On the coupling between ridged and rectangular waveguide via a non-offset longitudinal slot

Von der Fakultät für Ingenieurwissenschaften der
Abteilung Elektrotechnik und Informationstechnik
der Universität Duisburg-Essen

zur Erlangung des akademischen Grades

Doktor der Ingenieurwissenschaften

genehmigte Dissertation

von

Maria Pardalopoulou
aus
Athen, Griechenland

1. Gutachter: Prof. Dr.-Ing. Klaus Solbach
2. Gutachter: Prof. Dr. sc. techn. Daniel Erni
Tag der mündlichen Prüfung: 20.10.2011

Contents

I. Mathematical Symbols

$\overrightarrow{A}$	Magnetic Vector Potential
$\overrightarrow{E}$	Electric Field
$\overrightarrow{e}_{TE_i}$, $\overrightarrow{h}_{TE_i}$	Eigenvector of the TE_i Waveguide Eigenmode
$\overrightarrow{e}_{TM_i}$, $\overrightarrow{h}_{TM_i}$	Eigenvector of the TM_i Waveguide Eigenmode
ε	Electric Permitivity
f	Frequency
$\overrightarrow{F}$	Electric Vector Potential
$\overline{\overline{G}}(\overrightarrow{r}, \overrightarrow{r}')$	Dyadic Green Function
$G(\overrightarrow{r}, \overrightarrow{r}')$	Scalar Green Function
$\overrightarrow{H}$	Magnetic Field
$\overrightarrow{J}$	Electric Surface Current Density
k_0	Propagation Constant in free space
λ	Wavelength in free space
λ_g	Wavelength inside a Waveguide
$\overrightarrow{L}$	Complementary Non-Solenoidal Term
$\overrightarrow{M}$	Magnetic Surface Current Density
$\overrightarrow{n}$	Normal Vector to a Surface
μ	Magnetic Permeability
Φ	Electric Scalar Potential
ρ	Surface Charge Density
$\overrightarrow{r}$	Observation Point Vector
$\overrightarrow{r}'$	Source Point Vector
$\overrightarrow{s}$	Tangential Vector to a Surface
ψ_{h0}	Constant Mode inside a Magnetic Current carrying Waveguide
ω	Angular Frequency

Chapter 1

Introduction

The present thesis was conducted in the scope of a project aiming at the advancement of design- and production- technologies for millimeter wave modules on the basis of metalized plastics. The radiating elements, designed for this antenna employ a novel concept in the area of waveguide discontinuities and coupling, which is also the subject of the current thesis.
In the past decades a great amount of research has been conducted on the study of transmission line discontinuities and their application in structures like antennas, filters, couplers etc. Transmission line discontinuities like apertures or obstacles inside various kinds of waveguides, cavities or coaxial lines have been employed in order to guarantee electromagnetic behavior with specific characteristics [1] - [14]. The requirements for the electromagnetic behavior of the system determined the kind and the properties of the implemented discontinuities. A great variety of equivalent circuits with lumped or shunt elements have been developed for modeling the transmission line discontinuities. The circuit elements represent the effect of each aperture or obstacle on the overall regulation and distribution of the electromagnetic energy inside the waveguide configuration. Many of these circuits were accurate and very useful for engineering purposes, especially when the involved discontinuities are single apertures or posts with simple geometrical shapes. Therefore such applications have been very popular in the past years. Typical examples are slot arrays, waveguide slot-couplers, steps in waveguides or post-tuned filters.

The evolution of applications in the microwave area, however, increased the demand on more compact and complicated structures, which could not be accurately represented by the simplified older models. A better understanding of the electromagnetic behavior of such configurations required a closer study of the electromagnetic fields that are generated in the vicinity of the waveguide discontinuities. The complexity of these systems is also reflected into the mathematical equations that express the scattered fields, thus making their computation more difficult. To this purpose, various numerical techniques like the Moment Method, the Finite Element Method, the Finite Difference Time Domain method, the Boundary-Element method and many others have been developed and improved over the years. These techniques have been widely used until nowadays, because they can provide accuracy, relatively short computational time and numerical stability.

The waveguide structure, that will be investigated in the present work, was part of the project BMBF Verbundvorhaben "Adaptive Kommunikations-Module" (aKoM) led by the Daimler Chrysler/ Ulm, now part of EADS. In Chapter 2 a brief description of the antenna structure will be presented and the theoretical model for the thesis will be determined. The integral equations for the theoretical model will be derived in Chapter 3. The numerical methods that were employed for the computation of the electromagnetic fields inside the waveguides will be examined in Chapter 4, whereas Chapter 5 deals with solution convergence issues. In that chapter, specific theoretical data will be compared against a test model that was constructed in the University of Duisburg-Essen. Finally, in Chapter 6 the results of the theoretical computations will be demonstrated.

Chapter 2

Description of the 'aKoM' configuration

The aim of the project was the design of a flat antenna, applicable to point-to-point communications. The antenna is operating in the frequency range 37-39.5 GHz and its construction is based upon metalized plastics technology. The initial concept involved an array antenna that should meet criteria like high gain, wide bandwidth, low sidelobes and design suitable for low-cost plastics technology. Moreover, the antenna should also exhibit a performance compatible with the ETSI-Specifications. Taking all these factors into account, the design concept that emerged as the best one, was a planar array antenna with integration of radiators, waveguide feeding networks and HF electronics in three layers of metalized plastics, which are bonded together. Radiation takes place at the open-ends of rectangular waveguides, coupled to the radiator rows through slots. The design aspects of the antenna that are relevant to the present thesis involve the junction between the radiator elements and their feeding networks, which occupy the higher layer.

Starting with the description of the array architecture, it should be stated that the antenna consists of 640 open end radiating rectangular waveguides, distributed in 32 rows of 20 radiating elements. The antenna is divided into two identical subarrays as illustrated in Figure 2.1(a).

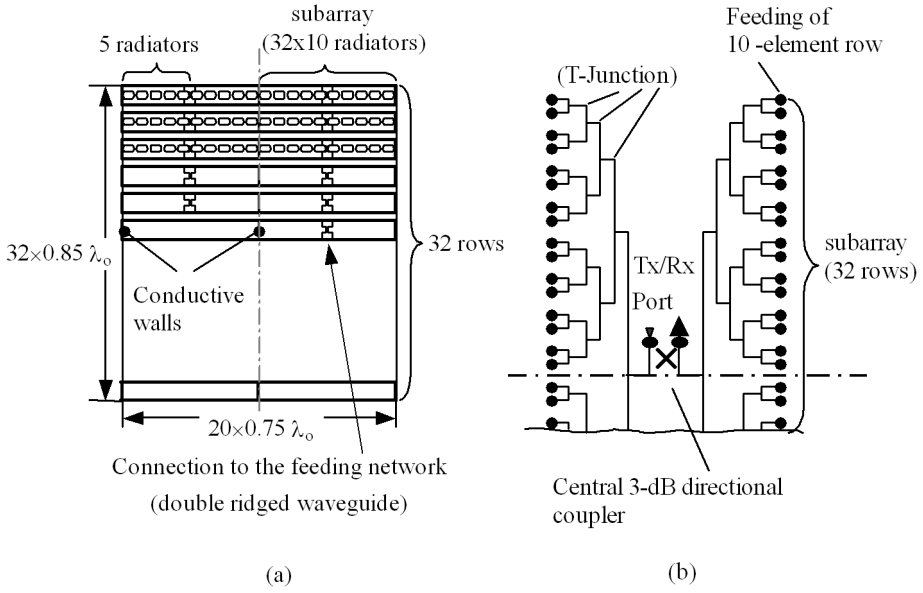

Figure 2.1 Array architecture. (a) Configuration of the higher layer bearing the radiating rows and the radiating elements. (b) Configuration of the middle layer embodying the feeding network

The subarrays consist of 32 rows with 10 radiators each. Every radiating rectangular waveguide forms a T-junction with its row. Each row is short-circuited at its ends and is fed at its center through a tree-form feeding network, which is placed at the middle layer. The feeding networks are arranged in a way, that uniform amplitude distribution over the array antenna be ensured, thus meeting the demand for high gain. The lowest layer is occupied by the 3-dB directional coupler, which distributes the power symmetrically to both subarrays. The coupling between the two higher layers is achieved through double ridged waveguides, which are positioned vertical to the planes of the layers.

Even though rectangular waveguides were favored as radiating elements, ridged waveguides were employed for the feeding network and the row configuration. Ridged waveguides were chosen mainly due to constructional reasons, because they possess small cross-sections. In this manner, the spacing between parallel waveguides could be large enough to enable tight bonding between the layers. Moreover, the use of ridged waveguides as radiating rows ensures a relatively compact array antenna, thus avoiding the appearance of grating lobes.

The entire structure is mounted under a 45-tilt angle, as demonstrated in Figure 2.2.

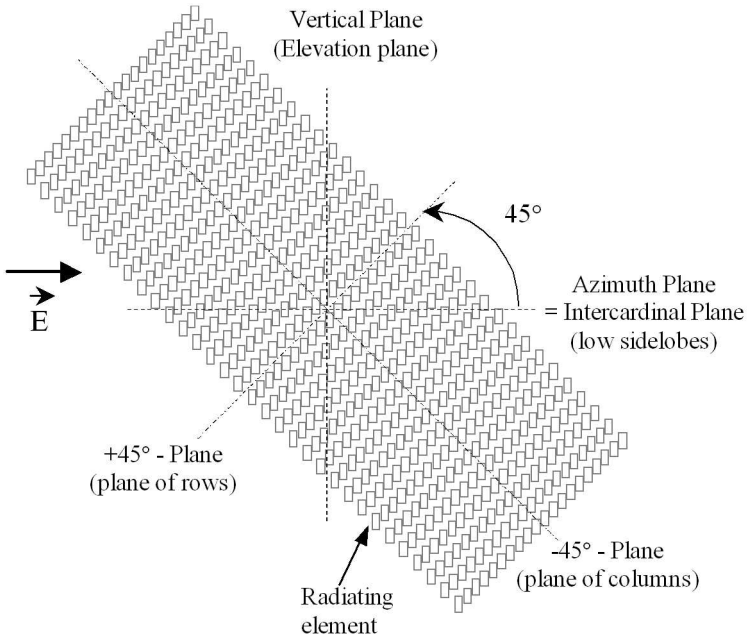

Figure 2.2 Array alignment. The entire array is rotated 45° with respect to the azimuth or the elevation plane. Each radiator has an additional 45° tilt

This alignment was dictated by the ETSI requirement for low side lobes in the azimuth plane. In order to meet such a requirement, the azimuth plane should coincide with an intercardinal plane, which forms a 45° angle with the planes of the rows and the columns of the array. Such a configuration, however, leads to deviations from the desired vertical polarization. Therefore, every waveguide radiator has an additional 45°-tilt with respect to the intercardinal planes, so that vertical polarization is finally achieved.

One of the most important issues of the designing procedure, was the optimization of the coupling between the radiating element and its row. As already mentioned, the radiation takes place at the open ends of rectangular waveguides, which are coupled to the ridged waveguide rows via T-junctions. Such a configuration, involving only one radiating element, is shown in Figure 2.3.

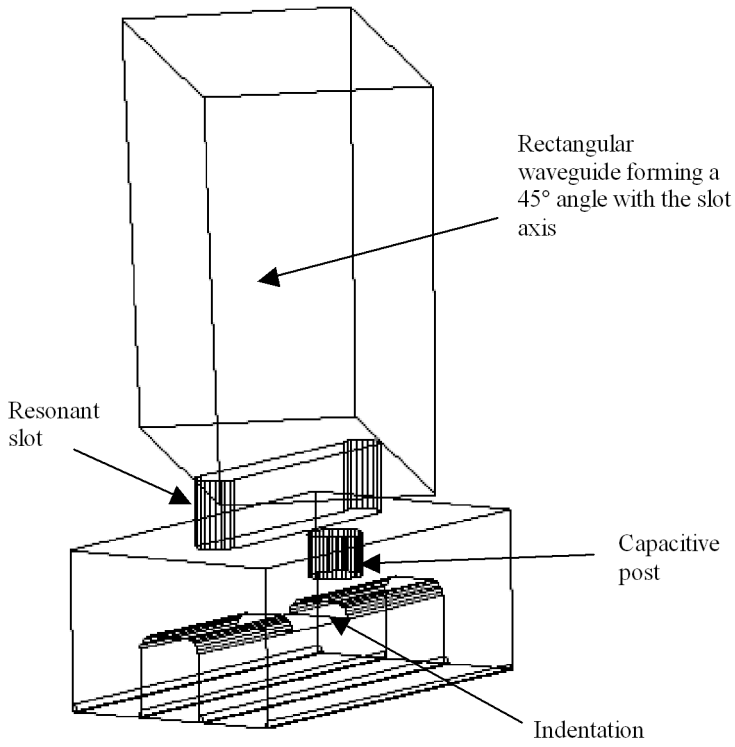

Figure 2.3 Junction of one radiating element with the ridged waveguide row.

The structure depicted in the previous figure is the exact radiator model used for the simulation, which was performed with the Agilent software HFSS (High Frequency Structure Simulator). In this model many constructional details were taken into account, in order to simulate their effect on the overall electromagnetic performance of the configuration. For this reason, the ridge has rounded edges and the rectangular waveguide has a slight "horn" form.

From Figure 2.3 it becomes apparent that the electromagnetic energy flows from the ridged to the rectangular waveguide through a resonant slot. Because of constructional restrictions, the edges of the slot should be rounded. The slot forms a 45°- angle with the symmetry planes of the rectangular waveguide, due to the additional tilt of the rectangular waveguide for the purpose of vertical polarization. As far as the ridged waveguide is concerned, the slot is located at the center line of its broad wall in the longitudinal direction. The alignment of the slot deviates from the usual configuration of slotted array antennas, where the slots are alternately displaced from the center-line of the waveguide at certain offsets [89] - [99]. Actually, this configuration was the first concept considered for the 'aKoM' antenna, but was quickly rejected because it would lead to a such placement of the radiating waveguides, that would cause the appearance of grating lobes. Therefore, the long axis of the slot had to coincide with the center line of the ridged waveguide broad wall. The major side-effect of this alignment, however, would be the lack of coupling between the waveguides, because the current flowing on the ridged waveguide wall is symmetric about the slot axis and can't induce any electric field on the aperture. The problem was dealt with, by attaching a small capacitive post to the ridged waveguide broad wall on one side of the slot. The higher order modes, generated by the post, disturb the symmetry of the current and enable the excitation of fields on the slot aperture, which ensure the transition of electromagnetic energy from the row to the radiator. The presence of the post inside the ridged waveguide affected the resonant behavior of the slot, due to its capacitive reactance and, therefore, had to be compensated for. The solution was the insertion

of an indentation on the ridge underneath the slot. In this manner, the inductive reactance of the indentation could counterbalance the capacitance of the post, if its geometrical dimensions were adjusted properly.

The geometrical dimensions of the discontinuities inside the ridged waveguide, namely the slot, the post and the indentation, determined, to a great extend, the electromagnetic performance of the radiator element. In particular, dimensions like the slot length or the post height were very critical, since slight changes in their values could "intensify" or "weaken" the coupling between the waveguides. The role of these parameters will be discussed to a greater detail in Chapter 6, where the corresponding results will be presented. At this point, however, it could be stated that the geometrical dimensions of the ridged waveguide discontinuities were also adjustable parameters, which were investigated during the design process, so that optimum performance is achieved.

The optimum performance of the radiator element is determined by the radiation requirements for the entire antenna, one of which is vertical polarization. To this purpose, it must be ensured that only one mode will propagate inside the rectangular waveguide, namely the TE_{10} mode. This can be achieved, if the rectangular waveguide has a minimum length, so that all evanescent modes excited at the vicinity of the slot attenuate. The minimum value for the length was found to be in the order of a half waveguide-wavelength. In this case the cross-polarization is held under 20dB over the entire frequency range. However, the length of the rectangular waveguide is also a parameter, which should be treated carefully, since the rectangular waveguide acts as a polarization twist and an impedance transformer at the same time. More specifically, the reflection coefficient of the radiating aperture is transformed to the slot plane through the rectangular waveguide section and is further transformed through the slot into the feeding ridged waveguide. Therefore, the value of the rectangular waveguide length controls the effect of the radiation impedance on the radiator row.

The open-end reflection coefficient, which also includes the mutual coupling effects of the large array, was another major issue during the design process. In order to approximate the mutual coupling effects on a radiating element not near the end of the array, an infinite array antenna was assumed and the model of a virtual waveguide simulator was employed [15] - [20]. The basic concept of the waveguide simulator is the introduction of electric walls at planes, where the tangential electric field of the array antenna is null. It is possible to arrange the conductive walls in a way that they form a cell or a waveguide, which is infinitely extended into free space. The walls do not perturb the field distribution, but their presence is justified by certain field symmetries. Once the walls are present, the field outside the waveguide may be completely ignored. In this way, a part of the infinite array is isolated and the mutual coupling effects between its radiating elements approximate the mutual coupling effects between the radiating elements of the entire antenna.

The waveguide simulator that was used in this project is shown in Figure 2.4. It consists of two parallel magnetic walls and two electric walls. The implementation of magnetic walls reflecting the proper field symmetry is only possible in field theoretical simulation. Conventional waveguide simulators are limited to electric walls and therefore can not simulate broadside radiation. The choice of the waveguide cross-section was based upon the form of the antenna grid. The grid is not exactly triangular, since the radiating elements are not aligned on the same line, due to their 45 tilt. However, the assumption of a proper triangular grid was proven to yield satisfactory results about the reflection coefficient at the radiating apertures. Considering the symmetry planes of the triangular grid, the smallest cross-section for the waveguide simulator is the one depicted in the picture. Both electric and magnetic walls bisect two neighboring radiating elements, forming a cross section made of one quarter of each element.

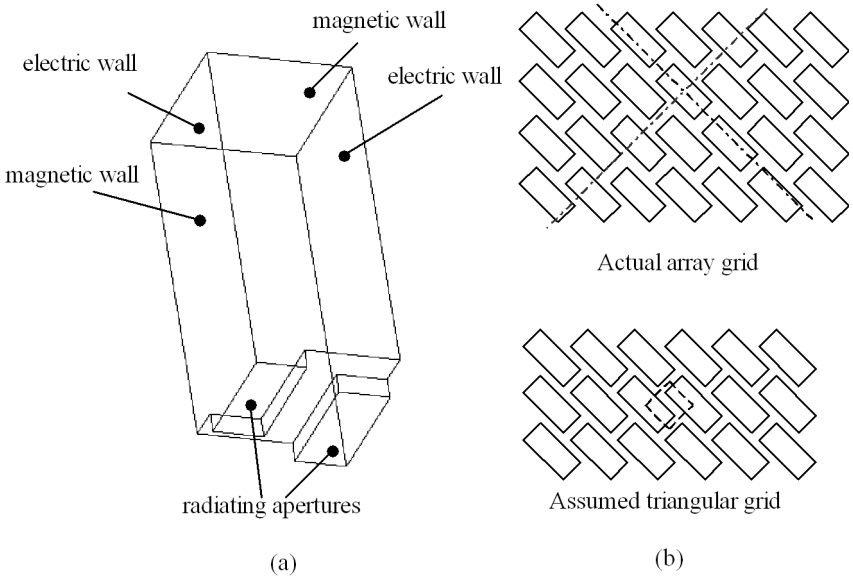

Figure 2.4 Waveguide simulator with the corresponding fragments of two neighboring radiating apertures

Figure 2.4 also depicts the HFSS model that was used for the waveguide simulator. The structure was simulated as a three-port configuration, where all ports (waveguide simulator and the two radiating waveguides) are considered to be terminated with a matched load. HFSS yielded the S-matrix of the three-port structure. Combination of the reflection coefficient for the excitation of only one radiating aperture with the transmission coefficient between the two apertures determines the reflection coefficient of each radiating aperture.

The radiation impedance is superimposed to the reactances introduced by the discontinuities inside the ridged waveguide. The total impedance of each radiator element should be controlled in a way that good matching of the radiator row to the feeding network be ensured for the entire frequency range. The proper tuning of the radiator element impedance through adjustments of certain geometrical dimensions was the basic goal of the design procedure. To this purpose, the electromagnetic behavior of an entire radiating row for various combinations of these geometrical dimensions had to be simulated. Each radiator row, however, is a complicated structure, which consists of ten identical radiator elements arranged in the following manner: The distance between adjacent slots is half a ridged waveguide length and the posts are staggered about the center line. Moreover, the slots close to the row ends are located quarter of a ridged waveguide length from the short circuited waveguide walls. In this way, the standing waves that are formed inside the ridged waveguide excite all ten slots in phase with equal amplitude. In addition, the connection of the radiator row to the feeding network is realized via a T-junction between a single and a double ridged waveguide. This junction had to be optimized as well, so that the reflection coefficient on the double ridged waveguide port be held low throughout the entire frequency range.

The above description states clearly that the simulation of a row with HFSS would be extremely time consuming and would not yield accurate results. For this reason it was necessary to segment the radiator row into smaller parts, which can be accurately simulated under HFSS. The first part was the T-junction between the ridged and the rectangular waveguide, involving the slot, the post and the indentation. This structure, like the waveguide simulator structure, was simulated as a three-port configuration, where all ports are well matched. The waveguide simulator was the second part simulated under HFSS and the last part was the T-junction at the feeding point of the radiator row. The model used for simulating the T-junction under HFSS is depicted in Figure 2.5. In this model two radiators are employed. The purpose of that was to examine to what extend the higher

order modes, which are excited in the vicinity of the waveguide junction, affect the field inside the radiating waveguides. The results from the electromagnetic simulation showed that the distortion to the slot fields due to the evanescent modes is negligible. Again, each port of the configuration is considered to be terminated with a matched load.

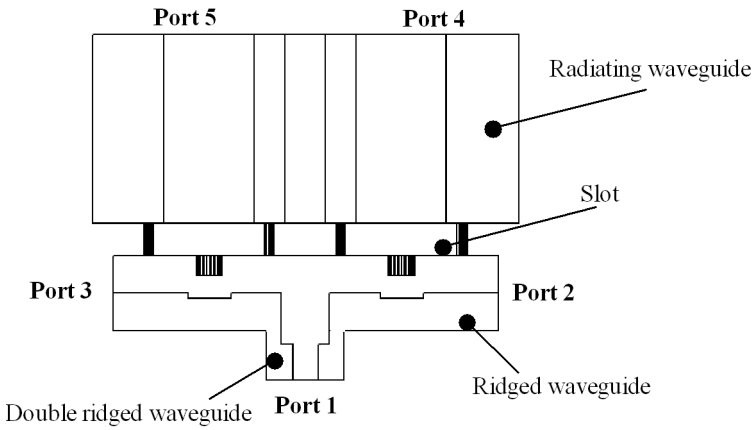

Figure 2.5 HFSS model of ridged waveguide T-junction with two radiating elements

The S-matrix data, obtained by HFSS for all structures, are imported to a network analysis tool (Agilent ADS) and are combined in the following way: The ridged waveguide ports of adjacent radiators are connected together and the open-end reflection coefficient, which is computed by the waveguide simulator scattering parameters, is applied to the rectangular waveguide port. The two ends of the row are short-circuited, whereas the feeding junction is inserted in its middle. In this manner, a one-port configuration emerged, which represented the entire radiator row. For the verification purposes, a similar test model was constructed and measured. The test model was produced on milled metal technology and was scaled, in order to operate in the X-band. The agreement of the ADS and the measurement results was good, confirming the validity of the design procedure.

The concept employed for the slot coupler of the radiator element was new. Therefore, it was intriguing to investigate the behavior of the electromagnetic fields that are produced by the combination of waveguide discontinuities like slot and post inside any structure similar to the 'aKoM' configuration. In the next chapters a model will be developed for the computation of the field quantities that are generated by a longitudinal slot and a metalic post inside a single ridged waveguide at the presence of a coupled rectangular waveguide. The radiation phenomena and the impact of the indentation were not included, for the sake of simplicity. The theoretical background along with the necessary mathematical formulations will be provided in the next chapter.

Chapter 3

Integral Equations for the 'aKoM' configuration

The novelty in the 'aKoM' structure lies in the combination of a centered slot and a cylindrical metallic post, which is employed in order to initiate the coupling mechanism between the ridged and the rectangular waveguide. Both slot and post represent waveguide discontinuities, which give rise to evanescent modes and cause scattering phenomena. The scope of this work is to analytically compute the scattered fields and to examine their impact on the electromagnetic behavior of the structure. In Chapter 3 an analysis is performed for the general case, where both slot and post are arbitrarily positioned inside the ridged waveguide. The integral equations that determine the scattered fields, along with the corresponding dyadic Green functions are derived. The chapter is concluded with the analysis for the 'aKoM' configuration.

3.1 Mathematical formulations for the waveguide fields

3.1.1 Theory

Figure 3.1 depicts the structure of the coupled waveguides. The slot and the post are also illustrated.

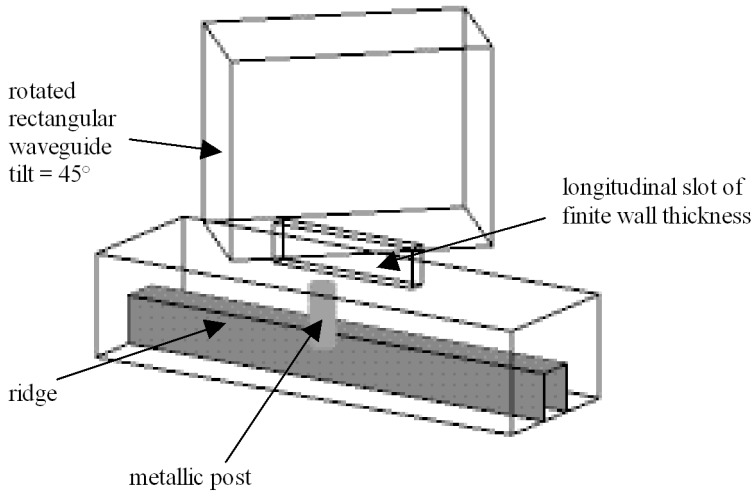

Figure 3.1 Waveguide slot coupler with metallic post

The finite wall thickness of the slot formulates a narrow rectangular waveguide, coupled to the ridged and the twisted rectangular waveguide via two apertures, namely 'Slot 1' and 'Slot 2' re-

spectively, as illustrated in Figure 3.2.

Slot 1 ensures the transition of energy between the ridged and the narrow rectangular waveguide through its electric field. Likewise, the electric field that is present at Slot 2 enables the coupling of the narrow and the twisted rectangular waveguide. The fields of both apertures are generated by the electric current distributions, flowing on these waveguide walls, where the apertures reside.

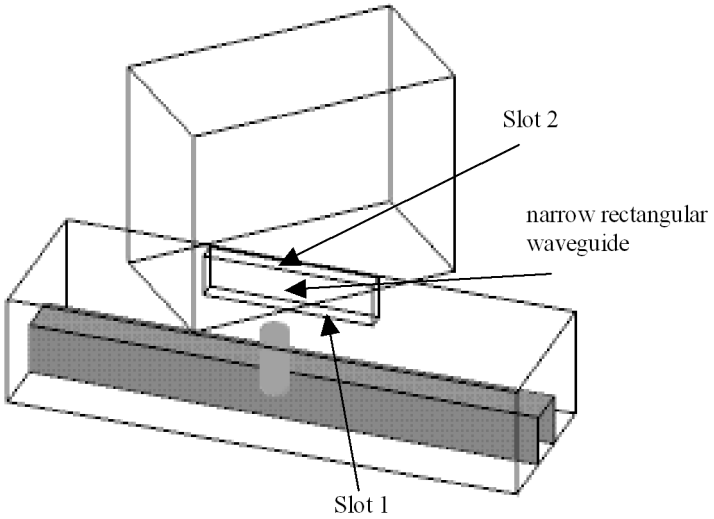

Figure 3.2 Apertures of the waveguide coupler

The excitation of the aperture electric field requires that the current distributions across the long slot edges be unsymmetric [86]. In the case of the 'aKoM' configuration, this condition is not satisfied for Slot 1, since the long axis of the slot coincides with the symmetry axis for the electric current on the ridged waveguide broad wall. The problem is dealt with, through insertion of the metallic post near the aperture: The post, which is illuminated by the incident wave inside the ridged waveguide, introduces an additional current density that perturbs the current symmetry of the upper broad wall, leading to the excitation of the aperture electric field. Consequently, in the 'aKoM' configuration the metallic post is responsible for the coupling between the ridged and the narrow rectangular waveguide. The special features of the 'aKoM' structure will be studied at a later section of the present chapter.

In a more general case, where the slot is located at an offset from the center line of the ridged waveguide broad wall, the slot would be excited even without the aid of the metallic scatterer, but the presence of the latter could alter the slot behavior, according to application specific characteristics. The coupling mechanism between the aperture and the post is the same, regardless of the post or the slot position and is based on the superposition of the scattered fields that each waveguide discontinuity produces [28]. Therefore, the theoretical study of the coupling requires the determination of the relationships between the exciting causes (post surface current, aperture electric field) and the resulting scattered fields. In the following sections of the present chapter, the analysis for the determination of the scattered fields will be presented. The appropriate mathematical formulations will be derived on the basis of suitable dyadic Green functions, which describe the excitation of each discontinuity inside a ridged or a rectangular waveguide.

3.1.2 Surface equivalent theorem - Maxwell Equations

The starting point for the derivation of the mathematical formulations is the application of the Schelkunoff's surface - equivalent theorem [21], according to which a scatterer may be replaced by equivalent electric or magnetic current distributions. The surface-equivalent theorem will be applied separately on each waveguide discontinuity.

Before applying Schelkunoff's theorem, it should be stated that both the ridged and the twisted rectangular waveguides are illuminated by incident waves ($\overrightarrow{E}_{inc1},\ \overrightarrow{H}_{inc1}$) and ($\overrightarrow{E}_{inc2}, \overrightarrow{H}_{inc2}$) respectively. The generating sources of the incident waves are located far from the metallic post and the slot, so that they will have no impact on the electromagnetic performance of the structure under study. Moreover, in the proceeding analysis it is assumed that all waves exhibit a $e^{-j\omega t}$ time dependency. The time dependency is suppressed.

- **Metallic Scatterer**

  The presence of electric and magnetic fields inside the ridged waveguide cause the excitation of a surface current density **J** on the closed surface of the post. Current **J** constitutes the source of a scattered wave ($\overrightarrow{E}_{s_p}, \overrightarrow{H}_{s_p}$), which is composed of higher order ridged waveguide modes. The overall fields in the waveguide region exterior to the post equal the sum of the scattered field ($\overrightarrow{E}_{p_s}, \overrightarrow{H}_{p_s}$) and the field that is incident on the post ($\overrightarrow{E}_{p_{inc}},\ \overrightarrow{H}_{p_{inc}}$):

$$\overrightarrow{E}_t = \overrightarrow{E}_{p_s} + \overrightarrow{E}_{p_{inc}} \quad (3.1a)$$
$$\overrightarrow{H}_t = \overrightarrow{H}_{p_s} + \overrightarrow{H}_{p_{inc}} \quad (3.1b)$$

  Since the scatterer is a conducting body, there are no fields in its interior region.

  According to Schelkunoff's theorem, the total field exterior to the post will not be disturbed, if a proper surface current density $\overrightarrow{J}_p$ is introduced on the closed surface of the scatterer and the scatterer itself is removed. $\overrightarrow{J}_p$ should be chosen in such a manner that it represents the discontinuity of the magnetic field intensity across the scatterer surface:

$$\overrightarrow{J}_p = \overrightarrow{n}_p \times (\overrightarrow{H}_e - \overrightarrow{H}_i)$$

  where $\overrightarrow{n}_p$ is the outward normal vector to the post surface, $\overrightarrow{H}_e$ is the magnetic field intensity just outside the post and $\overrightarrow{H}_i$ is the magnetic field intensity in its interior region. Since $\overrightarrow{H}_i = 0$ and $\overrightarrow{H}_e = \overrightarrow{H}_t$, the preceding equation may be written in the form:

$$\overrightarrow{J}_p = \overrightarrow{n}_p \times \overrightarrow{H}_t|_{\substack{'just'outside \\ the\ post\ surface}} \quad (3.2)$$

  In other words, the equivalent surface current density is considered to give rise to the $\overrightarrow{E}_{s_p}$ field outside the post and to the $-\overrightarrow{E}_{p_{inc}}$ field inside the post. In this way the boundary condition, regarding the continuity of the tangential electric field across the surface of the post is satisfied. The corresponding mathematical formulation is:

$$\overrightarrow{E}_t \cdot \overrightarrow{s}_p = (\overrightarrow{E}_{p_{inc}} + \overrightarrow{E}_{p_s}) \cdot \overrightarrow{s}_p = 0\ |_{post\ surface} \quad (3.3)$$

  where $\overrightarrow{s}_p$ is the tangential vector to the conducting surface.
  The scattered fields may be expressed in terms of the magnetic vector potential $\overrightarrow{A}$, which is produced by the electric current of the post. The relevant relationships are:

$$\overrightarrow{E}_{p_s}(\overrightarrow{r}) = -j\omega\mu[\overrightarrow{A}(\overrightarrow{r}) + \tfrac{1}{k_0^2}\nabla\nabla\cdot\overrightarrow{A}(\overrightarrow{r})] \quad (3.4)$$
$$\overrightarrow{H}_{p_s}(\overrightarrow{r}) = \nabla \times \overrightarrow{A}(\overrightarrow{r}) \quad (3.5)$$

  k_0 is the propagation constant in free space: $k_0^2 = \omega\epsilon\mu$
  $\omega = 2\pi f$, f is the operating frequency
  ϵ is the electric permitivity: $\epsilon \approx 8.8541878 \times 10^{-12}$ F/m
  μ is the magnetic permeability: $\mu = 4\pi 10^{-7}$ H/m

Enforcement of the Maxwell equations leads to the following expressions for the scattered field in the region exterior to the post:

$$\nabla \times \overrightarrow{E}_{p_s}(\overrightarrow{r}) = -j\omega\mu\overrightarrow{H}_{p_s}(\overrightarrow{r}) \quad (3.6a)$$
$$\nabla \times \overrightarrow{H}_{p_s}(\overrightarrow{r}) = j\omega\epsilon\overrightarrow{E}_{p_s}(\overrightarrow{r}) + \overrightarrow{J}_p(\overrightarrow{r}) \quad (3.6b)$$
$$\nabla \cdot [\epsilon\overrightarrow{E}_{p_s}(\overrightarrow{r})] = \overrightarrow{\rho}_e(\overrightarrow{r}) \quad (3.6c)$$

where $\overrightarrow{\rho}_e$ is the surface charge density. $\overrightarrow{\rho}_e$ is defined by the continuity equation:

$$\overrightarrow{\rho}_e(\overrightarrow{r}) = -\tfrac{1}{j\omega}\nabla_s \cdot \overrightarrow{J}_p(\overrightarrow{r}) \quad (3.6d)$$

∇_s is the surface divergence operator.
Combination of (3.4) (3.5) and (3.6) yields:

$$\nabla^2\overrightarrow{A}(\overrightarrow{r}) + k_0^2\overrightarrow{A}(\overrightarrow{r}) = -\overrightarrow{J}_p(\overrightarrow{r}) \quad (3.7a)$$
$$\nabla \times \nabla \times \overrightarrow{E}_{p_s}(\overrightarrow{r}) - k_0^2\overrightarrow{E}_{p_s}(\overrightarrow{r}) = -j\omega\mu\overrightarrow{J}_p(\overrightarrow{r}) \quad (3.7b)$$
$$\nabla \times \nabla \times \overrightarrow{H}_{p_s}(\overrightarrow{r}) - k_0^2\overrightarrow{H}_{p_s}(\overrightarrow{r}) = \nabla \times \overrightarrow{J}_p(\overrightarrow{r}) \quad (3.7c)$$

- **Apertures**

As already mentioned, the finite wall thickness of the slot dictates the segmentation of the entire structure into the three domains that are depicted in Figure 3.3.

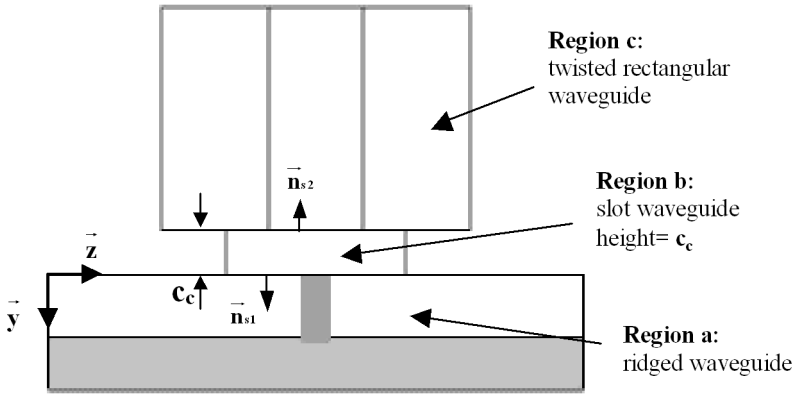

Figure 3.3 Waveguide junction

Region a represents the ridged waveguide, region b is the narrow slot waveguide and region c lies within the twisted rectangular waveguide. According to Schelkunoff's surface equivalence principle, a slot aperture that separates two adjacent regions may be substituted by a perfect short and a pair of magnetic current sheets that are located 'just' below and above the aperture plane. The magnetic currents are surrogates for the aperture electric fields [106] - [108]. More specifically, the aperture Slot 1 is short-circuited and a magnetic current sheet $\overrightarrow{M1}$ of equal dimensions is placed just below the aperture, at $y = 0^+$, so that it belongs to region a.

The proper choice for $\overrightarrow{M1}$ is:

$$\overrightarrow{M1} = \overrightarrow{E}_{Slot1} \times \overrightarrow{n}_{s1} \quad (3.8)$$

where $\overrightarrow{E}_{Slot1}$ is the electric field intensity at Slot 1 and $\overrightarrow{n}_{s1}$ is the vector normal to the aperture pointing to the interior of the ridged waveguide.

$\overrightarrow{M1}$ is responsible for the excitation of evanescent modes inside the ridged waveguide, which compose the slot-scattered field ($\overrightarrow{E}_{s_s}$, $\overrightarrow{H}_{s_s}$). The scattered fields are expressed with the aid

of the electric vector potential $\overrightarrow{F}$ according to the equations:

$$\overrightarrow{E}_{s_s}(\overrightarrow{r}) = -\nabla \times \overrightarrow{F}(\overrightarrow{r}) \quad (3.9)$$
$$\overrightarrow{H}_{s_s}(\overrightarrow{r}) = -j\omega\epsilon[\overrightarrow{F}(\overrightarrow{r}) + \tfrac{1}{k_0^2}\nabla\nabla \cdot \overrightarrow{F}(\overrightarrow{r})] \quad (3.10)$$

The scattered fields and their generating magnetic current relate to each other via the Maxwell equations:

$$\nabla \times \overrightarrow{E}_{s_s}(\overrightarrow{r}) = -j\omega\mu\overrightarrow{H}_{s_s}(\overrightarrow{r}) - \overrightarrow{M1}(\overrightarrow{r}) \quad (3.11a)$$
$$\nabla \times \overrightarrow{H}_{s_s}(\overrightarrow{r}) = j\omega\epsilon\overrightarrow{E}_{s_s}(\overrightarrow{r}) \quad (3.11b)$$
$$\nabla \cdot [\mu\overrightarrow{H}_{s_s}(\overrightarrow{r})] = \overrightarrow{\rho}_{m1}(\overrightarrow{r}) \quad (3.11c)$$

where $\overrightarrow{\rho}_{m1}$ is the surface magnetic charge density. $\overrightarrow{\rho}_{m1}$ is defined by the continuity equation:

$$\overrightarrow{\rho}_{m1}(\overrightarrow{r}) = -\tfrac{1}{j\omega}\nabla_s \cdot \overrightarrow{M1}(\overrightarrow{r}) \quad (3.11d)$$

After the combination of (3.9), (3.10) and (3.11) the following equations are obtained:

$$\nabla^2\overrightarrow{F}(\overrightarrow{r}) + k_0^2\overrightarrow{F}(\overrightarrow{r}) = -\overrightarrow{M1}(\overrightarrow{r}) \quad (3.12a)$$
$$\nabla \times \nabla \times \overrightarrow{H}_{s_s}(\overrightarrow{r}) - k_0^2\overrightarrow{H}_{s_s}(\overrightarrow{r}) = -j\omega\epsilon\overrightarrow{M1}(\overrightarrow{r}) \quad (3.12b)$$
$$\nabla \times \nabla \times \overrightarrow{E}_{s_s}(\overrightarrow{r}) - k_0^2\overrightarrow{E}_{s_s}(\overrightarrow{r}) = -\nabla \times \overrightarrow{M1}(\overrightarrow{r}) \quad (3.12c)$$

The presence of $\overrightarrow{M1}$ requires the insertion of a magnetic current sheet $-\overrightarrow{M1}$ at plane $y = 0^-$, so that the conditions of the surface equivalence principal be fulfilled. The magnetic current $-\overrightarrow{M1}$ excites scattered fields inside the slot waveguide that satisfy equations similar to (3.9)-(3.12). The boundary condition, which must apply across the aperture, is the continuity of the overall tangential magnetic field. This condition is mathematically formulated in the following manner:

$$\overrightarrow{H}_{s_{inc}} \cdot \overrightarrow{s}_{s1} + \overrightarrow{H}_{s_s} \cdot \overrightarrow{s}_{s1} = \overrightarrow{H}_c \cdot \overrightarrow{s}_{s2} \quad |_{y=0} \quad (3.13)$$

where $\overrightarrow{H}_{s_{inc}}$ is the ridged waveguide magnetic field incident to the slot and $\overrightarrow{H}_c$ is the total magnetic field inside the slot waveguide.
Vectors $\overrightarrow{s}_{s1}$ and $\overrightarrow{s}_{s2}$ are tangential to the slot aperture at planes $y = 0^+$ and $y = 0^-$ respectively.

In a similar manner, Slot 2 is shorted and a pair of magnetic current sheets $\overrightarrow{M2}$ and $-\overrightarrow{M2}$ is placed at $y = c_c^-$ and $y = c_c^+$ respectively. $\overrightarrow{M2}$ is the source of evanescent waveguide modes inside the twisted rectangular waveguide, which is now transformed to a semi-infinite waveguide. $\overrightarrow{M2}$ is defined by the expression:

$$\overrightarrow{M2} = \overrightarrow{E}_{Slot2} \times \overrightarrow{n}_{s2} \quad (3.14)$$

where $\overrightarrow{E}_{Slot2}$ is the electric field intensity at Slot 2 and $\overrightarrow{n}_{s2}$ is the vector normal to the slot aperture pointing to the interior of region c. The equations that apply for Slot 2 are similar to expressions (3.9) - (3.12):

$$\overrightarrow{E}_{rw_s}(\overrightarrow{r}) = -\nabla \times \overrightarrow{F}_{rw_s}(\overrightarrow{r}) \quad (3.15)$$
$$\overrightarrow{H}_{rw_s}(\overrightarrow{r}) = -j\omega\epsilon[\overrightarrow{F}_{rw_s}(\overrightarrow{r}) + \tfrac{1}{k_0^2}\nabla\nabla \cdot \overrightarrow{F}_{rw_s}(\overrightarrow{r})] \quad (3.16)$$
$$\nabla \times \overrightarrow{E}_{rw_s}(\overrightarrow{r}) = -j\omega\mu\overrightarrow{H}_{rw_s}(\overrightarrow{r}) - \overrightarrow{M2}(\overrightarrow{r}) \quad (3.17a)$$
$$\nabla \times \overrightarrow{H}_{rw_s}(\overrightarrow{r}) = j\omega\epsilon\overrightarrow{E}_{rw_s}(\overrightarrow{r}) \quad (3.17b)$$
$$\nabla \cdot [\mu\overrightarrow{H}_{rw_s}(\overrightarrow{r})] = \overrightarrow{\rho}_{m2}(\overrightarrow{r}) \quad (3.17c)$$

$\overrightarrow{F}_{s_{rw}}$ is the electric vector potential and $\overrightarrow{E}_{s_{rw}}$, $\overrightarrow{H}_{s_{rw}}$ are the electric and magnetic field intensities inside the twisted rectangular waveguide respectively.

$\overrightarrow{\rho}_{m2}$ is the surface charge density, defined by the continuity equation:

$$\overrightarrow{\rho}_{m2}(\overrightarrow{r}) = -\frac{\nabla_s \cdot \overrightarrow{M2}(\overrightarrow{r})}{j\omega} \quad (3.17d)$$

Combination of (3.11a) and (3.11b) yields:

$$\nabla^2 \overrightarrow{F}_{s_{rw}}(\overrightarrow{r}) + k_0^2 \overrightarrow{F}_{s_{rw}}(\overrightarrow{r}) = -\overrightarrow{M2}(\overrightarrow{r}) \quad (3.18a)$$
$$\nabla \times \nabla \times \overrightarrow{H}_{s_{rw}}(\overrightarrow{r}) - k_0^2 \overrightarrow{H}_{s_{rw}}(\overrightarrow{r}) = -j\omega\epsilon\overrightarrow{M2}(\overrightarrow{r}) \quad (3.18b)$$
$$\nabla \times \nabla \times \overrightarrow{E}_{s_{rw}}(\overrightarrow{r}) - k_0^2 \overrightarrow{E}_{s_{rw}}(\overrightarrow{r}) = -\nabla \times \overrightarrow{M2}(\overrightarrow{r}) \quad (3.18c)$$

The magnetic current $-\overrightarrow{M2}$ excites additional scattered fields inside the slot waveguide, which are superimposed to the ones produced by $-\overrightarrow{M1}$. Furthermore, implementation of Schelkunoff's surface equivalence principal, suggests that region b is transformed to a rectangular cavity excited by the magnetic currents $-\overrightarrow{M1}$ and $-\overrightarrow{M2}$. Consequently, the magnetic field at any point inside the rectangular cavity equals the sum of magnetic fields $\overrightarrow{H}_{c1}$ and $\overrightarrow{H}_{c2}$ generated by $-\overrightarrow{M1}$ and $-\overrightarrow{M2}$ respectively:

$$\begin{aligned} &\overrightarrow{H}_{inc2} \cdot \overrightarrow{s}_{s_{rw}} + \overrightarrow{H}_{s_{rw}} \cdot \overrightarrow{s}_{s_{rw}} = \overrightarrow{H}_c \cdot \overrightarrow{s}_{sc} \ \ |_{y=-c_c} \Rightarrow \\ &\overrightarrow{H}_{inc2} \cdot \overrightarrow{s}_{s_{rw}} + \overrightarrow{H}_{s_{rw}} \cdot \overrightarrow{s}_{s_{rw}} = \overrightarrow{H}_{c1} \cdot \overrightarrow{s}_{sc} + \overrightarrow{H}_{c2} \cdot \overrightarrow{s}_{sc} \ \ |_{y=-c_c} \end{aligned} \quad (3.19)$$

$\overrightarrow{H}_{inc2}$ is the incident magnetic field inside the twisted rectangular waveguide and vectors $\overrightarrow{s}_{sc}$, $\overrightarrow{s}_{s_{rw}}$ are tangential to the Slot 2 at planes $y = -c_c^+$ and $y = -c_c^-$ respectively.

The expressions that have been obtained by the implementation of the surface-equivalence principal constitute the basis for the derivation of the integral equations, which will determine the scattered fields inside the waveguides. The derivation procedure is carried out in the next section.

3.1.3 Integral Equations for the combined structure

From the preceding analysis, it becomes obvious that three kinds of fields exist in the ridged waveguide region near the slot and the post:

($\overrightarrow{E}_{inc1}$, $\overrightarrow{H}_{inc1}$)**:** The ridged waveguide incident field, induced by an external source with no impact on the configuration slot-post.

($\overrightarrow{E}_{p_s}$, $\overrightarrow{H}_{p_s}$)**:** The field induced by the electric current of the post surface.

($\overrightarrow{E}_{s_s}$, $\overrightarrow{H}_{s_s}$)**:** The field induced by the magnetic current that represents the aperture electric field.

Superposition of all fields yields the overall field inside the ridged waveguide:

$$\overrightarrow{E}_s = \overrightarrow{E}_{inc1} + \overrightarrow{E}_{s_s} + \overrightarrow{E}_{p_s} \quad (3.20a)$$
$$\overrightarrow{H}_s = \overrightarrow{H}_{inc1} + \overrightarrow{H}_{s_s} + \overrightarrow{H}_{p_s} \quad (3.20b)$$

Field ($\overrightarrow{E}_s$ $\overrightarrow{H}_s$) is subject to the following boundary conditions:
The electric field tangential to the post surface should vanish at the points of the surface:

$$\overrightarrow{E}_s \cdot \overrightarrow{s}_p = 0|_{\substack{post \\ surface}} \Rightarrow (\overrightarrow{E}_{inc1} + \overrightarrow{E}_{s_s} + \overrightarrow{E}_{s_p}) \cdot \overrightarrow{s}_p = 0|_{\substack{post \\ surface}} \quad (3.21)$$

Additionally, in view of (3.2) the total magnetic field intensity must satisfy the following condition just outside the surface of the post:

$$\begin{aligned} &\overrightarrow{J}_p = \overrightarrow{n}_p \times \overrightarrow{H}_s|_{\substack{post \\ surface^+}} \Rightarrow \\ &\overrightarrow{J}_p = \overrightarrow{n}_p \times (\overrightarrow{H}_{inc1} + \overrightarrow{H}_{s_s} + \overrightarrow{H}_{s_p})|_{\substack{post \\ surface^+}} \end{aligned} \quad (3.22)$$

The component of $\overrightarrow{H}_s$ that is tangential to Slot 1 must equal the tangential magnetic field inside the rectangular cavity, at the aperture points:

$$\overrightarrow{H}_s \cdot \overrightarrow{s}_{s1} = \overrightarrow{H}_c \cdot \overrightarrow{s}_{s2}|_{Slot1} \Rightarrow$$
$$(\overrightarrow{H}_{inc1} + \overrightarrow{H}_{s_s} + \overrightarrow{H}_{s_p}) \cdot \overrightarrow{s}_{s1} = \overrightarrow{H}_{c1} \cdot \overrightarrow{s}_{s2} + \overrightarrow{H}_{c2} \cdot \overrightarrow{s}_{s2}|_{Slot1} \quad (3.23)$$

Moreover, all the field quantities of the structure must satisfy the Dirichlet boundary conditions that stand for the interior of the waveguides and waveguide walls, namely:

$$\overrightarrow{n} \cdot \overrightarrow{H} = 0 \ |_{waveguide\ walls} \quad (3.24a)$$
$$\overrightarrow{n} \times \overrightarrow{E} = 0 \ |_{waveguide\ walls} \quad (3.24b)$$
$$\nabla \cdot \overrightarrow{H} = 0 \ |_{waveguide\ walls} \quad (3.24c)$$

where $\overrightarrow{n}$ is the inward normal vector to the waveguide walls.
Expressions (3.21) and (3.23) along with condition (3.19) form the system of equations, the solution of which will yield the total scattered fields. An equivalent system of equations may be formulated if expression (3.22) is employed, instead of (3.21). This matter will be discussed in the last section of the present chapter.
The fields produced at the post and the slot are related to their generating current sources via the expressions (3.7), (3.12) and (3.18). Such equations may be solved with the aid of proper dyadic Green functions, which are defined as follows [46] - [56]:

- $\nabla^2 \overline{\overline{G}}_N(\overrightarrow{r}, \overrightarrow{r}') + k_0^2 \overline{\overline{G}}_N(\overrightarrow{r}, \overrightarrow{r}') = -I\delta(\overrightarrow{r} - \overrightarrow{r}')$, with respect to equations (3.7a), (3.12a) and (3.18a)
- $\nabla \times \nabla \overline{\overline{G}}_k^{\,l}(\overrightarrow{r}, \overrightarrow{r}') + k_0^2 \overline{\overline{G}}_k^{\,l}(\overrightarrow{r}, \overrightarrow{r}') = I\delta(\overrightarrow{r} - \overrightarrow{r}')$, with respect to equations (3.7b), (3.12b) and (3.18b)
- $\nabla \times \nabla \overline{\overline{G}}_k^{\,l}(\overrightarrow{r}, \overrightarrow{r}') + k_0^2 \overline{\overline{G}}_k^{\,l}(\overrightarrow{r}, \overrightarrow{r}') = \nabla \times I\delta(\overrightarrow{r} - \overrightarrow{r}')$, with respect to equations (3.7c), (3.12c) and (3.18c)

Function $\overline{\overline{G}}_N(\overrightarrow{r}, \overrightarrow{r}')$ designates the electric or the magnetic vector potential at a point r, due to an magnetic or a electric current density located at point r'. In a similar manner, function $\overline{\overline{G}}_k^{\,l}(\overrightarrow{r}, \overrightarrow{r}')$ represents the corresponding electric or magnetic fields. Indices N, k and l are explained below:

$$N = \begin{cases} \text{A indicates magnetic vector potential} \\ \text{F indicates electric vector potential} \end{cases}$$

$$k = \begin{cases} \text{H indicates magnetic field intensity} \\ \text{E indicates electric field intensity} \end{cases}$$

$$l = \begin{cases} \text{m indicates magnetic current} \\ \text{e indicates electric current} \end{cases}$$

$I = \overrightarrow{x} \cdot \overrightarrow{x}' + \overrightarrow{y} \cdot \overrightarrow{y}' + \overrightarrow{z} \cdot \overrightarrow{z}'$ is the unitary dyad.

Since the dyadic Green functions $\overline{\overline{G}}_N(\overrightarrow{r}, \overrightarrow{r}')$, $\overline{\overline{G}}_k^{\,l}(\overrightarrow{r}, \overrightarrow{r}')$ determine the field quantities (vector potentials of field intensities) that are generated by impulse current distributions, the scattered fields resulting from arbitrary surface current densities, may be expressed in the following way:

$$\overrightarrow{A}(\overrightarrow{r}) = \iint_{S_p} \overline{\overline{G}}_A(\overrightarrow{r}, \overrightarrow{r}') \cdot J(\overrightarrow{r}')ds' \quad (3.25a)$$
$$\overrightarrow{F}(\overrightarrow{r}) = \iint_{S_p} \overline{\overline{G}}_F(\overrightarrow{r}, \overrightarrow{r}') \cdot M(\overrightarrow{r}')ds' \quad (3.25b)$$

$$\overrightarrow{E}(\overrightarrow{r})= -\iint_{S_a} \overline{\overline{G}}_E^m(\overrightarrow{r},\overrightarrow{r}')\cdot\overrightarrow{M}(\overrightarrow{r}')ds' - j\omega\mu\iint_{S_p}\overline{\overline{G}}_E^e(\overrightarrow{r},\overrightarrow{r}')\cdot\overrightarrow{J}(\overrightarrow{r}')ds' =$$
$$= -\nabla\times\iint_{S_a}\overline{\overline{G}}_F(\overrightarrow{r},\overrightarrow{r}')\cdot\overrightarrow{M}(\overrightarrow{r}')ds' - j\omega\mu[\iint_{S_p}\overline{\overline{G}}_A(\overrightarrow{r},\overrightarrow{r}')\cdot\overrightarrow{J}(\overrightarrow{r}')ds'+$$
$$+\tfrac{1}{k_0^2}\nabla\nabla\iint_{S_p}\overline{\overline{G}}_A(\overrightarrow{r},\overrightarrow{r}')\cdot\overrightarrow{J}(\overrightarrow{r}')ds'] \quad (3.25c)$$

$$\overrightarrow{H}(\overrightarrow{r})= \iint_{S_p} \overline{\overline{G}}_H^e(\overrightarrow{r},\overrightarrow{r}')\cdot\overrightarrow{J}(\overrightarrow{r}')ds' - j\omega\varepsilon\iint_{S_a}\overline{\overline{G}}_H^m(\overrightarrow{r},\overrightarrow{r}')\cdot\overrightarrow{M}(\overrightarrow{r}')ds' =$$
$$= \nabla\times\iint_{S_p}\overline{\overline{G}}_A(\overrightarrow{r},\overrightarrow{r}')\cdot\overrightarrow{J}(\overrightarrow{r}')ds' - j\omega\varepsilon[\iint_{S_a}\overline{\overline{G}}_F(\overrightarrow{r},\overrightarrow{r}')\cdot\overrightarrow{M}(\overrightarrow{r}')ds'+$$
$$+\tfrac{1}{k_0^2}\nabla\nabla\iint_{S_a}\overline{\overline{G}}_F(\overrightarrow{r},\overrightarrow{r}')\cdot\overrightarrow{M}(\overrightarrow{r}')ds'] \quad (3.25d)$$

The above Green functions satisfy the following equations [53] :

$$\nabla^2\overline{\overline{G}}_A(\overrightarrow{r},\overrightarrow{r}')+k_o^2\overline{\overline{G}}_A(\overrightarrow{r},\overrightarrow{r}')=-I\delta(\overrightarrow{r}-\overrightarrow{r}') \quad (3.26a)$$
$$\nabla^2\overline{\overline{G}}_F(\overrightarrow{r},\overrightarrow{r}')+k_o^2\overline{\overline{G}}_F(\overrightarrow{r},\overrightarrow{r}')=-I\delta(\overrightarrow{r}-\overrightarrow{r}') \quad (3.26b)$$
$$\nabla\times\nabla\times\overline{\overline{G}}_E^{\,e}(\overrightarrow{r},\overrightarrow{r}')-k_o^2\,\overline{\overline{G}}_E^{\,e}(\overrightarrow{r},\overrightarrow{r}')=I\delta(\overrightarrow{r}-\overrightarrow{r}') \quad (3.26c)$$
$$\nabla\times\nabla\times\overline{\overline{G}}_H^{\,e}(\overrightarrow{r},\overrightarrow{r}')-k_o^2\,\overline{\overline{G}}_H^{\,e}(\overrightarrow{r},\overrightarrow{r}')=\nabla\times I\delta(\overrightarrow{r}-\overrightarrow{r}') \quad (3.26d)$$
$$\nabla\times\nabla\times\overline{\overline{G}}_E^{\,m}(\overrightarrow{r},\overrightarrow{r}')-k_o^2\,\overline{\overline{G}}_E^{\,m}(\overrightarrow{r},\overrightarrow{r}')=-\nabla\times I\delta(\overrightarrow{r}-\overrightarrow{r}') \quad (3.26e)$$
$$\nabla\times\nabla\times\overline{\overline{G}}_H^{\,m}(\overrightarrow{r},\overrightarrow{r}')-k_o^2\,\overline{\overline{G}}_H^{\,m}(\overrightarrow{r},\overrightarrow{r}')=I\delta(\overrightarrow{r}-\overrightarrow{r}') \quad (3.26f)$$

Additionally:

$$\overline{\overline{G}}_E^{\,e}=\nabla^2\overline{\overline{G}}_A+\tfrac{1}{k_0^2}\overline{\overline{G}}_A \quad (3.27a)$$
$$\overline{\overline{G}}_H^{\,m}=\nabla^2\overline{\overline{G}}_F+\tfrac{1}{k_0^2}\overline{\overline{G}}_F \quad (3.27b)$$
$$\overline{\overline{G}}_E^{\,m}=-\nabla\times\overline{\overline{G}}_F \quad (3.27c)$$
$$\overline{\overline{G}}_H^{\,e}=\nabla\times\overline{\overline{G}}_A \quad (3.27d)$$
$$\nabla\times\overline{\overline{G}}_E^{\,e}=\overline{\overline{G}}_H^{\,e} \quad (3.27e)$$
$$\nabla\times\overline{\overline{G}}_H^{\,e}=k_0^2\overline{\overline{G}}_E^{\,e}+I\delta(\overrightarrow{r}-\overrightarrow{r}') \quad (3.27f)$$
$$\nabla\times\overline{\overline{G}}_E^{\,m}=k_0^2\overline{\overline{G}}_H^{\,m}+I\delta(\overrightarrow{r}-\overrightarrow{r}') \quad (3.27g)$$
$$\nabla\times\overline{\overline{G}}_H^{\,m}=\overline{\overline{G}}_E^{\,m} \quad (3.27h)$$

Expressions (3.25) are valid for fields inside a waveguide only when the dyadic Green functions satisfy boundary conditions similar to the ones given by (3.24):

$$\overrightarrow{n}\cdot\overline{\overline{G}}_E^{\,l}=0\ |_{waveguide\ walls} \quad (3.28a)$$
$$\overrightarrow{n}\times\nabla\times\overline{\overline{G}}_H^{\,l}=0\ |_{waveguide\ walls} \quad (3.28b)$$

$l=e,m$

Substitution of equations (3.25) in expressions (3.19), (3.21) and (3.23) leads to the formulations:

$$-\overrightarrow{E}_{inc1}(\overrightarrow{r}_p)\cdot\overrightarrow{s}_p=-j\omega\mu\iint_{S_p}\overline{\overline{G}}_E^e(\overrightarrow{r}_p,\overrightarrow{r}'_p)\cdot\overrightarrow{J}_p(\overrightarrow{r}'_p)ds'_p\cdot\overrightarrow{s}_p-$$
$$-\iint_{Slot1}\overline{\overline{G}}_E^m(\overrightarrow{r}_p,\overrightarrow{r}'_{s1})\cdot\overrightarrow{M}1(\overrightarrow{r}'_{s1})ds'_{s1}\cdot\overrightarrow{s}_p\ |_{\substack{post\\surface}} \quad (3.29a)$$

$$-\overrightarrow{E}_{inc1}(\overrightarrow{r}_p)\cdot\overrightarrow{s}_p=-j\omega\mu[\iint_{S_p}\overline{\overline{G}}_A(\overrightarrow{r}_p,\overrightarrow{r}'_p)\cdot\overrightarrow{J}_p(\overrightarrow{r}'_p)ds'_p+$$
$$+\tfrac{1}{k_o^2}\nabla\nabla\cdot\iint_{S_p}\overline{G}_A(\overrightarrow{r}_p,\overrightarrow{r}'_p)\cdot\overrightarrow{J}_p(\overrightarrow{r}'_p)ds'_p]\cdot\overrightarrow{s}_p+$$
$$-\nabla\times\iint_{Slot1}\overline{\overline{G}}_F(\overrightarrow{r}_p,\overrightarrow{r}'_{s1})\cdot\overrightarrow{M}1(\overrightarrow{r}'_{s1})ds'_{s1}\cdot\overrightarrow{s}_p\ |_{\substack{post\\surface}} \quad (3.29b)$$

$$-\overrightarrow{H}_{inc1}(\overrightarrow{r}_{s1})\cdot\overrightarrow{s}_{s1}=\iint_{S_p}\overline{\overline{G}}^{e}_{H}(\overrightarrow{r}_{s1},\overrightarrow{r}'_{p})\cdot\overrightarrow{J}_{p}(\overrightarrow{r}'_{p})ds'_{p}\cdot\overrightarrow{s}_{s1}-$$
$$-j\omega\varepsilon[\iint_{Slot1}\overline{\overline{G}}^{m}_{H}(\overrightarrow{r}_{s1},\overrightarrow{r}'_{s1})\cdot\overrightarrow{M}1(\overrightarrow{r}'_{s1})ds'_{s1}\cdot\overrightarrow{s}_{s1}+$$
$$+\iint_{Slot1}\overline{\overline{G}}^{m}_{H_c}(\overrightarrow{r}_{s1},\overrightarrow{r}'_{s1})\cdot\overrightarrow{M}1(\overrightarrow{r}'_{s1})ds'_{s1}\cdot\overrightarrow{s}_{s2}+$$
$$+\iint_{Slot2}\overline{\overline{G}}^{m}_{H_c}(\overrightarrow{r}_{s1},\overrightarrow{r}'_{s2})\cdot\overrightarrow{M}2(\overrightarrow{r}'_{s2})ds'_{s2}\cdot\overrightarrow{s}_{s2}]\mid_{Slot1}\quad(3.30a)$$

$$-\overrightarrow{H}_{inc1}(\overrightarrow{r}_{s1})\cdot\overrightarrow{s}_{s1}=\nabla\times\iint_{S_p}\overline{\overline{G}}_{A}(\overrightarrow{r}_{s1},\overrightarrow{r}'_{p})\cdot\overrightarrow{J}_{p}(\overrightarrow{r}'_{p})ds'_{p}\cdot\overrightarrow{s}_{s1}-$$
$$-j\omega\varepsilon[\iint_{Slot1}\overline{\overline{G}}_{F}(\overrightarrow{r}_{s1},\overrightarrow{r}'_{s1})\cdot\overrightarrow{M}1(\overrightarrow{r}'_{s1})ds'_{s1}+$$
$$+\tfrac{1}{k_o^2}\nabla\nabla\cdot\iint_{Slot1}\overline{\overline{G}}_{F}(\overrightarrow{r}_{s1},\overrightarrow{r}'_{s1})\cdot\overrightarrow{M}1(\overrightarrow{r}'_{s1})ds'_{s1}]\cdot\overrightarrow{s}_{s1}-$$
$$-j\omega\varepsilon[\iint_{Slot1}\overline{\overline{G}}_{Fc}(\overrightarrow{r}_{s1},\overrightarrow{r}'_{s1})\cdot\overrightarrow{M}1(\overrightarrow{r}'_{s1})ds'_{s1}+$$
$$+\tfrac{1}{k_o^2}\nabla\nabla\cdot\iint_{Slot1}\overline{\overline{G}}_{Fc}(\overrightarrow{r}_{s1},\overrightarrow{r}'_{s1})\cdot\overrightarrow{M}1(\overrightarrow{r}'_{s1})ds'_{s1}]\cdot\overrightarrow{s}_{s2}-$$
$$-j\omega\varepsilon[\iint_{Slot2}\overline{\overline{G}}_{Fc}(\overrightarrow{r}_{s1},\overrightarrow{r}'_{s2})\cdot\overrightarrow{M}2(\overrightarrow{r}'_{s2})ds'_{s2}+$$
$$+\tfrac{1}{k_o^2}\nabla\nabla\cdot\iint_{Slot2}\overline{\overline{G}}_{Fc}(\overrightarrow{r}_{s1},\overrightarrow{r}'_{s2})\cdot\overrightarrow{M}2(\overrightarrow{r}'_{s2})ds'_{s2}]\cdot\overrightarrow{s}_{s2}\mid_{Slot1}\quad(3.30b)$$

$$-\overrightarrow{H}_{inc2}(\overrightarrow{r}_{s2})\cdot\overrightarrow{s}_{s_{rw}}=-j\omega\varepsilon[\iint_{Slot1}\overline{\overline{G}}^{m}_{H_c}(\overrightarrow{r}_{s2},\overrightarrow{r}'_{s1})\cdot\overrightarrow{M}1(\overrightarrow{r}'_{s1})ds'_{s1}\cdot\overrightarrow{s}_{sc}+$$
$$+\iint_{Slot2}\overline{\overline{G}}^{m}_{H_c}(\overrightarrow{r}_{s2},\overrightarrow{r}'_{s2})\cdot\overrightarrow{M}2(\overrightarrow{r}'_{s2})ds'_{s2}\cdot\overrightarrow{s}_{sc}+$$
$$+\iint_{Slot2}\overline{\overline{G}}^{m}_{H_{s_{rw}}}(\overrightarrow{r}_{s2},\overrightarrow{r}'_{s2})\cdot\overrightarrow{M}2(\overrightarrow{r}'_{s2})ds'_{s2}\cdot\overrightarrow{s}_{s_{rw}}]\mid_{Slot2}\quad(3.31a)$$

$$-\overrightarrow{H}_{inc2}(\overrightarrow{r}_{s2})\cdot\overrightarrow{s}_{s_{rw}}=j\omega\epsilon[\iint_{Slot2}\overline{\overline{G}}_{F_c}(\overrightarrow{r}_{s2},\overrightarrow{r}'_{s1})\cdot\overrightarrow{M}1(\overrightarrow{r}'_{s1})\,ds'_{s1}+$$
$$+\tfrac{1}{k_0^2}\nabla\nabla\cdot\iint_{Slot2}\overline{\overline{G}}_{F_c}(\overrightarrow{r}_{s2},\overrightarrow{r}'_{s1})\cdot\overrightarrow{M}1(\overrightarrow{r}'_{s1})\,ds'_{s1}]\cdot\overrightarrow{s}_{rc}-$$
$$-j\omega\epsilon[\iint_{Slot2}\overline{\overline{G}}_{F_c}(\overrightarrow{r}_{s2},\overrightarrow{r}'_{s2})\cdot\overrightarrow{M}2(\overrightarrow{r}'_{s2})\,ds'_{s2}+$$
$$+\tfrac{1}{k_0^2}\nabla\nabla\cdot\iint_{Slot2}\overline{\overline{G}}_{F_c}(\overrightarrow{r}_{s2},\overrightarrow{r}'_{s2})\cdot\overrightarrow{M}2(\overrightarrow{r}'_{s2})\,ds'_{s2}]\cdot\overrightarrow{s}_{rc}-$$
$$-j\omega\epsilon[\tfrac{1}{k_0^2}\nabla\nabla\cdot\iint_{Slot2}\overline{\overline{G}}_{F_{s_{rw}}}(\overrightarrow{r}_{s2},\overrightarrow{r}'_{s2})\cdot\overrightarrow{M}2(\overrightarrow{r}'_{s2})\,ds'_{s2}+$$
$$+\iint_{Slot2}\overline{\overline{G}}_{F_{s_{rw}}}(\overrightarrow{r}_{s2},\overrightarrow{r}'_{s2})\cdot\overrightarrow{M}2(\overrightarrow{r}'_{s2})\,ds'_{s2}]\cdot\overrightarrow{s}_{s_{rw}}\mid_{Slot2}\quad(3.31b)$$

where:

$\overline{\overline{G}}_{F_c}$: Electric vector potential dyadic Green function inside the rectangular cavity.

$\overline{\overline{G}}_{F_{s_{rw}}}$: Electric vector potential dyadic Green function inside the semi-infinite rectangular waveguide.

$\overline{\overline{G}}^{m}_{H_{rc}}$: Magnetic dyadic Green function for the magnetic current inside the rectangular cavity.

$\overline{\overline{G}}^{m}_{H_{s_{rw}}}$: Magnetic dyadic Green function for the magnetic current inside the semi-infinite rectangular waveguide.

$\overrightarrow{r}_p$: Points on the post surface.

$\overrightarrow{r}_{s1}$: Points on Slot 1.

$\overrightarrow{r}_{s2}$: Points on Slot 2.

Equations (3.29), (3.30) and (3.31) constitute a system of three integral equations with three unknowns, namely the current densities $\overrightarrow{J}_p$, $\overrightarrow{M1}$ and $\overrightarrow{M2}$. These equations describe the relationship among the fields inside any structure that bears a resemblance to the 'aKoM' configuration. More specifically, the determination of the above current densities yields the scattered fields inside a waveguide that contains a metallic scatterer of arbitrary shape and is coupled to another waveguide via an aperture of arbitrary orientation and finite wall thickness. Equations (3.29), (3.30) and (3.31) apply, regardless of the relative position of the coupled waveguides and the locations of the slot and the metallic scatterer.

Solution of the former equations requires the derivation of all dyadic Green functions involved. Even though the derivation procedure will be analyzed at a later section of the present work, it can be stated at this point that some dyadic Green functions exhibit high singularities, especially when the observation point lies in the close vicinity of the source point. Particularly in the cases where the integrals may not be evaluated analytically, but resort must be taken to numerical methods, the singularities are more difficult to handle. The explanation lies in the presence of the differential operators inside the integral equations: the accuracy of the numerical methods is not guaranteed, if successive differentiations follow a numerical integration. For this reason it is often desired to interchange the sequence of integration and differentiation, so that the derivatives be computed analytically. This procedure, however, is not allowed, because it can lead to violation of the Leibnitz's rule, especially when source and observation points almost coincide [57]. For this reason it would be convenient, if equivalent integral equations were derived, where at least one derivative were brought inside the integral. This is accomplished via the mixed potential formulation, which employs the combination of vector and scalar potentials [57], [76]. The mixed potential formulation will be adapted for the integral equation relevant to the post surface, because these integrals may not be computed analytically, in contrast to the integrals involving the magnetic current. The derivation of the mixed potential formulation is presented below:

Combination of equations (3.5) and (3.6a) yields:

$$\nabla \times \overrightarrow{E}_{s_p} = -j\omega\mu\nabla \times \overrightarrow{A} \Rightarrow$$
$$\overrightarrow{E}_{s_p} = -j\omega\mu\overrightarrow{A} + \nabla\Phi_e$$

where Φ_e is a scalar potential function and is related to the surface charge density via the equation:

$$\nabla^2\Phi_e(\overrightarrow{r}) + k_0^2\Phi_e(\overrightarrow{r}) = -\rho_e(\overrightarrow{r})$$

In addition, the Lorenz gauge is valid:

$$\nabla \cdot \overrightarrow{A}(\overrightarrow{r}) = -j\omega\epsilon\Phi_e(\overrightarrow{r})$$

In a homogeneous medium Φ_e may also be expressed in terms of a scalar Green function:

$$\Phi_e(\overrightarrow{r}) = \epsilon \iint\limits_{\substack{scatterer \\ surface}} G_{\Phi_e}(\overrightarrow{r}, \overrightarrow{r}')\rho_\varepsilon(\overrightarrow{r}')ds' \quad (3.32)$$

Derivation of $G_{\Phi_e}(\overrightarrow{r}, \overrightarrow{r}')$ can be found in Appendix B.

Incorporation of (3.32) into equation (3.29b) yields:

$$-\overrightarrow{E}_{inc1}(\overrightarrow{r}_p)\cdot\overrightarrow{s}_p = -j\omega\mu \iint\limits_{S_p} \overline{\overline{G}}_A(\overrightarrow{r}_p, \overrightarrow{r}'_p)\cdot\overrightarrow{J}_p(\overrightarrow{r}'_p)ds'_p\cdot\overrightarrow{s}_p - \\ -\nabla\iint\limits_{S_p} G_{\Phi_e}(\overrightarrow{r_p}, \overrightarrow{r_p}')\nabla_s\cdot\overrightarrow{J_p}(\overrightarrow{r}')\,ds'_p\cdot\overrightarrow{s}_p + \\ -\nabla\times\iint\limits_{Slot1}\overline{\overline{G}}_F(\overrightarrow{r}_p, \overrightarrow{r}'_{s1})\cdot\overrightarrow{M}1(\overrightarrow{r}'_{s1})ds'_{s1}\cdot\overrightarrow{s}_p \;|_{\substack{post\\surface}} \quad (3.33)$$

Since expressions (3.29) and (3.33) are equivalent, (3.33) may replace (3.29a) or (3.29b) in the final system of equations. The combination of (3.33) (3.31) and (3.30) will be denoted as the MPIE method throughout the rest of this work, whereas the system that constitutes of equations (3.29) (3.31) and (3.30) is denoted as the EFIE method. In general the MPIE method produces more stable solutions than the EFIE method and is often preferred for the solution of scattering problems. Later on it will be proven, that in this particular problem both the EFIE and the MPIE methods lead to the same integral equation.

3.2 Derivation of the Dyadic Green Functions

Implementation of either the MPIE or the EFIE method requires the determination of the involved Green functions. It is a logical choice to expand all Green functions in terms of waveguide and cavity eigenvectors. In this way, all boundary conditions concerning the waveguide walls are automatically satisfied. Furthermore, the eigenfunction representation of Green function offers the possibility to handle the singular behavior of some Green functions by means of delta functions, instead of computing principal value integrals [56]. The principal-value method is mostly employed in the case of free space or unbounded media, where the Green functions are evaluated in closed form and the involved volume surface integrals do not converge. In such cases, a small exclusion volume surface S_δ containing the source point is defined. Subtraction of the exclusion volume surface integral from the overall Green volume surface integral leads to a principal-value integral, which is convergent when $S_\delta \to 0$. The principal value integral with respect to the Green functions has been the subject of numerous studies [47] - [49], [52], [54] - [56]. In the following section it will be evident that the effect of principal-value integral is inherent in the eigenfunction representation of the Green function.

The expansion of Green functions in terms of waveguide or cavity eigenvectors, however, raises an issue regarding the completeness of the modal expansion of some dyadic Green functions [46], [50], [51], [53], [57] . The issue becomes clear when the divergence operator is applied on both members of (3.26c). Recognizing that $\nabla\cdot I\delta(\overrightarrow{r}-\overrightarrow{r}') \neq 0$ for $\overrightarrow{r}=\overrightarrow{r}'$, it is concluded that the divergence of $\overline{\overline{G}}_E^{\,e}$ does not equal zero, when the source and the observation point coincide. Since all waveguide modes are divergenceless everywhere in the waveguide interior, it becomes obvious that superposition of waveguide eigenvectors alone does not suffice for the correct representation of the electric Green function. Additional terms are required so that the non-solenoidal nature of $\overline{\overline{G}}_E^{\,e}$ is retained. The same applies for $\overline{\overline{G}}_H^{\,m}$, $\overline{\overline{G}}_F$ and $\overline{\overline{G}}_A$.

All Green functions are derived after the Ohm-Rayleigh method [46]. In this section, the derivation of functions $\overline{\overline{G}}_A$ and $\overline{\overline{G}}_F$ will be demonstrated. Derivation of the rest dyadic Green functions is performed in Appendix B.

3.2.1 Dyadic Green function for the magnetic vector potential

The function $\overline{\overline{G}}_A$ satisfies the equation:

$$\nabla^2\overline{\overline{G}}_A(\overrightarrow{r}, \overrightarrow{r}') + k_0^2\overline{\overline{G}}_A(\overrightarrow{r}, \overrightarrow{r}') = -I\delta(\overrightarrow{r}-\overrightarrow{r}') \;|_{\substack{inside\ the\\waveguide}} \quad (3.34)$$

According to the Ohm-Rayleigh method, the term on the right side of (3.34) is expanded on the following sets of eigenvectors:

$$\begin{array}{ll}
\overrightarrow{e}_{TE_i}(\overrightarrow{r},h) = e^{jhz}\nabla_t g_i(x,y)\times\overrightarrow{z} & \text{(TE modes)}\\
\overrightarrow{e}_{TM_i}(\overrightarrow{r},h) = jhe^{jhz}\nabla_t f_i(x,y) + k^2_{C_{TMi}} f_i(x,y)e^{jhz}\cdot\overrightarrow{z} & \text{(TM modes)}\\
\overrightarrow{L}_{TM_i}(\overrightarrow{r},h) = \nabla(f_i(x,y)e^{jhz}) & \text{(non-solenoidal term)}
\end{array}$$

∇_t denotes divergence with respect to the transverse coordinates and $g_i(x,y)$, $f_i(x,y)$, $k^2_{C_{TMi}}$ have been defined in Appendix A. The Cartesian coordinate system for the ridged waveguide is analysed in Appendix C. Term $\overrightarrow{L}_{TM_i}$ is the complementary non-solenoidal term, which represents the solution to the homogeneous vector Helmholtz equation:

$$\overrightarrow{L}_{TM_i} + (k^2_{C_{TMi}} + h^2)\overrightarrow{L}_{TM_i} = 0$$

All vectors posses the following orthogonal properties:

$$\iint_{S_w}\int_{-\infty}^{\infty} \overrightarrow{e}_{TE_i}(\overrightarrow{r},h)\overrightarrow{e}_{TE_n}(\overrightarrow{r},-h')\,dz\,ds = \delta(h-h')\delta_{i,n}2\pi \tag{3.35a}$$

$$\iint_{S_w}\int_{-\infty}^{\infty} \overrightarrow{e}_{TM_i}(\overrightarrow{r},h)\overrightarrow{e}_{TM_n}(\overrightarrow{r},-h')\,dz\,ds = (k^2_{C_{TMi}}+h^2)\delta(h-h')\delta_{i,n}2\pi \tag{3.35b}$$

$$\iint_{S_w}\int_{-\infty}^{\infty} \overrightarrow{L}_{TM_i}(\overrightarrow{r},h)\overrightarrow{L}_{TM_n}(\overrightarrow{r},-h')\,dz\,ds = \frac{k^2_{C_{TMi}}+h^2}{k^2_{C_{TMi}}}\delta(h-h')\delta_{i,n}2\pi \tag{3.35c}$$

$$\iint_{S_w}\int_{-\infty}^{\infty} \overrightarrow{e}_{TE_i}(\overrightarrow{r},h)\overrightarrow{e}_{TM_n}(\overrightarrow{r},-h')\,dz\,ds = 0 \tag{3.35d}$$

$$\iint_{S_w}\int_{-\infty}^{\infty} \overrightarrow{e}_{TM_i}(\overrightarrow{r},h)\overrightarrow{L}_{TM_n}(\overrightarrow{r},-h')\,dz\,ds = j(h-h')k^2_{C_{TMi}}\delta(h-h')\delta_{i,n}2\pi \tag{3.35e}$$

$$\iint_{S_w}\int_{-\infty}^{\infty} \overrightarrow{e}_{TE_i}(\overrightarrow{r},h)\overrightarrow{L}_{TM_n}(\overrightarrow{r},-h')\,dz\,ds = 0 \tag{3.35f}$$

where S_w is the waveguide cross-section and $\delta_{i,n} = \begin{cases} 1 & ,i=n \\ 0 & ,i\neq n \end{cases}$

Expression (3.35e) suggests that eigenvectors $\overrightarrow{e}_{TM_i}(\overrightarrow{r},h)$ and $\overrightarrow{L}_{TM_n}(\overrightarrow{r},h)$ are not orthogonal in the spatial domain. This problem, however, is not encountered when the h domain is considered:

$$\int_{-\infty}^{\infty}\iint_{S_w}\int_{-\infty}^{\infty} \overrightarrow{e}_{TM_i}(\overrightarrow{r},h)\overrightarrow{L}_{TM_n}(\overrightarrow{r},-h')\,dz\,ds\;dh = 0$$

Expansion of term $I\delta(\overrightarrow{r}-\overrightarrow{r}')$ leads to:

$$\begin{aligned} I\delta(\overrightarrow{r}-\overrightarrow{r}') = \int_{-\infty}^{\infty} dh\{\sum_j [B_j(h)\overrightarrow{e}_{TM_j}(\overrightarrow{r},h) + C_j(h)\overrightarrow{L}_{TM_j}(\overrightarrow{r},h)] + \\ + \sum_i A_i(h)\overrightarrow{e}_{TE_i}(\overrightarrow{r},h)\} \end{aligned} \tag{3.36}$$

where $A_i(h)$, $B_j(h)$ and $C_j(h)$ are unknown coefficients to be determined. Multiplication of both members of (3.36) with $\overrightarrow{e}_{TE_i}(\overrightarrow{r},h)$, integration over the volume of the waveguide V and incorporation of (3.35) yields:

$$\iiint_V \overrightarrow{e}_{TE_k}(\overrightarrow{r},-h')\delta(\overrightarrow{r}-\overrightarrow{r}')dxdydz = \int_{-\infty}^{\infty} dhA_k(h)\delta(h-h')2\pi \Rightarrow$$

$$A_k(h) = \frac{\overrightarrow{e}_{TE_k}(\overrightarrow{r}',-h)}{2\pi}$$

In a similar way the values for coefficients $B_k(h)$ and $C_k(h)$ are obtained:

$$B_k(h) = \frac{\overrightarrow{e}_{TM_k}(\overrightarrow{r}',-h)}{2\pi(k^2_{C_{TMk}}+h^2)}$$
$$C_k(h) = \frac{\overrightarrow{L}_{TM_k}(\overrightarrow{r}',-h)k^2_{C_{TMk}}}{2\pi(k^2_{C_{TMk}}+h^2)}$$

Equation (3.36) becomes:

$$I\delta(\overrightarrow{r}-\overrightarrow{r}') = \int_{-\infty}^{\infty} dh\{\sum_i \frac{\overrightarrow{e}_{TE_i}(\overrightarrow{r}',-h)\overrightarrow{e}_{TE_i}(\overrightarrow{r},h)}{2\pi} + \\ + \sum_j [\frac{\overrightarrow{e}_{TM_j}(\overrightarrow{r}',-h)\overrightarrow{e}_{TM_j}(\overrightarrow{r},h)}{2\pi(k^2_{C_{TM_j}}+h^2)} + \\ + \frac{k^2_{C_{TM_j}}\overrightarrow{L}_{TM_j}(\overrightarrow{r}',-h)\overrightarrow{L}_{TM_j}(\overrightarrow{r},h)}{2\pi(k^2_{C_{TM_j}}+h^2)}]\} \quad (3.37)$$

or

$$\delta(\overrightarrow{r}-\overrightarrow{r}')\overrightarrow{x}\,\overrightarrow{x}' = \int_{-\infty}^{\infty} dh\{\sum_i [\frac{e^{j*h*(z-z')}}{2\pi}\frac{\partial g_i(x,y)}{\partial y}\frac{\partial g_i(x',y')}{\partial y'}] + \\ + \sum_j [\frac{e^{j*h*(z-z')}}{2\pi}\frac{\partial f_j(x,y)}{\partial x}\frac{\partial f_j(x',y')}{\partial x'}]\}\overrightarrow{x}\,\overrightarrow{x}' \Rightarrow$$
$$\delta(\overrightarrow{r}-\overrightarrow{r}')\overrightarrow{x}\,\overrightarrow{x}' = [\sum_i \frac{\partial g_i(x,y)}{\partial y}\frac{\partial g_i(x',y')}{\partial y'} + \\ + \sum_j \frac{\partial f_j(x,y)}{\partial x}\frac{\partial f_j(x',y')}{\partial x'}]\delta(z-z')\overrightarrow{x}\,\overrightarrow{x}' \quad (3.37a)$$

$$\delta(\overrightarrow{r}-\overrightarrow{r}')\overrightarrow{y}\,\overrightarrow{y}' = \int_{-\infty}^{\infty} dh\{\sum_i [\frac{e^{jh(z-z')}}{2\pi}\frac{\partial g_i(x,y)}{\partial x}\frac{\partial g_i(x',y')}{\partial x'}] + \\ + \sum_j [\frac{e^{jh(z-z')}}{2\pi}\frac{\partial f_j(x,y)}{\partial y}\frac{\partial f_j(x',y')}{\partial y'}]\}\overrightarrow{y}\,\overrightarrow{y}' \Rightarrow$$
$$\delta(\overrightarrow{r}-\overrightarrow{r}')\overrightarrow{y}\,\overrightarrow{y}' = [\sum_i \frac{\partial g_i(x,y)}{\partial x}\frac{\partial g_i(x',y')}{\partial x'} + \\ + \sum_j \frac{\partial f_j(x,y)}{\partial y}\frac{\partial f_j(x',y')}{\partial y'}]\delta(z-z')\overrightarrow{y}\,\overrightarrow{y}' \quad (3.37b)$$

$$\delta(\overrightarrow{r}-\overrightarrow{r}')\overrightarrow{z}\,\overrightarrow{z}' = \int_{-\infty}^{\infty} dh \sum_j [\frac{e^{jh(z-z')}}{2\pi}k^2_{C_{TMj}}f_j(x,y)f_j(x',y')]\overrightarrow{z}\,\overrightarrow{z}' \Rightarrow$$
$$\delta(\overrightarrow{r}-\overrightarrow{r}')\overrightarrow{z}\,\overrightarrow{z}' = \sum_j [k^2_{C_{TMj}}f_j(x,y)f_j(x',y')]\delta(z-z')\overrightarrow{z}\,\overrightarrow{z}' \quad (3.37c)$$

The next step is to expand the unknown Green function in the following way:

$$\overline{\overline{G}}_A(\overrightarrow{r},\overrightarrow{r}') = \frac{1}{2\pi}\int_{-\infty}^{\infty} dh\{\sum_i a_i(h)\overrightarrow{e}_{TE_i}(\overrightarrow{r}',-h)\overrightarrow{e}_{TE_i}(\overrightarrow{r},h) + \\ + \sum_j [b_j(h)\frac{\overrightarrow{e}_{TM_j}(\overrightarrow{r}',-h)\overrightarrow{e}_{TM_j}(\overrightarrow{r},h)}{(k^2_{C_{TM_j}}+h^2)} + \\ + c_j(h)\frac{k^2_{C_{TM_j}}\overrightarrow{L}_{TM_j}(\overrightarrow{r}',-h)\overrightarrow{L}_{TM_j}(\overrightarrow{r},h)}{(k^2_{C_{TM_j}}+h^2)}]\} \quad (3.38)$$

The unknown coefficients $a_i(h)$, $b_j(h)$ and $c_j(h)$ are determined after substitution of (3.37) and (3.38) into (3.34) and implementation of the following conditions:

$$\nabla^2\overrightarrow{e}_{TE_i}(\overrightarrow{r},h) = -\nabla\times\nabla\times\overrightarrow{e}_{TE_i}(\overrightarrow{r},h) = -(k^2_{C_{TEj}}+h^2)\overrightarrow{e}_{TE_i}(\overrightarrow{r},h)$$
$$\nabla^2\overrightarrow{e}_{TM_j}(\overrightarrow{r},h) = -\nabla\times\nabla\times\overrightarrow{e}_{TM_j}(\overrightarrow{r},h) = -(k^2_{C_{TM_j}}+h^2)\overrightarrow{e}_{TM_j}(\overrightarrow{r},h)$$
$$\nabla^2\overrightarrow{L}_{TM_j}(\overrightarrow{r},h) = \nabla\nabla\cdot\overrightarrow{L}_{TM_j}(\overrightarrow{r},h) = -(k^2_{C_{TM_j}}+h^2)\overrightarrow{L}_{TM_j}(\overrightarrow{r},h)$$

The resulting coefficients are:

$$b_k(h) = c_k(h) = \frac{1}{k^2_{C_{TM_j}} + h^2 + k_0^2}$$
$$a_k(h) = \frac{1}{k^2_{C_{TE_j}} + h^2 + k_0^2}$$

The expression for $\overline{\overline{G}}_A(\overrightarrow{r}, \overrightarrow{r}')$ takes the form:

$$\begin{aligned}\overline{\overline{G}}_A(\overrightarrow{r}, \overrightarrow{r}') =& \frac{1}{2\pi} \int_{-\infty}^{\infty} dh \{ \sum_i \frac{\overrightarrow{e}_{TE_i}(\overrightarrow{r}', -h)\, \overrightarrow{e}_{TE_i}(\overrightarrow{r}, h)}{k^2_{C_{TEi}} + h^2 - k_o^2} + \\ &+ \sum_j [\frac{\overrightarrow{e}_{TM_j}(\overrightarrow{r}', -h)\, \overrightarrow{e}_{TM_j}(\overrightarrow{r}, h)}{(k^2_{C_{TM_j}} + h^2)(k^2_{C_{TM_j}} + h^2 - k_o^2)} + \\ &+ \frac{k^2_{C_{TMj}}\, \overrightarrow{L}_{TM_j}(\overrightarrow{r}', -h)\, \overrightarrow{L}_{TM_j}(\overrightarrow{r}, h)}{(k^2_{C_{TM_j}} + h^2)(k^2_{C_{TM_j}} + h^2 - k_o^2)}] \} \end{aligned} \quad (3.39)$$

The Fourier integral of (3.39) may be evaluated in a closed form by applying the method of contour integration. All terms of the integrand have two poles at $h = \pm\sqrt{k_0^2 - k^2_{C_k}}$ and they fulfill the requirement of the Jordan lemma at infinity. After the implementation of the contour integration the final expression for $\overline{\overline{G}}_A(\overrightarrow{r}, \overrightarrow{r}')$ is obtained:

$$\begin{aligned}\overline{\overline{G}}_A(\overrightarrow{r}, \overrightarrow{r}') =& -j \sum_i \frac{\overrightarrow{e}_{TE_i}(\overrightarrow{r}', \pm\gamma_{TE_i})\, \overrightarrow{e}_{TE_i}(\overrightarrow{r}, \mp\gamma_{TE_i})}{2\gamma_{TE_i}} - \\ &- j \sum_j [\frac{\overrightarrow{e}_{TM_j}(\overrightarrow{r}', \pm\gamma_{TM_j})\, \overrightarrow{e}_{TM_j}(\overrightarrow{r}, \mp\gamma_{TM_j})}{2\gamma_{TM_j} k_o^2} + \\ &+ \frac{k^2_{C_{TMj}}\, \overrightarrow{L}_{TM_j}(\overrightarrow{r}', -h)\, \overrightarrow{L}_{TM_j}(\overrightarrow{r}, h)}{2\gamma_{TM_j} k_o^2}] \end{aligned} \quad (3.40)$$

The upper line in the summations refers to the case where $z > z'$ whereas the bottom line stands for $z < z'$. The elements of $\overline{\overline{G}}_A(\overrightarrow{r}, \overrightarrow{r}')$ are cited below:

$$\begin{aligned} G_{A_{xx}}(\overrightarrow{r}, \overrightarrow{r}') =& -j \sum_i \frac{\partial g_i(x,y)}{\partial y} \frac{\partial g_i(x',y')}{\partial y'} \frac{e^{-j\gamma_{TE_i}|z-z'|}}{2\gamma_{TE_i}} - \\ &- j \sum_j \frac{\partial f_j(x,y)}{\partial x} \frac{\partial f_j(x',y')}{\partial x'} \frac{e^{-j\gamma_{TM_j}|z-z'|}}{2\gamma_{TM_j}} \end{aligned} \quad (3.41a)$$

$$\begin{aligned} G_{A_{xy}}(\overrightarrow{r}, \overrightarrow{r}') =& j \sum_i \frac{\partial g_i(x,y)}{\partial y} \frac{\partial g_i(x',y')}{\partial x'} \frac{e^{-j\gamma_{TE_i}|z-z'|}}{2\gamma_{TE_i}} - \\ &- j \sum_j \frac{\partial f_j(x,y)}{\partial x} \frac{\partial f_j(x',y')}{\partial y'} \frac{e^{-j\gamma_{TM_j}|z-z'|}}{2\gamma_{TM_j}} \end{aligned} \quad (3.41b)$$

$$G_{A_{xz}}(\overrightarrow{r}, \overrightarrow{r}') = 0 \quad (3.41c)$$

$$\begin{aligned} G_{A_{yy}}(\overrightarrow{r}, \overrightarrow{r}') =& -j \sum_i \frac{\partial g_i(x,y)}{\partial x} \frac{\partial g_i(x',y')}{\partial x'} \frac{e^{-j\gamma_{TE_i}|z-z'|}}{2\gamma_{TE_i}} - \\ &- j \sum_j \frac{\partial f_j(x,y)}{\partial y} \frac{\partial f_j(x',y')}{\partial y'} \frac{e^{-j\gamma_{TM_j}|z-z'|}}{2\gamma_{TM_j}} \end{aligned} \quad (3.41d)$$

$$\begin{aligned} G_{A_{yx}}(\overrightarrow{r}, \overrightarrow{r}') =& j \sum_i \frac{\partial g_i(x,y)}{\partial x} \frac{\partial g_i(x',y')}{\partial y'} \frac{e^{-j\gamma_{TE_i}|z-z'|}}{2\gamma_{TE_i}} - \\ &- j \sum_j \frac{\partial f_j(x,y)}{\partial y} \frac{\partial f_j(x',y')}{\partial x'} \frac{e^{-j\gamma_{TM_j}|z-z'|}}{2\gamma_{TM_j}} \end{aligned} \quad (3.41e)$$

$$G_{A_{yz}}(\overrightarrow{r}, \overrightarrow{r}') = 0 \quad (3.41f)$$

$$G_{A_{zx}}(\overrightarrow{r}, \overrightarrow{r}') = 0 \quad (3.41g)$$

$$G_{A_{zy}}(\overrightarrow{r}, \overrightarrow{r}') = 0 \quad (3.41h)$$

$$G_{A_{zz}}(\overrightarrow{r}, \overrightarrow{r}') = -j \sum_j k^2_{C_{TM_j}} f_j(x,y) f_j(x',y') \frac{e^{-j\gamma_{TM_j}|z-z'|}}{2\gamma_{TM_j}} \quad (3.41i)$$

3.2.2 Dyadic Green Function for the electric vector potential

The Green function $\overline{\overline{G}}_F$ is derived in a similar way. The implementation of the Ohm-Rayleigh method results to the expansion of $\overline{\overline{G}}_F$ into sets of eigenvectors that represent the magnetic fields of the modes inside the waveguide. Again, in the case of $\overline{\overline{G}}_F$ an extra set of non-solenoidal eigenvectors is employed. However, these three sets of eigenvectors do not suffice for the complete representation of $\overline{\overline{G}}_F$. This is attributed to the presence of an additional term, which is introduced when a longitudinal aperture is milled on a waveguide wall [103], [104] . The presence of the additional term becomes evident, when the z-component of equation $\nabla \times \overrightarrow{E} = -j\omega\mu\overrightarrow{H}$ is examined:

$$\begin{aligned} &\overrightarrow{z} \cdot \nabla \times \overrightarrow{E} = -j\omega\mu \overrightarrow{z} \cdot \overrightarrow{H} \Rightarrow \\ &\nabla \cdot (\overrightarrow{E} \times \overrightarrow{z}) = -j\omega\mu \overrightarrow{z} \cdot \overrightarrow{H} \end{aligned}$$

Integration of the above equation over the waveguide cross-section, application of the divergence theorem and enforcement of the vector identity $\overrightarrow{n}_w \cdot (\overrightarrow{E} \times \overrightarrow{z}) = \overrightarrow{z} \cdot (\overrightarrow{n}_w \times \overrightarrow{E})$ yields:

$$\begin{aligned} &\iint_S \nabla \cdot (\overrightarrow{E} \times \overrightarrow{z}) ds = -j\omega\mu \iint_S \overrightarrow{z} \cdot \overrightarrow{H} ds \Rightarrow \\ &\int_c \overrightarrow{n}_w \cdot (\overrightarrow{E} \times \overrightarrow{z}) dc = -j\omega\mu \int_S \int \overrightarrow{z} \cdot \overrightarrow{H} ds \Rightarrow \\ &\overrightarrow{z} \cdot \int_c (\overrightarrow{n}_w \times \overrightarrow{E}) dc = -j\omega\mu \overrightarrow{z} \cdot \int_S \int H_z ds \end{aligned}$$

where C is the waveguide circumference and $\overrightarrow{n}_w$ is the unitary vector normal to the waveguide walls.
If H_z is expanded in terms of waveguide eigenvectors, then the right member of the preceding expression always vanishes, whereas the left member does not equal null, due to the electric field inside the aperture. Consequently, an additional term for the magnetic field must be present

$$\begin{aligned} &H_z = \psi_{h0}(x,y,z) + \sum_{n=1} \overrightarrow{h}_{TE_n}(x,y,z)\overrightarrow{z} \Rightarrow \\ &\int_c (\overrightarrow{n}_w \times \overrightarrow{E}) dc = -j\omega\mu \iint_S \psi_{h0}(x,y,z) ds - j\omega\mu \sum_{n=1} \iint_S \overrightarrow{h}_{TE_n}(x,y,z)\overrightarrow{z} ds \Rightarrow \\ &\int_c (\overrightarrow{n}_w \times \overrightarrow{E}) dc = -j\omega\mu \iint_S \psi_{h0}(x,y,z) ds \Rightarrow \\ &\psi_{h0}(z) = -\tfrac{1}{j\omega\mu S} \int_c (\overrightarrow{n}_w \times \overrightarrow{E}) dc \qquad (3.42) \end{aligned}$$

Equation (3.42) indicates that term ψ_{h0} is directed along the z-axis and does not vary with the transverse coordinates. It should be pointed out that term ψ_{h0} does not appear when magnetic currents flow in the interior volume of the waveguide. If such currents are present, then the integral in (3.42) vanishes and so does ψ_{h0}. Term ψ_{h0} has also no influence on the waveguide electric field, therefore it cannot be produced by electric currents. ψ_{h0} is excited only by aperture scatterers and, as stated by equation (3.42), exists in the region 'under the aperture' or 'above the aperture', depending on the geometry of the structure under study.
Embodying the condition $\overrightarrow{n}_w \times \overrightarrow{E} = -\overrightarrow{M}$, equation (3.42) becomes:

$$\psi_{h0}(z) = \frac{1}{j\omega\mu S} \int\limits_{\substack{aperture \\ width}} M(x,y,z) dc$$

where the integration is performed with respect to x or y, depending on the location of the aperture inside the waveguide. The preceding equation may be written in the following manner:

$$\begin{aligned} &\psi_{h0}(z) = \tfrac{1}{j\omega\mu S} \int\limits_{\substack{aperture \\ length}} \int\limits_{\substack{aperture \\ width}} M1(x',y',z')\delta(z'-z) dc' dz' \Rightarrow \\ &\psi_{h0}(z) = \tfrac{1}{j\omega\mu S} \int\int\limits_{\substack{aperture \\ surface}} M1(x',y',z')\delta(z'-z) dc' dz' \end{aligned}$$

This expression will be used for the derivation of $\overline{\overline{G}}_{\mathrm{F}}$
$\overline{\overline{G}}_{\mathrm{F}}$ satisfies the equation:

$$\nabla^2\overline{\overline{G}}_F(\overrightarrow{r},\overrightarrow{r}') + k_o^2\,\overline{\overline{G}}_F(\overrightarrow{r},\overrightarrow{r}') = -I\delta(\overrightarrow{r}-\overrightarrow{r}') \qquad (3.43)$$

Term $I\delta(\overrightarrow{r}-\overrightarrow{r}')$ is expressed as the sum of ψ_{h0} and a series of the waveguide eigenvectors that are stated below.

$$\begin{array}{ll}
\overrightarrow{h}_{TE_i}(\overrightarrow{r},h) = jhe^{jhz}\nabla_t g_i(x,y) + k_{C_{TEi}}^2 g_i(x,y)e^{jhz}\overrightarrow{z} & \text{(TE modes)}\\
\overrightarrow{h}_{TM_i}(\overrightarrow{r},h) = e^{jhz}\nabla_t f_i(x,y)\times\overrightarrow{z} & \text{(TM modes)}\\
\overrightarrow{L}_{TE_i}(\overrightarrow{r},h) = \nabla(g_i(x,y)e^{jhz}) & \text{(non-solenoidal terms)}
\end{array}$$

$g_i(x,y)$, $f_i(x,y)$ and $k_{C_{TEi}}^2$ have been defined in Appendix A and $\overrightarrow{L}_{TE_i}$ satisfies the equation:

$$\nabla^2\overrightarrow{L}_{TE_i} + (k_{C_{TEi}}^2 + h^2)\overrightarrow{L}_{TE_i} = 0$$

The following orthogonality conditions are valid:

$$\iint_S\int_{-\infty}^{\infty}\overrightarrow{h}_{TE_i}(\overrightarrow{r},h)\overrightarrow{h}_{TE_n}(\overrightarrow{r},-h')dsdz = (k_{C_{TEi}}^2+h^2)\delta(h-h')\delta_{i,n}2\pi \qquad (3.44a)$$

$$\iint_S\int_{-\infty}^{\infty}\overrightarrow{h}_{TM_i}(\overrightarrow{r},h)\overrightarrow{h}_{TM_n}(\overrightarrow{r},-h')dsdz = \delta(h-h')\delta_{i,n}2\pi \qquad (3.44b)$$

$$\iint_S\int_{-\infty}^{\infty}\overrightarrow{L}_{TE_i}(\overrightarrow{r},h)\overrightarrow{L}_{TE_n}(\overrightarrow{r},-h')dsdz = \frac{(k_{C_{TEi}}^2+h^2)}{k_{C_{TEi}}^2}\delta(h-h')\delta_{i,n}2\pi \qquad (3.44c)$$

$$\iint_S\int_{-\infty}^{\infty}\overrightarrow{h}_{TE_i}(\overrightarrow{r},h)\overrightarrow{h}_{TM_n}(\overrightarrow{r},-h')dsdz = 0 \qquad (3.44d)$$

$$\iint_S\int_{-\infty}^{\infty}\overrightarrow{h}_{TE_i}(\overrightarrow{r},h)\overrightarrow{L}_{TE_n}(\overrightarrow{r},-h')dsdz = jk_{C_{TEi}}^2(h-h')\delta(h-h')\delta_{i,n}2\pi \qquad (3.44e)$$

$$\iint_S\int_{-\infty}^{\infty}\overrightarrow{h}_{TM_i}(\overrightarrow{r},h)\overrightarrow{L}_{TE_n}(\overrightarrow{r},-h')dsdz = 0 \qquad (3.44f)$$

Vectors $\overrightarrow{L}_{TE}$ and $\overrightarrow{h}_{TE}$ are orthogonal in the h domain, as indicated by the proceeding expression:

$$\int_{-\infty}^{\infty}\iint_S\int_{-\infty}^{\infty}\overrightarrow{h}_{TE_i}(\overrightarrow{r},h)\overrightarrow{L}_{TE_i}(\overrightarrow{r},-h')dsdzdh = 0$$

Term $I\delta(\overrightarrow{r}-\overrightarrow{r}')$ becomes:

$$\begin{aligned}
I\delta(\overrightarrow{r}-\overrightarrow{r}') = \int_{-\infty}^{\infty} dh\{\sum_i[A_i(h)\overrightarrow{h}_{TE_i}(\overrightarrow{r},h) + C_i(h)\overrightarrow{L}_{TE_i}(\overrightarrow{r},h)] + \\
+\sum_j B_j(h)\overrightarrow{h}_{TM_j}(\overrightarrow{r},h)\} + D\tfrac{1}{S}\delta(z-z')\overrightarrow{z} \qquad (3.45)
\end{aligned}$$

For the determination of D, both members of (3.45) are multiplied with $\frac{1}{S}\overrightarrow{z}$ and integrated over the waveguide volume:

$$D = 1$$

The unknown coefficients $A_i(h)$, $B_j(h)$ and $C_i(h)$ are determined after multiplication of both members of (3.45) with $\overrightarrow{h}_{TE_k}(\overrightarrow{r}',-h)$, $\overrightarrow{h}_{TM_k}(\overrightarrow{r}',-h)$ and $\overrightarrow{L}_{TE_k}(\overrightarrow{r}',-h)$ respectively and integration over the waveguide volume:

$$A_k(h) = \frac{\overrightarrow{h}_{TE_k}(\overrightarrow{r}',-h)}{2\pi(k^2_{C_{TEk}}+h^2)}$$
$$B_k(h) = \frac{\overrightarrow{h}_{TM_k}(\overrightarrow{r}',-h)}{2\pi}$$
$$C_k(h) = \frac{\overrightarrow{L}_{TE_k}(\overrightarrow{r}',-h)k^2_{C_{TMk}}}{2\pi(k^2_{C_{TMk}}+h^2)}$$

Equation (3.45) takes the form:

$$I\delta(\overrightarrow{r}-\overrightarrow{r}') = \int_{-\infty}^{\infty} dh\{\sum_i [\frac{\overrightarrow{h}_{TE_i}(\overrightarrow{r}',-h)}{2\pi(k^2_{C_{TEi}}+h^2)}\overrightarrow{h}_{TE_i}(\overrightarrow{r},h)+ \\ +\frac{\overrightarrow{L}_{TE_i}(\overrightarrow{r}',-h)k^2_{C_{TEi}}}{2\pi(k^2_{C_{TEi}}+h^2)}\overrightarrow{L}_{TE_i}(\overrightarrow{r},h)]+ \\ +\sum_j \frac{\overrightarrow{h}_{TM_j}(\overrightarrow{r}',-h)}{2\pi}\overrightarrow{h}_{TM_j}(\overrightarrow{r},h)\} + \tfrac{1}{S}\delta(z-z')\overrightarrow{z}\overrightarrow{z}' \qquad (3.46)$$

The unknown function $\overline{\overline{G}}_F$ is expanded in the following way:

$$\overline{\overline{G}}_F(\overrightarrow{r},\overrightarrow{r}') = \int_{-\infty}^{\infty} dh\{\sum_i [a_i(h)\frac{\overrightarrow{h}_{TE_i}(\overrightarrow{r}',-h)}{2\pi(k^2_{C_i}+h^2)}\overrightarrow{h}_{TE_i}(\overrightarrow{r},h)+ \\ +c_i(h)\frac{\overrightarrow{L}_{TE_i}(\overrightarrow{r}',-h)k^2_{C_i}}{2\pi(k^2_{C_i}+h^2)}\overrightarrow{L}_{TE_i}(\overrightarrow{r},h)]+ \\ +\sum_j b_j(h)\frac{\overrightarrow{h}_{TM_j}(\overrightarrow{r}',-h)}{2\pi}\overrightarrow{h}_{TM_j}(\overrightarrow{r},h)\} + d\tfrac{1}{S}\delta(z-z')\overrightarrow{z}\overrightarrow{z}' \qquad (3.47)$$

The unknown coefficients $a_i(h)$, $b_j(h)$, $c_i(h)$ and d are determined after substitution of (3.46) and (3.47) into (3.43) and implementation of the following conditions:

$$\nabla^2\overrightarrow{h}_{TE_i}(\overrightarrow{r},h) = -\nabla\times\nabla\times\overrightarrow{h}_{TE_i}(\overrightarrow{r},h) = -(k^2_{C_{TEi}}+h^2)\overrightarrow{h}_{TE_i}(\overrightarrow{r},h)$$
$$\nabla^2\overrightarrow{h}_{TM_i}(\overrightarrow{r},h) = -\nabla\times\nabla\times\overrightarrow{h}_{TM_i}(\overrightarrow{r},h) = -(k^2_{C_{TM_i}}+h^2)\overrightarrow{h}_{TM_i}(\overrightarrow{r},h)$$
$$\nabla^2\overrightarrow{L}_{TE_i}(\overrightarrow{r},h) = \nabla\nabla\cdot\overrightarrow{L}_{TE_i}(\overrightarrow{r},h) = -(k^2_{C_{TEi}}+h^2)\overrightarrow{L}_{TE_i}(\overrightarrow{r},h)$$

The resulting coefficients are:

$$a_k(h) = c_k(h) = \frac{1}{k^2_{C_{TEk}}+h^2-k^2_o}$$
$$b_k(h) = \frac{1}{k^2_{C_{TMk}}+h^2-k^2_o}$$
$$d = -\tfrac{1}{k^2_o}$$

Equation (3.47) is rewritten in the form:

$$\overline{\overline{G}}_F(\overrightarrow{r},\overrightarrow{r}') = \int_{-\infty}^{\infty} dh\{\sum_i \frac{1}{k^2_{C_{TEi}}+h^2-k^2_o}[\frac{\overrightarrow{h}_{TE_i}(\overrightarrow{r}',-h)\overrightarrow{h}_{TE_i}(\overrightarrow{r},h)}{2\pi(k^2_{C_{TEi}}+h^2)}+ \\ +\frac{k^2_{C_{TEi}}\overrightarrow{L}_{TE_i}(\overrightarrow{r}',-h)\overrightarrow{L}_{TE_i}(\overrightarrow{r},h)}{2\pi(k^2_{C_{TEi}}+h^2)}]+ \\ +\sum_j \frac{\overrightarrow{h}_{TM_j}(\overrightarrow{r}',-h)\overrightarrow{h}_{TM_j}(\overrightarrow{r},h)}{2\pi(k^2_{C_{TMj}}+h^2-k^2_o)}\} + \tfrac{1}{S}\delta(z-z')\overrightarrow{z}\overrightarrow{z}'$$

The integral in the above equation is evaluated in closed form. The result is:

$$\overline{\overline{G}}_F(\overrightarrow{r},\overrightarrow{r}') = -j\sum_i [\frac{\overrightarrow{h}_{TE_i}(\overrightarrow{r},\mp\gamma_{TE_i})\overrightarrow{h}_{TE_i}(\overrightarrow{r}',\pm\gamma_{TE_i})}{2\gamma_{TE_i}k^2_o}+ \\ +\frac{k^2_{C_{TEi}}\overrightarrow{L}_{TE_i}(\overrightarrow{r},\mp\gamma_{TE_i})\overrightarrow{L}_{TE_i}(\overrightarrow{r}',\pm\gamma_{TE_i})}{2\gamma_{TE_i}k^2_o}]- \\ -j\sum_j \frac{\overrightarrow{h}_{TM_j}(\overrightarrow{r}',\pm\gamma_{TM_j})}{2\gamma_{TM_j}}\overrightarrow{h}_{TM_j}(\overrightarrow{r},\mp\gamma_{TM_j}) + \tfrac{1}{S}\delta(z-z')\overrightarrow{z}\overrightarrow{z}'$$

The upper line in the summations refers to the case where z¿z' whereas the bottom line stands for $z < z'$.
The elements of $\overline{\overline{G}}_F(\overrightarrow{r}, \overrightarrow{r}')$ are listed below:

$$G_{F_{xx}}(\overrightarrow{r}, \overrightarrow{r}') = -j \sum_i \frac{\partial g_i(x,y)}{\partial x} \frac{\partial g_i(x',y')}{\partial x'} \frac{e^{-j\gamma_{TE_i}|z-z'|}}{2\gamma_{TE_i}} - \\ -j \sum_j \frac{\partial f_j(x,y)}{\partial y} \frac{\partial f_j(x',y')}{\partial y'} \frac{e^{-j\gamma_{TM_j}|z-z'|}}{2\gamma_{TM_j}} \quad (3.48a)$$

$$G_{F_{xy}}(\overrightarrow{r}, \overrightarrow{r}') = -j \sum_i \frac{\partial g_i(x,y)}{\partial x} \frac{\partial g_i(x',y')}{\partial y'} \frac{e^{-j\gamma_{TE_i}|z-z'|}}{2\gamma_{TE_i}} + \\ +j \sum_j \frac{\partial f_j(x,y)}{\partial y} \frac{\partial f_j(x',y')}{\partial x'} \frac{e^{-j\gamma_{TM_j}|z-z'|}}{2\gamma_{TM_j}} \quad (3.48b)$$

$$G_{F_{xz}}(\overrightarrow{r}, \overrightarrow{r}') = 0 \quad (3.48c)$$

$$G_{F_{yx}}(\overrightarrow{r}, \overrightarrow{r}') = -j \sum_i \frac{\partial g_i(x,y)}{\partial y} \frac{\partial g_i(x',y')}{\partial x'} \frac{e^{-j\gamma_{TE_i}|z-z'|}}{2\gamma_{TE_i}} - \\ -j \sum_j \frac{\partial f_j(x,y)}{\partial x} \frac{\partial f_j(x',y')}{\partial y'} \frac{e^{-j\gamma_{TM_j}|z-z'|}}{2\gamma_{TM_j}} \quad (3.48d)$$

$$G_{F_{yy}}(\overrightarrow{r}, \overrightarrow{r}') = -j \sum_i \frac{\partial g_i(x,y)}{\partial y} \frac{\partial g_i(x',y')}{\partial y'} \frac{e^{-j\gamma_{TE_i}|z-z'|}}{2\gamma_{TE_i}} - \\ -j \sum_j \frac{\partial f_j(x,y)}{\partial x} \frac{\partial f_j(x',y')}{\partial x'} \frac{e^{-j\gamma_{TM_j}|z-z'|}}{2\gamma_{TM_j}} \quad (3.48e)$$

$$G_{F_{yz}}(\overrightarrow{r}, \overrightarrow{r}') = 0 \quad (3.48f)$$

$$G_{F_{zx}}(\overrightarrow{r}, \overrightarrow{r}') = 0 \quad (3.48g)$$

$$G_{F_{zy}}(\overrightarrow{r}, \overrightarrow{r}') = 0 \quad (3.48h)$$

$$G_{F_{zz}}(\overrightarrow{r}, \overrightarrow{r}') = -j \sum_i k^2_{C_{TEi}} g_i(x,y) g_i(x',y') \frac{e^{-j\gamma_{TE_i}|z-z'|}}{2\gamma_{TE_i}} + \\ +\frac{1}{S}\delta(z-z')\overrightarrow{z}\,\overrightarrow{z}' \quad (3.48i)$$

Equations (3.41) and (3.48) represent the dyadic Green functions inside a ridged waveguide for arbitrary electric and magnetic currents. The remaining dyadic Green functions are derived in Appendix B.

3.3 'aKoM' configuration: Geometry - Integral Equations

At this point, the special features of the 'aKoM' configuration must be taken into account, so that the Green functions be accordingly modified. The geometry and the orientation of the components that constitute the 'aKoM' structure dictate the introduction of two additional coordinate systems: a cylindrical coordinate system and a Cartesian coordinate system, rotated 45 degrees about the initial one.

- **Cylindrical coordinate system**

  Figure 3.4 illustrates the employed cylindrical coordinate system. The coupling slot and the rectangular waveguide are omitted for the sake of simplicity. The use of the specific cylindrical coordinate system is imposed by the shape of the metallic scatterer and concerns all relevant field quantities inside the ridged waveguide.

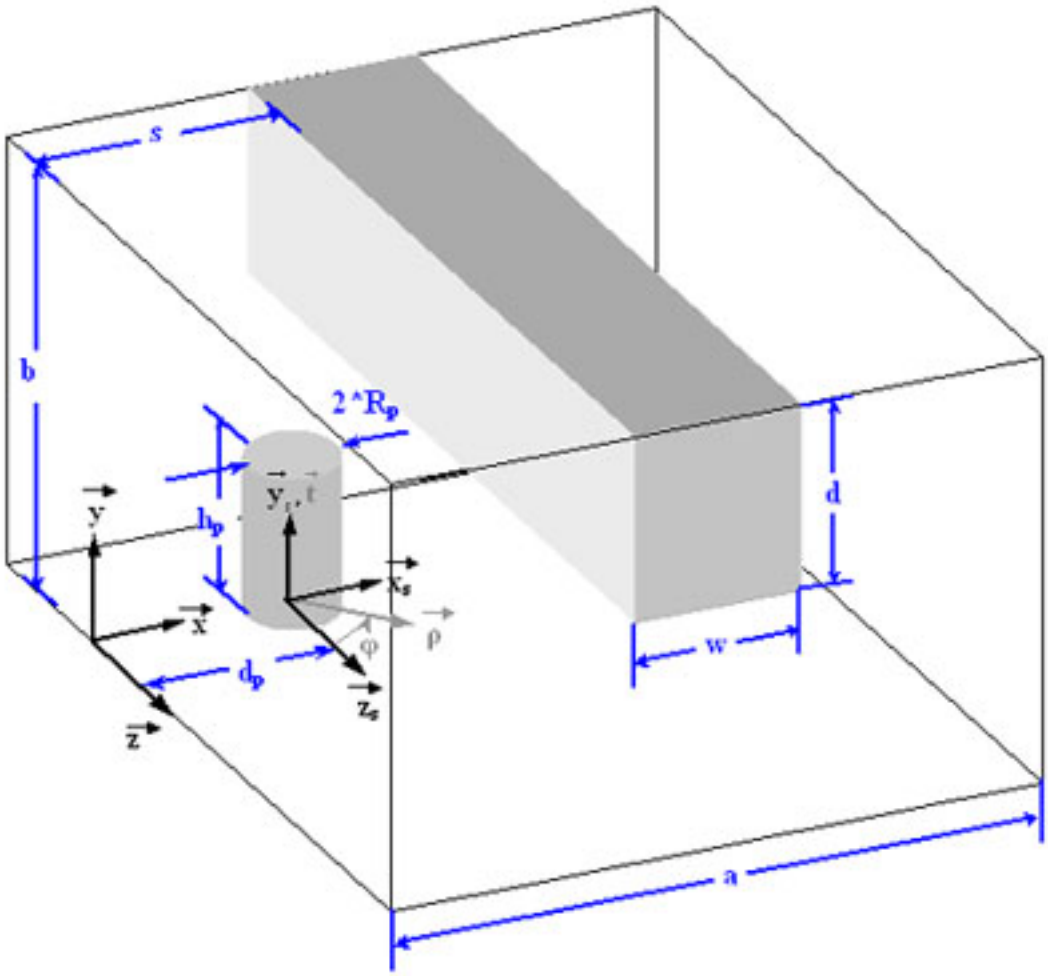

Figure 3.4 Coordinate systems for the 'aKoM' configuration

As viewed in Figure 3.4, the origin of the cylindrical coordinate system is shifted in the x-direction from the origin of the ridged waveguide Cartesian coordinate system, so that axis t coincides with the post axis. d_p is the distance of the post axis from the vertical waveguide wall, R_p is the post radius and h_p is the post height. The ridged waveguide dimensions are also depicted in Figure 3.4. The relationships between the unitary vectors of the cylindrical and the Cartesian coordinate systems are:

$$\begin{pmatrix} \rho \\ t \\ \varphi \end{pmatrix} = \begin{pmatrix} \sin(\varphi) & \cos(\varphi) & 0 \\ 0 & 0 & 1 \\ \cos(\varphi) & -\sin(\varphi) & 0 \end{pmatrix} \begin{pmatrix} x_s \\ y_s \\ z_s \end{pmatrix} \Rightarrow$$

$$\Rightarrow \begin{cases} \overrightarrow{\rho} = \overrightarrow{x}_s \sin(\varphi) + \overrightarrow{z}_s \cos(\varphi) \\ \overrightarrow{t} = \overrightarrow{y}_s \\ \overrightarrow{\varphi} = \overrightarrow{x}_s \cos(\varphi) - \overrightarrow{z}_s \sin(\varphi) \end{cases} , \varphi = \tan^{-1}(\frac{x_s}{z_s}) \quad (3.49)$$

The coordinate system x_s, y_s, z_s is defined in the following manner:

$$\begin{cases} x_s = x - d_p \\ y_s = y \\ z_s = z \end{cases}$$

All field quantities inside the ridged waveguide are expressed in the new coordinate system via the transformation equation:

$$\begin{pmatrix} B_\rho \\ B_t \\ B_\varphi \end{pmatrix} = \begin{pmatrix} \sin(\varphi) & \cos(\varphi) & 0 \\ 0 & 0 & 1 \\ \cos(\varphi) & -\sin(\varphi) & 0 \end{pmatrix} \begin{pmatrix} B_x \\ B_y \\ B_z \end{pmatrix} \quad (3.50)$$

Moreover, the Green functions related to the fields inside the ridged waveguide are subject to similar transformation equations:

$$\overline{\overline{G}}_{\rho t\varphi} = T\overline{\overline{G}}_{xyz}T'^{T} \quad (3.51)$$

where:

$$T = \begin{pmatrix} \sin(\varphi) & \cos(\varphi) & 0 \\ 0 & 0 & 1 \\ \cos(\varphi) & -\sin(\varphi) & 0 \end{pmatrix}$$

$$T'^{T} = \begin{pmatrix} \sin(\varphi') & 0 & \cos(\varphi') \\ \cos(\varphi') & 0 & -\sin(\varphi') \\ 0 & 1 & 0 \end{pmatrix}$$

$$\overline{\overline{G}}_{\rho t\varphi} = \begin{pmatrix} G_{\rho\rho} & G_{\rho t} & G_{\rho\varphi} \\ G_{\varphi\rho} & G_{\varphi t} & G_{\varphi\varphi} \\ G_{t\rho} & G_{tt} & G_{t\varphi} \end{pmatrix}$$

$$\overline{\overline{G}}_{xyz} = \begin{pmatrix} G_{xx} & G_{xy} & G_{xz} \\ G_{yx} & G_{yy} & G_{yz} \\ G_{zx} & G_{zy} & G_{zz} \end{pmatrix}$$

φ refers to the observation point,
φ' refers to the source point.

- **Rotated Cartesian coordinate system**

The rotated Cartesian coordinate system is depicted in Figure 3.5, where the top view of the 'aKoM' configuration is demonstrated. The interior of the ridged waveguide is omitted for the sake of simplicity. In Figure 3.5 (b) the dimensions of the slot and the rectangular waveguide are illustrated.

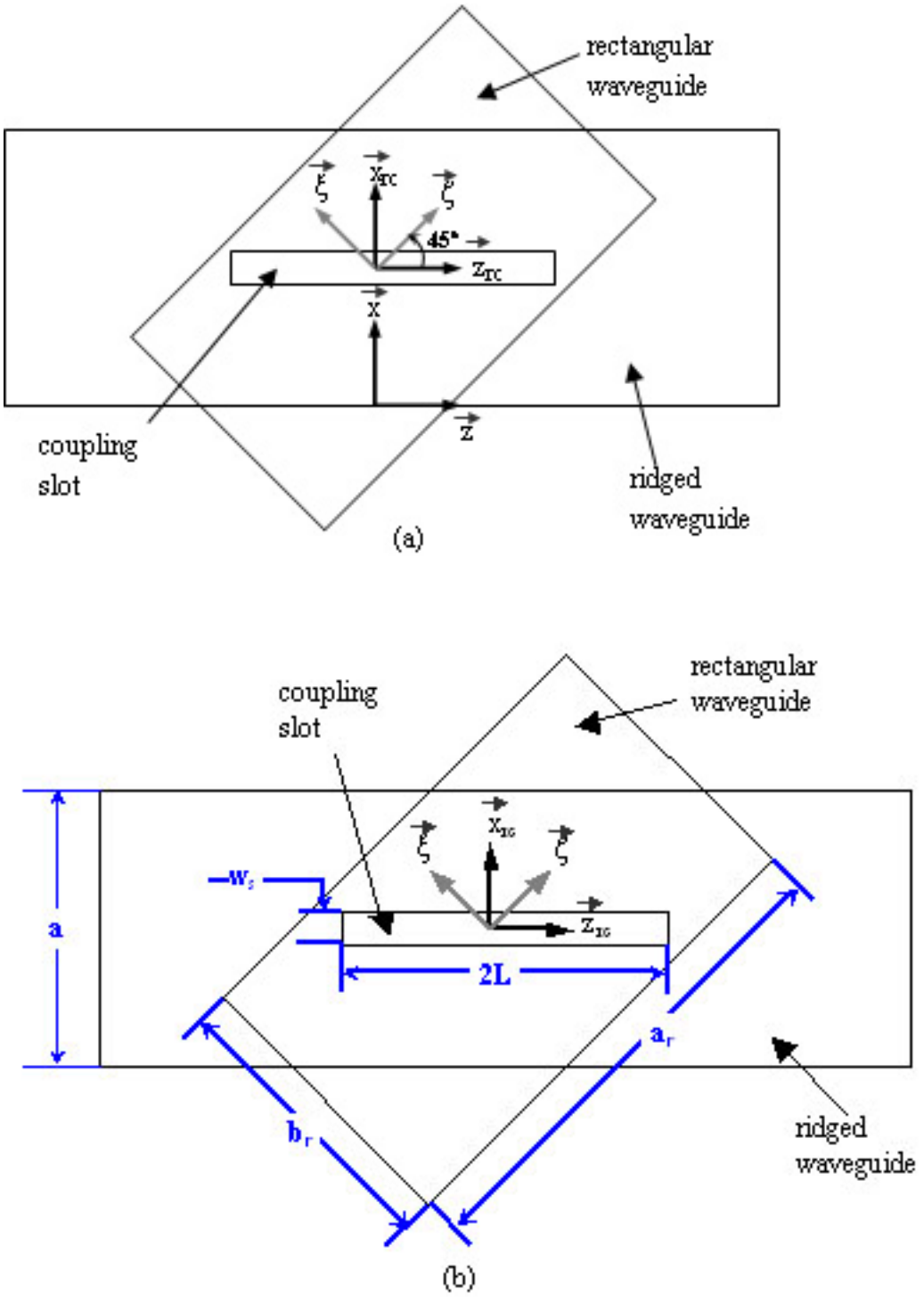

Figure 3.5(a),(b): 'aKoM' configuration - top view

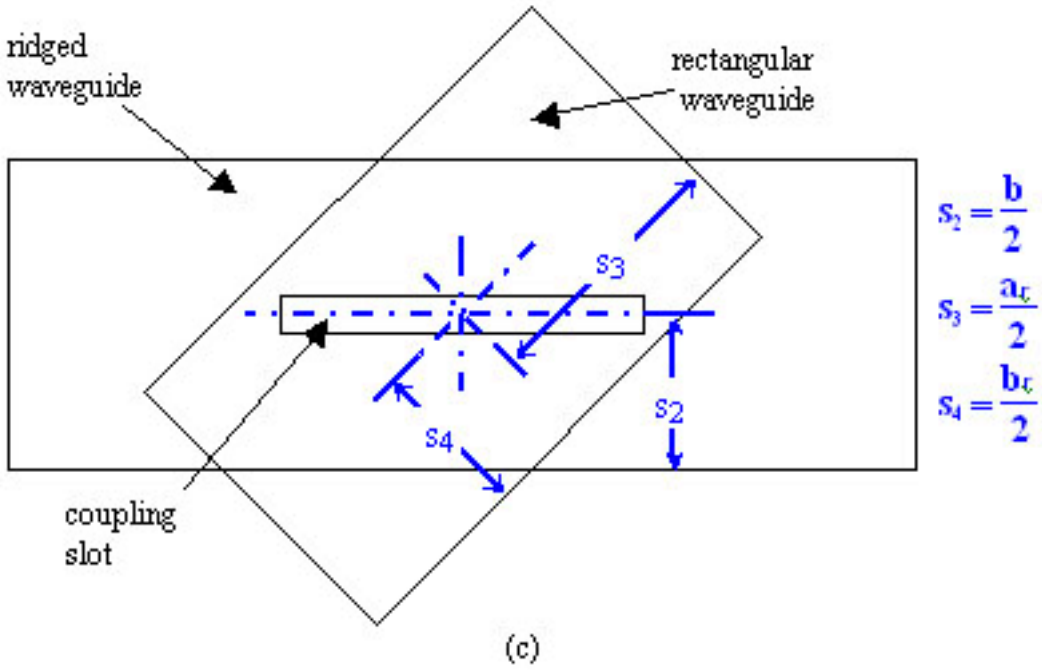

Figure 3.5(c) 'aKoM' configuration - top view

The use of coordinate system ζ, ξ, η is dictated by the orientation of the slot with regard to the semi-infinite rectangular waveguide. The magnetic fields inside the rectangular waveguide will be expressed in terms of ζ, ξ and η coordinates. Figure 3.5 indicates that the coordinate system ζ, ξ, η is rotated at a 45 tilt with regard to the Cartesian coordinate system z_{rc}, x_{rc}, y_{rc} that is shifted $\frac{a}{2}$ from the ridged waveguide coordinate system. Coordinate system z_{rc}, x_{rc}, y_{rc} serves to express all field quantities inside the rectangular cavity. The transformation relationships between all three Cartesian coordinate systems are stated below:

$$\begin{pmatrix} \zeta \\ \xi \\ \eta \end{pmatrix} = \begin{pmatrix} \cos(45°) & \sin(45°) & 0 \\ -\sin(45°) & \cos(45°) & 0 \\ 0 & 0 & 1 \end{pmatrix} \begin{pmatrix} z_{rc} \\ x_{rc} \\ y_{rc} \end{pmatrix}$$

$$\Rightarrow \begin{pmatrix} \zeta \\ \xi \\ \eta \end{pmatrix} = \begin{pmatrix} \frac{\sqrt{2}}{2} & \frac{\sqrt{2}}{2} & 0 \\ -\frac{\sqrt{2}}{2} & \frac{\sqrt{2}}{2} & 0 \\ 0 & 0 & 1 \end{pmatrix} \begin{pmatrix} z_{rc} \\ x_{rc} \\ y_{rc} \end{pmatrix} \Rightarrow$$

$$\Rightarrow \begin{cases} \overrightarrow{\zeta} = \overrightarrow{z}_{rc}\frac{\sqrt{2}}{2} + \overrightarrow{x}_{rc}\frac{\sqrt{2}}{2} \\ \overrightarrow{\xi} = -\overrightarrow{z}_{rc}\frac{\sqrt{2}}{2} + \overrightarrow{x}_{rc}\frac{\sqrt{2}}{2} \\ \overrightarrow{\eta} = \overrightarrow{y}_{rc} \end{cases} \qquad (3.52)$$

The coordinate system for the rectangular cavity is defined in the following way:

$$\begin{cases} x_{rc} = x - \frac{a}{2} \\ y_{rc} = y \\ z_{rc} = z \end{cases}$$

All field quantities inside the rectangular waveguide are subject to the transformation equation:

$$\begin{pmatrix} B_\zeta \\ B_\xi \\ B_\eta \end{pmatrix} = \begin{pmatrix} \frac{\sqrt{2}}{2} & \frac{\sqrt{2}}{2} & 0 \\ -\frac{\sqrt{2}}{2} & \frac{\sqrt{2}}{2} & 0 \\ 0 & 0 & 1 \end{pmatrix} \begin{pmatrix} B_z \\ B_x \\ B_y \end{pmatrix} \qquad (3.53)$$

Likewise, the relevant Green functions are transformed in the following manner:

$$\overline{\overline{G}}_{\zeta\xi\eta} = \mathrm{P}\overline{\overline{G}}_{zxy}\mathrm{P}'^{T} \qquad (3.54)$$

where:

$$\mathrm{P} = \begin{pmatrix} \frac{\sqrt{2}}{2} & \frac{\sqrt{2}}{2} & 0 \\ -\frac{\sqrt{2}}{2} & \frac{\sqrt{2}}{2} & 0 \\ 0 & 0 & 1 \end{pmatrix}$$

$$\mathrm{P}'^{T} = \begin{pmatrix} \frac{\sqrt{2}}{2} & -\frac{\sqrt{2}}{2} & 0 \\ \frac{\sqrt{2}}{2} & \frac{\sqrt{2}}{2} & 0 \\ 0 & 0 & 1 \end{pmatrix}$$

$$\overline{\overline{G}}_{\zeta\xi\eta} = \begin{pmatrix} G_{\zeta\zeta} & G_{\zeta\xi} & G_{\zeta\eta} \\ G_{\xi\zeta} & G_{\xi\xi} & G_{\xi\eta} \\ G_{\eta\zeta} & G_{\eta\xi} & G_{\eta\eta} \end{pmatrix}$$

$$\overline{\overline{G}}_{zxy} = \begin{pmatrix} G_{zz} & G_{zx} & G_{zy} \\ G_{xz} & G_{xx} & G_{xy} \\ G_{yz} & G_{yx} & G_{yy} \end{pmatrix}$$

Usually, in the case of a thin cylindrical post inside a rectangular waveguide, the circumferential currents are neglected, since their contribution to the total scattered field is very small compared to the contribution of the current directed along the cylinder axis [29], [34], [36]. However, when the cylindrical post is located inside a ridged waveguide, the circumferential current must be accounted for, even if the post is thin. This is mainly due to the nature of the ridged waveguide eigenvectors [129] , which, contrary to the rectangular waveguide eigenvectors, constitute of both transverse field components, even in the case of mode TE_{10}. As indicated by the expressions for the waveguide eigenvectors in Appendix A, the x-component of the TE_{10} electric field becomes comparable to the dominant y-component at the points near the vertical waveguide walls. Therefore, the circumferential currents that are produced by the x-component have a non-negligible impact on the overall scattered field, especially when the entire post resides inside the trough region. Consideration of the circumferential currents leads to the splitting of condition (3.21) into two equations, each for one component of the post current. In this manner, the system of equations for MPIE or EFIE comprises of four equations with four unknowns, namely J_t, J_φ, $M1$ and $M2$. The final formulations will result, after all field quantities are expressed in terms of the appropriate coordinate systems. The field intensities, relevant to the electric current may be analyzed into their components via equations (3.50):

$$\overrightarrow{J}_p = J_t\overrightarrow{t} + J_\varphi\overrightarrow{\varphi} \quad (3.55a)$$
$$\overrightarrow{E}_{inc} = E_{inc_t}\overrightarrow{t} + E_{inc_\varphi}\overrightarrow{\varphi} + e_{inc_\rho}\overrightarrow{\rho} \quad (3.55b)$$
$$\overrightarrow{E}_{sc} = E_{sp_t}\overrightarrow{t} + E_{sp_\varphi}\overrightarrow{\varphi} + E_{sp_\rho}\overrightarrow{\rho} \quad (3.55c)$$
$$\overrightarrow{H}_{inc} = H_{inc_t}\overrightarrow{t} + H_{inc_\varphi}\overrightarrow{\varphi} + H_{inc_\rho}\overrightarrow{\rho} \quad (3.55d)$$
$$\overrightarrow{H}_{s_p} = H_{sp_t}\overrightarrow{t} + H_{sp_\varphi}\overrightarrow{\varphi} + H_{sp_\rho}\overrightarrow{\rho} \quad (3.55e)$$
$$\overrightarrow{A} = A_t\overrightarrow{t} + A_\varphi\overrightarrow{\varphi} + A_\rho\overrightarrow{\rho} \quad (3.55f)$$

In contrast to the electric current density, the magnetic current is assumed to have only one component, namely the component parallel to the slot axis. This assumption is justified by the fact that the slot width is very small compared to the slot length. The orientation of the slot dictates the following relationships:
ridged waveguide:

$$\overrightarrow{M}1 = M1\overrightarrow{z}$$
$$\overrightarrow{H}_s = Hs_x\overrightarrow{x} + Hs_y\overrightarrow{y} + Hs_z\overrightarrow{z}$$

rectangular cavity:

$$\begin{aligned}
-\overrightarrow{M1} &= -M1\overrightarrow{z} \\
\overrightarrow{H}_{c1} &= Hc1_z\overrightarrow{z} + Hc1_x\overrightarrow{x} + Hc1_y\overrightarrow{y} \\
-\overrightarrow{M2} &= -M2\overrightarrow{z} \\
\overrightarrow{H}_{c2} &= Hc2_z\overrightarrow{z} + Hc2_x\overrightarrow{x} + Hc2_y\overrightarrow{y}
\end{aligned}$$

semi-infinite rectangular waveguide:

$$\begin{aligned}
\overrightarrow{M}2 &= M2\overrightarrow{\zeta} \\
\overrightarrow{H}_{s_{rw}} &= Hs_{rw_\zeta}\overrightarrow{\zeta} + Hs_{rw_\xi}\overrightarrow{\xi} + Hs_{rw_\eta}\overrightarrow{\eta}
\end{aligned}$$

The transformation of all field quantities into the appropriate coordinate systems is performed analytically in Appendix C. At this point particular attention will be paid to equation (C.11), which can be rewritten in the following manner:

$$\Rightarrow \begin{cases}
H_{ss_\rho}(\overrightarrow{r}) = -j\omega\varepsilon[\frac{1}{k_o^2}\sin(\varphi)\frac{\partial^2}{\partial x\partial z}\int\limits_{-L}^{L}\int\limits_{-\frac{w}{2}}^{\frac{w}{2}} G_{F_{zz}}(\overrightarrow{r},\overrightarrow{r_{s1}}')M1(\overrightarrow{r_{s1}}')dx'_{s1}dz'_{s1}+ \\
\qquad + \int\limits_{-L}^{L}\int\limits_{-\frac{w}{2}}^{\frac{w}{2}} G_{F_{zz}}(\overrightarrow{r},\overrightarrow{r_{s1}}')M1(\overrightarrow{r_{s1}}')dx'_{s1}dz'_{s1}+ \\
\qquad +\frac{1}{k_o^2}\cos(\varphi)\frac{\partial^2}{\partial z^2}\int\limits_{-L}^{L}\int\limits_{-\frac{w}{2}}^{\frac{w}{2}} G_{F_{zz}}(\overrightarrow{r},\overrightarrow{r_{s1}}')M1(\overrightarrow{r_{s1}}')dx'_{s1}dz'_{s1}] \\
H_{ss_t}(\overrightarrow{r}) = -\frac{j\omega\varepsilon}{k_o^2}\frac{\partial^2}{\partial y\partial z}\int\limits_{-L}^{L}\int\limits_{-\frac{w}{2}}^{\frac{w}{2}} G_{F_{zz}}(\overrightarrow{r},\overrightarrow{r_{s1}}')M1(\overrightarrow{r_{s1}}')dx'_{s1}dz'_{s1} \\
H_{ss_\varphi}(\overrightarrow{r}) = -j\omega\varepsilon[\frac{1}{k_o^2}\cos(\varphi)\frac{\partial^2}{\partial x\partial z}\int\limits_{-L}^{L}\int\limits_{-\frac{w}{2}}^{\frac{w}{2}} G_{F_{zz}}(\overrightarrow{r},\overrightarrow{r_{s1}}')M1(\overrightarrow{r_{s1}}')dx'_{s1}dz'_{s1}- \\
\qquad - \int\limits_{-L}^{L}\int\limits_{-\frac{w}{2}}^{\frac{w}{2}} G_{F_{zz}}(\overrightarrow{r},\overrightarrow{r_{s1}}')M1(\overrightarrow{r_{s1}}')dx'_{s1}dz'_{s1}- \\
\qquad -\frac{1}{k_o^2}\sin(\varphi)\frac{\partial^2}{\partial z^2}\int\limits_{-L}^{L}\int\limits_{-\frac{w}{2}}^{\frac{w}{2}} G_{F_{zz}}(\overrightarrow{r},\overrightarrow{r_{s1}}')M1(\overrightarrow{r_{s1}}')dx'_{s1}dz'_{s1}]
\end{cases}$$

It has already been stated that the slot of the 'aKoM' structure lies symmetrically about the longitudinal axis of the ridged waveguide broad wall. The position of the slot justifies the assumption of a magnetic current distribution, which is also symmetric about the z-axis. Incorporation of such a magnetic current distribution in equation (C.11) leads to the elimination of the integral with respect to the x coordinate for the odd TE modes of the ridged waveguide. Since the ridged waveguide TM modes have no impact on the magnetic current and the resulting scattered field, the presence of the slot may only influence the even TE modes inside the ridged waveguide. Moreover, if the incident wave constitutes only of the dominant TE_{01} mode, then it becomes apparent that the excitation of the aperture is enabled exclusively by the evanescent even TE modes that are produced by the electric current on the post surface. This remark summarizes the main concept of the 'aKoM' configuration. Finally, it must be mentioned that the operating frequency allows the propagation of the TE_{01} mode only inside the ridged waveguide. The twisted rectangular waveguide is excited exclusively by the slot ($\overrightarrow{E}_{inc2} = 0, \overrightarrow{H}_{inc2} = 0$). After all necessary transformations are performed the final integral equations are obtained:

MPIE:

t-directed electric field on the post surface

$$\begin{aligned}E_{inc_t}(\overrightarrow{r_p}) = &-j\omega\mu\{\int_0^{h_p}\int_0^{2\pi}[G_{A_{tt}}(\overrightarrow{r_p},\overrightarrow{r_p}')J_t(\overrightarrow{r_p}')+G_{A_{t\varphi}}(\overrightarrow{r_p},\overrightarrow{r_p}')J_\varphi(\overrightarrow{r_p}')]R_p dt_p' d\varphi_p'+\\ &+\tfrac{1}{k_0^2}\tfrac{\partial}{\partial t_p}\int_0^{h_p}\int_0^{2\pi}G_{\Phi_\varepsilon}(\overrightarrow{r_p},\overrightarrow{r_p}')[\tfrac{\partial J_t(\overrightarrow{r_p}')}{\partial t_p'}+\tfrac{1}{R_p}\tfrac{\partial J_\varphi(\overrightarrow{r_p}')}{\partial \varphi_p'}]R_p dt_p' d\varphi_p'\}-\\ &-\tfrac{\partial}{\partial x_p}\int_{-L}^{L}\int_{\frac{a}{2}-\frac{w}{2}}^{\frac{a}{2}+\frac{w}{2}}G_{F_{zz}}(\overrightarrow{r_p},\overrightarrow{r_{s1}}')M1(\overrightarrow{r_{s1}}')dz_{s1}'dx_{s1}' \quad (3.56a)\end{aligned}$$

ϕ-directed electric field on the post surface

$$\begin{aligned}E_{inc_\varphi}(\overrightarrow{r_p}) = &-j\omega\mu\{\int_0^{h_p}\int_0^{2\pi}[G_{A_{\varphi t}}(\overrightarrow{r_p},\overrightarrow{r_p}')J_t(\overrightarrow{r_p}')+G_{A_{\varphi\varphi}}(\overrightarrow{r_p},\overrightarrow{r_p}')J_\varphi(\overrightarrow{r_p}')]R_p dt_p' d\varphi_p'+\\ &+\tfrac{1}{R_p k_0^2}\tfrac{\partial}{\partial \varphi_p}\int_0^{h_p}\int_0^{2\pi}G_{\Phi_\varepsilon}(\overrightarrow{r_p},\overrightarrow{r_p}')[\tfrac{\partial J_t(\overrightarrow{r_p}')}{\partial t_p'}+\tfrac{1}{R_p}\tfrac{\partial J_\varphi(\overrightarrow{r_p}')}{\partial \varphi_p'}]R_p dt_p' d\varphi_p'\}-\\ &-\tfrac{cos\varphi_p}{R_p}\tfrac{\partial}{\partial y_p}\int_{-L}^{L}\int_{\frac{a}{2}-\frac{w}{2}}^{\frac{a}{2}+\frac{w}{2}}G_{F_{zz}}(\overrightarrow{r_p},\overrightarrow{r_{s1}}')M1(\overrightarrow{r_{s1}}')dz_{s1}'dx_{s1}' \quad (3.56b)\end{aligned}$$

z-directed magnetic field across Slot 1

$$\begin{aligned}H_{inc_z}(\overrightarrow{r_{s1}}) = &\tfrac{\partial}{\partial y_{s1}}\{\sin\varphi\int_0^{h_p}\int_0^{2\pi}[G_{A_{\rho t}}(\overrightarrow{r_{s1}},\overrightarrow{r_p}')J_t(\overrightarrow{r_p}')+\\ &+G_{A_{\rho\varphi}}(\overrightarrow{r_{s1}},\overrightarrow{r_p}')J_\varphi(\overrightarrow{r_p}')]R_p dt_p' d\varphi_p'+\\ &+\cos\varphi\int_0^{h_p}\int_0^{2\pi}[G_{A_{\varphi t}}(\overrightarrow{r_{s1}},\overrightarrow{r_p}')J_t(\overrightarrow{r_p}')+\\ &+G_{A_{\varphi\varphi}}(\overrightarrow{r_{s1}},\overrightarrow{r_p}')J_\varphi(\overrightarrow{r_p}')]R_p dt_p' d\varphi_p'\}+\\ &+\tfrac{\partial}{\partial x_{s1}}\int_0^{h_p}\int_0^{2\pi}[G_{A_{tt}}(\overrightarrow{r_{s1}},\overrightarrow{r_p}')J_t(\overrightarrow{r_p}')+\\ &+G_{A_{t\varphi}}(\overrightarrow{r_{s1}},\overrightarrow{r_p}')J_\varphi(\overrightarrow{r_p}')]R_p dt_p' d\varphi_p'-\\ &-j\omega\varepsilon[\int_{-L}^{L}\int_{\frac{a}{2}-\frac{w}{2}}^{\frac{a}{2}+\frac{w}{2}}G_{Fc_{zz}}(\overrightarrow{r_{s1}},\overrightarrow{r_{s1}}')M1(\overrightarrow{r_{s1}}')dz_{s1}'dx_{s1}'+\\ &+\tfrac{1}{k_0^2}\tfrac{\partial^2}{\partial z_{s1}^2}\int_{-L}^{L}\int_{\frac{a}{2}-\frac{w}{2}}^{\frac{a}{2}+\frac{w}{2}}G_{Fc_{zz}}(\overrightarrow{r_{s1}},\overrightarrow{r_{s1}}')M1(\overrightarrow{r_{s1}}')dz_{s1}'dx_{s1}']-\\ &-j\omega\varepsilon\int_{-L}^{L}\int_{\frac{a}{2}-\frac{w}{2}}^{\frac{a}{2}+\frac{w}{2}}G^m_{Hsrc_{zz}}(\overrightarrow{r_{s1}},\overrightarrow{r_{s1}}')M1(\overrightarrow{r_{s1}}')dz_{s1}'dx_{s1}'-\\ &-j\omega\varepsilon\int_{-L}^{L}\int_{\frac{a}{2}-\frac{w}{2}}^{\frac{a}{2}+\frac{w}{2}}G^m_{Hsrc_{zz}}(\overrightarrow{r_{s1}},\overrightarrow{r_{s2}}')M2(\overrightarrow{r_{s2}}')dz_{s2}'dx_{s2}' \quad (3.56c)\end{aligned}$$

z-directed magnetic field across Slot 2

$$\begin{aligned}0 = &-j\omega\varepsilon\int_{-L}^{L}\int_{\frac{a}{2}-\frac{w}{2}}^{\frac{a}{2}+\frac{w}{2}}G^m_{Hsrc_{zz}}(\overrightarrow{r_{s2}},\overrightarrow{r_{s1}}')M1(\overrightarrow{r_{s1}}')dz_{s1}'dx_{s1}'-\\ &-j\omega\varepsilon\int_{-L}^{L}\int_{\frac{a}{2}-\frac{w}{2}}^{\frac{a}{2}+\frac{w}{2}}G^m_{Hsrc_{zz}}(\overrightarrow{r_{s2}},\overrightarrow{r_{s2}}')M2(\overrightarrow{r_{s2}}')dz_{s2}'dx_{s2}'-\\ &-\tfrac{j\omega\varepsilon}{2}\int_{-L}^{L}\int_{\frac{a}{2}-\frac{w}{2}}^{\frac{a}{2}+\frac{w}{2}}[G^m_{Hsrw_{\zeta\zeta}}(\overrightarrow{r_{s2}},\overrightarrow{r_{s2}}')+G^m_{Hsrw_{\zeta\xi}}(\overrightarrow{r_{s2}},\overrightarrow{r_{s2}}')+\\ &+G^m_{Hsrw_{\xi\zeta}}(\overrightarrow{r_{s2}},\overrightarrow{r_{s2}}')+G^m_{Hsrw_{\xi\xi}}(\overrightarrow{r_{s2}},\overrightarrow{r_{s2}}')]M2(\overrightarrow{r_{s2}}')d\zeta_{s2}'d\xi_{s2}' \quad (3.56d)\end{aligned}$$

EFIE:

t-directed electric field on the post surface

$$\begin{aligned}E_{inc_t}(\overrightarrow{r_p}) = &-j\omega\mu\{\int_0^{h_p}\int_0^{2\pi}[G_{A_{tt}}(\overrightarrow{r_p},\overrightarrow{r_p}')J_t(\overrightarrow{r_p}')+\\ &+G_{A_{t\varphi}}(\overrightarrow{r_p},\overrightarrow{r_p}')J_\varphi(\overrightarrow{r_p}')]R_p dt_p' d\varphi_p' +\\ &+\tfrac{1}{k_0^2}\tfrac{\partial}{\partial t_p}\nabla\cdot\int_0^{h_p}\int_0^{2\pi}\overline{\overline{G}}_A(\overrightarrow{r_p},\overrightarrow{r_p}')\cdot\overrightarrow{J}(\overrightarrow{r_p}')R_p dt_p' d\varphi_p'\}-\\ &-\tfrac{\partial}{\partial x_p}\int_{-L}^{L}\int_{\frac{a}{2}-\frac{w}{2}}^{\frac{a}{2}+\frac{w}{2}}G_{F_{zz}}(\overrightarrow{r_p},\overrightarrow{r_{s1}}')M1(\overrightarrow{r_{s1}}')dz_{s1}'dx_{s1}' \quad (3.57a)\end{aligned}$$

ϕ-directed electric field on the post surface

$$\begin{aligned}E_{inc_\varphi}(\overrightarrow{r_p}) = &-j\omega\mu\{\int_0^{h_p}\int_0^{2\pi}[G_{A_{\varphi t}}(\overrightarrow{r_p},\overrightarrow{r_p}')J_t(\overrightarrow{r_p}')+\\ &+G_{A_{\varphi\varphi}}(\overrightarrow{r_p},\overrightarrow{r_p}')J_\varphi(\overrightarrow{r_p}')]R_p dt_p' d\varphi_p' +\\ &+\tfrac{1}{R_p k_0^2}\tfrac{\partial}{\partial\varphi_p}\nabla\cdot\int_0^{h_p}\int_0^{2\pi}\overline{\overline{G}}_A(\overrightarrow{r_p},\overrightarrow{r_p}')\cdot\overrightarrow{J}(\overrightarrow{r_p}')R_p dt_p' d\varphi_p'\}-\\ &-\tfrac{cos\varphi_p}{R_p}\tfrac{\partial}{\partial y_p}\int_{-L}^{L}\int_{\frac{a}{2}-\frac{w}{2}}^{\frac{a}{2}+\frac{w}{2}}G_{F_{zz}}(\overrightarrow{r_p},\overrightarrow{r_{s1}}')M1(\overrightarrow{r_{s1}}')dz_{s1}'dx_{s1}' \quad (3.57b)\end{aligned}$$

z-directed magnetic field across Slot 1

As in MPIE

z-directed magnetic field across Slot 2

As in MPIE

Expressions (3.57) are more complicated than the MPIE expressions, due to the presence of an additional differentiation operator, introduced by the divergence of the magnetic vector potential. For this reason, further handling of the EFIE expressions is necessary. This procedure will be performed below:

According to the analysis in Appendix C, the divergence of $A(\rho,t,\varphi)$ is expressed in the following manner:

$$\nabla\cdot\overrightarrow{A}(\rho,t,\varphi) = \tfrac{1}{\rho}\tfrac{\partial[\rho A_\rho(\rho,t,\varphi)]}{\partial\rho} + \tfrac{1}{\rho}\tfrac{\partial A_\varphi(\rho,t,\varphi)}{\partial\varphi} + \tfrac{A_t(\rho,t,\varphi)}{\partial t} \quad (3.58)$$

where the functions A_ρ, A_t and A_φ are defined as:

$$\begin{aligned}A_\rho(\rho,t,\varphi) = &\int_0^{h_p}\int_0^{2\pi}G_{A_{\rho t}}(\rho,t,\varphi,R_p',t_p',\varphi_p')J_t(R_p',t_p',\varphi_p')R_p' dt_p' d\varphi_p' +\\ &+\int_0^{h_p}\int_0^{2\pi}G_{A_{\rho\varphi}}(\rho,t,\varphi,R_p',t_p',\varphi_p')J_\varphi(R_p',t_p',\varphi_p')R_p' dt_p' d\varphi_p'\end{aligned}$$

$$\begin{aligned}A_t(\rho,t,\varphi) = &\int_0^{h_p}\int_0^{2\pi}G_{A_{tt}}(\rho,t,\varphi,R_p',t_p',\varphi_p')J_t(R_p',t_p',\varphi_p')R_p' dt_p' d\varphi_p' +\\ &+\int_0^{h_p}\int_0^{2\pi}G_{A_{t\varphi}}(\rho,t,\varphi,R_p',t_p',\varphi_p')J_\varphi(R_p',t_p',\varphi_p')R_p' dt_p' d\varphi_p'\end{aligned}$$

$$A_\varphi(\rho,t,\varphi) = \int_0^{h_p}\int_0^{2\pi} G_{A_{\varphi t}}(\rho,t,\varphi,R'_p,t'_p,\varphi'_p)J_t(R'_p,t'_p,\varphi'_p)R'_p dt'_p d\varphi'_p + \\ + \int_0^{h_p}\int_0^{2\pi} G_{A_{\varphi\varphi}}(\rho,t,\varphi,R'_p,t'_p,\varphi'_p)J_\varphi(R'_p,t'_p,\varphi'_p)R'_p dt'_p d\varphi'_p$$

As a first step, the derivatives with respect to the cylindrical coordinates must be transformed to derivatives with respect to the cartesian coordinate system. This is easily done, if the following transformation relationships are taken into account:

$$\frac{\partial B}{\partial \rho} = \sin\varphi\frac{\partial B}{\partial x} + \cos\varphi\frac{\partial B}{\partial z}$$

$$\frac{\partial B}{\partial \varphi} = \rho\cos\varphi\frac{\partial B}{\partial x} - \rho\sin\varphi\frac{\partial B}{\partial z}$$

Each term of $\nabla\cdot\overrightarrow{A}$ is evaluated seperatelly:

$$\frac{1}{\rho}\frac{\partial[\rho A(\overrightarrow{r})]}{\partial\rho} = \frac{1}{\rho}[\rho\sin\varphi\frac{\partial A(\overrightarrow{r})}{\partial x} + \rho\cos\varphi\frac{\partial A(\overrightarrow{r})}{\partial z}] \Rightarrow$$

$$\frac{1}{\rho}\frac{\partial[\rho A(\overrightarrow{r})]}{\partial\rho} = \sin\varphi\frac{\partial}{\partial x}[\int_0^{h_p}\int_0^{2\pi} G_{A_{\rho t}}(\overrightarrow{r},\overrightarrow{r}'_p)J_t(\overrightarrow{r}'_p)R'_p dt'_p d\varphi_p + \\ + \int_0^{h_p}\int_0^{2\pi} G_{A_{\rho\varphi}}(\overrightarrow{r},\overrightarrow{r}'_p)J_\varphi(\overrightarrow{r}'_p)R'_p dt'_p d\varphi'_p] + \\ + \cos\varphi\frac{\partial}{\partial z}[\int_0^{h_p}\int_0^{2\pi} G_{A_{\rho t}}(\overrightarrow{r},\overrightarrow{r}'_p)J_t(\overrightarrow{r}'_p)R'_p dt'_p d\varphi_p + \\ + \int_0^{h_p}\int_0^{2\pi} G_{A_{\rho\varphi}}(\overrightarrow{r},\overrightarrow{r}'_p)J_\varphi(\overrightarrow{r}'_p)R'_p dt'_p d\varphi'_p] \Rightarrow$$

$$\frac{1}{\rho}\frac{\partial[\rho A(\overrightarrow{r})]}{\partial\rho} = \frac{\partial}{\partial x}\{\int_0^{h_p}\int_0^{2\pi} \sin^2\varphi G_{A_{xy}}(\overrightarrow{r},\overrightarrow{r}'_p)J_t(\overrightarrow{r}'_p)R'_p dt'_p d\varphi'_p + \\ + \int_0^{h_p}\int_0^{2\pi} [G_{A_{xx}}(\overrightarrow{r},\overrightarrow{r}'_p)\sin^2\varphi\cos\varphi'_p - \\ - G_{A_{zz}}(\overrightarrow{r},\overrightarrow{r}'_p)\cos\varphi\sin\varphi\sin\varphi'_p]J_\varphi(\overrightarrow{r}'_p)R'_p dt'_p d\varphi'_p\} + \\ + \frac{\partial}{\partial z}\{\int_0^{h_p}\int_0^{2\pi} \cos\varphi\sin\varphi G_{A_{xy}}(\overrightarrow{r},\overrightarrow{r}'_p)J_t(\overrightarrow{r}'_p)R'_p dt'_p d\varphi_p + \\ + \int_0^{h_p}\int_0^{2\pi} [G_{A_{xx}}(\overrightarrow{r},\overrightarrow{r}'_p)\cos\varphi\sin\varphi\cos\varphi'_p \\ - G_{A_{zz}}(\overrightarrow{r},\overrightarrow{r}'_p)\cos^2\varphi\sin\varphi'_p]J_\varphi(\overrightarrow{r}'_p)R'_p dt'_p d\varphi'_p\} \quad (3.59a)$$

$$\frac{1}{\rho}\frac{\partial A(\overrightarrow{r})}{\partial\varphi} = \cos\varphi\frac{\partial A(\overrightarrow{r})}{\partial x} - \sin\varphi\frac{\partial A(\overrightarrow{r})}{\partial z} \Rightarrow$$

$$\begin{aligned}\frac{1}{\rho}\frac{\partial A(\overrightarrow{r})}{\partial\varphi} =& \cos\varphi\frac{\partial}{\partial x}[\int_0^{h_p}\int_0^{2\pi} G_{A_{\varphi t}}(\overrightarrow{r},\overrightarrow{r}'_p)J_t(\overrightarrow{r}'_p)R'_p dt'_p d\varphi_p +\\ &+\int_0^{h_p}\int_0^{2\pi} G_{A_{\varphi\varphi}}(\overrightarrow{r},\overrightarrow{r}'_p)J_\varphi(\overrightarrow{r}'_p)R'_p dt'_p d\varphi'_p] -\\ &-\sin\varphi\frac{\partial}{\partial z}[\int_0^{h_p}\int_0^{2\pi} G_{A_{\varphi t}}(\overrightarrow{r},\overrightarrow{r}'_p)J_t(\overrightarrow{r}'_p)R'_p dt'_p d\varphi_p +\\ &+\int_0^{h_p}\int_0^{2\pi} G_{A_{\varphi\varphi}}(\overrightarrow{r},\overrightarrow{r}'_p)J_\varphi(\overrightarrow{r}'_p)R'_p dt'_p d\varphi'_p] \Rightarrow\end{aligned}$$

$$\begin{aligned}\frac{1}{\rho}\frac{\partial A(\overrightarrow{r})}{\partial\varphi} =& \frac{\partial}{\partial x}\{\int_0^{h_p}\int_0^{2\pi}\cos^2\varphi G_{A_{xy}}(\overrightarrow{r},\overrightarrow{r}'_p)J_t(\overrightarrow{r}'_p)R'_p dt'_p d\varphi'_p +\\ &+\int_0^{h_p}\int_0^{2\pi}[G_{A_{xx}}(\overrightarrow{r},\overrightarrow{r}'_p)\cos^2\varphi\cos\varphi'_p +\\ &+G_{A_{zz}}(\overrightarrow{r},\overrightarrow{r}'_p)\cos\varphi\sin\varphi\sin\varphi'_p]J_\varphi(\overrightarrow{r}'_p)R'_p dt'_p d\varphi'_p\} -\\ &-\frac{\partial}{\partial z}\{\int_0^{h_p}\int_0^{2\pi}\cos\varphi\sin\varphi G_{A_{xy}}(\overrightarrow{r},\overrightarrow{r}'_p)J_t(\overrightarrow{r}'_p)R'_p dt'_p d\varphi_p +\\ &+\int_0^{h_p}\int_0^{2\pi}[G_{A_{xx}}(\overrightarrow{r},\overrightarrow{r}'_p)\cos\varphi\sin\varphi\cos\varphi'_p\\ &-G_{A_{zz}}(\overrightarrow{r},\overrightarrow{r}'_p)\sin^2\varphi\sin\varphi'_p]J_\varphi(\overrightarrow{r}'_p)R'_p dt'_p d\varphi'_p\} \quad (3.59b)\end{aligned}$$

$$\begin{aligned}\frac{\partial A(\overrightarrow{r})}{\partial t} =& \frac{\partial}{\partial y}[\int_0^{h_p}\int_0^{2\pi} G_{A_{tt}}(\overrightarrow{r},\overrightarrow{r}'_p)J_t(\overrightarrow{r}'_p)R'_p dt'_p d\varphi_p +\\ &+\int_0^{h_p}\int_0^{2\pi} G_{A_{t\varphi}}(\overrightarrow{r},\overrightarrow{r}'_p)J_\varphi(\overrightarrow{r}'_p)R'_p dt'_p d\varphi'_p] \Rightarrow\end{aligned}$$

$$\begin{aligned}\frac{\partial A(\overrightarrow{r})}{\partial t} =& \frac{\partial}{\partial y}[\int_0^{h_p}\int_0^{2\pi} G_{A_{yy}}(\overrightarrow{r},\overrightarrow{r}'_p)J_t(\overrightarrow{r}'_p)R'_p dt'_p d\varphi'_p +\\ &+\int_0^{h_p}\int_0^{2\pi} G_{A_{yx}}(\overrightarrow{r},\overrightarrow{r}'_p)J_\varphi(\overrightarrow{r}'_p)\cos\varphi'_p R'_p dt'_p d\varphi'_p] \quad (3.59c)\end{aligned}$$

Insertion of (3.59a), (3.59b) and (3.59c) into (3.58) yields:

$$\begin{aligned}\nabla\overrightarrow{A}(\overrightarrow{r}) =& \frac{\partial}{\partial x}\int_0^{h_p}\int_0^{2\pi} G_{A_{xy}}(\overrightarrow{r},\overrightarrow{r}'_p)J_t(\overrightarrow{r}'_p)R'_p dt'_p d\varphi'_p +\\ &+\frac{\partial}{\partial y}\int_0^{h_p}\int_0^{2\pi} G_{A_{yy}}(\overrightarrow{r},\overrightarrow{r}'_p)J_t(\overrightarrow{r}'_p)R'_p dt'_p d\varphi'_p +\\ &+\frac{\partial}{\partial y}\int_0^{h_p}\int_0^{2\pi} G_{A_{yx}}(\overrightarrow{r},\overrightarrow{r}'_p)\cos\varphi'_p J_\varphi(\overrightarrow{r}'_p)R'_p dt'_p d\varphi'_p\\ &+\frac{\partial}{\partial x}\int_0^{h_p}\int_0^{2\pi} G_{A_{xx}}(\overrightarrow{r},\overrightarrow{r}'_p)\cos\varphi'_p J_\varphi(\overrightarrow{r}'_p)R'_p dt'_p d\varphi'_p\\ &-\frac{\partial}{\partial z}\int_0^{h_p}\int_0^{2\pi} G_{A_{zz}}(\overrightarrow{r},\overrightarrow{r}'_p)\sin\varphi'_p J_\varphi(\overrightarrow{r}'_p)R'_p dt'_p d\varphi'_p \quad (3.60)\end{aligned}$$

At this stage, it is allowed to change the sequence of differentiation and integration, since these operands refer to different variables. Moreover, if all the Green functions are analyzed with the aid

of the expressions (3.41), then the expression will take the form :

$$\begin{aligned}\nabla\cdot\overrightarrow{A}(\overrightarrow{r}) = &\int_0^{h_p}\int_0^{2\pi}[\sum_{k=0}^{K} j\frac{\partial^2 g(\overrightarrow{u})}{\partial x\partial y}\frac{\partial g(\overrightarrow{u}'_p)}{\partial x'_p}\frac{e^{-j\gamma_{TEk}|z-R'_p\cos\varphi'_p|}}{2\gamma_{TEk}} - \\ &- \sum_{k=1}^{K} j\frac{\partial^2 f(\overrightarrow{u})}{\partial x^2}\frac{\partial f(\overrightarrow{u}'_p)}{\partial y'_p}\frac{e^{-j\gamma_{TMk}|z-R'_p\cos\varphi'_p|}}{2\gamma_{TMk}} - \\ &- \sum_{k=0}^{K} j\frac{\partial^2 g(\overrightarrow{u})}{\partial y\partial x}\frac{\partial g(\overrightarrow{u}'_p)}{\partial y'_p}\frac{e^{-j\gamma_{TEk}|z-R'_p\cos\varphi'_p|}}{2\gamma_{TEk}} - \\ &- \sum_{k=1}^{K} j\frac{\partial^2 f(\overrightarrow{u})}{\partial y^2}\frac{\partial f(\overrightarrow{u}'_p)}{\partial y'_p}\frac{e^{-j\gamma_{TMk}|z-R'_p\cos\varphi'_p|}}{2\gamma_{TMk}}]J_t(\overrightarrow{r}'_p)R'_p dt'_p d\varphi'_p + \\ &+ \int_0^{h_p}\int_0^{2\pi}\{\sum_{k=1}^{K} j\frac{K^2_{C_{TMk}}}{2\gamma_{TMk}}f(\overrightarrow{u})f(\overrightarrow{u}'_p)\frac{\partial e^{-j\gamma_{TEk}|z-R'_p\cos\varphi'_p|}}{\partial z}\sin\varphi'_p + \\ &+ [\sum_{k=0}^{K} j\frac{\partial^2 g(\overrightarrow{u})}{\partial x\partial y}\frac{\partial g(\overrightarrow{u}'_p)}{\partial y'_p}\frac{e^{-j\gamma_{TEk}|z-R'_p\cos\varphi'_p|}}{2\gamma_{TEk}} - \\ &- \sum_{k=1}^{K} j\frac{\partial^2 f(\overrightarrow{u})}{\partial y^2}\frac{\partial f(\overrightarrow{u}'_p)}{\partial x'_p}\frac{e^{-j\gamma_{TMk}|z-R'_p\cos\varphi'_p|}}{2\gamma_{TMk}} - \\ &- \sum_{k=0}^{K} j\frac{\partial^2 g(\overrightarrow{u})}{\partial x\partial y}\frac{\partial g(\overrightarrow{u}'_p)}{\partial y'_p}\frac{e^{-j\gamma_{TEk}|z-R'_p\cos\varphi'_p|}}{2\gamma_{TEk}} - \\ &- \sum_{k=1}^{K} j\frac{\partial^2 f(\overrightarrow{u})}{\partial x^2}\frac{\partial f(\overrightarrow{u}'_p)}{\partial x'_p}\frac{e^{-j\gamma_{TMk}|z-R'_p\cos\varphi'_p|}}{2\gamma_{TMk}}]\cos\varphi'_p\}J_\varphi(\overrightarrow{r}'_p)R'_p dt'_p d\varphi'_p \Rightarrow\end{aligned}$$

$$\nabla\cdot\overrightarrow{A}(\overrightarrow{r}) = I1 + I2 \quad (3.61)$$

where:

$$I1(\overrightarrow{r}) = \int_0^{h_p}\int_0^{2\pi}\sum_{k=1}^{K} jK^2_{C_{TMk}}f(\overrightarrow{u})\frac{\partial f(\overrightarrow{u}'_p)}{\partial y'_p}\frac{e^{-j\gamma_{TEk}|z-R'_p\cos\varphi'_p|}}{2\gamma_{TEk}}J_t(\overrightarrow{r}'_p)R'_p dt'_p d\varphi'_p$$

$$\begin{aligned}I2(\overrightarrow{r}) = &\int_0^{h_p}\int_0^{2\pi}[\sum_{k=1}^{K} j\frac{K^2_{C_{TMk}}}{2\gamma_{TMk}}f(\overrightarrow{u})f(\overrightarrow{u}'_p)\frac{\partial e^{-j\gamma_{TEk}|z-R'_p\cos\varphi'_p|}}{\partial z}\sin\varphi'_p + \\ &+ \sum_{k=1}^{K} jK^2_{C_{TMk}}f(\overrightarrow{u})\frac{\partial f(\overrightarrow{u}'_p)}{\partial x'_p}\frac{e^{-j\gamma_{TMk}|z-R'_p\cos\varphi'_p|}}{2\gamma_{TMk}}\cos\varphi'_p]J_\varphi(\overrightarrow{r}'_p)R'_p dt'_p d\varphi'_p\end{aligned}$$

and

$$\begin{aligned}x_p &= R'_p\sin\varphi'_p \\ z_p &= R'_p\cos\varphi'_p \\ \overrightarrow{u} &= (x, y) \\ \overrightarrow{u}'_p &= (R'_p\sin\varphi'_p, t'_p)\end{aligned}$$

It is possible to rewrite term $\frac{\partial e^{-j\gamma_{TMk}|z-R'_p\cos\varphi'_p|}}{\partial z}$ in the form:

$$\frac{\partial e^{-j\gamma_{TEk}|z-R'_p\cos\varphi'_p|}}{\partial z} = -\frac{\partial e^{-j\gamma_{TMk}|z-R'_p\cos\varphi'_p|}}{\partial z'_p}$$

Under this condition, integral $I2$ takes the form:

$$I2(\overrightarrow{r}) = \int_0^{h_p}\int_0^{2\pi}\sum_{k=1}^{K} j\frac{K^2_{C_{TMk}}}{2\gamma_{TMk}} f(\overrightarrow{u})[-f(\overrightarrow{u}'_p)\frac{\partial e^{-j\gamma_{TEk}|z-R'_p\cos\varphi'_p|}}{\partial z}\sin\varphi'_p + \\ + \frac{\partial f(\overrightarrow{u}'_p)}{\partial x'_p} e^{-j\gamma_{TMk}|z-R'_p\cos\varphi'_p|}\cos\varphi'_p]J_\varphi(\overrightarrow{r}'_p)dt'_p d\varphi'_p \Rightarrow$$

$$I2(\overrightarrow{r}) = \int_0^{h_p}\int_0^{2\pi}\sum_{k=1}^{K} j\frac{K^2_{C_{TMk}}}{2\gamma_{TMk}} f(\overrightarrow{u})\frac{\partial[f(\overrightarrow{u}'_p)e^{-j\gamma_{TMk}|z-R'_p\cos\varphi'_p|}]}{\partial\varphi'_p} J_\varphi(\overrightarrow{r}'_p)dt'_p d\varphi'_p \Rightarrow$$

$$I2(\overrightarrow{r}) = \int_0^{h_p}\int_0^{2\pi}\frac{\partial}{\partial\varphi'_p}[\sum_{k=1}^{K} j\frac{K^2_{C_{TMk}}}{2\gamma_{TMk}} f(\overrightarrow{u})f(\overrightarrow{u}'_p)e^{-j\gamma_{TMk}|z-R'_p\cos\varphi'_p|}]J_\varphi(\overrightarrow{r}'_p)dt'_p d\varphi'_p$$

Implementation of integration by parts on the previous expression yields:

$$I2(\overrightarrow{r}) = \left[\int_0^{h_p}\sum_{k=1}^{K} j\frac{K^2_{C_{TMk}}}{2\gamma_{TMk}} f(\overrightarrow{u})f(\overrightarrow{u}'_p)e^{-j\gamma_{TMk}|z-R'_p\cos\varphi'_p|}J_\varphi(\overrightarrow{r}'_p)dt'_p\right]_0^{2\pi} - \\ - \int_0^{h_p}\int_0^{2\pi}\sum_{k=1}^{K} j\frac{K^2_{C_{TMk}}}{2\gamma_{TMk}} f(\overrightarrow{u})f(\overrightarrow{u}'_p)e^{-j\gamma_{TMk}|z-R'_p\cos\varphi'_p|}\frac{\partial J_\varphi(\overrightarrow{r}'_p)}{\partial\varphi'_p}dt'_p d\varphi'_p \Rightarrow$$

$$I2(\overrightarrow{r}) = \int_0^{h_p}\sum_{k=1}^{K} j\frac{K^2_{C_{TMk}}}{2\gamma_{TMk}} f(\overrightarrow{u})f(0,t'_p)e^{-j\gamma_{TMk}|z-R'_p|}J_\varphi(0,t'_p,R'_p)dt'_p - \\ - \int_0^{h_p}\sum_{k=1}^{K} j\frac{K^2_{C_{TMk}}}{2\gamma_{TMk}} f(\overrightarrow{u})f(0,t'_p)e^{-j\gamma_{TMk}|z-R'_p|}J_\varphi(0,t'_p,R'_p)dt'_p - \\ - \int_0^{h_p}\int_0^{2\pi}\sum_{k=1}^{K} j\frac{K^2_{C_{TMk}}}{2\gamma_{TMk}} f(\overrightarrow{u})f(\overrightarrow{u}'_p)e^{-j\gamma_{TMk}|z-R'_p\cos\varphi'_p|}\frac{\partial J_\varphi(\overrightarrow{r}'_p)}{\partial\varphi'_p}dt'_p d\varphi'_p \Rightarrow$$

$$I2(\overrightarrow{r}) = -\int_0^{h_p}\int_0^{2\pi}\sum_{k=1}^{K} j\frac{K^2_{C_{TMk}}}{2\gamma_{TMk}} f(\overrightarrow{u})f(\overrightarrow{u}'_p)e^{-j\gamma_{TMk}|z-R'_p\cos\varphi'_p|}\frac{\partial J_\varphi(\overrightarrow{r}'_p)}{\partial\varphi'_p}dt'_p d\varphi'_p$$

If expression (B.50) is taken into account, it becomes obvious that:

$$I2(\overrightarrow{r}) = \int_0^{h_p}\int_0^{2\pi} G_{\Phi_\varepsilon}(\overrightarrow{r},\overrightarrow{r}'_p)\frac{\partial J_\varphi(\overrightarrow{r}'_p)}{\partial\varphi'_p}dt'_p d\varphi'_p \quad (3.62)$$

In a similar way integral $I1(\overrightarrow{r})$ may be expressed in terms of the Green function for the electric scalar potential. More specifically:
Integration by parts:

$$I1(\overrightarrow{r}) = \left[\int_0^{2\pi}\sum_{k=1}^{K} j\frac{K^2_{C_{TMk}}}{2\gamma_{TMk}} f(\overrightarrow{u})f(\overrightarrow{u}'_p)e^{-j\gamma_{TMk}|z-R'_p\cos\varphi'_p|}J_t(\overrightarrow{r}'_p)R'_p d\varphi'_p\right]_0^{h_p} - \\ - \int_0^{h_p}\int_0^{2\pi}\sum_{k=1}^{K} jK^2_{C_{TMk}} f(\overrightarrow{u})f(\overrightarrow{u}'_p)\frac{e^{-j\gamma_{TEk}|z-R'_p\cos\varphi'_p|}}{2\gamma_{TEk}}\frac{\partial J_t(\overrightarrow{r}'_p)}{\partial t'_p}R'_p dt'_p d\varphi'_p \Rightarrow$$

$$I1(\overrightarrow{r}) = \int_0^{2\pi}\sum_{k=1}^{K} j\frac{K^2_{C_{TMk}}}{2\gamma_{TMk}} f(\overrightarrow{u})[f(R'_p\sin\varphi'_p,h_p)J_t(R'_p,h_p,\varphi'_p) - \\ - f(R'_p\sin\varphi'_p,0)J_t(R'_p,0,\varphi'_p)]e^{-j\gamma_{TMk}|z-R'_p\cos\varphi'_p|}d\varphi'_p - \\ - \int_0^{h_p}\int_0^{2\pi}\sum_{k=1}^{K} jK^2_{C_{TMk}} f(\overrightarrow{u})f(\overrightarrow{u}'_p)\frac{e^{-j\gamma_{TEk}|z-R'_p\cos\varphi'_p|}}{2\gamma_{TEk}}\frac{\partial J_t(\overrightarrow{r}'_p)}{\partial t'_p}R'_p dt'_p d\varphi'_p$$

In view of expressions (A.63)-(A.70) and the boundary condition: $J_t(R'_p, h_p, \varphi'_p) = 0$ the previous equation becomes:

$$I1(\overrightarrow{r}) = \int_0^{h_p} \int_0^{2\pi} G_{\Phi_\varepsilon}(\overrightarrow{r}, \overrightarrow{r}'_p) \frac{\partial J_t(\overrightarrow{r}'_p)}{\partial t'_p} R'_p dt'_p d\varphi'_p \quad (3.63)$$

The final expression for $\nabla \cdot \overrightarrow{A}$ is obtained with the combination of (3.61), (3.62) and (3.63):

$$(3.61) \overset{(3.62),\ (3.63)}{\Rightarrow}$$

$$\nabla \cdot \overrightarrow{A}(\overrightarrow{r}) = \int_0^{h_p} \int_0^{2\pi} G_{\Phi_\varepsilon}(\overrightarrow{r}, \overrightarrow{r}'_p)[\frac{\partial J_t(\overrightarrow{r}'_p)}{\partial t'_p} + \frac{1}{R'_p} \frac{\partial J_t(\overrightarrow{r}'_p)}{\partial \varphi'_p}] R'_p dt'_p d\varphi'_p \Rightarrow$$

$$\nabla \cdot \overrightarrow{A}(\overrightarrow{r}) = \int_0^{h_p} \int_0^{2\pi} G_{\Phi_\varepsilon}(\overrightarrow{r}, \overrightarrow{r}'_p) \nabla_s \cdot \overrightarrow{J}(\overrightarrow{r}'_p) R'_p dt'_p d\varphi'_p \quad (3.64)$$

Expression (3.64) is another formulation of the Lorenz Gauge. Therefore, it is only reasonable to expect that insertion of (3.64) into equations (3.57a) and (3.57b) results to equations (3.56a) and (3.56b) respectvely. The above equations will be used, in order to compute the unknown current densities and the resulting scattered fields. This procedure will be performed with the aid of numerical methods and it will be presented in Chapter 4.

Chapter 4

Numerical Solution

In Chapter 3, the Field Integral Equations for the "aKoM" configuration were derived. The complexity of the involved integrals inhibits their solution in closed form. As a result resort must be taken to numerical methods. Numerical techniques generally require more computation than the analytical methods, but they have proved to be very powerful EM analysis tools. In the present Chapter, the numerical techniques employed for the solution of the "aKoM" scattering problem will be presented and analyzed. The corresponding results will be cited in Chapters 5 and 6.

4.1 Moment Method

In the past years much effort has been dedicated to developing and enhancing the numerical techniques, in order to ensure the reliability of their results. A number of different numerical methods and techniques for solving electromagnetic problems are available, like the Finite Element Method [119] - [124], the Moment Method (MoM), the Boundary Element Method [117], [118], the Mode Matching techniques [6], [14], [79], [26], [27], [43], [45], Image techniques, accounting for the waveguide side walls [29], [39], [42], the Transmission Line Method (TLM), etc. Since each method can be characterized based on its strengths and limitations, it is expected that some methods are more appropriate for particular types of problems, than others. The method that was employed in the present work is the Moment Method [24], [63] - [66], [69], [80], [81]. This choice was mainly dictated by the analysis of Chapter 3. Implementation of another numerical technique would require a different theoretical analysis, which would be equivalent to the current one.

The Method of Moments is a technique for solving complex integral equations of the form:

$$y = f(x) \qquad (4.1)$$

The Moment Method is based on the transformation of the former complex equation into a system of simpler linear equations, employing the method of weighted residuals. The weighted residual techniques begin by establishing a set of trial solution functions with one or more variables, depending on the kind of the initial equation. The residuals are a measure of the difference between the trial solution and the true solution. The variable parameters are determined in a manner that guarantees a best fit of the trial functions based on a minimization of the residuals.

The first step in the Moment Method solution process is to expand the unknown quantity x into a finite sum of basis functions.

$$x = \sum_{m}^{M} x_m b_m \qquad (4.2)$$

where b_m is the m^{th} basis function and x_m is an unknown coefficient. Next, a set of M linearly independent weighting (or testing) functions, w_n, is defined. Both sides of the initial equation are multiplied with each testing function, forming a set of independent equations of the form:

$$< w_n, y >=< w_n, f(x) >, \;\; n = 1, 2, ...M \qquad (4.3)$$

where the symbol <> denotes inner product.

By expanding x using Equation (4.2), the following set of M equations with M unknowns is obtained:

$$< w_n, y >= \sum_{m=1}^{M} < w_n, f(x_m, b_m) >, \;\; n = 1, 2, ...M \qquad (4.4)$$

The equivalent matrix form is:

$$\mathbf{Y} = A\mathbf{X} \qquad (4.5)$$

where:
A is a MxM matrix: $A_{ij} =< w_j, f(b_i) >$,
X is a Mx1 matrix: $X_j = x_j$,
Y is a Mx1 matrix: $Y_i =< w_i, y >$,

In the following section the Moment Method will be applied to the 'aKoM' configuration.

4.2 Application of the Moment Method to the 'aKoM' Structure

One of the most important issues in the implementation of the MoM is the selection of basis and test functions. In the case of thin obstacles inside waveguides constant current distributions were often employed as basis and testing functions, in order to reduce the computation time and effort. The application of constant current distribution on the scatterer surface may be allowed, if the dimensions of the scatterer are substantially smaller compared to the wavelength and the waveguide dimensions, since the yielded results exhibit good agreement with the measured ones. This approximation, however, leads to inaccurate results, when applied to larger scatterers. In such cases, proper non constant current distributions must be assumed, so that the non-negligible variation of the current over the scatterer surface is accounted for. The selection of the test/ basis functions is determined by many factors such as the fulfillment of all boundary conditions that exist on the scatterer surface and the continuity of the electric currents. Clearly, the optimal choice of the basis / test functions is one that resembles the unknown distributions and leads to convergent solutions with the fewest number of terms in the expansion. An additional criterion is the shortest computation time. Unfortunately, true optimality imposes restrictions on the generality of the solution procedure. In practice, therefore, the choice involves compromise. The issue of selecting the appropriate test/ basis functions will be analyzed in detail in the following section.

4.2.1 Expansion Functions

Variation of the electrical current over the surface of the cylindrical metallic post indicates variation with respect to the post height and the post contour (the azimuth angle φ). The latter has usually been neglected, in case the metallic post diameter is significantly smaller than the length of the waveguide broad wall [34], [39]. In many cases, the thin post has been approximated with a flat strip that is 1.8d (d: post diameter) wide [29], [31] - [33] , [37]. The current solution addresses the scattered field generated by a post of arbitrary diameter, therefore the angular variation must be accounted for. It is legitimate to consider that the angular variation is decoupled from the t-variation (the variation along the post axis). Therefore, both components of the electric current

flowing on the surface of the 'aKoM' metallic post may be expressed in the following manner:

$$J_t(\varphi,t) = \varphi_t(\varphi)b_t(t) \qquad (4.6a)$$
$$J_\varphi(\varphi,t) = \varphi_\varphi(\varphi)b_\varphi(t) \qquad (4.6b)$$

Functions $\varphi_t(\varphi)$ and $\varphi_\varphi(\varphi)$ represent the angular variation, whereas functions $b_t(t)$ and $b_\varphi(t)$ express the t-variation of J_t and J_φ respectively.

An appropriate choice for $\varphi_t(\varphi)$ and $\varphi_\varphi(\varphi)$, indicated by the cylindrical shape of the 'aKoM' post, is the expansion on Fourier series:

$$\varphi_t(\varphi) = \sum_{n=-N}^{N} A_n e^{j2\pi n\varphi} \qquad (4.7a)$$
$$\varphi_\varphi(\varphi) = \sum_{m=-M}^{M} B_m e^{j2\pi m\varphi} \qquad (4.7b)$$

In the above equations, A_n, B_m are unknown weighting coefficients and M, N are the numbers of the expansion functions respectively.

While entire domain functions are employed for the $\varphi-$dependency of the electric currents, sub-domain functions are proved to be a good choice for the variation over the post height. Sub-domain basis functions are defined over a domain of an integral operator L, so that they are vanishing over a part of this domain.

The surface of the post is divided into a number of horizontal strips, as depicted in Figure 4.1 and each strip bears its own current. The strip current distributions must be chosen in such a way, that the continuity of the post current across the edges of each strip is ensured. The total current equals the superposition of the strip currents.

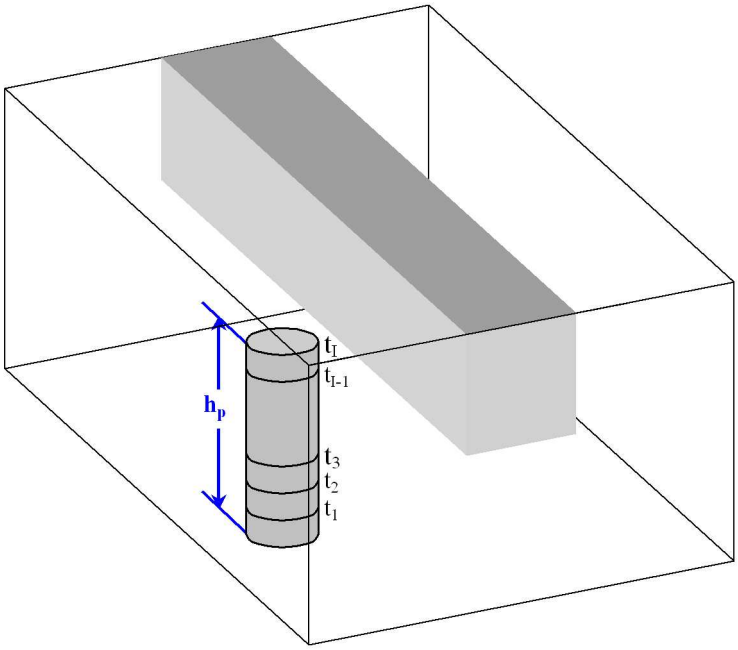

Figure 4.1 Segmentation of metallic post into horizontal stripes

Traditionally, sub-domain expansions have been favored because of their geometric flexibility, easier evaluation of the multiple integrals arising in the MM technique and their ability to handle localized

surface features in scattering problems. Such a surface feature in the 'aKoM' case is the corner junction between the post and the waveguide broad wall. Continuity of the electric current at these points must be ensured. Moreover, the t-component of the electric current must vanish at the free end of the post ($t = h_p$), in case of a capacitive scatterer. This condition must be satisfied because the electric current flowing on the bottom of the cylindrical post is considered to be negligible. In an opposite case, continuity of the electric current across the edge should be the valid boundary condition, indicating that J_t does not vanish at $t = h_p$.

Sub-domain expansions like the rooftop functions or the piecewise sinusoidal functions satisfy all conditions that apply on the post surface and, furthermore, give well-conditioned matrices [72], [67] - [69], [75], [78]. The corresponding mathematical formulations are:

$$b_t(t) = \sum_{i=1}^{I} C_i b_{t_i}(t) \qquad (4.8)$$

C_i: unknown weighting coefficient.
I: number of expansion functions or number of horizontal stripes

- **Piecewise Sinusoidal Functions:**
  If $0 \leq t \leq t_1$:

$$b_{t_i}(t) = \begin{cases} \frac{sin[l_t(t_1 - t)]}{sin(l_t t_1)} & , \quad 0 \leq t \leq t_1 \\ 0 & , \quad \text{elsewhere} \end{cases} \qquad (4.9a)$$

  else

$$b_{t_i}(t) = \begin{cases} \frac{sin[l_t(t - t_{i-1})]}{sin[l_t(t_i - t_{i-1})]} & , \quad t_{i-1} \leq t \leq t_i, \ 2 \leq i \leq I-1 \\ \frac{sin[l_t(t_{i+1} - t)]}{sin[l_t(t_{i+1} - t_i)]} & , \quad t_i \leq t \leq t_{i+1}, \ 2 \leq i \leq I-1 \\ 0 & , \quad \text{elsewhere} \end{cases} \qquad (4.9b)$$

  where: l_t is a constant that can be defined arbitrarily and I is the number of expansion functions.

  In case the post extends until the bottom of the ridged waveguide, an additional term must be included:

$$b_{t_i}(t) = \begin{cases} \frac{sin[l_t(t - t_{I-1})]}{sin[l_t(t_I - t_{I-1})]} & , \quad t_{I-1} \leq t \leq h_{rw} \\ 0 & , \quad \text{elsewhere} \end{cases} \qquad (4.9c)$$

  where: h_{rw} is the ridged waveguide height. This extra term ensures the continuity of the current as it flows from the post to the waveguide wall and vice versa.

- **Rooftop Functions:**
  If $0 \leq t \leq t_1$:

$$b_{t_i}(t) = \begin{cases} \frac{t_1 - t}{t_1} & , \quad 0 \leq t \leq t_1 \\ 0 & , \quad \text{elsewhere} \end{cases} \qquad (4.10a)$$

else

$$b_{t_i}(t) = \begin{cases} \frac{t-t_{i-1}}{t_i-t_{i-1}} & , \quad t_{i-1} \leq t \leq t_i, \ 2 \leq i \leq I-1 \\ \\ \frac{t_{i+1}-t}{t_{i+1}-t_i} & , \quad t_i \leq t \leq t_{i+1}, \ 2 \leq i \leq I-1 \\ \\ 0 & , \quad \text{elsewhere} \end{cases} \qquad (4.10b)$$

The additional term for the case of the inductive post is:

$$b_{t_i}(t) = \begin{cases} \frac{t-t_{I-1}}{t_I-t_{I-1}} & , \quad t_{I-1} \leq t \leq h_{rw} \\ \\ 0 & , \quad \text{elsewhere} \end{cases} \qquad (4.10c)$$

Both piecewise sinusoidal and rooftop functions span over two adjacent horizontal stripes. The former equations indicate that continuity across the common edge and across the edges of the neighboring stripes is guaranteed. It may also be easily understood that the passage from the post to the waveguide broad wall is expressed through the half piecewise functions, defined in the interval $0 \leq t \leq t_1$. In this manner, it is ensured that J_t does not vanish at the corner junction between the post and the waveguide wall. The above equations represent the general case, where the horizontal strips do not have the same width ($t_{i+1} - t_i \neq t_i - t_{i-1}$). Due to computational reasons, it is convenient however to segment the surface into stripes of the same width, which is defined as $\Delta h = \frac{h_p}{I}$ The choice of the appropriate number of stripes I will be discussed later.

Alternatively, entire domain trigonometrical functions were considered for the expansion of b_t. A typical example of such an expansion is cited below [24]:

$$\begin{cases} b_{t_1} = sin\, k(h_p - t) \\ b_{t_2} = sin\, k(h_p - t) + a[1 - cos\, k(h_p - t)] \end{cases}$$

where $k = \frac{2\pi}{\lambda}$, $\lambda = \frac{c}{f}$, f is the operating frequency and a is a normalization coefficient given by:

$$a = -\frac{\int_0^{h_p} [sin\, k(h_p - t)]^2 dt}{\int_0^{h_p} sin\, k(h_p - t)[1 - cos\, k(h_p - t)] dt}$$

It was found that generally both sub-domain and entire domain functions yielded similar results in cases of thin posts, where the circumferential current was so weak that could be neglected. However, adaptation of entire domain functions for b_t in case of a thicker post would require utilization of entire domain functions also for $b_\varphi(t)$. After several computations, it was concluded that the implementation of entire domain functions for both b_t and $b_\varphi(t)$ led to less accurate results compared to the sub-domain expansion.

Contrary to $b_t(t)$, the selection of expansion functions for $b_\varphi(t)$ is not subject to any special restriction, except for the smooth transition of the circumferential electric current from the post to the waveguide broad wall.
For the function $b_\varphi(t)$ pulse functions are selected:

$$b_\varphi(t) = \sum_{i=1}^{I} D_j b_{\varphi_i}(t) \qquad (4.11)$$

where

$$b_{\varphi_j}(t) = \begin{cases} 1 & , \quad (i-1)\Delta h \leq t \leq i\Delta h \\ 0 & , \quad \text{elsewhere} \end{cases} \qquad (4.12)$$

D_j is an unknown weighting coefficient.

The process of selecting the expansion functions is concluded with the choice for the magnetic currents. The magnetic currents will be expanded on entire domain basis functions. The reason for that is mainly the nature of the Green Functions representing these currents, which allows analytical computation of the involved integrals. The basis functions must satisfy the condition that the magnetic currents vanish at the ends of each slot. The corresponding mathematical formulations are listed below:

$$M1_b(z) = \sum_{q=1}^{Q} T_q sin[\tfrac{q\pi}{2L}(L+z)],\ -L \leq z \leq L \quad (4.13)$$

$$M2_b(z) = \sum_{p=1}^{P} K_p sin[\tfrac{p\pi}{2L}(L+z)],\ -L \leq z \leq L \quad (4.14)$$

K_p and T_q are unknown weighting coefficients and P, Q are the number of the expansion functions. For the sake of simplicity, it is assumed that P=Q. The magnetic currents are assumed to be constant across the slot and to vary only with the longitudinal coordinate. This assumption is justified by the fact that the slot is so narrow that its width is negligible compared to its length [105]- [111], [116].

4.2.2 Test Functions

The choice of the testing functions is as important as the choice of the expansion functions. As will be demonstrated at a later section of this chapter, the proper selection of weighting functions may contribute to the formulation of less complicated system of linear equations. This can be achieved, if the testing functions posses one, two or more degrees of differentiability. In such a case, the testing functions may 'eliminate' the singular behavior that is introduced by the differential operators, which are present in the integral equations, especially in the equations involved in the EFIE [71], [72]. The differentiability of the testing functions may allow the implementation of integration by parts, which subsequently leads to the reduction of the number of successive differentiations applied on the Green function.

An appropriate set of weighting functions would be the set of expansion functions, provided that the latter posses the afore mentioned degrees of differentiability. This technique is called the Galerkin method and constitutes one of the most popular techniques. The Galerkin method is often preferred due to the numerical stability it guarantees and the computational economy it may introduce. This is also the method that has been favored in the present work for all unknown current distributions.

Alternativelly, point matching has also been applied for the t-variation of J_φ. Point matching employs Delta functions for the testing, where the center of each Dirac function is located at the center of the corresponding pulse. Even though the Dirac functions simplified computations to a great extend, they were rejected because they led to the the ill-conditioning of matrix A (EFIE case). The ill-conditioning of matrix A is attributed to the effect of the $\nabla\nabla\cdot$ operator: Whenever operator $\nabla\nabla\cdot$ is combined with the Dirac functions, singularities are introduced, since the latter posses no degree of differentiability.

The weighting functions that were chosen (Galerkin method) are listed below:

$$J_t(\varphi,t) \quad : \quad w_t(t_p,\varphi_p) = \sum_{n=-N}^{N} e^{-j2\pi n\varphi} t_t(t) \quad (4.15)$$

$$J_\varphi(\varphi,t) \quad : \quad w_\varphi(t_p,\varphi_p) = \sum_{m=-M}^{M} e^{-j2\pi m\varphi} t_\varphi(t) \quad (4.16)$$

$$M1(z) \quad : \quad M1_w(z) = \sum_{q=1}^{Q} sin[\frac{q\pi}{2L}(L+z)] \qquad (4.17)$$

$$M2(z) \quad : \quad M2_w(z) = \sum_{p=1}^{P} sin[\frac{p\pi}{2L}(L+z)] \qquad (4.18)$$

where: $t_t(t) = b_t(t)$ and $t_\varphi(t) = b_\varphi(t)$.

4.3 Numerical Solution

The determination of the test and the basis functions completes the first step in the MM technique. The second major issue is the formulation of the set of linear equations, which involves the evaluation of the arising multiple integrals. This procedure will be presented in this section.

Insertion of the expansion functions into equations (3.56) and formulation of the inner products with the testing functions, leads to the expressions:

t-directed electric field on the post surface

$$\begin{aligned} & R_p \int_0^{h_p} \int_0^{2\pi} w_t(t_p,\varphi_p) E_{inc_t}(t_p,\varphi_p) dt_p d\varphi_p = \\ & = -j\omega\mu R_p [\int_0^{h_p} \int_0^{2\pi} w_t(t_p,\varphi_p) A_t(t_p,\varphi_p) dt_p d\varphi_p + \\ & + \tfrac{1}{k_0^2} \int_0^{h_p} \int_0^{2\pi} w_t(t_p,\varphi_p) \tfrac{\partial \varphi_\varepsilon(t_p,\varphi_p)}{\partial t_p} dt_p d\varphi_p - \\ & - \int_0^{h_p} \int_0^{2\pi} w_t(t_p,\varphi_p) F_t(t_p,\varphi_p) dt_p d\varphi_p \quad (4.19a) \end{aligned}$$

where:

$$\begin{aligned} A_t(t_p,\varphi_p) = & \int_0^{h_p} \int_0^{2\pi} G_{A_{tt}}(t_p,\varphi_p|t'_p,\varphi'_p) f_t(t'_p,\varphi'_p) dt'_p d\varphi'_p + \\ & + \int_0^{h_p} \int_0^{2\pi} G_{A_{t\varphi}}(t_p,\varphi_p|t'_p,\varphi'_p) f_\varphi(t'_p,\varphi'_p) dt'_p d\varphi'_p \Rightarrow \end{aligned}$$

$$\varphi_\varepsilon(t_p,\varphi_p) = R_p \int_0^{h_p} \int_0^{2\pi} G_{\varphi_\varepsilon}(t_p,\varphi_p|t'_p,\varphi'_p) [\frac{1}{R_p} \frac{\partial f_\varphi(t'_p,\varphi'_p)}{\partial \varphi'_p} + \frac{\partial f_t(t'_p,\varphi'_p)}{\partial t'_p}] dt'_p d\varphi'_p$$

$$F_t(t_p,\varphi_p) = \frac{\partial}{\partial x_p} \int_{-L}^{L} \int_{\frac{a}{2}-\frac{w}{2}}^{\frac{a}{2}+\frac{w}{2}} G_{F_{zz}}(t_p,\varphi_p|z'_{s1},x'_{s1}) M1_b(z'_{s1}) dz'_{s1} dx'_{s1}$$

R_p: Post Radius

φ-directed electric field on the post surface

$$R_p \int_0^{h_p}\int_0^{2\pi} w_\varphi(t_p,\varphi_p)E_{inc_\varphi}(t_p,\varphi_p)dt_p d\varphi_p =$$
$$= -j\omega\mu R_p[\int_0^{h_p}\int_0^{2\pi} w_\varphi(t_p,\varphi_p)A_\varphi(t_p,\varphi_p)dt_p d\varphi_p +$$
$$+\tfrac{1}{R_p k_0^2}\int_0^{h_p}\int_0^{2\pi} w_\varphi(t_p,\varphi_p)\tfrac{\partial\varphi_\varepsilon(t_p,\varphi_p)}{\partial\varphi_p}dt_p d\varphi_p] -$$
$$-\int_0^{h_p}\int_0^{2\pi} w_\varphi(t_p,\varphi_p)F_\varphi(t_p,\varphi_p)dt_p d\varphi_p \quad (4.19b)$$

where:

$$A_\varphi(t_p,\varphi_p) = \int_0^{h_p}\int_0^{2\pi} G_{A_{\varphi t}}(t_p,\varphi_p|t'_p,\varphi'_p)f_t(t'_p,\varphi'_p)R_p dt'_p d\varphi'_p +$$
$$+\int_0^{h_p}\int_0^{2\pi} G_{A_{\varphi\varphi}}(t_p,\varphi_p|t'_p,\varphi'_p)f_\varphi(t'_p,\varphi'_p)R_p dt'_p d\varphi'_p$$

$$F_\varphi(t_p,\varphi_p) = \frac{cos\varphi_p}{R_p}\frac{\partial}{\partial y_p}\int_{-L}^{L}\int_{\frac{a}{2}-\frac{w}{2}}^{\frac{a}{2}+\frac{w}{2}} G_{F_{zz}}(t_p,\varphi_p|z'_{s1},x'_{s1})M1_b(z'_{s1})dz'_{s1}dx'_{s1}$$

z-directed magnetic field across Slot 1

$$\int_{-L}^{L}\int_{\frac{a}{2}-\frac{w}{2}}^{\frac{a}{2}+\frac{w}{2}} M1_w(z_{s1})H_{inc_z}(z_{s1},x_{s1})dz_{s1}dx_{s1} =$$
$$= \int_{-L}^{L}\int_{\frac{a}{2}-\frac{w}{2}}^{\frac{a}{2}+\frac{w}{2}} M1_w(z_{s1})H_{J_t}(z_{s1},x_{s1})dz_{s1}dx_{s1} +$$
$$+\int_{-L}^{L}\int_{\frac{a}{2}-\frac{w}{2}}^{\frac{a}{2}+\frac{w}{2}} M1_w(z_{s1})H_{J_\varphi}(z_{s1},x_{s1})dz_{s1}dx_{s1} -$$
$$-j\omega\varepsilon\int_{-L}^{L}\int_{\frac{a}{2}-\frac{w}{2}}^{\frac{a}{2}+\frac{w}{2}} M1_w(z_{s1})H_1(z_{s1},x_{s1})dz_{s1}dx_{s1} -$$
$$-j\omega\varepsilon\int_{-L}^{L}\int_{\frac{a}{2}-\frac{w}{2}}^{\frac{a}{2}+\frac{w}{2}} M1_w(z_{s1})H_2(z_{s1},x_{s1})dz_{s1}dx_{s1} \quad (4.19c)$$

where:

$$H_{J_t}(z_{s1},x_{s1}) = \sin\varphi_{s1}\frac{\partial}{\partial y_{s1}}\int_0^{h_p}\int_0^{2\pi} G_{A_{\rho t}}(z_{s1},x_{s1}|t'_p,\varphi'_p)f_t(t'_p,\varphi'_p)R_p dt'_p d\varphi'_p +$$
$$-\cos\varphi_{s1}\frac{\partial}{\partial y_{s1}}\int_0^{h_p}\int_0^{2\pi} G_{A_{\varphi t}}(z_{s1},x_{s1}|t'_p,\varphi'_p)f_t(t'_p,\varphi'_p)R_p dt'_p d\varphi'_p +$$
$$+\frac{\partial}{\partial x_{s1}}\int_0^{h_p}\int_0^{2\pi} G_{A_{tt}}(z_{s1},x_{s1}|t'_p,\varphi'_p)f_t(t'_p,\varphi'_p)R_p dt'_p d\varphi'_p$$

$$H_{J_\varphi}(z_{s1},x_{s1}) = \sin\varphi_{s1}\frac{\partial}{\partial y_{s1}}\int_0^{h_p}\int_0^{2\pi} G_{A_{\rho\varphi}}(z_{s1},x_{s1}|t'_p,\varphi'_p)f_\varphi(t'_p,\varphi'_p)R_p dt'_p d\varphi'_p + \\ -\cos\varphi_{s1}\frac{\partial}{\partial y_{s1}}\int_0^{h_p}\int_0^{2\pi} G_{A_{\varphi\varphi}}(z_{s1},x_{s1}|t'_p,\varphi'_p)f_\varphi(t'_p,\varphi'_p)R_p dt'_p d\varphi'_p + \\ +\frac{\partial}{\partial x_{s1}}\int_0^{h_p}\int_0^{2\pi} G_{A_{t\varphi}}(z_{s1},x_{s1}|t'_p,\varphi'_p)f_\varphi(t'_p,\varphi'_p)R_p dt'_p d\varphi'_p$$

$$H_1(z_{s1},x_{s1}) = \int_{-L}^{L}\int_{\frac{a}{2}-\frac{w}{2}}^{\frac{a}{2}+\frac{w}{2}} G_{F_{zz}}(z_{s1},x_{s1}|z'_{s1},x'_{s1})M1_b(z'_{s1})dz'_{s1}dx'_{s1} + \\ +\frac{1}{k_0^2}\frac{\partial^2}{\partial z_{s1}^2}\int_{-L}^{L}\int_{\frac{a}{2}-\frac{w}{2}}^{\frac{a}{2}+\frac{w}{2}} G_{F_{zz}}(z_{s1},x_{s1}|z'_{s1},x'_{s1})M1_b(z'_{s1})dz'_{s1}dx'_{s1}$$

$$H_2(z_{s1},x_{s1}) = \int_{-L}^{L}\int_{\frac{a}{2}-\frac{w}{2}}^{\frac{a}{2}+\frac{w}{2}} G_{F_{zz}}(z_{s1},x_{s1}|z'_{s1},x'_{s1})M2_b(z'_{s2})dz'_{s2}dx'_{s2} + \\ +\frac{1}{k_0^2}\frac{\partial^2}{\partial z_{s1}^2}\int_{-L}^{L}\int_{\frac{a}{2}-\frac{w}{2}}^{\frac{a}{2}+\frac{w}{2}} G_{F_{zz}}(z_{s1},x_{s1}|z'_{s2},x'_{s1})M2_b(z'_{s2})dz'_{s2}dx'_{s2}$$

z-directed magnetic field across Slot 2

$$0 = j\omega\varepsilon\int_{-L}^{L}\int_{\frac{a}{2}-\frac{w}{2}}^{\frac{a}{2}+\frac{w}{2}} M2_w(\zeta_{s2},\eta_{s2})H_{srw}(\zeta_{s2},\eta_{s2})d\zeta_{s2}d\eta_{s2} - \\ -j\omega\varepsilon\int_{-L}^{L}\int_{\frac{a}{2}-\frac{w}{2}}^{\frac{a}{2}+\frac{w}{2}} M2_w(z_{s2})H_1(z_{s2},x_{s2})dz_{s2}dx_{s2} - \\ -j\omega\varepsilon\int_{-L}^{L}\int_{\frac{a}{2}-\frac{w}{2}}^{\frac{a}{2}+\frac{w}{2}} M2_w(z_{s2})H_2(z_{s2},x_{s2})dz_{s2}dx_{s2} \quad (4.19d)$$

where:

$$H_{srw}(\zeta_{s2},\eta_{s2}) = \frac{1}{2}[\int_{-L}^{L}\int_{\frac{a}{2}-\frac{w}{2}}^{\frac{a}{2}+\frac{w}{2}} G_{H_{zz}}(\zeta_{s2},\eta_{s2}|\zeta'_{s2},\eta'_{s2})M2_b(\zeta'_{s2},\eta'_{s2})d\zeta'_{s2}d\eta'_{s2} + \\ +\int_{-L}^{L}\int_{\frac{a}{2}-\frac{w}{2}}^{\frac{a}{2}+\frac{w}{2}} G_{H_{xz}}(\zeta_{s2},\eta_{s2}|\zeta'_{s2},\eta'_{s2})M2_b(\zeta'_{s2},\eta'_{s2})d\zeta'_{s2}d\eta'_{s2} + \\ +\int_{-L}^{L}\int_{\frac{a}{2}-\frac{w}{2}}^{\frac{a}{2}+\frac{w}{2}} G_{H_{zx}}(\zeta_{s2},\eta_{s2}|\zeta'_{s2},\eta'_{s2})M2_b(\zeta'_{s2},\eta'_{s2})d\zeta'_{s2}d\eta'_{s2} + \\ +\int_{-L}^{L}\int_{\frac{a}{2}-\frac{w}{2}}^{\frac{a}{2}+\frac{w}{2}} G_{H_{xx}}(\zeta_{s2},\eta_{s2}|\zeta'_{s2},\eta'_{s2})M2_b(\zeta'_{s2},\eta'_{s2})d\zeta'_{s2}d\eta'_{s2}]$$

The expressions for the Green functions in equations (4.19) are presented in Appendices B and C. As already discussed in Chapter 3, equations (4.19) include operations such as integration followed by differentiation. Some of these integrals, like the ones involving the magnetic currents, may be easily evaluated analytically. In this case the subsequent differentiation may be performed without any difficulty. On the other hand, the integrals involving the electric currents present two difficulties:

a) Analytical integration of A_t, A_φ or φ_ε is almost impossible, thus forcing the use of approximations.

b) The differentiation of the above mentioned functions yields non continuous functions, which introduce singularities.

For these reasons, certain manipulations are necessary for the simplification of the computations. The necessity for further handling of the equations relevant to the electric field may become apparent if attention is paid to expression (4.19b). Differentiation of φ_ε with respect to φ_p will generate the non continuous function because of term: $\frac{e^{-j\gamma_{TEi}|r_p\cos\varphi_p - r'_p\cos\varphi'_p|}}{2\gamma_{TEi}}$.
Implementation of integration by parts on (4.19b) yields:

$$
\begin{aligned}
&(4.19b) \Rightarrow R_p \int_0^{h_p}\int_0^{2\pi} w_\varphi(t_p,\varphi_p)E_{inc_\varphi}(t_p,\varphi_p)dt_p d\varphi_p = \\
&= -j\omega\mu R_p\{\int_0^{h_p}\int_0^{2\pi} w_\varphi(t_p,\varphi_p)G_{A_\varphi}(t_p,\varphi_p)dt_p d\varphi_p + \\
&+\tfrac{1}{R_p k_0^2}[\int_0^{h_p} w_\varphi(t_p,2\pi)G_{\varphi_\varepsilon}(t_p,2\pi)dt_p - \int_0^{h_p} w_\varphi(t_p,0)G_{\varphi_\varepsilon}(t_p,0)dt_p] - \\
&-\tfrac{1}{R_p k_0^2}\int_0^{h_p}\int_0^{2\pi} G_{\varphi_\varepsilon}(t_p,\varphi_p)\tfrac{\partial w_\varphi(t_p,\varphi_p)}{\partial\varphi_p}dt_p d\varphi_p\} - \\
&-\int_0^{h_p}\int_0^{2\pi} w_\varphi(t_p,\varphi_p)G_{F_\varphi}(t_p,\varphi_p)dt_p d\varphi_p \Rightarrow
\end{aligned}
$$

$$
\begin{aligned}
&R_p \int_0^{h_p}\int_0^{2\pi} w_\varphi(t_p,\varphi_p)E_{inc_\varphi}(t_p,\varphi_p)dt_p d\varphi_p = \\
&= -j\omega\mu R_p\{\int_0^{h_p}\int_0^{2\pi} w_\varphi(t_p,\varphi_p)G_{A_\varphi}(t_p,\varphi_p)dt_p d\varphi_p - \\
&-\tfrac{1}{R_p k_0^2}\int_0^{h_p}\int_0^{2\pi} G_{\varphi_\varepsilon}(t_p,\varphi_p)\tfrac{\partial w_\varphi(t_p,\varphi_p)}{\partial\varphi_p}dt_p d\varphi_p - \\
&-\int_0^{h_p}\int_0^{2\pi} w_\varphi(t_p,\varphi_p)G_{F_\varphi}(t_p,\varphi_p)dt_p d\varphi_p \quad (4.19e)
\end{aligned}
$$

Insertion of the appropriate expansion and weighting function into the above expressions leads to the transformation of the initial system of four integral equations with four unknowns into a set of (M+N)xI+2xP linear equations with (M+N)xI+2xP unknown variables. The system of linear equations is expressed in the following matrix form:

$$B = AX \qquad (4.20)$$

where (M+N)xI+2xP vector B represents all incident fields, (M+N)xI+2xP vector X represents all unknown expansion coefficients for the current distributions and ((M+N)xI+2xP)x((M+N)xI+2xP) matrix A results from the manipulations of the Green functions. All sub-matrices are defined analytically in Appendix D.

The question that arises at this point is the proper choice of numbers for the test or basis functions. Theoretically, the series of the test/ basis functions should be infinite, in order to constitute the optimum representation for the unknown current densities. However, these series must be truncated for the enabling of further computational manipulations. The number of terms in the expansion functions should be large enough to ensure satisfactory approximation of the unknown current densities, but should not exceed a limit, above which numerical instabilities may emerge. Such instabilities relate to the ill-conditioning of matrix A. When A is ill-conditioned, it cannot be

correctly inverted, thus leading to a non accurate solution.

Such a behavior has also been observed in the current work. More specifically, the choices of truncation number I, which concerns the functions representing the t-dependency of J_t, are crucial for the convergence of the solution. These functions play a very important role, since the contribution of J_t into the scattered electric field of the post is the most significant one.

As it will be demonstrated in Chapter 5, if a relatively large number of terms inside b_t or b_φ is assumed, then the solution of the system will not converge. The reason for this is a relation between the truncation number of the expansion function and the number of summation terms assumed for each ridged waveguide eigenvector. According to the analysis in Appendix A, the ridged waveguide eigenmodes are represented by summations with infinite terms. Like the expansion functions, the infinite series of the ridged waveguide eigenmodes must be truncated. These truncated summations are employed for all further calculations such as the derivation of all dyadic Green functions inside the ridged waveguide. The number N of terms in the truncated series is important, since it affects the sensitivity of the Green function kernel to spatial oscillations [81]. Therefore, a small value of N leads to a Green function kernel, which may not respond to the rapid spatial variations, that are introduced by expansion functions of many summation terms. Such a case would lead to an ill-conditioned matrix A and inaccurate results for the current densities, as will be discussed in Chapter 5. At this stage of the analysis, a compromise must be made. The number of terms in the eigenmodes series must be large enough to ensure proper representation of all field quantities inside the ridged waveguide, but should not exceed a limit, above which all computations require excessive amount of time and storage capacity. Consequently, the number N imposes a restriction to the value of number I, so that ill-conditioning phenomena be avoided.

The elements of matrices A and B are computed with MATLAB. The inversion of A is also performed with MATLAB based on the LU factorization technique. According to LU factorization the square matrix A may be expressed as a product of two triangular matrices:

$$A = LU$$

U is an upper triangular matrix and L is a permutation of lower triangular matrix.
The inverse of A is obtained by the product of the inverse matrices of L and U, according to the relationship:

$$A^{-1} = U^{-1}L^{-1}$$

The solution of the linear system in equation (4.20) performed in two steps:

$$Y = L^{-1}B$$

$$X = U^{-1}Y$$

The solution of each set of equations is performed easily by means of backward and forward substitution, since triangular matrices are involved.

All issues concerning matters of convergence and numerical stability will be reported in Chapter 5, while the results of the theoretical analysis and the simulating process will be presented in Chapter 6.

Chapter 5

Convergence of Numerical Results - Model Verification

The aim of the theoretical analysis that was conducted in chapter 3, was the determination of the unknown electric current distribution on the post surface and the computation of the electric field on the slot aperture. Both field quantities are very difficult to measure, especially when the dimensions of the configuration are as small as in the 'aKoM' case. Therefore, the S parameters were employed for the comparison of the simulation and the theoretical results. The S parameters of both the theoretical and the simulation model are directly computed by the electric and 'magnetic' currents of the structure. Consequently, good agreement between the simulated and the theoretically computed S parameters can verify the accuracy of the theoretical model. In the present chapter emphasis is given to the convergence of the computed results. A complete set of results will presented in the next chapter.

At this point it should be reminded that the 'aKoM' radiating element is analyzed as a three port configuration where only one ridged waveguide port is excited by the dominating TE_{10} mode and all other waveguide ports are assumed to be terminated with a matched load. The same configuration has been designed and simulated with program HFSS (High Frequency Simulator), which employs the Finite Element Method (FEM). As already mentioned in chapter 4, the Finite Element Method is one of the most popular numerical techniques that approach field scattering and radiation problems. The first step in FEM is the division of the configuration volume into a number of smaller homogeneous pieces or elements. The model contains information about the device geometry, material constraints, excitations and boundary conditions. The dimensions of the elements may vary, so that the elements can be very small near discontinuities or much larger elsewhere. In this way, geometrical details which have an impact on the electromagnetic behavior of the structure can be accounted for. The elements are chosen in a way that a simple (often linear) variation of the interior field may be assumed. The aim of the finite-element method is the computation of the field quantities at the so called nodes, the corners of the elements. To this purpose variational techniques are utilized, which work by minimizing an expression that describes the energy associated with the configuration under analysis.

The simulation results of the FEM are directly compared to the data, obtained by the implementation of the Moment Method on the 'aKoM' theoretical model. All theoretical computations, including the determination of the ridged waveguide relevant quantities (cutoff frequencies, eigenvectors and normalization coefficients) and the elements of the Moment Method Matrix, have been performed with MATLAB.

Additional to the simulation data, experimental results have been provided for a structure that involves only the ridged waveguide and the metallic post. The aim of this experiment was to verify

the accuracy of both HFSS and MATLAB results against measured data. To that purpose, it was not necessary to construct a structure similar to the 'aKoM' element, which was a difficult task. Instead, a test structure (Figure 5.16) was constructed, which consists of a rectangular waveguide containing a tapered ridge at both sides. The presence of the tapered ridge ensures proper adjustment of the test structure to the adaptors of the network analyzer. The test structure is scaled so that it operates in the frequency range: 8-12 GHz. The post is represented by a tuning screw of large diameter. The test structure was constructed and measured in the Institute for Microwave and RF-Technology of the University of Duisburg-Essen.

5.1 Convergence of the numerical results

Figure 5.1 depicts the three port configuration that was simulated under HFSS and analyzed with MATLAB. The ridged waveguide ports are designated as ports 1 and 2 whereas the rectangular waveguide port is port 3.

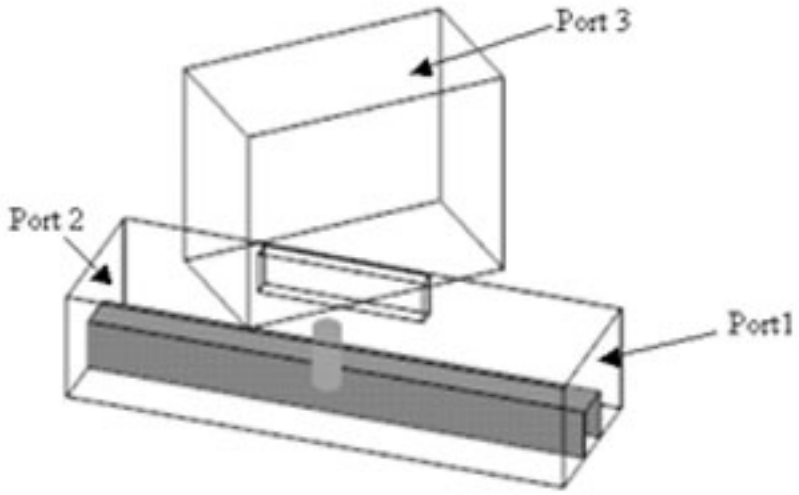

Figure 5.1 'aKoM' configuration: The 3-port model that is used for the HFSS simulation and the theoretical calculation.

A typical example of the diagrams that will be presented in chapter 6 is shown in Figure 5.2.

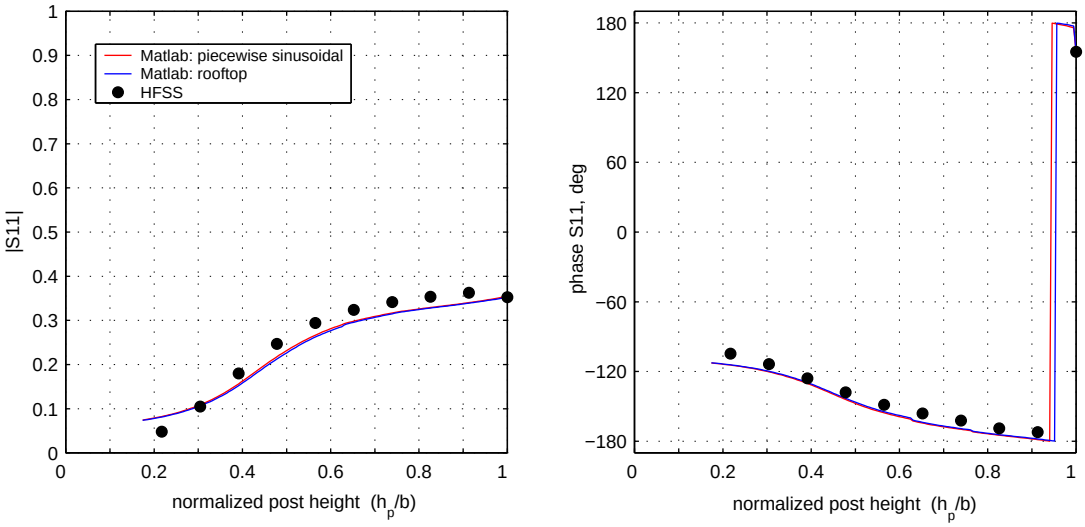

Figure 5.2 Variation of $S11$ with the post height, f=38.25 GHz, MPIE

These curves refer to the "aKoM" structure and illustrate the dependency of $S11$ on the post height, at frequency 38.25 GHz. The values of all geometrical dimensions are listed in Table 5.1:

ridged waveguide width (w_{rgw})	3.4 mm
ridged waveguide height (h_{rgw})	2.3 mm
ridge width (w_r)	1 mm
ridge height (h_r)	1.17 mm
post radius (r)	0.3 mm
post offset (d)	1.1 mm
slot length (l_s)	4 mm
slot width (w_s)	0.4 mm
branch waveguide length(t)	1 mm
rectangular waveguide width (w_{rcw})	7.11 mm
rectangular waveguide height (h_{rcw})	3.555 mm

Table 5.1 Geometrical dimensions of the 'aKoM' structure

Each of the above diagrams includes three curves: the dotted line corresponds to the HFSS simulation results, whereas the two solid lines represent MATLAB results. Both MATLAB curves have been computed using the same test and basis functions for the magnetic current and the J_φ current. Their difference lies on the weight and expansion functions employed for the y- variation of the J_y current. More specifically, the weight and expansion functions used for each current are listed below:

1. Magnetic current M1:
   - test function given by expression (4.17), where P=15.
   - basis function given by expression (4.13), where Q=15.
2. Magnetic current M2:
   - test function given by expression (4.18), where P=15.
   - basis function given by expression (4.14), where Q=15.

3. Electric current J_φ:
   - test function given by expression (4.16), where M=5 and t_φ is defined in (4.11).
   - basis function given by expression (4.7b), where M=5 and b_φ is defined in (4.11).
4. Electric current J_y:
   - test function given by expression (4.15), where M=5 and t_y:
     - red curve: Piecewise sinusoidal functions defined in (5.1)
     - blue curve: Pulse functions defined in (5.3)
   - basis function given by expression (4.7a), where M=5 and b_y:
     - red curve: Piecewise sinusoidal functions defined in (5.1)
     - blue curve: Rooftop functions defined in (5.2)

Piecewise sinusoidal functions:

$$b_{t_i}(t) = \begin{cases} \frac{sin[k_0(t_1-t)]}{sin(k_0\Delta t)} & , \ 0 \le t \le \Delta t \\ 0 & , \ \text{elsewhere} \end{cases} \qquad (5.1a)$$

and

$$b_{t_i}(t) = \begin{cases} \frac{sin[k_0(t-t_{i-1})]}{sin[k_0(\Delta t)]} & , \ t_{i-1} \le t \le t_i, \ 2 \le i \le N \\ \frac{sin[k_0(t_{i+1}-t)]}{sin[k_0(\Delta t)]} & , \ t_i \le t \le t_{i+1}, \ 2 \le i \le N \\ 0 & , \ \text{elsewhere} \end{cases} \qquad (5.1b)$$

where: $k_0 = \frac{2\pi}{\lambda}, \lambda = \frac{c}{f}, f = 38.25GHz$

Rooftop functions:

$$b_{t_i}(t) = \begin{cases} \frac{t_1-t}{\Delta t} & , \ 0 \le t \le \Delta t \\ 0 & , \ \text{elsewhere} \end{cases} \qquad (5.2a)$$

and

$$b_{t_i}(t) = \begin{cases} \frac{t-t_{i-1}}{\Delta t} & , \ t_{i-1} \le t \le t_i, \ 2 \le i \le N \\ \frac{t_{i+1}-t}{\Delta t} & , \ t_i \le t \le t_{i+1}, \ 2 \le i \le N \\ 0 & , \ \text{elsewhere} \end{cases} \qquad (5.2b)$$

Pulse functions:

$$t_{t_i}(t) = \begin{cases} 1 & , \ 0 \le t \le \Delta t \\ 0 & , \ \text{elsewhere} \end{cases} \qquad (5.3a)$$

and

$$t_{t_i}(t) = \begin{cases} 1 & , \ t_{i-1} + \frac{\Delta t}{2} \le t \le t_{i+1} - \frac{\Delta t}{2}, \ 2 \le i \le N \\ 0 & , \ \text{elsewhere} \end{cases} \qquad (5.3b)$$

In both cases, the post surface is segmented into N horizontal stripes of the same width Δt : $\Delta t = \frac{h_p}{N}$, h_p is the post height.

The number N of terms in t_φ, b_φ, t_y and b_y is set to 4 for this computation.

At this point the values of M, P, Q and N will be discussed. As already mentioned in Chapter 4, the choice for the number of test/ expansion functions is very important, because the convergence of the solution depends on it. The most critical number is N, the number of test/expansion functions for the axial variation of current J_t. The significance of N can be demonstrated by the following diagrams:

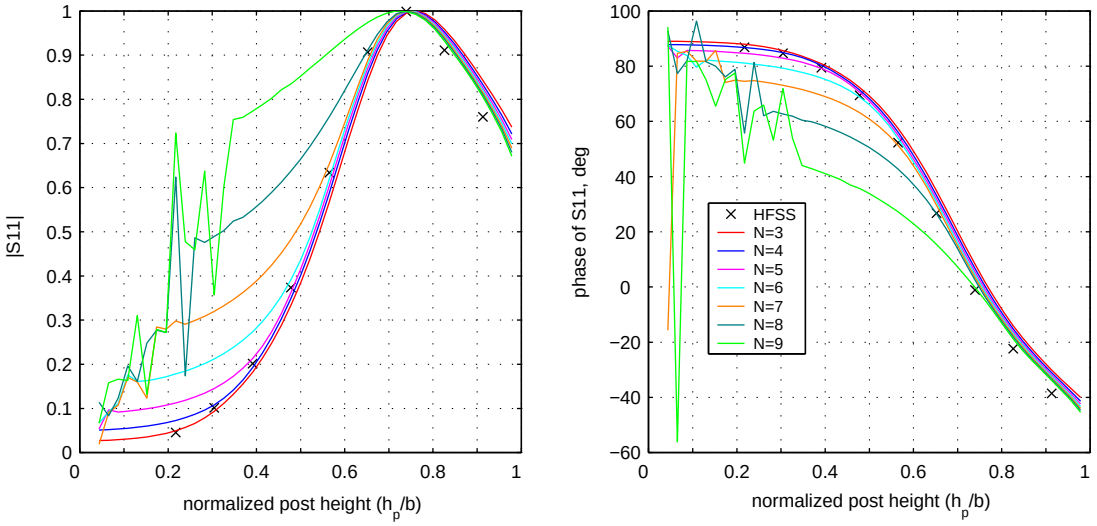

Figure 5.3a $S11$ vs h_p for various values of N ("aKoM", 12 terms deployed in eigenvector expansion, 279 modes)

The diagrams of Figure 5.3a illustrate the variation of $S11$ with respect to the post height for a configuration that consists only of a ridged waveguide and a metallic post. In this case the slot and the twisted waveguide have been omitted, since their presence does not have an impact on the choice of N. The geometrical dimensions of the ridged waveguide and the post are listed in Table 5.1. The phase of S11 has been computed at a $\frac{\lambda_{wg}}{4}$ distance away from the post center. In each diagram the amplitude and the phase of $S11$ are calculated using different number of piecewise sinusoidal functions for the expansion. It is evident that when N receives large values, the results become inaccurate, especially for short posts. Similar curves would have been obtained if the combination of rooftop - pulse functions were employed. Moreover, the remaining S parameters exhibit the same behavior as $S11$. The corresponding diagrams are omitted.

The reason for this behavior may become apparent if the eigenvectors of the ridged waveguide are examined. The relevant expressions are listed in Appendix A. For example, expression (A.59) represents the ridged waveguide eigenvectors in the trough region for the TE even modes: Each eigenvector is composed of an infinite sum of terms:

$$\overrightarrow{E}_i(x,y,z) = -j\omega\mu[-\sum_{n=1}^{\infty} N_{n1}\tfrac{n\pi}{b}\cos(\alpha_{n1t}x)\sin(\tfrac{n\pi}{b}y)\overrightarrow{x} + \\ + \sum_{n=0}^{\infty} N_{n1}\alpha_{n1t}\sin(\alpha_{n1t}x)\cos(\tfrac{n\pi}{b}y)\overrightarrow{y}]e^{-j\gamma_\iota z}$$

Even though the variation of each eigenvector with respect to y is given by an infinite Fourier series, the actual sensitivity of that particular eigenvector towards oscillations in the y-direction may be quite limited, if
a) the higher order Fourier coefficients are very small or
b) higher order Fourier terms are not considered at all for further computations (i.e. Dyadic Green Functions).
Case a is clearly the case of the eigenvectors with low cutoff frequency. These modes are dominated by the lower order Fourier terms and, as a result, are not particularly sensitive to rapid variations in

the y-direction. Bearing in mind that short posts give rise to evanescent modes with relatively low cutoff frequency, it becomes clear why the selection of a large value for N causes the ill-conditioning of the system matrix and leads to inaccurate results.

Case b can be presented by the comparison between the diagramms of Figures 5.3a and 5.3b. The curves in Figure 5.3a have been computed with eigenvectors consisting of 12 terms (order=11) in the trough region, whereas the results of Figure 5.3b have been computed with eigenvectors consisting of 8 terms (order=7). In both cases, 279 evanescent modes were considered.

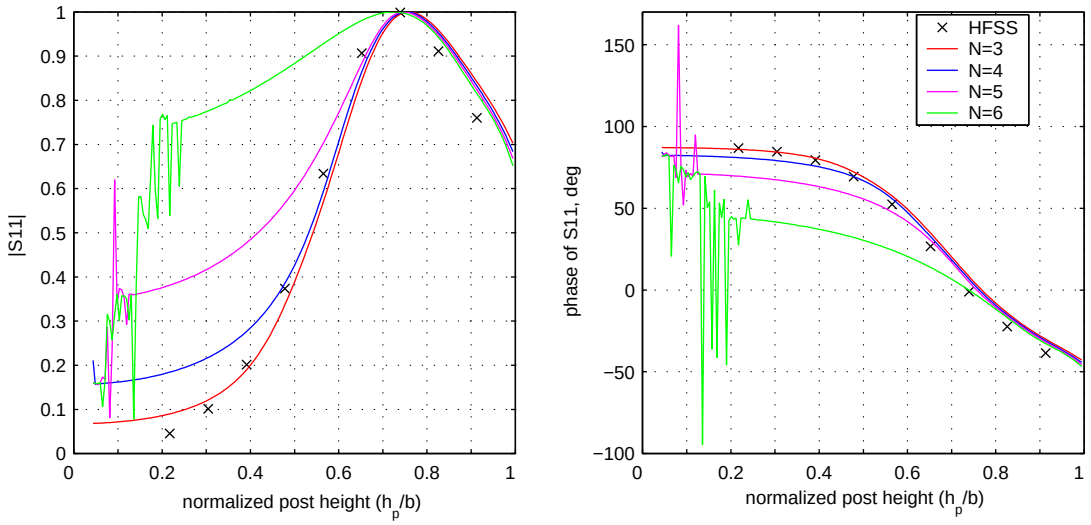

Figure 5.3b $S11$ vs h_p for various values of N ("aKoM", 8 terms deployed in eigenvector expansion, 279 modes)

Study of Figures 5.3a and 5.3b reveals that the combination N=6 - order=11 (Figure 5.3a, cyan line) produces similar results as the combination N=4 - order=8 (Figure 5.3b, blue line): The MATLAB results deviate from the HFSS results in the case of small posts ($h_p < 0.4h_{rgw}$, h_{rgw}: ridged waveguide height), but exhibit good agreement for larger posts. Furthermore, parallelizations can be observed between N=8 - order=11 (Figure 5.3a) and N=5 - order=8 (Figure 5.3b) or N=9 - order=11 (Figure 5.3a) and N=6 - order=8 (Figure 5.3b). In these cases, it is also evident that the choice of N is causing the ill-conditioning of the system matrix for small posts, yielding totally inaccurate results.

From the above, it becomes clear that there is a dependency between the number of truncated Fourier terms of the eigenvectors and the value of N. This dependency seems to affect mainly the small posts, since the MATLAB solution converges and exhibits good agreement to the HFSS solution for larger posts regardles the value of N. However, it should be further investgated, if there is also a certain relation between N and the order of the Fourier series that has an impact on the larger posts. Indeed this relation exists, as demonstrated by Figures 5.4a (order=11, 12 terms in the trough region) and 5.4b (order=7, 8 terms in the trough region). Clearly, when the value of N exceeds the order of the truncated Fouries series, the MATLAB results are completely inaccurate for all post heights, including the case $h_p = h_{rgw}$. In the cases of N=11 (Figure 5.4a) and N=7 (Figure 5.4b) the MATLAB results coincide with the HFSS results for the long posts ($h_p >= 0.9h_{rgw}$). The conclusion that can be drawn by the curves of Figures 5.4a and 5.4b is that the ultimate upper limit for N should be the order of the truncated Fouries series. This conclusion is in agreement with the analysis of Chapter 4.

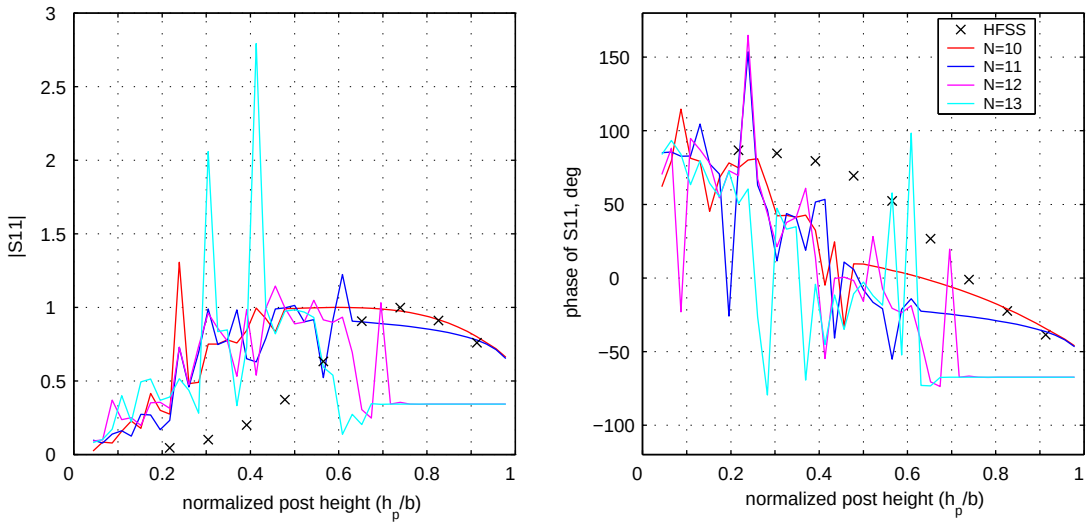

Figure 5.4a $S11$ vs h_p for very large values of N ("aKoM", 12 terms deployed in eigenvector expansion, 279 modes)

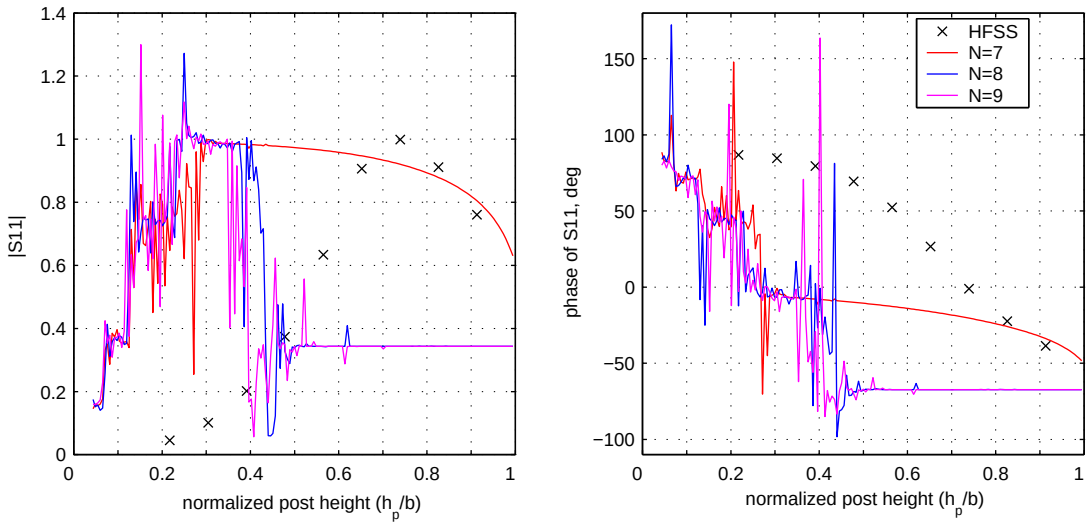

Figure 5.4b $S11$ vs h_p for very large values of N ("aKoM", 8 terms deployed in eigenvector expansion, 279 modes)

At this point, it would be interesting to examine whether the values of post radius or post offset have any impact on the value of N. To this purpose, the following diagrams will be presented:

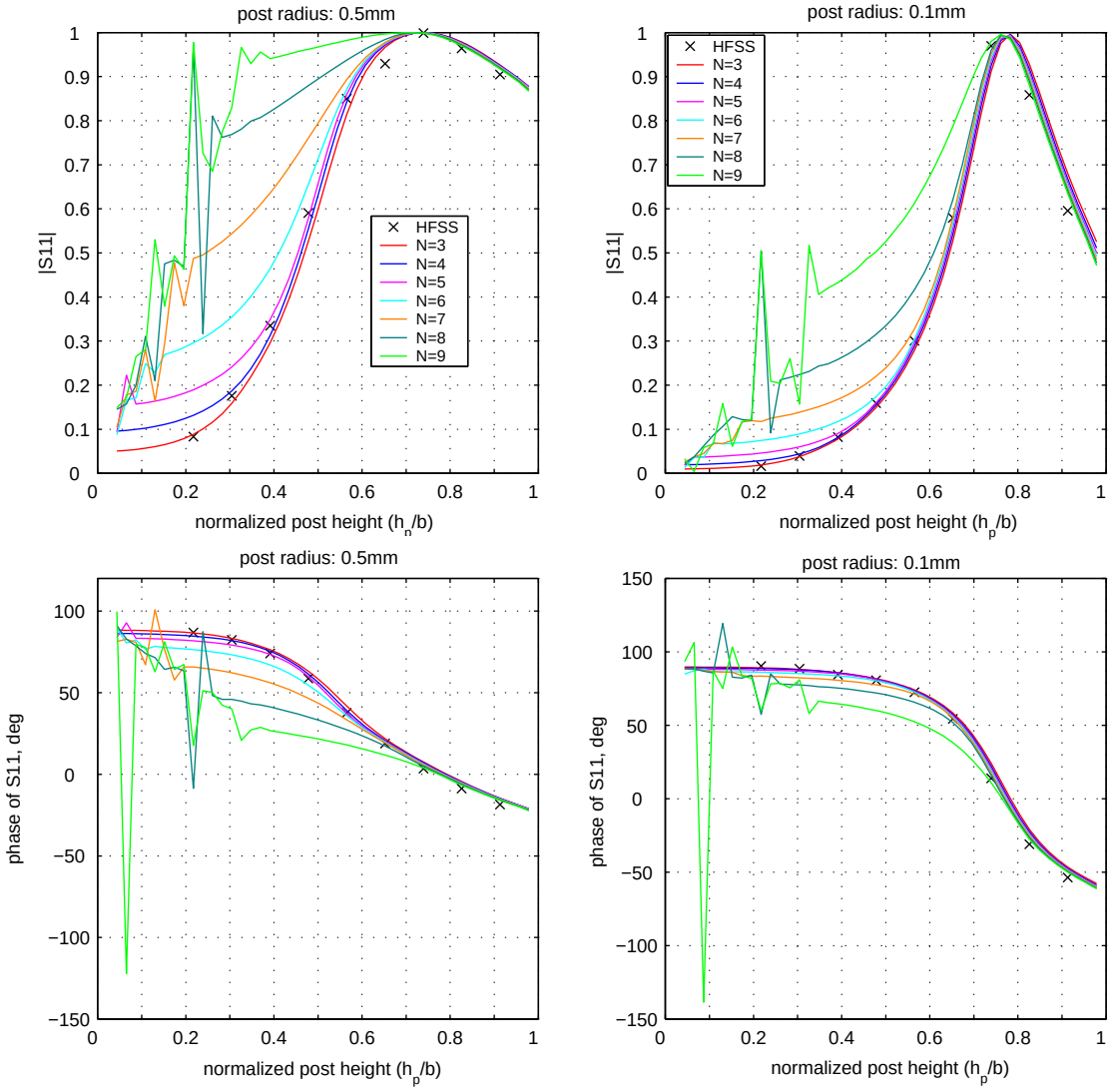

Figure 5.5 $S11$ vs h_p for various values of N and post radius ("aKoM"). Post offset: 1.1mm, N<10

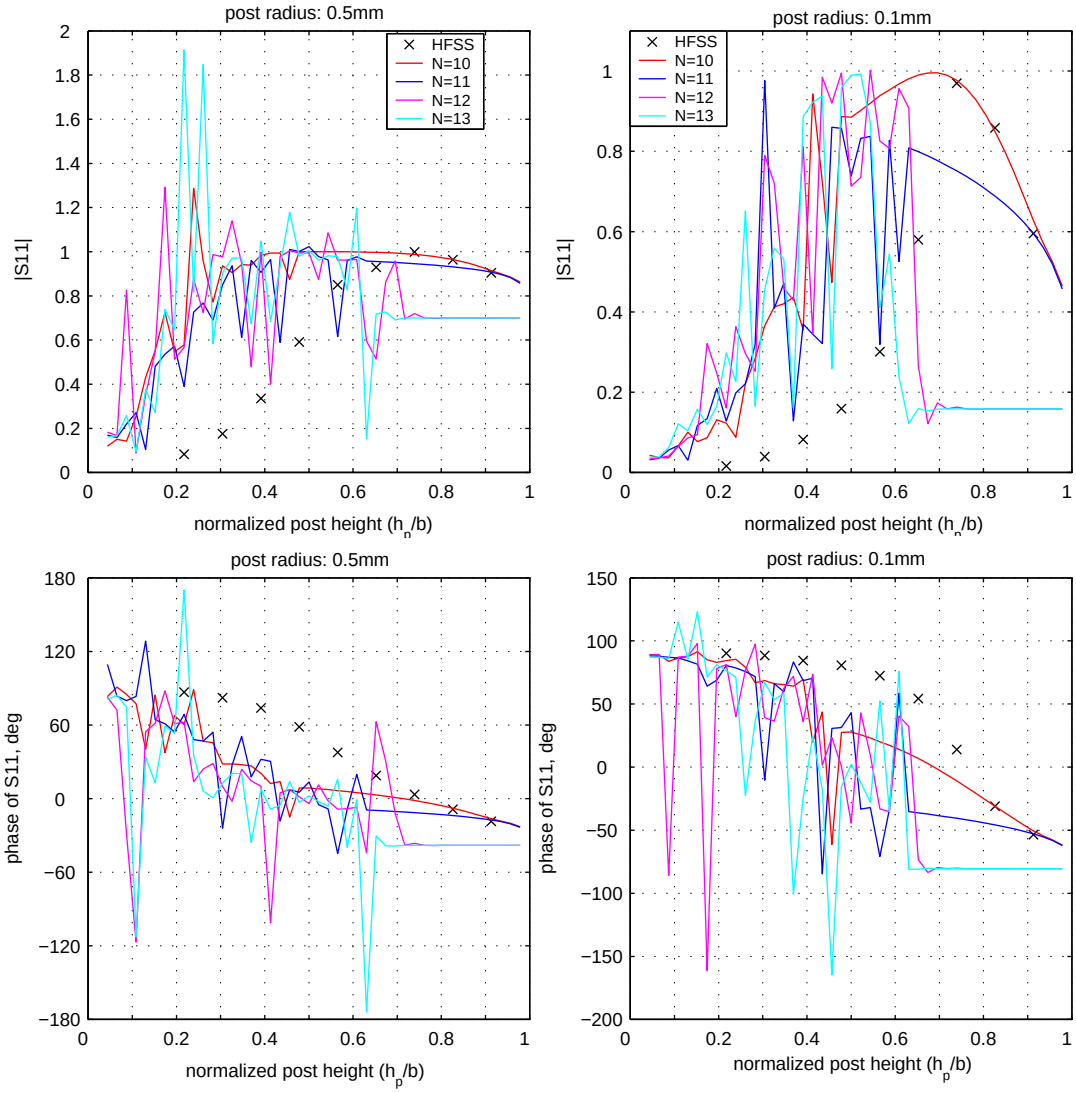

Figure 5.6 $S11$ vs h_p for various values of N and post radius ("aKoM"). Post offset: 1.1mm, N≥10

Figures 5.5 and 5.6 illustrate the effect of N on the variation of $S11$ with respect to the post height in the cases of a thick and a thin post. Comparison of Figures 5.3-5.6 may lead to the conclusion that the convergence of the solution is not substantially affected by the value of the post radius. The most significant difference between the thin and the thick post is observed for relatively small values of the post height (h_p <1.1mm). In this case, the configuration containing a thin post responds to the increase of N in a more stable way. However, if the value of N exceeds a limit, then the solution for the thin post also begins to diverge. The post radius seems to play no role at all, when the post height receives larger values. In such cases, the system can withstand greater values of N, but there is also an upper limit for these values.

Similar comments may be made on the system behavior, when the impact of the post offset is considered. Figures 5.7 and 5.8 present two groups of curves, which have been computed for two different post offset values. The post offset in these computations is defined as the distance of the post axis to the center line of the ridged waveguide broad wall.

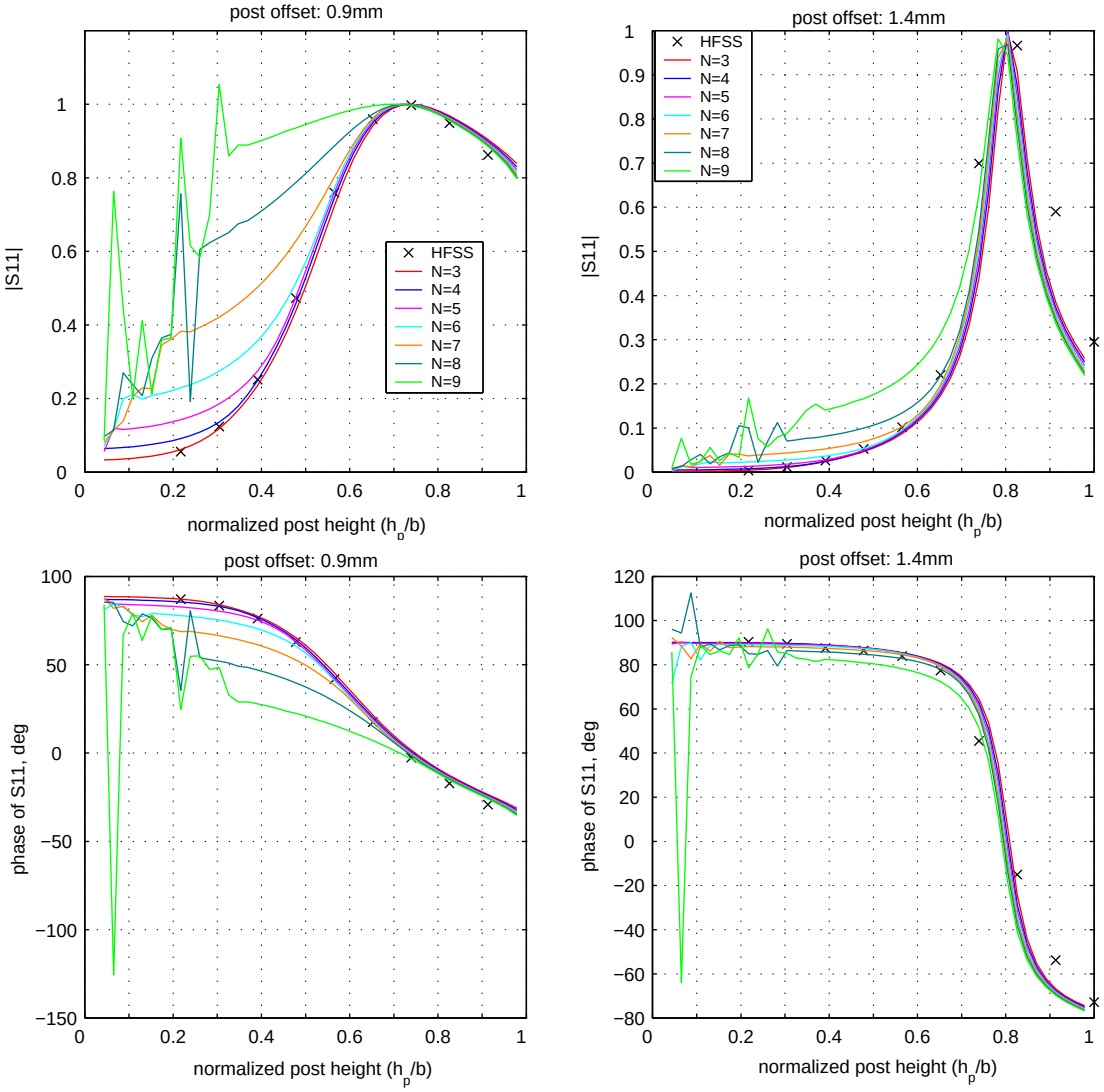

Figure 5.7 $S11$ vs h_p for various values of N and post offset ("aKoM"). Post radius: 0.2mm, N<10

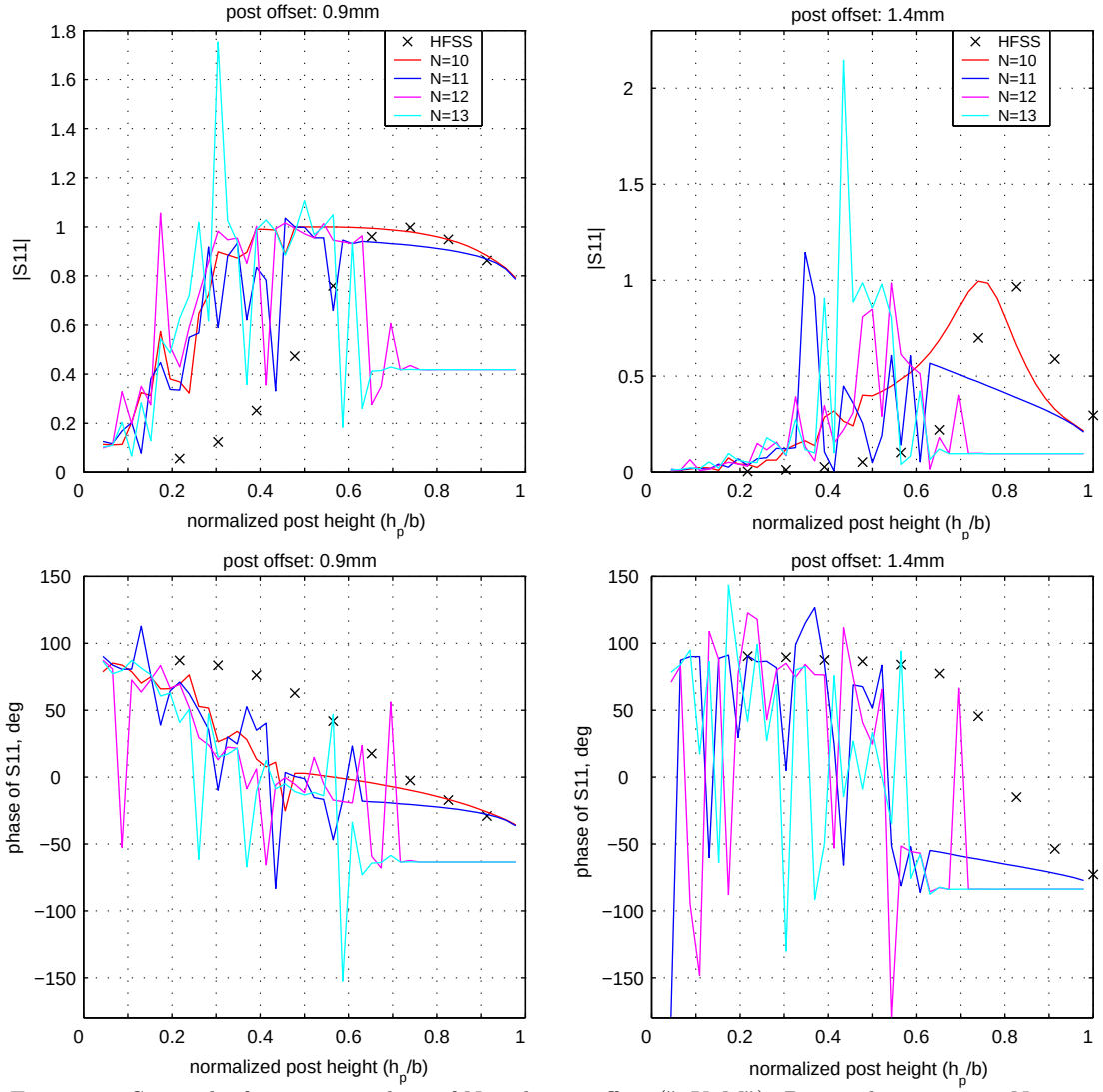

Figure 5.8 $S11$ vs h_p for various values of N and post offset ("aKoM"). Post radius: 0.2mm, N≥10

The value of post offset seems to have a greater impact on the solution convergence than the value of post radius. From the above curves it becomes clear that the solution is more stable when the post lies far from the ridge regardless of the post height value. However, there is also a limit in the values of N, beyond which the solution begins to diverge.

The most important conclusion drawn by Figures 5.3-5.8 is that of all parameters relative to the post, it is the height that mainly determines the proper value for N. Therefore, it is only reasonable to try to derive a general "relationship" between N and the post height, which would apply for any microwave structure containing a post inside a ridged waveguide. In this way, the selection of N may be made safely, leading to convergent solutions for the S parameters. Since it is quite difficult to formulate mathematical equations that describe the relationship between N and the post height, it could be sufficient to determine an "empirical" rule. This rule has been defined after studying the behavior of various configurations similar to the "aKoM". To this purpose the following structures were employed:

- Large configuration (l.c.)

ridged waveguide width (w_{rgw})	109.2 mm
ridged waveguide height (h_{rgw})	54.6 mm
ridge width (w_r)	32 mm
ridge height (h_r)	32 mm
post radius (r_p)	10 mm
post offset (d_p)	35 mm

Table 5.2: Characteristics of the ridged waveguide for the large configuration. Frequency range: 1.7-2.3 GHz

- Medium configuration (m.c.)

ridged waveguide width (w_{rgw})	22.86 mm
ridged waveguide height (h_{rgw})	10.16 mm
ridge width (w_r)	6 mm
ridge height (h_r)	5 mm
post radius (r_p)	0.95 mm
post offset (d_p)	7.43 mm

Table 5.3: Characteristics of the ridged waveguide for the medium configuration. Frequency range: 8-12 GHz

- Small configuration (s.c.)

ridged waveguide width (w_{rgw})	3.4 mm
ridged waveguide height (h_{rgw})	2.3 mm
ridge width (w_r)	1 mm
ridge height (h_r)	1.17 mm
post radius (r_p)	0.2 mm
post offset (d_p)	1 mm

Table 5.4: Characteristics of the ridged waveguide for the small configuration (aKoM). Frequency range: 37-39.5 GHz

Study of all three configurations revealed that the results are satisfactory, when the following relationship applies:

$$\frac{N}{N_t} \approx \frac{h_p}{h_{rgw}}$$

where N_t is the order of the last term in the truncated series of each eigenmode. This condition will be satisfied if N receives values given by:

$$N = round(\frac{N_t h_p}{h_{rgw}}) \quad (5.4)$$

Function round rounds its argument to the nearest integer. In case the ratio $\frac{N_t h_p}{h_{rgw}}$ lies equally between two successive integers, then both integers should provide satisfactory results. The $|S11|$ convergence with respect to N for each configuration will be presented in the diagrams of Figure 5.9

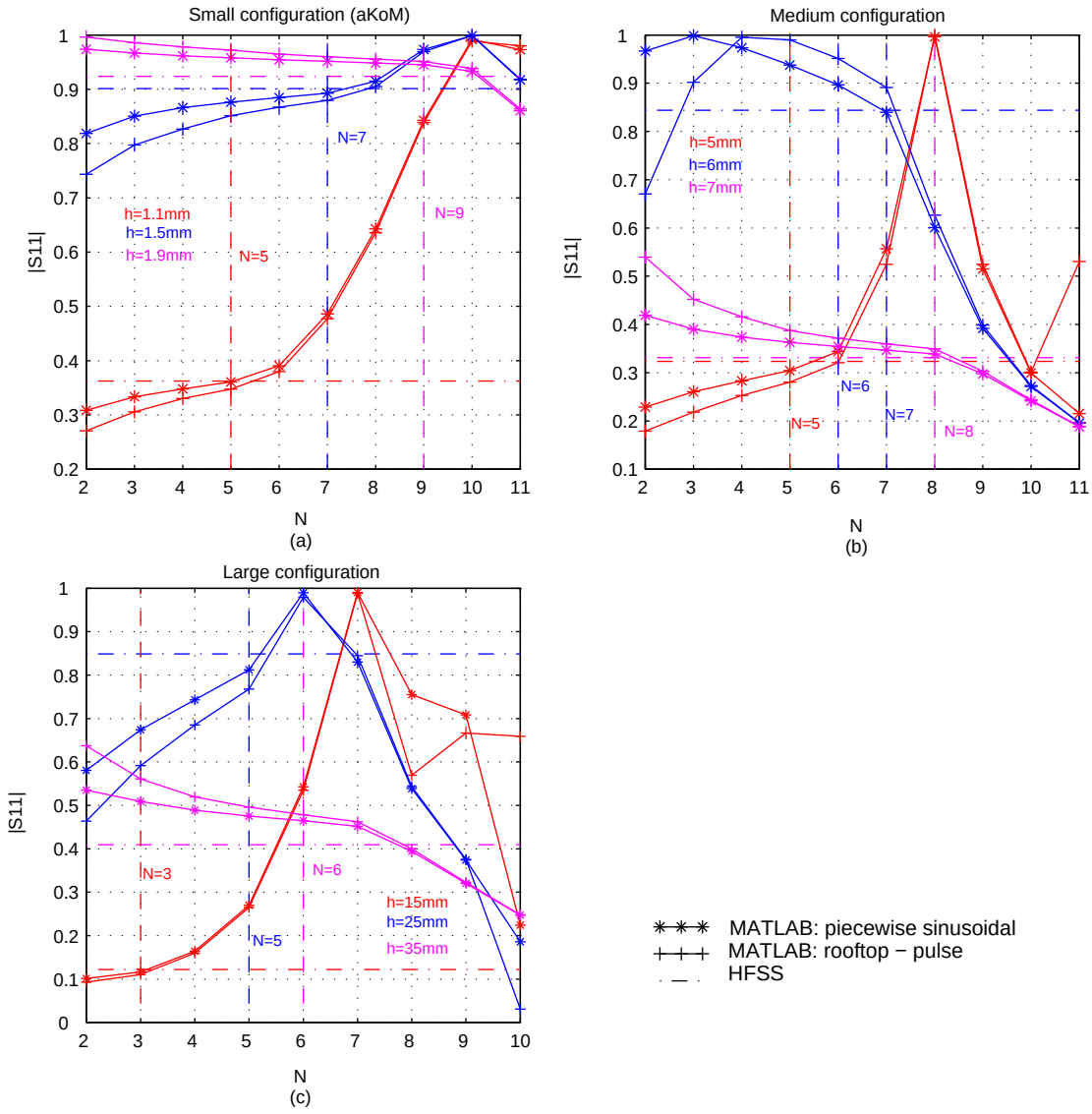

Figure 5.9 $|S11|$ convergence for various values of post height.(a) frequency: 38.25GHz,(b) frequency: 10GHz,(c) frequency: 2GHz

For the small and medium configuration 12 terms (order=11) were considered in the truncated series of the eigenmodes, whereas the large configuration was computed with 11 terms (order=10). Three post height values were selected for each configuration:

- post height smaller than resonance height
  s.c.: $h = 1.1mm => N = 5$, m.c.: $h = 5mm => N = 5$, l.c.: $h = 15mm => N = 3$
- post height close to resonance height
  s.c.: $h = 1.5mm => N = 7$, m.c.: $h = 6mm => N = 6$ or $N = 7$, l.c.: $h = 25mm => N = 5$
- post height longer than resonance height
  s.c.: $h = 1.9mm => N = 9$, m.c.: $h = 7mm => N = 8$, l.c.: $h = 35mm => N = 6$

The resonance height is defined as the height, where S11 is purely real and its amplitude reaches unity.

The common remark for all three configurations is the good agreement between MATLAB and HFSS values for $S11$, when N receives the value of (5.4). This is valid also for the medium configuration, when the post is 6mm long. In this case equation (5.4) yields $N = 6.496$, which indicates that both values 6 and 7 can lead to accurate results. Indeed, the blue curves of Figure 5.9 (b) and especially the curve corresponding to the piecewise sinusoidal equations indicate that the MATLAB values lie very close to the HFSS result. In all cases, the MATLAB $S11$ values approach the corresponding HFSS values at a relatively smooth rate, while N reaches up to the (5.4) value. Once N exceeds this value, the MATLAB results for $S11$ begin to strongly deviate from the HFSS results. An additional comment can be made on the large configuration: In this case the MATLAB computations were conducted with eigenvectors consisting of 11 terms (order =10), because less evanescent modes were considered. Therefore, equation (5.4) yields lower values for N, compared to the other two configurations. The impact of the lower N values on the $S11$ computations is reflected in the blue curves of Figure 5.9(c), where the MATLAB values approach the HFSS values slightly more 'abruptly'.

A similar effect can also be observed for the small or the medium configuration, if less higher order modes are assumed for the determination of the scattering matrix. Consideration of less evanescent modes automatically means lower order of the truncated ridged waveguide eigenvectors, as the evanescent eigenmodes with higher cutoff frequency are the ones that contain higher order terms with non negligible amplitude. Consequently, when such eigenmodes are excluded from the scattering matrix computation, then the expansion functions deploying high N values will clearly produce non convergent solutions, since these expansion functions assume rapid variation of the electric current in the axial direction, which can't be 'absorbed' by the dyadic Green functions of the scattering matrix. Therefore consideration of more evanescent modes in the computation leads to larger values of N, suitable for convergent solution. This effect is demonstrated by the curves of Figures 5.10.

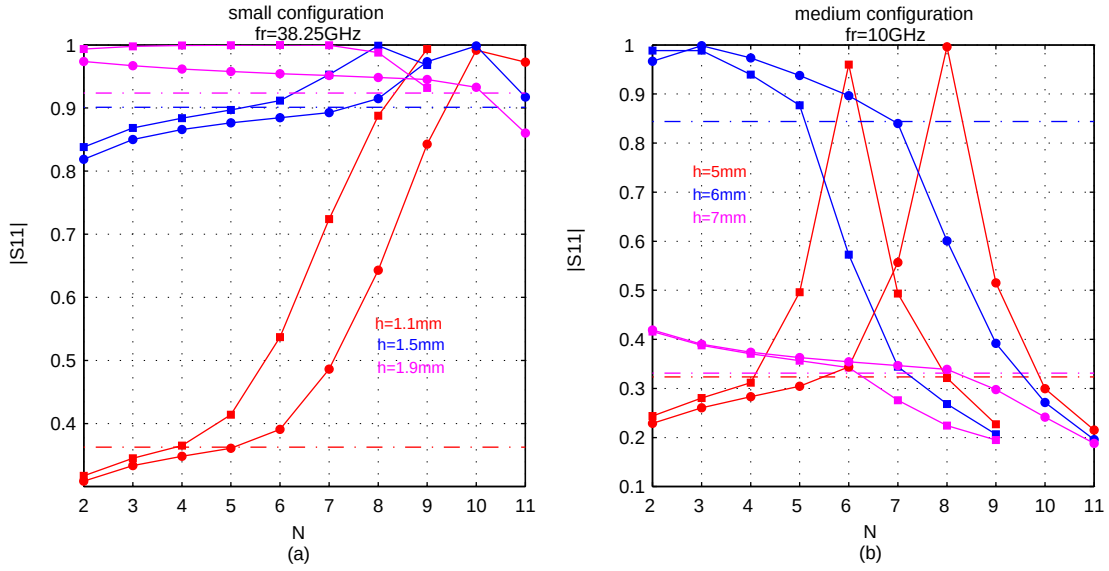

Figure 5.10 Computation of $|S11|$ vs N for various values of h_p, using different number of evanescent modes: (a) small configuration, circled line: 12 terms in Fourier series - 279 evanescent modes, $h = 1.1mm$ => $N = 5$, $h = 1.5mm$ => $N = 7$, $h = 1.9mm$ => $N = 9$, squared line: 10 terms in Fourier series - 173 evanescent modes, $h = 1.1mm$ => $N = 4$, $h = 1.5mm$ => $N = 6$, $h = 1.9mm$ => $N = 7$, dash-doted line: HFSS

(b) medium configuration, circled line: 12 terms in Fourier series - 396 evanescent modes, $h = 5mm$ => $N = 5$, $h = 6mm$ => $N = 6$ or $N = 7$, $h = 7mm$ => $N = 8$, squared line: 10 terms in Fourier series - 241 evanescent modes, $h = 5mm$ => $N = 4$, $h = 6mm$ => $N = 5$, $h = 7mm$ => $N = 6$, dash-doted line: HFSS

Figure 5.10 suggests that even when equation (5.4) yields low values for N, the computed $S11$ results are very close to the HFSS results. It will be shown later that for the medium configuration the HFSS and MATLAB results are in very good agreement with measured data.

The rule of (5.4) should also be tested against frequency. The corresponding curves for all three configurations are listed below:

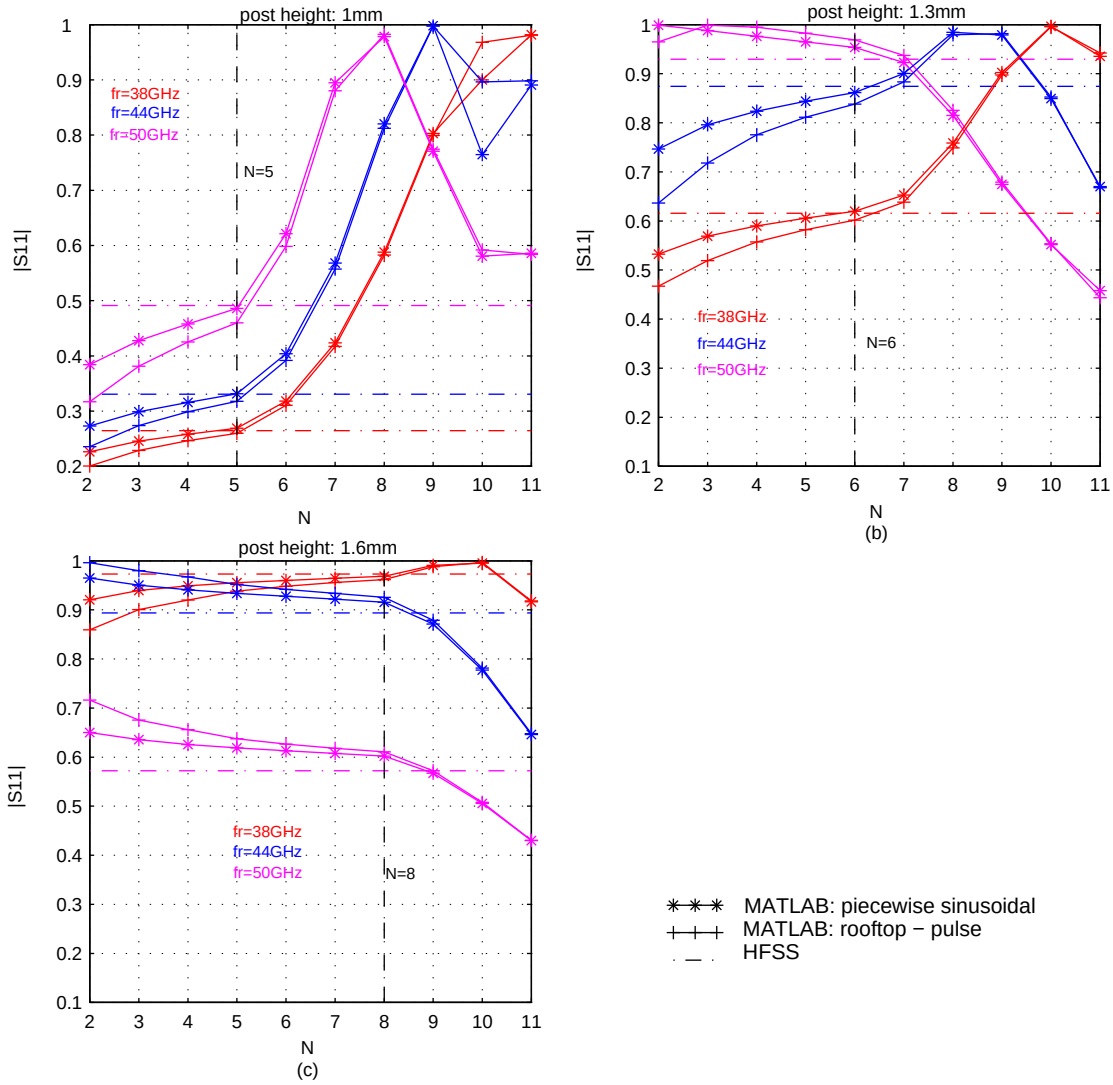

Figure 5.11 Small configuration, $|S11|$ convergence for various values of frequency. (a) post height: 1mm, (b) post height: 1.3mm, (c) post height: 1.6mm

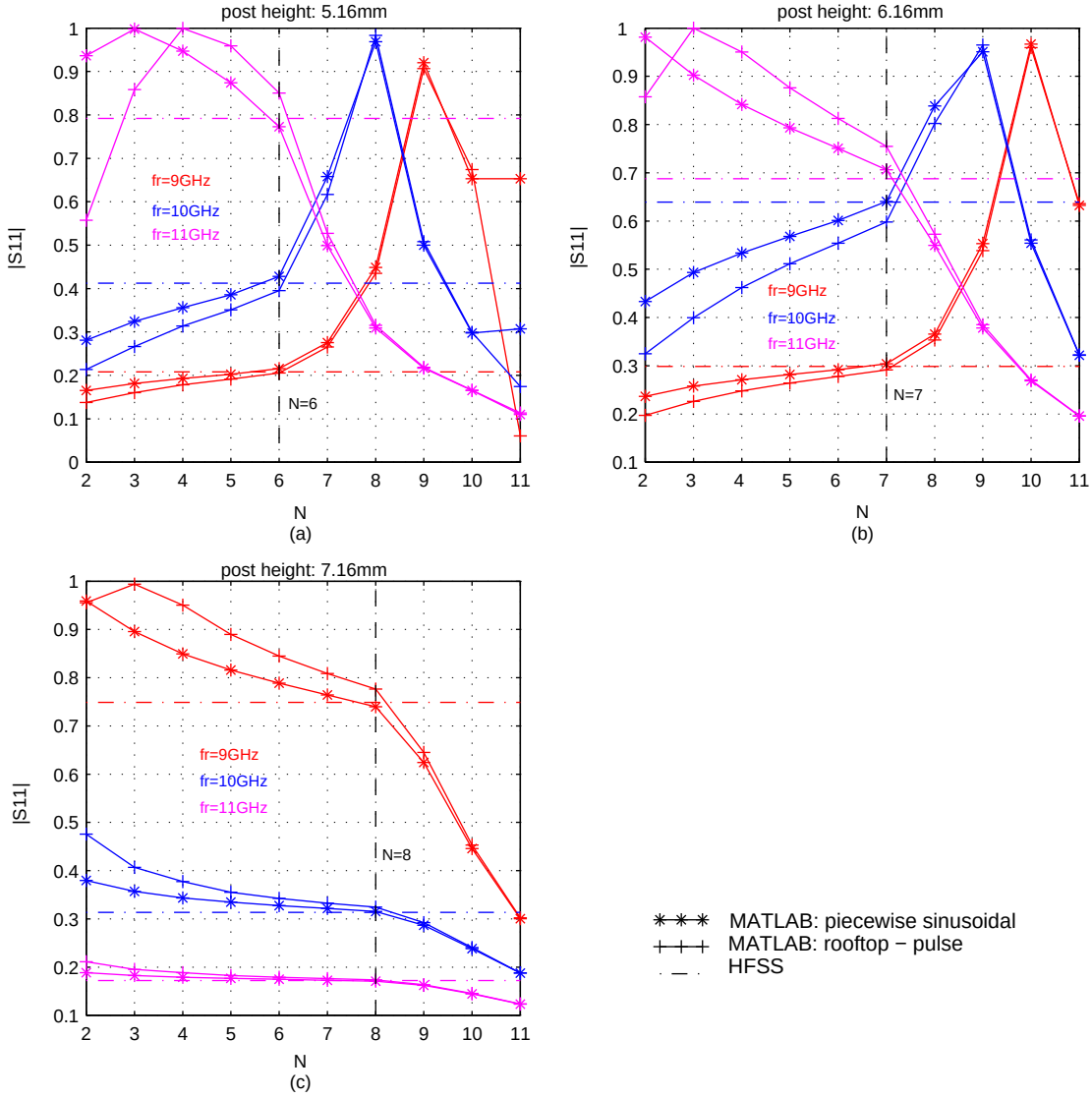

Figure 5.12 Medium configuration, $|S11|$ convergence for various values of frequency. (a) post height: 5.16mm, (b) post height: 6.16mm, (c) post height: 7.16mm

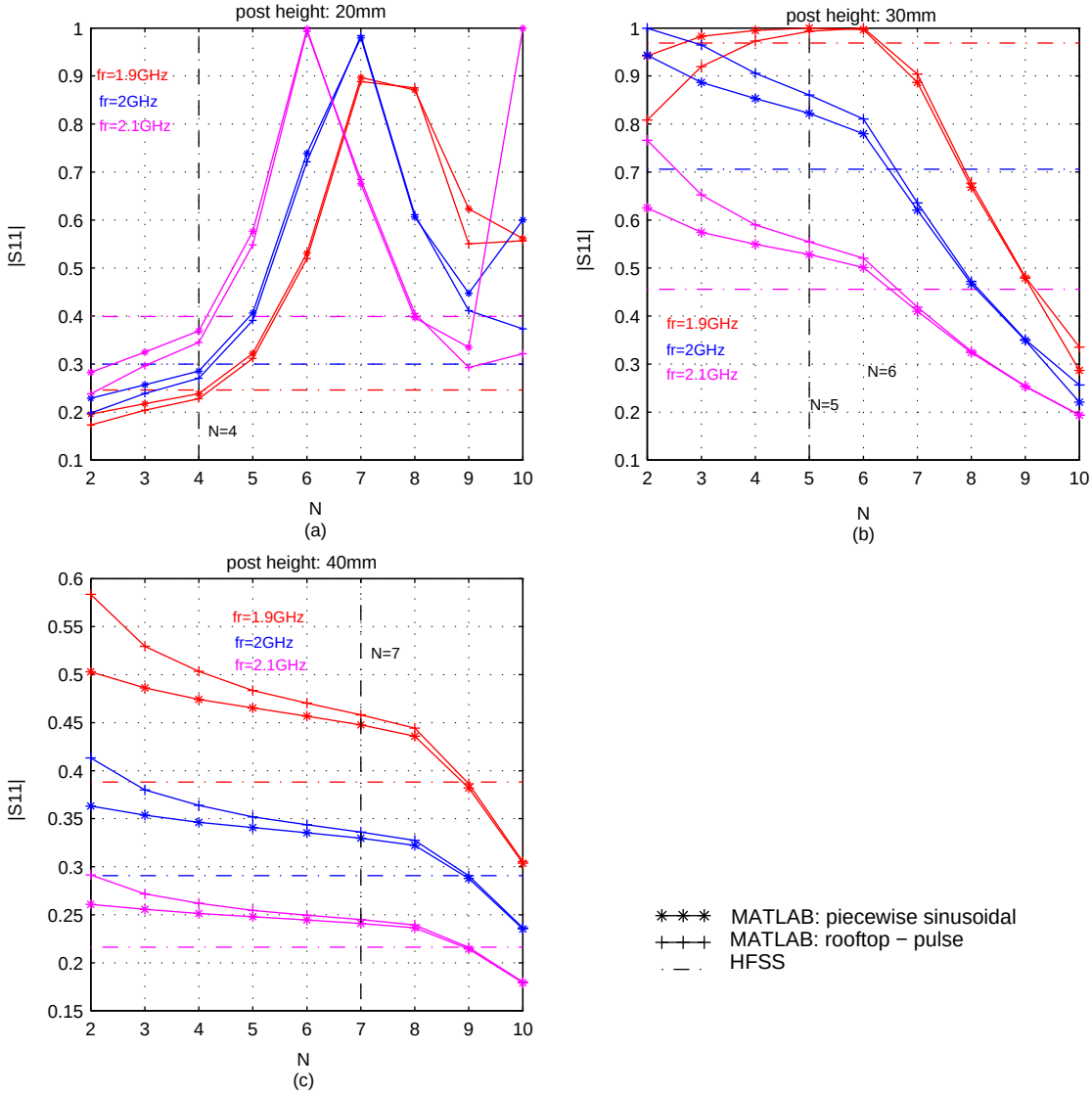

Figure 5.13 Large configuration, $|S11|$ convergence for various values of frequency. (a) post height: 20mm, (b) post height: 30mm, (c) post height: 40mm

The selection of post height values was based on the pattern of Figure 5.9. From the above graphics it becomes evident that the convergence (rate) for $S11$ is not affected by the frequency. Furthermore, expression (5.4) seems to be valid for all configurations, yielding results close to the HFSS results.

Contrary to N, the selection of the number of expansion and weight functions for the angular variation of both J_y and J_φ was an easy issue, since the solution converges very fast. This rapid convergence is demonstrated in the following diagrams, where the variation of S11 with respect to M (order of exponential terms representing the angular variation) for various post heights is depicted.

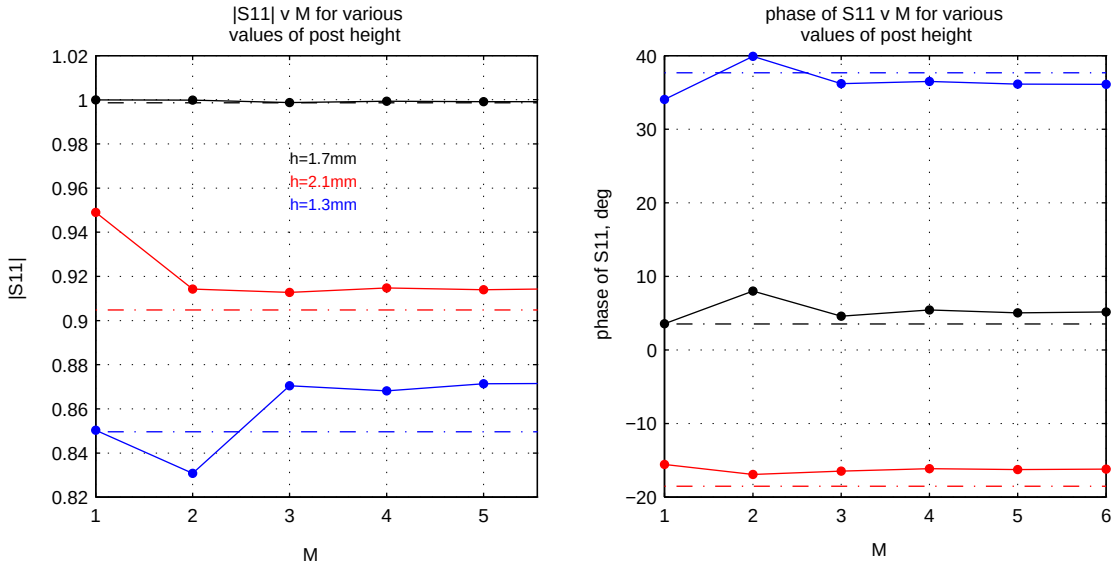

Figure 5.14 Convergence with respect to M: MPIE, pwsn functions for J_t small configuration, post radius:0.5mm, post offset:1.1mm

The results of Figure 5.14 have been computed for a thick post, where the angular variation of the electric currents J_ϕ and J_t is expected to be more intense, compared to a thinner post. Even in this case, the solution converges very fast. The results, which will be presented in the next chapter, have been computed, assuming that M=5.

Similar to the case of M, the number of magnetic current terms P was also easily chosen upon. The following curves present the effect of P on the convergence of the solution. It can be easily recognized that when P exceeds 7, convergence is ensured. The number of M varies between 3 and 10, in cases of structures containing longitudinal slot couplers between dissimilar waveguides. 3 test/basis functions are used in [106]-[108], 5 in [106]-[108], [109], [110] and [116] and 10 in [106].

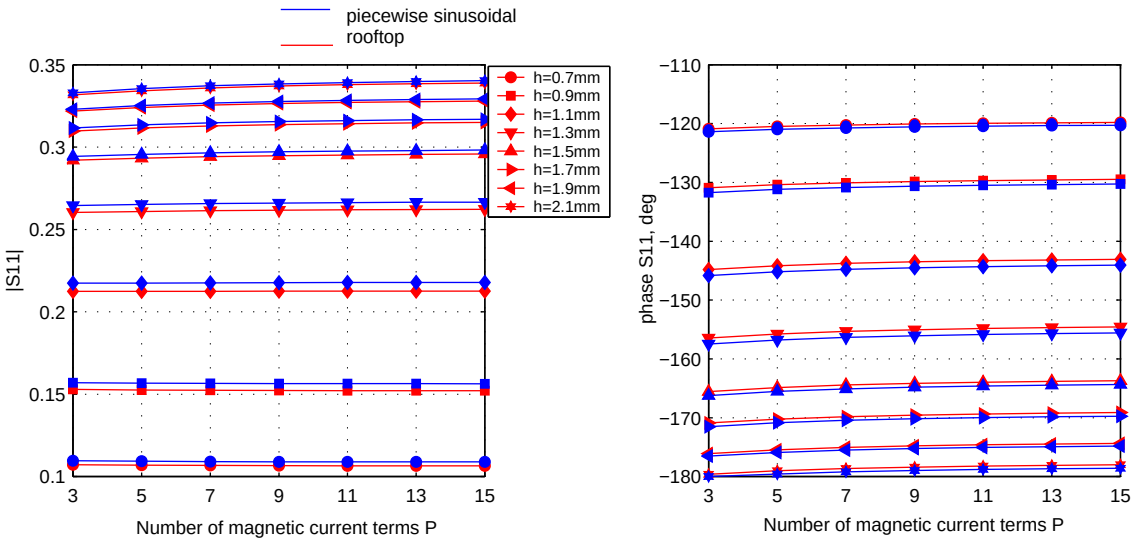

Figure 5.15 Convergence with respect to P: MPIE method
post radius:0.5mm, post offset:1.1mm, slot length:4mm, slot width:0.4mm, slot thickness:1mm

In the present work the magnetic current was modeled with 9 terms.

5.2 Verification

As already mentioned in the beginning of the present chapter, a test structure was constructed and measured. The measurements were compared against the computed results obtained by HFSS (FEM) and MATLAB (MoM). The test structure is depicted in the following Figure.

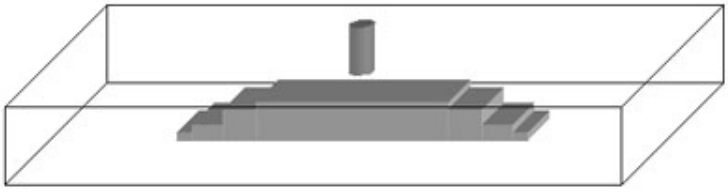

Figure 5.16(a) General view of the test structure

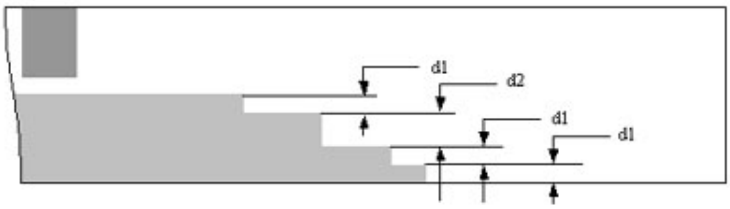

Figure 5.16(b) Side view of the test structure

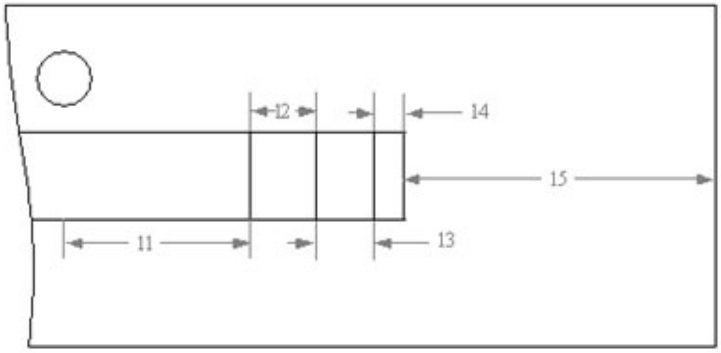

Figure 5.16(c) Top view of the test structure

The tapered ridged waveguide was necessary, in order to adjust the test structure to the rectangular flanges that were employed for the measurement. The geometrical dimensions of the test structure were chosen in a way that the structure operates in the frequency range 8-12GHz. For the determination of dimensions d1, d2, l1, l2, l3, l4 and l5 a structure consisting of only the rectangular waveguide and the tapered ridge was simulated under HFSS. The aim was to find the appropriate values for these dimensions that ensure $|S11| \simeq 0$ and $|S12| \simeq 1$ for the entire frequency range. These values along with the remaining waveguide dimensions are presented in the table below:

ridged waveguide width (w_{rgw})	22.86 mm
ridged waveguide height (h_{rgw})	10.16 mm
ridge width (w_r)	6 mm
ridge height (h_r)	5 mm
post radius (r_p)	2 mm
post offset (d_p)	7.43 mm
d1	1 mm
d2	2 mm
l1	34 mm
l2	8 mm
l3	8 mm
l4	4 mm
l5	34 mm

Table 5.5: Dimensions of the test structure. Frequency range: 8-12 GHz

The above dimensions provided an adaptor that ensured good matching between the ridged and the rectangular waveguides. Measurements were performed on this adaptor. The results are presented in the below diagram, where the red line represents the measured $|S11|$ and the blue line corresponds to the reflection coefficient that was obtained by the HFSS simulation. The diagram verifies the smooth transition from the ridged to the rectangular waveguide due to the the presence of the tapered ridge, since the reflection coefficient of the structure receives very low values throughout the entire frequency range.

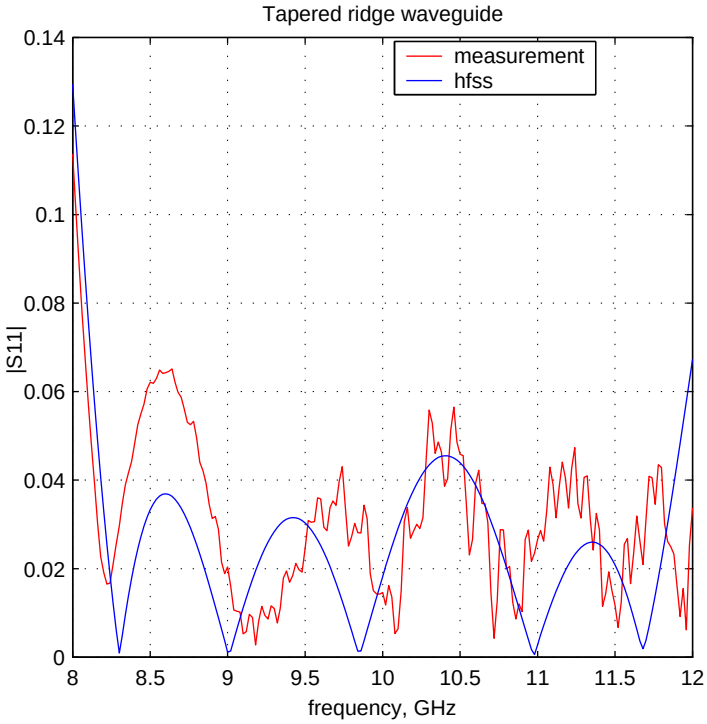

Figure 5.17 Reflection coefficient of the tapered ridge waveguide. The post is not present in the structure.

For the verification of the theoretical against the experimental data, the following computations were made:

- a) Ridged waveguide with cylindrical post:
  In this case the tapered end of the ridge was not considered. All computations were performed under the assumption that the ridged waveguide ports were terminated to a matched load. The S-parameters of this structure were computed under HFSS (FEM) and MATLAB (MoM).

For the MATLAB computation both piecewise sinusoidal and rooftop test/ basis functions were employed. The relevant curves are designated with blue.

- b) Rectangular waveguide containing the tapered ridge and the cylindrical post (actual test structure):
  The S-parameters were computed under HFSS (FEM). The corresponding curves are designated with magenta.

The results of both measurement and computations are presented in Figure 5.18, for two different values of post height:

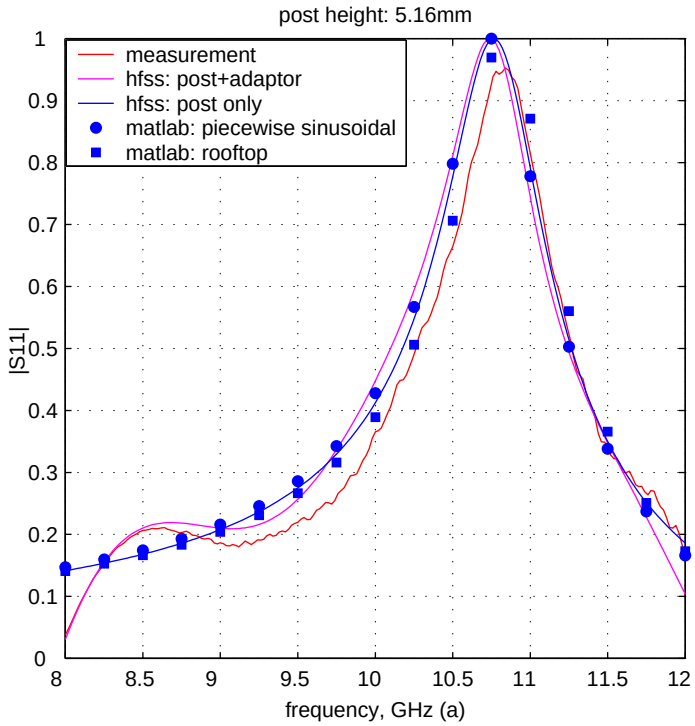

Figure 5.18a Computed and measured $|S11|$ of the test structure. Post height: 5.16mm

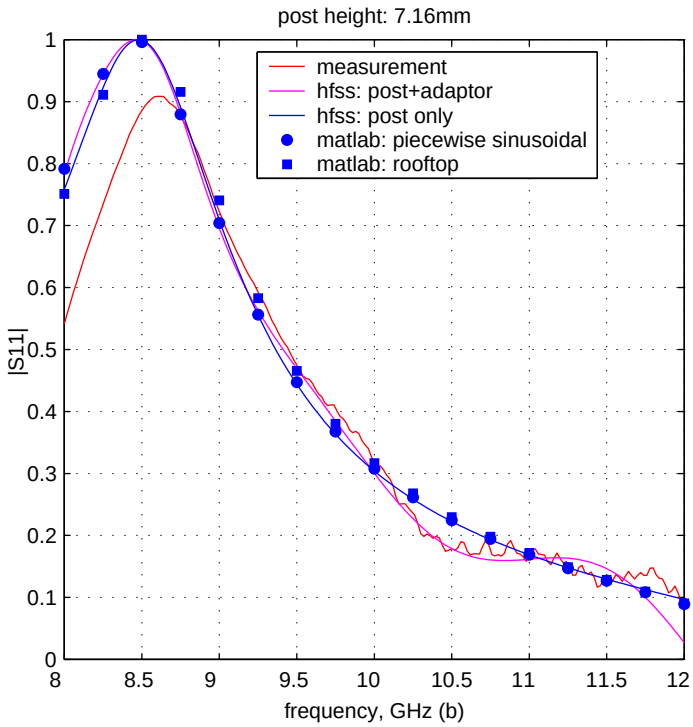

Figure 5.18b Computed and measured $|S11|$ of the test structure. Post height: 7.16mm

The diagrams of Figure 5.18 verify the excellent agreement between the theoretical computations (FEM and MoM). Even the purple line, which corresponds to case b), almost coincides with the blue lines for the frequencies between 9 and 12 GHz. The measurements also exhibit good agreement to the theoretical curves. Small deviations between the measured and the computed data are observed for frequencies lower than the resonant frequency, especially in the case of post height= 7.16mm. These deviations are mainly attributed to the attenuation and power loss inside the ridged and the rectangular waveguides of the measured structure, which never allow the red curve (measured data for $|S11|$) to reach unity at resonance. Contrary to that, both HFSS and MATLAB computations were performed under the two conditions:
(a) there are no losses inside the waveguides and
(b) all waveguide ports are terminated at a matched load.

Furthermore, it wasn't possible to achieve 100% accuracy in setting the post or even the ridge height to the desired value during measurement. Such slight variations in the post or ridge height value are responsible for small deviations between the theoretical and the experimental data. Figure 5.19 can verify the sensitivity of the $S11$ against minor post height variations.

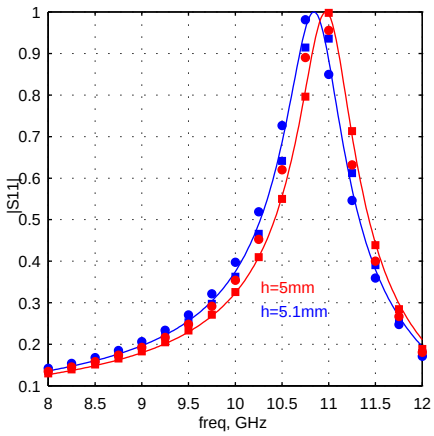

Figure 5.19: Computed $|S11|$ of the test structure for two post height values. Solid line: HFSS. Circled line: MATLAB, piecewise sinusoidal test/ basis functions. Squared line: MATLAB, rooftop test/ basis functions.

In the above Figure the HFSS and MATLAB results are presented for post height values 5mm and 5.1mm. A slight change in the post height (2%) can cause a small frequency shift (approximately 1.2% in this case). The increased sensitivity of the structure against the post height value will be demonstrated to a great extend in Chapter 6. The equations of Appendix A also demonstrate the sensitivity of the electromagnetic fields inside the ridged waveguide against the ridge height.

Despite the slight deviations in the amplitude values, a basic conclusion that emerges from Figure 5.18 is the fact that the theoretical models can predict the resonant frequency of the structure with good accuracy. Additionally, the computed and the measured curves exhibit the same variation with frequency and the same dependency on the post height value. Based on these remarks, it would be safe to state that the results of Figure 5.18 verify the validity of the both FEM and MoM theoretical models.

Chapter 6

Analysis of computed results

The role of parameters, like frequency or geometrical dimensions, on determining the electromagnetic behavior of the 'aKoM' structure will be presented and analyzed in the present chapter. To this purpose, sets of results will be demonstrated, which indicate the impact of the system parameters on the reflection and transmission coefficients. For the sake of simplicity, the effect of each geometrical dimension will be discussed separately in the following sections. The results have been computed by implementation of the MoM on the theoretical model of Figure 5.1. All the remarks or constraints described in Chapters 4 and 5 have been taken into account during the theoretical computations. The computed data will be compared against simulated data that are obtained by HFSS. The same model is used for the HFSS simulation. The basic assumption there is that all ports are terminated with a well-matched load.

6.1 Slot length - Post height

According to the analysis of the preceding chapters, the most critical dimensions are the slot length and the post height, because they control the magnetic and the electric current respectively. Due to the special characteristics of the 'aKoM' configuration, these two parameters will be examined together. The significance of these dimensions becomes quite clear by the diagrams below. The curves of Figure 6.1(a) illustrate the impact of the slot length on the variation of ridged waveguide reflection coefficient $S11$ with respect to the post height. The phase of $S11$ has been computed at a distance: $\frac{\lambda_{wg}}{2}$ from the waveguide discontinuities (level z=0), where $\lambda_{wg} = \frac{2\pi}{\gamma_{wg}}$

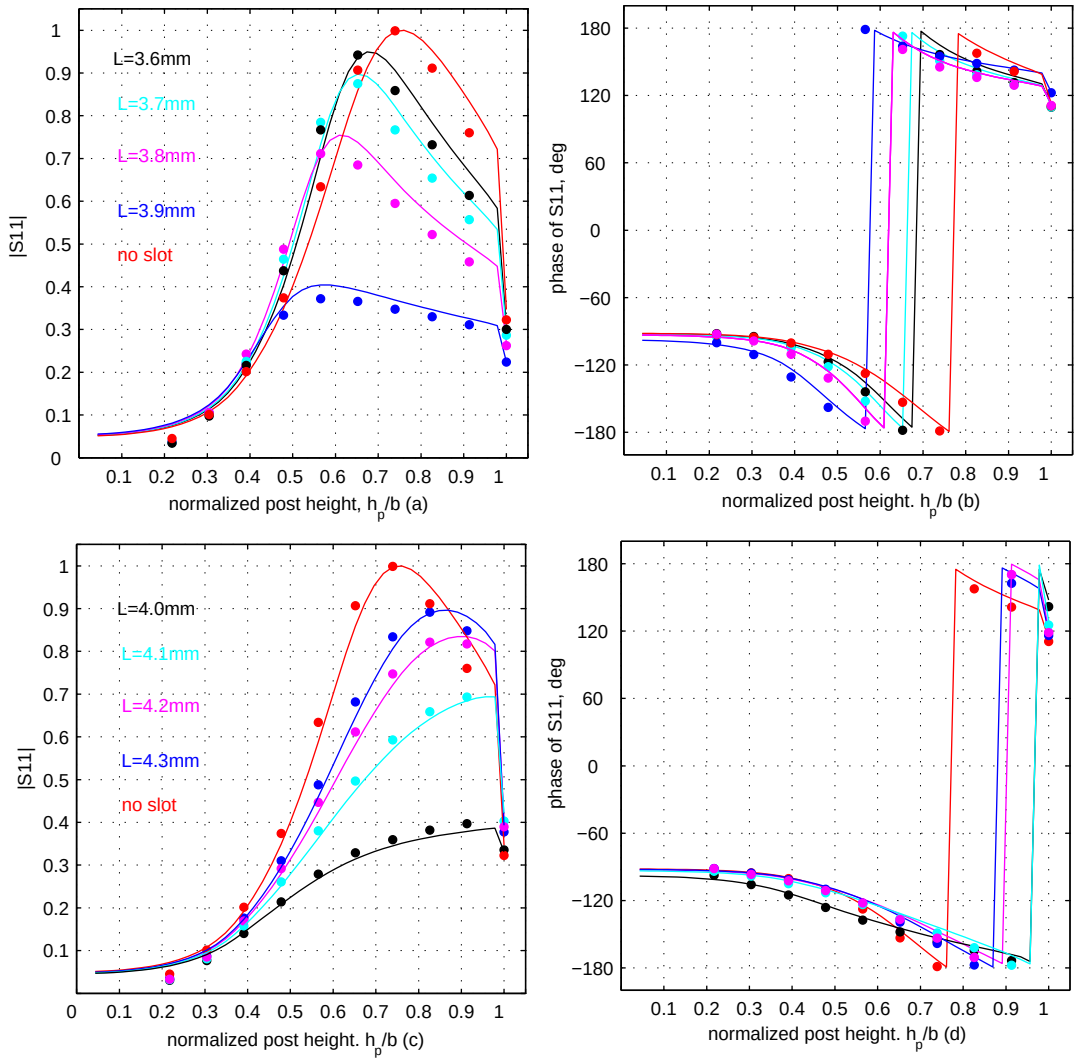

Figure 6.1: Variation of $S11$ with respect to the post height for various slot length values. Solid line: MATLAB, (MPIE method), Points: HFSS, L: slot length
(a),(b): slots shorter than half a wavelength.($f = 38.25GHz$, $\frac{\lambda}{2} = 3.92mm$)
(c),(d): slots longer than half a wavelength.($f = 38.25GHz$, $\frac{\lambda}{2} = 3.92mm$)
aKoM configuration: post radius: 0.3mm, post offset: 1.1mm, slot width: 0.4mm, slot thickness: 1mm

In the diagrams of Figure 6.1, the red curves refer to the case where no slot is present. The reason for including the red curves is the fact that they deviate substantially from the other curves, indicating the significant role of the slot length value in the scattered field inside the ridged waveguide. In the case of a resonating slot (slot length $\approx$ half wavelength), the reflection coefficient $S11$ no longer receives values close to unity. This is a reasonable result, since the magnetic current on the slot aperture introduces an inductive reactance, which partly compensates for the capacitive behavior of the metallic post. Therefore, the total reactance inside the ridged waveguide will be reduced, yielding lower values for the amplitude of $S11$.

Moreover, as the slot length drifts from half a wavelength, the inductive reactance becomes smaller and after a point can be neglected. This behavior is observed in the diagrams of Figure 6.1, where the lines representing non resonant slots tend to approach the red curve (no slot). Consequently, the maximum energy flow from one waveguide to the other takes place in the case of a resonant slot, as can be easily seen by the S31 curves that are presented in Figure 6.2. In both Figures the

computed data (MATLAB) exhibit good agreement with the HFSS-simulation results.

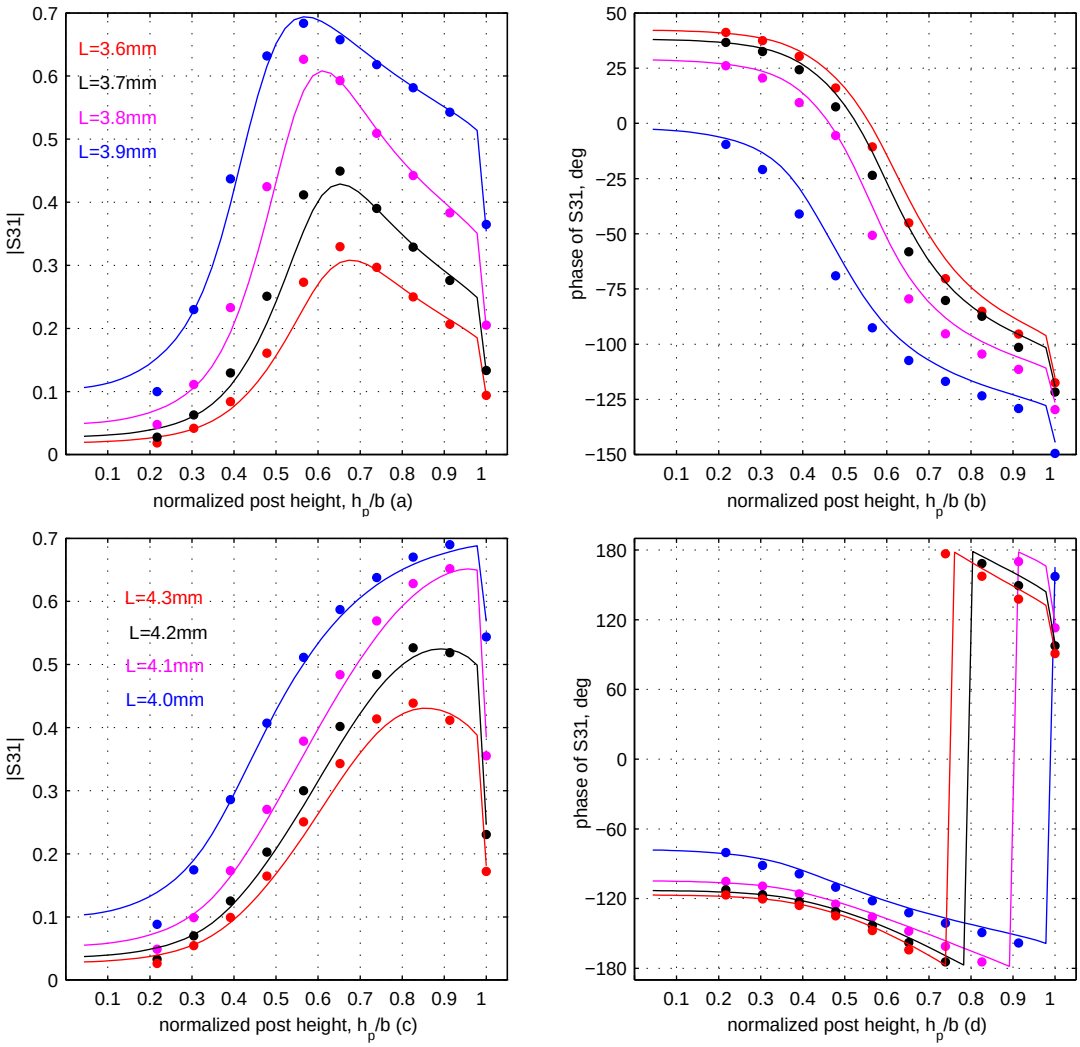

Figure 6.2: Variation of $S31$ with respect to the post height for various slot length values. Solid line: MATLAB, (MPIE method), Points: HFSS, L: slot length.
(a),(b): slots shorter than half a wavelength.($f = 38.25GHz$, $\frac{\lambda}{2} = 3.92mm$)
(c),(d): slots longer than half a wavelength.($f = 38.25GHz$, $\frac{\lambda}{2} = 3.92mm$)
aKoM configuration: post radius: 0.3mm, post offset: 1.1mm, slot width: 0.4mm, slot thickness: 1mm

Since the amplitude of $S11$ never equals unity in the presence of a coupling slot, the resonant post height or the resonant frequency can not be defined according to the classical manner [23], [8] for the 'aKoM' case. Likewise, the typical definition of the resonant slot length based on the backscattering or the forward scattering off the slot [105]-[108], may not be directly applied to the 'aKoM' configuration, because the scattered TE_{10} mode is induced by the post and not by the slot. Consequently, it would only make sense to try and determine pairs of values for the slot length and the post height, which provide resonance characteristics to the structure. A typical example of such data is presented in Figure 6.3. At this point it should be stated that, since both backward and forward scattered TE_{10} field inside the ridged waveguide can be computed, in some cases the resonant pairs are determined according to both definitions. However, the determination based on the backscattered wave phase is preferred for most of the computations in the proceeding sections. All these definitions apply in the case where only one ridged waveguide port is excited. Alternatively, resonant pairs may be determined, if only the rectangular waveguide port is excited and the ridged

waveguide ports are considered to be terminated with matched load. Specific diagrams of this kind will not be presented in the current work, since it is possible to recognize these resonances from other provided diagrams.

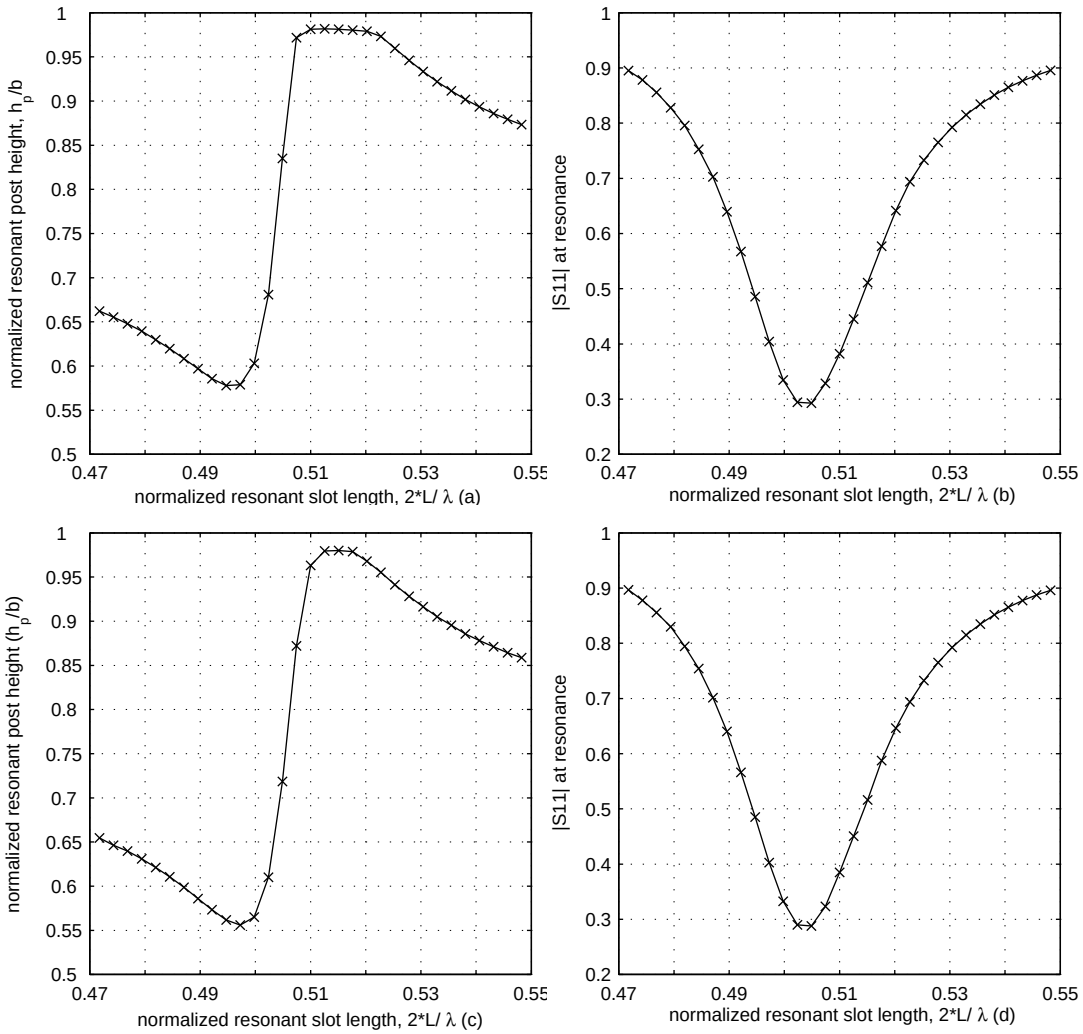

Figure 6.3: (a) Variation of resonant post height with resonant slot length (back-scattered field).
(b) Variation of $|S11|$ at resonance with resonant slot length (back-scattered field).
(c) Variation of resonant post height with resonant slot length (forward-scattered field).
(d) Variation of $|S11|$ at resonance with resonant slot length (forward-scattered field).
MATLAB: Post radius: 0.3mm, post offset:1.1, slot width:0.4mm, slot thickness:1mm, frequency:38.25GHz.

Figures 6.3(a) and (b) show the pairs of post height and slot length for which the backscattered TE_{10} mode is out of phase with the incident TE_{10} mode at level $z = 0$. The condition for the computation of the last two diagrams was the 180 degrees phase difference between the forward scattered TE_{10} mode and the incident TE_{10} mode at level $z = 0$. Comparison between Figure 6.3(a) and Figure 6.3(c) shows that the different definitions of resonance do not significantly alter the values of the resonant pairs. The curves of Figure 6.3(b) and Figure 6.3(d) are practically identical. These diagrams suggest that for the given geometrical dimensions, the discontinuities inside the waveguide may be represented by a nearly perfect shunt element [107].

A first comment on Figures 6.3(a) and (c) is the relatively limited range of post height values, that allow resonance. A similar restriction does not apply to the slot length, as long as it varies between 0.47λ and 0.55λ. For the specific configuration, resonance is possible only if the post height values

vary between $0.57b$ and $0.983b$ (back-scattered field) or $0.556b$ and $0.979b$ (forward-scattered field). The reason for this is related to the special characteristics of the "aKoM" configuration: The slot is excited by the evanescent even TE modes that are generated by the post. When the post is quite short these modes are too weak to generate a substantial electric field on the slot aperture. Therefore, the presence of the slot in case of posts shorter than $0.3b$ barely has an impact on $S11$, as depicted in Figure 6.1. As the post height increases, the scattered field due to the evanescent even TE modes is intensified and couples more vividly with the slot. Beyond a certain post height value the proper conditions for resonance are met. These conditions are eliminated, once the post height value approximates the ridged waveguide height. In this case the post alone would represent an inductive obstacle inside the ridged waveguide, as shown by Figure 6.1(b) or Figure 6.1(d). Thereafter, both ridged waveguide discontinuities produce inductive reactance, thus not allowing the imaginary part of the reflection or the transmission coefficient to equal zero. The upper and lower limits of the post height values, beyond which resonance is no longer possible, depend mainly on the post dimensions. This issue will be discussed later on in this chapter. However, at this point it could be interesting to examine the following diagram:

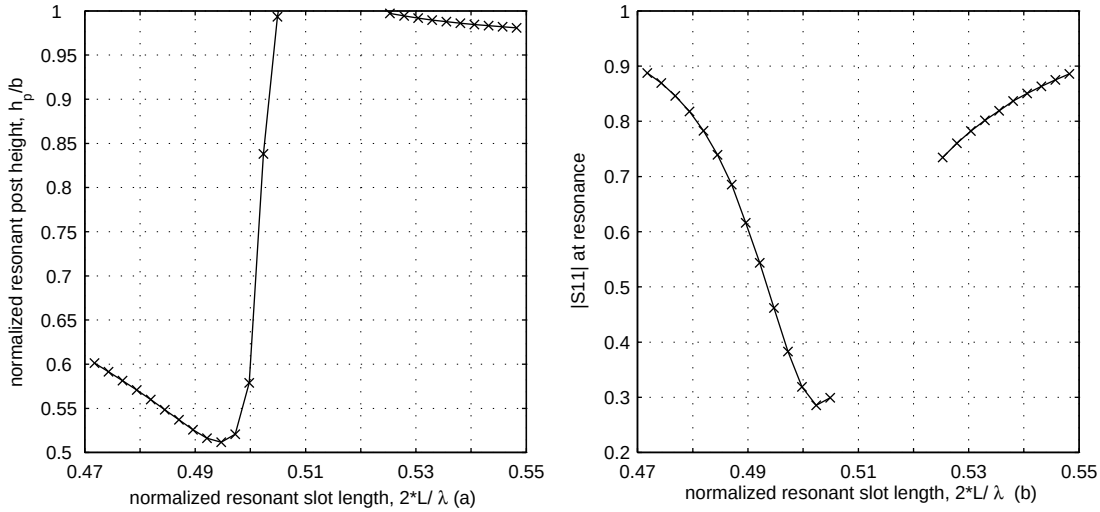

Figure 6.4: (a) Variation of resonant post height with resonant slot length (back-scattered field). (b) Variation of $|S11|$ at resonance with resonant slot length (back-scattered field). MATLAB: Post radius: 0.5mm, post offset:1.1, slot width:0.4mm, slot thickness:1mm, frequency:38.25GHz.

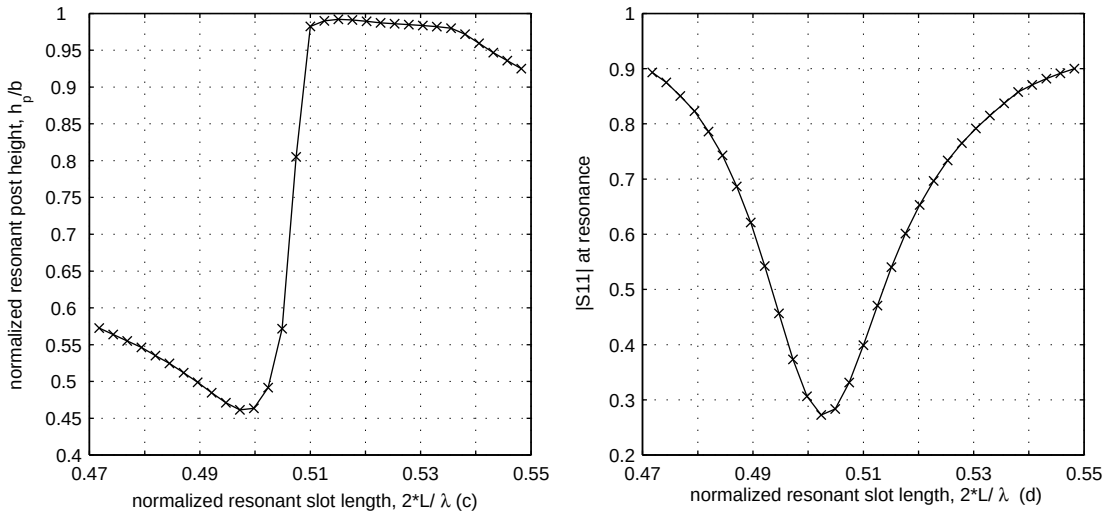

Figure 6.4: (c) Variation of resonant post height with resonant slot length (forward-scattered field). (d) Variation of $|S11|$ at resonance with resonant slot length (forward-scattered field). MATLAB: Post radius: 0.5mm, post offset:1.1mm, slot width:0.4mm, slot thickness:1mm, frequency:38.25GHz.

Contrary to the diagrams of Figure 6.3(a) and (b), the curves of Figures 6.4(a) and (b) are "interrupted" for the slot length range: $[0.505\lambda..0.524\lambda]$. For these values resonance is not possible at frequency 38.25GHz, according to the back-scattered wave definition. This is not the case for the forward-scattered wave definition, where the curves are continuous throughout the entire resonant slot length range, indicating that resonance is always reached. According to Figure 6.4(c), the normalized resonant post height values lie close to unity for the range of resonant slot length, for which resonance based on backscattered wave is not possible. From the above results, it becomes clear that the interaction between a thick post (Figure 6.4) and the slot can no longer be represented by a shunt element inside the waveguide, especially when the slot length receives values greater than 0.49λ.

As the post height transcends the threshold for resonance, there exists a certain range of values, where the post height is combined with only one slot length value and yield resonant characteristics to the structure. According to Figure 6.3(a) this range extends from $0.663b$ to $0.883b$ (approximately 53% of the entire resonance range) for this specific structure. Similar results are obtained by Figure 6.3(c): post height values from $0.655b$ to $0.86b$ (48% of the resonance range) match with only one slot length at resonance. The corresponding slot length values are slightly greater than half the wavelength and range from 0.5017λ to 0.5055λ (Figure 6.3(a)) or between 0.5036λ and 0.5072λ (Figure 6.3(c)). Both Figures 6.3(a) and (c) demonstrate the increased sensitivity of the resonant post height against slight variations of the resonant slot length, when the latter lies in this narrow range. For those pairs the amplitude of $S11$ at resonance reaches its lowest possible values, as shown in Figure 6.3(b) or Figure 6.3(d).

Post height values outside the above ranges may be combined with two different slot length values and achieve resonance. However, the $|S11|$ values are different for each of these pairs, as seen by Figures 6.3(b) and (d). This effect is demonstrated at a greater detail in Figures 6.5 and 6.6. Each diagram in those Figures presents the variation of every S-parameter amplitude with post height for two slot length values that combine with the same post height value at resonance, based on backscattered field definition. Figure 6.5 depicts the S parameters for slot lengths 3.86mm (0.49215λ) and 3.91mm (0.49853λ). In this case, resonance is achieved when the post height becomes 1.35mm ($0.5869b$). The electric current distribution at resonance is illustrated in Figure 6.6 for each slot length . The curves of Figure 6.7 are computed for slot lengths: 4mm (0.51λ)

and 4.1mm (0.52275λ). The resonant post height for these slot length values is 2.25mm (0.9913b). Figure 6.8 presents the corresponding electric current distributions.

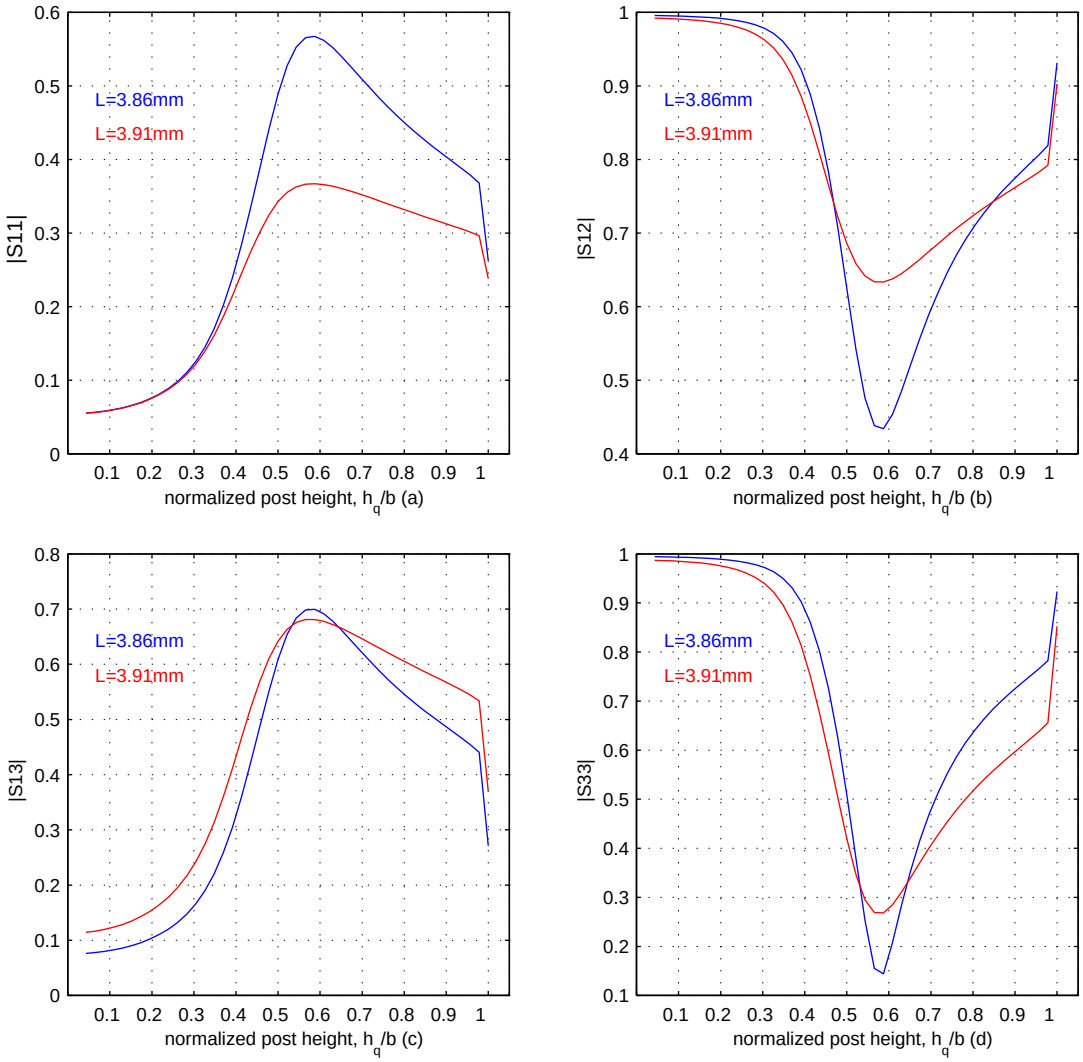

Figure 6.5: Variation of $|S11|$, $|S12|$, $|S31|$ and $|S33|$ with post height for slots shorter than 0.5λ. MATLAB: Post radius: 0.3mm, post offset:1.1, slot width:0.4mm, slot thickness:1mm

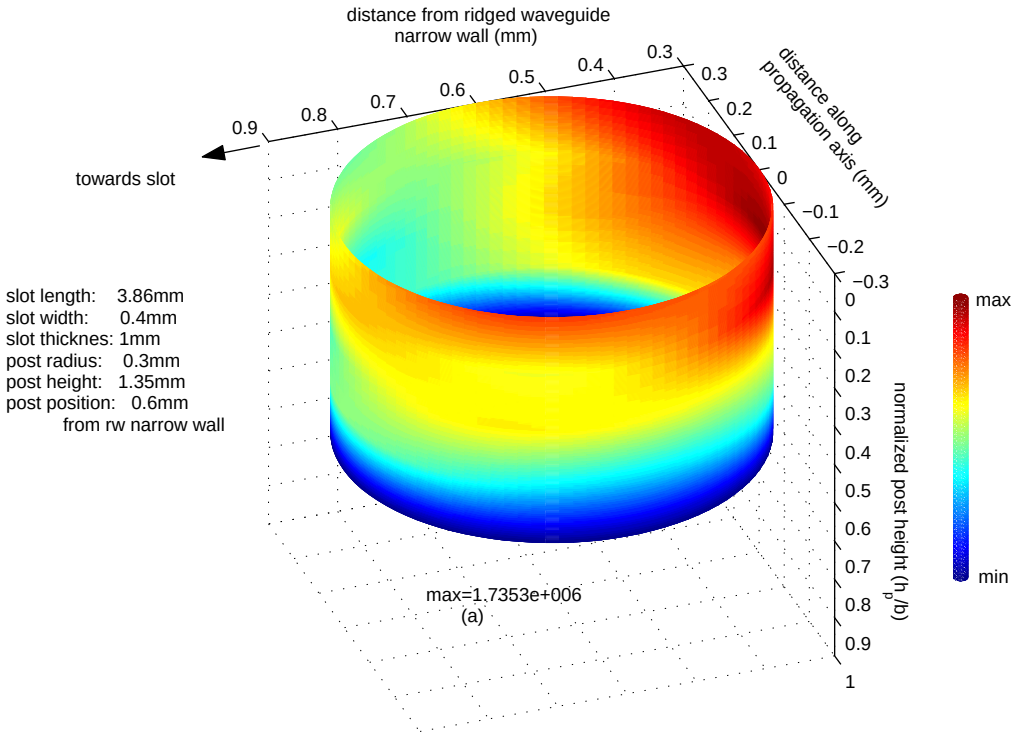

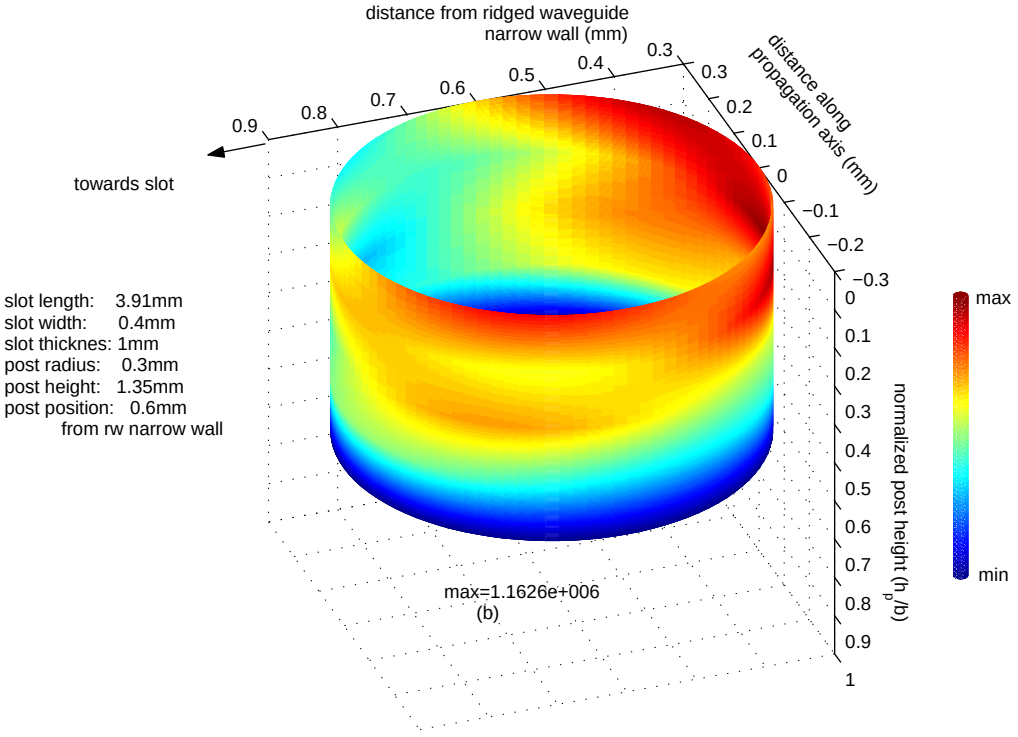

Figure 6.6: Electric current distribution across the post surface at resonance for slots shorter than 0.5λ. MATLAB.

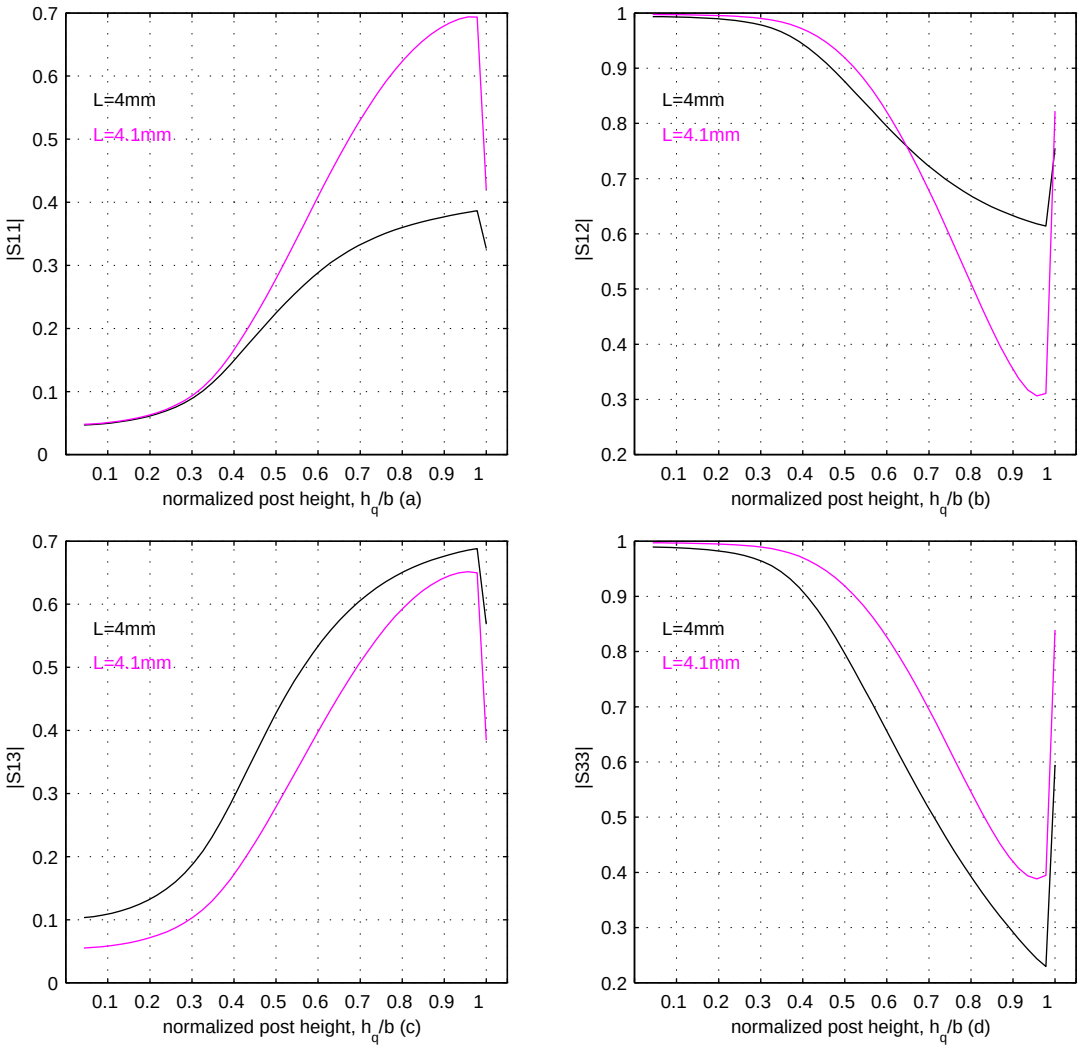

Figure 6.7: Variation of $|S11|$, $|S12|$, $|S31|$ and $|S33|$ with post height for slots longer than 0.5λ. MATLAB: Post radius: 0.3mm, post offset:1.1, slot width:0.4mm, slot thickness:1mm

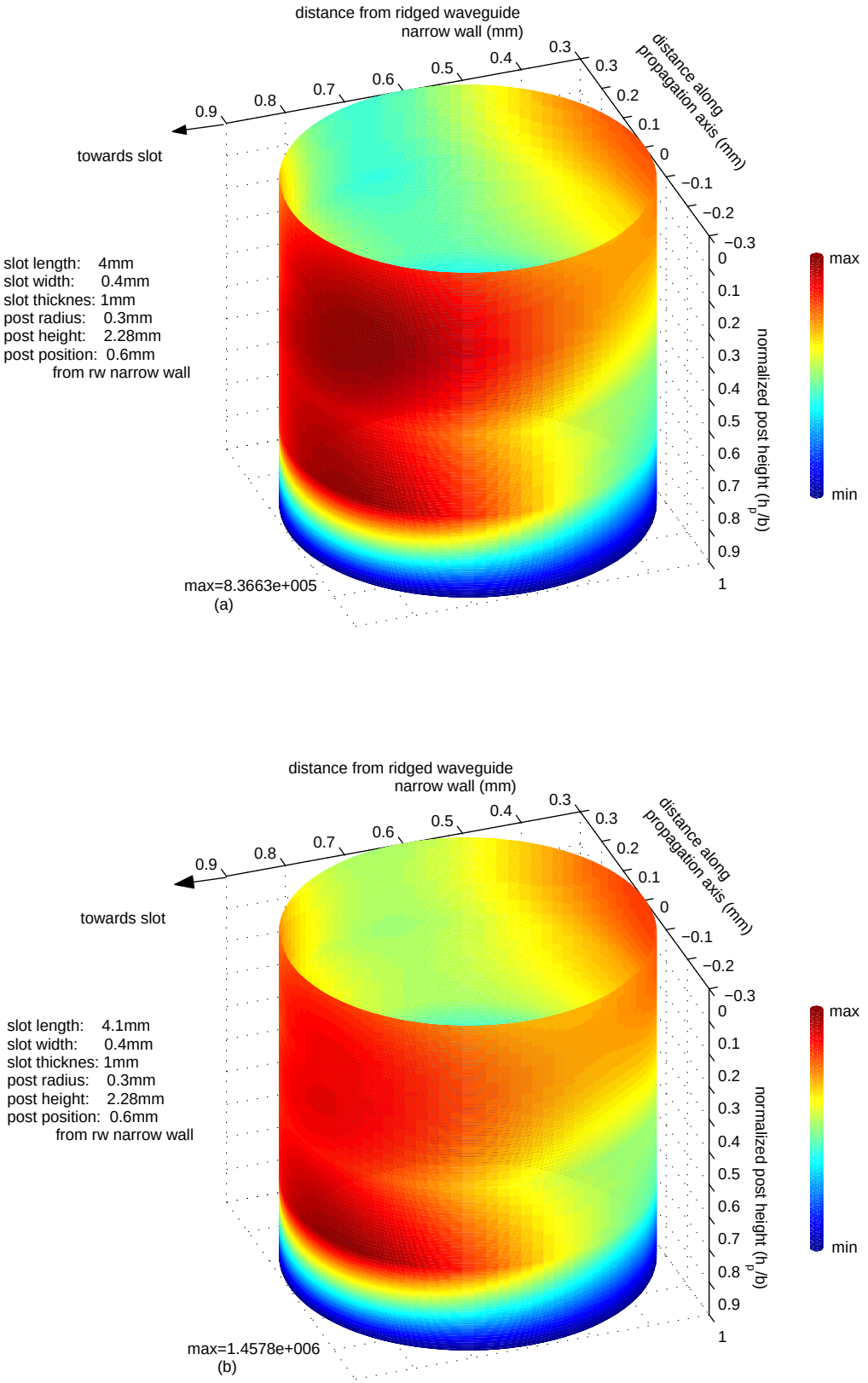

Figure 6.8: Electric current distribution across the post surface at resonance for slots longer than 0.5λ. MATLAB.

The first comment on these diagrams is that at resonance the amplitudes of $S11$ and $S12$ receive their maximum and minimum values respectively. This is consistent with the definition of the

resonant post height. Furthermore, the values of $|S13|$ and $|S33|$ reach their maximum and minimum respectively at resonance. This is also consistent with the definition of the resonant slot length. Figure 6.6 states that the electric surface current receives its highest values at the side of the post, which is closer to the waveguide narrow wall, while it becomes quite weak at the side closer to the slot. Figure 6.8 demonstrates the exact opposite behavior. Even though the currrent distributions are very similar for each resonant pair, the maximum current values are increased as the slot length approaches 0.5λ. In that case also the values of $|S11|$ or $|S12|$ at resonance exhibit substantial decrease or increase correspondingly. The amplitude of $|S13|$ appears to be less affected by the different slot length values, indicating that the energy flow from the ridged to the rectangular waveguide and vice versa at resonance is more or less the same for any resonant pair of post height and slot length. Likewise, the values of $|S33|$ at resonance do not present as great a dependency as the $|S11|$ or $|S12|$ values on the slot length. The loose dependency between resonant slot length and $|S13|$ or $|S33|$ may yield certain degrees of freedom at the design of similar configurations, especially when more attention is paid to the coupling between the two waveguides and the matching of the ridged waveguide is of secondary role. However, this dependency will become more intense, if the slot length value deviates significantly from the half wavelength. In such a case, the value of $|S13|$ is decreasing, as also depicted in Figure 6.2, indicating that negligible or no coupling between the two waveguides takes place.

6.2 Slot width

In the analysis of Chapter 3 the assumption was made that the magnetic current consists of only one longitudinal component that, additionally, does not vary with the slot width, because the latter is considerably smaller than the slot length. However, it could be of interest to examine, if and how the variations on the slot width may affect the overall performance of the structure. The below diagrams demonstrate the variation of the S parameters with frequency for different values of slot width. The post dimensions, the slot length and the slot thickness are kept constant. The phases of all S parameters have been computed at a distance: $\frac{\lambda_{wg}}{2}$ from the waveguide discontinuities, where $\lambda_{wg} = \frac{2\pi}{\gamma_{wg}}$.

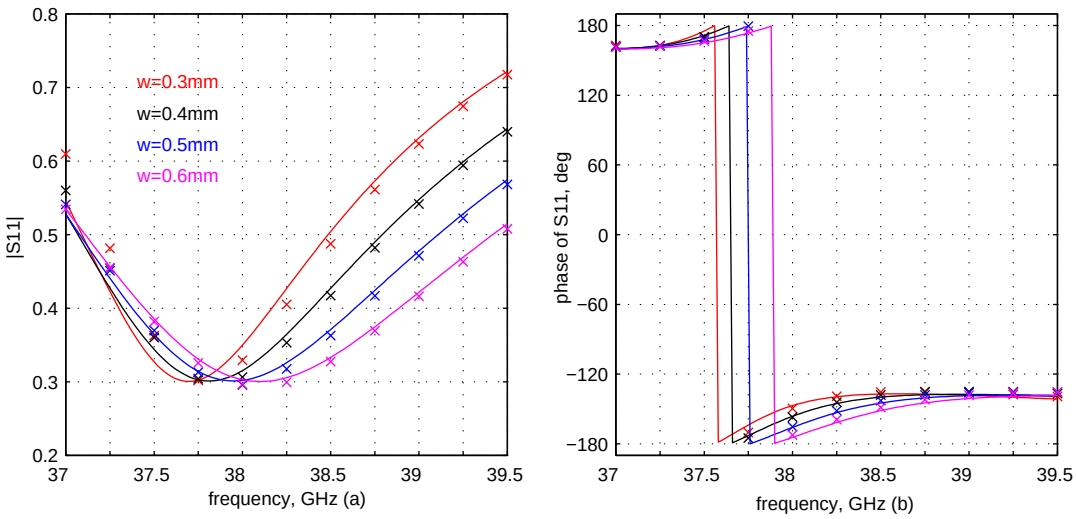

Figure 6.9: Variation of S parameters with respect to frequency for various values of slot width (w). Post radius:0.5mm, post offset: 1.1mm, post height:1.5mm, slot length: 4mm, slot thickness:1mm. Solid line: HFSS, Points: MATLAB.

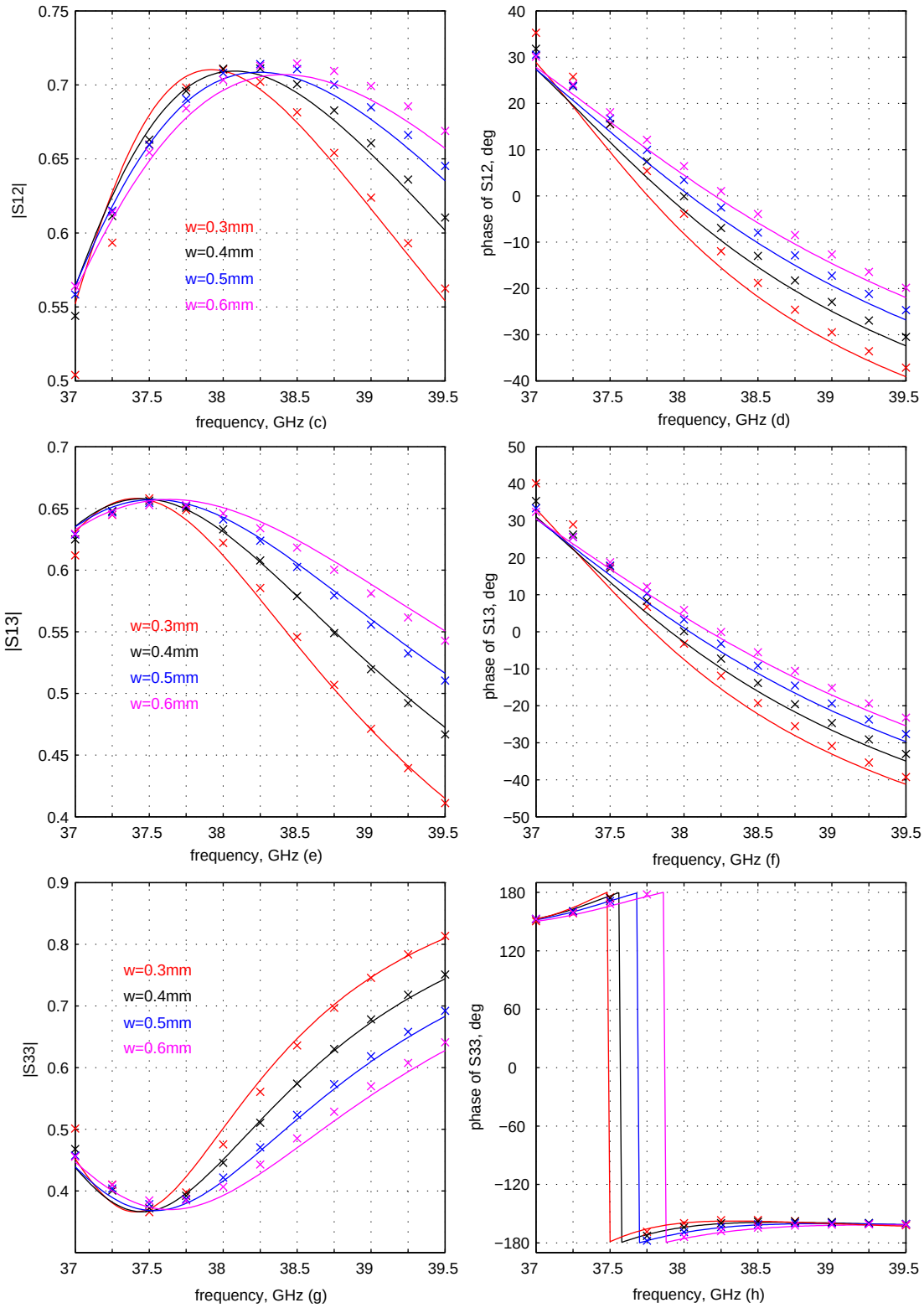

Figure 6.9: Variation of S parameters with respect to frequency for various values of slot width (w). Post radius:0.5mm, post offset: 1.1mm, post height:1.5mm, slot length: 4mm, slot thickness:1mm. Solid line: HFSS, Points: MATLAB.

Figure 6.9 suggests that there is a relatively limited impact of the slot width value on the frequency variation of the S parameters at the lower frequencies. A first remark on the above graphs is the slightly greater bandwidth that is allowed by the wider slots. This observation becomes more apparent in the $|S13|$ and $|S13|$ curves, where the values almost coincide at the lower frequencies and deviate substantially from each other at frequencies close to 39.5GHz. The wider slots exhibit smaller phase variation around and off-resonance. Similar characteristic is observed at any offset longitudinal slot that couples two waveguides [107].

The curves representing the amplitudes of the S parameters exhibit very slight 'shifts' to higher frequencies as the slot width increases, but their minimum ($|S11|$ and $|S33|$) or maximum ($|S12|$ and $|S13|$) values are not changed. The frequency shifts, especially in the phases of $S11$ and $S33$ for the wider slots, indicate that the specific slot length and post height values (0.51λ and 0.65217b respectively) combine and yield resonant characteristics at higher frequencies. This conclusion emerges also from Figure 6.10, which presents the effect of the slot width on the resonant behavior of the structure. The diagrams have been computed at frequency 38.25 GHz.

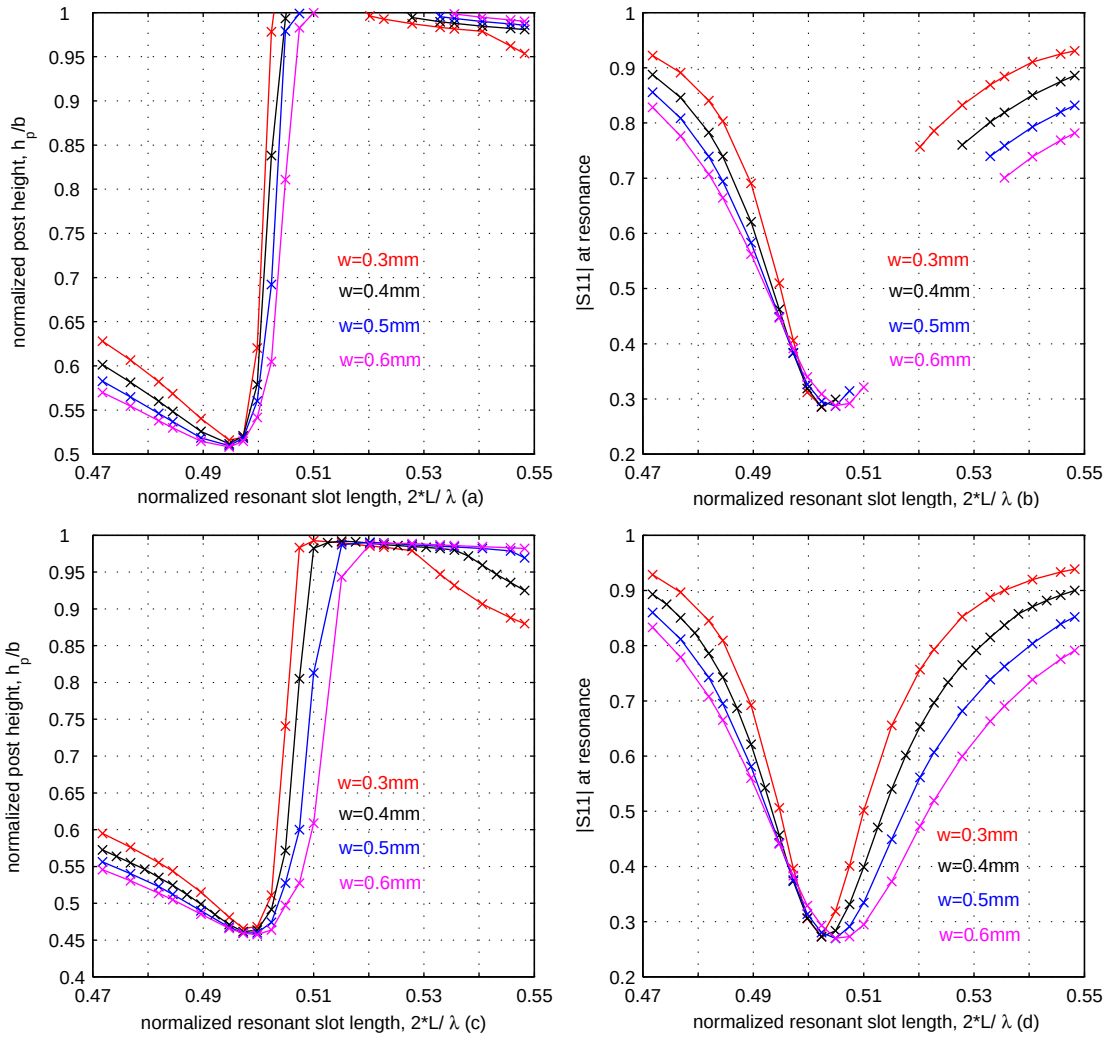

Figure 6.10: Impact of slot width on resonance slot length and post height.
(a) Variation of resonant post height with resonant slot length, backward scattered wave.
(b) Variation of $|S11|$ at resonance with resonant slot length, backward scattered wave.
(c) Variation of resonant post height with resonant slot length, forward scattered wave.
(d) Variation of $|S11|$ at resonance with resonant slot length, forward scattered wave.
MATLAB: Post radius: 0.5mm, post offset:1.1, slot thickness:1mm, frequency:38.25GHz

According to Figures 6.10(a) and (c) the variation in the slot width does not modify the threshold for the resonant post height and also has no effect on the corresponding length value of the resonant slot. Even though the slot width has no impact at the range of resonant post height values, its reduction causes the limitation of the values that uniquely combine with one slot length at resonance. Based on backscattered wave definition, these values occupy 67% of the entire resonant height range for slot width 0.3mm, while this percentage becomes 85.5% at slot width: 0.6mm. The corresponding percentages for the forward-scattered wave definition are 54% at slot width 0.3mm against 82% for slot width 0.6mm. While the post receives values within these ranges, the thicker slots cause the slight shift of the resonant length towards higher values, which is in agreement with the results of Figure 6.9(b). This behavior is also typical for structures consisting of two rectangular waveguides that are coupled via a longitudinal slot [107].

Like the results of Figure 6.4, the curves of Figure 6.10 have been computed for post height radius 0.5mm. Therefore, there is a region of normalized slot length values, for which resonance according to the backscattered wave definition can not be achieved for any post height value. These regions become larger and are shifted towards greater slot length values as the slot width increases. When the slot length receives greater values, resonance is possible again for large values of post height. In this case the resonant post height decreases slower for thicker posts.

In general, the thinner slots introduce an increased sensitivity of the resonant post height against the resonant slot length. In case of thinner posts, slight changes in the resonant length trigger more acute changes in the post height, especially when the latter lies in the range of values that match to only one resonant slot length. Similar observation can be made on the impact of slot width on $|S11|$ at resonance as depicted in Figures 6.10(b) and (d). From these diagrams it becomes clear that the thinner slots produce sharper curves for $|S11|$ at resonance. The minimum values of $|S11|$ however are almost unaffected by the slot width value, which is consistent with the conclusions that were drawn by the amplitude curves of Figure 6.9. Furthermore, these values are slightly shifted to higher normalized resonant slot lengths as the slot width is increased, justifying the small frequency shift that was observed in Figure 6.9(a). As expected, $|S11|$ receives its minimum values at post height values that combine with only one resonant slot length, regardless of the slot width value.

Some of the previous conclusions may be verified by the diagrams of Figure 6.11, which present the variation of S parameters with frequency for two different values of post height and slot width. The amplitude curves of all S parameters are broader and slightly shifted to higher frequencies in the presence of wider slots, like the corresponding curves of Figure 6.9. The data for post height 1.9mm ($0.826b$) confirm the increase of normalized resonant slot length for wider slots, in case the resonant post height matches only one resonant slot length. Post height value 1.1mm ($0.478b$) lies below the threshold for backward-scattered field resonance that applies to this configuration. Hence no such resonance is observed. In case of forward-scattered field resonance however, the post height value 1.1mm is slightly higher than the threshold value of Figure 6.10(c), indicating that resonance is possible for two different values of normalized slot length. This is confirmed by Figure 6.11(d), where the phase of S12, $h_p = 1.1mm$, equals zero at two different frequencies.

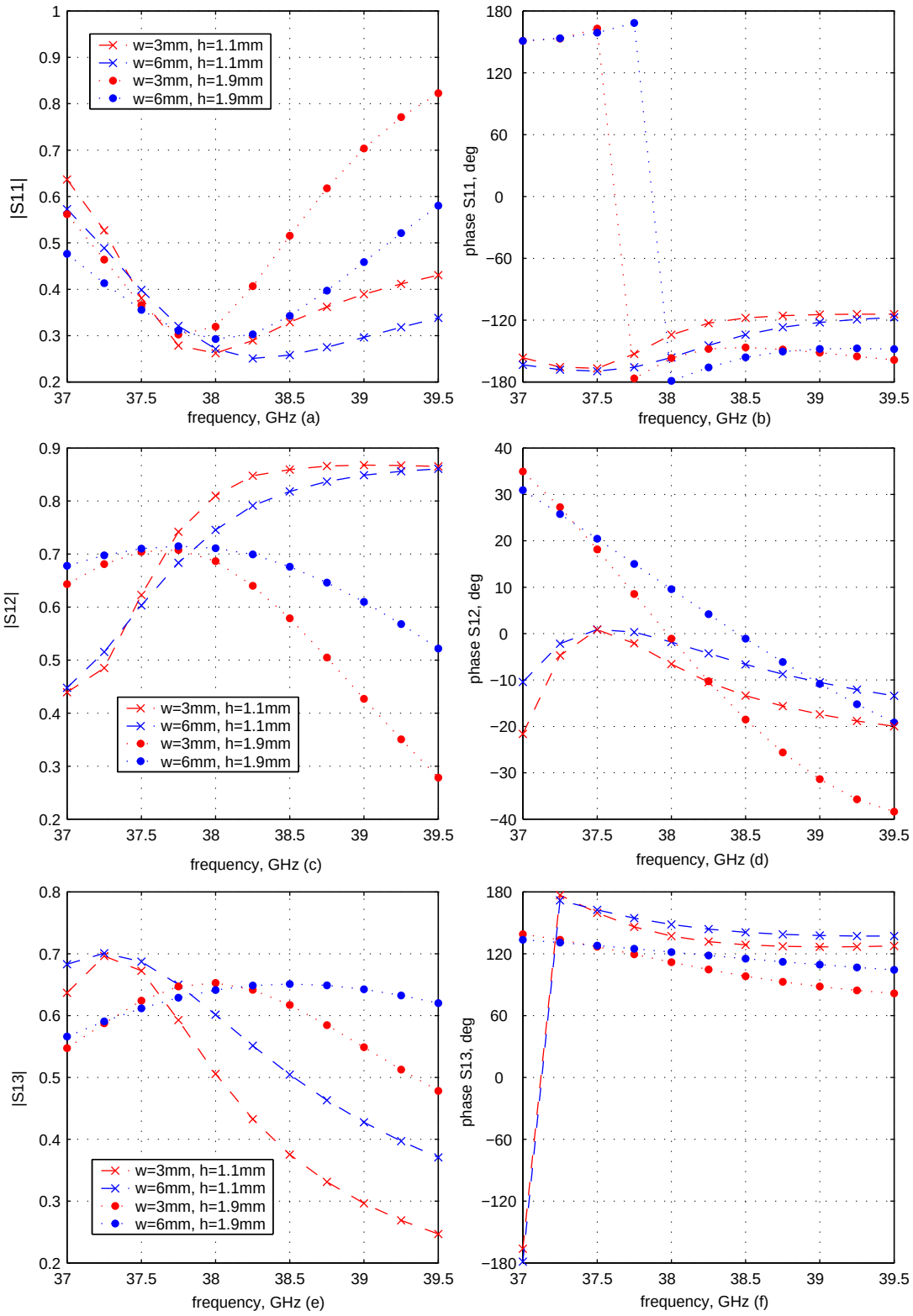

Figure 6.11: Variation of S parameters with respect to frequency for various values of slot width (w) and post height(h). MATLAB, Post radius:0.5mm, post offset: 1.1mm, slot length: 4mm, slot thickness:1mm.

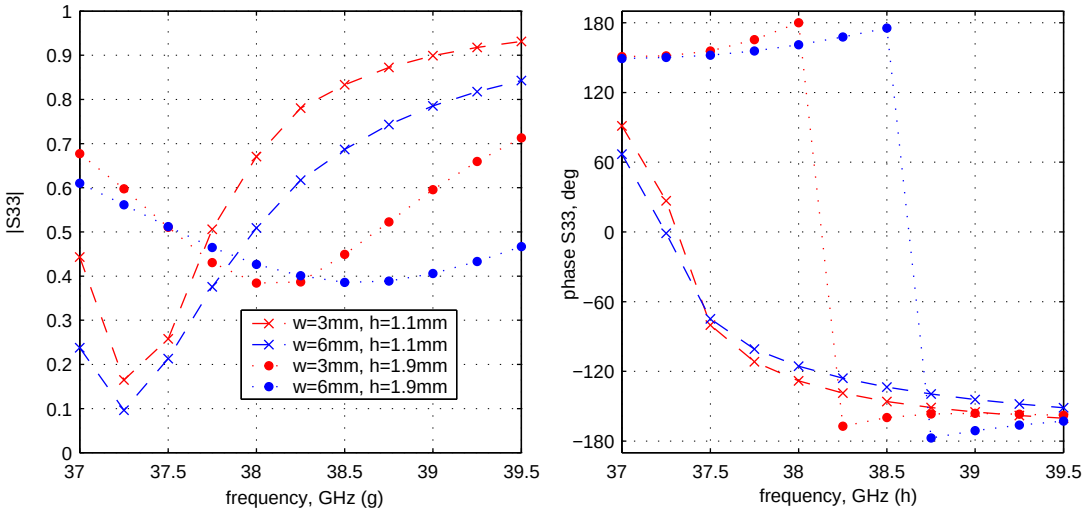

Figure 6.11: Variation of S parameters with respect to frequency for various values of slot width (w) and post height(h). MATLAB, Post radius:0.5mm, post offset: 1.1mm, slot length: 4mm, slot thickness:1mm.

Figure 6.12 concludes the analysis on the effect of slot width on the performance of the structure by presenting the impact of the slot width on the variation of S parameters with post height for constant slot length and frequency. The most obvious observation is the lack of resonance according to backward-scattered field definition in case of thin slots for the specific normalized slot length, as demonstrated by Figure 6.12(b). Only the widest slot (w=0.6mm) can yield resonant characteristics to the structure for the specified frequency (38.25 GHz). The curves of the $S11$ phase are fully consistent with Figure 6.10: ratio $\frac{2*L}{\lambda}$ becomes 0.51 for slot length 4mm and frequency 38.25 GHz. According to Figure 6.10(a), for this slot length value resonance can never be achieved, while the slot width is smaller than 0.6mm. On the other hand, forward-scattered resonance is possible for all slot width values, as depicted by Figure 6.12(d). As anticipated from Figure 6.10(c), for the given normalized slot length the resonant post height value is increased as the slot becomes thinner.

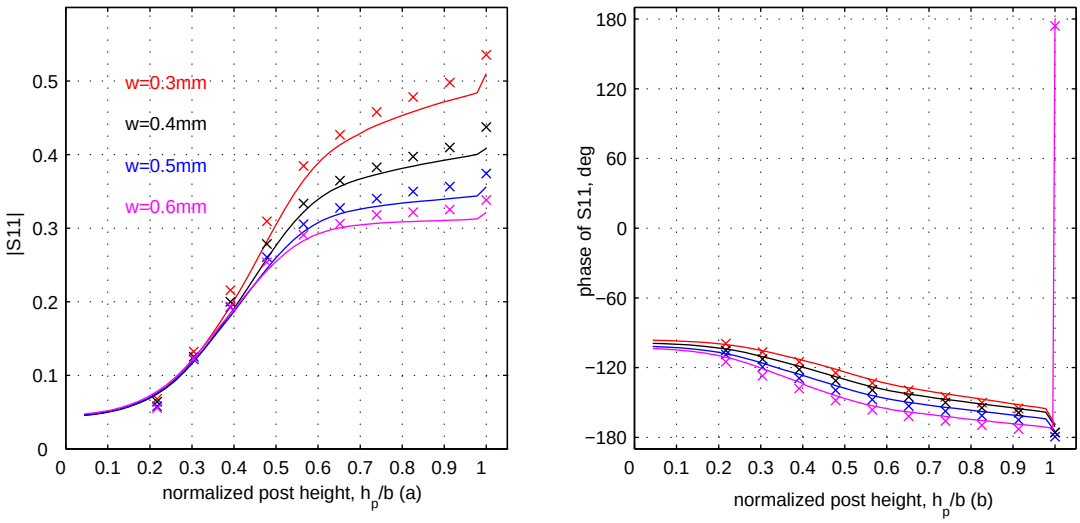

Figure 6.12: Variation of S parameters with the post height for various slot width values. Solid line: MATLAB, (MPIE method), Points: HFSS. Post radius: 0.5mm, post offset: 1.1mm, slot length: 4mm, slot thickness: 1mm, frequency:38.25GHz

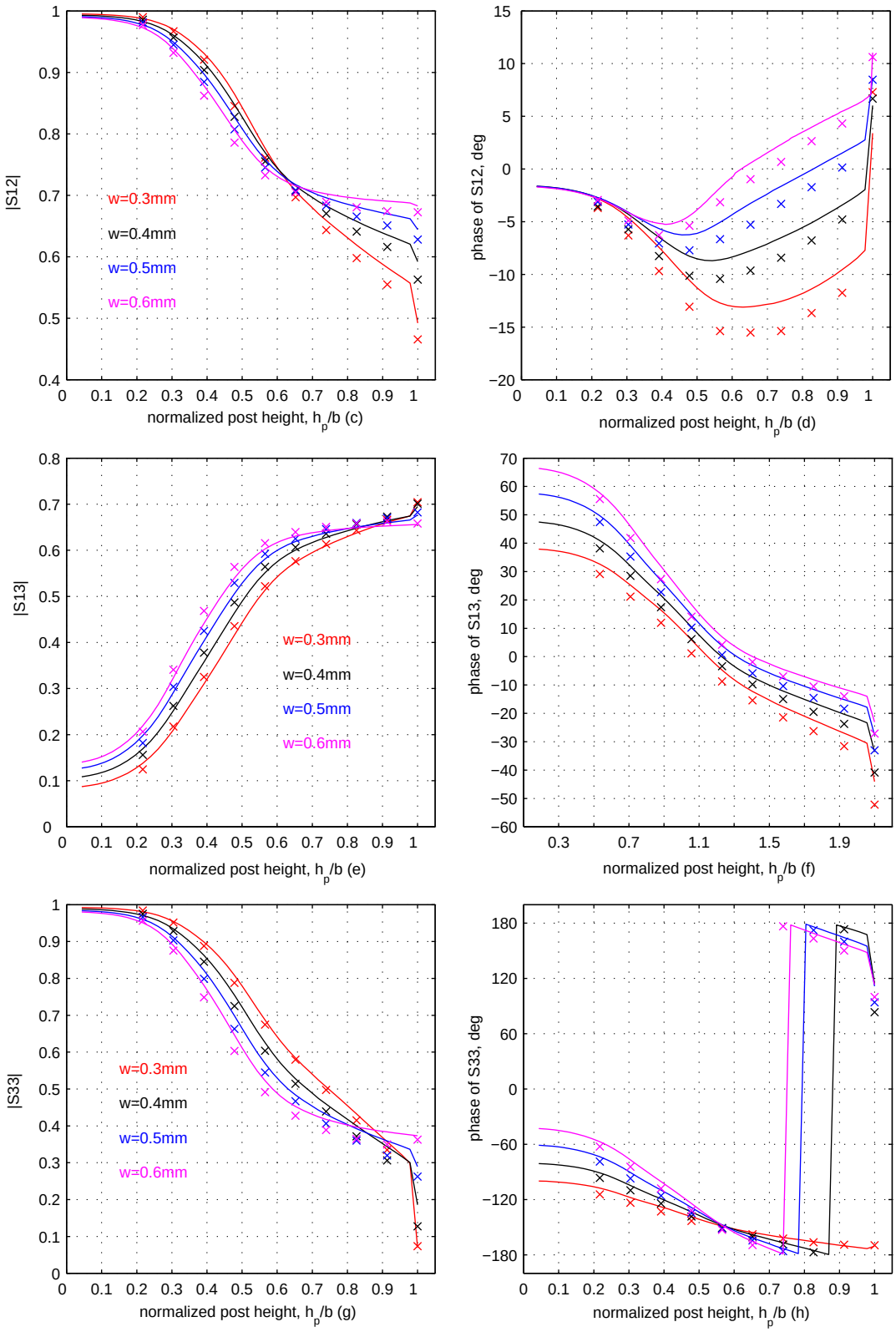

Figure 6.12: Variation of S parameters with the post height for various slot width values. Solid line: MATLAB, (MPIE method), Points: HFSS. Post radius: 0.5mm, post offset: 1.1mm, slot length: 4mm, slot thickness: 1mm, frequency:38.25GHz

The amplitude of S11 decreases as the slot becomes wider and seems to have a greater dependency on the slot width than the amplitude of any other S parameter. Thinner slots cause the amplitudes of S11 and S12 to span over a greater range of values. $|S33|$ and especially $|S13|$ seem to be affected by the slot width value at low or medium values of post height. The coupling is slightly intensified in the presence of a wider slot, as shown by Figure 6.12(e). The impact on slot width on the $|Sx3|$ parameters (x=1,2,3) weakens as the post height receives great values, according to Figure 6.12(e) and Figure 6.12(g), indicating that the energy flow from the ridged to the rectangular waveguide is only slightly dependant on the slot width values in the presence of a long post.

6.3 Slot thickness

Based on the analysis of Chapter 3, it is anticipated that the slot thickness has a greater impact on the system performance than the slot width. The graphs of Figure 6.13 illustrate the effect of the slot thickness on the variation of S parameters with frequency, when the post dimensions, the slot length and width are constant.

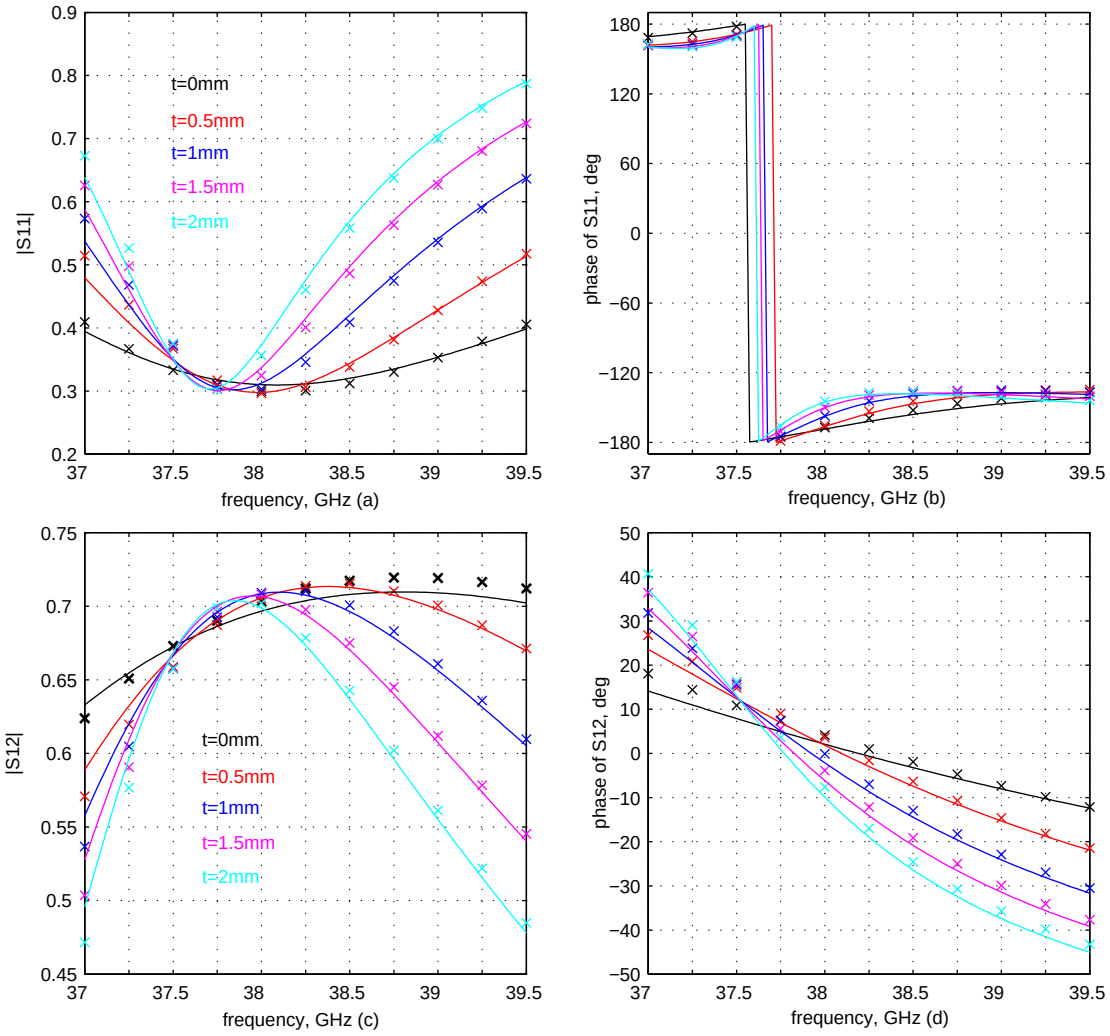

Figure 6.13: Variation of S parameters with respect to frequency for various values of slot thickness (t). Post radius:0.5mm, post offset: 1.1mm, post height:1.5mm, slot length: 4mm, slot width:0.4mm. Solid line: HFSS, Points: MATLAB.

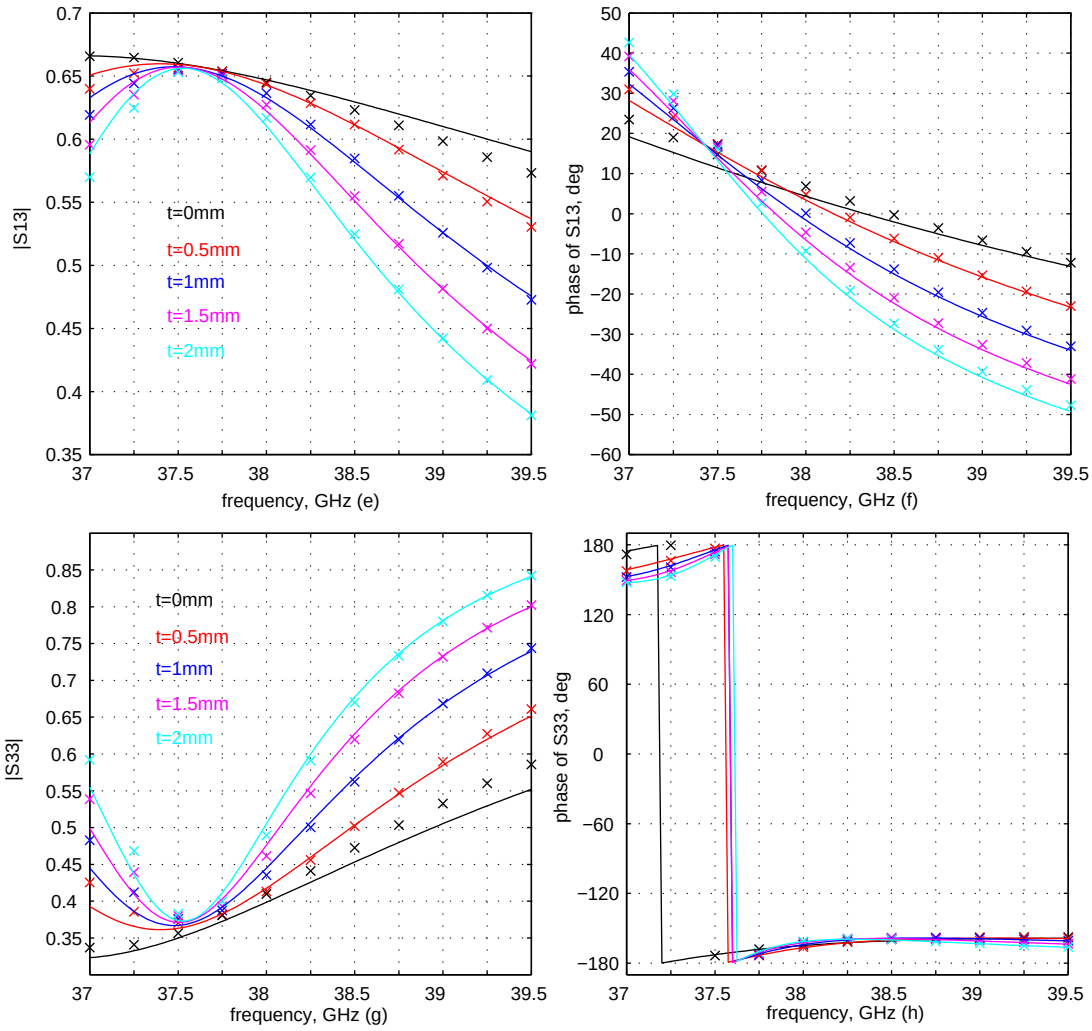

Figure 6.13: Variation of S parameters with respect to frequency for various values of slot thickness (t). Post radius:0.5mm, post offset: 1.1mm, post height:1.5mm, slot length: 4mm, slot width:0.4mm. Solid line: HFSS, Points: MATLAB.

The first conclusion that can be drawn by the diagrams of Figure 6.13 is that slot thickness mostly effects the bandwidth of the structure, whereas the minimum or maximum values of the S parameters exhibit only slight differences. All curves representing the amplitudes of the S parameters become broader as the slot thickness decreases. This behavior is demonstrated to the greatest extend, when the slot thickness is eliminated. In addition, according to Figure 6.13(b) the phase of $S11$ exhibits smaller variation around resonance for thinner slots. These characteristics are consistent with the characteristics of any structure containing a slot coupler between dissimilar waveguides [116], [107], also in the case where the slot is located at the narrow wall of the primary waveguide [109]. The basic deviation from such structures is the lack of major frequency shift in the maximum values of $|S13|$, [116], which can be attributed to the presence of the post. The frequency shifts in the 'aKoM' structure are mostly observed in $|S11|$ or $|S12|$, where the minimum or maximum values respectively are reached at lower frequencies as the slot thickness increases.

A closer observation of Figure 6.13(b) reveals that resonance, based on backward-scattered wave, is slightly shifted to lower frequencies as the slot thickness increases. However, this does not apply to the zero slot thickness case, where resonance is achieved at the lowest frequency. This behavior is validated by the curves of Figure 6.14, where the combination of slot length and post value at

resonance is presented. According to Figure 6.14(a), resonance is reached at a smaller ratio $\frac{2*L}{\lambda}$ for zero slot thickness, when the resonant post height is 1.5mm (0.65217b). For the same post height value, the resonant slot length is only slightly shifted to lower values as the slot thickness increases, which is in agreement with the comment on the curves of Figure 6.13. Additionally, Figure 6.14(c) is consistent with Figure 6.13(d), indicating that resonance according to forward-scattered field at $\frac{h_p}{b} = 0.65217$ is achieved for higher normalized slot length values when the slot thickness decreases.

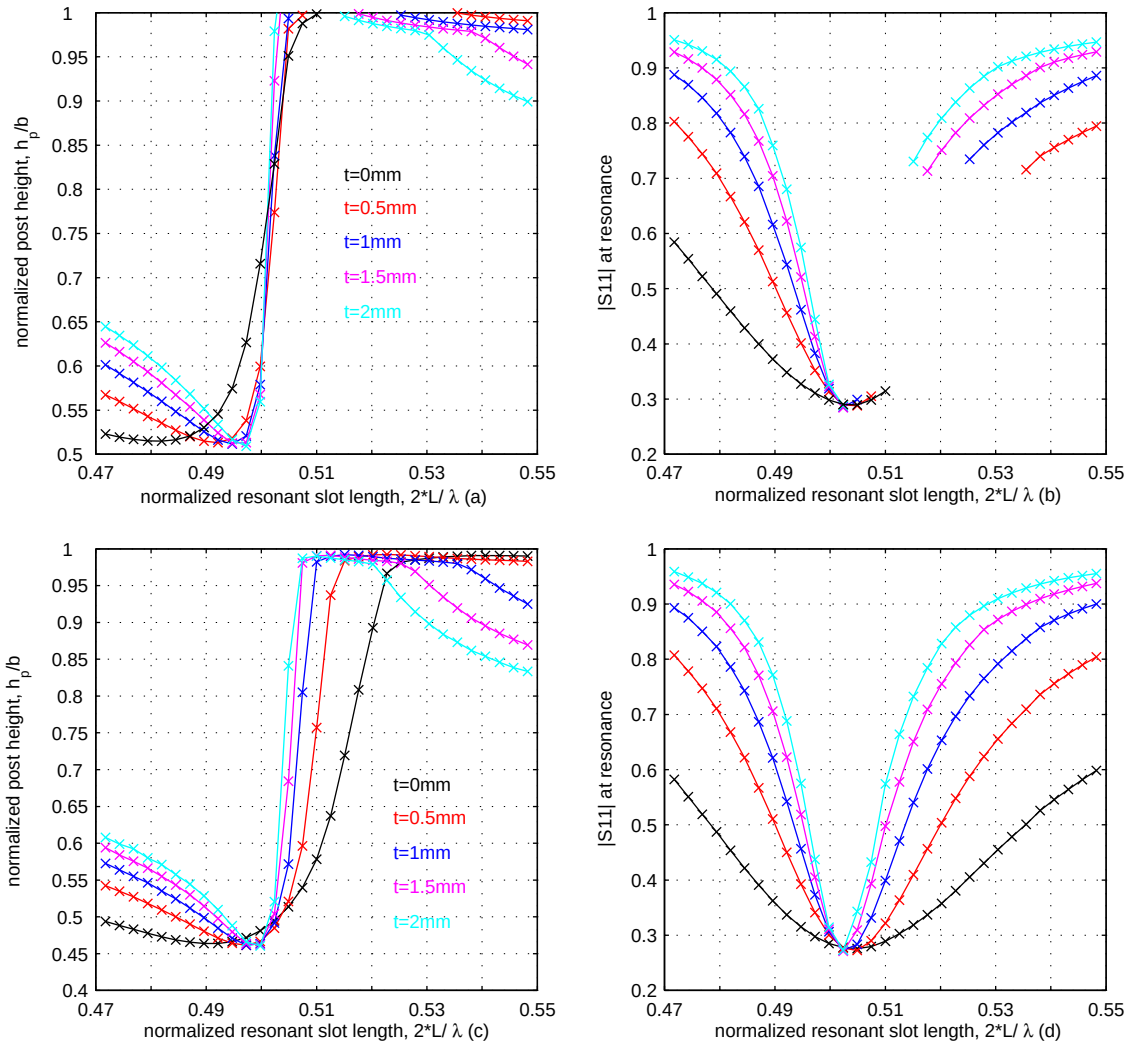

Figure 6.14: Impact of slot thickness on resonance slot length and post height.
(a) Variation of resonant post height with resonant slot length, backward scattered wave.
(b) Variation of $|S11|$ at resonance with resonant slot length, backward scattered wave.
(c) Variation of resonant post height with resonant slot length, forward scattered wave.
(d) Variation of $|S11|$ at resonance with resonant slot length, forward scattered wave.
MATLAB: Post radius: 0.5mm, post offset:1.1, slot width:0.4mm, frequency:38.25GHz

From Figure 6.14(a) and Figure 6.14(c) it becomes clear that the shape of the curve representing the pairs of slot length and post height at resonance is altered when the slot thickness equals zero. In this case, for slot length values varying from 0.47λ to 0.487λ (backward-scattered wave) or between 0.47λ and 0.497λ (forward-scattered wave), the corresponding resonant post height values concentrate in a very small range from 0.514b to 0.523b (backward-scattered wave) or 0.464b to 0.494b (forward-scattered wave), very close to the threshold that allows resonance. For a similar normalized slot length value range (0.47λ to 0.492λ, backward-scattered wave or 0.47λ to 0.497λ,

forward-scattered wave), the resonant post height values are almost linearly decreasing in case of finite slot thickness. The slope of the curves increases for thicker slots. The increased finite wall thickness shifts the resonant slot length to higher values, if $2L < \frac{\lambda}{2}$. Similar dependency of resonant slot length on slot thickness is also verified at any structure containing two dissimilar waveguides coupled via an offset longitudinal slot [100], [107].

When the slot thickness equals zero, the post height values, that combine with only one slot length at resonance, lie inside a great range, which in this case spans between $0.523b$ and b (backward-scattered field) or $0.494b$ and $0.99b$ (forward-scattered field). Resonance according to backward scattered field is not possible for normalized slot length values inside the range $[0.5102, 0.55]$, but it will be observed again at greater values of slot length, which extend beyond the range of Figure 6.14(a). When the slot becomes thicker, then this range of normalized slot length values is significantly reduced, as shown in Figure 6.14(a). The range of unique pairs at resonance is considerably reduced as the slot thickness increases: 87% (backward-scattered field) or 0.83% (forward-scattered field) of the entire resonant post height range for slot thickness 0.5mm against 52% (backward-scattered field) or 0.426% (forward-scattered field) when slot thickness equals 2mm. The corresponding resonant slot length range is also shrunk for thicker slots. Especially, in the case of slot thickness 2mm, Figure 6.14(a), this range is practically narrowed down to an extremely small area around value 0.501λ. The performance of such a structure is very sensitive to any slight variations in the resonant slot length. This increased sensitivity may account for the acute sharpness of those curves in Figure 6.13, Figure 6.14(b) and Figure 6.14(d) that represent slot thickness 2mm. $|S11|$ at resonance receives lower values as the slot thickness decreases for almost all the resonant pairs of slot length and post height. This behavior deviates substantially from the behavior of a typical slot coupler structure, where the backscattered $|S11|$ is independent on the slot thickness [107]. The exception is a small range around the minimum value of $|S11|$, where $|S11|$ is practically insensitive to the slot thickness. These values are reached, when the resonant post height is matched to only one resonant slot length.

The curves of Figure 6.15 present the variation of S parameters with respect to frequency for different values of post height and slot thickness. The remaining geometrical dimensions as well as the frequency are constant:

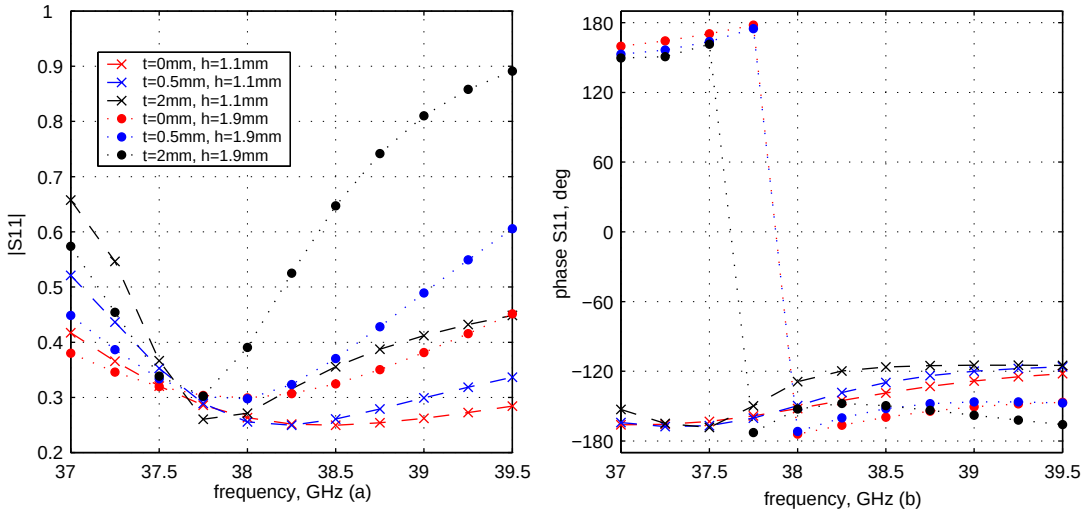

Figure 6.15: Variation of S parameters with respect to frequency for various values of slot thickness (t) and post height(h). MATLAB, Post radius:0.5mm, post offset: 1.1mm, slot length: 4mm, slot width:0.4mm, frequency:38.25GHz.

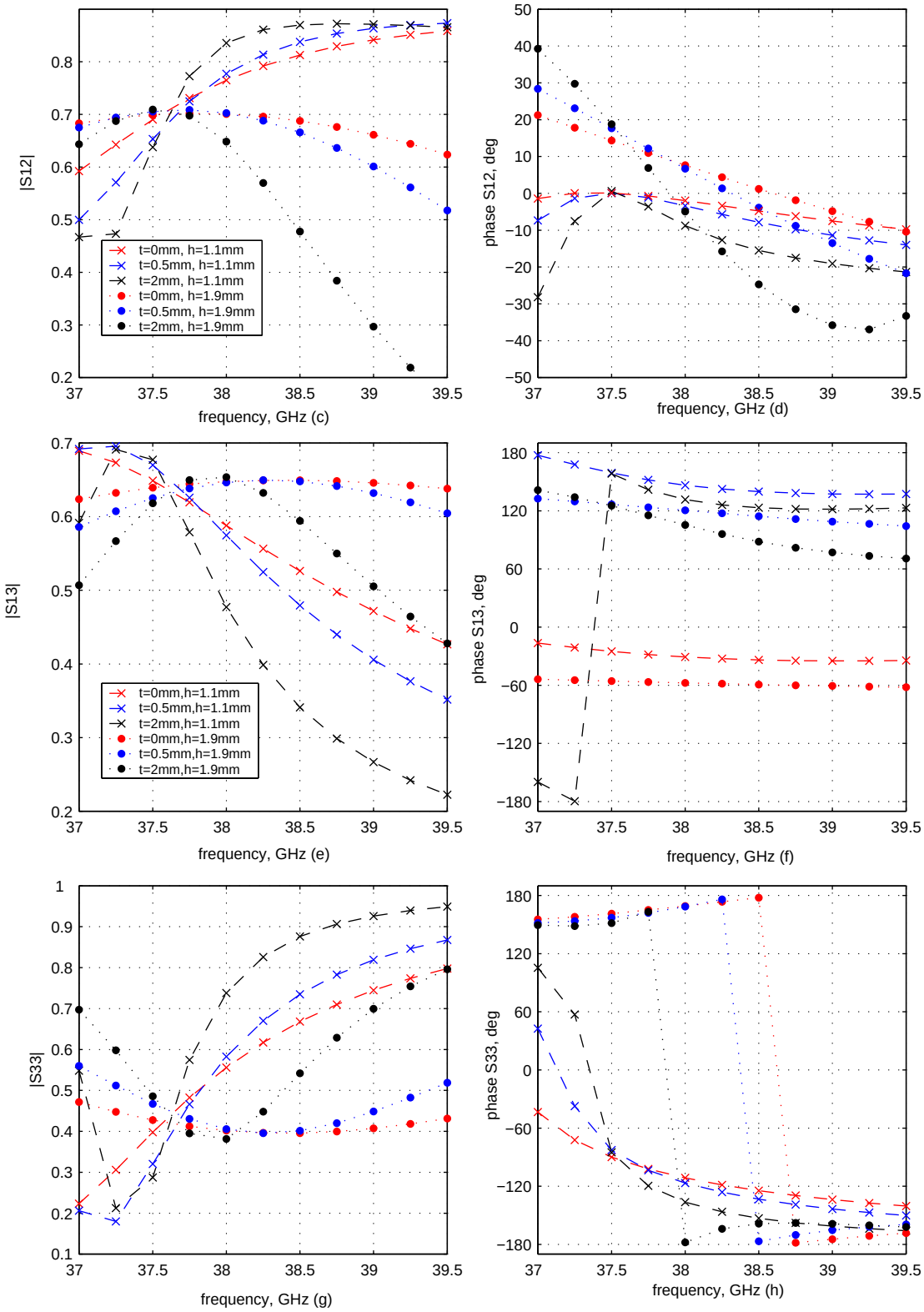

Figure 6.15: Variation of S parameters with respect to frequency for various values of slot thickness (t) and post height(h). MATLAB, Post radius:0.5mm, post offset: 1.1mm, slot length: 4mm, slot width:0.4mm, frequency:38.25GHz.

The diagrams of Figure 6.15 state clearly that the bandwidth becomes more narrow for thicker slots for all post height values, which is consistent with the results of Figure 6.14(a). The high post (post height=1.9mm) causes a small shift to lower frequency for $|S11|$, when the slot becomes thick enough (slot thickness=2mm). The S11 phase diagram is consistent with the curves of Figure 6.14 as far as resonance is concerned, since for post height $0.826b$ (1.9mm) the resonant slot length is smaller for greater slot thickness values. Figure 6.15(d) is also consistent with the results of Figure 6.14(c), since forward-scattered resonance is observed for two different normalized resonant length values at h_p=1.1mm. In the case of back-scattered resonance, this post height value lies below the resonant post height range.

The interaction between post height and slot thickness is demonstrated more clearly in the diagrams of Figure 6.16. These curves were computed for constant frequency (38.25 GHz) and slot length 4mm (0.51λ).

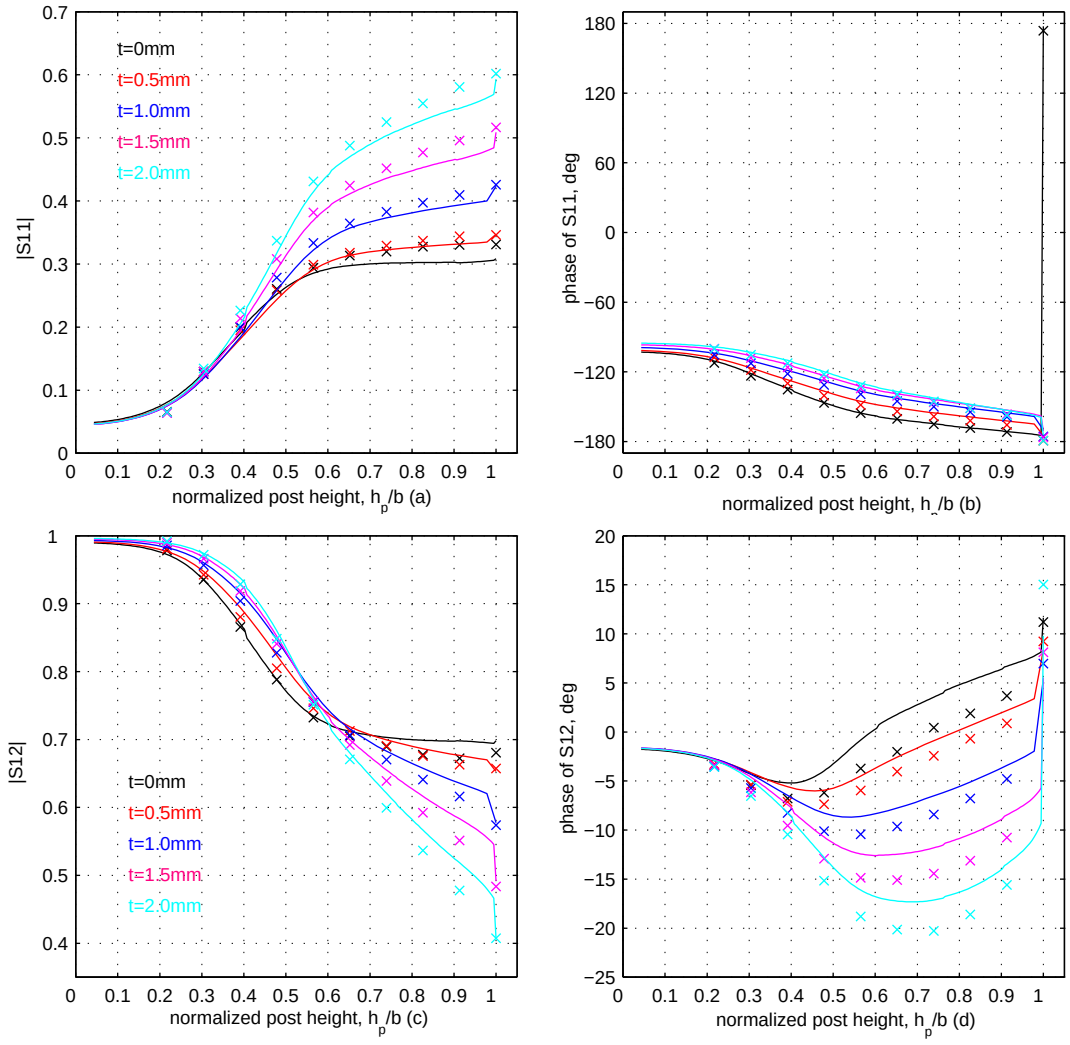

Figure 6.16: Variation of S parameters with the post height for various slot width values. Solid line: MATLAB, (MPIE method), Points: HFSS. Post radius: 0.5mm, post offset: 1.1mm, slot length: 4mm, slot width: 0.4mm

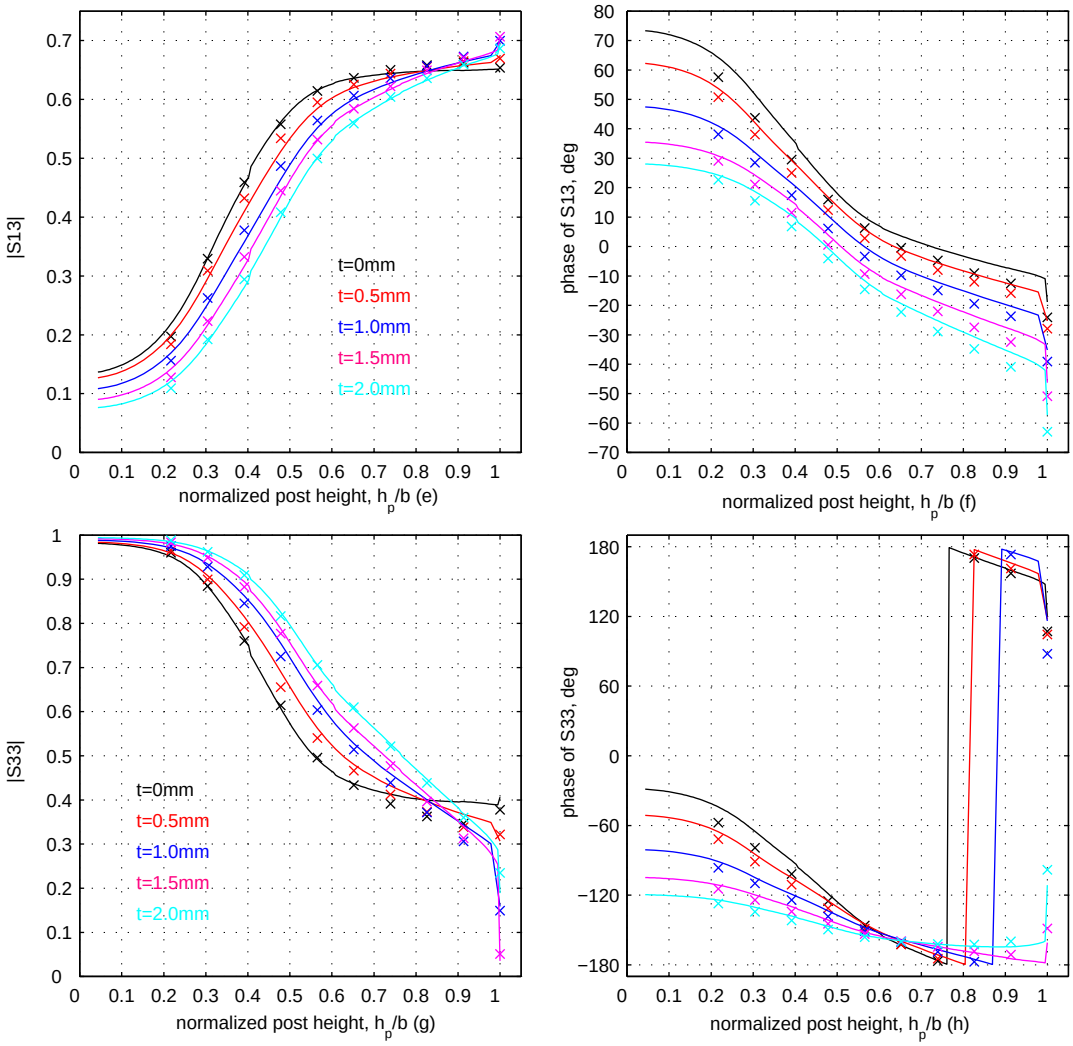

Figure 6.16: Variation of S parameters with the post height for various slot width values. Solid line: MATLAB, (MPIE method), Points: HFSS. Post radius: 0.5mm, post offset: 1.1mm, slot length: 4mm, slot width: 0.4mm

The impact of slot thickness on the variation of S parameters with post height resembles the impact of slot width. More specifically, Figure 6.16(a) states that the increase in slot thickness introduces higher values of $|S11|$, when the post becomes longer than a certain value (in this case: 0.391b). The results of Figure 6.16(a) are also consistent with the results of Figure 6.13(a), Figure 6.14(b) and Figure 6.15(a). Like $|S11|$, also $|S12|$ is affected by the slot thickness value in the presence of a long post. However, the $|Sx3|$ parameters seem to exhibit a dependency on the slot thickness, only when the post height receives relatively low or medium values, as depicted in Figure 6.16(e) and Figure 6.16(g). When the post height approaches the ridged waveguide height, then the slot thickness does not play an important role on the amplitudes of the coupling coefficient (S13). According to Figure 6.14, for the given values of frequency and slot length resonance based on back-scattered field is possible only when slot thickness equals zero. This is verified by the S11 phase diagram of Figure 6.16. Additionally, resonance according to the forward-scattered field is possible for all slot thickness values, as demonstrated by Figure 6.14(c) and Figure 6.16(d).

6.4 Post Radius

The previous sections contained remarks on the significance of dimensions like post height, slot length, width and thickness. The remaining parameters that affect the electromagnetic behavior of the 'aKoM' structure are the post radius and the post offset from the ridged waveguide center line. In this section the impact of the post radius is examined. Figure 6.17 illustrates the variation of the S parameters with respect to frequency for various values of post radius. All other dimensions (post height, slot length, thickness and width) are constant.

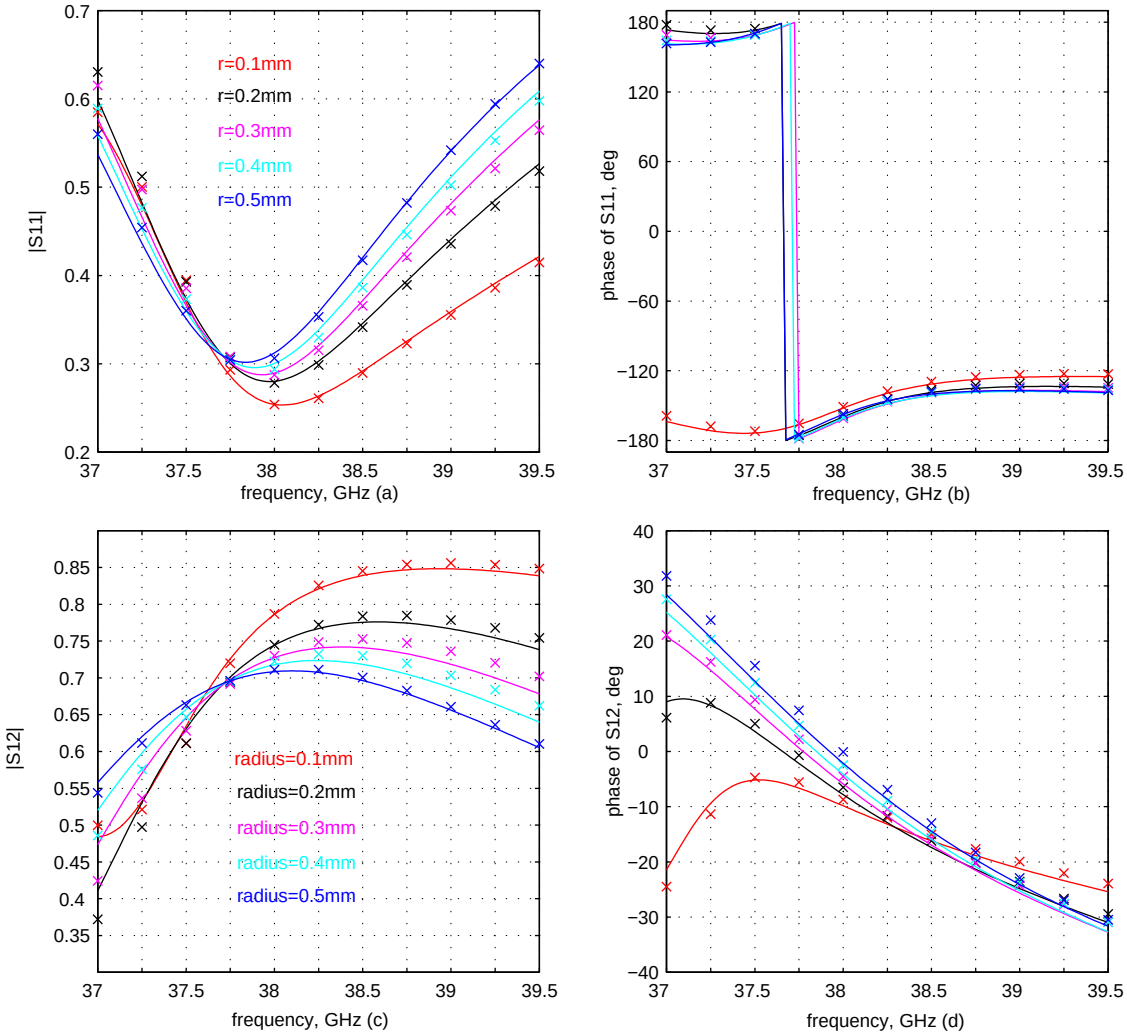

Figure 6.17: Variation of S parameters with respect to frequency for various values of post radius (r). Post offset: 1.1mm, post height:1.5mm, slot length: 4mm, slot width: 0.4mm, slot thickness:1mm. Solid line: HFSS, Points: MATLAB.

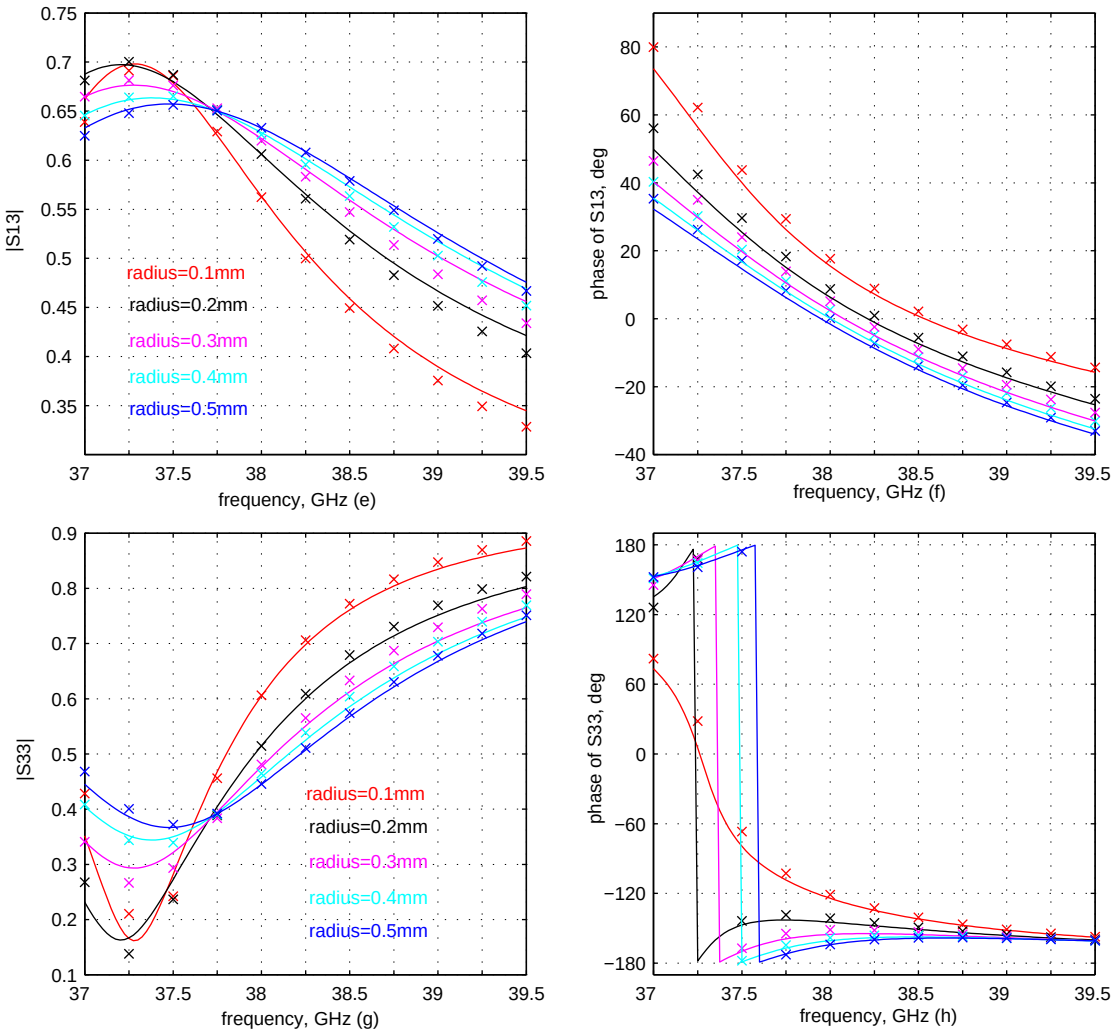

Figure 6.17: Variation of S parameters with respect to frequency for various values of post radius (r). Post offset: 1.1mm, post height:1.5mm, slot length: 4mm, slot width: 0.4mm, slot thickness:1mm. Solid line: HFSS, Points: MATLAB.

Figures 6.17(d) and 6.17(f) reveal that the phases of $S12$ and $S13$ receive similar values throughout the entire frequency bandwidth for the thicker posts. This behavior is usually required at antenna configurations with amplitude attenuation for low side-lobes. When the post radius is decreasing, then the values of $S12$ and $S13$ phases lie quite far from each other, particularly for the lower frequencies.

The effect of the post radius on the S parameters can be examined if two frequency ranges are considered: the frequencies below resonance and the $S12$ and $S13$ frequencies above resonance. In the former range the thicker posts introduce lower values for $|S11|$, $|S13|$ and higher values for $|S12|$, $|S33|$. The opposite comment applies to the second frequency range. The case of r=0.1mm is excluded from the above rule, since resonance is not possible for the specified post height, slot length and frequency range. This post height lies below the range of resonant height values, as shown in Figure 6.18(a). However, when r=0.1mm, then the amplitude values follow the rule for frequencies higher than 37.7GHz. The radius value modifies the bandwidth of the S parameters. In the case of thicker posts, the $|S11|$ curve is sharper, whereas the $|Sx3|$ curves become broader. Figure 6.17(a) indicates that the minimum values for $|S11|$ are slightly increased for thicker posts. The impact of post radius on $S33$, however, is more intense, since a decrease in the post radius

produces a non negligible decrease in the minimum value of $|S33|$. The variation in post radius does not cause a significant frequency shift in the minimum or maximum values of the S parameter amplitudes. Consistently, the resonance frequency also seems to be little affected by the changes in post radius, for the given post height value. In general, it could be stated that the impact of the post radius regarding the frequency shift is similar to the impact of the slot width or thickness.

The role of the post radius on the resonant behavior of the system will be demonstrated in the diagrams of Figure 6.18:

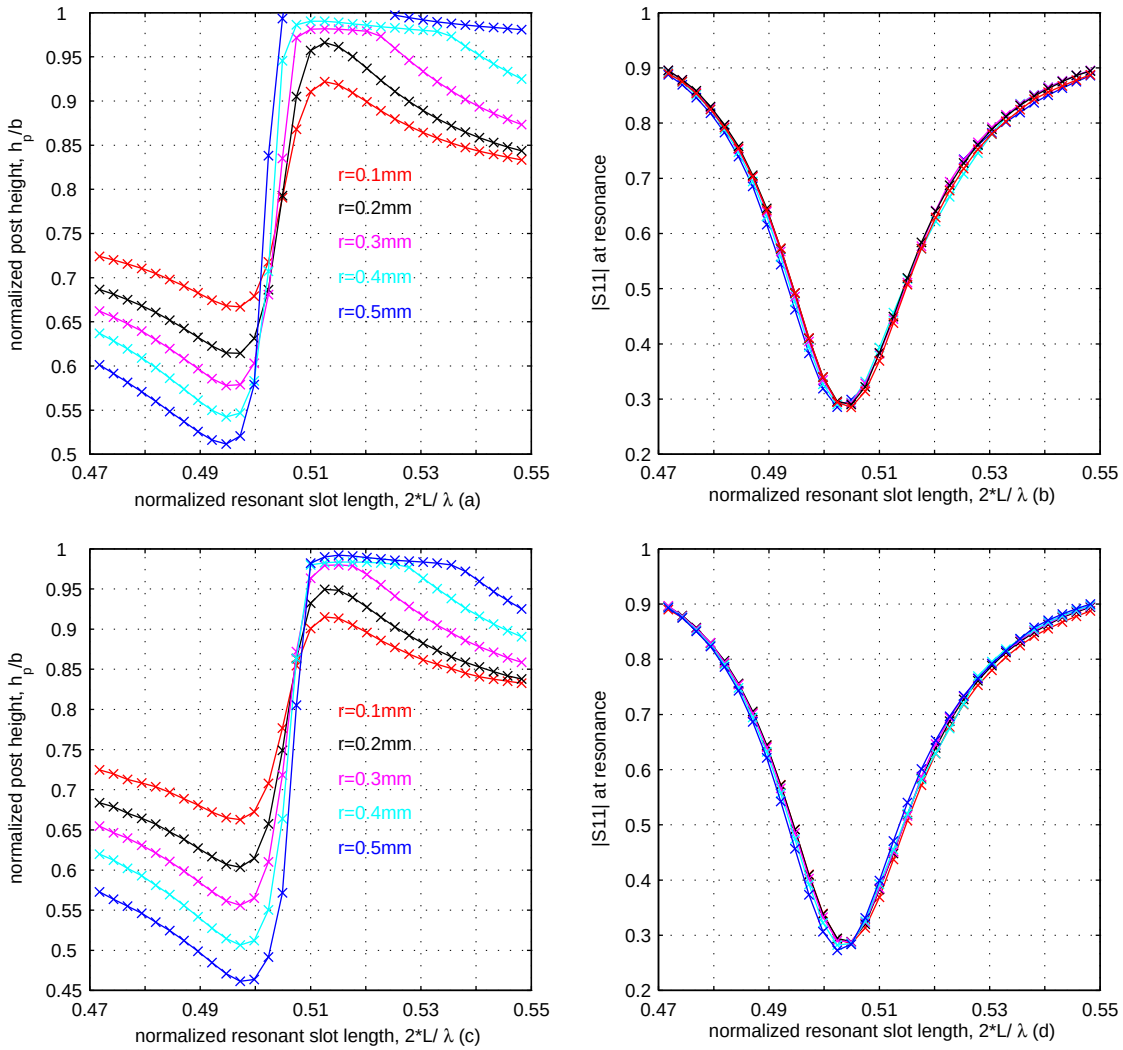

Figure 6.18: Impact of post radius on resonance slot length and post height.
(a) Variation of resonant post height with resonant slot length, backward scattered wave.
(b) Variation of $|S11|$ at resonance with resonant slot length, backward scattered wave.
(c) Variation of resonant post height with resonant slot length, forward scattered wave.
(d) Variation of $|S11|$ at resonance with resonant slot length, forward scattered wave.
MATLAB: Post radius: post offset:1.1mm, slot width:0.4mm, slot thickness:1mm, frequency:38.25GHz

The most obvious comment on the above diagrams is the independency of $|S11|$ at resonance on the radius value for the entire range of length values of the resonant slot. These diagrams are quite different than the corresponding diagrams of Figure 6.10 or Figure 6.14, where the slot width or thickness respectively introduce different values of $|S11|$ at resonance. However, Figure 6.18(a) indicates that the $|S11|$ curve for post radius 0.5mm is "interrupted" for a region of slot length values.

The role of post radius becomes more clear in Figures 6.18(a) and (c). The thinner posts provide continuous curves throughout the entire range of normalized slot lengths and, additionally, cause the reduction of the upper limit in the resonant post height values, while the lower limit is also significantly increased. In this way the entire range of the resonant post height is considerably reduced in case of thinner posts. As a result, the range for resonant post height values that combine with one resonant slot length is also shrunk: 44% of the entire resonant post range for r=0.1mm against 64.3% for r=0.4mm (resonance based on back-scattered wave) or 42.8% for r=0.1mm against 56.9% for r=0.4mm (resonance based on forward-scattered wave). The corresponding range of slot length values however appears to be almost unaffected by the changes in the post radius. This conclusion is also confirmed by Figures 6.18(b) and (d), where the lowest values of $|S11|$ almost coincide for all the post radius values. For this range, the sensitivity of the resonant post height against small variations of slot length is slightly increased at thicker posts. When the slot length becomes longer, the resonant post height receives lower values for thinner posts. In general, the thinner posts yield curves, which can be considered more "symmetric" about the area of the unique resonant pairs.

The interaction between post radius and post height for a frequency range will be presented in Figure 6.19. The slot dimensions as well as the post offset are constant. The results have been computed for frequency 38.25GHz.

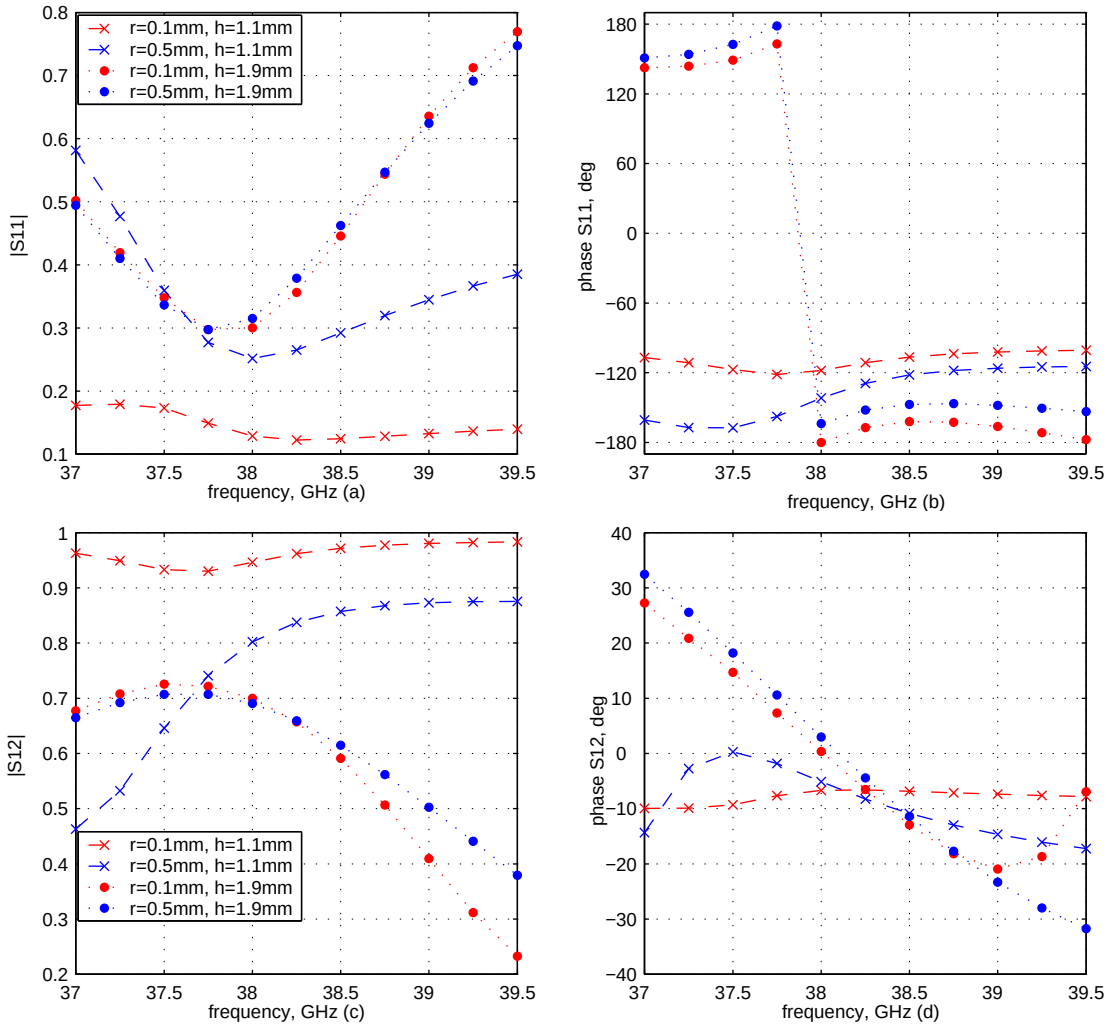

Figure 6.19: Variation of S parameters with respect to frequency for various values of post radius (r) and post height(h). MATLAB, Post offset: 1.1mm, slot length: 4mm, slot width:0.4mm, slot thickness:1mm.

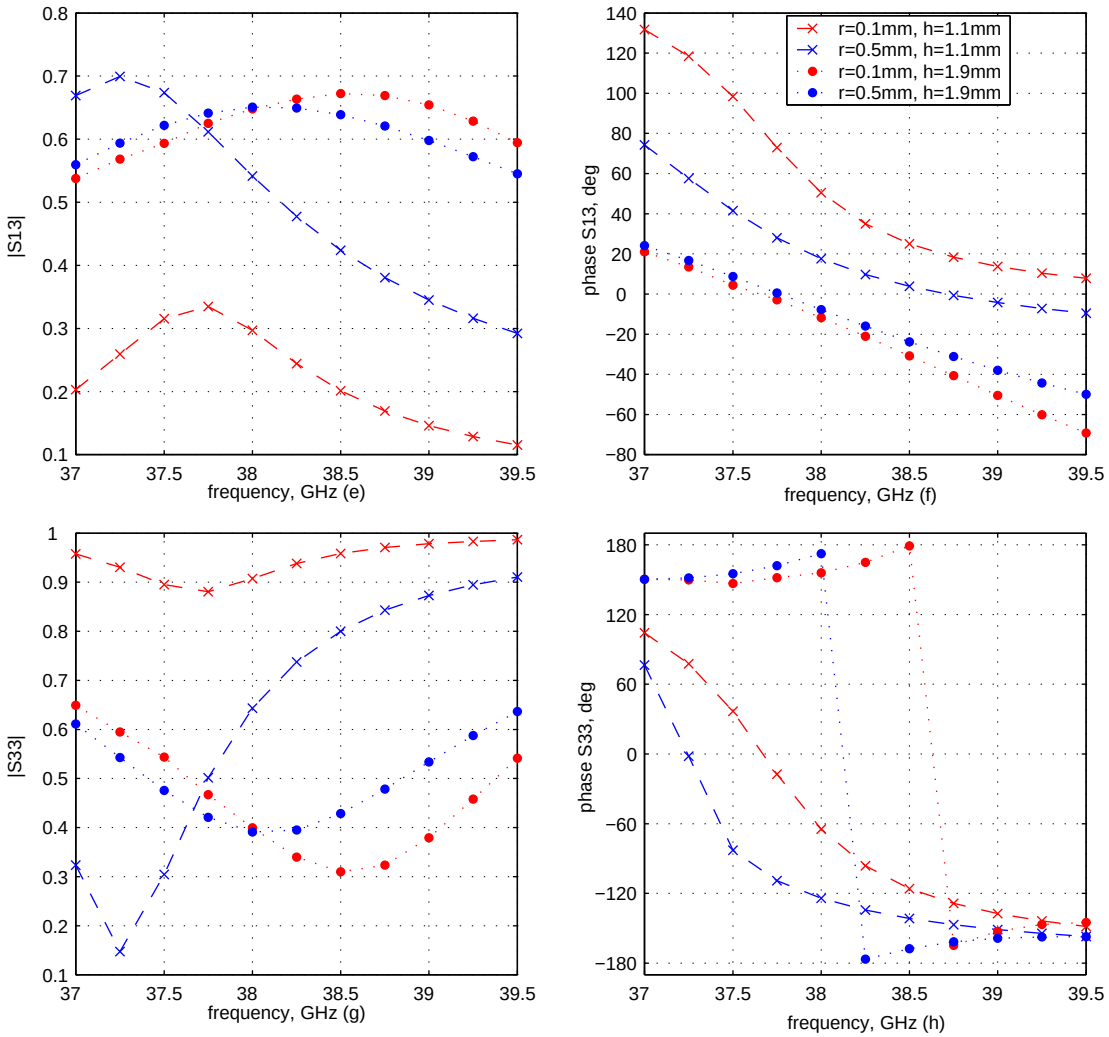

Figure 6.19: Variation of S parameters with respect to frequency for various values of post radius (r) and post height(h). MATLAB, Post offset: 1.1mm, slot length: 4mm, slot width:0.4mm, slot thickness:1mm.

The amplitude curves representing the two different values of radius lie quite far from each other throughout the entire frequency range if h_p=1.1mm (0.4782b). The deviation between these two kinds of curves in Figure 6.19 is even greater than in Figure 6.17. For the dimensions of the 'aKoM' structure, a post of height 1.1mm is considered a short post. If, additionally, the radius receives a low value like 0.1mm then the post represents a very small discontinuity inside the ridged waveguide, incapable of generating many evanescent modes. Therefore the electric field induced on the slot aperture is not strong enough to enable large energy flow from one waveguide to the other. All of this is clearly depicted in the above diagrams, where the $|S13|$ curve for r=0.1mm lies much lower than the $|S13|$ curve for r=0.5mm for the entire frequency range under study. The amplitudes of $S12$ and $S33$ receive greater values, when the radius is decreased, whereas $|S11|$ values are kept at a very low level for small radius.

From Figure 6.19 it becomes clear that the impact of the radius on the S parameters is very limited throughout the entire frequency range, if the post is quite long . Only S33 seems to be more affected by the variation of radius in terms of both amplitude and phase. In this case, the lower radius value causes a shift of the S33 curves to higher frequencies. In addition, Figure 6.19(b) demonstrates the second resonance (back-scattered field) in case of r=0.1mm, $h_p = 1.9mm$. This result is consistent with Figure 6.18(a), according to which post height value 1.9mm is combined with normalized

slot length values 0.5058 and 0.549 at resonance. Figure 6.19(d) also demonstrates the resonance according to forward-scattered wave for the long post (h_p=1.9mm) and the case r=0.5mm and h_p=1.1mm. For r=0.1mm and h_p=1.1mm resonance is not possible as stated by Figure 6.18(c). When the post becomes quite long, the thinner posts are almost as capable of exciting higher order modes as the thicker ones. For this reason the interaction of both thin or thick posts with the slot is practically the same. This is presented in a more clear way in the following diagrams, where parameters like frequency, post offset and slot dimensions are constant and only the post height and radius are modified.

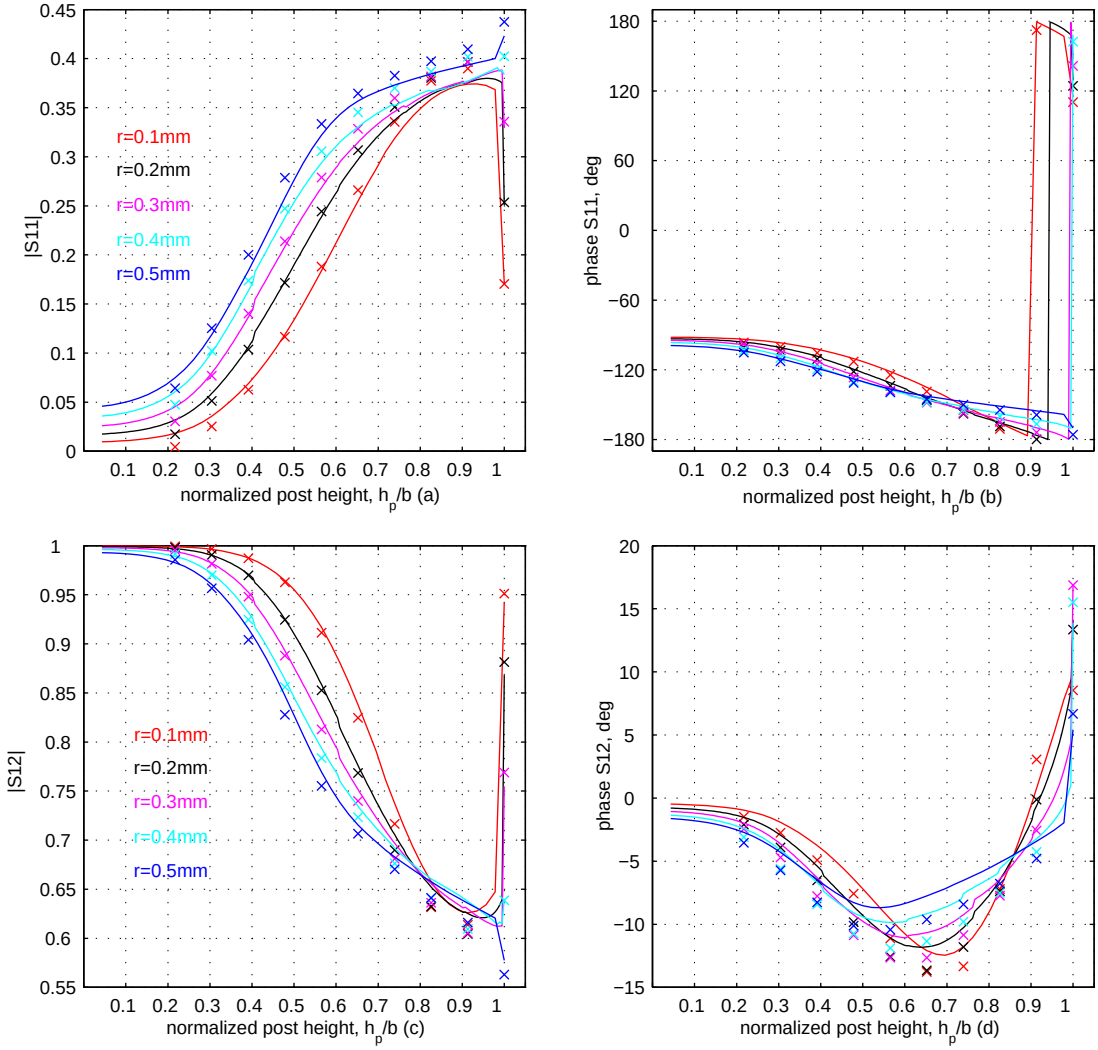

Figure 6.20: Variation of S parameters with the post height for various post radii. Solid line: MATLAB, (MPIE method), Points: HFSS. Post offset: 1.1mm, slot length: 4mm, slot width: 0.4mm, slot thickness: 1mm

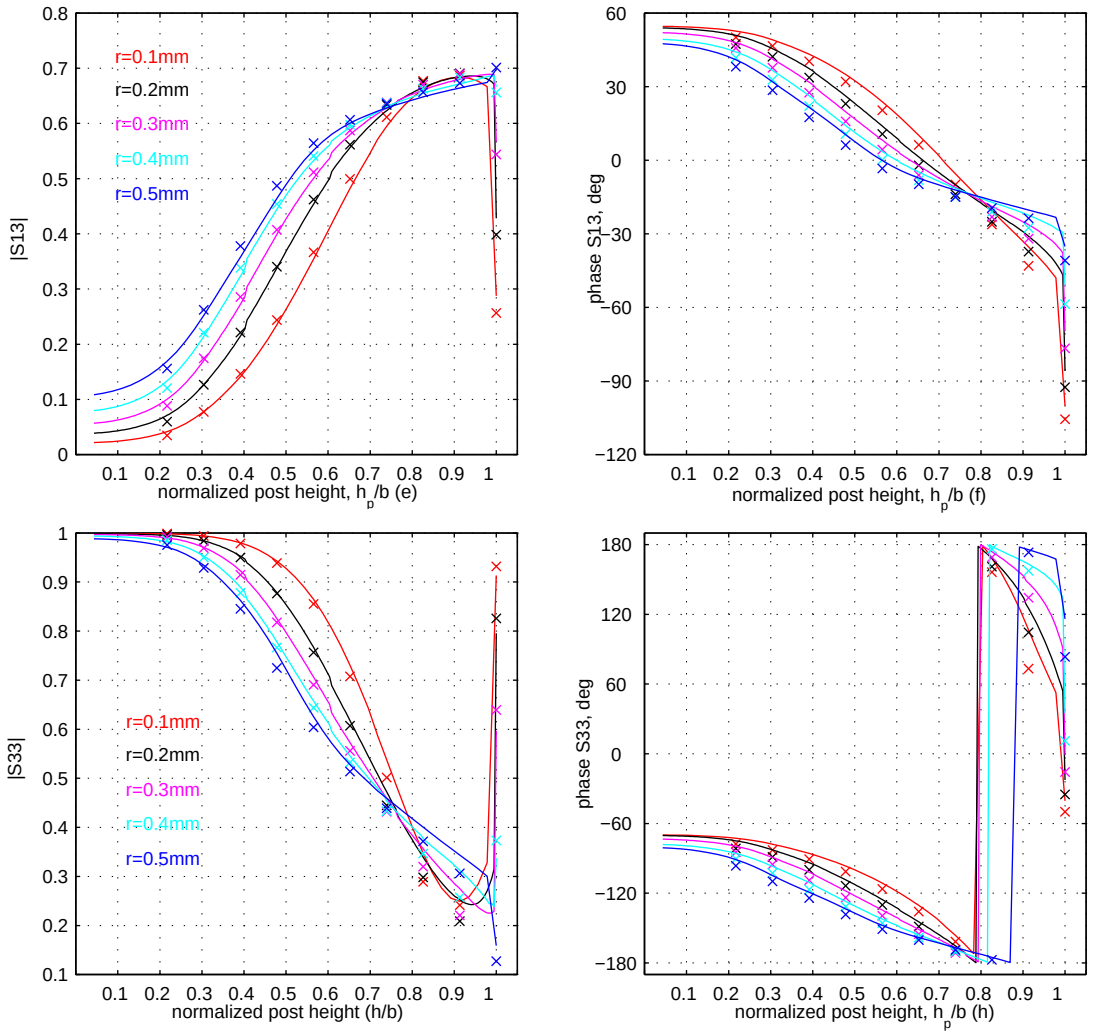

Figure 6.20: Variation of S parameters with the post height for various post radii. Solid line: MATLAB, (MPIE method), Points: HFSS. Post offset: 1.1mm, slot length: 4mm, slot width: 0.4mm, slot thickness: 1mm

Figure 6.20 confirms the reduced effect of radius on the S parameters in the presence of a long post, since for all S parameters, except for S33, the curves almost converge for the post height values between 0.75b and 0.95b. The curves begin to deviate from each other again, when the post becomes inductive ($h = b$). As expected by Figure 6.18(a), for the given normalized slot length (0.51) resonance is achieved at higher post height values as the radius increases. Similar behavior is also observed in a configuration consisting of a rectangular waveguide that contains a cylindrical post [35], [1]. In case of r=0.5mm resonance (back-scattered field) is not possible for any post height value, which is confirmed by Figure 6.20(b). Figure 6.20(d) is in accordance to Figure 6.18(c) indicating that resonance based on forward-scattered wave is possible for all radius values. The values of $|S11|$ at resonance almost coincide for all radius values and concentrate around 0.39, verifying the conclusions of Figure 6.18(b) and Figure 6.18(d). Furthermore, the amplitude curves become more sharp as the radius decreases. This could be attributed to the smaller resonant post height value range in case of thinner posts.

6.5 Post offset

The present chapter is concluded with the analysis on the effect of the post offset. The first diagrams depict the variation of all S parameters with frequency for various values of post offset, whereas the remaining parameters are constant. In the below diagrams the post offset is defined as the distance of the post center from the center line of the ridged waveguide broad wall.

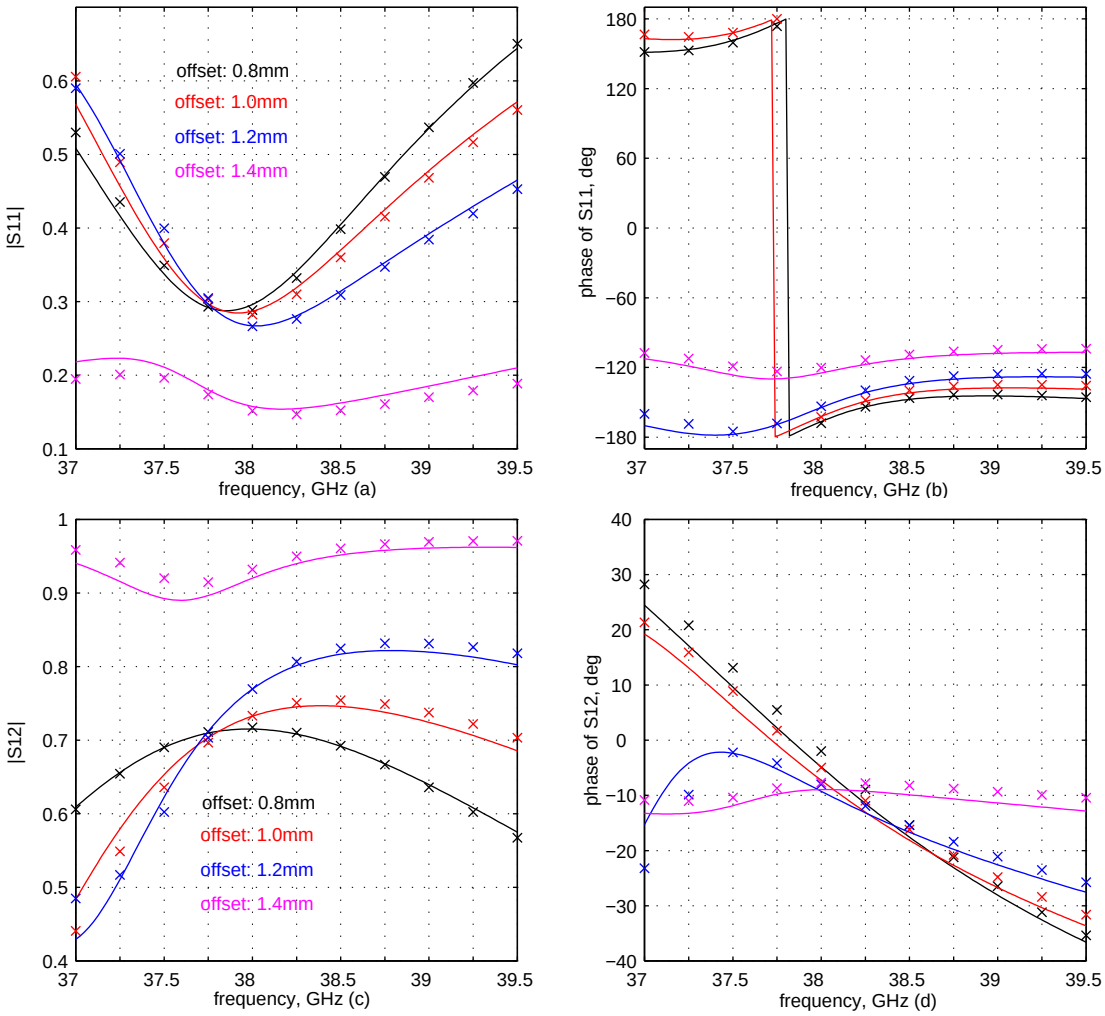

Figure 6.21: Variation of S parameters with respect to frequency for various values of post offset (d). Post radius: 0.2mm, post height:1.5mm, slot length: 4mm, slot width: 0.4mm, slot thickness:1mm. Solid line: HFSS, Points: MATLAB.

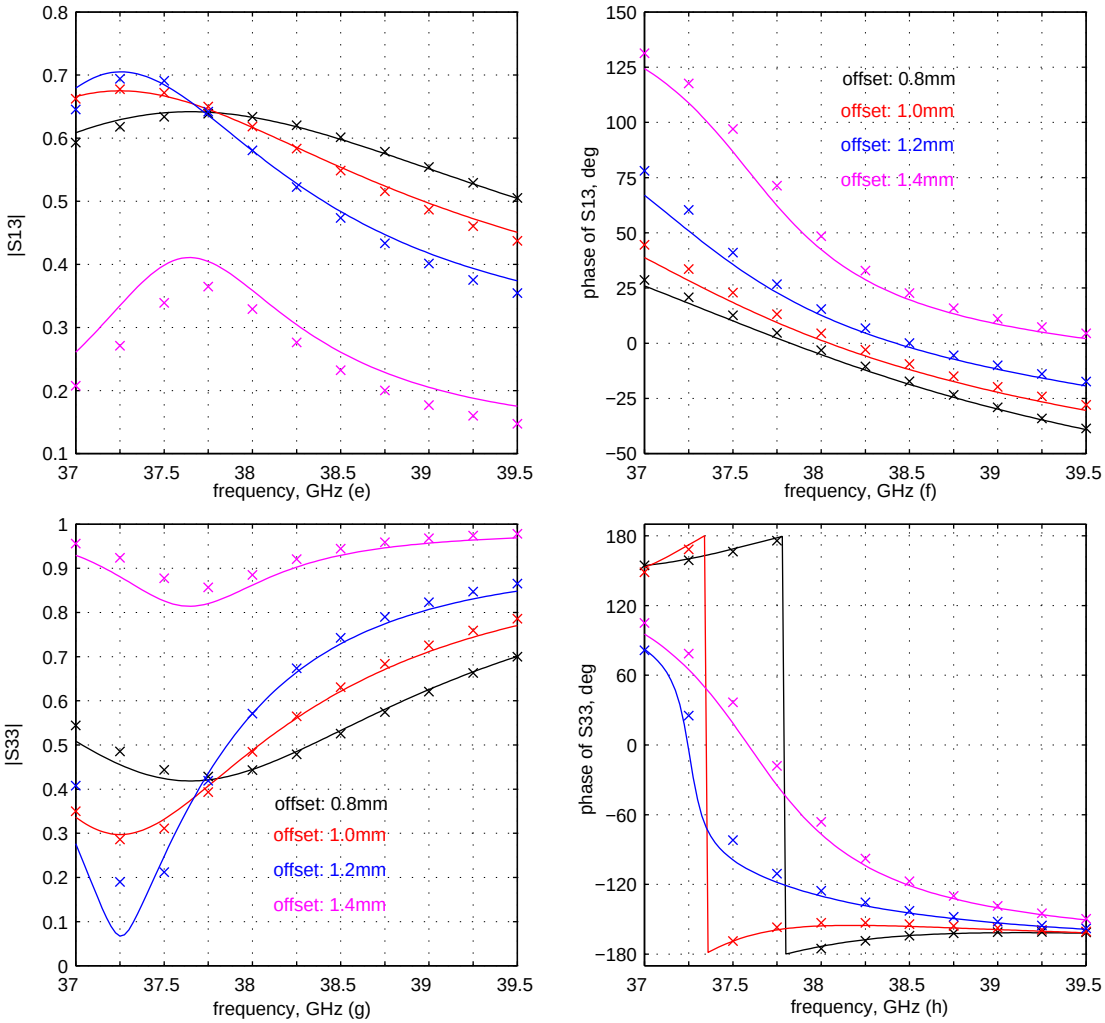

Figure 6.21: Variation of S parameters with respect to frequency for various values of post offset (d). Post radius: 0.2mm, post height:1.5mm, slot length: 4mm, slot width: 0.4mm, slot thickness:1mm. Solid line: HFSS, Points: MATLAB.

For the given post height value the reflection coefficient $|S11|$ sustains very low values throughout the entire frequency range, when the post lies very close to the ridged waveguide side wall (post offset: 1.4mm), while $|S12|$ values vary from 0.87 to 1, indicating the generation of weak scattered fields by the post. According to the equations of Appendix A, this is an expected result, since the incident ridged waveguide field attenuates close to the narrow ridged waveguide wall, thus inducing weak electric current on the post surface. The consequence from the poor post excitation is the low interaction between slot and post, which reflects upon the $|S13|$ and $|S33|$ curves in case of post offset:1.4mm.

As the post approaches the slot, then the post offset begins to have an impact on the S parameters similar to the impact of the post radius demonstrated in Figure 6.17. In general, the effect of small post offsets can be parallelized to the effect of the large radius, since in both cases the electric current produced scattered field is intensified. Figure 6.21 also suggests that resonance capability is restricted, when the post offset increases. This behavior will be examined closer in the following diagrams.

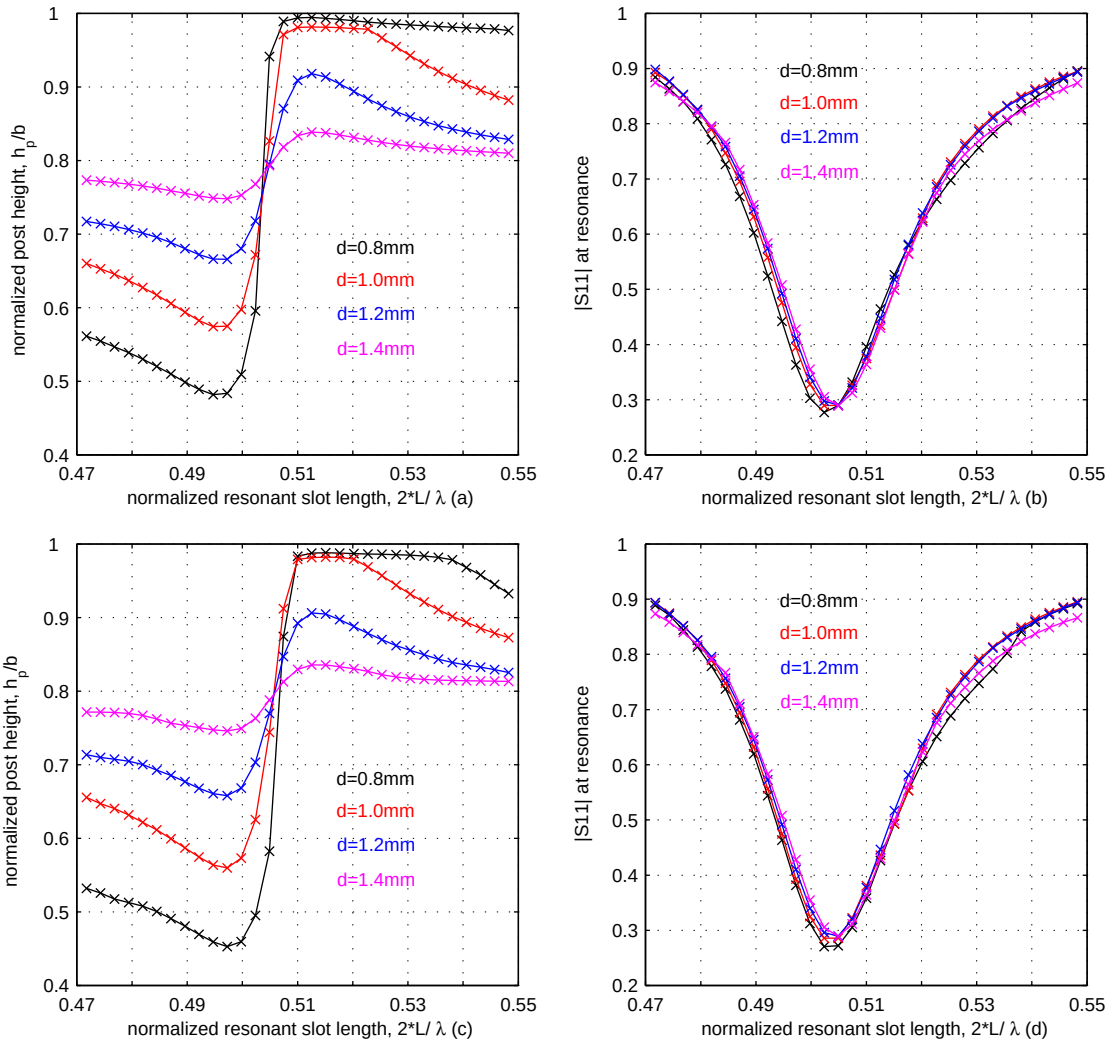

Figure 6.22: Impact of post offset on resonance slot length and post height.
(a) Variation of resonant post height with resonant slot length.
(b) Variation of $|S11|$ at resonance with resonant slot length.
(c) Variation of resonant post height with resonant slot length, forward scattered wave.
(d) Variation of $|S11|$ at resonance with resonant slot length, forward scattered wave.
MATLAB: Post radius: 0.2mm, slot width:0.4mm, slot thickness:1mm, frequency:38.25GHz

The effect of the post offset on the resonant pairs of slot length and post height is similar to the radius effect, but more acute. More specifically, a large post offset reduces drastically the range of resonant post height values. These values cluster in a small range between 0.76b and 0.853b in case of d=1.4mm. The resonant post height range for d=0.8mm, which spans from 0.48b to 0.99b, is almost five times bigger. Furthermore, at larger post offset, the range of post height values that uniquely combine with one slot length value is significantly shrunk and occupies a smaller percent of the entire range: 40.45% (or 46.53% for the forward scattered wave) at post offset 1.4mm against 82.76% (or 74.85% based on the forward scattered wave) at post offset 0.8mm. The corresponding range of slot length values is practically unaffected by the variations of post offset. This conclusion is also drawn by Figure 6.22(b). Especially for this range, the resonant post height becomes less sensitive to resonant slot length changes as post offset increases. When the resonant slot becomes longer, then the resonant post height receives lower values for smaller post offset. This is consistent with the post offset effect on the frequency variation of the resonant post height, in case of a structure that constitutes of a rectangular waveguide containing a hollow cylindrical post [35].

The interaction between post offset, post height and frequency is illustrated in Figure 6.23. For those results the slot dimensions and the post radius were constant.

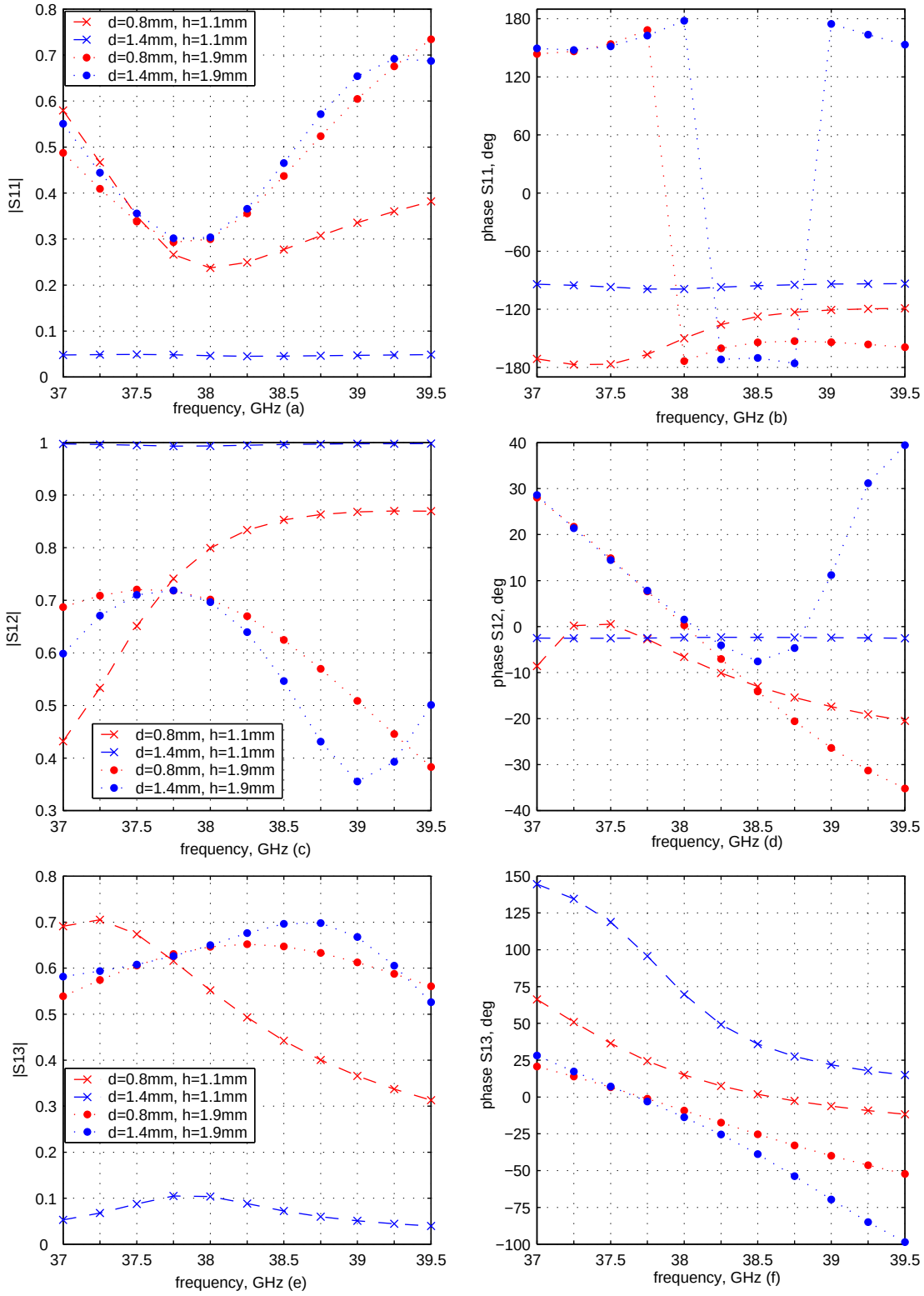

Figure 6.23: Variation of S parameters with respect to frequency for various values of post offset (d) and post height(h). MATLAB, Post radius:0.2mm, slot length: 4mm, slot width:0.4mm, slot thickness:1mm.

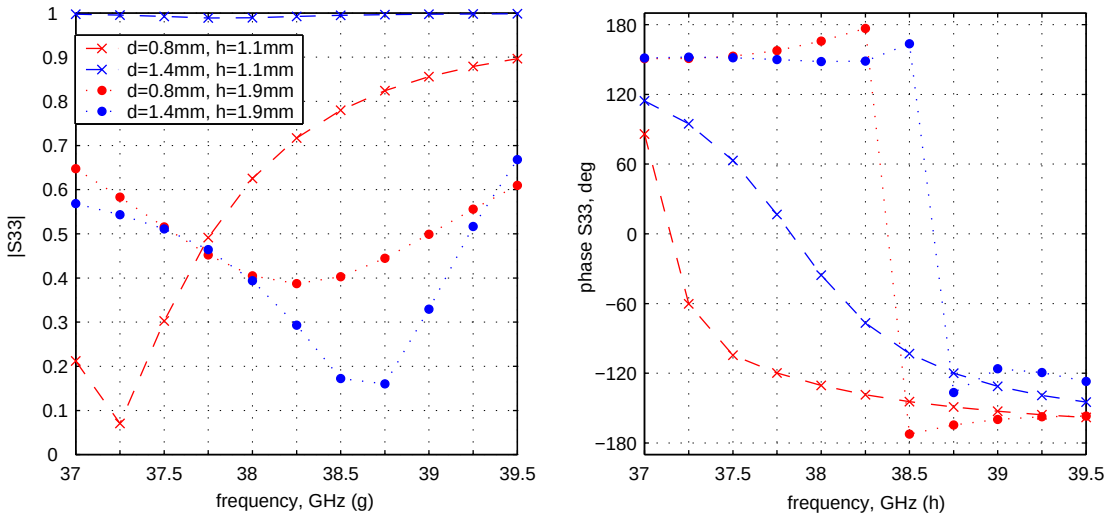

Figure 6.23: Variation of S parameters with respect to frequency for various values of post offset (d) and post height(h). MATLAB, Post radius:0.2mm, slot length: 4mm, slot width:0.4mm, slot thickness:1mm.

As anticipated, the curves for d=1.4mm, h_p=1.1mm are practically straight horizontal lines. $|S12|$ and $|S33|$ almost approach unity, indicating that no coupling between the two waveguides takes place. In case of d=0.8mm and h_p=1.1mm the coupling becomes significant and comparable to the case where h_p=1.9mm, as suggested by the $|S33|$ curves. The increase in post height introduces a great shift towards higher frequencies for $|Sx3|$ coefficients. When the post height receives the value 1.9mm, then the amplitude curves representing different post offset values do not deviate substantially from each other. Only the $|S33|$ curves for d=1.4mm receive significantly lower values in a small frequency range around 38.75GHz. Moreover, in Figure 6.23(b) a second resonance is observed in the case d=1.4mm, $h_p = 1.9mm$. This result is in agreement with Figure 6.22(a), since post height value 1.9mm combines with slot length values 0.5082λ and 0.5242λ at resonance.

Figure 6.24 presents the variation of the S parameters with h_p for various post offset values. The slot dimensions, the frequency and the post radius are not modified.

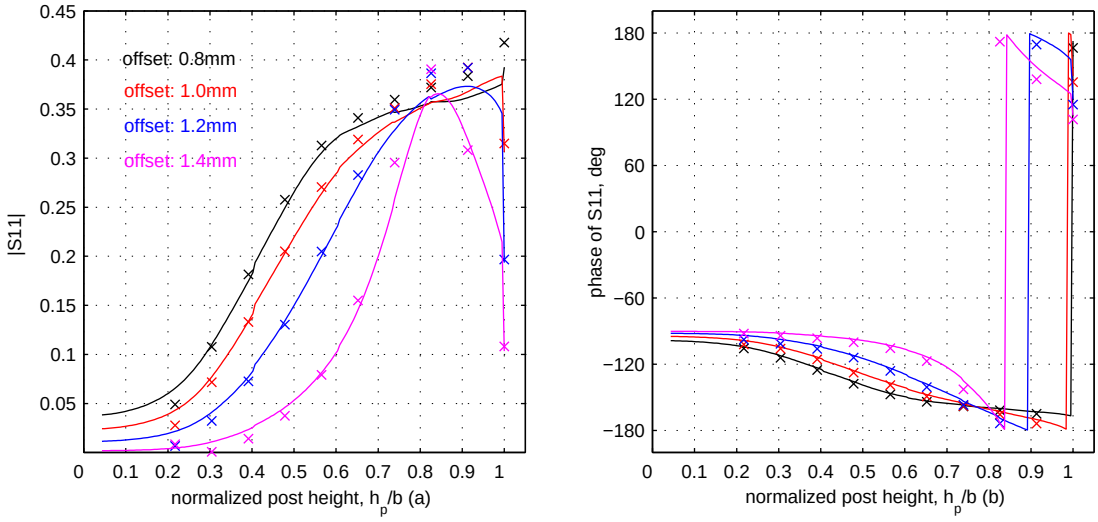

Figure 6.24: Variation of S parameters with the post height for various values of post offset (d). Post radius: 0.2mm, post height:1.5mm, slot length: 4mm, slot width: 0.4mm, slot thickness:1mm, frequency:38.25. Solid line: HFSS, Points: MATLAB.

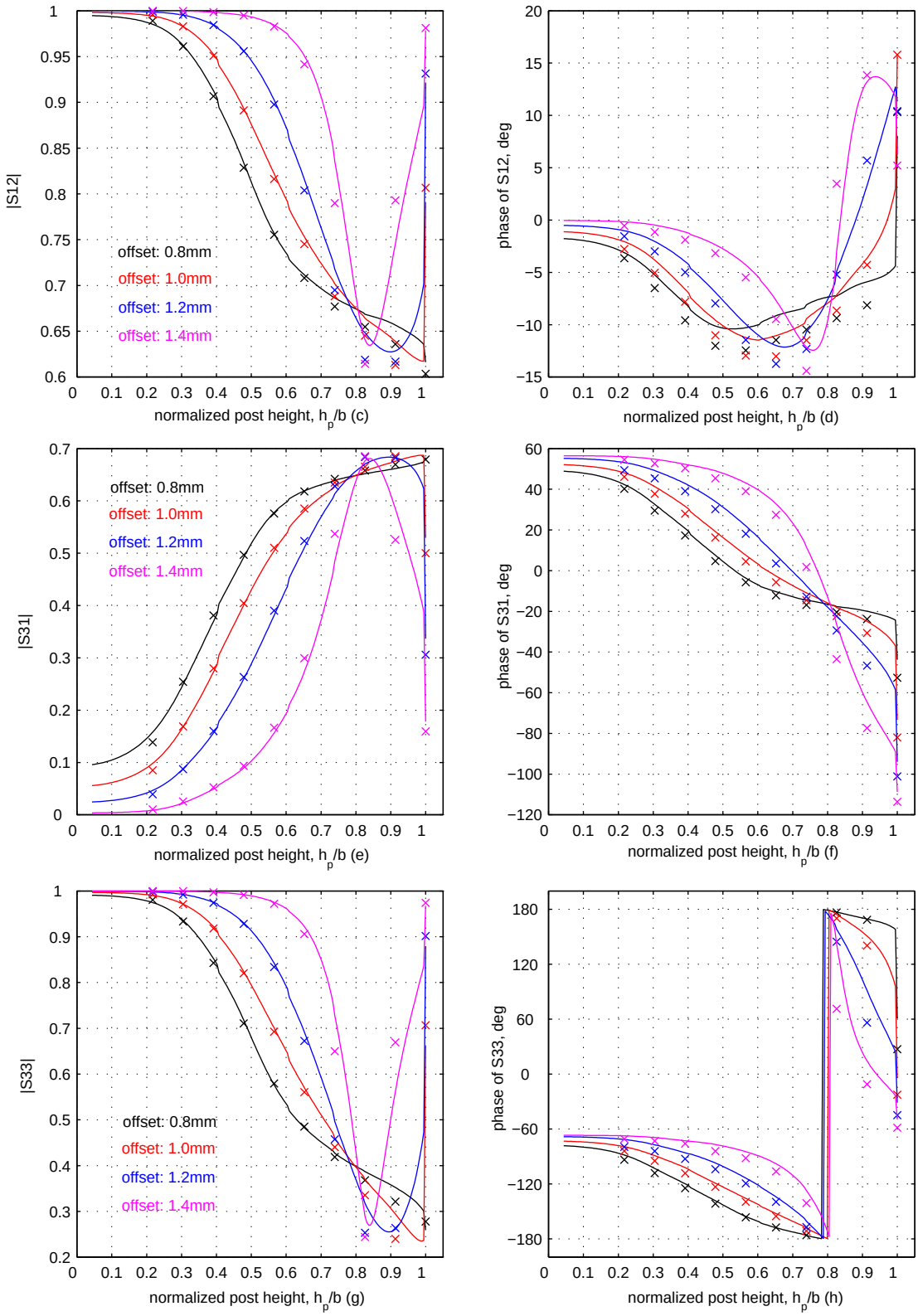

Figure 6.24: Variation of S parameters with the post height for various values of post offset (d). Post radius: 0.2mm, post height:1.5mm, slot length: 4mm, slot width: 0.4mm, slot thickness:1mm, frequency:38.25. Solid line: HFSS, Points: MATLAB.

The above results clearly demonstrate the increased sharpness of the curves, at great post offset. Such a behavior has also been observed in case of a rectangular waveguide containing a cylindrical post [35]. $|S11|$ and $|S13|$ values decrease for short or medium posts that are located close to the ridged waveguide side wall, suggesting a weak interaction between slot and post. The coupling however becomes intense at resonance, where the amplitude values of all S parameters are practically independent on the post offset. The limited bandwidth at smaller post offset values is also obvious in the curves representing the phases of all S parameters. For the given normalized slot length (0.51λ), resonance is achieved in the presence of shorter posts, which is also consistent with the results of Figure 6.22(a).

At the end of the current chapter, a comment should be made on the agreement between the simulated (HFSS) and the computed (MATLAB) results. In all cases, both HFSS and MATLAB curves presented the same dependency on the respective input variables. In most of the cases, the numerical values of the MATLAB and the HFSS results exhibited very good agreement. In a few cases, however, there were small differences in the values of these curves. These differences may be attributed to a number of factors. The number of eigenmodes considered for the MATLAB computations is definitely an important factor, as discussed in Chapter 5. Additionally, the number of considered truncated terms for the ridged waveguide eigenvectors plays also a very important role in regulating the approximation errors in the MATLAB computations. According to Chapter 5 and Appendix A, the agreement between the computated and the actual data is improved as this number is increased, but the complexity of the calculations imposes an upper limit there, hence introducing small approximation errors. Finally, the HFSS results are obtained by implementation of the Finite Element Method, that involves a number of successive, adaptive iterations. Logically, a great number of iterations yields more accurate results, but at the same time it increases the requirements on computational efficiency and makes the simulation extremelly time-consuming. Therefore, this number does not receive very high values, suggesting that additional but small approximation errors are contained in the computations.

The diagrams of Chapter 6 clearly state that the S matrix of the structure is very sensitive to small variations of the geometrical dimension values. As a consequence, the major challenge in constructing a structure like 'aKoM' is the accuracy of the geometrical dimensions. If the tolerance in certain lengths exceeds 10% then with all probability, the electromagnetic behavior of the system will be altered. As far as the post is concerned, the value of 10% can be considered too high. This conclusion is also drawn by Figure 5.19, where the increase of the post height by 2% introduces a non negligible frequency shift in the peak of s11 amplitude

Figure 6.25 presents the computated and measured results for two variations of the 'aKoM' configuration. The ridged waveguide dimensions are the same for both configurations, whereas the differences in the slot and post related dimensions do not exceed 10%. Table 6.1 lists all the relevant data.

	configuration 1	configuration 2
post radius (r)	0.3 mm	0.33 mm
post offset (d)	1.1 mm	1.1 mm
post height (h_p)	1.6 mm	1.65 mm
slot length (l_s)	4 mm	3.8 mm
slot width (w_s)	0.4 mm	0.4 mm
branch waveguide length(t)	1 mm	1.1 mm

Table 6.1 Geometrical dimensions of the 'aKoM' structure

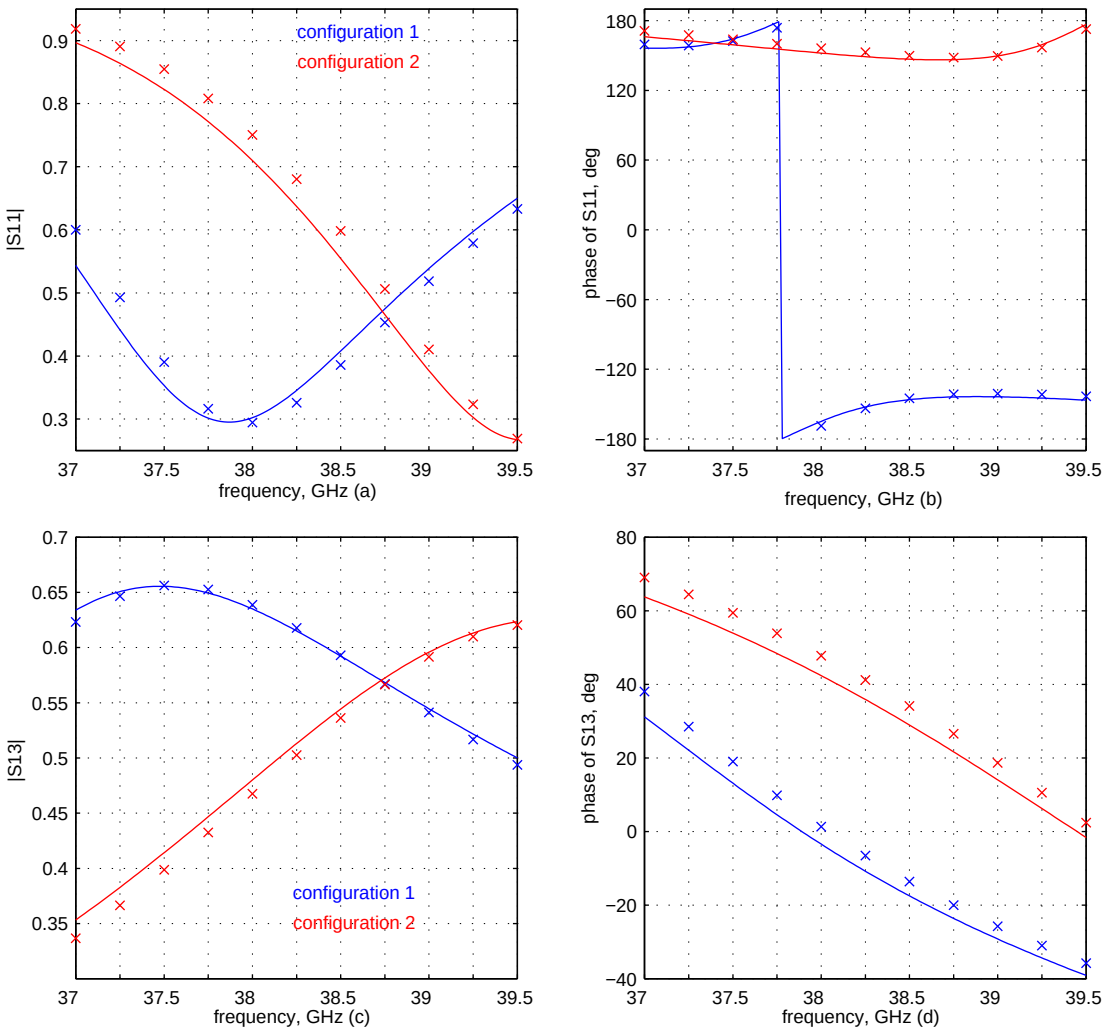

Figure 6.25: S11 and S13 coefficients against frequency for two configurations Solid line: HFSS, Points: MATLAB.

Even though parameters like post offset and slot width have the same values at both configurations, the differences between the S parameters are significant, especially in terms of frequency shift. Figure 6.25 (a) and (b) reveal that the resonance frequency is shifted by more than 50% of the considered frequency bandwidth. The impact on the phase of $S13$ is also intense, as shown in Figure 6.25 (d), where an almost constant deviation of approximately 40 degrees is observed throughout the entire frequency bandwidth.

Chapter 7

Summary

In the previous chapters the characteristics of a novel configuration were analyzed. The novelty of the structure lies on the fact that a longitudinal slot, which was used for the coupling between a ridged and a rectangular waveguide, was placed on the center of the ridged waveguide broad wall. Since the location of the slot did not allow its excitation by the incident TE_{10} ridged waveguide eigenmode, an additional obstacle had to be placed inside the ridged waveguide. The role of this obstacle was to disturb the symmetric E-field about the center line of the ridged waveguide broad wall and, hence, induce an E-field on the slot aperture. The obstacle that was used to this purpose was a metallic post, which was mounted to the upper ridged waveguide wall at a small offset away from the slot.

In Chapter 3 an attempt was made to formulate the mathematical equations that completely define the fields inside a ridged waveguide containing a longitudinal coupling slot and a metallic post at arbitrary positions. This procedure was based on Schelkunoff's surface-equivalent theorem, which suggests the replacement of a scattering body with the equivalent electric or magnetic current distributions. In this way, the post was represented by the electric current flowing on its surface, whereas the slot was replaced by a magnetic current. Application of the proper boundary conditions in conjunction with the Maxwell equations yielded a system of equations that could calculate the scattered fields inside the waveguides. The solution of these equations required the utilization of the dyadic Green functions, which were proven a very powerful tool for this purpose. The implementation of the dyadic Green functions led to the Mixed Potential Integral Equations and the Electric Field Integral Equations of the system. As expected, both methods produced the same system of integral equations. After the integral equations for the general case were fully defined, the special features of the 'aKoM' configurations were taken into account by imposing the proper geometric conditions.

The next step was the determination of the numerical method that had to be deployed for the solution of the system of equations. The theoretical analysis had implied that the Method of Moments would be the most appropriate method for the particular problem. The basic issue there was the choice of suitable basis and test functions, which could satisfy the boundary conditions and guarantee numerical stability. To this purpose, both entire and sub-domain expansion/ test functions were employed: the magnetic currents were expanded in entire-domain sinusoidal series, the circumferential electrical post current was expressed as a sum of Fourier series, while piecewise sinusoidal and roof-top functions were used for the electrical current that was parallel to the post axis.

The issue of convergence was the next major topic. The number of expansion/ test functions had to be determined, especially for the electric current parallel to the post axis. This was the most challenging part of the present work, as there had been only very few references in the literature regarding the formulation and the behavior of Dyadic Green functions inside a ridged waveguide and most of them concerned very thin obstacles, thus allowing assumptions, which could not be

applied in the 'aKoM' case. To this purpose two additional configurations were examined: a large one operating in frequency range 1.7-2.3GHz and a medium configuration operating in frequency range 8-12GHz. Both configurations consisted of only a metallic post inside a ridged waveguide. Study of the results on all configurations and comparison with the corresponding simulated data, obtained by HFSS, led to a new, empirical rule, which can predict the values of S parameters with satisfying accuracy. The medium configuration was also constructed and measured in the University of Duisburg-Essen. The agreement between the measured and the computed data was very good (Figure 5.18).

After the issues of numerical stability and convergence were studied, the impact of the post and slot geometrical dimensions on the electromagnetic performance of the 'aKoM' configuration had to be investigated. For this reason computations were performed applying the Moment Method on the theoretical model of Chapter 3. The computed results were always compared against simulated data, produced by HFSS by means of the Finite Element Method. The computed and the simulated results exhibited very good agreement. All the computations of Chapter 6 clearly state that the S parameters are controlled by the values of the post and slot geometrical dimensions, particularly the post height and the slot width. Therefore, the fine tuning of the geometrical dimensions can achieve the desired performance in terms of waveguide coupling and proper matching, depending on the respective requirements.

Appendix A

Modal expansion in a ridged waveguide

The 'aKoM' ridged waveguide is a waveguide with a single ridge, located symmetrically about the center of the broad wall. Its geometry can be viewed in Figure A.1. The z-direction is considered to be the direction of wave propagation inside the waveguide. Furthermore, the waveguide is not filled with any dielectric material. Montgomery [129] suggested an efficient way to calculate the cutoff frequencies as well as the normalization coefficients of the eigenmodes inside a ridged waveguide. The same procedure has been employed for the purpose of the present dissertation.

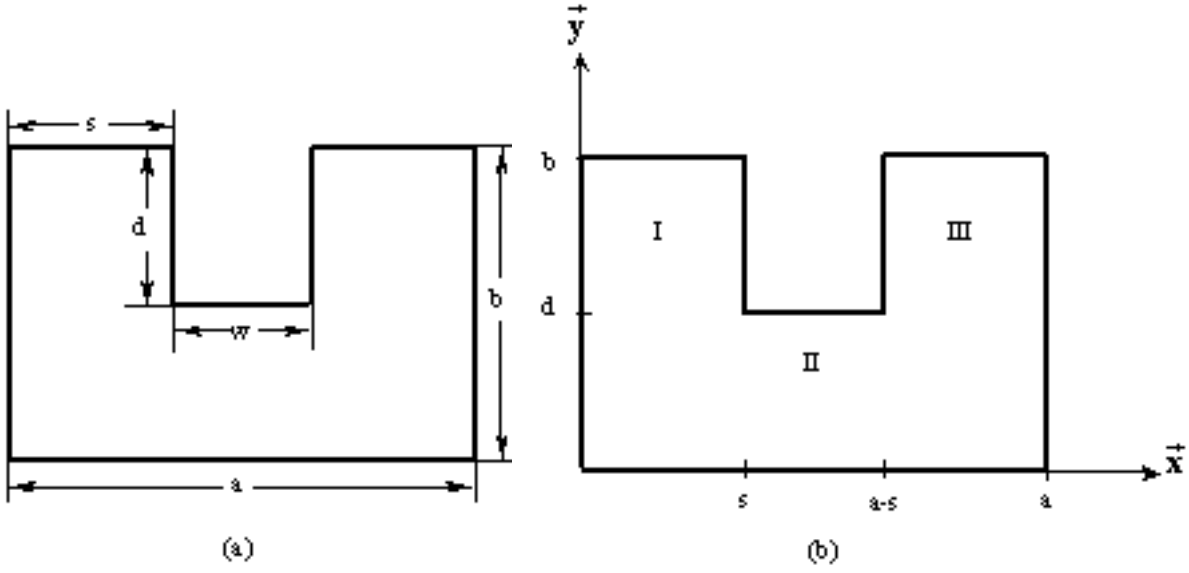

Figure A.1 Ridged waveguide. (a) Dimensions of the ridged waveguide. (b) Coordinate system

According to Montgomery's method, the space inside the waveguide can be separated into the three regions that are depicted in Figure A.1(b). The regions are defined in the following way:

Region I: 0 x s, 0 y b (trough region)
Region II: s x a-s, 0 y d (gap)
Region III: a-s x a, 0 y b (trough region)

The ridged waveguide eigenmodes are classified in TE and TM modes, depending on the kind of scalar potential, which generates them. The scalar potential for the t eigenmode may be expressed

in the following way:

$$\psi_{\mathrm{pit}}(\mathrm{x},\mathrm{y},\mathrm{z}) = \mathrm{g}_{\mathrm{pit}}(\mathrm{x},\mathrm{y})\varphi_{\mathrm{pt}}(\mathrm{z})$$

where ψ_{pit} is a function of the transverse coordinates and φ_{pt} depends only on the z coordinate. Indices p and i are explained below:

$$\mathrm{p} = \begin{cases} \text{h indicates magnetic scalar potential} \\ \text{e indicates electric scalar potential} \end{cases}$$

$$\mathrm{i} = \begin{cases} \text{1 indicates scalarpotential for region I} \\ \text{2 indicates scalarpotential for region II} \\ \text{3 indicates scalarpotential for region III} \end{cases}$$

The scalar potential satisfies the wave equation:

$$\nabla^2\psi_{\mathrm{pit}} + \mathrm{k}_{\mathrm{o}}^2\psi_{\mathrm{pit}} = 0 \Rightarrow \frac{\partial^2\psi_{\mathrm{pit}}}{\partial \mathrm{x}^2} + \frac{\partial^2\psi_{\mathrm{pit}}}{\partial \mathrm{y}^2} + \frac{\partial^2\psi_{\mathrm{pit}}}{\partial \mathrm{z}^2} + \mathrm{k}_{\mathrm{o}}^2\psi_{\mathrm{pit}} = 0$$

where k_0 is the propagation constant in free space.

$$\mathrm{k}_{\mathrm{o}}^2 = \omega^2\varepsilon\mu$$

The previous expression can be analyzed in the following equations:

$$\frac{\partial^2 \mathrm{g}_{\mathrm{pit}}}{\partial \mathrm{x}^2} + \frac{\partial^2 \mathrm{g}_{\mathrm{pit}}}{\partial \mathrm{y}^2} + \mathrm{k}_{\mathrm{C_t}}^2 \mathrm{g}_{\mathrm{pit}} = 0 \qquad (A.1)$$

$$\frac{\partial^2 \varphi_{\mathrm{pt}}}{\partial \mathrm{z}^2} + \gamma_{\mathrm{t}}^2 \varphi_{\mathrm{pt}} = 0 \qquad (A.2)$$

where $\mathrm{k}_{\mathrm{C_t}}$ is the ridged waveguide eigenvalue that corresponds to the t waveguide mode and γ_t is the propagation constant inside the ridged waveguide for the same mode.

$$\mathrm{k}_{\mathrm{C_t}}^2 = \mathrm{k}_{\mathrm{o}}^2 - \gamma_{\mathrm{t}}^2$$

The electric and magnetic fields of each eigenmode are related to the scalar potential according to the following formulas:

- TE Modes:

$$\vec{\mathbf{E}}_{\mathrm{i}}(\mathrm{x},\mathrm{y},\mathrm{z}) = -\mathrm{j}\omega\mu\varphi_{\mathrm{i}}(\mathrm{z})\nabla \mathrm{g}_{\mathrm{hi}}(\mathrm{x},\mathrm{y}) \times \vec{\mathbf{z}} \qquad (A.3)$$

$$\vec{\mathbf{H}}_{\mathrm{i}}(\mathrm{x},\mathrm{y},\mathrm{z}) = \frac{d\varphi_{\mathrm{i}}(\mathrm{z})}{d\mathrm{z}} \nabla \mathrm{g}_{\mathrm{hi}}(\mathrm{x},\mathrm{y}) + \mathrm{k}_{\mathrm{C_t}}^2 \mathrm{g}_{\mathrm{hi}}(\mathrm{x},\mathrm{y})\varphi_{\mathrm{i}}(\mathrm{z})\vec{\mathbf{z}} \qquad (A.4)$$

- TM Modes:

$$\vec{\mathbf{E}}_{\mathrm{i}}(\mathrm{x},\mathrm{y},\mathrm{z}) = \frac{d\varphi_{\mathrm{i}}(\mathrm{z})}{d\mathrm{z}} \nabla \mathrm{g}_{\mathrm{ei}}(\mathrm{x},\mathrm{y}) + \mathrm{k}_{\mathrm{C_t}}^2 \mathrm{g}_{\mathrm{ei}}(\mathrm{x},\mathrm{y})\varphi_{\mathrm{i}}(\mathrm{z})\vec{\mathbf{z}} \qquad (A.5)$$

$$\vec{\mathbf{H}}_{\mathrm{i}}(\mathrm{x},\mathrm{y},\mathrm{z}) = \mathrm{j}\omega\varepsilon\varphi_{\mathrm{i}}(\mathrm{z})\nabla \mathrm{g}_{\mathrm{ei}}(\mathrm{x},\mathrm{y}) \times \vec{\mathbf{z}} \qquad (A.6)$$

A.1 TE Modes

The transverse eigenvectors for the t TE mode are:

$$\overrightarrow{\mathrm{e}}_{\mathrm{TE_t}}=\nabla \mathrm{g_{ht}(x,y)} \times \overrightarrow{\mathbf{z}}$$

$$\overrightarrow{\mathrm{h}}_{\mathrm{TE_t}}=\frac{\gamma_{\mathrm{t}}}{\omega\mu}\overrightarrow{\mathbf{z}} \times \overrightarrow{\mathrm{e}}_{\mathrm{TE_t}}$$

Orthogonality condition:

$$\int\int_{S_w} \overrightarrow{\mathrm{e}}_{\mathrm{TE_t}} \overrightarrow{\mathrm{e}}_{\mathrm{TE_s}} dS = \delta_{t,s}$$

where S_w is the waveguide cross-section and

$$\delta_{\mathrm{t,s}}=\begin{cases} 1, \mathrm{t}=\mathrm{s} \\ 0, \mathrm{t}\neq\mathrm{s} \end{cases}$$

A.1.1 Odd TE Modes

In case of odd TE modes, the electric field is symmetric about plane $\mathrm{x}=\frac{\mathrm{a}}{2}$, which is considered as a magnetic wall. In order to determine the expressions for the ridged waveguide eigenvectors, the following boundary conditions must be taken into account:

Region I:

$$\begin{cases} \mathrm{E_x(x,0,z)}=0, 0\leq\mathrm{x}\leq\mathrm{s} \\ \mathrm{E_x(x,b,z)}=0, 0\leq\mathrm{x}\leq\mathrm{s} \\ \mathrm{E_y(0,y,z)}=0, 0\leq\mathrm{y}\leq\mathrm{b} \\ \mathrm{E_y(s,y,z)}=0, \mathrm{d}\leq\mathrm{y}\leq\mathrm{b} \end{cases} \quad (A.7)$$

Region III:

$$\begin{cases} \mathrm{E_x(x,0,z)}=0, \mathrm{a}-\mathrm{s}\leq\mathrm{x}\leq\mathrm{a} \\ \mathrm{E_x(x,b,z)}=0, \mathrm{a}-\mathrm{s}\leq\mathrm{x}\leq\mathrm{a} \\ \mathrm{E_y(a,y,z)}=0, 0\leq\mathrm{y}\leq\mathrm{b} \\ \mathrm{E_y(a-s,y,z)}=0, \mathrm{d}\leq\mathrm{y}\leq\mathrm{b} \end{cases} \quad (A.8)$$

Region II: .

$$\begin{cases} \mathrm{E_x(x,0,z)}=0, \mathrm{s}\leq\mathrm{x}\leq\mathrm{a}-\mathrm{s} \\ \mathrm{E_x(x,d,z)}=0, \mathrm{s}\leq\mathrm{x}\leq\mathrm{a}-\mathrm{s} \\ \mathrm{E_x}(\frac{\mathrm{a}}{2},\mathrm{y,z})=0, 0\leq\mathrm{y}\leq\mathrm{d\ (magnetic\ wall)} \end{cases} \quad (A.9)$$

Each eigenvector must satisfy the wave equation (A.1). It is obvious that equation (A.1) has a solution of the form:

$$\mathrm{g_{hit}(x,y)}=\sum_{\mathrm{n}=0}^{\infty}[\mathrm{A_{ni}cos}(\alpha_{\mathrm{nit}}\mathrm{x})+\mathrm{B_{ni}sin}(\alpha_{\mathrm{nit}}\mathrm{x})][\mathrm{C_{ni}cos}(\beta_{\mathrm{nit}}\mathrm{y})+\mathrm{D_{ni}sin}(\beta_{\mathrm{nit}}\mathrm{y})] \quad (A.10)$$

where: $\mathrm{k}_{\mathrm{C_t}}^2=\alpha_{\mathrm{nit}}^2+\beta_{\mathrm{nit}}^2$.
Implementation of the boundary conditions for each region leads to the final expressions for the scalar potential:

Region I:

For $0\leq x \leq s$:

$$E_x(x,0)=0 \overset{(A.3)}{\Rightarrow} \frac{\partial g_{h1t}(x,y)}{\partial y}=0|_{y=0} \Rightarrow D_{n1}=0$$

For $0\leq y \leq b$:

$$E_y(0,y)=0 \overset{(A.3)}{\Rightarrow} \frac{\partial g_{h1t}(x,y)}{\partial x}=0|_{x=0} \Rightarrow B_{n1}=0$$

For $0\leq x \leq s$:

$$E_x(x,b)=0 \overset{(A.3)}{\Rightarrow} \frac{\partial g_{h1t}(x,y)}{\partial y}=0|_{y=b} \Rightarrow b_{n1t}=\frac{n\pi}{b}$$

$$k_{C_t}^2=\alpha_{n1t}^2+\beta_{n1t}^2 \Rightarrow \alpha_{n1t}=\begin{cases} \sqrt{k_{C_t}^2-\left(\frac{n\pi}{b}\right)^2}, k_{C_t}\geq\frac{n\pi}{b} \\ -j\sqrt{\left(\frac{n\pi}{b}\right)^2-k_{C_t}^2}, k_{C_t}\leq\frac{n\pi}{b} \end{cases}$$

Substitution of the previous results into (A.10) yields the expressions for the magnetic scalar potential and the corresponding eigenvectors in region I:

$$g_{h1t}(x,y)=\sum_{n=0}^{\infty} N_{n1}\cos(\alpha_{n1t}x)\cos(\frac{n\pi}{b}y) \qquad (A.11)$$

where N_{n1} is a normalization coefficient that will be determined later.

Region II:

For $s\leq x \leq a\text{-}s$:

$$E_x(x,0)=0 \overset{(A.3)}{\Rightarrow} \frac{\partial g_{h2t}(x,y)}{\partial y}=0|_{y=0} \Rightarrow D_{m2}=0$$

For $s\leq x \leq a\text{-}s$:

$$E_x(x,d)=0 \overset{(A.3)}{\Rightarrow} \frac{\partial g_{h2t}(x,y)}{\partial y}=0|_{y=d} \Rightarrow b_{m2t}=\frac{m\pi}{d}$$

For $0\leq y \leq d$:

$$E_x(\frac{a}{2},y)=0 \overset{(A.3)}{\Rightarrow} \frac{\partial g_{h2t}(x,y)}{\partial y}=0|_{x=\frac{a}{2}} \Rightarrow \begin{cases} A_{m2}=\sin(a_{m2t}\frac{a}{2}) \\ B_{m2}=-\cos(a_{m2t}\frac{a}{2}) \end{cases}$$

$$k_{Ct}^2=\alpha_{m2t}^2+\beta_{m2t}^2 \Rightarrow \alpha_{m2t}=\begin{cases} \sqrt{k_{Ct}^2-\left(\frac{m\pi}{d}\right)^2}, k_{Ct}\geq\frac{m\pi}{d} \\ -j\sqrt{\left(\frac{m\pi}{d}\right)^2-k_{Ct}^2}, k_{Ct}\leq\frac{m\pi}{d} \end{cases}$$

Substitution of the previous results into (A.10) yields the expressions for the magnetic scalar potential and the corresponding eigenvectors in region II:

$$g_{h2t}(x,y)=\sum_{m=0}^{\infty} N_{m2}\sin[\alpha_{m2t}(\frac{a}{2}-x)]\cos(\frac{m\pi}{d}y) \qquad (A.12)$$

where N_{m2} is a normalization coefficient.

Region III:

For a-s$\leq$ x $\leq$a:

$$E_x(x,0)=0 \overset{(A.3)}{\Rightarrow} \frac{\partial g_{h3t}(x,y)}{\partial y}=0|_{y=0} \Rightarrow D_{n3}=0$$

For 0$\leq$ y $\leq$d:

$$E_y(0,y)=0 \overset{(A.3)}{\Rightarrow} \frac{\partial g_{h3t}(x,y)}{\partial x}=0|_{x=0} \Rightarrow B_{n3}=0$$

$$E_y(a,y)=0 \overset{(A.3)}{\Rightarrow} \frac{\partial g_{h3t}(x,y)}{\partial x}=0|_{x=a} \Rightarrow \begin{cases} A_{n3}=\cos(a_{n3t}a) \\ B_{n3}=\sin(a_{n3t}a) \end{cases}$$

For a-s$\leq$ x $\leq$a:

$$E_x(x,b)=0 \overset{(A.3)}{\Rightarrow} \frac{\partial g_{h3t}(x,y)}{\partial y}=0|_{y=b} \Rightarrow b_{n3t}=\frac{n\pi}{b}$$

$$k_{Ct}^2=\alpha_{n3t}^2+\beta_{n3t}^2 \Rightarrow \alpha_{n3t}=\begin{cases} \sqrt{k_{Ct}^2-\left(\frac{n\pi}{b}\right)^2}, k_{Ct} \geq \frac{n\pi}{b} \\ -j\sqrt{\left(\frac{n\pi}{b}\right)^2-k_{Ct}^2}, k_{Ct} \leq \frac{n\pi}{b} \end{cases}$$

Substitution of the previous results into (A.10) yields the expressions for the magnetic scalar potential and the corresponding eigenvectors in region III:

$$g_{h3t}(x,y)=\sum_{n=0}^{\infty} N_{n3}\cos[\alpha_{n3t}(x-a)]\cos(\frac{n\pi}{b}y) \qquad (A.13)$$

where N_{n3} is a normalization coefficient, which together with coefficients N_{m2} and N_{n1} will be determined later.
Due to the magnetic wall at plane $x=\frac{a}{2}$ the following condition must be valid:

$$\overrightarrow{e}_{TEt}(x,y)\overrightarrow{y}=\overrightarrow{e}_{TEt}(a-x,y)\overrightarrow{y}$$

The condition is automatically satisfied if $N_{n3}=N_{n1}$
The next step is to calculate the waveguide eigenvalues k_{C_t} as well as the normalization coefficients. For this purpose the continuity of the fields across the planes $x=s$ and $x=a-s$ must be taken into account. More specifically, at the border between the trough region and the gap, the fields present no singularity and the expressions that represent them, must ensure the smooth transition from one region to the other. The mathematical formulations of the above remarks are:
For $0 \leq y \leq d$

$$\begin{cases} g_{h1t}(s,y)=g_{h2t}(\frac{a}{2}-s,y) \\ \vec{E}_{1t}(s,y,z)=\vec{E}_{2t}(\frac{a}{2}-s,y,z) \\ \vec{H}_{1t}(s,y,z)=\vec{H}_{2t}(\frac{a}{2}-s,y,z) \end{cases} \qquad (A.14)$$

$$\begin{cases} g_{h2t}(s-\frac{a}{2},y)=g_{h3t}(a-s,y) \\ \vec{E}_{2t}(s-\frac{a}{2},y,z)=\vec{E}_{3t}(a-s,y,z) \\ \vec{H}_{2t}(s-\frac{a}{2},y,z)=\vec{H}_{3t}(a-s,y,z) \end{cases} \qquad (A.15)$$

The magnetic scalar potential and the y-component of the E-field will be examined. The y-component of the E-field is expanded as a Fourier series:

$$E_{yb}(s,y)=\begin{cases} \sum_{p=0}^{\infty} C_p\cos(\frac{p\pi}{d}y), 0 \leq y \leq d \\ 0, d \leq y \leq b \end{cases}$$

The following conditions must be satisfied:

$$\mathrm{E_{y1}(s,y)=E_{yb}(s,y)}\Rightarrow$$
$$\sum_{n=0}^{\infty}\mathrm{N_{n1}}\alpha_{\mathrm{n1t}}\sin(\alpha_{\mathrm{n1t}}\mathrm{s})\cos(\tfrac{\mathrm{n}\pi}{\mathrm{b}}\mathrm{y})=\sum_{p=0}^{\infty}\mathrm{C_p}\cos(\tfrac{\mathrm{p}\pi}{\mathrm{d}}\mathrm{y}) \qquad (A.16)$$

$$\mathrm{E_{y2}(s,y)=E_{yb}(s,y)}\Rightarrow$$
$$\sum_{m=0}^{\infty}\mathrm{N_{m2}}\alpha_{\mathrm{m2t}}\cos[\alpha_{\mathrm{m2t}}(\tfrac{\mathrm{a}}{2}-\mathrm{s})]\cos(\tfrac{\mathrm{m}\pi}{\mathrm{d}}\mathrm{y})=\sum_{p=0}^{\infty}\mathrm{C_p}\cos(\tfrac{\mathrm{p}\pi}{\mathrm{d}}\mathrm{y}) \qquad (A.17)$$

Multiplication of both sides of (A.16) with $\cos(\frac{\mathrm{l}\pi}{\mathrm{d}}\mathrm{y})$ and integration with respect to y from 0 to b lead to the expression:

$$\mathrm{N_{n1}}\alpha_{\mathrm{n1t}}\sin(\alpha_{\mathrm{n1t}}\mathrm{s})\varepsilon_{\mathrm{n}}\frac{\mathrm{b}}{2}=\int_0^{\mathrm{d}}\sum_{l=0}^{\infty}\mathrm{C_l}\cos(\frac{\mathrm{l}\pi}{\mathrm{d}}\mathrm{y})\cos(\frac{\mathrm{n}\pi}{\mathrm{b}}\mathrm{y})\mathrm{dy} \qquad (A.18)$$

Similarly, multiplication of both sides of (A.17) with $\cos(\frac{\mathrm{l}\pi}{\mathrm{d}}\mathrm{y})$ and integration with respect to y from 0 to d lead to the expression:

$$\mathrm{N_{m2}}\alpha_{\mathrm{m2t}}\cos[\alpha_{\mathrm{m2t}}(\frac{\mathrm{a}}{2}-\mathrm{s})]=\mathrm{C_m} \qquad (A.19)$$

where:

$$\varepsilon_{\mathrm{q}}=\begin{cases}1, \mathrm{q}\neq 0\\ 2, \mathrm{q}=0\end{cases}$$

Continuity of the magnetic scalar potential yields:

$$\sum_{n=0}^{\infty}\mathrm{N_{n1}}\cos(\alpha_{\mathrm{n1t}}\mathrm{x})\cos(\frac{\mathrm{n}\pi}{\mathrm{b}}\mathrm{y})=\sum_{m=0}^{\infty}\mathrm{N_{m2}}\sin[\alpha_{\mathrm{m2t}}(\frac{\mathrm{a}}{2}-\mathrm{s})]\cos(\frac{\mathrm{m}\pi}{\mathrm{d}}\mathrm{y}) \qquad (A.20)$$

After substitution of (A.18) and (A.19) into (A.20) the following expression is obtained:

$$\sum_{m=0}^{\infty}\frac{\sin[\alpha_{\mathrm{m2t}}(\frac{\mathrm{a}}{2}-\mathrm{s})]\cos(\frac{\mathrm{m}\pi}{\mathrm{d}}\mathrm{y})\mathrm{C_m}}{\alpha_{\mathrm{m2t}}\cos[\alpha_{\mathrm{m2t}}(\frac{\mathrm{a}}{2}-\mathrm{s})]}=$$
$$\sum_{n=0}^{\infty}\frac{2\cos(\alpha_{\mathrm{n1t}}\mathrm{s})\cos(\frac{\mathrm{n}\pi}{\mathrm{b}}\mathrm{y})}{\alpha_{\mathrm{n1t}}\sin(\alpha_{\mathrm{n1t}}\mathrm{s})\varepsilon_{\mathrm{n}}\mathrm{b}}\int_0^{\mathrm{d}}\sum_{l=0}^{\infty}\mathrm{C_l}\cos(\frac{\mathrm{l}\pi}{\mathrm{d}}\mathrm{y})\cos(\frac{\mathrm{n}\pi}{\mathrm{b}}\mathrm{y})\mathrm{dy}$$

Both members of the former equation are multiplied with $\cos(\frac{\mathrm{p}\pi}{\mathrm{d}}\mathrm{y})$ and integrated with respect to y from 0 to d, thus yielding the matrix equation, which determines the ridged waveguide eigenvalues for the odd TE modes:

$$\mathbf{H}_{\mathrm{TE}}^{\mathrm{odd}}\mathbf{C}=\mathbf{0} \qquad (A.21)$$

The matrix elements are:

$$\mathbf{H}_{\mathrm{TE_{i,j}}}^{\mathrm{odd}}=\frac{\tan[\alpha_{\mathrm{m2t}}(\frac{\mathrm{a}}{2}-\mathrm{s})]\mathrm{d}\varepsilon_{\mathrm{n}}\delta_{\mathrm{i,j}}}{2\alpha_{\mathrm{m2t}}}-\sum_{n=0}^{\infty}\frac{2\cot(\alpha_{\mathrm{n1t}}\mathrm{s})}{\alpha_{\mathrm{n1t}}\varepsilon_{\mathrm{n}}\mathrm{b}}\mathrm{P_{in}}\mathrm{P_{jn}}$$

where:

$$\mathrm{P_{in}}=\int_0^{\mathrm{d}}\cos(\tfrac{\mathrm{i}\pi}{\mathrm{d}}\mathrm{y})\cos(\tfrac{\mathrm{n}\pi}{\mathrm{b}}\mathrm{y})\mathrm{dy}$$
$$\mathrm{P_{jn}}=\int_0^{\mathrm{d}}\cos(\tfrac{\mathrm{i}\pi}{\mathrm{d}}\mathrm{y})\cos(\tfrac{\mathrm{n}\pi}{\mathrm{b}}\mathrm{y})\mathrm{dy}$$

The roots of equation (A.21) can be found graphically and they represent the waveguide eigenvalues. The corresponding eigenvectors [C] in association with the orthogonality condition will be used to determine the normalization coefficients $\mathrm{N_{m2}}$ and $\mathrm{N_{n1}}$, as indicated by expressions (A.18) and (A.19).

A.1.2 Even TE modes

In case of even TE modes the plane $x = \frac{a}{2}$ is considered as an electric wall. The boundary conditions in regions III and I for the TE odd modes apply also in the case of the TE even modes. Therefore, the eigenvectors inside the trough region can be expressed by (A.11) and (A.13). The only difference in the boundary conditions in region II emerges from the presence of the electric wall at plane $x = \frac{a}{2}$:

Region II:

$$\begin{cases} E_x(x,0,z) = 0, s \le x \le a - s \\ E_x(x,d,z) = 0, s \le x \le a - s \\ E_y(\frac{a}{2},y,z) = 0, 0 \le y \le d \text{ (electric wall)} \end{cases}$$

All eigenvectors inside region II must satisfy the wave equation (A.1). The solution is written in the form:

$$g_{h2t}(x,y) = \sum_{m=0}^{\infty} [A_{m2}\cos(\alpha_{m2t}x) + B_{m2}\sin(\alpha_{m2t}x)][C_{m2}\cos(\beta_{m2t}y) + D_{m2}\sin(\beta_{m2t}y)] \qquad (A.23)$$

where: $k_{Ct}^2 = \alpha_{m2t}^2 + \beta_{m2t}^2$
Implementation of the boundary conditions:
For $s \le x \le a - s$:

$$E_x(x,0) = 0 \overset{(A.3)}{\Rightarrow} \frac{\partial g_{h2t}(x,y)}{\partial y} = 0|_{y=0} \Rightarrow D_{m2} = 0$$

For $s \le x \le a - s$:

$$E_x(x,d) = 0 \overset{(A.3)}{\Rightarrow} \frac{\partial g_{h2t}(x,y)}{\partial y} = 0|_{y=d} \Rightarrow b_{m2t} = \frac{m\pi}{d}$$

For $0 \le y \le d$:

$$E_y(\frac{a}{2},y) = 0 \overset{(A.3)}{\Rightarrow} \frac{\partial g_{h2t}(x,y)}{\partial x} = 0|_{x=\frac{a}{2}} \Rightarrow \begin{cases} A_{m2} = \cos(\alpha_{m2t}\frac{a}{2}) \\ B_{m2} = \sin(\alpha_{m2t}\frac{a}{2}) \end{cases}$$

$$k_{C_t}^2 = \alpha_{m2t}^2 + \beta_{m2t}^2 \Rightarrow \alpha_{m2t} = \begin{cases} \sqrt{k_{C_t}^2 - \left(\frac{m\pi}{d}\right)^2}, k_{C_t} \ge \frac{m\pi}{d} \\ -j\sqrt{\left(\frac{m\pi}{d}\right)^2 - k_{C_t}^2}, k_{C_t} \le \frac{m\pi}{d} \end{cases}$$

Substitution of the previous results into (A.23) yields the expressions for the magnetic scalar potential and the corresponding eigenvectors in region II:

$$g_{h2t}(x,y) = \sum_{m=0}^{\infty} N_{m2}\cos[\alpha_{m2t}(\frac{a}{2} - x)]\cos(\frac{m\pi}{d}y) \qquad (A.24)$$

The normalization coefficient N_{m2} will be determined later.
Due to the electric wall at plane $x = \frac{a}{2}$ the following condition must apply:

$$\vec{e}_{TEt}(x,y)\vec{y} = -\vec{e}_{TEt}(a - x,y)\vec{y}$$

The condition is automatically satisfied if $N_{n1} = -N_{n3}$ The waveguide eigenvalues and the normalization coefficients are determined by the implementation of the field continuity conditions at planes $x = s$ and $x = a - s$. The continuity conditions are given by expressions (A.14) and (A.15). The y-component of the E-field is expanded as a Fourier series:

$$E_{yb}(s,y)=\begin{cases}\sum\limits_{p=0}^{\infty} C_p\cos(\frac{p\pi}{d}y), 0\le y\le d\\ 0, d\le y\le b\end{cases}$$

The following conditions must be satisfied:

$$E_{y1}(s,y)=E_{yb}(s,y)\Rightarrow$$
$$\sum_{n=0}^{\infty} N_{n1}\alpha_{n1t}\sin(\alpha_{n1t}s)\cos(\tfrac{n\pi}{b}y)=\sum_{p=0}^{\infty} C_p\cos(\tfrac{p\pi}{d}y) \qquad (A.25)$$

$$E_{y2}(s,y)=E_{yb}(s,y)\Rightarrow$$
$$-\sum_{m=0}^{\infty} N_{m2}\alpha_{m2t}\sin[\alpha_{m2t}(\tfrac{a}{2}-s)]\cos(\tfrac{m\pi}{d}y)=\sum_{p=0}^{\infty} C_p\cos(\tfrac{p\pi}{d}y) \qquad (A.26)$$

Multiplication of both sides of (A.25) with $\cos(\frac{l\pi}{d})$ and integration with respect to y from 0 to b lead to the expression:

$$N_{n1}\alpha_{n1t}\sin(\alpha_{n1t}s)\varepsilon_n\frac{b}{2}=\int_0^d\sum_{l=0}^{\infty} C_l\cos(\frac{l\pi}{d}y)\cos(\frac{n\pi}{b}y)dy \qquad (A.27)$$

Similarly, multiplication of both sides of (A.26) with $\cos(\frac{l\pi}{d})$ and integration with respect to y from 0 to d lead to the expression:

$$-N_{m2}\alpha_{m2t}\sin[\alpha_{m2t}(\frac{a}{2}-s)]=C_m \qquad (A.28)$$

where: $\varepsilon_q=\begin{cases}1, q\neq 0\\ 2, q=0\end{cases}$

Continuity of the magnetic scalar potential:

$$\sum_{n=0}^{\infty} N_{n1}\cos(\alpha_{n1t}x)\cos(\frac{n\pi}{b}y)=\sum_{m=0}^{\infty} N_{m2}\cos[\alpha_{m2t}(\frac{a}{2}-s)]\cos(\frac{m\pi}{d}y) \qquad (A.29)$$

Substitution of (A.27) and (A.28) into (A.29) yields:

$$\sum_{m=0}^{\infty}\frac{\cos[\alpha_{m2t}(\frac{a}{2}-s)]\cos(\frac{m\pi}{d}y)C_m}{\alpha_{m2t}\sin[\alpha_{m2t}(\frac{a}{2}-s)]}=$$
$$-\sum_{n=0}^{\infty}\frac{2\cos(\alpha_{n1t}s)\cos(\frac{n\pi}{b}y)}{\alpha_{n1t}\sin(\alpha_{n1t}s)\varepsilon_n b}\int_0^d\sum_{l=0}^{\infty} C_l\cos(\tfrac{l\pi}{d}y)\cos(\tfrac{n\pi}{b}y)dy$$

The matrix equation that determines the ridged waveguide eigenvalues for the even TE modes is obtained after multiplication of both sides of the former equation with $\cos(\frac{p\pi}{d})$ and integration with respect to y from 0 to d:

$$\mathbf{H}_{TE}^{even}\mathbf{C}=\mathbf{0} \qquad (A.30)$$

The matrix elements are:

$$\mathbf{H}_{TE_{i,j}}^{even}=\frac{\cot[\alpha_{m2t}(\frac{a}{2}-s)]d\varepsilon_n\delta_{i,j}}{2\alpha_{m2t}}+\sum_{n=0}^{\infty}\frac{2\cot(\alpha_{n1t}s)}{\alpha_{n1t}\varepsilon_n b}P_{in}P_{jn}$$

where:

$$P_{in}=\int_0^d \cos(\tfrac{i\pi}{d}y)\cos(\tfrac{n\pi}{b}y)dy$$
$$P_{jn}=\int_0^d \cos(\tfrac{i\pi}{d}y)\cos(\tfrac{n\pi}{b}y)dy$$

The waveguide eigenvalues result from the graphical solution of (A.30). The corresponding eigenvectors [C] contribute to the determination of coefficients N_{m2} and N_{n1}, according to expressions (A.27) and (A.28).

A.2 TM Modes

The transverse eigenvectors for the t TM mode are:

$$\overrightarrow{e}_{TM_t}=\frac{\gamma_t}{\omega\varepsilon}\nabla g_{et}(x,y)$$
$$\overrightarrow{h}_{TM_t}=\nabla g_{et}(x,y)\times\overrightarrow{z}$$

Orthogonality condition:

$$\int\int_{S_w} e_{TM_t}e_{TM_s}dS=\delta_{t,s}$$

A.2.1 Odd TM Modes

In case of odd TM modes the plane $x=\frac{a}{2}$ is considered as magnetic wall. The boundary conditions for all regions are:

Region I:

$$\begin{cases} E_x(x,0,z)=0, 0\le x\le s \\ E_x(x,b,z)=0, 0\le x\le s \\ E_y(0,y,z)=0, 0\le y\le b \\ E_y(s,y,z)=0, 0\le y\le b \end{cases} \quad (A.31)$$

Region II:

$$\begin{cases} E_x(x,0,z)=0, a-s\le x\le a \\ E_x(x,b,z)=0, a-s\le x\le a \\ E_y(a,y,z)=0, 0\le y\le b \\ E_y(a-s,y,z)=0, 0\le y\le b \end{cases} \quad (A.32)$$

Region II:

$$\begin{cases} E_x(x,0,z)=0, s\le x\le a-s \\ E_x(x,d,z)=0, s\le x\le a-s \\ E_x(\frac{a}{2},y,z)=0, 0\le y\le b \text{ (magnetic wall)} \end{cases} \quad (A.33)$$

Each eigenvector must satisfy the wave equation (A.1). The solution of (A.1) has the form:

$$g_{eit}(x,y)=\sum_{n=0}^{\infty}[A_{ni}\cos(\alpha_{nit}x)+B_{ni}\sin(\alpha_{nit}x)][C_{ni}\cos(\beta_{nit}y)+D_{ni}\sin(\beta_{nit}y)] \quad (A.34)$$

where: $k_{Ct}^2=\alpha_{nit}^2+\beta_{nit}^2$
Implementation of the boundary conditions for each region leads to the final expressions for the

scalar potential:

Region I:
For $0 \leq x \leq s$:

$$E_x(x,0) = 0 \overset{(A.5)}{\Rightarrow} \frac{\partial g_{e1t}(x,y)}{\partial x} = 0|_{y=0} \Rightarrow C_{n1} = 0$$

For $0 \leq y \leq b$:

$$E_y(0,y) = 0 \overset{(A.5)}{\Rightarrow} \frac{\partial g_{e1t}(x,y)}{\partial y} = 0|_{x=0} \Rightarrow A_{n1} = 0$$

For $0 \leq x \leq s$:

$$E_x(x,b) = 0 \overset{(A.5)}{\Rightarrow} \frac{\partial g_{e1t}(x,y)}{\partial x} = 0|_{y=b} \Rightarrow b_{n1t} = \frac{n\pi}{b}$$

$$k_{C_t}^2 = \alpha_{n1t}^2 + \beta_{n1t}^2 \Rightarrow \alpha_{n1t} = \begin{cases} \sqrt{k_{C_t}^2 - \left(\frac{n\pi}{b}\right)^2}, k_{C_t} \geq \frac{n\pi}{b} \\ -j\sqrt{\left(\frac{n\pi}{b}\right)^2 - k_{C_t}^2}, k_{C_t} \leq \frac{n\pi}{b} \end{cases}$$

Substitution of the previous results into (A.34) yields the expressions for the magnetic scalar potential and the corresponding eigenvectors in region I:

$$g_{e1t}(x,y) = \sum_{n=1}^{\infty} M_{n1} \cos(\alpha_{n1t} x) \sin(\frac{n\pi}{b} y) \qquad (A.35)$$

Coefficient M_{n1} will be determined at a later stage.
Region II:
For $s \leq x \leq a - s$:

$$E_x(x,0) = 0 \overset{(A.5)}{\Rightarrow} \frac{\partial g_{e2t}(x,y)}{\partial x} = 0|_{y=0} \Rightarrow C_{m2} = 0$$

For $s \leq x \leq a - s$:

$$E_x(x,d) = 0 \overset{(A.5)}{\Rightarrow} \frac{\partial g_{e2t}(x,y)}{\partial x} = 0|_{y=d} \Rightarrow b_{m2t} = \frac{m\pi}{d}$$

For $0 \leq y \leq b$:

$$E_x(\frac{a}{2}, y) = 0 \overset{(A.5)}{\Rightarrow} \frac{\partial g_{e2t}(x,y)}{\partial x} = 0|_{x=\frac{a}{2}} \Rightarrow \begin{cases} A_{m2} = \cos(a_{m2t}\frac{a}{2}) \\ B_{m2} = \sin(a_{m2t}\frac{a}{2}) \end{cases}$$

$$k_{C_t}^2 = \alpha_{m2t}^2 + \beta_{m2t}^2 \Rightarrow \alpha_{m2t} = \begin{cases} \sqrt{k_{C_t}^2 - \left(\frac{m\pi}{d}\right)^2}, k_{C_t} \geq \frac{m\pi}{d} \\ -j\sqrt{\left(\frac{m\pi}{d}\right)^2 - k_{C_t}^2}, k_{C_t} \leq \frac{m\pi}{d} \end{cases}$$

Substitution of the previous results into (A.34) yields the expressions for the magnetic scalar potential and the corresponding eigenvectors in region II:

$$g_{e2t}(x,y) = \sum_{m=1}^{\infty} M_{m2} \cos[\alpha_{m2t}(\frac{a}{2} - x)] \sin(\frac{m\pi}{d} y) \qquad (A.36)$$

where M_{m2} is a normalization coefficient.

Region III:
For $a - s \leq x \leq a$:

$$E_x(x,0) = 0 \overset{(A.5)}{\Rightarrow} \frac{\partial g_{e3t}(x,y)}{\partial x} = 0|_{y=0} \Rightarrow C_{n3} = 0$$

For $0 \leq y \leq d$:

$$E_y(a,y) = 0 \overset{(A.5)}{\Rightarrow} \frac{\partial g_{e3t}(x,y)}{\partial y} = 0|_{x=a} \Rightarrow \begin{cases} A_{n3} = -\sin(a_{n3t}a) \\ B_{n3} = \cos(a_{n3t}a) \end{cases}$$

For $a - s \leq x \leq a$:

$$E_x(x,b) = 0 \overset{(A.5)}{\Rightarrow} \frac{\partial g_{e3t}(x,y)}{\partial x} = 0|_{y=b} \Rightarrow b_{n3t} = \frac{n\pi}{b}$$

$$k_{C_t}^2 = \alpha_{n3t}^2 + \beta_{n3t}^2 \Rightarrow \alpha_{n3t} = \begin{cases} \sqrt{k_{C_t}^2 - \left(\frac{n\pi}{b}\right)^2}, k_{C_t} \geq \frac{n\pi}{b} \\ -j\sqrt{\left(\frac{n\pi}{b}\right)^2 - k_{C_t}^2}, k_{C_t} \leq \frac{n\pi}{b} \end{cases}$$

Substitution of the previous results into (A.34) yields the expressions for the magnetic scalar potential and the corresponding eigenvectors in region I:

$$g_{e3t}(x,y) = \sum_{n=1}^{\infty} M_{n3} \sin[\alpha_{n3t}(x-a)] \cos(\frac{n\pi}{b}y) \qquad (A.37)$$

where M_{n3} is a normalization coefficient.
Due to the magnetic wall at plane $x = \frac{a}{2}$ the following condition must be satisfied:

$$\overrightarrow{e}_{TEt}(x,y)\overrightarrow{y} = \overrightarrow{e}_{TEt}(a-x,y)\overrightarrow{y}$$

The condition is automatically satisfied if $M_{n1} = M_{n3}$
Computation of the waveguide eigenvalues k_{C_t} and the normalization coefficients is performed, after taking the conditions for the continuity of the fields into consideration:

For $0 \leq y \leq d$

$$\begin{cases} g_{e1t}(s,y) = g_{e2t}(\frac{a}{2} - s, y) \\ \vec{E}_{1t}(s,y,z) = \vec{E}_{2t}(\frac{a}{2} - s, y, z) \\ \vec{H}_{1t}(s,y,z) = \vec{H}_{2t}(\frac{a}{2} - s, y, z) \end{cases}$$

$$\begin{cases} g_{e2t}(s - \frac{a}{2}, y) = g_{e3t}(a - s, y) \\ \vec{E}_{2t}(s - \frac{a}{2}, y, z) = \vec{E}_{3t}(a - s, y, z) \\ \vec{H}_{2t}(s - \frac{a}{2}, y, z) = \vec{H}_{3t}(a - s, y, z) \end{cases}$$

The y-component of the H-field and the electric scalar potential will be examined. The electric scalar potential at plane $x = s$ is expanded as a Fourier series:

$$g_{eb}(s,y) = \begin{cases} \sum_{q=1}^{\infty} C_q \sin(\frac{q\pi}{d}y), 0 \leq y \leq d \\ 0, d \leq y \leq b \end{cases}$$

The following conditions must be satisfied:

$$g_{e1i}(s,y) = g_{eb}(s,y) \Rightarrow$$
$$\sum_{n=1}^{\infty} M_{n1}\sin(\alpha_{n1t}s)\sin(\tfrac{n\pi}{b}y) = \sum_{q=1}^{\infty} C_q \sin(\tfrac{q\pi}{d}y) \qquad (A.40)$$

$$g_{e2i}(s,y) = g_{eb}(s,y) \Rightarrow$$
$$\sum_{m=1}^{\infty} M_{m2}\cos[\alpha_{m2t}(\tfrac{a}{2}-s)]\sin(\tfrac{m\pi}{b}y) = \sum_{q=1}^{\infty} C_q \sin(\tfrac{q\pi}{d}y) \qquad (A.41)$$

Multiplication of both sides of (A.40) with $\sin(\frac{s\pi}{d})$ and integration with respect to y from 0 to b lead to the expression:

$$M_{n1}\sin(\alpha_{n1t}s)\frac{b}{2} = \int_0^d \sum_{s=1}^{\infty} C_s \sin(\frac{s\pi}{d}y)\sin(\frac{n\pi}{b}y)dy \qquad (A.42)$$

Similarly, multiplication of both sides of (A.41) with $\sin(\frac{s\pi}{d})$ and integration with respect to y from 0 to d lead to the expression:

$$M_{s2}\cos[\alpha_{s2t}(\frac{a}{2}-s)] = C_s \qquad (A.43)$$

Continuity of the y-component of the H-field:

$$H_{y1}(s,y) = H_{y2}(s,y) \overset{(A.6)}{\Rightarrow} \tfrac{\partial g_{e1t}}{\partial x}|_{x=s} = \tfrac{\partial g_{e2t}}{\partial x}|_{x=s} \Rightarrow$$
$$\sum_{n=1}^{\infty} M_{n1}\alpha_{n1t}\cos(\alpha_{n1t}s)\sin(\tfrac{n\pi}{b}y) = \sum_{m=1}^{\infty} M_{m2}\alpha_{m2t}\sin[\alpha_{m2t}(\tfrac{a}{2}-s)]\sin(\tfrac{m\pi}{d}y) \qquad (A.44)$$

Substitution of (A.42) and (A.43) into (A.44) yields:

$$\sum_{m=1}^{\infty} \frac{\alpha_{m2t}\sin[\alpha_{m2t}(\frac{a}{2}-s)]\sin(\frac{m\pi}{d}y)C_m}{\cos[\alpha_{m2t}(\frac{a}{2}-s)]} =$$
$$\sum_{n=1}^{\infty} \frac{2\alpha_{n1t}\cos(\alpha_{n1t}s)\sin(\frac{n\pi}{b}y)}{\sin(\alpha_{n1t}s)b} \int_0^d \sum_{s=1}^{\infty} C_s \sin(\tfrac{s\pi}{d}y)\sin(\tfrac{n\pi}{b}y)dy$$

Both members of the preceding expression are multiplied with $\sin(\frac{s\pi}{d})$ and integrated with respect to y from 0 to d, thus yielding the matrix equation, which determines the ridged waveguide eigenvalues for the odd TM modes:

$$\mathbf{H}_{TM}^{odd}\mathbf{C} = \mathbf{0} \qquad (A.45)$$

The matrix elements are:

$$\mathbf{H}_{TM_{i,j}}^{odd} = \frac{\tan[\alpha_{m2t}(\frac{a}{2}-s)]\alpha_{m2t}d\delta_{i,j}}{2} - \sum_{n=0}^{\infty} \frac{2\alpha_{n1t}\cot(\alpha_{n1t}s)}{b} P_{in}P_{jn}$$

where:

$$P_{in} = \int_0^d \sin(\frac{i\pi}{d}y)\sin(\frac{n\pi}{b}y)dy$$

$$P_{jn} = \int_0^d \sin(\frac{j\pi}{d}y)\sin(\frac{n\pi}{b}y)dy$$

The roots of equation (A.45) represent the waveguide eigenvalues and can be found graphically. The corresponding eigenvectors [C] in association with the orthogonality condition will be used to determine the normalization coefficients M_{n1} and M_{m2}, as indicated by expressions (A.42) and (A.43).

A.2.2 Even TM Modes

In case of even TM modes the plane $x = \frac{a}{2}$ is considered as electric wall. The boundary conditions for regions III and I are the ones that apply in the case of odd TM modes. The only difference is observed in region II due to the presence of the electric wall.

Region II:

$$\begin{cases} E_x(x,0,z) = 0, s \le x \le a - s \\ E_x(x,d,z) = 0, s \le x \le a - s \\ E_y(\frac{a}{2},y,z) = 0, 0 \le y \le b \text{ (electric wall)} \end{cases} \qquad (A.46)$$

Each eigenvector must satisfy the wave equation (A.1). Equation (A.1) has a solution of the form:

$$g_{eit}(x,y) = \sum_{n=0}^{\infty} [A_{ni}\cos(\alpha_{nit}x) + B_{ni}\sin(\alpha_{nit}x)][C_{ni}\cos(\beta_{nit}y) + D_{ni}\sin(\beta_{nit}y)] \qquad (A.47)$$

where: $k_{Ct}^2 = \alpha_{nit}^2 + \beta_{nit}^2$
Implementation of the boundary conditions for each region leads to the final expressions for the eigenvectors:
Region II:

For $s \le x \le a - s$:

$$E_x(x,0) = 0 \overset{(A.5)}{\Rightarrow} \frac{\partial g_{e2t}(x,y)}{\partial x} = 0|_{y=0} \Rightarrow C_{m2} = 0$$

For $s \le x \le a - s$:

$$E_x(x,d) = 0 \overset{(A.5)}{\Rightarrow} \frac{\partial g_{e2t}(x,y)}{\partial x} = 0|_{y=d} \Rightarrow b_{m2t} = \frac{m\pi}{d}$$

For $0 \le y \le d$:

$$E_x(\frac{a}{2},y) = 0 \overset{(A.5)}{\Rightarrow} \frac{\partial g_{e2t}(x,y)}{\partial y} = 0|_{x=\frac{a}{2}} \Rightarrow \begin{cases} A_{m2} = \sin(a_{m2t}\frac{a}{2}) \\ B_{m2} = -\cos(a_{m2t}\frac{a}{2}) \end{cases}$$

$$k_{C_t}^2 = \alpha_{m2t}^2 + \beta_{m2t}^2 \Rightarrow \alpha_{m2t} = \begin{cases} \sqrt{k_{C_t}^2 - \left(\frac{m\pi}{d}\right)^2}, k_{C_t} \ge \frac{m\pi}{d} \\ -j\sqrt{\left(\frac{m\pi}{d}\right)^2 - k_{C_t}^2}, k_{C_t} \le \frac{m\pi}{d} \end{cases}$$

Substitution of the previous results into (A.47) yields the expressions for the electric scalar potential and the corresponding eigenvectors in region II:

$$g_{e2t}(x,y) = \sum_{m=1}^{\infty} M_{m2}\sin[\alpha_{m2t}(\frac{a}{2} - x)]\sin(\frac{m\pi}{d}y) \qquad (A.48)$$

where M_{m2} is a normalization coefficient.
Due to the electric wall at plane $x = \frac{a}{2}$ the following condition must be satisfied:

$$\vec{e}_{TMt}(x,y)\vec{y} = -\vec{e}_{TMt}(a - x,y)\vec{y}$$

The condition is automatically satisfied if $M_{n1} = -M_{n3}$
For the determination of the waveguide eigenvalues k_{C_t} and the normalization coefficients, the continuity conditions (A.38) and (A.39) are taken into consideration. The electric scalar potential at

plane $x = s$ is expanded as a Fourier series:

$$\mathrm{g_{eb}(s,y)} = \begin{cases} \sum\limits_{\mathrm{q=1}}^{\infty} \mathrm{C_q sin(\frac{q\pi}{d} y)}, 0 \le \mathrm{y} \le \mathrm{d} \\ 0, \mathrm{d} \le \mathrm{y} \le \mathrm{b} \end{cases}$$

The following conditions must be satisfied:

$$\mathrm{ge1i(s,y) = geb(s,y)} \Rightarrow$$
$$\sum_{\mathrm{n=1}}^{\infty} \mathrm{M_{n1} sin(\alpha_{n1t} s) sin(\frac{n\pi}{b} y)} = \sum_{\mathrm{q=1}}^{\infty} \mathrm{C_q sin(\frac{q\pi}{d} y)} \qquad (A.49)$$

$$\mathrm{ge2i(s,y) = geb(s,y)} \Rightarrow$$
$$\sum_{\mathrm{m=1}}^{\infty} \mathrm{N_{m2} sin[\alpha_{m2t}(\frac{a}{2} - s)] sin(\frac{m\pi}{b} y)} = \sum_{\mathrm{q=1}}^{\infty} \mathrm{C_q sin(\frac{q\pi}{d} y)} \qquad (A.50)$$

Multiplication of both sides of (A.49) with $\mathrm{sin(\frac{s\pi}{d})}$ and integration with respect to y from 0 to b lead to the expression:

$$\mathrm{M_{n1} sin(\alpha_{n1t} s)} \frac{\mathrm{b}}{2} = \int_0^{\mathrm{d}} \sum_{\mathrm{s=1}}^{\infty} \mathrm{C_s sin(\frac{s\pi}{d} y) sin(\frac{n\pi}{b} y) dy} \qquad (A.51)$$

Similarly, multiplication of both sides of (A.50) with $\mathrm{sin(\frac{s\pi}{d})}$ and integration with respect to y from 0 to d lead to the expression:

$$\mathrm{M_{s2} sin[\alpha_{s2t}(\frac{a}{2} - s)]} = \mathrm{C_s} \qquad (A.52)$$

Continuity of the y-component of the H-field:

$$\mathrm{H_{y1}(s,y) = H_{y2}(s,y)} \overset{(A.6)}{\Rightarrow} \mathrm{\frac{\partial g_{e1t}}{\partial x}|_{x=s} = \frac{\partial g_{e2t}}{\partial x}|_{x=s}} \Rightarrow$$
$$\sum_{\mathrm{n=1}}^{\infty} \mathrm{M_{n1} \alpha_{n1t} cos(\alpha_{n1t} s) sin(\frac{n\pi}{b} y)} = -\sum_{\mathrm{m=1}}^{\infty} \mathrm{M_{m2} \alpha_{m2t} cos[\alpha_{m2t}(\frac{a}{2} - s)] sin(\frac{m\pi}{d} y)} \qquad (A.53)$$

Substitution of (A.51) and (A.52) into (A.53) yields:

$$\sum_{\mathrm{m=1}}^{\infty} \mathrm{\frac{\alpha_{m2t} cos[\alpha_{m2t}(\frac{a}{2} - s)] sin(\frac{m\pi}{d} y) C_m}{sin[\alpha_{m2t}(\frac{a}{2} - s)]}} =$$
$$-\sum_{\mathrm{n=1}}^{\infty} \mathrm{\frac{2\alpha_{n1t} cos(\alpha_{n1t} s) sin(\frac{n\pi}{b} y)}{sin(\alpha_{n1t} s) b}} \int_0^{\mathrm{d}} \sum_{\mathrm{s=1}}^{\infty} \mathrm{C_s sin(\frac{s\pi}{d} y) sin(\frac{n\pi}{b} y) dy}$$

The matrix equation that determines the ridged waveguide eigenvalues for the even TE modes is obtained after multiplication of both sides of the former equation with $\mathrm{sin(\frac{s\pi}{d})}$ and integration with respect to y from 0 to d:

$$\mathbf{H}_{\mathrm{TM}}^{\mathrm{even}} \mathbf{C} = \mathbf{0} \qquad (A.54)$$

The matrix elements are:

$$\mathbf{H}_{\mathrm{TM_{i,j}}}^{\mathrm{even}} = \frac{\mathrm{cot[\alpha_{m2t}(\frac{a}{2} - s)] \alpha_{m2t} d\delta_{i,j}}}{2} + \sum_{\mathrm{n=0}}^{\infty} \mathrm{\frac{2\alpha_{n1t} cot(\alpha_{n1t} s)}{b}} \mathrm{P_{in} P_{jn}}$$

where:

$$P_{in}=\int_0^d \sin(\frac{i\pi}{d}y)\sin(\frac{n\pi}{b}y)dy$$

$$P_{jn}=\int_0^d \sin(\frac{j\pi}{d}y)\sin(\frac{n\pi}{b}y)dy$$

The roots of equation (A.54) can be found graphically and they represent the waveguide eigenvalues. The corresponding eigenvectors [C] in association with the orthogonality condition will be used to determine the normalization coefficients M_{n1} and M_{m2}, as indicated by expressions (A.51) and (A.52).

Finally, the analytical expressions for the eigenvectors of all waveguide modes are cited below:

1. **Odd TE Modes**

   - trough region:

$$\overrightarrow{E}_i(x,y,z) = -j\omega\mu[-\sum_{n=1}^{\infty} N_{n1}\tfrac{n\pi}{b}\cos(\alpha_{n1t}x)\sin(\tfrac{n\pi}{b}y)\overrightarrow{x}+ \\ +\sum_{n=0}^{\infty} N_{n1}\alpha_{n1t}\sin(\alpha_{n1t}x)\cos(\tfrac{n\pi}{b}y)\overrightarrow{y}]e^{-j\gamma_\iota z} \qquad (A.55)$$

$$\overrightarrow{H}_i(x,y,z) = [j\gamma_t\sum_{n=0}^{\infty} N_{n1}\alpha_{n1t}\sin(\alpha_{n1t}x)\cos(\tfrac{n\pi}{b}y)\overrightarrow{x}+ \\ +j\gamma_t\sum_{n=1}^{\infty} N_{n1}\tfrac{n\pi}{b}\cos(\alpha_{n1t}x)\sin(\tfrac{n\pi}{b}y)\overrightarrow{y}+ \\ +k_{Ct}^2\sum_{n=0}^{\infty} N_{n1}\cos(\alpha_{n1t}x)\cos(\tfrac{n\pi}{b}y)\overrightarrow{z}]e^{-j\gamma_\iota z} \qquad (A.56)$$

   - gap:

$$\overrightarrow{E}_i(x,y,z) = -j\omega\mu\{-\sum_{m=1}^{\infty} N_{m2}\tfrac{m\pi}{d}\sin[\alpha_{m2t}(\tfrac{a}{2}-x)]\sin(\tfrac{m\pi}{d}y)\overrightarrow{x}+ \\ +\sum_{m=0}^{\infty} N_{m2}\alpha_{m2t}\cos[\alpha_{m2t}(\tfrac{a}{2}-x)]\cos(\tfrac{m\pi}{d}y)\overrightarrow{y}\}e^{-j\gamma_\iota z} \qquad (A.57)$$

$$\overrightarrow{H}_i(x,y,z) = \{j\gamma_t\sum_{m=0}^{\infty} N_{m2}\alpha_{m2t}\cos[\alpha_{m2t}(\tfrac{a}{2}-x)]\cos(\tfrac{m\pi}{d}y)\overrightarrow{x}+ \\ +j\gamma_t\sum_{m=1}^{\infty} N_{m2}\tfrac{m\pi}{d}\sin[\alpha_{m2t}(\tfrac{a}{2}-x)]\sin(\tfrac{m\pi}{d}y)\overrightarrow{y}+ \\ +k_{Ct}^2\sum_{m=0}^{\infty} N_{m2}\sin[\alpha_{m2t}(\tfrac{a}{2}-x)]\cos(\tfrac{m\pi}{d}y)\overrightarrow{z}\}e^{-j\gamma_\iota z} \qquad (A.58)$$

2. **Even TE Modes**

   - trough region:

$$\overrightarrow{E}_i(x,y,z) = -j\omega\mu[-\sum_{n=1}^{\infty} N_{n1}\tfrac{n\pi}{b}\cos(\alpha_{n1t}x)\sin(\tfrac{n\pi}{b}y)\overrightarrow{x}+ \\ +\sum_{n=0}^{\infty} N_{n1}\alpha_{n1t}\sin(\alpha_{n1t}x)\cos(\tfrac{n\pi}{b}y)\overrightarrow{y}]e^{-j\gamma_\iota z} \qquad (A.59)$$

$$\overrightarrow{H}_i(x,y,z) = [j\gamma_t \sum_{n=0}^{\infty} N_{n1}\alpha_{n1t}\sin(\alpha_{n1t}x)\cos(\tfrac{n\pi}{b}y)\overrightarrow{x} +$$
$$+j\gamma_t \sum_{n=1}^{\infty} N_{n1}\tfrac{n\pi}{b}\cos(\alpha_{n1t}x)\sin(\tfrac{n\pi}{b}y)\overrightarrow{y} +$$
$$+k_{Ct}^2 \sum_{n=0}^{\infty} N_{n1}\cos(\alpha_{n1t}x)\cos(\tfrac{n\pi}{b}y)\overrightarrow{z}]e^{-j\gamma_\iota z} \qquad (A.60)$$

- gap:

$$\overrightarrow{E}_i(x,y,z) = -j\omega\mu\{-\sum_{m=1}^{\infty} N_{m2}\tfrac{m\pi}{d}\cos[\alpha_{m2t}(\tfrac{a}{2}-x)]\sin(\tfrac{m\pi}{d}y)\overrightarrow{x} -$$
$$-\sum_{m=0}^{\infty} N_{m2}\alpha_{m2t}\sin[\alpha_{m2t}(\tfrac{a}{2}-x)]\cos(\tfrac{m\pi}{d}y)\overrightarrow{y}\}e^{-j\gamma_\iota z} \qquad (A.61)$$

$$\overrightarrow{H}_i(x,y,z) = \{-j\gamma_t \sum_{m=0}^{\infty} N_{m2}\alpha_{m2t}\sin[\alpha_{m2t}(\tfrac{a}{2}-x)]\cos(\tfrac{m\pi}{d}y)\overrightarrow{x} +$$
$$+j\gamma_t \sum_{m=1}^{\infty} N_{m2}\tfrac{m\pi}{d}\cos[\alpha_{m2t}(\tfrac{a}{2}-x)]\sin(\tfrac{m\pi}{d}y)\overrightarrow{y} +$$
$$+k_{Ct}^2 \sum_{m=0}^{\infty} N_{m2}\cos[\alpha_{m2t}(\tfrac{a}{2}-x)]\cos(\tfrac{m\pi}{d}y)\overrightarrow{z}\}e^{-j\gamma_\iota z} \qquad (A.62)$$

3. **Odd TM Modes**

- trough region:

$$\overrightarrow{E}_i(x,y,z) = [-j\gamma_t \sum_{n=1}^{\infty} M_{n1}\alpha_{n1t}\cos(\alpha_{n1t}x)\sin(\tfrac{n\pi}{b}y)\overrightarrow{x} -$$
$$-j\gamma_t \sum_{n=1}^{\infty} M_{n1}\tfrac{n\pi}{b}\sin(\alpha_{n1t}x)\cos(\tfrac{n\pi}{b}y)\overrightarrow{y} +$$
$$+k_{Ct}^2 \sum_{n=1}^{\infty} M_{n1}\sin(\alpha_{n1t}x)\sin(\tfrac{n\pi}{b}y)\overrightarrow{z}]e^{-j\gamma_\iota z} \qquad (A.63)$$

$$\overrightarrow{H}_i(x,y,z) = j\omega\varepsilon[\sum_{n=1}^{\infty} M_{n1}\tfrac{n\pi}{b}\sin(\alpha_{n1t}x)\cos(\tfrac{n\pi}{b}y)\overrightarrow{x} +$$
$$+\sum_{n=1}^{\infty} M_{n1}\alpha_{n1t}\cos(\alpha_{n1t}x)\sin(\tfrac{n\pi}{b}y)\overrightarrow{y}]e^{-j\gamma_\iota z} \qquad (A.64)$$

- gap:

$$\overrightarrow{E}_i(x,y,z) = \{-j\gamma_t \sum_{m=1}^{\infty} M_{m2}\alpha_{m2t}\sin[\alpha_{m2t}(\tfrac{a}{2}-x)]\sin(\tfrac{m\pi}{d}y)\overrightarrow{x} -$$
$$-j\gamma_t \sum_{m=1}^{\infty} M_{m2}\tfrac{m\pi}{d}\cos[\alpha_{m2t}(\tfrac{a}{2}-x)]\cos(\tfrac{m\pi}{d}y)\overrightarrow{y} +$$
$$+k_{Ct}^2 \sum_{m=1}^{\infty} M_{m2}\cos[\alpha_{m2t}(\tfrac{a}{2}-x)]\sin(\tfrac{m\pi}{d}y)\overrightarrow{z}\}e^{-j\gamma_\iota z} \qquad (A.65)$$

$$\overrightarrow{H}_i(x,y,z) = j\omega\varepsilon\{\sum_{m=1}^{\infty} M_{m2}\tfrac{m\pi}{d}\cos[\alpha_{m2t}(\tfrac{a}{2}-x)]\cos(\tfrac{m\pi}{d}y)\overrightarrow{x} -$$
$$-\sum_{m=1}^{\infty} M_{m2}\alpha_{m2t}\sin[\alpha_{m2t}(\tfrac{a}{2}-x)]\sin(\tfrac{m\pi}{d}y)\overrightarrow{y}\}e^{-j\gamma_\iota z} \qquad (A.66)$$

4. **Even TM Modes**

- trough region:

$$\overrightarrow{E}_i(x,y,z) = [-j\gamma_t \sum_{n=1}^{\infty} M_{n1}\alpha_{n1t}\cos(\alpha_{n1t}x)\sin(\tfrac{n\pi}{b}y)\overrightarrow{x} -$$
$$-j\gamma_t \sum_{n=1}^{\infty} M_{n1}\tfrac{n\pi}{b}\sin(\alpha_{n1t}x)\cos(\tfrac{n\pi}{b}y)\overrightarrow{y} +$$
$$+k_{Ct}^2 \sum_{n=1}^{\infty} M_{n1}\sin(\alpha_{n1t}x)\sin(\tfrac{n\pi}{b}y)\overrightarrow{z}]e^{-j\gamma_\iota z} \qquad (A.67)$$

$$\overrightarrow{H}_i(x,y,z) = j\omega\varepsilon[\sum_{n=1}^{\infty} M_{n1}\tfrac{n\pi}{b}\sin(\alpha_{n1t}x)\cos(\tfrac{n\pi}{b}y)\overrightarrow{x} +$$
$$+\sum_{n=1}^{\infty} M_{n1}\alpha_{n1t}\cos(\alpha_{n1t}x)\sin(\tfrac{n\pi}{b}y)\overrightarrow{y}]e^{-j\gamma_\iota z} \qquad (A.68)$$

- gap:

$$\overrightarrow{E}_i(x,y,z) = \{j\gamma_t \sum_{m=1}^{\infty} M_{m2}\alpha_{m2t}\cos[\alpha_{m2t}(\tfrac{a}{2}-x)]\sin(\tfrac{m\pi}{d}y)\overrightarrow{x} -$$
$$-j\gamma_t \sum_{m=1}^{\infty} M_{m2}\tfrac{m\pi}{d}\sin[\alpha_{m2t}(\tfrac{a}{2}-x)]\cos(\tfrac{m\pi}{d}y)\overrightarrow{y} +$$
$$+k_{Ct}^2 \sum_{m=1}^{\infty} M_{m2}\sin[\alpha_{m2t}(\tfrac{a}{2}-x)]\sin(\tfrac{m\pi}{d}y)\overrightarrow{z}\}e^{-j\gamma_\iota z} \qquad (A.69)$$

$$\overrightarrow{H}_i(x,y,z) = j\omega\varepsilon\{\sum_{m=1}^{\infty} M_{m2}\tfrac{m\pi}{d}\sin[\alpha_{m2t}(\tfrac{a}{2}-x)]\cos(\tfrac{m\pi}{d}y)\overrightarrow{x} +$$
$$+\sum_{m=1}^{\infty} M_{m2}\alpha_{m2t}\cos[\alpha_{m2t}(\tfrac{a}{2}-x)]\sin(\tfrac{m\pi}{d}y)\overrightarrow{y}\}e^{-j\gamma_\iota z} \qquad (A.70)$$

Appendix B

Dyadic Green Functions for the 'aKoM' waveguides

In Chapter 3 the dyadic Green functions relevant to the vector potentials inside a ridged waveguide have been derived. The corresponding Green functions for the rectangular waveguide may be derived according to the same procedure. The only difference lies in the fact that the 'aKoM' rectangular waveguide is assumed to be a semi-infinite waveguide, since the side, where the slot resides, is covered by a metallic surface. The Green functions for such a waveguide will be determined on the grounds of the Green function for the infinite waveguide.

B.1 Dyadic Green Functions inside a rectangular waveguide

B.1.1 Dyadic Green Function for the electric vector potential

The coordinate system of the rectangular waveguide are depicted in Fig.B.1.

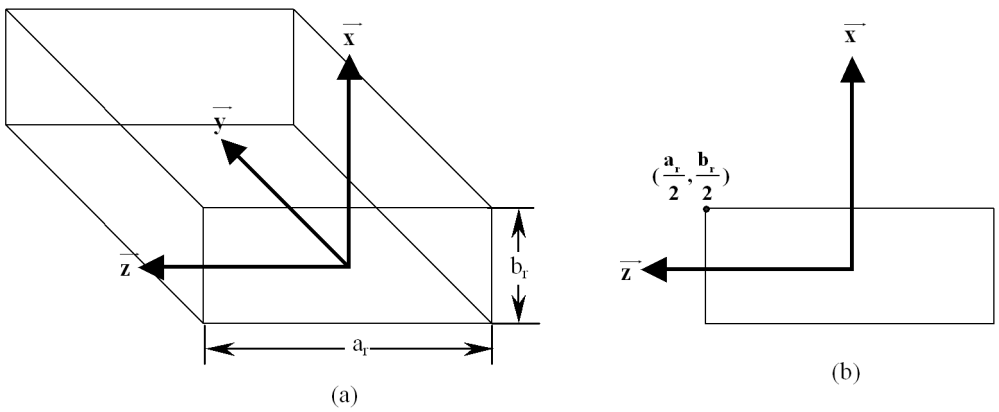

Figure B.1 Coordinate system of the rectangular waveguide

The coordinate system is selected in this manner, so that the analysis is adjusted to the orientation of the actual 'aKoM' rectangular waveguide.

The procedure for the derivation of $\overline{\overline{G}}_{Frw}$ (dyadic Green function for the electric vector potential inside a rectangular waveguide) is performed according to the Ohm-Rayleigh method. $\overline{\overline{G}}_{Frw}$ satis-

fies the equation:

$$\nabla^2\overline{\overline{G}}_{Frw}(\overrightarrow{r},\overrightarrow{r}') + k_o^2\,\overline{\overline{G}}_{Frw}(\overrightarrow{r},\overrightarrow{r}') = -I\delta(\overrightarrow{r}-\overrightarrow{r}') \quad (B.1)$$

$\overline{\overline{G}}_{Frw}$ will be expanded on the rectangular waveguide eigenvectors:

$$\overrightarrow{h}_{TE_{nm}}(\overrightarrow{r},h) = jhe^{jhy}\nabla_t g_{nm}(z,x) + k_{C_{nm}}^2 g_{nm}(z,x)e^{jhy}\overrightarrow{y}$$
$$\overrightarrow{h}_{TM_{nm}}(\overrightarrow{r},h) = e^{jhy}\nabla_t f_{nm}(z,x)\times\overrightarrow{y}$$

where

$$g_{nm}(z,x) = \cos[k_z(z+\tfrac{a_r}{2})]\cos[k_x(x+\tfrac{b_r}{2})] \quad (B.2a)$$
$$f_{nm}(z,x) = \sin[k_z(z+\tfrac{a_r}{2})]\sin[k_x(x+\tfrac{b_r}{2})] \quad (B.2b)$$

and $k_z = \frac{n\pi}{a_r}$, $k_x = \frac{m\pi}{b_r}$

The vector sets will be completed with the non-solenoidal set:

$$\overrightarrow{L}_{nm}(\overrightarrow{r},h) = \nabla(g_{nm}(z,x)e^{jhy})$$

where:

$$\nabla^2\overrightarrow{L}_{nm} + (k_{C_{nm}}^2 + h^2)\overrightarrow{L}_{nm} = 0$$

and the term ψ_{hrw0}, which is present in the case of magnetic currents $\overrightarrow{M}_{rw}$ flowing on the waveguide walls, parallel to the propagation direction.
Term ψ_{hrw0} is given by the equation:

$$\psi_{hrw0}(y) = -\frac{1}{j\omega\mu S}\int\limits_{\substack{aperture\\surface}}\overrightarrow{M}_{rw}(y')\delta(y'-y)dy'dc$$

where $dc = dx$ or $dc = dz$, depending on the location of the aperture.
The orthogonality conditions between the eigenvector sets are:

$$\iiint\limits_{S}\int\limits_{-\infty}^{\infty}\overrightarrow{h}_{TE_{nm}}(\overrightarrow{r},h)\overrightarrow{h}_{TE_{n'm'}}(\overrightarrow{r},-h')dsdy = \begin{cases} H_{nm}k_{C_{nm}}^2(k_{C_{nm}}^2+h^2)\delta(h-h'), \\ \qquad n=n' \text{ and } m=m' \\ 0,\ n\neq n' \text{ or } m\neq m' \end{cases} \quad (B.3a)$$

$$\iiint\limits_{S}\int\limits_{-\infty}^{\infty}\overrightarrow{h}_{TM_{nm}}(\overrightarrow{r},h)\overrightarrow{h}_{TM_{n'm'}}(\overrightarrow{r},-h')dsdy = \begin{cases} Hk_{C_{nm}}^2\delta(h-h'),\ n=n' \\ \qquad \text{and } m=m' \\ 0,\ n\neq n' \text{ or } m\neq m' \end{cases} \quad (B.3b)$$

$$\iiint\limits_{S}\int\limits_{-\infty}^{\infty}\overrightarrow{L}_{nm}(\overrightarrow{r},h)\overrightarrow{L}_{n'm'}(\overrightarrow{r},-h')dsdy = \begin{cases} H_{nm}(k_{C_{nm}}^2+h^2)\delta(h-h')2\pi, \\ \qquad n=n' \text{ and } m=m' \\ 0,\ n\neq n' \text{ or } m\neq m' \end{cases} \quad (B.3c)$$

$$\iiint\limits_{S}\int\limits_{-\infty}^{\infty}\overrightarrow{h}_{TM_{nm}}(\overrightarrow{r},h)\overrightarrow{h}_{TE_{nm}}(\overrightarrow{r},-h')dsdy = 0 \quad (B.3d)$$

$$\iiint\limits_{S}\int\limits_{-\infty}^{\infty}\overrightarrow{h}_{TE_{nm}}(\overrightarrow{r},h)\overrightarrow{L}_{n'm'}(\overrightarrow{r},-h')dsdy = \begin{cases} k_{C_{nm}}^2 H_{nm}(h-h')\delta(h-h')2\pi, \\ \qquad n=n' \text{ and } m=m' \\ 0,\ n\neq n' \text{ or } m\neq m' \end{cases} \quad (B.3e)$$

$$\iint_S \int_{-\infty}^{\infty} \overrightarrow{h}_{TM_{nm}}(\overrightarrow{r},h)\overrightarrow{L}_{nm}(\overrightarrow{r},-h')dsdy = 0 \qquad (B.3f)$$

$$H_{nm} = 2\pi\frac{a_r b_r}{4}\epsilon_n\epsilon_m$$
$$H = 2\pi\frac{a_r b_r}{4}$$

$$\varepsilon_n = \begin{cases} 2, & n = 0 \\ 1, & n \neq 0 \end{cases}$$

In the h-domain, eigenvectors $\overrightarrow{h}_{TE_{nm}}$ and $\overrightarrow{L}_{nm}$ are orthogonal and, therefore, may be used as basis vectors for the expansion of $\overline{\overline{G}}_{Frw}$.
Term $I\delta(\overrightarrow{r} - \overrightarrow{r}')$ is written in the following way:

$$I\delta(\overrightarrow{r} - \overrightarrow{r}') = \int_{-\infty}^{\infty} \sum_n \sum_m [A_{nm}(h)\overrightarrow{h}_{TE_{nm}}(\overrightarrow{r},h) + B_{nm}(h)\overrightarrow{h}_{TM_{nm}}(\overrightarrow{r},h) + C_{nm}(h)\overrightarrow{L}_{nm}(\overrightarrow{r},h)]dh + D\frac{1}{S}\delta(y-y')\overrightarrow{y} \qquad (B.4)$$

For the determination of D, both members of (B.4) are multiplied with $\frac{1}{S}\overrightarrow{y}$ and integrated over the cavity volume:

$$D = 1$$

Enforcement of the orthogonality properties (B.4) into (B.5) leads to the determination of the unknown coefficients $A_{nm}(h)$, $B_{nm}(h)$ and $C_{nm}(h)$:

$$A_{nm}(h) = \frac{2\overrightarrow{h}_{TE_{nm}}(\overrightarrow{r}',-h)}{\pi(k_{C_{nm}}^2+h^2)a_r b_r \varepsilon_n \varepsilon_m k_{C_{nm}}^2}$$
$$B_{nm}(h) = \frac{2\overrightarrow{h}_{TM_{nm}}(\overrightarrow{r}',-h)}{\pi a_r b_r k_{C_{nm}}^2}$$
$$C_{nm}(h) = \frac{2\overrightarrow{L}_{nm}(\overrightarrow{r}',-h)}{\pi a_r b_r \varepsilon_n \varepsilon_m (k_{C_{nm}}^2+h^2)}$$

Equation (B.3) takes the form:

$$I\delta(\overrightarrow{r} - \overrightarrow{r}') = \int_{-\infty}^{\infty} \sum_n \sum_m [\frac{2\overrightarrow{L}_{nm}(\overrightarrow{r},h)\overrightarrow{L}_{nm}(\overrightarrow{r}',-h)}{\varepsilon_n\varepsilon_m(k_{C_{nm}}^2+h^2)\pi a_r b_r} + \frac{2\overrightarrow{h}_{TM_{nm}}(\overrightarrow{r},h)\overrightarrow{h}_{TM_{nm}}(\overrightarrow{r}',-h)}{k_{C_{nm}}^2\pi a_r b_r} + \frac{2\overrightarrow{h}_{TE_{nm}}(\overrightarrow{r},h)\overrightarrow{h}_{TE_{nm}}(\overrightarrow{r}',-h)}{(k_{C_{nm}}^2+h^2)\varepsilon_n\varepsilon_m k_{C_{nm}}^2\pi a_r b_r}]dh + \frac{1}{S}\delta(y-y')\overrightarrow{y}\,\overrightarrow{y}' \qquad (B.6)$$

The unknown function $\overline{\overline{G}}_{Frw}$. is expanded in the following way:

$$\overline{\overline{G}}_{Frw}(\overrightarrow{r},\overrightarrow{r}') = \int_{-\infty}^{\infty} \sum_n \sum_m [A_{nm}(h)\frac{2\overrightarrow{h}_{TE_{nm}}(\overrightarrow{r},h)\overrightarrow{h}_{TE_{nm}}(\overrightarrow{r}',-h)}{(k_{C_{nm}}^2+h^2)\varepsilon_n\varepsilon_m k_{C_{nm}}^2\pi a_r b_r} + B_{nm}(h)\frac{2\overrightarrow{h}_{TM_{nm}}(\overrightarrow{r},h)\overrightarrow{h}_{TM_{nm}}(\overrightarrow{r}',-h)}{\pi a_r b_r k_{C_{nm}}^2} + C_{nm}(h)\frac{2\overrightarrow{L}_{nm}(\overrightarrow{r}',-h)\overrightarrow{L}_{nm}(\overrightarrow{r},h)}{\pi a_r b_r \varepsilon_n \varepsilon_m (k_{C_{nm}}^2+h^2)}]dh + \frac{1}{S}d\delta(y-y')\overrightarrow{y}\,\overrightarrow{y}' \qquad (B.7)$$

The unknown coefficients $A_{nm}(h)$, $B_{nm}(h)$, $C_{nm}(h)$ and d are determined after substitution of (B.5) and (B.6) into (B.1) and implementation of the following conditions:

$$\nabla^2 \overrightarrow{h}_{TE_{nm}}(\overrightarrow{r},h) = -\nabla\times\nabla\times\overrightarrow{h}_{TE_{nm}}(\overrightarrow{r},h) = -(k_{C_{nm}}^2+h^2)\overrightarrow{h}_{TE_{nm}}(\overrightarrow{r},h)$$
$$\nabla^2 \overrightarrow{h}_{TM_{nm}}(\overrightarrow{r},h) = -\nabla\times\nabla\times\overrightarrow{h}_{TM_{nm}}(\overrightarrow{r},h) = -(k_{C_{nm}}^2+h^2)\overrightarrow{h}_{TM_{nm}}(\overrightarrow{r},h)$$
$$\nabla^2 \overrightarrow{L}_{TE_{nm}}(\overrightarrow{r},h) = \nabla\nabla\cdot\overrightarrow{L}_{TE_{nm}}(\overrightarrow{r},h) = -(k_{C_{nm}}^2+h^2)\overrightarrow{L}_{TE_{nm}}(\overrightarrow{r},h)$$

The resulting coefficients are:

$$A_{nm}(h) = B_{nm}(h) = C_{nm}(h) = \frac{1}{k_{C_{nm}}^2 + h^2 - k_o^2}$$

$$d = -\frac{1}{k_o^2}$$

Insertion of the coefficient values into equation (B.6) yields:

$$\begin{aligned}\overline{\overline{G}}_{Frw}(\overrightarrow{r},\overrightarrow{r}') = \int_{-\infty}^{\infty} dh \sum_n \sum_m \frac{2}{(k_{C_{nm}}^2+h^2-k_o^2)\pi a_r b_r}\Big[\frac{\overrightarrow{h}_{TE_{nm}}(\overrightarrow{r},h)\overrightarrow{h}_{TE_{nm}}(\overrightarrow{r}',-h)}{(k_{C_{nm}}^2+h^2)\varepsilon_n\varepsilon_m k_{C_{nm}}^2} + \\ + \frac{2\overrightarrow{h}_{TM_{nm}}(\overrightarrow{r},h)\overrightarrow{h}_{TM_{nm}}(\overrightarrow{r}',-h)}{k_{C_{nm}}^2} + \frac{\overrightarrow{L}_{nm}(\overrightarrow{r},h)\overrightarrow{L}_{nm}(\overrightarrow{r}',-h)}{\varepsilon_n\varepsilon_m(k_{C_{nm}}^2+h^2)}\Big] - \\ - \frac{1}{k_o^2 S}\delta(y-y')\overrightarrow{y}\overrightarrow{y}' \qquad (B.8)\end{aligned}$$

The integral in the above equation may be evaluated by direct application of the residue theorem, since every term satisfies the Jordan lemma. The result is:

$$\begin{aligned}\overline{\overline{G}}_{Frw}(\overrightarrow{r},\overrightarrow{r}') = \frac{-2j}{a_r b_r}\sum_n \sum_m \Big[\frac{\overrightarrow{h}_{TE_{nm}}(\overrightarrow{r},\mp\gamma_{nm})\overrightarrow{h}_{TE_{nm}}(\overrightarrow{r}',\pm\gamma_{nm})}{\gamma_{nm}\varepsilon_n\varepsilon_m k_o^2 k_{C_{nm}}^2} + \\ + \frac{\overrightarrow{L}_{nm}(\overrightarrow{r},\mp\gamma_{nm})\overrightarrow{L}_{nm}(\overrightarrow{r}',\pm\gamma_{nm})}{\gamma_{nm}\varepsilon_n\varepsilon_m k_0^2} + \\ + \frac{\overrightarrow{h}_{TM_{nm}}(\overrightarrow{r},\mp\gamma_{nm})\overrightarrow{h}_{TM_{nm}}(\overrightarrow{r}',\pm\gamma_{nm})}{\gamma_{nm}k_{C_{nm}}^2}\Big] - \\ - \overrightarrow{y}\,\overrightarrow{y}'\frac{1}{k_o^2 S}\delta(y-y') \qquad (B.9)\end{aligned}$$

The upper line in the summations refers to the case where y¿y', whereas the bottom line stands for $y < y'$.

Expression (B.9) represents the dyadic Green function for the electric vector potential inside an infinite rectangular waveguide. All nine elements of $\overline{\overline{G}}_{Frw}$ are listed below:

$$\begin{aligned}
\overline{\overline{G}}_{Frw_{zz}}(\overrightarrow{r},\overrightarrow{r}') &= -j\sum_{n=0}^{\infty}\sum_{m=0}^{\infty}\frac{\partial g_{nm}(z,x)}{\partial z}\frac{\partial g_{nm}(z',x')}{\partial z}\frac{e^{-j\gamma_{nm}|y-y'|}}{\gamma_{nm}a_r b_r\varepsilon_n\varepsilon_m} \\
\overline{\overline{G}}_{Frw_{zx}}(\overrightarrow{r},\overrightarrow{r}') &= 0 \\
\overline{\overline{G}}_{Frw_{xz}}(\overrightarrow{r},\overrightarrow{r}') &= 0 \\
\overline{\overline{G}}_{Frw_{xx}}(\overrightarrow{r},\overrightarrow{r}') &= -j\sum_{n=0}^{\infty}\sum_{m=0}^{\infty}\frac{\partial g_{nm}(z,x)}{\partial x}\frac{\partial g_{nm}(z',x')}{\partial x}\frac{e^{-j\gamma_{nm}|y-y'|}}{\gamma_{nm}a_r b_r\varepsilon_n\varepsilon_m} \\
\overline{\overline{G}}_{Frw_{yz}}(\overrightarrow{r},\overrightarrow{r}') &= 0 \\
\overline{\overline{G}}_{Frw_{yx}}(\overrightarrow{r},\overrightarrow{r}') &= 0 \\
\overline{\overline{G}}_{Frw_{yy}}(\overrightarrow{r},\overrightarrow{r}') &= -j\sum_{n=0}^{\infty}\sum_{m=0}^{\infty}k_{C_{nm}}^2 g_{nm}(z,x)g_{nm}(z',x')\frac{e^{-j\gamma_{nm}|y-y'|}}{\gamma_{nm}a_r b_r\varepsilon_n\varepsilon_m} \\
&\quad + \frac{1}{S}\delta(y-y')
\end{aligned}$$

$$\begin{aligned}
\overline{\overline{G}}_{Frw_{zy}}(\overrightarrow{r},\overrightarrow{r}') &= 0 \\
\overline{\overline{G}}_{Frw_{xy}}(\overrightarrow{r},\overrightarrow{r}') &= 0
\end{aligned}$$

B.1.2 Electric dyadic Green Function generated by magnetic current

Infinite rectangular waveguide

The electric field inside the rectangular waveguide satisfies the equation:

$$\nabla \times \nabla \times \overrightarrow{E} - k_o^2 \overrightarrow{E} = \nabla \times \overrightarrow{M}$$

The Green function $\overline{\overline{G}}^m_{E_{rw}}(\overrightarrow{r}, \overrightarrow{r}')$ must satisfy a similar equation:

$$\nabla \times \nabla \times \overline{\overline{G}}^m_{E_{rw}}(\overrightarrow{r}, \overrightarrow{r}') - k_o^2 \overline{\overline{G}}^m_{E_{rw}}(\overrightarrow{r}, \overrightarrow{r}') = \nabla \times I\delta(\overrightarrow{r} - \overrightarrow{r}') \quad (B.10)$$

In this case, vector $\overrightarrow{L}_{nm}$ is not used for the expansion of $I\delta(\overrightarrow{r} - \overrightarrow{r}')$, because there is no need for a non-solenoidal eigenvector set, since $\nabla \cdot \overrightarrow{E}(\overrightarrow{r}') = 0$ everywhere inside a waveguide that carries magnetic currents. Moreover, when the electric dyadic Green function is examined, the term ψ_{hrw0} is not included in the expansion series, since it has no impact on the electric field. The right side of (B.10) is expanded on the wave vectors for the electric field:

$$\overrightarrow{e}_{TE_{nm}}(\overrightarrow{r}, h) = e^{jhy} \nabla_t g_{nm}(z, x) \times \overrightarrow{y} \qquad (TE\,Modes)$$

$$\overrightarrow{e}_{TM_{nm}}(\overrightarrow{r}, h) = jhe^{jhy} \nabla_t f_{nm}(z, x) + k^2_{C_{nm}} f_{nm}(z, x) e^{jhy} \overrightarrow{y} \qquad (TM\,Modes)$$

where functions $g_{nm}(z, x)$ and $f_{nm}(z, x)$ have been defined by equations (B.2)

The orthogonality conditions are:

$$\iint_S \int_{-\infty}^{\infty} \overrightarrow{e}_{TE_{nm}}(\overrightarrow{r}, h) \overrightarrow{e}_{TE_{n'm'}}(\overrightarrow{r}, -h') ds dz = \begin{cases} k^2_{C_{nm}} H_{nm} \delta(h - h'), \ n = n' \\ \qquad\qquad and\ m = m' \\ 0, \ n \neq n' \ or \ m \neq m' \end{cases} \quad (B.11a)$$

$$\iint_S \int_{-\infty}^{\infty} \overrightarrow{e}_{TM_{nm}}(\overrightarrow{r}, h) \overrightarrow{e}_{TM_{n'm'}}(\overrightarrow{r}, -h') ds dz = \begin{cases} k^2_{C_{nm}} H(k^2_{C_{nm}} + h^2) \delta(h - h'), \\ \qquad\qquad n = n' \ and \ m = m' \\ 0, \ n \neq n' \ or \ m \neq m' \end{cases} \quad (B.11b)$$

$$\iint_S \int_{-\infty}^{\infty} \overrightarrow{e}_{TM_{nm}}(\overrightarrow{r}, h) \overrightarrow{e}_{TE_{n'm'}}(\overrightarrow{r}, -h') ds dz = 0 \quad (B.11c)$$

The expression for $\bigtriangledown \times I\delta(\overrightarrow{r} - \overrightarrow{r}')$ is:

$$\nabla \times I\delta(\overrightarrow{r} - \overrightarrow{r}') = \int_{-\infty}^{\infty} \sum_n \sum_m [A_{nm}(h) \overrightarrow{e}_{TE_{nm}}(\overrightarrow{r}, h) + B_{nm}(h) \overrightarrow{e}_{TM_{nm}}(\overrightarrow{r}, h)] dh \quad (B.12)$$

Both members of expression (B.12) are multiplied with $\overrightarrow{e}_{TE_{n'm'}}(\overrightarrow{r}, -h)$ and integrated over the waveguide volume:

$$\iiint_V \overrightarrow{e}_{TE_{n'm'}}(\overrightarrow{r}, -h) \nabla \times I\delta(\overrightarrow{r} - \overrightarrow{r}') dv =$$

$$= \iiint_V dv \int_{-\infty}^{\infty} \sum_n \sum_m \overrightarrow{e}_{TE_{n'm'}}(\overrightarrow{r}, -h) [A_{nm}(h) \overrightarrow{e}_{TE_{nm}}(\overrightarrow{r}, h) + B_{nm}(h) \overrightarrow{e}_{TM_{nm}}(\overrightarrow{r}, h)] dh =$$

$$= \int_{-\infty}^{\infty} A_{nm}(h) k_{C_{nm}}^2 \frac{a_r b_r}{4} \varepsilon_n \varepsilon_m (k_{C_{nm}}^2 + h^2) \delta(h - h') 2\pi dh \qquad (B.13)$$

Application of the dyadic identity: $\nabla \cdot (\overrightarrow{a} \times \overline{\overline{b}}) = -\overrightarrow{a} \nabla \times \overline{\overline{b}} + \overline{\overline{b}} \nabla \times \overrightarrow{a}$ and the divergence theorem:

$$\iiint_V \nabla \cdot \overrightarrow{B} dv = \oiint_S (\overrightarrow{n} \times \overrightarrow{B}) ds$$

on the left side of (B.13) yields:

$$\iiint_V \overrightarrow{e}_{TE_{n'm'}}(\overrightarrow{r}, -h) \nabla \times I\delta(\overrightarrow{r} - \overrightarrow{r}') dv =$$

$$= \int\int_V \int \nabla \cdot [\overrightarrow{e}_{TE_{n'm'}}(\overrightarrow{r}, -h) \times I\delta(\overrightarrow{r} - \overrightarrow{r}')] dv +$$
$$+ \int\int_V \int \nabla \times \overrightarrow{e}_{TE_{n'm'}}(\overrightarrow{r}, -h) I\delta(\overrightarrow{r} - \overrightarrow{r}') dv =$$

$$= \oiint_S \overrightarrow{n} \cdot [\overrightarrow{e}_{TE_{n'm'}}(\overrightarrow{r}, -h) \times I\delta(\overrightarrow{r} - \overrightarrow{r}')] ds + \nabla' \times \overrightarrow{e}_{TE_{n'm'}}(\overrightarrow{r'}, -h)$$

The surface integral in the above expression vanishes because $\overrightarrow{r}'$ is located inside the volume V. In view of the preceding equation, expression (B.13) becomes:

$$A_{nm}(h) = \frac{2\nabla' \times \overrightarrow{e}_{TE_{n'm'}}(\overrightarrow{r'}, -h)}{k_{C_{nm}}^2 a_r b_r \varepsilon_n \varepsilon_m \pi} = \frac{2\overrightarrow{h}_{TE_{n'm'}}(\overrightarrow{r'}, -h)}{k_{C_{nm}}^2 a_r b_r \varepsilon_n \varepsilon_m \pi}$$

In a similar way:

$$B_{nm}(h) = \frac{2\nabla' \times \overrightarrow{e}_{TM_{n'm'}}(\overrightarrow{r'}, -h)}{k_{C_{nm}}^2 a_r b_r \pi (k_{C_{nm}}^2 + h^2)} = \frac{2\overrightarrow{h}_{TM_{n'm'}}(\overrightarrow{r'}, -h)}{k_{C_{nm}}^2 a_r b_r \pi}$$

Equation (B.12) becomes

$$\nabla \times I\delta(\overrightarrow{r} - \overrightarrow{r}') = \int_{-\infty}^{\infty} \sum_n \sum_m [\frac{2\overrightarrow{h}_{TE_{n'm'}}(\overrightarrow{r'}, -h)}{k_{C_{nm}}^2 a_r b_r \varepsilon_n \varepsilon_m \pi} \overrightarrow{e}_{TE_{nm}}(\overrightarrow{r}, h) +$$
$$+ \frac{2\overrightarrow{h}_{TM_{n'm'}}(\overrightarrow{r'}, -h)}{k_{C_{nm}}^2 * a_r * b_r * \pi} \overrightarrow{e}_{TM_{nm}}(\overrightarrow{r}, h)] dh \qquad (B.14)$$

The unknown Green function is expressed in the following way:

$$\overline{\overline{G}}_{E_{rw}}^m(\overrightarrow{r}, \overrightarrow{r}') = \int_{-\infty}^{\infty} \sum_n \sum_m [A_{nm}(h) \frac{2\overrightarrow{e}_{TE_{nm}}(\overrightarrow{r}, h) \overrightarrow{h}_{TE_{n'm'}}(\overrightarrow{r}', -h)}{k_{C_{nm}}^2 a_r b_r \varepsilon_n \varepsilon_m \pi} +$$
$$+ B_{nm}(h) \frac{2\overrightarrow{e}_{TM_{nm}}(\overrightarrow{r}, h) \overrightarrow{h}_{TM_{n'm'}}(\overrightarrow{r'}, -h)}{k_{C_{nm}}^2 a_r b_r \pi}] dh \qquad (B.15)$$

The unknown coefficients $A_{nm}(h)$ and $B_{nm}(h)$ are determined after substitution of (B.15) and (B.14) into (B.10) and implementation of the following conditions:

$$\nabla \times \nabla \times \overrightarrow{e}_{TE_{nm}}(\overrightarrow{r}, h) = (k_{C_{nm}}^2 + h^2) \overrightarrow{e}_{TE_{nm}}(\overrightarrow{r}, h)$$

$$\nabla \times \nabla \times \overrightarrow{e}_{TM_{nm}}(\overrightarrow{r}, h) = (k_{C_{nm}}^2 + h^2) \overrightarrow{e}_{TM_{nm}}(\overrightarrow{r}, h)$$

The result is:

$$A_{nm}(h) = B_{nm}(h) = \frac{1}{k_{C_{nm}}^2 + h^2 - k_o^2}$$

Equation (B.15) becomes:

$$\overline{\overline{G}}_{E_{rw}}^m(\overrightarrow{r}, \overrightarrow{r}') = \int_{-\infty}^{\infty} \sum_n \sum_m \frac{2}{k_{C_{nm}}^2 + h^2 - k_o^2} [\frac{\overrightarrow{e}_{TE_{nm}}(\overrightarrow{r}, h)\, \overrightarrow{h}_{TE_{n'm'}}(\overrightarrow{r}', -h)}{k_{C_{nm}}^2 a_r b_r \varepsilon_n \varepsilon_m \pi} + \\ + \frac{\overrightarrow{e}_{TM_{nm}}(\overrightarrow{r}, h)\, \overrightarrow{h}_{TM_{n'm'}}(\overrightarrow{r}', -h)}{k_{C_{nm}}^2 a_r b_r \pi}] dh$$

The integral in the above expression may be evaluated by the method of contour integration. Both terms of the integrand satisfy the Jordan lemma and have two poles in $h = \pm\sqrt{k_o^2 - k_{C_{nm}}^2}$. The final expression for $\overline{\overline{G}}_E^m(\overrightarrow{r}, \overrightarrow{r}')$ is:

$$\overline{\overline{G}}_{E_{rw}}^m(\overrightarrow{r}, \overrightarrow{r}') = \sum_n \sum_m [-j \frac{2\, \overrightarrow{h}_{TE_{nm}}(\overrightarrow{r}', \pm\gamma_{nm})\, \overrightarrow{e}_{TE_{nm}}(\overrightarrow{r}, \mp\gamma_{nm})}{k_{C_{nm}}^2 a_r b_r \varepsilon_n \varepsilon_m \gamma_{nm}} - \\ - j \frac{2\, \overrightarrow{h}_{TM_{n'm'}}(\overrightarrow{r}', \pm\gamma_{nm})\, \overrightarrow{e}_{TM_{nm}}(\overrightarrow{r}, \mp\gamma_{nm})}{k_{C_{nm}}^2 a_r b_r \gamma_{nm}}] \qquad (B.16)$$

Equation (B.16) defines the electric dyadic Green function generated by magnetic current inside an infinite rectangular waveguide.

Semi-infinite rectangular waveguide

The electric Green function $\overline{\overline{G}}_{E_{srw}}^m(\overrightarrow{r}, \overrightarrow{r}')$ for the magnetic current inside a semi-infinite rectangular waveguide is determined according to the method proposed by Tai. The semi-infinite waveguide has the same transverse dimensions as the infinite waveguide. The Green function $\overline{\overline{G}}_{E_{srw}}^m$ for the semi-infinite waveguide is expressed with the aid of $\overline{\overline{G}}_{E_{rw}}^m$:

$$\overline{\overline{G}}_{E_{srw}}^m = \overline{\overline{G}}_{E_{rw}}^m + \overline{\overline{G}}_1^m \qquad (B.17)$$

where:

$$\overline{\overline{G}}_1^m(\overrightarrow{r}, \overrightarrow{r'}) = -j \sum_n \sum_m [A_e \frac{2\, \overrightarrow{h}_{TE_{nm}}(\overrightarrow{r'}, \gamma_{nm})\, \overrightarrow{e}_{TE_{nm}}(\overrightarrow{r}, \gamma_{nm})}{k_{C_{nm}}^2 a_r b_r \varepsilon_n \varepsilon_m \gamma_{nm}} + \\ + A_m \frac{2\, \overrightarrow{h}_{TM_{nm}}(\overrightarrow{r'}, \gamma_{nm})\, \overrightarrow{e}_{TM_{nm}}(\overrightarrow{r}, \gamma_{nm})}{k_{C_{nm}}^2 a_r b_r \gamma_{nm}}]$$

and A_m, A_e are unknown coefficients that are determined by implementation of the boundary condition: $\overrightarrow{y} \times \overrightarrow{E} = 0$ at plane $y = 0$:

$$\overrightarrow{y} \times \overrightarrow{E} = 0 \Rightarrow \overrightarrow{y} \times \overline{\overline{G}}_{E_{srw}}^m = 0 \Rightarrow$$

$$\Rightarrow \begin{cases} \overrightarrow{y} \times [\overrightarrow{e}_{TE_{nm}}(\overrightarrow{r}, -\gamma_{nm})\, \overrightarrow{h}_{TE_{nm}}(\overrightarrow{r'}, \gamma_{nm}) + \\ + A_e\, \overrightarrow{e}_{TE_{nm}}(\overrightarrow{r}, \gamma_{nm})\, \overrightarrow{h}_{TE_{nm}}(\overrightarrow{r'}, \gamma_{nm})] = 0|_{y=0} \\ \overrightarrow{y} \times [\overrightarrow{e}_{TM_{nm}}(\overrightarrow{r}, -\gamma_{nm})\, \overrightarrow{h}_{TM_{nm}}(\overrightarrow{r'}, \gamma_{nm}) + \\ + A_m\, \overrightarrow{e}_{TM_{nm}}(\overrightarrow{r}, \gamma_{nm})\, \overrightarrow{h}_{TM_{nm}}(\overrightarrow{r'}, \gamma_{nm})] = 0|_{y=0} \end{cases} \Rightarrow$$

$$\Rightarrow \begin{cases} A_e = -1 \\ A_m = 1 \end{cases}$$

Equation (B.17) is rewritten in the following way:
for $y < y'$:

$$\overline{\overline{G}}^{m}_{E_{srw}}(\overrightarrow{r},\overrightarrow{r}') = \sum_{n}^{\infty}\sum_{m}^{\infty}\{-j2\frac{\overrightarrow{e}_{TE_{nm}}(\overrightarrow{r},\gamma_{nm})[\overrightarrow{h}_{TE_{nm}}(\overrightarrow{r'},-\gamma_{nm})-\overrightarrow{h}_{TE_{nm}}(\overrightarrow{r'},\gamma_{nm})]}{k^2_{C_{nm}}a_r b_r \varepsilon_n \varepsilon_m \gamma_{nm}} - \\ -j2\frac{\overrightarrow{e}_{TM_{nm}}(\overrightarrow{r},\gamma_{nm})[\overrightarrow{h}_{TM_{nm}}(\overrightarrow{r'},-\gamma_{nm})+\overrightarrow{h}_{TM_{nm}}(\overrightarrow{r'},\gamma_{nm})]}{k^2_{C_{nm}}a_r b_r \gamma_{nm}}\} \quad (B.18a)$$

for $y > y'$:

$$\overline{\overline{G}}^{m}_{E_{srw}}(\overrightarrow{r},\overrightarrow{r}') = \sum_{n}^{\infty}\sum_{m}^{\infty}\{-j2\frac{\overrightarrow{h}_{TE_{nm}}(\overrightarrow{r}',\gamma_{nm})[\overrightarrow{e}_{TE_{nm}}(\overrightarrow{r},-\gamma_{nm})-\overrightarrow{e}_{TE_{nm}}(\overrightarrow{r},\gamma_{nm})]}{k^2_{C_{nm}}a_r b_r \varepsilon_n \varepsilon_m \gamma_{nm}} - \\ -j2\frac{\overrightarrow{h}_{TM_{nm}}(\overrightarrow{r}',\gamma_{nm})[\overrightarrow{e}_{TM_{nm}}(\overrightarrow{r},-\gamma_{nm})+\overrightarrow{e}_{TM_{nm}}(\overrightarrow{r},\gamma_{nm})]}{k^2_{C_{nm}}a_r b_r \gamma_{nm}}\} \quad (B.18b)$$

Two new sets of eigenvectors are introduced:

$$\overrightarrow{e}^{o}_{TE_{nm}}(\overrightarrow{r},\gamma_{nm}) = \nabla \times \{g_{nm}(z,x)\sin(\gamma_{nm}y)\overrightarrow{y}\} \Rightarrow$$

$$\overrightarrow{e}^{o}_{TE_{nm}}(\overrightarrow{r},\gamma_{nm}) = \overrightarrow{z}\frac{\partial g_{nm}(z,x)}{\partial x}\sin(\gamma_{nm}y) - \overrightarrow{x}\frac{\partial g_{nm}(z,x)}{\partial z}\sin(\gamma_{nm}y) \quad (B.19a)$$

$$\overrightarrow{e}^{o}_{TM_{nm}}(\overrightarrow{r},\gamma_{nm}) = \nabla \times \nabla \times \{f_{nm}(z,x)\cos(\gamma_{nm}y)\overrightarrow{y}\} \Rightarrow$$

$$\overrightarrow{e}^{o}_{TM_{nm}}(\overrightarrow{r},\gamma_{nm}) = -\overrightarrow{z}\gamma_{nm}\frac{\partial f_{nm}(z,x)}{\partial z}\sin(\gamma_{nm}y) - \\ -\overrightarrow{x}\gamma_{nm}\frac{\partial f_{nm}(z,x)}{\partial x}\sin(\gamma_{nm}y) + \overrightarrow{y}k^2_{C_{nm}}f_{nm}(z,x)\cos(\gamma_{nm}y) \quad (B.19b)$$

The new eigenvectors are related to the waveguide eigenvectors via the following expressions:

$$-2j\overrightarrow{e}^{o}_{TE_{nm}}(\overrightarrow{r},\gamma_{nm}) = \overrightarrow{e}_{TE_{nm}}(\overrightarrow{r},-\gamma_{nm}) - \overrightarrow{e}_{TE_{nm}}(\overrightarrow{r},\gamma_{nm}) \quad (B.20a)$$

$$2\overrightarrow{e}^{o}_{TM_{nm}}(\overrightarrow{r},\gamma_{nm}) = \overrightarrow{e}_{TM_{nm}}(\overrightarrow{r},-\gamma_{nm}) + \overrightarrow{e}_{TM_{nm}}(\overrightarrow{r},\gamma_{nm}) \quad (B.20a)$$

The corresponding expressions for the magnetic fields are:

$$\overrightarrow{h}^{o}_{TE_{nm}}(\overrightarrow{r},\gamma_{nm}) = \nabla \times \overrightarrow{e}^{o}_{TE_{nm}}(\overrightarrow{r},\gamma_{nm}) \Rightarrow$$

$$\overrightarrow{h}^{o}_{TE_{nm}}(\overrightarrow{r},\gamma_{nm}) = \overrightarrow{z}\gamma_{nm}\frac{\partial g_{nm}(z,x)}{\partial z}\cos(\gamma_{nm}y) + \overrightarrow{x}\gamma_{nm}\frac{\partial g_{nm}(z,x)}{\partial x}\cos(\gamma_{nm}y) + \\ +\overrightarrow{y}k^2_{C_{nm}}g_{nm}(z,x)\sin(\gamma_{nm}y) \quad (B.21a)$$

$$\overrightarrow{h}^{o}_{TM_{nm}}(\overrightarrow{r},\gamma_{nm}) = \nabla \times [f_{nm}(z,x)\cos(\gamma_{nm}y)\overrightarrow{y}] \Rightarrow$$

$$\overrightarrow{h}^{o}_{TM_{nm}}(\overrightarrow{r},\gamma_{nm}) = \overrightarrow{z}\frac{\partial f_{nm}(z,x)}{\partial x}\cos(\gamma_{nm}y) - \overrightarrow{x}\frac{\partial f_{nm}(z,x)}{\partial z}\cos(\gamma_{nm}y) \quad (B.21b)$$

The following expressions are valid:

$$-2j\overrightarrow{h}^{o}_{TE_{nm}}(\overrightarrow{r},\gamma_{nm}) = \overrightarrow{h}_{TE_{nm}}(\overrightarrow{r},-\gamma_{nm}) - \overrightarrow{h}_{TE_{nm}}(\overrightarrow{r},\gamma_{nm}) \quad (B.22a)$$

$$2\overrightarrow{h}^{o}_{TM_{nm}}(\overrightarrow{r},\gamma_{nm}) = \overrightarrow{h}_{TM_{nm}}(\overrightarrow{r},-\gamma_{nm}) + \overrightarrow{h}_{TM_{nm}}(\overrightarrow{r},\gamma_{nm}) \quad (B.22b)$$

In view of expressions (B.20) and (B.22), equations (B.18) take the final form for $\overline{\overline{G}}^m_{Esrw}$: for $y < y'$:

$$\overline{\overline{G}}^m_{E_{srw}}(\overrightarrow{r},\overrightarrow{r}') = -j4\sum_n^\infty\sum_m^\infty [-j\frac{\overrightarrow{e}_{TE_{nm}}(\overrightarrow{r},\gamma_{nm})\overrightarrow{h}^o_{TE_{nm}}(\overrightarrow{r'},\gamma_{nm})}{k^2_{C_{nm}}a_r b_r\varepsilon_n\varepsilon_m\gamma_{nm}} + \\ + \frac{\overrightarrow{e}_{TM_{nm}}(\overrightarrow{r},\gamma_{nm})\overrightarrow{h}^o_{TM_{nm}}(\overrightarrow{r'},\gamma_{nm})}{k^2_{C_{nm}}a_r b_r\gamma_{nm}}] \quad (B.23a)$$

for $y > y'$:

$$\overline{\overline{G}}^m_{E_{srw}}(\overrightarrow{r},\overrightarrow{r}') = -j4\sum_n^\infty\sum_m^\infty [-j\frac{\overrightarrow{h}_{TE_{nm}}(\overrightarrow{r}',\gamma_{nm})\overrightarrow{e}^o_{TE_{nm}}(\overrightarrow{r},\gamma_{nm})}{k^2_{C_{nm}}a_r b_r\varepsilon_n\varepsilon_m\gamma_{nm}} + \\ + \frac{\overrightarrow{h}_{TM_{nm}}(\overrightarrow{r}',\gamma_{nm})\overrightarrow{e}^o_{TM_{nm}}(\overrightarrow{r},\gamma_{nm})}{k^2_{C_{nm}}a_r b_r\gamma_{nm}}] \quad (B.23b)$$

The elements of $\overline{\overline{G}}^m_{Esrw}$ are listed below:

$$G^m_{Esrw_{zz}} = 0$$

$$G^m_{Esrw_{zx}} = \begin{cases} -j4\sum_n^\infty\sum_m^\infty [-j\frac{\partial g_{nm}(z,x)}{\partial x}\frac{\partial g_{nm}(z',x')}{\partial x'} - \\ -j\frac{\partial f_{nm}(z,x)}{\partial z}\frac{\partial f_{nm}(z',x')}{\partial z'}]\frac{e^{j\gamma_{nm}y}\cos(\gamma_{nm}y')}{k^2_{C_{nm}}a_r b_r\varepsilon_n\varepsilon_m}, y < y' \\ -j4\sum_n^\infty\sum_m^\infty [\frac{\partial g_{nm}(z,x)}{\partial x}\frac{\partial g_{nm}(z',x')}{\partial x'} + \\ +\frac{\partial f_{nm}(z,x)}{\partial z}\frac{\partial f_{nm}(z',x')}{\partial z'}]\frac{e^{j\gamma_{nm}y}\sin(\gamma_{n,m}y)}{k^2_{C_{nm}}a_r b_r\varepsilon_n\varepsilon_m}, y > y' \end{cases} \Rightarrow$$

$$G^m_{Esrw_{zx}} = 2\sum_n^\infty\sum_m^\infty [\frac{\partial g_{nm}(z,x)}{\partial x}\frac{\partial g_{nm}(z',x')}{\partial x'} + \\ + \frac{\partial f_{nm}(z,x)}{\partial z}\frac{\partial f_{nm}(z',x')}{\partial z'}]\frac{[e^{j\gamma_{nm}(y+y')} - sign(y-y')e^{-j\gamma_{nm}|y-y'|}]}{k^2_{C_{nm}}a_r b_r\varepsilon_n\varepsilon_m}$$

$$G^m_{Esrw_{zy}} = \begin{cases} -j4\sum_n^\infty\sum_m^\infty [-j\frac{\partial g_{nm}(z,x)}{\partial x}g_{nm}(z',x')\frac{e^{j\gamma_{nm}y}\sin(\gamma_{nm}y')}{a_r b_r\varepsilon_n\varepsilon_m\gamma_{nm}}], y < y' \\ -j4\sum_n^\infty\sum_m^\infty [-j\frac{\partial g_{nm}(z,x)}{\partial x}g_{nm}(z',x')\frac{e^{j\gamma_{nm}y'}\sin(\gamma_{nm}y)}{a_r b_r\varepsilon_n\varepsilon_m\gamma_{nm}}], y > y' \end{cases} \Rightarrow$$

$$G^m_{Esrw_{zy}} = 2j\sum_n^\infty\sum_m^\infty \frac{\partial g_{nm}(z,x)}{\partial x}g_{nm}(z',x')\frac{(e^{j\gamma_{nm}(y+y')} - e^{-j\gamma_{nm}|y-y'|})}{a_r b_r\varepsilon_n\varepsilon_m\gamma_{nm}}$$

$$G^m_{Esrw_{xz}} = \begin{cases} -j4\sum_n^\infty\sum_m^\infty [j\frac{\partial g_{nm}(z,x)}{\partial z}\frac{\partial g_{nm}(z',x')}{\partial z'} + \\ +j\frac{\partial f_{nm}(z,x)}{\partial x}\frac{\partial f_{nm}(z',x')}{\partial x'}]\frac{e^{j\gamma_{nm}y}\cos(\gamma_{nm}y')}{k^2_{C_{nm}}a_r b_r\varepsilon_n\varepsilon_m}, y < y' \\ -j4\sum_n^\infty\sum_m^\infty [-\frac{\partial g_{nm}(z,x)}{\partial z}\frac{\partial g_{nm}(z',x')}{\partial z'} - \\ -\frac{\partial f_{nm}(z,x)}{\partial x}\frac{\partial f_{nm}(z',x')}{\partial x'}]\frac{e^{j\gamma_{nm}y}\sin(\gamma_{n,m}y)}{k^2_{C_{nm}}a_r b_r\varepsilon_n\varepsilon_m}, y > y' \end{cases} \Rightarrow$$

$$G^m_{Esrw_{xz}} = 2\sum_n^\infty\sum_m^\infty [\frac{\partial g_{nm}(z,x)}{\partial z}\frac{\partial g_{nm}(z',x')}{\partial z'} + \\ + \frac{\partial f_{nm}(z,x)}{\partial x}\frac{\partial f_{nm}(z',x')}{\partial x'}]\frac{[e^{j\gamma_{nm}(y+y')} - sign(y-y')e^{-j\gamma_{nm}|y-y'|}]}{k^2_{C_{nm}}a_r b_r \varepsilon_n \varepsilon_m}$$

$$G^m_{Esrw_{xx}} = 0$$

$$G^m_{Esrw_{xy}} = \begin{cases} -j4\sum_n^\infty\sum_m^\infty j\frac{\partial g_{nm}(z,x)}{\partial z}g_{nm}(z',x')\frac{e^{j\gamma_{nm}y}\sin(\gamma_{nm}y')}{a_r b_r \varepsilon_n \varepsilon_m \gamma_{nm}}, y < y' \\ -j4\sum_n^\infty\sum_m^\infty j\frac{\partial g_{nm}(z,x)}{\partial z}g_{nm}(z',x')\frac{e^{j\gamma_{nm}y'}\sin(\gamma_{nm}y)}{a_r b_r \varepsilon_n \varepsilon_m \gamma_{nm}}, y > y' \end{cases} \Rightarrow$$

$$G^m_{Esrw_{xy}} = -2j\sum_n^\infty\sum_m^\infty \frac{\partial g_{nm}(z,x)}{\partial z}g_{nm}(z',x')\frac{(e^{j\gamma_{nm}(y+y')} - e^{-j\gamma_{nm}|y-y'|})}{a_r b_r \varepsilon_n \varepsilon_m \gamma_{nm}}$$

$$G^m_{Esrw_{yz}} = \begin{cases} -j4\sum_n^\infty\sum_m^\infty f_{nm}(z,x)\frac{\partial f_{nm}(z',x')}{\partial x'}\frac{e^{j\gamma_{nm}y}\cos(\gamma_{nm}y')}{a_r b_r \gamma_{nm}}, y < y' \\ -j4\sum_n^\infty\sum_m^\infty f_{nm}(z,x)\frac{\partial f_{nm}(z',x')}{\partial x'}\frac{e^{j\gamma_{nm}y'}\cos(\gamma_{nm}y)}{a_r b_r \gamma_{nm}}, y > y' \end{cases} \Rightarrow$$

$$G^m_{Esrw_{yz}} = -2j\sum_n^\infty\sum_m^\infty f_{nm}(z,x)\frac{\partial f_{nm}(z',x')}{\partial x'}\frac{(e^{j\gamma_{nm}(y+y')} + e^{-j\gamma_{nm}|y-y'|})}{a_r b_r \gamma_{nm}}$$

$$G^m_{Esrw_{yx}} = \begin{cases} j4\sum_n^\infty\sum_m^\infty f_{nm}(z,x)\frac{\partial f_{nm}(z',x')}{\partial z'}\frac{e^{j\gamma_{nm}y}\cos(\gamma_{nm}y')}{a_r b_r \gamma_{nm}}, y < y' \\ j4\sum_n^\infty\sum_m^\infty f_{nm}(z,x)\frac{\partial f_{nm}(z',x')}{\partial z'}\frac{e^{j\gamma_{nm}y'}\cos(\gamma_{nm}y)}{a_r b_r \gamma_{nm}}, y > y' \end{cases} \Rightarrow$$

$$G^m_{Esrw_{yx}} = 2j\sum_n^\infty\sum_m^\infty f_{nm}(z,x)\frac{\partial f_{nm}(z',x')}{\partial z'}\frac{(e^{j\gamma_{nm}(y+y')} + e^{-j\gamma_{nm}|y-y'|})}{a_r b_r \gamma_{nm}}$$

$$G^m_{Esrw_{yy}} = 0$$

For the derivation of the elements of $\overline{\overline{G}}^m_{Hsrw}$ the following conditions will be employed:

$$t_1(y,y') = \frac{[e^{j\gamma_{nm}(y+y')} - sign(y-y')e^{-j\gamma_{nm}|y-y'|}]}{2j} = \begin{cases} -j\cos(\gamma_{nm}y')e^{j\gamma_{nm}y}, y < y' \\ \sin(\gamma_{nm}y)e^{j\gamma_{nm}y'}, y > y' \end{cases}$$

$$t_2(y,y') = \frac{(e^{j\gamma_{nm}(y+y')} - e^{-j\gamma_{nm}|y-y'|})}{2j} = \begin{cases} \sin(\gamma_{nm}y')e^{j\gamma_{nm}y}, y < y' \\ \sin(\gamma_{nm}y)e^{j\gamma_{nm}y'}, y > y' \end{cases}$$

$$t_3(y,y') = \frac{(e^{j\gamma_{nm}(y+y')} + e^{-j\gamma_{nm}|y-y'|})}{2} = \begin{cases} \cos(\gamma_{nm}y')e^{j\gamma_{nm}y}, y < y' \\ \cos(\gamma_{nm}y)e^{j\gamma_{nm}y'}, y > y' \end{cases}$$

$$t_4(y,y') = \frac{[e^{j\gamma_{nm}(y+y')} + sign(y-y')e^{-j\gamma_{nm}|y-y'|}]}{2}$$

The rotation of $\overline{\overline{G}}^m_{E_{srw}}$ with respect to the non-primed variables leads to the expression for $\overline{\overline{G}}^m_{H_{srw}}$ according to the condition (3.27g)

$$\overline{\overline{G}}^m_{H_{srw}}(\overrightarrow{r},\overrightarrow{r}') = \frac{1}{k_o^2}[\nabla \times \overline{\overline{G}}^m_{E_{srw}}(\overrightarrow{r},\overrightarrow{r}') - I\delta(\overrightarrow{r}-\overrightarrow{r}')]$$

If $\overline{\overline{G}}^m_{H_1}(\overrightarrow{r},\overrightarrow{r}') = \nabla \times \overline{\overline{G}}^m_{E_{srw}}(\overrightarrow{r},\overrightarrow{r}')$, then the elements of $\overline{\overline{G}}^m_{H_1}(\overrightarrow{r},\overrightarrow{r}')$ are:

$$\begin{aligned}G^m_{H_1zz}(\overrightarrow{r},\overrightarrow{r}') = &\sum_n^\infty\sum_m^\infty [\frac{\partial g_{nm}(z,x)}{\partial z}\frac{\partial g_{nm}(z',x')}{\partial z'} + \\ &+\frac{\partial f_{nm}(z,x)}{\partial x}\frac{\partial f_{nm}(z',x')}{\partial x'}]\frac{4\delta(y-y')}{k^2_{C_{nm}}a_rb_r\varepsilon_n\varepsilon_m} - \\ &-\sum_n^\infty\sum_m^\infty [\frac{\partial g_{nm}(z,x)}{\partial z}\frac{\partial g_{nm}(z',x')}{\partial z'} + \\ &+\frac{\partial f_{nm}(z,x)}{\partial x}\frac{\partial f_{nm}(z',x')}{\partial x'}\frac{k_o^2}{\gamma_{nm}}]\frac{4jt_3(y,y')}{k^2_{C_{nm}}a_rb_r\varepsilon_n\varepsilon_m}\end{aligned}$$

$$G^m_{H_1zx}(\overrightarrow{r},\overrightarrow{r}') = j\sum_{\mathrm{n}}^\infty\sum_{\mathrm{m}}^\infty \frac{\partial \mathrm{f_{n,m}(z,x)}}{\partial \mathrm{x}}\frac{\partial \mathrm{f_{n,m}(z',x')}}{\partial \mathrm{z}'}\frac{4\mathrm{t_3(y,y')}}{\mathrm{a_r b_r \varepsilon_n \varepsilon_m \gamma_{n,m}}}$$

$$G^m_{H_1zy}(\overrightarrow{r},\overrightarrow{r}') = -\sum_n^\infty\sum_m^\infty \frac{\partial g_{nm}(z,x)}{\partial z}g_{nm}(z',x')\frac{4t_4(y,y')}{a_rb_r\varepsilon_n\varepsilon_m}$$

$$G^m_{H_1xz}(\overrightarrow{r},\overrightarrow{r}') = j\sum_n^\infty\sum_m^\infty \frac{\partial f_{nm}(z,x)}{\partial z}\frac{\partial f_{nm}(z',x')}{\partial x'}\frac{4t_3(y,y')}{a_rb_r\varepsilon_n\varepsilon_m\gamma_{nm}}$$

$$\begin{aligned}G^m_{H_1xx}(\overrightarrow{r},\overrightarrow{r}') = = &\sum_n^\infty\sum_m^\infty [\frac{\partial g_{nm}(z,x)}{\partial x}\frac{\partial g_{nm}(z',x')}{\partial x'} + \\ &+\frac{\partial f_{nm}(z,x)}{\partial z}\frac{\partial f_{nm}(z',x')}{\partial z'}]\frac{4\delta(y-y')}{k^2_{C_{nm}}a_rb_r\varepsilon_n\varepsilon_m} - \\ &-\sum_n^\infty\sum_m^\infty [\frac{\partial g_{nm}(z,x)}{\partial x}\frac{\partial g_{nm}(z',x')}{\partial x'} + \\ &+\frac{\partial f_{nm}(z,x)}{\partial z}\frac{\partial f_{nm}(z',x')}{\partial z'}\frac{k_o^2}{\gamma_{nm}}]\frac{4jt_3(y,y')}{k^2_{C_{nm}}a_rb_r\varepsilon_n\varepsilon_m}\end{aligned}$$

$$G^m_{H_1xy}(\overrightarrow{r},\overrightarrow{r}') = -\sum_n^\infty\sum_m^\infty \frac{\partial g_{nm}(z,x)}{\partial x}g_{nm}(z',x')\frac{4t_4(y,y')}{a_rb_r\varepsilon_n\varepsilon_m}$$

$$\begin{aligned}G^m_{H_1yz}(\overrightarrow{r},\overrightarrow{r}') = &\sum_n^\infty\sum_m^\infty [\frac{\partial^2 g_{nm}(z,x)}{\partial z^2}\frac{\partial g_{nm}(z',x')}{\partial z'} + \\ &+\frac{\partial^2 f_{nm}(z,x)}{\partial z\partial x}\frac{\partial f_{nm}(z',x')}{\partial x'}]\frac{4jt_1(y,y')}{k^2_{C_{nm}}a_rb_r\varepsilon_n\varepsilon_m} = \\ &= -\sum_n^\infty\sum_m^\infty g_{nm}(z,x)\frac{\partial g_{nm}(z',x')}{\partial z'}\frac{4jt_1(y,y')}{k^2_{C_{nm}}a_rb_r\varepsilon_n\varepsilon_m}\end{aligned}$$

$$G^m_{H_1yx}(\overrightarrow{r},\overrightarrow{r}') = \sum_n^\infty \sum_m^\infty [\frac{\partial^2 g_{nm}(z,x)}{\partial z^2}\frac{\partial g_{nm}(z',x')}{\partial x'} + \\ + \frac{\partial^2 f_{nm}(z,x)}{\partial z \partial x}\frac{\partial f_{nm}(z',x')}{\partial z'}] \frac{4jt_1(y,y')}{k^2_{C_{nm}} a_r b_r \varepsilon_n \varepsilon_m} = \\ = -\sum_n^\infty \sum_m^\infty g_{nm}(z,x)\frac{\partial g_{nm}(z',x')}{\partial x' -} \frac{4jt_1(y,y')}{k^2_{C_{nm}} a_r b_r \varepsilon_n \varepsilon_m}$$

$$G^m_{H_1yy}(\overrightarrow{r},\overrightarrow{r}') = -4\sum_n^\infty \sum_m^\infty g_{nm}(z,x) g_{nm}(z',x') \frac{t_2(y,y')}{a_r b_r \varepsilon_n \varepsilon_m \gamma_{nm}}$$

Terms $G^m_{H_1xx}(\overrightarrow{r},\overrightarrow{r}')$ and $G^m_{H_1zz}(\overrightarrow{r},\overrightarrow{r}')$ may be further analysed if expression (B.6) is taken into account. More specifically, evaluation of elements $\overrightarrow{z}\,\overrightarrow{z}'$ and $\overrightarrow{x}\,\overrightarrow{x}'$ in (B.6) yields:

$$\delta(\overrightarrow{r}-\overrightarrow{r}')\overrightarrow{z}\,\overrightarrow{z}' = \int_{-\infty}^{\infty} dh \frac{1}{\pi a_r b_r} \sum_n \sum_m [\frac{2e^{jh(y-y')}}{\varepsilon_n \varepsilon_m k^2_{C_{nm}}} \frac{\partial g_{nm}(z,x)}{\partial z}\frac{\partial g_{nm}(z',x')}{\partial z'} + \\ + \frac{2e^{jh(y-y')}}{k^2_{C_{nm}}} \frac{\partial f_{nm}(z,x)}{\partial z}\frac{\partial f_{nm}(z',x')}{\partial z'}]\overrightarrow{z}\,\overrightarrow{z}' \Rightarrow$$

$$\delta(\overrightarrow{r}-\overrightarrow{r}')\overrightarrow{z}\,\overrightarrow{z}' = \sum_n \sum_m [\frac{4}{\varepsilon_n \varepsilon_m k^2_{C_{nm}} a_r b_r} \frac{\partial g_{nm}(z,x)}{\partial z}\frac{\partial g_{nm}(z',x')}{\partial z'}\delta(y-y') + \\ + \frac{4}{k^2_{C_{nm}} a_r b_r} \frac{\partial f_{nm}(z,x)}{\partial x}\frac{\partial f_{nm}(z',x')}{\partial x'}\delta(y-y')]\overrightarrow{z}\,\overrightarrow{z}' \qquad (B.24a)$$

$$\delta(\overrightarrow{r}-\overrightarrow{r}')\overrightarrow{x}\,\overrightarrow{x}' = \int_{-\infty}^{\infty} dh \frac{1}{\pi a_r b_r} \sum_n \sum_m [\frac{2e^{jh(y-y')}}{\varepsilon_n \varepsilon_m k^2_{C_{nm}}} \frac{\partial g_{nm}(z,x)}{\partial x}\frac{\partial g_{nm}(z',x')}{\partial x'} + \\ + \frac{2e^{jh(y-y')}}{k^2_{C_{nm}}} \frac{\partial f_{nm}(z,x)}{\partial z}\frac{\partial f_{nm}(z',x')}{\partial z'}]\overrightarrow{x}\,\overrightarrow{x}' \Rightarrow$$

$$\delta(\overrightarrow{r}-\overrightarrow{r}')\overrightarrow{x}\,\overrightarrow{x}' = \sum_n \sum_m [\frac{4}{\varepsilon_n \varepsilon_m k^2_{C_{nm}} a_r b_r} \frac{\partial g_{nm}(z,x)}{\partial x}\frac{\partial g_{nm}(z',x')}{\partial x'}\delta(y-y') + \\ + \frac{4}{k^2_{C_{nm}} a_r b_r} \frac{\partial f_{nm}(z,x)}{\partial z}\frac{\partial f_{nm}(z',x')}{\partial z'}\delta(y-y')]\overrightarrow{x}\,\overrightarrow{x}' \qquad (B.24b)$$

Through substitution of (B.24) into the expressions for $G^m_{H_1,xx}(\overrightarrow{r},\overrightarrow{r}')$ and $G^m_{H_1,zz}(\overrightarrow{r},\overrightarrow{r}')$ the following relations are obtained:

$$G^m_{H_1,zz}(\overrightarrow{r},\overrightarrow{r}') = \delta(\overrightarrow{r}-\overrightarrow{r}') - \sum_n^\infty \sum_m^\infty [\frac{\partial g_{nm}(z,x)}{\partial z}\frac{\partial g_{nm}(z',x')}{\partial z'}\gamma_{nm} + \\ + \frac{\partial f_{nm}(z,x)}{\partial x}\frac{\partial f_{nm}(z',x')}{\partial x'}\frac{k_o^2}{\gamma_{nm}}] \frac{4jt_3(y,y')}{k^2_{C_{nm}} a_r b_r \varepsilon_n \varepsilon_m}$$

$$G^m_{H_1,xx}(\overrightarrow{r},\overrightarrow{r}') = \delta(\overrightarrow{r}-\overrightarrow{r}') - \sum_n^\infty \sum_m^\infty [\frac{\partial g_{nm}(z,x)}{\partial x}\frac{\partial g_{nm}(z',x')}{\partial x'}\gamma_{nm} + \\ + \frac{\partial f_{nm}(z,x)}{\partial z}\frac{\partial f_{nm}(z',x')}{\partial z'}\frac{k_o^2}{\gamma_{nm}}] \frac{4jt_3(y,y')}{k^2_{C_{nm}} a_r b_r \varepsilon_n \varepsilon_m}$$

Insertion of the expression for $G^m_{H_1}(\overrightarrow{r},\overrightarrow{r}')$ into condition (3.27g) leads to the determination of $G^m_{H_{srw}}(\overrightarrow{r},\overrightarrow{r}')$:

$$\overline{\overline{G}}^m_{H_{srw}}(\overrightarrow{r},\overrightarrow{r}') = \frac{1}{k_0^2}\overline{\overline{G}}^m_{H_1}(\overrightarrow{r},\overrightarrow{r}') - \frac{1}{k_0^2}\delta(\overrightarrow{r}-\overrightarrow{r}')\overrightarrow{y}\,\overrightarrow{y}' \qquad (B.25)$$

Rectangular cavity

Figure B.2 dedpicts the geometry and the coordinate system of the rectangular cavity

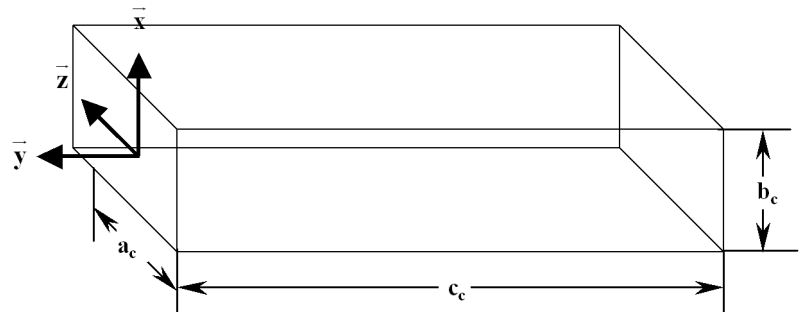

Figure B.2 Coordinate system of the rectangular cavity

The Green function $G^m_{E_{src}}(\overrightarrow{r},\overrightarrow{r}')$ for the cavity can be expressed with the aid of $G^m_{E_{srw}}(\overrightarrow{r},\overrightarrow{r}')$ via the following equation:

$$\overline{\overline{G}}^m_{E_{src}} = \overline{\overline{G}}^m_{E_{srw}} + \overline{\overline{G}}^m_2 \qquad (B.26)$$

where $G^m_2(\overrightarrow{r},\overrightarrow{r}')$ is defined as:

$$\overline{\overline{G}}^m_2(\overrightarrow{r},\overrightarrow{r'}) = \sum_n^\infty \sum_m^\infty [B_e \frac{4\,\overrightarrow{h}^o_{TE_{nm}}(\overrightarrow{r'},\gamma_{nm})\,\overrightarrow{e}^o_{TE_{nm}}(\overrightarrow{r},\gamma_{nm})}{k^2_{C_{nm}} a_c b_c \varepsilon_n \varepsilon_m \gamma_{nm}} + \\ + B_m \frac{4\,\overrightarrow{h}^o_{TM_{nm}}(\overrightarrow{r'},\gamma_{nm})\,\overrightarrow{e}^o_{TM_{nm}}(\overrightarrow{r},\gamma_{nm})}{k^2_{C_{nm}} a_c b_c \gamma_{nm}}]$$

The unknown coefficients B_e and B_m will be determined after implementation of the boundary condition $\vec{y} \times \vec{E} = 0$ at plane $y = -c_c$:

$$\overrightarrow{y} \times \overrightarrow{E} = 0|_{y=-c_c} \Rightarrow \overrightarrow{y} \times \overline{\overline{G}}^m_{E_{src}} = 0|_{y=-c_c} \Rightarrow$$

$$\begin{cases} \overrightarrow{y} \times [-\overrightarrow{h}^o_{TE_{nm}}(\overrightarrow{r'},\gamma_{nm})\overrightarrow{e}_{TE_{nm}}(\overrightarrow{r},\gamma_{nm}) + \\ + B_e \overrightarrow{h}^o_{TE_{nm}}(\overrightarrow{r'},\gamma_{nm})\overrightarrow{e}^o_{TE_{nm}}(\overrightarrow{r},\gamma_{nm})] = 0|_{y=c_c} \\ \overrightarrow{y} \times [-j\,\overrightarrow{h}^o_{TM_{nm}}(\overrightarrow{r'},\gamma_{nm})\overrightarrow{e}_{TM_{nm}}(\overrightarrow{r},\gamma_{nm}) + \\ + B_m \overrightarrow{h}^o_{TM_{nm}}(\overrightarrow{r'},\gamma_{nm})\overrightarrow{e}^o_{TM_{nm}}(\overrightarrow{r},\gamma_{nm})] = 0|_{y=c_c} \end{cases} \Rightarrow$$

$$\begin{cases} B_e = -\frac{e^{-j\gamma_{n,m}c_c}}{\sin(\gamma_{n,m}c_c)} \\ B_m = -\frac{e^{-j\gamma_{nm}c_c}}{\sin(\gamma_{nm}c_c)} \end{cases}$$

Insertion of the values for B_e and B_m into equation (B.26) leads to the expressions:
for $y < y'$:

$$\overline{\overline{G}}^m_{E_{srw}}(\overrightarrow{r},\overrightarrow{r}') = -j4 \sum_n^\infty \sum_m^\infty [-j \frac{\overrightarrow{e}_{TE_{nm}}(\overrightarrow{r},\gamma_{nm})\,\overrightarrow{h}^o_{TE_{nm}}(\overrightarrow{r'},\gamma_{nm})}{k^2_{C_{nm}} a_r b_r \varepsilon_n \varepsilon_m \gamma_{nm}} + \\ + \frac{\overrightarrow{e}_{TM_{nm}}(\overrightarrow{r},\gamma_{nm})\,\overrightarrow{h}^o_{TM_{nm}}(\overrightarrow{r'},\gamma_{nm})}{k^2_{C_{nm}} a_r b_r \gamma_{nm}}] - \\ - \sum_n^\infty \sum_m^\infty [\frac{4\,\overrightarrow{h}^o_{TE_{nm}}(\overrightarrow{r'},\gamma_{nm})\,\overrightarrow{e}^o_{TE_{nm}}(\overrightarrow{r},\gamma_{nm})e^{-j\gamma_{nm}c_c}}{k^2_{C_{nm}} a_r b_r \varepsilon_n \varepsilon_m \gamma_{nm} \sin(\gamma_{nm}c_c)} + \\ + \frac{4\,\overrightarrow{h}^o_{TM_{nm}}(\overrightarrow{r'},\gamma_{nm})\,\overrightarrow{e}^o_{TM_{nm}}(\overrightarrow{r},\gamma_{nm})e^{-j\gamma_{nm}c_c}}{k^2_{C_{nm}} a_r b_r \gamma_{nm} \sin(\gamma_{nm}c_c)}]$$

for $y > y'$:

$$\overline{\overline{G}}^{m}_{E_{srw}}(\overrightarrow{r},\overrightarrow{r}') = -j4\sum_{n}^{\infty}\sum_{m}^{\infty}[-j\frac{\overrightarrow{h}_{TE_{nm}}(\overrightarrow{r}',\gamma_{nm})\overrightarrow{e}^{o}_{TE_{nm}}(\overrightarrow{r},\gamma_{nm})}{k^2_{C_{nm}}a_r b_r \varepsilon_n \varepsilon_m \gamma_{nm}} + \frac{\overrightarrow{h}_{TM_{nm}}(\overrightarrow{r}',\gamma_{nm})\overrightarrow{e}^{o}_{TM_{nm}}(\overrightarrow{r},\gamma_{nm})}{k^2_{C_{nm}}a_r b_r \gamma_{nm}}] - \\ -\sum_{n}\sum_{m}[\frac{4\overrightarrow{h}^{o}_{TE_{nm}}(\overrightarrow{r}',\gamma_{nm})\overrightarrow{e}^{o}_{TE_{nm}}(\overrightarrow{r},\gamma_{nm})\mathrm{e}^{-\mathrm{j}\gamma_{\mathrm{n,m}}\mathrm{c_c}}}{k^2_{C_{nm}}a_r b_r \varepsilon_n \varepsilon_m \gamma_{nm}\sin(\gamma_{\mathrm{n,m}}\mathrm{c_c})} + \\ +\frac{4\overrightarrow{h}^{o}_{TM_{nm}}(\overrightarrow{r}',\gamma_{nm})\overrightarrow{e}^{o}_{TM_{nm}}(\overrightarrow{r},\gamma_{nm})\mathrm{e}^{-\mathrm{j}\gamma_{\mathrm{n,m}}\mathrm{c_c}}}{k^2_{C_{nm}}a_r b_r \gamma_{nm}\sin(\gamma_{\mathrm{n,m}}\mathrm{c_c})}]$$

The following relationships are valid:

$$\overrightarrow{e}_{TE_{nm}}(\overrightarrow{r},\gamma_{nm}) + \frac{e^{-j\gamma_{nm}c_c}}{\sin(\gamma_{nm}c_c)}\overrightarrow{e}^{o}_{TE_{nm}}(\overrightarrow{r},\gamma_{nm}) = \frac{\overrightarrow{e}^{o}_{TE_{nm}}(z,x,c_c+y,\gamma_{nm})}{\sin(\gamma_{nm}c_c)}$$

$$j\overrightarrow{e}_{TM_{nm}}(\overrightarrow{r},\gamma_{nm}) + \frac{e^{-j\gamma_{nm}c_c}}{\sin(\gamma_{nm}c_c)}\overrightarrow{e}^{o}_{TM_{nm}}(\overrightarrow{r},\gamma_{nm}) = \frac{\overrightarrow{e}^{o}_{TM_{nm}}(z,x,c_c+y,\gamma_{nm})}{\sin(\gamma_{nm}c_c)}$$

$$\overrightarrow{h}_{TE_{nm}}(\overrightarrow{r},\gamma_{nm}) + \frac{e^{-j\gamma_{nm}c_c}}{\sin(\gamma_{nm}c_c)}\overrightarrow{h}^{o}_{TE_{nm}}(\overrightarrow{r},\gamma_{nm}) = \frac{\overrightarrow{h}^{o}_{TE_{nm}}(z,x,c_c+y,\gamma_{nm})}{\sin(\gamma_{nm}c_c)}$$

$$j\overrightarrow{h}_{TM_{nm}}(\overrightarrow{r},\gamma_{nm}) + \frac{e^{-j\gamma_{nm}c_c}}{\sin(\gamma_{nm}c_c)}\overrightarrow{h}^{o}_{TM_{nm}}(\overrightarrow{r},\gamma_{nm}) = \frac{\overrightarrow{h}^{o}_{TM_{nm}}(z,x,c_c+y,\gamma_{nm})}{\sin(\gamma_{nm}c_c)}$$

Equation (B.26) becomes:
for $y < y'$

$$\overline{\overline{G}}^{m}_{E_{src}}(\overrightarrow{r},\overrightarrow{r}') = -4\sum_{n}^{\infty}\sum_{m}^{\infty}[\frac{\overrightarrow{h}^{o}_{TE_{nm}}(z',x',y',\gamma_{nm})\overrightarrow{e}^{o}_{TE_{nm}}(z,x,c_c+y,\gamma_{nm})}{k^2_{C_{nm}}a_c b_c \varepsilon_n \varepsilon_m \gamma_{nm}\sin(\gamma_{nm}c_c)} + \\ +\frac{\overrightarrow{h}^{o}_{TM_{nm}}(z',x',y',\gamma_{nm})\overrightarrow{e}^{o}_{TM_{nm}}(z,x,y+c_c,\gamma_{nm})}{k^2_{C_{nm}}a_c b_c \varepsilon_n \varepsilon_m \gamma_{nm}\sin(\gamma_{nm}c_c)}]$$

for $y > y'$

$$\overline{\overline{G}}^{m}_{E_{src}}(\overrightarrow{r},\overrightarrow{r}') = -4\sum_{n}^{\infty}\sum_{m}^{\infty}[\frac{\overrightarrow{e}^{o}_{TE_{nm}}(z,x,y,\gamma_{nm})\overrightarrow{h}^{o}_{TE_{nm}}(z',x',c_c+y',\gamma_{nm})}{k^2_{C_{nm}}a_c b_c \varepsilon_n \varepsilon_m \gamma_{nm}\sin(\gamma_{nm}c_c)} + \\ +\frac{\overrightarrow{e}^{o}_{TM_{nm}}(z,x,y,\gamma_{nm})\overrightarrow{h}^{o}_{TM_{nm}}(z',x',y'+c_c,\gamma_{nm})}{k^2_{C_{nm}}a_c b_c \varepsilon_n \varepsilon_m \gamma_{nm}\sin(\gamma_{nm}c_c)}]$$

The elements of $\overline{\overline{G}}^{m}_{E_{src}}(\overrightarrow{r},\overrightarrow{r}')$ are:

$$G^{m}_{E_{src}zz} = 0$$

$$G^{m}_{E_{src}zx} = \begin{cases} -4\sum_{n}^{\infty}\sum_{m}^{\infty}[\frac{\partial g_{nm}(z,x)}{\partial x}\frac{\partial g_{nm}(z',x')}{\partial x'} + \\ +\frac{\partial f_{nm}(z,x)}{\partial z}\frac{\partial f_{nm}(z',x')}{\partial z'}]\frac{\sin[\gamma_{nm}(y+c_c)]\cos(\gamma_{nm}y')}{k^2_{C_{nm}}a_c b_c \varepsilon_n \varepsilon_m \sin(\gamma_{nm}c_c)}, y < y' \\ -4\sum_{n}^{\infty}\sum_{m}^{\infty}[\frac{\partial g_{nm}(z,x)}{\partial x}\frac{\partial g_{nm}(z',x')}{\partial x'} + \\ +\frac{\partial f_{nm}(z,x)}{\partial z}\frac{\partial f_{nm}(z',x')}{\partial z'}]\frac{\cos[\gamma_{nm}(y'+c_c)]\sin(\gamma_{nm}y)}{k^2_{C_{nm}}a_c b_c \varepsilon_n \varepsilon_m \sin(\gamma_{nm}c_c)}, y > y' \end{cases} \Rightarrow$$

$$G^{m}_{E_{src}zx} = -4\sum_{n}^{\infty}\sum_{m}^{\infty}[\frac{\partial g_{nm}(z,x)}{\partial x}\frac{\partial g_{nm}(z',x')}{\partial x'} + \\ +\frac{\partial f_{nm}(z,x)}{\partial z}\frac{\partial f_{nm}(z',x')}{\partial z'}]\frac{s_3(y,y')}{k^2_{C_{nm}}a_c b_c \varepsilon_n \varepsilon_m \sin(\gamma_{nm}c_c)}$$

$$G^m_{E_{src}zy} = \begin{cases} -4\sum_n^\infty\sum_m^\infty [\frac{\partial g_{nm}(z,x)}{\partial x} g_{nm}(z',x') \frac{\sin[\gamma_{nm}(y+c_c)]\sin(\gamma_{nm}y')}{a_c b_c \varepsilon_n \varepsilon_m \gamma_{nm} \sin(\gamma_{nm}c_c)}], y < y' \\ -4\sum_n^\infty\sum_m^\infty [\frac{\partial g_{nm}(z,x)}{\partial x} g_{nm}(z',x') \frac{\sin[\gamma_{nm}(y'+c_c)]\sin(\gamma_{nm}y)}{a_c b_c \varepsilon_n \varepsilon_m \gamma_{nm} \sin(\gamma_{nm}c_c)}], y > y' \end{cases} \Rightarrow$$

$$G^m_{E_{src}zy} = -4\sum_n^\infty\sum_m^\infty \frac{\partial g_{nm}(z,x)}{\partial x} g_{nm}(z',x') \frac{s_2(y,y')}{a_c b_c \varepsilon_n \varepsilon_m \gamma_{nm} \sin(\gamma_{nm}c_c)}$$

$$G^m_{E_{src}xz} = \begin{cases} 4\sum_n^\infty\sum_m^\infty [\frac{\partial g_{nm}(z,x)}{\partial z} \frac{\partial g_{nm}(z',x')}{\partial z} + \\ + \frac{\partial f_{nm}(z,x)}{\partial x} \frac{\partial f_{nm}(z',x')}{\partial x'}] \frac{\sin[\gamma_{nm}(y+c_c)]\cos(\gamma_{nm}y')}{k^2_{C_{nm}} a_c b_c \varepsilon_n \varepsilon_m \sin(\gamma_{nm}c_c)}, y < y' \\ 4\sum_n^\infty\sum_m^\infty [\frac{\partial g_{nm}(z,x)}{\partial z} \frac{\partial g_{nm}(z',x')}{\partial z} + \\ + \frac{\partial f_{nm}(z,x)}{\partial x} \frac{\partial f_{nm}(z',x')}{\partial x'}] \frac{\cos[\gamma_{nm}(y'+c_c)]\sin(\gamma_{nm}y)}{k^2_{C_{nm}} a_c b_c \varepsilon_n \varepsilon_m \sin(\gamma_{nm}c_c)}, y > y' \end{cases} \Rightarrow$$

$$G^m_{E_{src}xz} = 4\sum_n^\infty\sum_m^\infty [\frac{\partial g_{nm}(z,x)}{\partial z} \frac{\partial g_{nm}(z',x')}{\partial z'} + \\ + \frac{\partial f_{nm}(z,x)}{\partial x} \frac{\partial f_{nm}(z',x')}{\partial x'}] \frac{s_3(y,y')}{k^2_{C_{nm}} a_c b_c \varepsilon_n \varepsilon_m \sin(\gamma_{nm}c_c)}$$

$$G^m_{E_{src}xx} = 0$$

$$G^m_{E_{src}xy} = \begin{cases} 4\sum_n^\infty\sum_m^\infty [\frac{\partial g_{nm}(z,x)}{\partial z} g_{nm}(z',x') \frac{\sin[\gamma_{nm}(y+c_c)]\sin(\gamma_{nm}y')}{a_c b_c \varepsilon_n \varepsilon_m \gamma_{nm} \sin(\gamma_{nm}c_c)}], y < y' \\ 4\sum_n^\infty\sum_m^\infty [\frac{\partial g_{nm}(z,x)}{\partial z} g_{nm}(z',x') \frac{\sin[\gamma_{nm}(y'+c_c)]\sin(\gamma_{nm}y)}{a_c b_c \varepsilon_n \varepsilon_m \gamma_{nm} \sin(\gamma_{nm}c_c)}], y > y' \end{cases} \Rightarrow$$

$$G^m_{E_{src}xy} = 4\sum_n^\infty\sum_m^\infty \frac{\partial g_{nm}(z,x)}{\partial z} g_{nm}(z',x') \frac{s_2(y,y')}{a_c b_c \varepsilon_n \varepsilon_m \gamma_{nm} \sin(\gamma_{nm}c_c)}$$

$$G^m_{E_{src}yz} = \begin{cases} -4\sum_n^\infty\sum_m^\infty f_{nm}(z,x) \frac{\partial f_{nm}(z',x')}{\partial x'} \frac{\cos[\gamma_{nm}(y+c_c)]\cos(\gamma_{nm}y')}{a_c b_c \gamma_{nm} \sin(\gamma_{nm}c_c)}, y < y' \\ -4\sum_n^\infty\sum_m^\infty f_{nm}(z,x) \frac{\partial f_{nm}(z',x')}{\partial x'} \frac{\cos[\gamma_{nm}(y'+c_c)]\cos(\gamma_{nm}y)}{a_c b_c \gamma_{nm} \sin(\gamma_{nm}c_c)}, y > y' \end{cases} \Rightarrow$$

$$G^m_{E_{src}yz} = -4\sum_n^\infty\sum_m^\infty f_{nm}(z,x) \frac{\partial f_{nm}(z',x')}{\partial x'} \frac{s_1(y,y')}{a_c b_c \gamma_{nm} \sin(\gamma_{nm}c_c)}$$

$$G^m_{E_{src}yx} = \begin{cases} 4\sum_n^\infty\sum_m^\infty f_{nm}(z,x) \frac{\partial f_{nm}(z',x')}{\partial z'} \frac{\cos[\gamma_{nm}(y+c_c)]\cos(\gamma_{nm}y')}{a_c b_c \gamma_{nm} \sin(\gamma_{nm}c_c)}, y < y' \\ 4\sum_n^\infty\sum_m^\infty f_{nm}(z,x) \frac{\partial f_{nm}(z',x')}{\partial z'} \frac{\cos[\gamma_{nm}(y'+c_c)]\cos(\gamma_{nm}y)}{a_c b_c \gamma_{nm} \sin(\gamma_{nm}c_c)}, y > y' \end{cases} \Rightarrow$$

$$G^m_{E_{src}yx} = 4\sum_n^\infty \sum_m^\infty f_{nm}(z,x)\frac{\partial f_{nm}(z',x')}{\partial z'}\frac{s_1(y,y')}{a_c b_c \gamma_{nm}\sin(\gamma_{nm}c_c)}$$

$$G^m_{E_{src}yy} = 0$$

where:

$$s_1(y,y') = \tfrac{\cos[\gamma_{nm}(y+y'+c_c)]+\cos[\gamma_{nm}(c_c-|y-y'|)]}{2} \Rightarrow$$

$$s_1(y,y') = \begin{cases} \cos[\gamma_{nm}(y+c_c)]\cos(\gamma_{nm}y'), y<y' \\ \cos(\gamma_{nm}y)\cos[\gamma_{nm}(y'+c_c)], y>y' \end{cases}$$

$$s_2(y,y') = \tfrac{\cos[\gamma_{nm}(y+y'+c_c)]-\cos[\gamma_{nm}(c_c-|y-y'|)]}{2} \Rightarrow$$

$$s_2(y,y') = \begin{cases} \sin[\gamma_{nm}(y+c_c)]\sin(\gamma_{nm}y'), y<y' \\ \sin(\gamma_{nm}y)\sin[\gamma_{nm}(y'+c_c)], y>y' \end{cases}$$

$$s_3(y,y') = \tfrac{\sin[\gamma_{nm}(c_c+y+y')]-sign(y-y')\sin[\gamma_{nm}(c_c-|y-y'|)]}{2} \Rightarrow$$

$$s_3(y,y') = \begin{cases} \sin[\gamma_{nm}(y+c_c)]\cos(\gamma_{nm}y'), y<y' \\ \sin(\gamma_{nm}y)\cos[\gamma_{nm}(y'+c_c)], y>y' \end{cases}$$

Additionally:

$$s_4(y,y') = \frac{\sin[\gamma_{nm}(c_c+y+y')]+sign(y-y')\sin[\gamma_{nm}(c_c-|y-y'|)]}{2}$$

The dyadic $\overline{\overline{G}}^m_{H_{src}}(\overrightarrow{r},\overrightarrow{r}')$ is derived in the same manner as $\overline{\overline{G}}^m_{E_{src}}(\overrightarrow{r},\overrightarrow{r}')$, namely according to equation:

$$\overline{\overline{G}}^m_{H_{src}}(\overrightarrow{r},\overrightarrow{r}') = \frac{1}{k_o^2}[\nabla\times\overline{\overline{G}}^m_{E_{src}}(\overrightarrow{r},\overrightarrow{r}') - I\delta(\overrightarrow{r}-\overrightarrow{r}')]$$

If $\overline{\overline{G}}^m_{H_2}(\overrightarrow{r},\overrightarrow{r}') = \nabla\times\overline{\overline{G}}^m_{E_{src}}(\overrightarrow{r},\overrightarrow{r}')$, then the elements of $\overline{\overline{G}}^m_{H_2}(\overrightarrow{r},\overrightarrow{r}')$ are:

$$\begin{aligned} G^m_{H_2zz}(\overrightarrow{r},\overrightarrow{r}') = {} & \tfrac{4}{a_r b_r}\sum_n^\infty\sum_m^\infty[\tfrac{\partial g_{nm}(z,x)}{\partial z}\tfrac{\partial g_{nm}(z',x')}{\partial z'} + \\ & + \tfrac{\partial f_{nm}(z,x)}{\partial x}\tfrac{\partial f_{nm}(z',x')}{\partial x'}]\tfrac{\delta(y-y')}{k^2_{C_{nm}}\varepsilon_n\varepsilon_m} - \\ & - \sum_n^\infty\sum_m^\infty[\tfrac{\partial g_{nm}(z,x)}{\partial z}\tfrac{\partial g_{nm}(z',x')}{\partial z'} + \\ & + \tfrac{\partial f_{nm}(z,x)}{\partial x}\tfrac{\partial f_{nm}(z',x')}{\partial x'}\tfrac{k_o^2}{\gamma_{nm}}]\tfrac{s_1(y,y')}{k^2_{C_{nm}}\varepsilon_n\varepsilon_m\sin(\gamma_{nm}c_c)} \overset{(B.24a)}{\Rightarrow} \end{aligned}$$

$$G^m_{H_2,zx}(\overrightarrow{r},\overrightarrow{r}') = 4\sum_n^\infty\sum_m^\infty \frac{\partial f_{nm}(z,x)}{\partial x}\frac{\partial f_{nm}(z',x')}{\partial z'}\frac{s_1(y,y')}{a_c b_c\gamma_{nm}\sin(\gamma_{nm}c_c)}$$

$$G^m_{H_2,zy}(\overrightarrow{r},\overrightarrow{r}') = 4\sum_n^\infty\sum_m^\infty \frac{\partial g_{nm}(z,x)}{\partial z}g_{nm}(z',x')\frac{s_4(y,y')}{a_c b_c\varepsilon_n\varepsilon_m\sin(\gamma_{nm}c_c)}$$

$$G^m_{H_2,xz}(\overrightarrow{r},\overrightarrow{r}') = 4\sum_n^\infty\sum_m^\infty \frac{\partial f_{nm}(z,x)}{\partial z}\frac{\partial f_{nm}(z',x')}{\partial x'}\frac{s_1(y,y')}{a_c b_c \gamma_{n,m}\sin(\gamma_{nm}c_c)}$$

$$\begin{aligned}G^m_{H_2xx}(\overrightarrow{r},\overrightarrow{r}') = &\tfrac{4}{a_r b_r}\sum_n^\infty\sum_m^\infty[\tfrac{\partial g_{nm}(z,x)}{\partial x}\tfrac{\partial g_{nm}(z',x')}{\partial x'}+\\ &+\tfrac{\partial f_{nm}(z,x)}{\partial z}\tfrac{\partial f_{nm}(z',x')}{\partial z'}]\tfrac{\delta(y-y')}{k^2_{C_{nm}}\varepsilon_n\varepsilon_m}-\\ &-\sum_n^\infty\sum_m^\infty[\tfrac{\partial g_{nm}(z,x)}{\partial x}\tfrac{\partial g_{nm}(z',x')}{\partial x'}+\\ &+\tfrac{\partial f_{nm}(z,x)}{\partial z}\tfrac{\partial f_{nm}(z',x')}{\partial z'}\tfrac{k_o^2}{\gamma_{nm}}]\tfrac{s_1(y,y')}{k^2_{C_{nm}}\varepsilon_n\varepsilon_m\sin(\gamma_{nm}c_c)}\overset{(B.24b)}{\Rightarrow}\end{aligned}$$

$$\begin{aligned}G^m_{H_2,xx}(\overrightarrow{r},\overrightarrow{r}') = &\delta(\overrightarrow{r}-\overrightarrow{r}') - \tfrac{4}{k^2_{C_{nm}}a_r b_r\varepsilon_n\varepsilon_m}\sum_n^\infty\sum_m^\infty[\tfrac{\partial g_{nm}(z,x)}{\partial x}\tfrac{\partial g_{nm}(z',x')}{\partial x'}\gamma_{nm}+\\ &+\tfrac{\partial f_{nm}(z,x)}{\partial z}\tfrac{\partial f_{nm}(z',x')}{\partial z'}\tfrac{k_o^2}{\gamma_{nm}}]\tfrac{s_1(y,y')}{\sin(\gamma_{nm}c_c)}\end{aligned}$$

$$G^m_{H_2,xy}(\overrightarrow{r},\overrightarrow{r}') = 4\sum_n^\infty\sum_m^\infty \tfrac{\partial g_{nm}(z,x)}{\partial x}g_{nm}(z',x')\tfrac{s_4(y,y')}{a_c b_c\varepsilon_n\varepsilon_m\sin(\gamma_{nm}c_c)}$$

$$\begin{aligned}G^m_{H_2,yz}(\overrightarrow{r},\overrightarrow{r}') = &\sum_n^\infty\sum_m^\infty[\tfrac{\partial^2 g_{nm}(z,x)}{\partial z^2}\tfrac{\partial g_{nm}(z',x')}{\partial z'}+\\ &+\tfrac{\partial^2 f_{nm}(z,x)}{\partial z\partial x}\tfrac{\partial f_{nm}(z',x')}{\partial x'}]\tfrac{4s_3(y,y')}{k^2_{C_{nm}}a_c b_c\varepsilon_n\varepsilon_m\sin(\gamma_{nm}c_c)} =\\ &= -4\sum_n^\infty\sum_m^\infty g_{nm}(z,x)\tfrac{\partial g_{nm}(z',x')}{\partial z'}\tfrac{s_3(y,y')}{a_c b_c\varepsilon_n\varepsilon_m\sin(\gamma_{nm}c_c)}\end{aligned}$$

$$\begin{aligned}G^m_{H_2,yx}(\overrightarrow{r},\overrightarrow{r}') = &\sum_n^\infty\sum_m^\infty[\tfrac{\partial^2 g_{nm}(z,x)}{\partial x^2}\tfrac{\partial g_{nm}(z',x')}{\partial x'}+\\ &+\tfrac{\partial^2 f_{nm}(z,x)}{\partial x\partial z}\tfrac{\partial f_{nm}(z',x')}{\partial z'}]\tfrac{4s_3(y,y')}{k^2_{C_{nm}}a_c b_c\varepsilon_n\varepsilon_m\sin(\gamma_{nm}c_c)} =\\ &= -4\sum_n^\infty\sum_m^\infty g_{nm}(z,x)\tfrac{\partial g_{nm}(z',x')}{\partial x'}\tfrac{s_3(y,y')}{a_c b_c\varepsilon_n\varepsilon_m\sin(\gamma_{nm}c_c)}\end{aligned}$$

$$G^m_{H_2,yy}(\overrightarrow{r},\overrightarrow{r}') = -4\sum_n^\infty\sum_m^\infty k^2_{C_{nm}}g_{nm}(z,x)g_{nm}(z',x')\frac{s_2(y,y')}{a_c b_c\varepsilon_n\varepsilon_m\gamma_{nm}\sin(\gamma_{nm}c_c)}$$

The final expression for $\overline{\overline{G}}^m_{H_{src}}$ is:

$$\overline{\overline{G}}^m_{H_{src}}(\overrightarrow{r},\overrightarrow{r}') = \frac{1}{k_0^2}\overline{\overline{G}}^m_{H_2}(\overrightarrow{r},\overrightarrow{r}') - \frac{1}{k_0^2}\delta(\overrightarrow{r}-\overrightarrow{r}')\overrightarrow{y}\,\overrightarrow{y}' \qquad (B.27)$$

Equation (B.27) determines the magnetic dyadic Green function for the magnetic current inside a rectangular cavity.

B.2 Dyadic Green Functions inside a ridged waveguide

B.2.1 Magnetic dyadic Green function generated by electric current

The magnetic field inside the ridged waveguide satisfies the equation:

$$\nabla \times \nabla \times \overrightarrow{H} - k_0^2 \overrightarrow{H} = \nabla \times \overrightarrow{J}$$

The Green function $\overline{\overline{G}}_H^e(r, r')$ must satisfy a similar equation:

$$\nabla \times \nabla \times \overline{\overline{G}}_H^e(r, r') - k_o^2 \overline{\overline{G}}_H^e(r, r') = \nabla \times I\delta(\overrightarrow{r} - \overrightarrow{r}') \quad (B.28)$$

Unlike the case of magnetic vector potential, vector $\overrightarrow{L}_{n,m}$ is not used for the expansion of $I\delta(\overrightarrow{r} - \overrightarrow{r}')$, because there is no need for a non-solenoidal eigenvector set, since $\nabla \cdot \overrightarrow{H}(\overrightarrow{r}') = 0$ everywhere inside a waveguide that carries electric currents.
The right side of (B.28) is expanded on the wave vectors for the electric field:

$$\overrightarrow{h}_{TE_i}(\overrightarrow{r}, h) = jhe^{jhz}\nabla_t g_i(x, y) + k_{Ci}^2 g_i(x, y)e^{jhz}\overrightarrow{z}$$
$$\overrightarrow{h}_{TM_i}(\overrightarrow{r}, h) = e^{jhz}\nabla_t f_i(x, y) \times \overrightarrow{z}$$

The orthogonality conditions are represented by equations (3.35).
Term $\nabla \times I\delta(\overrightarrow{r} - \overrightarrow{r}')$ is expanded in the following manner:

$$I\delta(\overrightarrow{r} - \overrightarrow{r}') = \int_{-\infty}^{\infty} dh[\sum_i A_i(h)\overrightarrow{h}_{TE_i}(\overrightarrow{r}, h) + \sum_j B_j(h)\overrightarrow{h}_{TM_j}(\overrightarrow{r}, h)] \quad (B.29)$$

Both members of expression (B.29) are multiplied with $\overrightarrow{h}_{TE_t}(\overrightarrow{r}, -h)$ and integrated over the waveguide volume:

$$\iiint_V \overrightarrow{h}_{TE_t}(\overrightarrow{r}, -h)\nabla \times I\delta(\overrightarrow{r} - \overrightarrow{r}')dv =$$
$$= \iiint_V dv \int_{-\infty}^{\infty} dh\, \overrightarrow{h}_{TE_t}(\overrightarrow{r}, -h)[\sum_i A_i(h)\overrightarrow{h}_{TE_i}(\overrightarrow{r}, h) + \sum_j B_j(h)\overrightarrow{h}_{TM_j}(\overrightarrow{r}, h)] \Rightarrow$$
$$\iiint_V \overrightarrow{h}_{TE_t}(\overrightarrow{r}, -h)\nabla \times I\delta(\overrightarrow{r} - \overrightarrow{r}')dv = \int_{-\infty}^{\infty} dh A_t(h)(k_{C_t}^2 + h^2)\delta(h - h')2\pi \quad (B.30)$$

Application of the dyadic identity: $\nabla \cdot (\overrightarrow{a} \times \overline{\overline{b}}) = -\overrightarrow{a}\nabla \times \overline{\overline{b}} + \overline{\overline{b}}\nabla \times \overrightarrow{a}$ and the divergence theorem:

$$\iiint_V \nabla \cdot \overrightarrow{B}dv = \oiint_S (\overrightarrow{n} \times \overrightarrow{B})ds$$

on the left side of (B.30) yields:

$$\iiint_V \overrightarrow{h}_{TE_t}(\overrightarrow{r}, -h)\nabla \times I\delta(\overrightarrow{r} - \overrightarrow{r}')dv =$$
$$-\iiint_V \nabla[\overrightarrow{h}_{TE_t}(\overrightarrow{r}, -h) \times I\delta(\overrightarrow{r} - \overrightarrow{r}')]dv + \iiint_V \nabla \overrightarrow{h}_{TE_t}(\overrightarrow{r}, -h)I\delta(\overrightarrow{r} - \overrightarrow{r}')]dv =$$
$$\oiint_S \overrightarrow{n} \cdot [\overrightarrow{h}_{TE_t}(\overrightarrow{r}, -h) \times I\delta(\overrightarrow{r} - \overrightarrow{r}')]ds + \nabla' \times \overrightarrow{h}_{TE_t}(\overrightarrow{r}', -h)$$

The surface integral in the above expression vanishes because $\overrightarrow{r}'$ is located inside the volume V
In view of the preceding equation, expression (B.30) becomes:

$$A_i(h) = \frac{\nabla' \times \overrightarrow{h}_{TE_i}(\overrightarrow{r'}, -h)}{(k_{C_{TEi}}^2 + h^2)2\pi} = \frac{\overrightarrow{e}_{TE_i}(\overrightarrow{r'}, -h)}{2\pi}$$

In a similar way:

$$B_i(h) = \frac{\nabla' \times \overrightarrow{h}_{TM_i}(\overrightarrow{r'}, -h)}{2\pi} = \frac{\overrightarrow{e}_{TM_i}(\overrightarrow{r'}, -h)}{2\pi}$$

Equation (B.29) becomes:

$$\nabla \times I\delta(\overrightarrow{r} - \overrightarrow{r}') = \int_{-\infty}^{\infty} dh[\sum_i \frac{\overrightarrow{e}_{TE_i}(\overrightarrow{r'}, -h)}{2\pi} \overrightarrow{h}_{TE_i}(\overrightarrow{r}, h) + \\ + \sum_j \frac{2\overrightarrow{e}_{TM_j}(\overrightarrow{r'}, -h)}{2\pi} \overrightarrow{h}_{TM_j}(\overrightarrow{r}, h)] \quad (B.31)$$

The unknown Green function is expressed in the following way:

$$\overline{\overline{G}}^e_H(\overrightarrow{r}, \overrightarrow{r}') = \int_{-\infty}^{\infty} dh[\sum_i a_i(h) \frac{\overrightarrow{e}_{TE_i}(\overrightarrow{r'}, -h)}{2\pi} \overrightarrow{h}_{TE_i}(\overrightarrow{r}, h) + \\ + \sum_j b_j(h) \frac{2\overrightarrow{e}_{TM_j}(\overrightarrow{r'}, -h)}{2\pi} \overrightarrow{h}_{TM_j}(\overrightarrow{r}, h)] \quad (B.32)$$

Insertion of (B.31) and (B.32) into (B.28) yields the values of the coefficients $a_i(h)$ and $b_j(h)$:

$$a_k(h) = \frac{1}{k^2_{C_{TEk}} + h^2 - k_o^2}$$
$$b_k(h) = \frac{1}{k^2_{C_{TMk}} + h^2 - k_o^2}$$

Equation (B.32) becomes:

$$\overline{\overline{G}}^e_H(\overrightarrow{r}, \overrightarrow{r}') = \frac{1}{2\pi} \int_{-\infty}^{\infty} dh[\sum_i \frac{\overrightarrow{h}_{TE_i}(\overrightarrow{r}, h)\overrightarrow{e}_{TE_i}(\overrightarrow{r}', -h)}{k^2_{C_{TEi}} + h^2 - k_o^2} + \\ + \sum_j \frac{\overrightarrow{h}_{TM_j}(\overrightarrow{r}, h)\overrightarrow{e}_{TM_j}(\overrightarrow{r}', -h)}{k^2_{C_{TMj}} + h^2 - k_o^2}]$$

The integral in the above expression may be evaluated by the method of contour integration. Both terms of the integrand satisfy the Jordan lemma and have two poles in $h = \pm\sqrt{k_o^2 - k^2_{C_k}} = \mp\gamma_k$.The final expression for $\overline{\overline{G}}^e_H(\overrightarrow{r}, \overrightarrow{r}')$ is:

$$\overline{\overline{G}}^e_H(\overrightarrow{r}, \overrightarrow{r}') = -j \sum_n \frac{\overrightarrow{e}_{TE_i - (\overrightarrow{r'}, \pm\gamma_{TE_i})} \overrightarrow{h}_{TE_i}(\overrightarrow{r}, \mp\gamma_{TE_i})}{2\gamma_{TE_i}} - \\ -j \sum_j \frac{\overrightarrow{e}_{TM_j}(\overrightarrow{r'}, \pm\gamma_{TM_j}) \overrightarrow{h}_{TM_j}(\overrightarrow{r}, \mp\gamma_{TM_j})}{2\gamma_{TM_j}} \quad (B.33)$$

Analytical expressions for the elements of $\overline{\overline{G}}^e_H$:

$$G^e_{H_{xx}}(\overrightarrow{r}, \overrightarrow{r}') = -\sum_i sign(z - z') \frac{\partial g_i(x,y)}{\partial y} \frac{\partial g_i(x',y')}{\partial y'} \frac{e^{-j\gamma_{TE_i}|z-z'|}}{2} - \\ -\sum_j sign(z - z') \frac{\partial f_j(x,y)}{\partial x} \frac{\partial f_j(x',y')}{\partial x'} \frac{e^{-j\gamma_{TM_j}|z-z'|}}{2}$$

$$G^e_{H_{xy}}(\overrightarrow{r}, \overrightarrow{r}') = -\sum_i sign(z - z') \frac{\partial g_i(x,y)}{\partial y} \frac{\partial g_i(x',y')}{\partial y'} \frac{e^{-j\gamma_{TE_i}|z-z'|}}{2} - \\ \sum_j sign(z - z') \frac{\partial f_j(x,y)}{\partial x} \frac{\partial f_j(x',y')}{\partial y'} \frac{e^{-j\gamma_{TM_j}z-z'|}}{2}$$

$$G^e_{H_{xz}}(\overrightarrow{r},\overrightarrow{r}') = -j\sum_i k^2_{C_{TEi}}\frac{\partial g_i(x,y)}{\partial y}g_i(x',y')\frac{e^{-j\gamma_{TE_i}|z-z'|}}{2\gamma_{TE_i}}$$

$$G^e_{H_{yx}}(\overrightarrow{r},\overrightarrow{r}') = \sum_i sign(z-z')\frac{\partial g_i(x,y)}{\partial x}\frac{\partial g_i(x',y')}{\partial y'}\frac{e^{-j\gamma_{TE_i}|z-z'|}}{2} + \\ + \sum_j sign(z-z')\frac{\partial f_j(x,y)}{\partial y}\frac{\partial f_j(x',y')}{\partial x'}\frac{e^{-j\gamma_{TM_j}|z-z'|}}{2}$$

$$G^e_{H_{yy}}(\overrightarrow{r},\overrightarrow{r}') = \sum_i sign(z-z')\frac{\partial g_i(x,y)}{\partial x}\frac{\partial g_i(x',y')}{\partial x'}\frac{e^{-j\gamma_{TE_i}|z-z'|}}{2} + \\ + \sum_j sign(z-z')\frac{\partial f_j(x,y)}{\partial y}\frac{\partial f_j(x',y')}{\partial y'}\frac{e^{-j\gamma_{TM_j}|z-z'|}}{2}$$

$$G^e_{H_{xz}}(\overrightarrow{r},\overrightarrow{r}') = j\sum_i k^2_{C_{TEi}}\frac{\partial g_i(x,y)}{\partial x}g_i(x',y')\frac{e^{-j\gamma_{TE_i}|z-z'|}}{2\gamma_{TE_i}}$$

$$G^e_{H_{zx}}(\overrightarrow{r},\overrightarrow{r}') = -j\sum_i k^2_{C_{TEi}}g_i(x,y)\frac{\partial g_i(x',y')}{\partial y'}\frac{e^{-j\gamma_{TE_i}|z-z'|}}{2\gamma_{TE_i}}$$

$$G^e_{H_{zy}}(\overrightarrow{r},\overrightarrow{r}') = j\sum_i k^2_{C_{TEi}}g_i(x,y)\frac{\partial g_i(x',y')}{\partial x'}\frac{e^{-j\gamma_{TE_i}|z-z'|}}{2\gamma_{TE_i}}$$

$$G^e_{H_{zz}}(\overrightarrow{r},\overrightarrow{r}') = 0$$

Equation (B.33) determines the magnetic dyadic Green function generated by electric current inside an infinite ridged waveguide.

B.2.2 Green Function for the electric scalar potential

As already mentioned in Chapter.2, the electric scalar potential Φ may be expressed in terms of a scalar Green function G_Φ via equation:

$$\Phi(\overrightarrow{r}) = \varepsilon\iint\limits_{\substack{scatterer\\surface}} G_\Phi(\overrightarrow{r},\overrightarrow{r}')\rho(\overrightarrow{r}')ds'$$

Since the electric scalar potential satisfies the equation $\nabla^2\Phi + k_o^2\,\Phi = -\rho$, the corresponding function $G_\Phi(\overrightarrow{r},\overrightarrow{r}')$ should also satisfy a similar equation:

$$\nabla^2 G_\Phi(\overrightarrow{r},\overrightarrow{r}') + k_o^2\,G_\Phi(\overrightarrow{r},\overrightarrow{r}') = -\delta(\overrightarrow{r}-\overrightarrow{r}') \qquad (B.34)$$

The derivation of G_Φ is also performed according to the Ohm-Rayleigh method. The appropriate eigenvector set for the expansion of G_Φ may be found if the Lorenz gauge $\nabla\cdot\overrightarrow{A} = j\omega\varepsilon\Phi$ is taken into account. From this condition it becomes evident that Φ constitutes the non-solenoidal part of the magnetic vector potential. Therefore the suitable vector set is:

$$\nabla\cdot\left(\frac{\overrightarrow{L}_{TMi}(\overrightarrow{r},h)}{k^2_{Ci}+h^2}\right) = \nabla\cdot\left(\frac{\nabla(f_i(x,y)e^{jhz})}{k^2_{Ci}+h^2}\right) = f_i(x,y)e^{jhz}$$

Orthogonality conditions:

$$\iiint_{\substack{waveguide\\volume}} f_i(x,y)e^{jhz} f_s(x,y)e^{-jh'z}dxdydz = 2\pi\delta_{t,s}\frac{\delta(h-h')}{k_{Ct}^2} \qquad (B.35)$$

Expansion of term $\delta(\overrightarrow{\mathbf{r}}-\overrightarrow{\mathbf{r}}')$:

$$\delta(\overrightarrow{r}-\overrightarrow{r}') = \int_{-\infty}^{\infty} dh \sum_i [A_i(h)f_i(x,y)e^{jhz}] \qquad (B.36)$$

The unknown coefficient $A_i(h)$ is determined by enforcement of condition (B.36) on the former equation:

$$A_i(h) = \frac{k_{C_i}^2}{2\pi} f_i(x',y')e^{-jhz'}$$

Equation (B.36) becomes:

$$\begin{aligned}&\delta(\overrightarrow{r}-\overrightarrow{r}') = \int_{-\infty}^{\infty} dh \sum_i [\tfrac{k_{Ci}^2}{2\pi} f_i(x',y')e^{-jhz'} f_i(x,y)e^{jhz}] \Rightarrow\\ &\delta(x-x')\delta(y-y') = \sum_i [k_{Ci}^2 f_i(x',y')f_i(x,y)]\end{aligned}$$

which is in total agreement with expression (3.59).
The unknown Green function is expanded in the following manner:

$$G_\Phi(\overrightarrow{r},\overrightarrow{r}') = \int_{-\infty}^{\infty} dh \sum_i [a(h)\frac{k_{C_i}^2}{2\pi} f_i(x',y')e^{-jhz'} f_i(x,y)e^{jhz}] \qquad (B.37)$$

Substitution of (B.36) into (B.34) yields the value of the unknown coefficient $a(h)$:

$$a(h) = \frac{1}{k_{C_i}^2 + h^2 - k_o^2}$$

In view of the preceding expression, equation (B.37) becomes:

$$G_\Phi(\overrightarrow{r},\overrightarrow{r}') = \int_{-\infty}^{\infty} dh \sum_i [\frac{1}{k_{C_i}^2 + h^2 - k_o^2}\frac{k_{C_i}^2}{2\pi} f_i(x',y')e^{-jhz'} f_i(x,y)e^{jhz}]$$

The integrand may be evaluated by the method of contour integration. The result is:

$$G_\Phi(\overrightarrow{r},\overrightarrow{r}') = -j\sum_i [\frac{k_{C_i}^2}{2\gamma_{TM_i}} f_i(x,y)f_i(x',y')e^{-jh|z-z'|}] \qquad (B.38)$$

Appendix C

Coordinate systems

C.1 Electric current - Cylindrical coordinate system

Each dyadic Green function for the electric current has the following elements:

$$\overline{\overline{G}} = G_{tt}\,\overrightarrow{t}\,\overrightarrow{t}' + G_{t\varphi}\,\overrightarrow{t}\,\overrightarrow{\varphi}' + G_{\rho t}\,\overrightarrow{\rho}\,\overrightarrow{t}' + G_{\rho\varphi}\,\overrightarrow{\rho}\,\overrightarrow{\varphi}' + G_{\varphi t}\,\overrightarrow{\varphi}\,\overrightarrow{t}' + G_{\varphi\varphi}\,\overrightarrow{\varphi}\,\overrightarrow{\varphi}' \qquad (C.1)$$

where: $\overline{\overline{G}} = \overline{\overline{G}}^{e}_{E}, \overline{\overline{G}}^{e}_{H}$ or $\overline{\overline{G}}_{\mathrm{A}}$.

Expression (C.1) is valid since the post current has $t-$ and $\varphi-$ components. The elements of the above Green functions are determined with the aid of expressions (3.41) or (B.33):

- Magnetic vector potential:

$$G_{A_{t\varphi}}\,\overrightarrow{t}\,\overrightarrow{\varphi}' = G_{A_{yx}}\cos(\varphi')\,\overrightarrow{y}\,\overrightarrow{x}' \qquad (C.2a)$$

$$G_{A_{\varphi t}}\,\overrightarrow{\varphi}\,\overrightarrow{t}' = G_{A_{xy}}\cos\varphi\,\overrightarrow{x}\,\overrightarrow{y}' \qquad (C.2b)$$

$$G_{A_{\rho t}}\,\overrightarrow{\rho}\,\overrightarrow{t}' = G_{A_{xy}}\sin\varphi\,\overrightarrow{x}\,\overrightarrow{y}' \qquad (C.2c)$$

$$G_{A_{\rho\varphi}}\,\overrightarrow{\rho}\,\overrightarrow{\varphi}' = G_{A_{xx}}\sin\varphi\cos(\varphi')\,\overrightarrow{x}\,\overrightarrow{x}' - G_{A_{zz}}\cos\varphi\sin(\varphi')\,\overrightarrow{z}\,\overrightarrow{z}' \qquad (C.2d)$$

$$G_{A_{\varphi\varphi}}\,\overrightarrow{\varphi}\,\overrightarrow{\varphi}' = G_{A_{xx}}\cos\varphi\cos(\varphi')\,\overrightarrow{x}\,\overrightarrow{x}' + G_{A_{zz}}\sin\varphi\sin(\varphi')\,\overrightarrow{z}\,\overrightarrow{z}' \qquad (C.2e)$$

- Electric field

$$G^e_{E_{t\varphi}}\,\overrightarrow{t}\,\overrightarrow{\varphi}' = G^e_{E_{yx}}\cos(\varphi')\,\overrightarrow{y}\,\overrightarrow{x}' - G^e_{E_{yz}}\sin(\varphi')\,\overrightarrow{y}\,\overrightarrow{z}' \tag{C.3a}$$

$$G^e_{M_{\rho t}}\,\overrightarrow{\rho}\,\overrightarrow{t}' = G^e_{E_{xy}}\sin\varphi\,\overrightarrow{x}\,\overrightarrow{y}' + G^e_{E_{zy}}\cos\varphi\,\overrightarrow{z}\,\overrightarrow{y}' \tag{C.3b}$$

$$G^e_{M_{\varphi t}}\,\overrightarrow{\varphi}\,\overrightarrow{t}' = G^e_{E_{xy}}\cos\varphi\,\overrightarrow{x}\,\overrightarrow{y}' - G^e_{E_{zy}}\sin\varphi\,\overrightarrow{z}\,\overrightarrow{y}' \tag{C.3c}$$

$$\begin{aligned} G^e_{M_{\varphi\varphi}}\,\overrightarrow{\varphi}\,\overrightarrow{\varphi}' = {} & G^e_{E_{xx}}\cos\varphi\cos(\varphi')\,\overrightarrow{x}\,\overrightarrow{x}' + G^e_{E_{zz}}\sin\varphi\sin(\varphi')\,\overrightarrow{z}\,\overrightarrow{z}' - \\ & - G^e_{E_{xz}}\cos\varphi\sin(\varphi')\,\overrightarrow{x}\,\overrightarrow{z}' - G^e_{E_{zx}}\sin\varphi\cos(\varphi')\,\overrightarrow{z}\,\overrightarrow{x}' \end{aligned} \tag{C.3d}$$

$$\begin{aligned} G^e_{M_{\rho\varphi}}\,\overrightarrow{\varphi}\,\overrightarrow{\varphi}' = {} & G^e_{E_{xx}}\sin\varphi\cos(\varphi')\,\overrightarrow{x}\,\overrightarrow{x}' - G^e_{E_{zz}}\cos\varphi\sin(\varphi')\,\overrightarrow{z}\,\overrightarrow{z}' - \\ & - G^e_{E_{xz}}\sin\varphi\sin(\varphi')\,\overrightarrow{x}\,\overrightarrow{z}' + G^e_{E_{zx}}\cos\varphi\cos(\varphi')\,\overrightarrow{z}\,\overrightarrow{x}' \end{aligned} \tag{C.3e}$$

In the preceding expressions, the coordinates of the source points (R', t', φ') have been incorporated. The equations that involve the magnetic vector potential employ the operands $\nabla\nabla\cdot$ and $\nabla\times$.For the cylindrical coordinates the operands are analysed in the following manner:

$$\begin{aligned} \nabla\nabla\cdot\overrightarrow{B} = {} & \overrightarrow{\rho}\{\tfrac{\partial}{\partial\rho}[\tfrac{\partial B_\rho}{\partial\rho} + \tfrac{1}{\rho}B_\rho] + \tfrac{\partial}{\partial\rho}(\tfrac{1}{\rho}\tfrac{\partial B_\varphi}{\partial\varphi}) + \tfrac{\partial}{\partial\rho}(\tfrac{\partial B_t}{\partial t})\} + \\ & + \overrightarrow{\varphi}\tfrac{1}{\rho}(\tfrac{\partial^2 B_\rho}{\partial\varphi\partial\rho} + \tfrac{1}{\rho}\tfrac{\partial B_\rho}{\partial\varphi} + \tfrac{1}{\rho}\tfrac{\partial^2 B_\varphi}{\partial\varphi^2} + \tfrac{\partial^2 B_t}{\partial\varphi\partial t}) + \\ & + \overrightarrow{t}(\tfrac{\partial^2 B_\rho}{\partial t\partial\rho} + \tfrac{1}{\rho}\tfrac{\partial B_\rho}{\partial t} + \tfrac{1}{\rho}\tfrac{\partial^2 B_\varphi}{\partial t\partial\varphi} + \tfrac{\partial^2 B_t}{\partial t^2}) \end{aligned}$$

$$\nabla\times\overrightarrow{B} = \overrightarrow{\rho}(\tfrac{1}{\rho}\tfrac{\partial B_t}{\partial\varphi} - \tfrac{\partial B_\varphi}{\partial t}) + \overrightarrow{\varphi}(\tfrac{\partial B_\rho}{\partial t} - \tfrac{\partial B_t}{\partial\rho}) + \overrightarrow{t}\,\tfrac{1}{\rho}[\tfrac{\partial B_\rho}{\partial\varphi} - \tfrac{\partial(\rho B_\varphi)}{\partial\rho}]$$

As already mentioned, particular attention must be paid to the sequence of differentiation and integration, since the interchange is not permitted when the observation and the source points lie close to one another. The relevant formulations are listed below:

$$\begin{aligned} E_{p_{s_t}}(\overrightarrow{r}) = {} & -j\omega\mu R_p \int\limits_{\substack{scatter\\surface}}\int [G_{A_{tt}}(\overrightarrow{r},\overrightarrow{r_p}')J_t(\overrightarrow{r_p}') + G_{A_{t\varphi}}(\overrightarrow{r},\overrightarrow{r_p}')J_\varphi(\overrightarrow{r_p}')]dt'_p d\varphi'_p + \\ & + \tfrac{1}{j\omega\varepsilon}\{\tfrac{\partial^2}{\partial t^2}\int\limits_{\substack{scatter\\surface}}\int [G_{A_{tt}}(\overrightarrow{r},\overrightarrow{r_p}')J_t(\overrightarrow{r_p}') + G_{A_{t\varphi}}(\overrightarrow{r},\overrightarrow{r_p}')J_\varphi(\overrightarrow{r_p}')]dt'_p d\varphi'_p + \\ & + \tfrac{1}{\rho}\tfrac{\partial^2}{\partial t\partial\rho}\int\limits_{\substack{scatter\\surface}}\int \rho[G_{A_{\rho t}}(\overrightarrow{r},\overrightarrow{r_p}')J_t(\overrightarrow{r_p}') + G_{A_{\rho\varphi}}(\overrightarrow{r},\overrightarrow{r_p}')J_\varphi(\overrightarrow{r_p}')]dt'_p d\varphi'_p + \\ & + \tfrac{1}{\rho}\tfrac{\partial^2}{\partial t\partial\varphi}\int\limits_{\substack{scatter\\surface}}\int [G_{A_{\varphi t}}(\overrightarrow{r},\overrightarrow{r_p}')J_t(\overrightarrow{r_p}') + G_{A_{\varphi\varphi}}(\overrightarrow{r},\overrightarrow{r_p}')J_\varphi(\overrightarrow{r_p}')]dt'_p d\varphi'_p\} + \end{aligned} \tag{C.4a}$$

$$\begin{aligned} E_{p_{s_\varphi}}(\overrightarrow{r}) = {} & -j\omega\mu R_p \int\limits_{\substack{scatter\\surface}}\int [G_{A_{\varphi t}}(\overrightarrow{r},\overrightarrow{r_p}')J_t(\overrightarrow{r_p}') + G_{A_{\varphi\varphi}}(\overrightarrow{r},\overrightarrow{r_p}')J_\varphi(\overrightarrow{r_p}')]dt'_p d\varphi'_p + \\ & + \tfrac{R_p}{j\omega\varepsilon}\tfrac{1}{\rho}\{\tfrac{1}{\rho}\tfrac{\partial^2}{\partial\varphi^2}\int\limits_{\substack{scatter\\surface}}\int [G_{A_{\varphi t}}(\overrightarrow{r},\overrightarrow{r_p}')J_t(\overrightarrow{r_p}') + G_{A_{\varphi\varphi}}(\overrightarrow{r},\overrightarrow{r_p}')J_\varphi(\overrightarrow{r_p}')]dt'_p d\varphi'_p + \\ & + \tfrac{1}{\rho}\tfrac{\partial^2}{\partial\varphi\partial\rho}\int\limits_{\substack{scatter\\surface}}\int \rho[G_{A_{\rho t}}(\overrightarrow{r},\overrightarrow{r_p}')J_t(\overrightarrow{r_p}') + G_{A_{\rho\varphi}}(\overrightarrow{r},\overrightarrow{r_p}')J_\varphi(\overrightarrow{r_p}')]dt'_p d\varphi'_p + \\ & + \tfrac{\partial^2}{\partial\varphi\partial t}\int\limits_{\substack{scatter\\surface}}\int [G_{A_{tt}}(\overrightarrow{r},\overrightarrow{r_p}')J_t(\overrightarrow{r_p}') + G_{A_{t\varphi}}(\overrightarrow{r},\overrightarrow{r_p}')J_\varphi(\overrightarrow{r_p}')]dt'_p d\varphi'_p\} \end{aligned} \tag{C.4b}$$

$$E_{p_{s_\rho}}(\overrightarrow{r}) = -j\omega\mu R_p \int\limits_{\substack{scatter\\surface}}\int [G_{A_{\rho t}}(\overrightarrow{r},\overrightarrow{r_p}')J_t(\overrightarrow{r_p}') + G_{A_{\rho\varphi}}(\overrightarrow{r},\overrightarrow{r_p}')J_\varphi(\overrightarrow{r_p}')]dt_p'd\varphi_p' -$$
$$-\frac{jR_p}{\omega\varepsilon}\{\frac{1}{\rho}\frac{\partial^2}{\partial\varphi\partial\rho}\int\limits_{\substack{scatter\\surface}}\int [G_{A_{\varphi t}}(\overrightarrow{r},\overrightarrow{r_p}')J_t(\overrightarrow{r_p}') + G_{A_{\varphi\varphi}}(\overrightarrow{r},\overrightarrow{r_p}')J_\varphi(\overrightarrow{r_p}')]R_p dt_p'd\varphi_p' +$$
$$+\frac{\partial}{\partial\rho}\{\frac{1}{\rho}\frac{\partial}{\partial\rho}\int\limits_{\substack{scatter\\surface}}\int \rho[G_{A_{\rho t}}(\overrightarrow{r},\overrightarrow{r_p}')J_t(\overrightarrow{r_p}') + G_{A_{\rho\varphi}}(\overrightarrow{r},\overrightarrow{r_p}')J_\varphi(\overrightarrow{r_p}')]R_p dt_p'd\varphi_p'\} +$$
$$+\frac{\partial^2}{\partial\rho\partial t}\int\limits_{\substack{scatter\\surface}}\int [G_{A_{tt}}(\overrightarrow{r},\overrightarrow{r_p}')J_t(\overrightarrow{r_p}') + G_{A_{t\varphi}}(\overrightarrow{r},\overrightarrow{r_p}')J_\varphi(\overrightarrow{r_p}')]R_p dt_p'd\varphi_p'\} \tag{C.4c}$$

$$H_{p_{s_t}}(\overrightarrow{r}) = \frac{1}{\rho}\frac{\partial}{\partial\varphi}\int\limits_{\substack{scatter\\surface}}\int [G_{A_{\rho t}}(\overrightarrow{r},\overrightarrow{r_p}')J_t(\overrightarrow{r_p}') + G_{A_{\rho\varphi}}(\overrightarrow{r},\overrightarrow{r_p}')J_\varphi(\overrightarrow{r_p}')]R_p dt_p'd\varphi_p' -$$
$$-\frac{\partial}{\partial\rho}\int\limits_{\substack{scatter\\surface}}\int [G_{A_{tt}}(\overrightarrow{r},\overrightarrow{r_p}')J_t(\overrightarrow{r_p}') + G_{A_{t\varphi}}(\overrightarrow{r},\overrightarrow{r_p}')J_\varphi(\overrightarrow{r_p}')]R_p dt_p'd\varphi_p' \qquad (C.5a)$$

$$H_{p_{s_\varphi}}(\overrightarrow{r}) = \frac{\partial}{\partial t}\int\limits_{\substack{scatter\\surface}}\int [G_{A_{\rho t}}(\overrightarrow{r},\overrightarrow{r_p}')J_t(\overrightarrow{r_p}') + G_{A_{\rho\varphi}}(\overrightarrow{r},\overrightarrow{r_p}')J_\varphi(\overrightarrow{r_p}')]R_p dt_p'd\varphi_p' -$$
$$-\frac{\partial}{\partial\rho}\int\limits_{\substack{scatter\\surface}}\int [G_{A_{tt}}(\overrightarrow{r},\overrightarrow{r_p}')J_t(\overrightarrow{r_p}') + G_{A_{t\varphi}}(\overrightarrow{r},\overrightarrow{r_p}')J_\varphi(\overrightarrow{r_p}')]R_p dt_p'd\varphi_p' \qquad (C.5b)$$

$$H_{p_{s_\rho}}(\overrightarrow{r}) = \frac{1}{\rho}\frac{\partial}{\partial\varphi}\int\limits_{\substack{scatter\\surface}}\int [G_{A_{tt}}(\overrightarrow{r},\overrightarrow{r_p}')J_t(\overrightarrow{r_p}') + G_{A_{t\varphi}}(\overrightarrow{r},\overrightarrow{r_p}')J_\varphi(\overrightarrow{r_p}')]R_p dt_p'd\varphi_p' -$$
$$-\frac{\partial}{\partial t}\int\limits_{\substack{scatter\\surface}}\int [G_{A_{\varphi t}}(\overrightarrow{r},\overrightarrow{r_p}')J_t(\overrightarrow{r_p}') + G_{A_{\varphi\varphi}}(\overrightarrow{r},\overrightarrow{r_p}')J_\varphi(\overrightarrow{r_p}')]R_p dt_p'd\varphi_p' \qquad (C.5c)$$

The equations for the mixed potential formulation are also adjusted to the cylindrical coordinate system. Combination of the expressions:

$$\overrightarrow{E}_{p_s} = -j\omega\mu\overrightarrow{A} + \nabla\Phi_e$$
$$\nabla\Phi_e = \overrightarrow{\rho}\frac{\partial\Phi_e}{\partial\rho} + \overrightarrow{\varphi}\frac{1}{\rho}\frac{\partial\Phi_e}{\partial\varphi} + \overrightarrow{t}\frac{\partial\Phi_e}{\partial t}$$
$$\nabla\cdot\overrightarrow{J} = \frac{1}{\rho}\frac{\partial J_\varphi}{\partial\varphi} + \frac{\partial J_t}{\partial t}$$

yields the modified equations:

$$E_{p_{s_t}}(\overrightarrow{r}) = -j\omega\mu\int\limits_{\substack{scatter\\surface}}\int [G_{A_{tt}}(\overrightarrow{r},\overrightarrow{r_p}')J_t(\overrightarrow{r_p}') + G_{A_{t\varphi}}(\overrightarrow{r},\overrightarrow{r_p}')J_\varphi(\overrightarrow{r_p}')]R_p dt_p'd\varphi_p' +$$
$$+\frac{\partial}{\partial t}\int\limits_{\substack{scatter\\surface}}\int G_{\Phi_e}(\overrightarrow{r},\overrightarrow{r_p}')[\frac{1}{\rho}\frac{\partial J_\varphi(\overrightarrow{r_p}')}{\partial\varphi} + \frac{\partial J_t(\overrightarrow{r_p}')}{\partial t}]R_p dt_p'd\varphi_p' \qquad (C.6a)$$

$$E_{p_{s_\varphi}}(\overrightarrow{r}) = -j\omega\mu\int\limits_{\substack{scatter\\surface}}\int [G_{A_{\varphi t}}(\overrightarrow{r},\overrightarrow{r_p}')J_t(\overrightarrow{r_p}') + G_{A_{\varphi\varphi}}(\overrightarrow{r},\overrightarrow{r_p}')J_\varphi(\overrightarrow{r_p}')]R_p dt_p'd\varphi_p' +$$
$$+\frac{1}{\rho}\frac{\partial}{\partial\varphi}\int\limits_{\substack{scatter\\surface}}\int G_{\Phi_e}(\overrightarrow{r},\overrightarrow{r_p}')[\frac{1}{\rho}\frac{\partial J_\varphi(\overrightarrow{r_p}')}{\partial\varphi} + \frac{\partial J_t(\overrightarrow{r_p}')}{\partial t}]R_p dt_p'd\varphi_p' \qquad (C.6b)$$

$$E_{p_{s_\rho}}(\overrightarrow{r}) = -j\omega\mu\int\limits_{\substack{scatter\\surface}}\int [G_{A_{\rho t}}(\overrightarrow{r},\overrightarrow{r_p}')J_t(\overrightarrow{r_p}') + G_{A_{\rho\varphi}}(\overrightarrow{r},\overrightarrow{r_p}')J_\varphi(\overrightarrow{r_p}')]R_p dt_p'd\varphi_p' +$$
$$+\frac{\partial}{\partial\rho}\int\limits_{\substack{scatter\\surface}}\int G_{\Phi_e}(\overrightarrow{r},\overrightarrow{r_p}')[\frac{1}{\rho}\frac{\partial J_\varphi(\overrightarrow{r_p}')}{\partial\varphi} + \frac{\partial J_t(\overrightarrow{r_p}')}{\partial t}]R_p dt_p'd\varphi_p' \qquad (C.6c)$$

C.2 Electric current - Cartesian coordinate system

The magnetic field produced by the electric current is part of the incident magnetic field on the slot. For this reason it is necessary to express the coordinates of the observation points via the Cartesian system of the cavity, whereas the cylindrical system of the post is employed for the coordinates of the source points.

$$\begin{pmatrix} H_x \\ H_y \\ H_z \end{pmatrix} = \begin{pmatrix} \rho\sin\varphi & \rho\cos\varphi & 0 \\ 0 & 0 & 1 \\ \rho\cos\varphi & -\rho\sin\varphi & 0 \end{pmatrix} \begin{pmatrix} H_\rho \\ H_t \\ H_\varphi \end{pmatrix} \Rightarrow$$

$$\Rightarrow \begin{cases} H_x = \sin\varphi H_\rho + \cos\varphi H_\varphi \\ H_y = H_t \\ H_z = \cos\varphi H_\rho - \sin\varphi H_\varphi \end{cases} \Rightarrow$$

$$\Rightarrow \begin{cases} H_x(\overrightarrow{r}) = \sin\varphi R_p \int\limits_{\substack{scatter \\ surface}} \int [G^e_{H_{\rho t}}(\overrightarrow{r},\overrightarrow{r_p}')J_t(\overrightarrow{r_p}') + G^e_{H_{\rho\varphi}}(\overrightarrow{r},\overrightarrow{r_p}')J_\varphi(\overrightarrow{r_p}')]dt_p' d\varphi_p' + \\ \qquad + \cos\varphi R_p \int\limits_{\substack{scatter \\ surface}} \int [G^e_{H_{\varphi t}}(\overrightarrow{r},\overrightarrow{r_p}')J_t(\overrightarrow{r_p}') + G^e_{H_{\varphi\varphi}}(\overrightarrow{r},\overrightarrow{r_p}')J_\varphi(\overrightarrow{r_p}')]dt_p' d\varphi_p' \\ H_y(\overrightarrow{r}) = \int\limits_{\substack{scatter \\ surface}} \int [G^e_{H_{tt}}(\overrightarrow{r},\overrightarrow{r_p}')J_t(\overrightarrow{r_p}') + G^e_{H_{t\varphi}}(\overrightarrow{r},\overrightarrow{r_p}')J_\varphi(\overrightarrow{r_p}')]R_p dt_p' d\varphi_p' \\ H_z(\overrightarrow{r}) = \sin\varphi R_p \int\limits_{\substack{scatter \\ surface}} \int [G^e_{H_{\rho t}}(\overrightarrow{r},\overrightarrow{r_p}')J_t(\overrightarrow{r_p}') + G^e_{H_{\rho\varphi}}(\overrightarrow{r},\overrightarrow{r_p}')J_\varphi(\overrightarrow{r_p}')]dt_p' d\varphi_p' - \\ \qquad - \cos\varphi R_p \int\limits_{\substack{scatter \\ surface}} \int [G^e_{H_{\varphi t}}(\overrightarrow{r},\overrightarrow{r_p}')J_t(\overrightarrow{r_p}') + G^e_{H_{\varphi\varphi}}(\overrightarrow{r},\overrightarrow{r_p}')J_\varphi(\overrightarrow{r_p}')]dt_p' d\varphi_p' \end{cases} \Rightarrow$$

$$\Rightarrow \begin{cases} H_x(\overrightarrow{r}) = R_p \int\limits_{\substack{scatter \\ surface}} \int [\sin\varphi G^e_{H_{\rho\varphi}}(\overrightarrow{r},\overrightarrow{r_p}')J_\varphi(\overrightarrow{r_p}') + \cos\varphi G^e_{H_{\varphi\varphi}}(\overrightarrow{r},\overrightarrow{r_p}')J_\varphi(\overrightarrow{r_p}')]dt_p' d\varphi_p' + \\ \qquad + R_p \int\limits_{\substack{scatter \\ surface}} \int G^e_{H_{xy}}(\overrightarrow{r},\overrightarrow{r_p}')J_t(\overrightarrow{r_p}')dt_p' d\varphi_p' \\ H_y(\overrightarrow{r}) = \int\limits_{\substack{scatter \\ surface}} \int [G^e_{H_{yy}}(\overrightarrow{r},\overrightarrow{r_p}')J_t(\overrightarrow{r_p}') + G^e_{H_{t\varphi}}(\overrightarrow{r},\overrightarrow{r_p}')J_\varphi(\overrightarrow{r_p}')]R_p dt_p' d\varphi_p' \\ H_z(\overrightarrow{r}) = R_p \int\limits_{\substack{scatter \\ surface}} \int [\cos\varphi G^e_{H_{\rho\varphi}}(\overrightarrow{r},\overrightarrow{r_p}')J_\varphi(\overrightarrow{r_p}') - \sin\varphi G^e_{H_{\varphi\varphi}}(\overrightarrow{r},\overrightarrow{r_p}')J_\varphi(\overrightarrow{r_p}')]dt_p' d\varphi_p' + \\ \qquad + R_p \int\limits_{\substack{scatter \\ surface}} \int G^e_{H_{zy}}(\overrightarrow{r},\overrightarrow{r_p}')J_t(\overrightarrow{r_p}')dt_p' d\varphi_p' \end{cases} \Rightarrow$$

$$\Rightarrow \begin{cases} H_x(\overrightarrow{r}) = R_p \int\limits_{\substack{scatter \\ surface}} \int [G^e_{H_{xx}}(\overrightarrow{r},\overrightarrow{r_p}')\cos(\varphi') - G^e_{H_{xz}}(\overrightarrow{r},\overrightarrow{r_p}')\sin(\varphi')]J_\varphi(\overrightarrow{r_p}')dt_p' d\varphi_p' + \\ \qquad + R_p \int\limits_{\substack{scatter \\ surface}} \int G^e_{H_{xy}}(\overrightarrow{r},\overrightarrow{r_p}')J_t(\overrightarrow{r_p}')dt_p' d\varphi_p' \\ H_y(\overrightarrow{r}) = R_p \int\limits_{\substack{scatter \\ surface}} \int G^e_{H_{yy}}(\overrightarrow{r},\overrightarrow{r_p}')J_t(\overrightarrow{r_p}')dt_p' d\varphi_p' + \\ \qquad + R_p \int\limits_{\substack{scatter \\ surface}} \int [G^e_{H_{yx}}(\overrightarrow{r},\overrightarrow{r_p}')\cos(\varphi') - G^e_{H_{yz}}(\overrightarrow{r},\overrightarrow{r_p}')\sin(\varphi')]J_\varphi(\overrightarrow{r_p}')dt_p' d\varphi_p' \\ H_z(\overrightarrow{r}) = R_p \int\limits_{\substack{scatter \\ surface}} \int [G^e_{H_{zx}}(\overrightarrow{r},\overrightarrow{r_p}')\cos(\varphi') + G^e_{H_{zy}}(\overrightarrow{r},\overrightarrow{r_p}')\sin(\varphi')]J_\varphi(\overrightarrow{r_p}')dt_p' d\varphi_p' \end{cases} \quad (C.8)$$

C.3 Magnetic current - Cylindrical coordinate system

The fields generated by the magnetic current of the slot influence the electric current on the post. Therefore, the Cartesian coordinate system of the cavity is employed for the source points, whereas the coordinates of the observation points are expressed in the cylindrical system of the post. Recognizing that the magnetic current has only a z-component, the electric field is obtained by the combination of (3.9) and (3.50):

$$\overrightarrow{E}_{s_s} = -\nabla \times \overrightarrow{F} \Rightarrow \overrightarrow{E}_{s_s} = -\nabla \times (F_z \overrightarrow{z}) \Rightarrow \overrightarrow{E}_{s_s} = -\overrightarrow{x}\frac{\partial F_z}{\partial y} + \overrightarrow{y}\frac{\partial F_z}{\partial x} \Rightarrow$$

$$\Rightarrow \overrightarrow{E}_{s_s} = -\overrightarrow{\rho}\sin\varphi\frac{\partial F_z}{\partial y} - \overrightarrow{\varphi}\cos\varphi\frac{\partial F_z}{\partial y} + \overrightarrow{y}\frac{\partial F_z}{\partial x} \Rightarrow$$

$$\Rightarrow \begin{cases} E_{s_{s_\rho}}(\overrightarrow{r}) = -\sin\varphi\frac{\partial}{\partial y}\underset{Slot1}{\int\int} G_{F_{zz}}(\overrightarrow{r},\overrightarrow{r_{s1}}')M1(\overrightarrow{r_{s1}}')dx'_{s1}dz'_{s1} \\ E_{s_{s_\varphi}}(\overrightarrow{r}) = -\cos\varphi\frac{\partial}{\partial y}\underset{Slot1}{\int\int} G_{F_{zz}}(\overrightarrow{r},\overrightarrow{r_{s1}}')M1(\overrightarrow{r_{s1}}')dx'_{s1}dz'_{s1} \\ E_{s_{s_t}}(\overrightarrow{r}) = \frac{\partial}{\partial x}\underset{Slot1}{\int\int} G_{F_{zz}}(\overrightarrow{r},\overrightarrow{r_{s1}}')M1(\overrightarrow{r_{s1}}')dx'_{s1}dz'_{s1} \end{cases}$$

The variables $x'_{s1}, y'_{s1}, z'_{s1}$ represent the coordinates of the magnetic current points.
The expression for the magnetic field $\overrightarrow{H}_{s_s}$ is:

$$\overrightarrow{H}_{s_s} = -j\omega\varepsilon[\overrightarrow{x}\frac{1}{k_o^2}\frac{\partial^2 F_z}{\partial x\partial z} + \overrightarrow{y}\frac{1}{k_o^2}\frac{\partial^2 F_z}{\partial y\partial z} + \overrightarrow{z}(F_z + \frac{1}{k_o^2}\frac{\partial^2 F_z}{\partial z^2})] \Rightarrow$$

$$\Rightarrow \overrightarrow{H}_{s_s} = -j\omega\varepsilon\{\overrightarrow{\rho}[\tfrac{1}{k_o^2}\tfrac{\partial^2 F_z}{\partial x\partial z}\sin\varphi + (F_z + \tfrac{1}{k_o^2}\tfrac{\partial^2 F_z}{\partial z^2})\cos\varphi] + \overrightarrow{t}\tfrac{1}{k_o^2}\tfrac{\partial^2 F_z}{\partial y\partial z} +$$
$$+\overrightarrow{\varphi}[\tfrac{1}{k_o^2}\tfrac{\partial^2 F_z}{\partial x\partial z}\cos\varphi - (F_z + \tfrac{1}{k_o^2}\tfrac{\partial^2 F_z}{\partial z^2})\sin\varphi]\} \Rightarrow$$

$$\Rightarrow \begin{cases} H_{s_{s_\rho}}(\overrightarrow{r}) = -j\omega\varepsilon[\underset{Slot1}{\int\int} G_{F_{zz}}(\overrightarrow{r},\overrightarrow{r_{s1}}')M1(\overrightarrow{r_{s1}}')dx'_{s1}dz'_{s1} + \\ \qquad +\frac{1}{k_o^2}\sin\varphi\frac{\partial^2}{\partial x\partial z}\underset{Slot1}{\int\int} G_{F_{zz}}(\overrightarrow{r},\overrightarrow{r_{s1}}')M1(\overrightarrow{r_{s1}}')dx'_{s1}dz'_{s1} + \\ \qquad +\frac{1}{k_o^2}\cos\varphi\frac{\partial^2}{\partial z^2}\underset{Slot1}{\int\int} G_{F_{zz}}(\overrightarrow{r},\overrightarrow{r_{s1}}')M1(\overrightarrow{r_{s1}}')dx'_{s1}dz'_{s1}] \\ H_{s_{s_t}}(\overrightarrow{r}) = (\overrightarrow{r}) = -\frac{j\omega\varepsilon}{k_o^2}\frac{\partial^2}{\partial y\partial z}\underset{Slot1}{\int\int} G_{F_{zz}}(\overrightarrow{r},\overrightarrow{r_{s1}}')M1(\overrightarrow{r_{s1}}')dx'_{s1}dz'_{s1} \\ H_{s_{s_\varphi}}(\overrightarrow{r}) = -j\omega\varepsilon[-\underset{Slot1}{\int\int} G_{F_{zz}}(\overrightarrow{r},\overrightarrow{r_{s1}}')M1(\overrightarrow{r_{s1}}')dx'_{s1}dz'_{s1} + \\ \qquad +\frac{1}{k_o^2}\cos\varphi\frac{\partial^2}{\partial x\partial z}\underset{Slot1}{\int\int} G_{F_{zz}}(\overrightarrow{r},\overrightarrow{r_{s1}}')M1(\overrightarrow{r_{s1}}')dx'_{s1}dz'_{s1} - \\ \qquad -\frac{1}{k_o^2}\sin\varphi\frac{\partial^2}{\partial z^2}\underset{Slot1}{\int\int} G_{F_{zz}}(\overrightarrow{r},\overrightarrow{r_{s1}}')M1(\overrightarrow{r_{s1}}')dx'_{s1}dz'_{s1}] \end{cases} \quad (C.9)$$

Equations (C.9) in association with expression (3.47) indicate that the slot couples only to the TE modes of the ridged waveguide, since only the zz component of $\overline{\overline{G}}_F$ is involved. The expressions that involve the magnetic vector potential are derived directly by equations (C.5) and (3.50):

$$
\Rightarrow \begin{cases}
H_{s_{s_x}} = R_p \frac{\partial}{\partial y}\{\cos\varphi[\int\limits_{\substack{scatter\\surface}}\int [G_{A_{\rho t}}(\overrightarrow{r},\overrightarrow{r_p}')J_t(\overrightarrow{r_p}') + G_{A_{\rho\varphi}}(\overrightarrow{r},\overrightarrow{r_p}')J_\varphi(\overrightarrow{r_p}')]dt_p' d\varphi_p' - \\
\quad -\sin\varphi \int\limits_{\substack{scatter\\surface}}\int [G_{A_{\varphi t}}(\overrightarrow{r},\overrightarrow{r_p}')J_t(\overrightarrow{r_p}') + G_{A_{\varphi\varphi}}(\overrightarrow{r},\overrightarrow{r_p}')J_\varphi(\overrightarrow{r_p}')]dt_p' d\varphi_p'\} - \\
\quad -\frac{\partial}{\partial z}\int\limits_{\substack{scatter\\surface}}\int [G_{A_{tt}}(\overrightarrow{r},\overrightarrow{r_p}')J_t(\overrightarrow{r_p}') + G_{A_{t\varphi}}(\overrightarrow{r},\overrightarrow{r_p}')J_\varphi(\overrightarrow{r_p}')]R_p dt_p' d\varphi_p' \\
H_{s_{s_y}} = \frac{R_p}{\rho}\{\frac{\partial}{\partial\varphi}\int\limits_{\substack{scatter\\surface}}\int [G_{A_{\rho t}}(\overrightarrow{r},\overrightarrow{r_p}')J_t(\overrightarrow{r_p}') + G_{A_{\rho\varphi}}(\overrightarrow{r},\overrightarrow{r_p}')J_\varphi(\overrightarrow{r_p}')]dt_p' d\varphi_p' - \\
\quad -R_p\frac{\partial}{\partial\rho}\int\limits_{\substack{scatter\\surface}}\int [G_{A_{tt}}(\overrightarrow{r},\overrightarrow{r_p}')J_t(\overrightarrow{r_p}') + G_{A_{t\varphi}}(\overrightarrow{r},\overrightarrow{r_p}')J_\varphi(\overrightarrow{r_p}')]R_p dt_p' d\varphi_p' \\
H_{s_{s_z}} = -R_p\frac{\partial}{\partial y}\{\sin\varphi\int\limits_{\substack{scatter\\surface}}\int [G_{A_{\rho t}}(\overrightarrow{r},\overrightarrow{r_p}')J_t(\overrightarrow{r_p}') + G_{A_{\rho\varphi}}(\overrightarrow{r},\overrightarrow{r_p}')J_\varphi(\overrightarrow{r_p}')]dt_p' d\varphi_p' + \\
\quad +\cos\varphi\int\limits_{\substack{scatter\\surface}}\int [G_{A_{\varphi t}}(\overrightarrow{r},\overrightarrow{r_p}')J_t(\overrightarrow{r_p}') + G_{A_{\varphi\varphi}}(\overrightarrow{r},\overrightarrow{r_p}')J_\varphi(\overrightarrow{r_p}')]dt_p' d\varphi_p'\} + \\
\quad +\frac{\partial}{\partial x}\int\limits_{\substack{scatter\\surface}}\int [G_{A_{tt}}(\overrightarrow{r},\overrightarrow{r_p}')J_t(\overrightarrow{r_p}') + G_{A_{t\varphi}}(\overrightarrow{r},\overrightarrow{r_p}')J_\varphi(\overrightarrow{r_p}')]R_p dt_p' d\varphi_p'
\end{cases} \qquad (C.10)
$$

C.4 Magnetic current - Cartesian coordinate system for the cavity

The fields produced by the magnetic currents inside the rectangular cavity are expressed in the corresponding Cartesian coordinate system and are obtained by equation (B.27):

$$H_{cn_z} = -j\omega\varepsilon \int\limits_{Slot1}\int G^m_{H_{zz}}(\overrightarrow{r},\overrightarrow{r}'_{sn})M_n(\overrightarrow{r_{sn}}')dx'_{sn}dz'_{sn} \qquad (C.11a)$$

$$H_{cn_x} = -j\omega\varepsilon \int\limits_{Slot1}\int G^m_{H_{xz}}(\overrightarrow{r},\overrightarrow{r}'_{sn})M_n(\overrightarrow{r_{sn}}')dx'_{sn}dz'_{sn} \qquad (C.11b)$$

$$H_{cn_y} = -j\omega\varepsilon \int\limits_{Slot1}\int G^m_{H_{yz}}(\overrightarrow{r},\overrightarrow{r}'_{sn})M_n(\overrightarrow{r_{sn}}')dx'_{sn}dz'_{sn} \qquad (C.11c)$$

where: $n = \begin{cases} 1, \text{ for upper slot aperture} \\ 2, \text{ for lower slot aperture} \end{cases}$

The coordinates of the source points are denoted as $z'_{sn}, x'_{sn}, y'_{sn}$.

C.5 Magnetic current - Rotated Cartesian coordinate system

The dyadic Green function for the magnetic field inside the semi-infinite rectangular waveguide has the following elements:

$$\overline{\overline{G}}^m_{Hsrw} = G^m_{Hsrw_{\zeta\zeta}}\overrightarrow{\zeta}\overrightarrow{\zeta}' + G^m_{Hsrw_{\xi\zeta}}\overrightarrow{\xi}\overrightarrow{\zeta}' + G^m_{Hsrw_{\eta\zeta}}\overrightarrow{\eta}\overrightarrow{\zeta}' \qquad (C.12)$$

Functions $G^m_{Hsrw_{\zeta\zeta}}$ and $G^m_{Hsrw_{\xi\zeta}}$ and are determined via equation (3.54):

$$G^m_{Hsrw_{\zeta\zeta}} = \tfrac{1}{2}G^m_{Hsrw_{zz}}\overrightarrow{z}\overrightarrow{z}' + \tfrac{1}{2}G^m_{Hsrw_{xz}}\overrightarrow{x}\overrightarrow{z}' + \tfrac{1}{2}G^m_{Hsrw_{zx}}\overrightarrow{z}\overrightarrow{x}' + \tfrac{1}{2}G^m_{Hsrw_{xx}}\overrightarrow{x}\overrightarrow{x}' \qquad (C.13a)$$

$$G^m_{Hsrw_{\xi\zeta}} = -\tfrac{1}{2}G^m_{Hsrw_{zz}}\overrightarrow{z}\overrightarrow{z}' - \tfrac{1}{2}G^m_{Hsrw_{xz}}\overrightarrow{x}\overrightarrow{z}' + \tfrac{1}{2}G^m_{Hsrw_{zx}}\overrightarrow{z}\overrightarrow{x}' + \tfrac{1}{2}G^m_{Hsrw_{xx}}\overrightarrow{x}\overrightarrow{x}' \qquad (C.13b)$$

$$G^m_{Hsrw_{\eta\zeta}} = \tfrac{\sqrt{2}}{2}G^m_{Hsrw_{yz}}\overrightarrow{y}\overrightarrow{z}' + \tfrac{\sqrt{2}}{2}G^m_{Hsrw_{yx}}\overrightarrow{y}\overrightarrow{x}' \qquad (C.13c)$$

The magnetic field $\overrightarrow{H}_{srw}$ is:

$$H_{srw_\zeta}(\overrightarrow{r}) = \frac{-j\omega\varepsilon}{2} \int\limits_{Slot2}\int [G^m_{Hsrw_{zz}}(\overrightarrow{r}, \overrightarrow{r}'_{s2}) + G^m_{Hsrw_{xz}}(\overrightarrow{r}, \overrightarrow{r}'_{s2}) + \\ + G^m_{Hsrw_{zx}}(\overrightarrow{r}, \overrightarrow{r}'_{s2}) + G^m_{Hsrw_{xx}}(\overrightarrow{r}, \overrightarrow{r}'_{s2})]M2(\overrightarrow{r_{s2}}')d\zeta'_{s2}d\xi'_{s2} \qquad (C.14a)$$

$$H_{srw_\xi}(\overrightarrow{r}) = \frac{-j\omega\varepsilon}{2} \int\limits_{Slot2}\int [-G^m_{Hsrw_{zz}}(\overrightarrow{r}, \overrightarrow{r}'_{s2}) - G^m_{Hsrw_{xz}}(\overrightarrow{r}, \overrightarrow{r}'_{s2}) + \\ + G^m_{Hsrw_{zx}}(\overrightarrow{r}, \overrightarrow{r}'_{s2}) + G^m_{Hsrw_{xx}}(\overrightarrow{r}, \overrightarrow{r_{s2}}')]M2(\overrightarrow{r}'_{s2})d\zeta'_{s2}d\xi'_{s2} \qquad (C.14b)$$

$$H_{srw_\eta}(\overrightarrow{r}) = \frac{-j\omega\varepsilon\sqrt{2}}{2} \int\limits_{Slot2}\int [G^m_{Hsrw_{yx}}(\overrightarrow{r}, \overrightarrow{r}'_{s2}) + G^m_{Hsrw_{yz}}(\overrightarrow{r}, \overrightarrow{r_{s2}}')]M2(\overrightarrow{r}'_{s2})d\zeta'_{s2}d\xi'_{s2} \qquad (C.14c)$$

The variables $\zeta'_{s2}, \xi'_{s2}, \eta'_{s2}$ represent the coordinates of the source points.
Function $\overline{\overline{G}}^m_{Hsrw}$ is given by expressions (B.25).

Appendix D

Computation of the matrix elements

Equation (4.6) may be rewritten in a more analytical form:

$$\begin{pmatrix} B_1 \\ B_2 \\ B_3 \\ 0 \end{pmatrix} = \begin{pmatrix} GE1 & GE2 & GE3 & 0 \\ GE4 & GE5 & GE6 & 0 \\ GE7 & GE8 & GE9 & GE10 \\ 0 & 0 & GE11 & GE12 \end{pmatrix} \begin{pmatrix} X_1 \\ X_2 \\ X_3 \\ X_4 \end{pmatrix} \qquad (D.1)$$

All matrices are defined below:

Matrix GE1: Impact of the t- directed electric current on the t- scattered electric field (ridged waveguide).

$$GE1 = \begin{pmatrix} GE1_{11} & GE1_{12} & ... & GE1_{1N} \\ GE1_{21} & GE1_{22} & ... & GE1_{2N} \\ . & . & . & . \\ . & . & . & . \\ . & . & . & . \\ GE1_{N1} & GE1_{N2} & ... & GE1_{NN} \end{pmatrix}$$

$GE1_{WS}$ are IxI matrixes defined in the following way:

$$GE1_{WS_{i,j}} = -j\omega\mu R_p^2 (F1_{WS_{ij}} + \frac{1}{k_o^2} F2_{WS_{ij}}) \qquad (D.2)$$

• $F1_{WS}$

$$F1_{WS_{ij}} = \int_0^{h_p} \int_0^{2\pi} e^{-jW\varphi_p} [t_{t_i}(t_p) \int_0^{h_p} \int_0^{2\pi} G_{A_{tt}}(\overrightarrow{r_p}|\overrightarrow{r_p}') e^{jS\varphi'_p} b_{t_j}(t'_p) dt'_p d\varphi'_p] dt_p d\varphi_p \qquad (D.2a)$$

where:

$$G_{A_{tt}}(\overrightarrow{r_p}|\overrightarrow{r_p}') \overset{(2.41)}{=} -j \sum_k^{K_e} \frac{\partial g_k(x_p,y_p)}{\partial x_p} \frac{\partial g_k(x'_p,y'_p)}{\partial x'_p} \frac{e^{-j\gamma_{TE_k}|z_p - z'_p|}}{2\gamma_{TE_k}} - \\ -j \sum_k^{K_m} \frac{\partial f_k(x_p,y_p)}{\partial y_p} \frac{\partial f_k(x'_p,y'_p)}{\partial y'_p} \frac{e^{-j\gamma_{TM_k}|z_p - z'_p|}}{2\gamma_{TM_k}}$$

$$x_p = R_p \sin\varphi_p$$
$$z_p = R_p \cos\varphi_p$$

and

$$g_k(x_p,y_p)=\begin{cases} \sum_{n=0}^{\infty} N_{k1n}\cos[k_{TE_{k1n}}d_p + x_p]\cos(\frac{n\pi}{b}y_p), \text{Odd TE, trough region} \\ \sum_{m=0}^{\infty} N_{k2m}\sin[k_{TE_{k2m}}(\frac{a}{2}-d_p-x_p)]\cos(\frac{m\pi}{d}y_p), \text{Odd TE, gap} \\ \sum_{n=0}^{\infty} N_{k1n}\cos[k_{TE_{k1n}}(d_p+x_p)]\cos(\frac{n\pi}{b}y_p), \text{Even TE, trough region} \\ \sum_{m=0}^{\infty} N_{k2m}\cos[k_{TE_{k2m}}(\frac{a}{2}-d_p-x_p)]\cos(\frac{m\pi}{d}y_p), \text{Even TE, gap} \end{cases}$$

$$f_k(x_p,y_p)=\begin{cases} \sum_{n=1}^{\infty} M_{k1n}\sin[k_{TM_{k1n}}(d_p+x_p]\sin(\frac{n\pi}{b}y_p), \text{Odd TM, trough region} \\ \sum_{m=1}^{\infty} M_{k2m}\cos[k_{TM_{k2m}}(\frac{a}{2}-d_p-x_p)]\sin(\frac{m\pi}{d}y_p), \text{Odd TM, gap} \\ \sum_{n=1}^{\infty} M_{k1n}\sin[k_{TM_{k1n}}(d_p+x_p)]\sin(\frac{n\pi}{b}y_p), \text{Even TM, trough region} \\ \sum_{m=0}^{\infty} M_{k2m}\sin[k_{TM_{k2m}}(\frac{a}{2}-d_p-x_p)]\sin(\frac{m\pi}{d}y_p), \text{Even TM, gap} \end{cases}$$

$$k_{TE_{k1n}} = \begin{cases} -j\sqrt{k_{TE_k}^2-(\frac{n\pi}{b})^2}, k_{TE_k} \geq \frac{n\pi}{b} \\ \sqrt{(\frac{n\pi}{b})^2-k_{TE_k}^2}, k_{TE_k} < \frac{n\pi}{b} \end{cases}$$

$$k_{TE_{k2m}} = \begin{cases} -j\sqrt{k_{TE_k}^2-(\frac{m\pi}{d})^2}, k_{TE_k} \geq \frac{m\pi}{d} \\ \sqrt{(\frac{m\pi}{d})^2-k_{TE_k}^2}, k_{TE_k} < \frac{m\pi}{d} \end{cases}$$

$$k_{TM_{k1n}} = \begin{cases} -j\sqrt{k_{TM_k}^2-(\frac{n\pi}{b})^2}, k_{TM_k} \geq \frac{n\pi}{b} \\ \sqrt{(\frac{n\pi}{b})^2-k_{TM_k}^2}, k_{TM_k} < \frac{n\pi}{b} \end{cases}$$

$$k_{TM_{k2m}} = \begin{cases} -j\sqrt{k_{TM_k}^2-(\frac{m\pi}{d})^2}, k_{TM_k} \geq \frac{m\pi}{d} \\ \sqrt{(\frac{m\pi}{d})^2-k_{TM_k}^2}, k_{TM_k} < \frac{m\pi}{d} \end{cases}$$

k_{TE_k} and k_{TM_k} are the cuttoff frequencies for the k- TE or TM eigenmode respectively.

- $F2_{WS}$

$$F2_{WS_{ij}} = \int_0^{h_p}\int_0^{2\pi} e^{-jW\varphi_p} t_{t_i}(t_p)\frac{\partial}{\partial y_p}\int_0^{h_p}\int_0^{2\pi} e^{jS\varphi_p}\frac{\partial G1(\overrightarrow{r}_p,\overrightarrow{r}'_p)}{\partial y'_p} b_{t_j}(t'_p)d\varphi'_p dt'_p d\varphi_p dt_p \qquad (D.2b)$$

where:

$$G1(\overrightarrow{r}_p,\overrightarrow{r}'_p) = \sum_k^{K_m} jk_{TM_k}^2 f_k(x_p,y_p)f_k(x'_p,y'_p)\frac{e^{-j\gamma_{TM_k}|z_p-z'_p|}}{2\gamma_{TM_k}}$$

Combination of (D.2a) and (D.2b) yields:

$$GE1_{WS_{ij}} = -j\omega\mu R_p^2 \int_0^{h_p}\int_0^{2\pi} e^{-jW\varphi_p} t_{t_i}(t_p) GR1_{S_j}(\overrightarrow{r_p}, \overrightarrow{r_p}')dt_p d\varphi_p \quad (D.3)$$

$$GR1_{S_j}(\overrightarrow{r_p}, \overrightarrow{r_p}') = \int_0^{h_p}\int_0^{2\pi} e^{jS\varphi_p'}[-j\sum_k^{K_e} \frac{\partial g_k(x_p,y_p)}{\partial x_p}\frac{\partial g_k(x_p',y_p')}{\partial x_p'}\frac{e^{-j\gamma_{TE_k}|z_p-z_p'|}}{2\gamma_{TE_k}} - j\sum_k^{K_m}\gamma_{TM_k}\frac{\partial f_k(x_p,y_p)}{\partial y_p}\frac{\partial f_k(x_p',y_p')}{\partial y_p'}\frac{e^{-j\gamma_{TM_k}|z_p-z_p'|}}{2k_0^2}]b_{t_j}(t_p')dt_p'd\varphi_p'$$

Matrix GE2: Impact of the φ- directed electric current on the t- scattered electric field (ridged waveguide).

$$GE2 = \begin{pmatrix} GE2_{11} & GE2_{12} & ... & GE2_{1N} \\ GE2_{21} & GE2_{22} & ... & GE2_{2N} \\ . & . & . & . \\ . & . & . & . \\ . & . & . & . \\ GE2_{N1} & GE2_{N2} & ... & GE2_{NN} \end{pmatrix}$$

$GE2_{WS}$ are IxI matrixes defined in the following way:

$$GE2_{WS_{i,j}} = -j\omega\mu R_p^2(G1_{WS_{ij}} + \frac{1}{R_p k_o^2} G2_{WS_{ij}}) \qquad (D.4)$$

• $G1_{WS}$

$$G1_{WS_{ij}} = \int_0^{h_p}\int_0^{2\pi} e^{-jW\varphi_p} t_{t_i}(t_p)dt_p d\varphi_p \int_0^{h_p}\int_0^{2\pi} G_{A_{t\varphi}}(\overrightarrow{r}_p|\overrightarrow{r}'_p) e^{jS\phi_p'} b_{\phi_j}(t_p')dt_p' d\varphi_p' \qquad (D.4a)$$

where:

$$G_{A_{t\varphi}}(\overrightarrow{r}_p|\overrightarrow{r}'_p) \overset{(C.4)}{=} G_{A_{yx}}(\overrightarrow{r}_p|\overrightarrow{r}'_p)\cos\varphi_p' \overset{(2.41)}{=} [j\sum_k^{K_e}\frac{\partial g_k(x_p,y_p)}{\partial x_p}\frac{\partial g_k(x_p',y_p')}{\partial y_p'}\frac{e^{-j\gamma_{TE_k}|z_p-z_p'|}}{2\gamma_{TE_k}} - j\sum_k^{K_m}\frac{\partial f_k(x_p,y_p)}{\partial y_p}\frac{\partial f_k(x_p',y_p')}{\partial x_p'}\frac{e^{-j\gamma_{TM_k}|z_p-z_p'|}}{2\gamma_{TM_k}}]\cos\varphi_p'$$

• $G2_{WS}$

$$G2_{WS_{ij}} = \int_0^{h_p}\int_0^{2\pi} e^{-jW\varphi_p} t_{t_i}(t_p)\frac{\partial}{\partial y_p}\int_0^{h_p}\int_0^{2\pi}\frac{\partial e^{jS\varphi_p'}}{\partial\varphi_p'} G1(\overrightarrow{r}_p|\overrightarrow{r}'_p) b_{\varphi_j}(t_p')d\varphi_p' dt_p' d\varphi_p dt_p \Rightarrow$$
$$G2_{WS_{ij}} = \int_0^{h_p}\int_0^{2\pi} e^{-jW\varphi_p} t_{t_i}(t_p)\frac{\partial}{\partial y_p}\int_0^{h_p}\int_0^{2\pi} jSe^{jS\varphi_p'} G1(\overrightarrow{r}_p|\overrightarrow{r}'_p) b_{\varphi_j}(t_p')d\varphi_p' dt_p' d\varphi_p dt_p \qquad (D.4b)$$

Combination of (D.4a) and (D.4b) yields:

$$GE2_{WS_{ij}} = -j\omega\mu R_p^2 \int_0^{h_p}\int_0^{2\pi} e^{-jW\varphi_p} t_{t_i}(t_p) GR2_{S_j}(\overrightarrow{r_p},\overrightarrow{r_p}')dt_p d\varphi_p \quad (D.5)$$

$$\begin{aligned} GE2_{S_j}(\overrightarrow{r_p},\overrightarrow{r_p}') = \int_0^{h_p}\int_0^{2\pi} e^{jS\varphi_p'} b_{t_j}(t_p')\{[j\sum_k^{K_e} \frac{\partial g_k(x_p,y_p)}{\partial x_p}\frac{\partial g_k(x_p',y_p')}{\partial y_p'}\frac{e^{-j\gamma_{TE_k}|z_p-z_p'|}}{2\gamma_{TE_k}} - \\ -j\sum_k^{K_m}\frac{\partial f_k(x_p,y_p)}{\partial y_p}\frac{\partial f_k(x_p',y_p')}{\partial x_p'}\frac{e^{-j\gamma_{TM_k}|z_p-z_p'|}}{2\gamma_{TM_k}}]\cos\varphi_p' - \\ -\frac{S}{R_p k_0^2}\sum_k^{K_m} k_{TM_k}^2 f_k(x_p,y_p) f_k(x_p',y_p')\frac{e^{-j\gamma_{TM_k}|z_p-z_p'|}}{2\gamma_{TM_k}}\}dt_p' d\varphi_p' \end{aligned}$$

Matrix GE3: Impact of the magnetic current on the t- scattered electric field (Slot1 - ridged waveguide).

$$GE3 = \begin{pmatrix} GE3_1 \\ GE3_2 \\ . \\ . \\ . \\ GE3_N \end{pmatrix}$$

$GE3_W$ are IxQ matrixes defined in the following way:

$$\begin{aligned} GE3_{W_{iq}} &= \int_0^{h_p}\int_0^{2\pi} e^{-jW\varphi_p}[t_{t_i}(t_p)\frac{\partial}{\partial x_p}\int_{-L}^{L}\int_{\frac{a}{2}-\frac{w}{2}}^{\frac{a}{2}+\frac{w}{2}} G_{F_{zz}}(\overrightarrow{r_p}|\overrightarrow{r_{s1}}')u_q(z_{s1}',x_{s1}')dz_{s1}'dx_{s1}']dt_p d\varphi_p = \\ &= \int_0^{h_p}\int_0^{2\pi} e^{-jW\varphi_p}[t_{t_i}(t_p)\int_{-L}^{L}\int_{\frac{a}{2}-\frac{w}{2}}^{\frac{a}{2}+\frac{w}{2}}\frac{\partial G_{F_{zz}}(\overrightarrow{r_p}|\overrightarrow{r_{s1}}')}{\partial x_p}u_q(z_{s1}',x_{s1}')dz_{s1}'dx_{s1}']dt_p d\varphi_p \end{aligned} \quad (D.6a)$$

where:

$$\frac{dG_{zz}(\overrightarrow{r_p}|\overrightarrow{r_{s1}}')}{\partial x_p} = -j\sum_k^{K_e} k_{TE_k}^2 \frac{\partial g_k(x_p,y_p)}{\partial x_p} g_k(x_{s1}',y_{s1}')\frac{e^{-j\gamma_{TE_k}|z_p-z_{s1}'|}}{2\gamma_{TE_k}}$$

and

$$u_q(z,x) = \sin[\frac{q\pi}{2L}(L+z)]$$

The integral:

$$I = \int_{-L}^{L}\int_{\frac{a}{2}-\frac{w}{2}}^{\frac{a}{2}+\frac{w}{2}}\frac{dG_{zz}(\overrightarrow{r_p}|\overrightarrow{r_{s1}}')}{\partial x_p}u_q(z_{s1}',x_{s1}')dz_{s1}'dx_{s1}'$$

may be expressed as a product of two linear integrals:

$$I = -j\sum_k^{K_e} k_{TE_k}^2 \frac{\partial g_k(x_p,y_p)}{\partial x_p} I_{k1} I_{k2_q}$$

Integrals I_{k1} and I_{k2_q} are defined in the following manner:

$$I_{k1} = \int_{\frac{a}{2}-\frac{w}{2}}^{\frac{a}{2}+\frac{w}{2}} g_k(x'_{s1}, y'_{s1})dx'$$

and

$$I_{k2_q} = \int_{-L}^{L} \frac{e^{-j\gamma_{TE_k}|z_p - z'_{s1}|}}{2\gamma_{TE_k}} \sin[\frac{q\pi}{2L}(L + z'_{s1})]dz'_{s1}$$

Both linear integrals may be evaluated analytically:

$$I_{k1} = \int_{\frac{a}{2}-\frac{w}{2}}^{\frac{a}{2}+\frac{w}{2}} g_k(x'_{s1}, y'_{s1})dx' \Rightarrow$$

$$I_{k1} = \int_{\frac{a}{2}-\frac{w}{2}}^{\frac{a}{2}+\frac{w}{2}} \sum_{m=0}^{M} N_{k2m} \cos[k_{TE_{k2m}}(\frac{a}{2} - x'_{s1})] \cos(\frac{m\pi}{d} y'_{s1})dx' \Rightarrow$$

$$I_{k1} = -\sum_{m=0}^{M} N_{k2m} \left[\frac{\sin[k_{TE_{k2m}}(\frac{a}{2} - x'_{s1})]}{k_{TE_{k2m}}}\right]_{\frac{a}{2}-\frac{w}{2}}^{\frac{a}{2}+\frac{w}{2}} \cos(\frac{m\pi}{d} y'_{s1}) \Rightarrow$$

$$I_{k1} = -\sum_{m=0}^{M} N_{k2m} \left[\frac{\sin(-k_{TE_{k2m}}\frac{w}{2})}{k_{TE_{k2m}}} - \frac{\sin(k_{TE_{k2m}}\frac{w}{2})}{k_{TE_{k2m}}}\right] \cos(\frac{m\pi}{d} y'_{s1}) \Rightarrow$$

$$I_{k1} = \sum_{m=0}^{M} 2N_{k2m} \frac{\sin(k_{TE_{k2m}}\frac{w}{2})}{k_{TE_{k2m}}} \cos(\frac{m\pi}{d} y'_{s1}) \quad (D.6b)$$

Integral I_{k2_q} may be split into two simpler integrals:

$$I_{k2_q} = I_{2a} + I_{2b}$$

where:

$$I_{k2a_q} = \int_{-L}^{z_p} \frac{e^{-j\gamma_{TE_k}(z_p - z'_{s1})}}{2\gamma_{TE_k}} \sin[\frac{q\pi}{2L}(L + z'_{s1})]dz'_{s1}$$
$$I_{k2b_q} = \int_{z_p}^{L} \frac{e^{j\gamma_{TE_k}(z_p - z'_{s1})}}{2\gamma_{TE_k}} \sin[\frac{q\pi}{2L}(L + z'_{s1})]dz'_{s1}$$

Evaluation of the integrals I_{k2a_q}, I_{k2b_q}:

$$I_{k2a_q} = -j \int_{-L}^{z_p} \frac{e^{-j\gamma_{TE_k}(z_p - z'_{s1})}}{4\gamma_{TE_k}} (e^{j\frac{q\pi}{2L}(L+z'_{s1})} - e^{-j\frac{q\pi}{2L}(L+z'_{s1})})dz'_{s1} \Rightarrow$$

$$I_{k2a_q} = -\frac{e^{-j\gamma_{TE_k}z_p}}{4\gamma_{TE_k}} \left[\frac{e^{j\gamma_{TE_k}z'_{s1}+\frac{jq\pi}{2L}(L+z'_{s1})}}{\gamma_{TE_k}+\frac{jq\pi}{2L}} - \frac{e^{j\gamma_{TE_k}z'_{s1}-\frac{jq\pi}{2L}(L+z'_{s1})}}{\gamma_{TE_k}-\frac{jq\pi}{2L}}\right]_{-L}^{z_p} \Rightarrow$$

$$I_{k2a_q} = -\frac{e^{-j\gamma_{TE_k}z_p}}{4\gamma_{TE_k}} (\frac{e^{j\gamma_{TE_k}z_p+\frac{jq\pi}{2L}(L+z_p)}}{\gamma_{TE_k}+\frac{jq\pi}{2L}} - \frac{e^{-j\gamma_{TE_k}L}}{\gamma_{TE_k}+\frac{jq\pi}{2L}} - \frac{e^{j\gamma_{TE_k}z_p-\frac{jq\pi}{2L}(L+z_p)}}{\gamma_{TE_k}-\frac{jq\pi}{2L}} +$$
$$+\frac{e^{-j\gamma_{TE_k}L}}{\gamma_{TE_k}-\frac{jq\pi}{2L}})$$

$$I_{k2b_q} = -j \int_{z_p}^{L} \frac{e^{j\gamma_{TE_k}(z_p - z'_{s1})}}{4\gamma_{TE_k}} (e^{j\frac{q\pi}{2L}(L+z'_{s1})} - e^{-j\frac{q\pi}{2L}(L+z'_{s1})}) dz'_{s1} \Rightarrow$$

$$I_{k2b_q} = -\frac{e^{j\gamma_{TE_k} z_p}}{4\gamma_{TE_k}} \left[\frac{e^{-j\gamma_{TE_k} z'_{s1} + j\frac{q\pi}{2L}(L+z'_{s1})}}{-\gamma_{TE_k} + \frac{q\pi}{2L}} + \frac{e^{-j\gamma_{TE_k} z'_{s1} - j\frac{q\pi}{2L}(L+z'_{s1})}}{\gamma_{TE_k} + \frac{q\pi}{2L}} \right]_{z_p}^{L} \Rightarrow$$

$$\begin{aligned} I_{k2b_q} = & -\frac{e^{j\gamma_{TE_k} z_p}}{4\gamma_{TE_k}} \left(\frac{e^{-j\gamma_{TE_k} L + jq\pi}}{-\gamma_{TE_k} + \frac{q\pi}{2L}} - \frac{e^{-j\gamma_{TE_k} z_p + j\frac{q\pi}{2L}(L+z_p)}}{-\gamma_{TE_k} + \frac{q\pi}{2L}} + \right. \\ & \left. + \frac{e^{-j\gamma_{TE_k} L - jq\pi}}{\gamma_{TE_k} + \frac{q\pi}{2L}} - \frac{e^{-j\gamma_{TE_k} z_p - j\frac{q\pi}{2L}(L+z_p)}}{\gamma_{TE_k} + \frac{q\pi}{2L}} \right) \end{aligned}$$

Combination of the above results leads to the following expression for integral I_{k2_q}

$$I_{k2_q} = \frac{q\pi}{2L\gamma_{TE_k}} \frac{e^{-j\gamma_{TE_k} L}(e^{j\gamma_{TE_k} z_p} e^{jq\pi} - e^{-j\gamma_{TE_k} z_p})}{\gamma_{TE_k}^2 - (\frac{q\pi}{2L})^2} - \frac{2j\sin[\frac{q\pi}{2L}(L+z_p)]}{\gamma_{TE_k}^2 - (\frac{q\pi}{2L})^2} \tag{D.6c}$$

The expression for the elements of $GE3$ is:

$$\begin{aligned} GE3_{W_{i,q}} = & -j \int_0^{h_p} \int_0^{2\pi} \sum_k^{K_e} k_{TE_k}^2 \frac{\partial g_k(x_p, y_p)}{\partial x_p} t_{t_i}(t_p) e^{-j2\pi W \varphi_p} [-\frac{j\sin[\frac{q\pi}{2L}(L+z_p)]}{\gamma_{TE_k}^2 - (\frac{q\pi}{2L})^2} + \\ & + \frac{q\pi}{4L\gamma_{TE_k}} \frac{e^{-j\gamma_{TE_k} L}(e^{j\gamma_{TE_k} z_p} e^{jq\pi} - e^{-j\gamma_{TE_k} z_p})}{\gamma_{TE_k}^2 - (\frac{q\pi}{2L})^2}] I_{k1} dt_p d\varphi_p \end{aligned}$$

Matrix GE4: Impact of the φ- directed electric current on the t- scattered electric field (ridged waveguide).

$$GE4 = \begin{pmatrix} GE4_{11} & GE4_{12} & ... & GE4_{1N} \\ GE4_{21} & GE4_{22} & ... & GE4_{2N} \\ . & . & . & . \\ . & . & . & . \\ . & . & . & . \\ GE4_{N1} & GE4_{N2} & ... & GE4_{NN} \end{pmatrix}$$

$GE4_{WS}$ are IxI matrixes defined in the following way:

$$GE4_{WS_{ij}} = -j\omega\mu R_p^2 [W1_{WS_{ij}} + \frac{1}{R_p k_0^2} W2_{WS_{ij}}] \quad (D.7)$$

• $W1_{WS}$

$$W1_{WS_{ij}} = \int_0^{h_p} \int_0^{2\pi} e^{-jW\varphi_p} [t_{\varphi_i}(t_p) \int_0^{h_p} \int_0^{2\pi} G_{A_{\varphi t}}(\overrightarrow{r_p} | \overrightarrow{r_p}') e^{jS\varphi'_p} b_{t_j}(t'_p) dt'_p d\varphi'_p] dt_p d\varphi_p \tag{D.7a}$$

where:

$$G_{A_{\varphi t}}(\overrightarrow{r}_p|\overrightarrow{r}'_p) = G_{A_{xy}}(\overrightarrow{r}_p|\overrightarrow{r}'_p)\cos\varphi_p \overset{(2.41)}{\Rightarrow}$$
$$G_{A_{\varphi t}}(\overrightarrow{r}_p|\overrightarrow{r}'_p) = j\sum_k^{K_e} \frac{\partial g_k(x_p,y_p)}{\partial y_p}\frac{\partial g_k(x'_p,y'_p)}{\partial x'_p}\frac{e^{-j\gamma_{TE_k}|z_p-z'_p|}}{2\gamma_{TE_k}}\cos\varphi_p -$$
$$-j\sum_k^{K_m} \frac{\partial f_k(x_p,y_p)}{\partial x_p}\frac{\partial f_k(x'_p,y'_p)}{\partial y'_p}\frac{e^{-j\gamma_{TM_k}|z_p-z'_p|}}{2\gamma_{TM_k}}\cos\varphi_p$$

• $W2_{WS}$

$$W2_{WS_{i,j}} = \int_0^{h_p}\int_0^{2\pi} \frac{\partial(e^{-jW\varphi_p})}{\partial\varphi_p}[t_{\varphi_i}(t_p)\int_0^{h_p}\int_0^{2\pi}\frac{\partial G1(\overrightarrow{r_p}|\overrightarrow{r_p}')}{\partial y'_p}e^{jS\varphi'_p}b_{t_j}(t'_p)dt'_p d\varphi'_p]dt_p d\varphi_p =$$
$$= \int_0^{h_p}\int_0^{2\pi}(-jW)e^{-jW\varphi_p}[t_{\varphi_i}(t_p)\int_0^{h_p}\int_0^{2\pi}\frac{\partial G1(\overrightarrow{r_p}|\overrightarrow{r_p}')}{\partial y'_p}e^{jS\varphi'_p}b_{t_j}(t'_p)dt'_p d\varphi'_p]dt_p d\varphi_p \tag{D.7b}$$

Combination of (D.7a) and (D.7b) yields:

$$GE4_{WS_{ij}} = -j\omega\mu R_p^2\int_0^{h_p}\int_0^{2\pi} e^{-jW\varphi_p}t_{t_i}(t_p)GR4_{S_j}(\overrightarrow{r_p},\overrightarrow{r_p}')dt_p d\varphi_p \quad (D.8)$$

$$GR4_{S_j}(\overrightarrow{r_p},\overrightarrow{r_p}') = \int_0^{h_p}\int_0^{2\pi} e^{jS\varphi'_p}b_{t_j}(t'_p)\{[j\sum_k^{K_e}\frac{\partial g_k(x_p,y_p)}{\partial y_p}\frac{\partial g_k(x'_p,y'_p)}{\partial x'_p}\frac{e^{-j\gamma_{TE_k}|z_p-z'_p|}}{2\gamma_{TE_k}} -$$
$$-j\sum_k^{K_m}\frac{\partial f_k(x_p,y_p)}{\partial x_p}\frac{\partial f_k(x'_p,y'_p)}{\partial y'_p}\frac{e^{-j\gamma_{TM_k}|z_p-z'_p|}}{2\gamma_{TM_k}}]\cos\varphi_p +$$
$$+\frac{W}{R_p k_0^2}\sum_k^{K_m} k_{TM_k}^2 f_k(x_p,y_p)\frac{\partial f_k(x'_p,y'_p)}{\partial y'_p}\frac{e^{-j\gamma_{TM_k}|z_p-z'_p|}}{2\gamma_{TM_k}}\}dt'_p d\varphi'_p$$

Matrix GE5: Impact of the φ- directed electric current on the φ- scattered electric field (ridged waveguide).

$$GE5 = \begin{pmatrix} GE5_{11} & GE5_{12} & ... & GE5_{1N} \\ GE5_{21} & GE5_{22} & ... & GE5_{2N} \\ . & . & . & . \\ . & . & . & . \\ . & . & . & . \\ GE5_{N1} & GE5_{N2} & ... & GE5_{NN} \end{pmatrix}$$

$GE5_{WS}$ are IxI matrixes defined in the following way:

$$GE5_{WS_{ij}} = -j\omega\mu R_p^2(H1_{WS_{ij}} + \frac{1}{R_p^2 k_0^2}H2_{WS_{ij}}) \quad (D.9)$$

• $H1_{WS}$

$$H1_{WS_{ij}} = \int_0^{h_p}\int_0^{2\pi} e^{-jW\varphi_p}[t_{\varphi_i}(t_p)\int_0^{h_p}\int_0^{2\pi} G_{A_{\varphi\varphi}}(\overrightarrow{r_p}|\overrightarrow{r_p}')e^{jS\varphi'_p}b_{\varphi_j}(t'_p)dt'_p d\varphi'_p]dt_p d\varphi_p \tag{D.9a}$$

where:

$$G_{A_{\varphi\varphi}}(\overrightarrow{r}_p|\overrightarrow{r}'_p) = G_{A_{xx}}(\overrightarrow{r}_p|\overrightarrow{r}'_p)\cos\varphi_p\cos\varphi'_p + G_{A_{zz}}(\overrightarrow{r}_p|\overrightarrow{r}'_p)\sin\varphi_p\sin\varphi'_p \overset{(2.5)}{=}$$
$$= -j\sum_k^{K_e}\frac{\partial g_k(x_p,y_p)}{\partial y_p}\frac{\partial g_k(x'_p,y'_p)}{\partial y'_p}\frac{e^{-j\gamma_{TE_k}|z_p-z'_p|}}{2\gamma_{TE_k}}\cos\varphi_p\cos\varphi'_p -$$
$$-j\sum_k^{K_m}\frac{\partial f_k(x_p,y_p)}{\partial x_p}\frac{\partial f_k(x'_p,y'_p)}{\partial x'_p}\frac{e^{-j\gamma_{TM_k}|z_p-z'_p|}}{2\gamma_{TM_k}}\cos\varphi_p\cos\varphi'_p -$$
$$-j\sum_k^{K_m}k^2_{TM_k}f_k(x_p,y_p)f_k(x'_p,y'_p)\frac{e^{-j\gamma_{TM_k}|z_p-z'_p|}}{2\gamma_{TM_k}}\sin\varphi_p\sin\varphi'_p$$

- $H2_{WS}$

$$H2_{WS_{ij}} = \int_0^{h_p}\int_0^{2\pi}\frac{\partial(e^{-jW\varphi_p})}{\partial\varphi_p}[t_{\varphi_i}(t_p)\int_0^{h_p}\int_0^{2\pi}G1(\overrightarrow{r_p}|\overrightarrow{r_p}')\frac{\partial(e^{jS\varphi'_p})}{\partial\varphi'_p}b_{\varphi_j}(t'_p)dt'_pd\varphi'_p]dt_pd\varphi_p =$$
$$= \int_0^{h_p}\int_0^{2\pi}(-jW)e^{-jW\varphi_p}[t_{\varphi_i}(t_p)\int_0^{h_p}\int_0^{2\pi}G1(\overrightarrow{r_p}|\overrightarrow{r_p}')jSe^{jS\varphi'_p}b_{\varphi_j}(t'_p)dt'_pd\varphi'_p]dt_pd\varphi_p \tag{D.9b}$$

Combination of (D.9a) and (D.9b) yields:

$$GE5_{WS_{ij}} = -j\omega\mu R_p^2\int_0^{h_p}\int_0^{2\pi}e^{-jW\varphi_p}t_{t_i}(t_p)GR5_{S_j}(\overrightarrow{r_p},\overrightarrow{r_p}')dt_pd\varphi_p \quad (D.10)$$

$$GE5_{S_j}(\overrightarrow{r_p},\overrightarrow{r_p}') = \int_0^{h_p}\int_0^{2\pi}e^{jS\varphi'_p}b_{t_j}(t'_p)\{[-j\sum_k^{K_e}\frac{\partial g_k(x_p,y_p)}{\partial y_p}\frac{\partial g_k(x'_p,y'_p)}{\partial y'_p}\frac{e^{-j\gamma_{TE_k}|z_p-z'_p|}}{2\gamma_{TE_k}} -$$
$$-j\sum_k^{K_m}\frac{\partial f_k(x_p,y_p)}{\partial x_p}\frac{\partial f_k(x'_p,y'_p)}{\partial x'_p}\frac{e^{-j\gamma_{TM_k}|z_p-z'_p|}}{2\gamma_{TM_k}}]\cos\varphi_p\cos\varphi'_p -$$
$$-j\sum_k^{K_m}k^2_{TM_k}f_k(x_p,y_p)f_k(x'_p,y'_p)\frac{e^{-j\gamma_{TM_k}|z_p-z'_p|}}{2\gamma_{TM_k}}\sin\varphi_p\sin\varphi'_p +$$
$$+j\frac{WS}{R_p^2k_0^2}\sum_k^{K_m}k^2_{TM_k}f_k(x_p,y_p)f_k(x'_p,y'_p)\frac{e^{-j\gamma_{TM_k}|z_p-z'_p|}}{2\gamma_{TM_k}}\}dt'_pd\varphi'_p$$

Matrix GE6: Impact of the magnetic current on the φ- scattered electric field (Slot1 - ridged waveguide).

$$GE6 = \begin{pmatrix} GE6_1 \\ GE6_2 \\ . \\ . \\ . \\ GE6_N \end{pmatrix}$$

$GE6_W$ are IxQ matrixes defined in the following way:

$$GE6_{W_{i,q}} = \int_0^{h_p}\int_0^{2\pi}e^{-jW\varphi_p}[t_{\varphi_i}(t_p)\cos\varphi_p\frac{\partial}{\partial y_p}\int_{-L}^{L}\int_{\frac{a}{2}-\frac{w}{2}}^{\frac{a}{2}+\frac{w}{2}}G_{F_{zz}}(\overrightarrow{r_p}|\overrightarrow{r_{s1}}')u_q(z'_{s1},x'_{s1})dz'_{s1}dx'_{s1}]dt_pd\varphi_p =$$
$$= \int_0^{h_p}\int_0^{2\pi}e^{-jW\varphi_p}[t_{\varphi_i}(t_p)\cos\varphi_p\int_{-L}^{L}\int_{\frac{a}{2}-\frac{w}{2}}^{\frac{a}{2}+\frac{w}{2}}\frac{\partial G_{F_{zz}}(\overrightarrow{r_p}|\overrightarrow{r_{s1}}')}{\partial y_p}u_q(z'_{s1},x'_{s1})dz'_{s1}dx'_{s1}]dt_pd\varphi_p$$

where:

$$\frac{dG_{zz}(\overrightarrow{r_p}|\overrightarrow{r_{s1}}')}{\partial y_p} = -j\sum_{k}^{K_e} k_{TE_k}^2 \frac{\partial g_k(x_p,y_p)}{\partial y_p} g_k(x'_{s1},y'_{s1}) \frac{e^{-j\gamma_{TE_k}|z_p-z'_{s1}|}}{2\gamma_{TE_k}}$$

and

$$u_q(z,x) = \sin[\frac{q\pi}{2L}(L+z)]$$

The integral:

$$I_\varphi = \int_{-L}^{L}\int_{\frac{a}{2}-\frac{w}{2}}^{\frac{a}{2}+\frac{w}{2}} \frac{dG_{zz}(\overrightarrow{r_p}|\overrightarrow{r_{s1}}')}{\partial y_p} u_q(z'_{s1},x'_{s1}) dz'_{s1}dx'_{s1}$$

may be expressed as a product of the two linear integrals I_{k1} and I_{k2_q}:

$$I_\varphi = -j\sum_{k}^{K_e} k_{TE_k}^2 \frac{\partial g_k(x_p,y_p)}{\partial y_p} I_{k1} I_{k2_q}$$

The resulting expression for the elements of $GE6$ is:

$$GE6_{W_{i,q}} = -j\int_0^{h_p}\int_0^{2\pi}\sum_{k}^{K_e} k_{TE_k}^2 \frac{\partial g_k(x_p,y_p)}{\partial y_p} t_{\varphi_i}(t_p) e^{-jW\varphi_p}\cos\varphi_p[-\frac{j\sin[\frac{q\pi}{2L}(L+z_p)]}{\gamma_{TE_k}^2-(\frac{q\pi}{2L})^2}+ \\ +\frac{q\pi}{4L\gamma_{TE_k}}\frac{e^{-j\gamma_{TE_k}L}(e^{j\gamma_{TE_k}z_p}e^{jq\pi}-e^{-j\gamma_{TE_k}z_p})}{\gamma_{TE_k}^2-(\frac{q\pi}{2L})^2}]I_{k1}dt_p d\varphi_p \quad (D.11)$$

Matrix GE7: Impact of the t- directed electric current on the scattered magnetic field (Slot1 - ridged waveguide).

$$GE7 = \begin{pmatrix} GE7_1 & GE7_2 & ... & GE7_N \end{pmatrix}$$

$GE7_S$ are PxI matrixes defined in the following way:

$$GE7_{S_{i,j}} = R_p(-M1_S - M2_S + M3_S) \quad (D.12)$$

• $M1_S$

$$M1_{S_{p,i}} = \int_{-L}^{L}\int_{\frac{a}{2}-\frac{w}{2}}^{\frac{a}{2}+\frac{w}{2}} v_p(z_{s1},x_{s1})[\sin\varphi'_p\frac{\partial}{\partial y_{s1}}\int_0^{h_p}\int_0^{2\pi} G_{A_{\rho t}}(\overrightarrow{r_{s1}}|\overrightarrow{r_p}')e^{jS\varphi'_p}b_{t_i}(t'_p)dt'_p d\varphi'_p]dz_{s1}dx_{s1} = \\ = \int_{-L}^{L}\int_{\frac{a}{2}-\frac{w}{2}}^{\frac{a}{2}+\frac{w}{2}} v_p(z_{s1},x_{s1})[\int_0^{h_p}\int_0^{2\pi}\frac{\partial G_{A_{xy}}(\overrightarrow{r_{s1}}|\overrightarrow{r_p}')}{\partial y_{s1}}\sin^2\varphi'_p e^{jS\varphi'_p}b_{t_i}(t'_p)dt'_p d\varphi'_p]dz_{s1}dx_{s1} \quad (D.12a)$$

• $M2_S$

$$M2_{S_{p,i}} = \int_{-L}^{L}\int_{\frac{a}{2}-\frac{w}{2}}^{\frac{a}{2}+\frac{w}{2}} v_p(z_{s1},x_{s1})[\cos\varphi'_p\frac{\partial}{\partial y_{s1}}\int_0^{h_p}\int_0^{2\pi} G_{A_{\varphi t}}(\overrightarrow{r_{s1}}|\overrightarrow{r_p}')e^{jS\varphi'_p}b_{t_i}(t'_p)dt'_p d\varphi'_p]dz_{s1}dx_{s1} = \\ = \int_{-L}^{L}\int_{\frac{a}{2}-\frac{w}{2}}^{\frac{a}{2}+\frac{w}{2}} v_p(z_{s1},x_{s1})[\int_0^{h_p}\int_0^{2\pi}\frac{\partial G_{A_{xy}}(\overrightarrow{r_{s1}}|\overrightarrow{r_p}')}{\partial y_{s1}}\cos^2\varphi'_p e^{jS\varphi'_p}b_{t_i}(t'_p)dt'_p d\varphi'_p]dz_{s1}dx_{s1} \quad (D.12b)$$

• $M3_S$

$$M3_{S_{p,i}} = \int_{-L}^{L} \int_{\frac{a}{2}-\frac{w}{2}}^{\frac{a}{2}+\frac{w}{2}} v_p(z_{s1}, x_{s1}) [\frac{\partial}{\partial x_{s1}} \int_0^{h_p} \int_0^{2\pi} G_{A_{tt}}(\overrightarrow{r_{s1}}|\overrightarrow{r_p}') e^{jS\varphi_p'} b_{t_i}(t_p') dt_p' d\varphi_p'] dz_{s1} dx_{s1} =$$
$$= \int_{-L}^{L} \int_{\frac{a}{2}-\frac{w}{2}}^{\frac{a}{2}+\frac{w}{2}} v_p(z_{s1}, x_{s1}) [\int_0^{h_p} \int_0^{2\pi} \frac{\partial G_{A_{yy}}(\overrightarrow{r_{s1}}|\overrightarrow{r_p}')}{\partial x_{s1}} e^{jS\varphi_p'} b_{t_i}(t_p') dt_p' d\varphi_p'] dz_{s1} dx_{s1} \qquad (D.12c)$$

where:

$$u_p(z) = \sin[\frac{q\pi}{2L}(L+z)]$$

Combination of (D.12a), (D.12b) and (D.12c) yields:

$$GE7_{S_{p,i}} = \int_{-L}^{L} \int_{\frac{a}{2}-\frac{w}{2}}^{\frac{a}{2}+\frac{w}{2}} u_p(z_{s1}, x_{s1}) \{ \int_0^{h_p} \int_0^{2\pi} [\frac{\partial G_{A_{yy}}(\overrightarrow{r_{s1}}|\overrightarrow{r_p}')}{\partial x_{s1}} -$$
$$- \frac{\partial G_{A_{xy}}(\overrightarrow{r_{s1}}|\overrightarrow{r_p}')}{\partial y_{s1}}] e^{jS\varphi_p'} b_{t_i}(t_p') dt_p' d\varphi_p' \} dz_{s1} dx_{s1} \Rightarrow$$

$$GE7_{S_{p,i}} = \int_{-L}^{L} \int_{\frac{a}{2}-\frac{w}{2}}^{\frac{a}{2}+\frac{w}{2}} v_p(z_{s1}, x_{s1}) \{ \int_0^{h_p} \int_0^{2\pi} [-j \sum_{TE_k}^{K} \frac{\partial^2 g_k(x_{s1}, y_{s1})}{\partial x_{s1}^2} \frac{\partial g_k(x_p', y_p')}{\partial x_p'} \frac{e^{-j\gamma_{TE_k}|z_{s1}-z_p'|}}{2\gamma_{TE_k}} -$$
$$-j \sum_{k}^{K_m} \frac{\partial^2 f_k(x_{s1}, y_{s1})}{\partial x_{s1} \partial y_{s1}} \frac{\partial f_k(x_p', y_p')}{\partial y_p'} \frac{e^{-j\gamma_{TM_k}|z_{s1}-z_p'|}}{2\gamma_{TM_k}} -$$
$$-j \sum_{k}^{K_e} \frac{\partial^2 g_k(x_{s1}, y_{s1})}{\partial y_{s1}^2} \frac{\partial g_k(x_p', y_p')}{\partial x_p'} \frac{e^{-j\gamma_{TE_k}|z_{s1}-z_p'|}}{2\gamma_{TE_k}} +$$
$$+j \sum_{k}^{K_m} \frac{\partial^2 f_k(x_{s1}, y_{s1})}{\partial x_{s1} \partial y_{s1}} \frac{\partial f_k(x_p', y_p')}{\partial y_p'} \frac{e^{-j\gamma_{TM_k}|z_{s1}-z_p'|}}{2\gamma_{TM_k}}] e^{jS\varphi_p'} b_{t_i}(t_p') dt_p' d\varphi_p' \} dz_{s1} dx_{s1} \Rightarrow$$

$$GE7_{S_{p,i}} = \int_{-L}^{L} \int_{\frac{a}{2}-\frac{w}{2}}^{\frac{a}{2}+\frac{w}{2}} u_p(z_{s1}, x_{s1}) \int_0^{h_p} \int_0^{2\pi} G_{H_{zy}}^e(\overrightarrow{r_{s1}}|\overrightarrow{r_p}') e^{jS\varphi_p'} b_{t_i}(t_p') dt_p' d\varphi_p' dz_{s1} dx_{s1}$$

where $G_{H_{zy}}^e$ is the $zy-$ element of the magnetic dyadic Green Function due to electical current and is defined by the formula:

$$G_{H_{zy}}^e(\overrightarrow{r_{s1}}|\overrightarrow{r_p}') = j \sum_{k}^{K_e} k_{TE_k}^2 g_k(x_{s1}, y_{s1}) \frac{\partial g_k(x_p', y_p')}{\partial x_p'} \frac{e^{-j\gamma_{TE_k}|z_{s1}-z_p'|}}{2\gamma_{TE_k}}$$

Since the observation points (slot apperture) lie far from the source points (post surface), it is possible to interchange the sequence of integrations with respect to φ' and z_{s1}:

$$GE7_{S_{p,i}} = \int_{\frac{a}{2}-\frac{w}{2}}^{\frac{a}{2}+\frac{w}{2}} \{ \int_0^{h_p} \int_0^{2\pi} [\int_{-L}^{L} u_p(z_{s1}, x_{s1}) G_{H_{zy}}^e(\overrightarrow{r_{s1}}|\overrightarrow{r_p}') dz_{s1}] e^{jS\varphi_p'} b_{t_i}(t_p') dt_p' d\varphi_p' \} dx_{s1}$$

The integrals with respect to the slot variables have already been evaluated. More specifically:

$$\int_{\frac{a}{2}-\frac{w}{2}}^{\frac{a}{2}+\frac{w}{2}} \sum_{k}^{K_e} k_{TE_k}^2 g_k(x_{s1}, y_{s1}) dx_{s1} = I_{k1}$$
$$\int_{-L}^{L} v_p(z_{s1}) \frac{e^{-j\gamma_{TE_k}|z_{s1}-z_p'|}}{2\gamma_{TE_k}} dz_{s1} = \int_{-L}^{L} \sin[\frac{p\pi}{2L}(z_{s1}+L)] \frac{e^{-j\gamma_{TE_k}|z_p'-z_{s1}|}}{2\gamma_{TE_k}} dz_{s1} = I_{k2_p}$$

The resulting expression for the elements of $GE7_{S_{p,i}}$ is

$$GE7_{S_{p,i}} = j \int_0^{h_p} \int_0^{2\pi} \frac{\partial g_k(x'_p, y'_p)}{\partial x'_p} b_{t_i}(t'_p) e^{jS\varphi'_p} I_{k2_p} I_{k1} dt'_p d\varphi'_p \quad (D.13)$$

Matrix GE8: Impact of the φ- directed electric current on the scattered magnetic field (Slot1 - ridged waveguide).

$$GE8 = \begin{pmatrix} GE8_1 & GE8_2 & \dots & GE8_M \end{pmatrix}$$

$GE8_S$ are PxJ matrixes defined in the following way:

$$GE8_{S_{i,j}} = R_p(-N1_S - N2_S + N3_S) \quad (D.14)$$

- $N1_S$

$$N1_{S_{p,i}} = \int_{-L}^{L} \int_{\frac{a}{2}-\frac{w}{2}}^{\frac{a}{2}+\frac{w}{2}} v_p(z_{s1}, x_{s1}) [\sin\varphi'_p \frac{\partial}{\partial y_{s1}} \int_0^{h_p} \int_0^{2\pi} G_{A_{\rho\phi}}(\overrightarrow{r_{s1}}|\overrightarrow{r_p}') b_{\varphi_i}(t'_p) dt'_p d\varphi'_p] dz_{s1} dx_{s1} =$$
$$= \int_{-L}^{L} \int_{\frac{a}{2}-\frac{w}{2}}^{\frac{a}{2}+\frac{w}{2}} v_p(z_{s1}, x_{s1}) [\int_0^{h_p} \int_0^{2\pi} [\frac{\partial G_{A_{xx}}(\overrightarrow{r_{s1}}|\overrightarrow{r_p}')}{\partial y_{s1}} \sin\varphi_p \cos\varphi'_p -$$
$$- \frac{\partial G_{A_{zz}}(\overrightarrow{r_{s1}}|\overrightarrow{r_p}')}{\partial y_{s1}} \cos\varphi'_p \sin\varphi'_p] \sin\varphi_p e^{jS\varphi'_p} b_{\varphi_i}(t'_p) dt'_p d\varphi'_p] dz_{s1} dx_{s1} \quad (D.14a)$$

- $N2_S$

$$N2_{S_{p,i}} = \int_{-L}^{L} \int_{\frac{a}{2}-\frac{w}{2}}^{\frac{a}{2}+\frac{w}{2}} v_p(z_{s1}, x_{s1}) [\cos\varphi_p \frac{\partial}{\partial y_{s1}} \int_0^{h_p} \int_0^{2\pi} G_{A_{\varphi\varphi}}(\overrightarrow{r_{s1}}|\overrightarrow{r_p}') b_{\varphi_i}(t'_p) dt'_p d\varphi'_p] dz_{s1} dx_{s1} =$$
$$= \int_{-L}^{L} \int_{\frac{a}{2}-\frac{w}{2}}^{\frac{a}{2}+\frac{w}{2}} v_p(z_{s1}, x_{s1}) [\int_0^{h_p} \int_0^{2\pi} [\frac{\partial G_{A_{xx}}(\overrightarrow{r_{s1}}|\overrightarrow{r_p}')}{\partial y_{s1}} \cos\varphi'_p \cos\varphi'_p +$$
$$+ \frac{\partial G_{A_{zz}}(\overrightarrow{r_{s1}}|\overrightarrow{r_p}')}{\partial y_{s1}} \sin\varphi'_p \sin\varphi'_p] \cos\varphi_p e^{jS\varphi'_p} b_{\varphi_i}(t'_p) dt'_p d\varphi'_p] dz_{s1} dx_{s1} \quad (D.14b)$$

- $N3_S$

$$N3_{S_{p,i}} = \int_{-L}^{L} \int_{\frac{a}{2}-\frac{w}{2}}^{\frac{a}{2}+\frac{w}{2}} v_p(z_{s1}, x_{s1}) [\frac{\partial}{\partial x_{s1}} \int_0^{h_p} \int_0^{2\pi} G_{A_{t\varphi}}(\overrightarrow{r_{s1}}|\overrightarrow{r_p}') b_{\varphi_i}(t'_p) dt'_p d\varphi'_p] dz_{s1} dx_{s1} =$$
$$= \int_{-L}^{L} \int_{\frac{a}{2}-\frac{w}{2}}^{\frac{a}{2}+\frac{w}{2}} v_p(z_{s1}, x_{s1}) [\int_0^{h_p} \int_0^{2\pi} \frac{\partial G_{A_{yx}}(\overrightarrow{r_{s1}}|\overrightarrow{r_p}')}{\partial x_{s1}} \cos\varphi'_p e^{jS\varphi'_p} b_{\varphi_i}(t'_p) dt'_p d\varphi'_p] dz_{s1} dx_{s1} \quad (D.14c)$$

Combination of (D.14a), (D.14b) and (D.14c) yields:

$$GE8_{S_{p,i}} = \int_{-L}^{L} \int_{\frac{a}{2}-\frac{w}{2}}^{\frac{a}{2}+\frac{w}{2}} u_p(z_{s1}, x_{s1}) \{ \int_0^{h_p} \int_0^{2\pi} [\frac{\partial G_{A_{yx}}(\overrightarrow{r_{s1}}|\overrightarrow{r_p}')}{\partial x_{s1}} -$$
$$- \frac{\partial G_{A_{xx}}(\overrightarrow{r_{s1}}|\overrightarrow{r_p}')}{\partial y_{s1}}] \cos\varphi'_p e^{jS\varphi'_p} b_{\varphi_i}(t'_p) dt'_p d\varphi'_p \} dz_{s1} dx_{s1} \Rightarrow$$

$$GE8_{S_{p,i}}=\int_{-L}^{L}\int_{\frac{a}{2}-\frac{w}{2}}^{\frac{a}{2}+\frac{w}{2}} v_p(z_{s1},x_{s1})\{\int_0^{h_p}\int_0^{2\pi}[j\sum_k^{K_e}\frac{\partial^2 g_k(x_{s1},y_{s1})}{\partial x_{s1}^2}\frac{\partial g_k(x'_p,y'_p)}{\partial y'_p}\frac{e^{-j\gamma_{TE_k}|z_p-z'_p|}}{2\gamma_{TE_k}}-$$
$$-j\sum_k^{K_m}\frac{\partial^2 f_k(x_{s1},y_{s1})}{\partial x_{s1}\partial y_{s1}}\frac{\partial f_k(x'_p,y'_p)}{\partial x'_p}\frac{e^{-j\gamma_{TM_k}|z_{s1}-z'_p|}}{2\gamma_{TM_k}}-$$
$$+j\sum_k^{K_e}\frac{\partial^2 g_k(x_{s1},y_{s1})}{\partial y_{s1}^2}\frac{\partial g_k(x'_p,y'_p)}{\partial y'_p}\frac{e^{-j\gamma_{TE_k}|z_{s1}-z'_p|}}{2\gamma_{TE_k}}+$$
$$+j\sum_k^{K_m}\frac{\partial^2 f_k(x_{s1},y_{s1})}{\partial x_{s1}\partial y_{s1}}\frac{\partial f_k(x'_p,y'_p)}{\partial x'_p}\frac{e^{-j\gamma_{TM_k}|z_{s1}-z'_p|}}{2\gamma_{TM_k}}]\cos\varphi'_p e^{jS\varphi'_p}b_{\varphi_i}(t'_p)dt'_p d\varphi'_p\}dz_{s1}dx_{s1}\Rightarrow$$

$$GE8_{S_{p,i}}=\int_{-L}^{L}\int_{\frac{a}{2}-\frac{w}{2}}^{\frac{a}{2}+\frac{w}{2}} u_p(z_{s1},x_{s1})\int_0^{h_p}\int_0^{2\pi} G^e_{H_{zx}}(\overrightarrow{r_{s1}}|\overrightarrow{r_p}')\cos\varphi' e^{jS\varphi'_p}b_{t_i}(t'_p)dt'_p d\varphi'_p dz_{s1}dx_{s1}$$

where $G^e_{H_{zx}}$ is the $zx-$ element of the magnetic dyadic Green Function due to electical current and is defined by:

$$G^e_{H_{zx}}(\overrightarrow{r_{s1}}|\overrightarrow{r_p}')=-j\sum_k^{K_e}k^2_{TE_k}g_k(x_{s1},y_{s1})\frac{\partial g_k(x'_p,y'_p)}{\partial y'_p}\frac{e^{-j\gamma_{TE_k}|z_{s1}-z'_p|}}{2\gamma_{TE_k}}$$

As in the case of $GE7$, interchange between the sequence of integrations with respect to z_{s1} and φ' leads to the final expression for $GE8_{S_{p,i}}$

$$GE8_{S_{p,i}}=-j\int_0^{h_p}\int_0^{2\pi}\frac{\partial g_k(x'_p,y'_p)}{\partial y'_p}\cos\varphi'_p b_{\varphi_i}(t'_p)e^{jS\varphi'_p}I_{k2_p}I_{k1}dt'_p d\varphi'_p \quad (D.15)$$

Matrix GE9: Impact of the magnetic current on the scattered magnetic field (Slot1 - ridged waveguide).

$GE9$ is a PxP matrix. It's elements are defined in the following way:

$$GE9_{p,q}=-j\omega\varepsilon(Q1_{p,q}+Q2_{p,q}) \quad (D.16)$$

• $Q1$

$$Q1_{p,q}=-j\omega\varepsilon\{\int_{-L}^{L}\int_{\frac{a}{2}-\frac{w}{2}}^{\frac{a}{2}+\frac{w}{2}} v(z_{s1},x_{s1})[\int_{-L}^{-L}\int_{\frac{a}{2}-\frac{w}{2}}^{\frac{a}{2}+\frac{w}{2}} G_{Fc_{zz}}(\overrightarrow{r_{s1}}|\overrightarrow{r_{s1}}')u_q(z'_{s1},x'_{s1})dx'_{s1}dz'_{s1}]dx_{s1}dz_{s1}+$$
$$+\frac{1}{k_0^2}\int_{-L}^{L}\int_{\frac{a}{2}-\frac{w}{2}}^{\frac{a}{2}+\frac{w}{2}} v(z_{s1},x_{s1})\frac{\partial^2}{\partial z_{s1}^2}[\int_{-L}^{-L}\int_{\frac{a}{2}-\frac{w}{2}}^{\frac{a}{2}+\frac{w}{2}} G_{Fc_{zz}}(\overrightarrow{r_{s1}}|\overrightarrow{r_{s1}}')u_q(z'_{s1},x'_{s1})dx'_{s1}dz'_{s1}]dx_{s1}dz_{s1}]\} \quad (D.16a)$$

where

$$G_{Fc_{zz}}(\overrightarrow{r_{s1}}|\overrightarrow{r_{s1}}')=-j\sum_k^{K_e}k^2_{TE_k}g_k(x_{s1},y_{s1})g_k(x'_{s1},y'_{s1})\frac{e^{-j\gamma_{TE_k}|z_{s1}-z'_{s1}|}}{2\gamma_{TE_k}}+$$
$$+\frac{1}{S}\delta(z_{s1}-z'_{s1})$$

The integrals of (D.16a) are evaluated analytically, based on exprssions (D.6b) and (D.6c). More specifically:

$$I_{k3_q} = \int_{-L}^{L}\int_{\frac{a}{2}-\frac{w}{2}}^{\frac{a}{2}+\frac{w}{2}} G_{Fc_{zz}}(\overrightarrow{r_{s1}}|\overrightarrow{r_{s1}}')u_q(z'_{s1},x'_{s1})dx'_{s1}dz'_{s1} \Rightarrow$$

$$I_{k3_q} = \int_{-L}^{L}\int_{\frac{a}{2}-\frac{w}{2}}^{\frac{a}{2}+\frac{w}{2}} \frac{1}{S}\delta(z_{s1}-z'_{s1})\sin[\tfrac{q\pi}{2L}(L+z'_{s1})]dx'_{s1}dz'_{s1} - j\sum_{k}^{K_e} k_{TE_k}^2 g_k(x_{s1},y_{s1})I_{k1}I_{k2_q} \Rightarrow$$

$$I_{k3_q} = -j\sum_{k}^{K_e} k_{TE_k}^2 g_k(x_{s1},y_{s1})I_{k1}I_{k2_q} + \tfrac{w}{S}\sin[\tfrac{q\pi}{2L}(L+z_{s1})]$$

$$I_{k4_q} = \tfrac{\partial^2}{\partial z_{s1}^2}\int_{-L}^{L}\int_{\frac{a}{2}-\frac{w}{2}}^{\frac{a}{2}+\frac{w}{2}} G_{Fc_{zz}}(\overrightarrow{r_{s1}}|\overrightarrow{r_{s1}}')u_q(z'_{s1},x'_{s1})dx'_{s1}dz'_{s1} \Rightarrow$$

$$I_{k4_q} = -j\sum_{k}^{K_e} k_{TE_k}^2 g_k(x_{s1},y_{s1})\tfrac{\partial^2 I_{k2_q}}{\partial z_{s1}^2}I_{k1} + \tfrac{w}{S}\tfrac{\partial^2 \sin[\frac{q\pi}{2L}(L+z_{s1})]}{\partial z_{s1}^2} \Rightarrow$$

$$I_{k4_q} = -j\sum_{k}^{K_e} k_{TE_k}^2 g_k(x_{s1},y_{s1})\tfrac{\partial^2 I_{k2_q}}{\partial z_{s1}^2}I_{k1} - \tfrac{w}{S}(\tfrac{q\pi}{2L})^2\sin[\tfrac{q\pi}{2L}(L+z_{s1})]$$

$$I_{k5_q} = \tfrac{\partial^2 I_{k2_q}}{\partial z_{s1}^2} \Rightarrow$$

$$I_{k5_q} = \tfrac{1}{\gamma_{TE_k}^2-(\frac{q\pi}{2L})^2}[\tfrac{q\pi e^{-j\gamma_{TE_k}L}}{4L\gamma_{TE_k}}(\tfrac{\partial^2 e^{j\gamma_{TE_k}z_{s1}}}{\partial z_{s1}^2}e^{jq\pi} - \tfrac{\partial^2 e^{-j\gamma_{TE_k}z_{s1}}}{\partial z_{s1}^2}) - j\tfrac{\partial^2 \sin[\frac{q\pi}{2L}(L+z_{s1})]}{\partial z_{s1}^2}] \Rightarrow$$

$$I_{k5_q} = -\tfrac{\gamma_{TE_k}q\pi}{4L}\tfrac{e^{-j\gamma_{TE_k}L}(e^{j\gamma_{TE_k}z_{s1}}e^{jq\pi}-e^{-j\gamma_{TE_k}z_{s1}})}{\gamma_{TE_k}^2-(\frac{q\pi}{2L})^2} + (\tfrac{q\pi}{2L})^2\tfrac{j\sin[\frac{q\pi}{2L}(L+z_{s1})]}{\gamma_{TE_k}^2-(\frac{q\pi}{2L})^2}$$

Insertion of the above results into (D.16) yields:

$$Q1_{p,q} = -j\omega\varepsilon[\int_{-L}^{L}\int_{\frac{a}{2}-\frac{w}{2}}^{\frac{a}{2}+\frac{w}{2}} v_p(z_{s1},x_{s1})I_{k3_q}dx_{s1}dz_{s1} + \tfrac{1}{k_o^2}\int_{-L}^{L}\int_{\frac{a}{2}-\frac{w}{2}}^{\frac{a}{2}+\frac{w}{2}} v_p(z_{s1},x_{s1})I_{k4_q}dx_{s1}dz_{s1}] \Rightarrow$$

$$\begin{aligned}Q1_{p,q} = &-j\omega\varepsilon\{\int_{\frac{a}{2}-\frac{w}{2}}^{\frac{a}{2}+\frac{w}{2}}\sum_{k}^{K_e} k_{TE_k}^2 g_k(x_{s1},y_{s1})I_{k1}[\int_{-L}^{L} v_p(z_{s1},x_{s1})I_{k3_q}dz_{s1}]dx_{s1} + \\ &+\tfrac{1}{k_o^2}\int_{\frac{a}{2}-\frac{w}{2}}^{\frac{a}{2}+\frac{w}{2}}\sum_{k}^{K_e} k_{TE_k}^2 g_k(x_{s1},y_{s1})I_{k1}[\int_{-L}^{L} v_p(z_{s1},x_{s1})I_{k5_q}dz_{s1}]dx_{s1} + \\ &+\tfrac{w^2}{S}\int_{-L}^{L} v_p(z_{s1},x_{s1})\sin[\tfrac{q\pi}{2L}(L+z_{s1})dz_{s1} - \\ &-\tfrac{w^2}{Sk_o^2}(\tfrac{q\pi}{2L})^2\int_{-L}^{L} v_p(z_{s1},x_{s1})\sin[\tfrac{q\pi}{2L}(L+z_{s1})dz_{s1}\} \Rightarrow\end{aligned}$$

$$\begin{aligned}Q1_{p,q} = &-j\omega\varepsilon\{\sum_{k}^{K_e} k_{TE_k}^2(I_{k1})^2\int_{-L}^{L}[v_p(z_{s1},x_{s1})I_{k3_q} + \tfrac{1}{k_o^2}v_p(z_{s1},x_{s1})I_{k5_q}]dz_{s1} + \\ &+\tfrac{w^2L\delta_{p,q}}{Sk_o^2}[k_o^2-(\tfrac{q\pi}{2L})^2]\}\quad (D.16b)\end{aligned}$$

where:

$$\delta_{p,q} = \begin{cases} 1, p = q \\ 0, p \neq q \end{cases}$$

Evaluation of the integrals in (D.16a):

$$I_{k6_{p,q}} = \int_{-L}^{L} v_p(z_{s1},x_{s1})I_{k2_q}dz_{s1} \Rightarrow$$

$$I_{k6_{p,q}} = \int_{-L}^{L} \sin[\tfrac{p\pi}{2L}(L+z_{s1})][\tfrac{q\pi e^{-j\gamma_{TE_k}L}}{4L\gamma_{TE_k}} \tfrac{(e^{j\gamma_{TE_k}z_{s1}}e^{jq\pi} - e^{-j\gamma_{TE_k}z_{s1}})}{\gamma_{TE_k}^2 - (\frac{q\pi}{2L})^2} - \tfrac{j\sin[\frac{q\pi}{2L}(L+z_{s1})]}{\gamma_{TE_k}^2 - (\frac{q\pi}{2L})^2}]dz_{s1} \Rightarrow$$

$$I_{k6_{p,q}} = \tfrac{q\pi e^{-j\gamma_{TE_k}L}}{4L\gamma_{TE_k}} \tfrac{(I_{k6a_{p,q}}e^{jq\pi} - I_{k6b_{p,q}})}{\gamma_{TE_k}^2 - (\frac{q\pi}{2L})^2} - \tfrac{jL\delta_{p,q}}{\gamma_{TE_k}^2 - (\frac{q\pi}{2L})^2}$$

$$I_{k6a_{p,q}} = \int_{-L}^{L} \sin[\tfrac{p\pi}{2L}(L+z_{s1})]e^{j\gamma_{TE_k}z_{s1}}dz_{s1} \Rightarrow$$

$$I_{k6a_{p,q}} = -\tfrac{j}{2}\int_{-L}^{L} e^{j\gamma_{TE_k}z_{s1}}(e^{j\frac{p\pi}{2L}(L+z_{s1})} - e^{-j\frac{p\pi}{2L}(L+z_{s1})})dz_{s1} \Rightarrow$$

$$I_{k6a_{p,q}} = -\tfrac{1}{2}\left[\tfrac{e^{j\gamma_{TE_k}z_{s1}+j\frac{p\pi}{2L}(L+z_{s1})}}{\gamma_{TE_k}+\frac{p\pi}{2L}} - \tfrac{e^{j\gamma_{TE_k}z_{s1}-j\frac{p\pi}{2L}(L+z_{s1})}}{\gamma_{TE_k}-\frac{p\pi}{2L}}\right]_{-L}^{L} \Rightarrow$$

$$I_{k6a_{p,q}} = -\tfrac{1}{2}(\tfrac{e^{j\gamma_{TE_k}L+jp\pi}}{\gamma_{TE_k}+\frac{p\pi}{2L}} - \tfrac{e^{-j\gamma_{TE_k}L}}{\gamma_{TE_k}+\frac{p\pi}{2L}} - \tfrac{e^{j\gamma_{TE_k}L+jp\pi}}{\gamma_{TE_k}-\frac{p\pi}{2L}} + \tfrac{e^{-j\gamma_{TE_k}L}}{\gamma_{TE_k}-\frac{p\pi}{2L}})$$

$$I_{k6a_{p,q}} = -\tfrac{p\pi}{2L}\tfrac{e^{-j\gamma_{TE_k}L} - e^{j\gamma_{TE_k}L+jp\pi}}{\gamma_{TE_k}^2 - (\frac{p\pi}{2L})^2}$$

$$I_{k6b_{p,q}} = \int_{-L}^{L} \sin[\tfrac{p\pi}{2L}(L+z_{s1})]e^{-j\gamma_{TE_k}z_{s1}}dz_{s1} \Rightarrow$$

$$I_{k6b_{p,q}} = \tfrac{-j}{2}\int_{-L}^{L} (e^{j\frac{p\pi}{2L}(L+z_{s1})} - e^{-j\frac{p\pi}{2L}(L+z_{s1})})e^{-j\gamma_{TE_k}z_{s1}}dz_{s1} \Rightarrow$$

$$I_{k6b_{p,q}} = -\tfrac{1}{2}\left[-\tfrac{e^{-j\gamma_{TE_k}z_{s1}+j\frac{p\pi}{2L}(L+z_{s1})}}{\gamma_{TE_k}-\frac{p\pi}{2L}} + \tfrac{e^{-j\gamma_{TE_k}z_{s1}-j\frac{p\pi}{2L}(L+z_{s1})}}{\gamma_{TE_k}+\frac{p\pi}{2L}}\right]_{-L}^{L} \Rightarrow$$

$$I_{k6b_{p,q}} = -\tfrac{1}{2}(-\tfrac{e^{-j\gamma_{TE_k}L+jp\pi}}{\gamma_{TE_k}-\frac{p\pi}{2L}} + \tfrac{e^{j\gamma_{TE_k}L}}{\gamma_{TE_k}-\frac{p\pi}{2L}} + \tfrac{e^{-j\gamma_{TE_k}L+jp\pi}}{\gamma_{TE_k}+\frac{p\pi}{2L}} - \tfrac{e^{j\gamma_{TE_k}L}}{\gamma_{TE_k}+\frac{p\pi}{2L}}) \Rightarrow$$

$$I_{k6b_{p,q}} = -\tfrac{p\pi}{2L}\tfrac{e^{j\gamma_{TE_k}L} - e^{-j\gamma_{TE_k}L+jp\pi}}{\gamma_{TE_k}^2 - (\frac{p\pi}{2L})^2}$$

$$I_{k6_{p,q}} = \frac{pq\pi^2}{8L^2\gamma_{TE_k}} \frac{[e^{-j\gamma_{TE_k}2L}(e^{jq\pi} + e^{jp\pi}) - e^{j(p+q)\pi} - 1]}{[\gamma_{TE_k}^2 - (\frac{q\pi}{2L})^2][\gamma_{TE_k}^2 - (\frac{p\pi}{2L})^2]} - \frac{jL\delta_{p,q}}{\gamma_{TE_k}^2 - (\frac{q\pi}{2L})^2}$$

$$I_{k7_{p,q}} = \int_{-L}^{L} v_p(z_{s1}, x_{s1})I_{k5_q}dz_{s1} \Rightarrow$$

$$I_{k7_{p,q}} = \int_{-L}^{L} \sin[\tfrac{p\pi}{2L}(L+z_{s1})]\{(\tfrac{q\pi}{2L})^2 \tfrac{j\sin[\frac{q\pi}{2L}(L+z_{s1})]}{\gamma_{TE_k}^2 - (\frac{q\pi}{2L})^2} - \\ - \tfrac{\gamma_{TE_k}q\pi e^{-j\gamma_{TE_k}L}}{4L} \tfrac{(e^{j\gamma_{TE_k}z_{s1}}e^{jq\pi} - e^{-j\gamma_{TE_k}z_{s1}})}{\gamma_{TE_k}^2 - (\frac{q\pi}{2L})^2}\}dz \Rightarrow$$

$$I_{k7_{p,q}} = (\tfrac{q\pi}{2L})^2 \tfrac{jL\delta_{p,q}}{\gamma_{TE_k}^2 - (\frac{q\pi}{2L})^2} - \tfrac{\gamma_{TE_k}q\pi e^{-j\gamma_{TE_k}L}}{4L} \tfrac{(I_{k6a_{p,q}}e^{jq\pi} - I_{k6b_{p,q}})}{\gamma_{TE_k}^2 - (\frac{q\pi}{2L})^2} \Rightarrow$$

$$I_{k7_{p,q}} = (\tfrac{q\pi}{2L})^2 \tfrac{jL\delta_{p,q}}{\gamma_{TE_k}^2 - (\frac{q\pi}{2L})^2} - \tfrac{pq\pi^2\gamma_{TE_k}}{8L^2} \tfrac{[e^{-j\gamma_{TE_k}2L}(e^{jq\pi} + e^{jp\pi}) - e^{j(p+q)\pi} - 1]}{[\gamma_{TE_k}^2 - (\frac{q\pi}{2L})^2][\gamma_{TE_k}^2 - (\frac{p\pi}{2L})^2]}$$

The final expression for $Q1_{q,p}$ is obtained after the insertion of the above results into (D.16a)

$$Q1_{p,q} = -j\omega\varepsilon\{\frac{w^2 L\delta_{p,q}}{Sk_o^2}[k_o^2-(\frac{q\pi}{2L})^2]+\frac{L\delta_{p,q}[k_o^2-(\frac{q\pi}{2L})^2]}{[\gamma_{TE_k}^2-(\frac{q\pi}{2L})^2]k_o^2}-$$
$$-j\sum_k^{K_e}(I_{k1})^2\frac{pq\pi^2k_{TE_k}^4}{8L^2k_o^2\gamma_{TE_k}}\frac{[e^{-j\gamma_{TE_k}2L}(e^{jq\pi}+e^{jp\pi})-e^{j(p+q)\pi}-1]}{[\gamma_{TE_k}^2-(\frac{q\pi}{2L})^2][\gamma_{TE_k}^2-(\frac{p\pi}{2L})^2]}\} \quad (D.16c)$$

• $Q2$

$$Q2_{p,q}=\int_{-L}^{L}\int_{\frac{a}{2}-\frac{w}{2}}^{\frac{a}{2}+\frac{w}{2}}v_p(z_{s1},x_{s1})\int_{-L}^{L}\int_{\frac{a}{2}-\frac{w}{2}}^{\frac{a}{2}+\frac{w}{2}}G^m_{Hrsc_{zz}}(\overrightarrow{r_{s1}}|\overrightarrow{r_{s1}}')u_q(z'_{s1},x'_{s1})dz'_{s1}dx'_{s1}dz_{s1}dx_{s1}$$

where:

$$G^m_{Hsrc_{zz}}(\overrightarrow{r_{s1}}|\overrightarrow{r_{s1}}')=-\frac{4}{2Lw}\sum_{t=1}^{\infty}\sum_{s=0}^{\infty}\frac{k_o^2-(\frac{t\pi}{2L})^2}{\gamma_{t,s}\varepsilon_t\varepsilon_s k_o^2}f1_{t,s}(z_{s1},x_{s1})f1_{t,s}(z'_{s1},x'_{s1})\frac{s_1(y_{s1},y'_{s1})}{\sin(\gamma_{t,s}c_c)},$$

$$f1_{t,s}(z_{s1},x_{s1})=\sin[\tfrac{t\pi}{2L}(z_{s1}+L)]\cos[\tfrac{s\pi}{w}(x_{s1}+\tfrac{w}{2})]$$

$$s1_{t,s}(y_{s1},y'_{s1})=\frac{\cos[\gamma_{t,s}(y_{s1}+y'_{s1}+c_c)]+\cos[\gamma_{t,s}(c_c-|y_{s1}-y'_{s1}|)]}{2} \quad (D.16d)$$

Expression (D.16d) may be written in the following manner:

$$Q2_{p,q}=-\frac{2}{Lw}\sum_{t=1}^{\infty}\sum_{s=0}^{\infty}\frac{k_o^2-(\frac{t\pi}{2L})^2}{\gamma_{t,s}\varepsilon_t\varepsilon_s k_o^2}I_{8_{t,s,p}}I_{8_{t,s,q}}\frac{s1_{t,s}(y_{s1},y'_{s1})}{\sin(\gamma_{t,s}c_c)},$$

$$I_{8_{t,s,q}}=\int_{-L}^{L}\int_{-\frac{w}{2}}^{\frac{w}{2}}f1_{t,s}(z'_{s1},x'_{s1})u_q(z'_{s1},x'_{s1})dx'_{s1}dz'_{s1}\Rightarrow$$
$$I_{8_{t,s,q}}=\int_{-L}^{L}\int_{-\frac{w}{2}}^{\frac{w}{2}}\sin[\tfrac{t\pi}{2L}(z'_{s1}+L)]\cos[\tfrac{s\pi}{w}(x'_{s1}+\tfrac{w}{2})]\sin[\tfrac{q\pi}{2L}(L+z'_{s1})]dx'_{s1}dz'_{s1}\Rightarrow$$
$$I_{8_{t,s,q}}=\int_{-L}^{L}\sin[\tfrac{t\pi}{2L}(z'_{s1}+L)]\sin[\tfrac{q\pi}{2L}(L+z'_{s1})]dz'_{s1}\int_{-\frac{w}{2}}^{\frac{w}{2}}\cos[\tfrac{s\pi}{w}(x'_{s1}+\tfrac{w}{2})]dx'_{s1}\Rightarrow$$
$$I_{8_{t,s,q}}=\begin{cases} wL\delta_{t,q}, s=0\\ 0, s\neq 0\end{cases}$$

and

$$I_{8_{t,s,p}}=\begin{cases} wL\delta_{t,p}, s=0\\ 0, s\neq 0\end{cases}$$

From the above results it is concluded that matrix Q2 is diagonal. Additionally, the position of the upper slot apperture (y=y'=0) must also be taken into account for the determination of $Q2_{p,p}$.

$$Q2_{p,p}=\frac{k_o^2-(\frac{p\pi}{2L})^2}{\gamma_{p,0}k_o^2}Lw\cot(\gamma_{p,0}c_c) \quad (D.16e)$$

Insertion of (D.16c) and (D.16e) into (D.16) leads to the expression for $GE9_{p,q}$

$$GE9_{q,p}=-j\omega\varepsilon\{\frac{L\delta_{p,q}}{k_o^2}[k_o^2-(\frac{p\pi}{2L})^2][\frac{w^2}{S}+\frac{\sum_k^{K_e}(I_{k1})^2}{[\gamma_{TE_k}^2-(\frac{p\pi}{2L})^2]}-\frac{w\cot(\gamma_{p,0}c_c)}{\gamma_{p,0}}]-$$
$$-j\sum_k^{K_e}(I_{k1})^2\frac{pq\pi^2k_{TE_k}^4}{8L^2k_o^2\gamma_{TE_k}}\frac{[e^{-j\gamma_{TE_k}2L}(e^{jq\pi}+e^{jp\pi})-e^{j(p+q)\pi}-1]}{[\gamma_{TE_k}^2-(\frac{q\pi}{2L})^2][\gamma_{TE_k}^2-(\frac{p\pi}{2L})^2]}\} \quad (D.17)$$

Matrix GE10: Impact of the magnetic current on the scattered magnetic field (Slot1 - rectangular cavity).

$GE10$ is a PxP matrix. It's elements are defined in the following way:

$$GE10_{p,q}=-j\omega\varepsilon\int_{-L}^{L}\int_{\frac{a}{2}-\frac{w}{2}}^{\frac{a}{2}+\frac{w}{2}} v_p(z_{s1},x_{s1})\int_{-L}^{L}\int_{\frac{a}{2}-\frac{w}{2}}^{\frac{a}{2}+\frac{w}{2}} G^m_{Hsrc_{zz}}(\overrightarrow{r_{s1}}|\overrightarrow{r_{s2}}')u_q(z'_{s2}x'_{s2})dx'_{s2}dz'_{s2}dx_{s1}dz_{s1} \Rightarrow$$

$$GE10_{p,q} = -j\omega\varepsilon\frac{wL\delta_{p,q}}{2k_o^2}[k_o^2-(\frac{p\pi}{2L})^2]\frac{s1_{p,p}(y_{s1},y'_{s2})}{\gamma_{p,0}\sin(\gamma_{p,0}c_c)} \Rightarrow$$

$$GE10_{p,q} = -j\omega\varepsilon\frac{wL\delta_{p,q}}{2k_o^2}[k_o^2-(\frac{p\pi}{2L})^2]\frac{s1_{p,p}(0,-c_c)}{\gamma_{p,0}\sin(\gamma_{p,0}c_c)} \Rightarrow$$

$$GE10_{p,q} = -j\omega\varepsilon\frac{wL\delta_{p,q}}{k_o^2}[k_o^2-(\frac{p\pi}{2L})^2]\frac{1}{\gamma_{p,0}\sin(\gamma_{p,0}c_c)} \quad (D.18)$$

Matrix GE11: Impact of magnetic current on the scattered magnetic field (Slot2 - rectangular cavity).

$GE11$ is a PxP matrix. It's elements are defined in the following way:

$$GE11_{p,q}=-j\omega\varepsilon\int_{-L}^{L}\int_{\frac{a}{2}-\frac{w}{2}}^{\frac{a}{2}+\frac{w}{2}} v_p(z_{s2},x_{s2})\int_{-L}^{L}\int_{\frac{a}{2}-\frac{w}{2}}^{\frac{a}{2}+\frac{w}{2}} G^m_{Hsrc_{zz}}(\overrightarrow{r_{s2}}|\overrightarrow{r_{s1}}')u_q(z'_{s1},x'_{s1})dx'_{s1}dz'_{s1}dx_{s2}dz_{s2} \Rightarrow$$

$$GE11_{p,q} = -j\omega\varepsilon\frac{wL\delta_{p,q}}{2k_o^2}[k_o^2-(\frac{p\pi}{2L})^2]\frac{s1_{p,p}(y_{s2},y'_{s1})}{\gamma_{p,0}\sin(\gamma_{p,0}c_c)} \Rightarrow$$

$$GE11_{p,q} = -j\omega\varepsilon\frac{wL\delta_{p,q}}{2k_o^2}[k_o^2-(\frac{p\pi}{2L})^2]\frac{s1_{p,p}(-c_c,0)}{\gamma_{p,0}\sin(\gamma_{p,0}c_c)} \Rightarrow$$

$$GE11_{p,q} = -j\omega\varepsilon\frac{wL\delta_{p,q}}{k_o^2}[k_o^2-(\frac{p\pi}{2L})^2]\frac{1}{\gamma_{p,0}\sin(\gamma_{p,0}c_c)} \quad (D.19)$$

Matrix GE12: Impact of magnetic current on the scattered magnetic field (Slot2 - rectangular waveguide).

$GE12$ is a PxP matrix. It's elements are defined in the following way:

$$GE12_{p,q}=-j\omega\varepsilon\frac{\sqrt{2}}{2}(R1_{p,q}+R2_{p,q}+R3_{p,q}+R4_{p,q}) \quad (D.20)$$

- $R1$

$$R1_{p,q} = \frac{\sqrt{2}}{2}\iint_{Slot2} v_p(\zeta_{s2},\xi_{s2})\iint_{Slot2} G^m_{Hsrw_{zz}}(\overrightarrow{r_{s2}}|\overrightarrow{r_{s2}}')u_q(\zeta'_{s2},\xi'_{s2})d\xi'_{s2}d\zeta'_{s2}d\xi_{s2}d\zeta_{s2}$$

where:

$$G^m_{Hsrw_{\zeta\zeta}}(\overrightarrow{r_{s2}}|\overrightarrow{r_{s2}}') = -\frac{4j}{a_r b_r}\sum_{m=1}^{\infty}\sum_{n=0}^{\infty}\frac{k_o^2-(\frac{m\pi}{a_r})^2}{\gamma_{m,n}\varepsilon_t\varepsilon_s k_o^2}f2_{m,n}(\zeta_{s2},\xi_{s2})f2_{m,n}(\zeta'_{s2},\xi'_{s2})t3_{m,n}(\eta_{s2},\eta'_{s2}),$$

$$f2_{m,n}(\zeta_{s2},\xi_{s2}) = \sin[\frac{m\pi}{a_r}(\zeta_{s2}+\frac{a_r}{2})]\cos[\frac{n\pi}{b_r}(\xi_{s2}+\frac{b_r}{2})]$$

$$t3_{m,n}(\eta_{s2},\eta'_{s2}) = \frac{(e^{j\gamma_{m,n}(\eta_{s2}+\eta'_{s2})}+e^{-j\gamma_{m,n}|\eta_{s2}-\eta'_{s2}|})}{2}$$

The factor $\frac{\sqrt{2}}{2}$ is included in the expression of $R1_{p,q}$, because term $R1_{p,q}$ represents the $\zeta-$ magnetic field that is generated by the $\zeta-$ slot magnetic current. According to the analysis in Appendix C, the $\zeta-$ and $\xi-$ components of the magnetic current are given by:

$$M_\zeta(\overrightarrow{r}_{s2}) = \frac{\sqrt{2}}{2} M2(\overrightarrow{r}_{s2})$$
$$M_\xi(\overrightarrow{r}_{s2}) = \frac{\sqrt{2}}{2} M2(\overrightarrow{r}_{s2})$$

As in the cases of GE9, GE10 and GE11, the integrals with respect to the primed variables may be computed independently from the integrals involving the non primed variables. Their product will yield the final expression for $R1_{p,q}$.
Since the test/ basis functions are expressed in terms of the ridged waveguide coordinate system, it is convinient to employ the same coordinate system for the eigenvectors of the twisted rectangular waveguide. The coresponding transformation relationships have been derived in Appendix C.

$$f2_{m,n}(z_{s2}, x_{s2}) \overset{(C.12)}{=} \sin[A_1(z_{s2}, x_{s2})] \cos[A_2(z_{s2}, x_{s2})],$$
$$A_1(z_{s2}, x_{s2}) = \frac{m\pi}{a_r}(\frac{\sqrt{2}}{2} z_{s2} + \frac{a_r}{2} - \frac{\sqrt{2}}{2} x_{s2} + \frac{\sqrt{2}}{4} a)$$
$$A_2(z_{s2}, x_{s2}) = \frac{n\pi}{b_r}(\frac{\sqrt{2}}{2} z_{s2} + \frac{b_r}{2} + \frac{\sqrt{2}}{2} x_{s2} - \frac{\sqrt{2}}{4} a)$$

$-$ Evaluation of the integral over the source points:

$$I_{s1_q} = \int\int_{Slot2} f2_{t,s}(z'_{s2}, x'_{s2}) u_q(z'_{s2}, x'_{s2}) dx'_{s2} dz'_{s2} \Rightarrow$$

$$I_{s1_q} = \int_{-L}^{L} \int_{\frac{a}{2}-\frac{w}{2}}^{\frac{a}{2}+\frac{w}{2}} f2_{t,s}(z'_{s2}, x'_{s2}) u_q(z'_{s2}) dx'_{s2} dz'_{s2} \Rightarrow$$

$$I_{s1_q} = \int_{-L}^{L} \int_{\frac{a}{2}-\frac{w}{2}}^{\frac{a}{2}+\frac{w}{2}} \sin[A_1(z'_{s2}, x'_{s2})] \cos[A_2(z'_{s2}, x'_{s2})] \sin[\frac{q\pi}{2L}(z'_{s2} + L)] dx'_{s2} dz'_{s2}$$

$$I_{s1_q} = \frac{1}{2} \int_{-L}^{L} \int_{\frac{a}{2}-\frac{w}{2}}^{\frac{a}{2}+\frac{w}{2}} \{\sin[A_1(z'_{s2}, x'_{s2}) + A_2(z'_{s2}, x'_{s2})] +$$
$$+ \sin[A_1(z'_{s2}, x'_{s2}) - A_2(z'_{s2}, x'_{s2})]\} \sin[\frac{q\pi}{2L}(z'_{s2} + L)] dx'_{s2} dz'_{s2} \Rightarrow$$

At this point, the following two cases must be distinguished:

I) $\frac{m\pi}{a_r} = \frac{n\pi}{b_r}$:

$$I_{s1a_q} = \frac{1}{2} \int_{-L}^{L} \int_{\frac{a}{2}-\frac{w}{2}}^{\frac{a}{2}+\frac{w}{2}} \{\sin[\frac{m\pi}{a_r}(\sqrt{2} z'_{s2} + \frac{a_r}{2} + \frac{b_r}{2})] +$$
$$+ \sin[\frac{m\pi}{a_r}(\frac{a_r}{2} - \frac{b_r}{2} - \sqrt{2} x'_{s2} + \frac{\sqrt{2}}{2} a)]\} \sin[\frac{q\pi}{2L}(z'_{s2} + L)] dx'_{s2} dz'_{s2} \Rightarrow$$

$$I_{s1a_q} = \frac{w}{2} \int_{-L}^{L} \sin[\frac{m\pi}{a_r}(\sqrt{2} z'_{s2} + \frac{a_r}{2} + \frac{b_r}{2})] \sin[\frac{q\pi}{2L}(z'_{s2} + L)] dz'_{s2} +$$
$$+ \frac{1}{2} \int_{-L}^{L} \sin[\frac{q\pi}{2L}(z'_{s2} + L)] \left[\frac{\cos[\frac{m\pi}{a_r}(\frac{a_r}{2} - \frac{b_r}{2} - \sqrt{2} x_{s2} + \frac{\sqrt{2}}{2} a)]}{\sqrt{2}\frac{m\pi}{a_r}} \right]_{\frac{a}{2}-\frac{w}{2}}^{\frac{a}{2}+\frac{w}{2}} dz'_{s2} \Rightarrow$$

$$I_{s1a_q} = \frac{w}{4} \int_{-L}^{L} \{\cos[\frac{q\pi}{2L}(z'_{s2} + L) - \frac{m\pi}{a_r}(\sqrt{2} z'_{s2} + \frac{a_r}{2} + \frac{b_r}{2})] -$$
$$- \cos[\frac{q\pi}{2L}(z'_{s2} + L) + \frac{m\pi}{a_r}(\sqrt{2} z'_{s2} + \frac{a_r}{2} + \frac{b_r}{2})]\} dz'_{s2} +$$
$$+ \frac{1}{2} \int_{-L}^{L} \sin[\frac{q\pi}{2L}(z'_{s2} + L)] \frac{\cos[\frac{m\pi}{a_r}(\frac{a_r}{2} - \frac{b_r}{2} - \frac{\sqrt{2}w}{2})]}{\sqrt{2}\frac{m\pi}{a_r}} dz'_{s2} -$$
$$- \frac{1}{2} \int_{-L}^{L} \sin[\frac{q\pi}{2L}(z'_{s2} + L)] \frac{\cos[\frac{m\pi}{a_r}(\frac{a_r}{2} - \frac{b_r}{2} + \frac{\sqrt{2}w}{2})]}{\sqrt{2}\frac{m\pi}{a_r}} dz'_{s2} \Rightarrow$$

$$I_{s1a_q}=\frac{w}{4}\left[\frac{\sin[\frac{q\pi}{2L}(z'_{s2}+L)-\frac{m\pi}{a_r}(\sqrt{2}z'_{s2}+\frac{a_r}{2}+\frac{b_r}{2})]}{\frac{q\pi}{2L}-\sqrt{2}\frac{m\pi}{a_r}}\right]_{-L}^{L}-$$
$$-\frac{w}{4}\left[\frac{\sin[\frac{q\pi}{2L}(z'_{s2}+L)+\frac{m\pi}{a_r}(\sqrt{2}z'_{s2}+\frac{a_r}{2}+\frac{b_r}{2})]}{\frac{q\pi}{2L}+\sqrt{2}\frac{m\pi}{a_r}}\right]_{-L}^{L}+$$
$$+\sqrt{2}\sin[\frac{m\pi}{a_r}(\frac{a_r}{2}-\frac{b_r}{2})]\sin(\frac{m\pi\sqrt{2}w}{2a_r})\frac{a_r}{m\pi}\frac{L}{q\pi}[1-\cos(q\pi)]\Rightarrow$$

$$I_{s1a_q}=\frac{w}{4}\frac{\sin[q\pi-\frac{m\pi}{a_r}(\sqrt{2}L+\frac{a_r}{2}+\frac{b_r}{2})]+\sin[\frac{m\pi}{a_r}(-\sqrt{2}L+\frac{a_r}{2}+\frac{b_r}{2})]}{\frac{q\pi}{2L}-\sqrt{2}\frac{m\pi}{a_r}}-$$
$$-\frac{w}{4}\frac{\sin[q\pi+\frac{m\pi}{a_r}(\sqrt{2}L+\frac{a_r}{2}+\frac{b_r}{2})]-\sin[\frac{m\pi}{a_r}(-\sqrt{2}L+\frac{a_r}{2}+\frac{b_r}{2})]}{\frac{q\pi}{2L}+\sqrt{2}\frac{m\pi}{a_r}}+$$
$$+\sqrt{2}\sin[\frac{(m-n)\pi}{2}]\sin(\frac{n\pi\sqrt{2}w}{2b_r})\frac{a_r}{m\pi}\frac{L}{q\pi}[1-\cos(q\pi)]\Rightarrow$$

$$I_{s1a_q}=\frac{w}{4}\frac{-\cos(q\pi)\sin[\frac{m\pi\sqrt{2}L}{a_r}+\frac{(m+n)\pi}{2}]+\sin[-\frac{m\pi\sqrt{2}L}{a_r}+\frac{(m+n)\pi}{2}]}{\frac{q\pi}{2L}-\sqrt{2}\frac{m\pi}{a_r}}-$$
$$-\frac{w}{4}\frac{\cos(q\pi)\sin[\frac{m\pi\sqrt{2}L}{a_r}+\frac{(m+n)\pi}{2}]-\sin[-\frac{m\pi\sqrt{2}L}{a_r}+\frac{(m+n)\pi}{2}]}{\frac{q\pi}{2L}+\sqrt{2}\frac{m\pi}{a_r}}+$$
$$+\sqrt{2}\sin[\frac{(m-n)\pi}{2}]\sin(\frac{n\pi\sqrt{2}w}{2b_r})\frac{a_r}{m\pi}\frac{L}{q\pi}[1-\cos(q\pi)]\Rightarrow$$

$$I_{s1a_q}=\frac{w}{4}\frac{q\pi}{L}\frac{\sin[-\frac{m\pi\sqrt{2}L}{a_r}+\frac{(m+n)\pi}{2}]-\cos(q\pi)\sin[\frac{m\pi\sqrt{2}L}{a_r}+\frac{(m+n)\pi}{2}]}{(\frac{q\pi}{2L})^2-2(\frac{m\pi}{a_r})^2}+$$
$$+\sqrt{2}\sin[\frac{(m-n)\pi}{2}]\sin(\frac{n\pi\sqrt{2}w}{2b_r})\frac{a_r}{m\pi}\frac{L}{q\pi}[1-\cos(q\pi)]\quad(D.21a)$$

II) $\frac{m\pi}{a_r}\neq\frac{n\pi}{b_r}$:

$$I_{s1b_q}=\frac{1}{2}\int_{-L}^{L}\sin[\frac{q\pi}{2L}(z'_{s2}+L)]\left[\frac{\cos[A_1(z'_{s2},x'_{s2})+A_2(z'_{s2},x'_{s2})]}{\frac{\sqrt{2}}{2}\frac{m\pi}{a_r}-\frac{\sqrt{2}}{2}\frac{n\pi}{b_r}}\right]_{\frac{a}{2}-\frac{w}{2}}^{\frac{a}{2}+\frac{w}{2}}dz'_{s2}+$$
$$+\frac{1}{2}\int_{-L}^{L}\sin[\frac{q\pi}{2L}(z'_{s2}+L)]\left[\frac{\cos[A_1(z'_{s2},x'_{s2})-A_2(z'_{s2},x'_{s2})]}{\frac{\sqrt{2}}{2}\frac{m\pi}{a_r}+\frac{\sqrt{2}}{2}\frac{n\pi}{b_r}}\right]_{\frac{a}{2}-\frac{w}{2}}^{\frac{a}{2}+\frac{w}{2}}dz'_{s2}\Rightarrow$$

$$I_{s1b_q}=\frac{\sqrt{2}}{2}\int_{-L}^{L}\sin[\frac{q\pi}{2L}(z'_{s2}+L)]\frac{\cos[(\frac{m\pi}{a_r}+\frac{n\pi}{b_r})\frac{\sqrt{2}z'_{s2}}{2}+\frac{\sqrt{2}w}{4}(\frac{n\pi}{b_r}-\frac{m\pi}{a_r})+\frac{(m+n)\pi}{2}]}{\frac{m\pi}{a_r}-\frac{n\pi}{b_r}}dz'_{s2}-$$
$$-\frac{\sqrt{2}}{2}\int_{-L}^{L}\sin[\frac{q\pi}{2L}(z'_{s2}+L)]\frac{\cos[(\frac{m\pi}{a_r}+\frac{n\pi}{b_r})\frac{\sqrt{2}z'_{s2}}{2}+\frac{\sqrt{2}w}{4}(\frac{-n\pi}{b_r}+\frac{m\pi}{a_r})+\frac{(m+n)\pi}{2}]}{\frac{m\pi}{a_r}-\frac{n\pi}{b_r}}dz'_{s2}+$$
$$+\frac{\sqrt{2}}{2}\int_{-L}^{L}\sin[\frac{q\pi}{2L}(z'_{s2}+L)]\frac{\cos[(\frac{m\pi}{a_r}-\frac{n\pi}{b_r})\frac{\sqrt{2}z'_{s2}}{2}-\frac{\sqrt{2}w}{4}(\frac{n\pi}{b_r}+\frac{m\pi}{a_r})+\frac{(m-n)\pi}{2}]}{\frac{m\pi}{a_r}+\frac{n\pi}{b_r}}dz'_{s2}-$$
$$-\frac{\sqrt{2}}{2}\int_{-L}^{L}\sin[\frac{q\pi}{2L}(z'_{s2}+L)]\frac{\cos[(\frac{m\pi}{a_r}-\frac{n\pi}{b_r})\frac{\sqrt{2}z'_{s2}}{2}+\frac{\sqrt{2}w}{4}(\frac{n\pi}{b_r}+\frac{m\pi}{a_r})+\frac{(m-n)\pi}{2}]}{\frac{m\pi}{a_r}+\frac{n\pi}{b_r}}dz'_{s2}\Rightarrow$$

$$I_{s1b_q}=\frac{\sqrt{2}}{2}\int_{-L}^{L}\sin[\frac{q\pi}{2L}(z'_{s2}+L)]\frac{2\sin[(\frac{m\pi}{a_r}+\frac{n\pi}{b_r})\frac{\sqrt{2}z'_{s2}}{2}+\frac{(m+n)\pi}{2}]\sin[\frac{\sqrt{2}w}{4}(\frac{m\pi}{a_r}-\frac{n\pi}{b_r})]}{\frac{m\pi}{a_r}-\frac{n\pi}{b_r}}dz'_{s2}+$$
$$+\frac{\sqrt{2}}{2}\int_{-L}^{L}\sin[\frac{q\pi}{2L}(z'_{s2}+L)]\frac{2\sin[(\frac{m\pi}{a_r}-\frac{n\pi}{b_r})\frac{\sqrt{2}z'_{s2}}{2}+\frac{(m-n)\pi}{2}]\sin[\frac{\sqrt{2}w}{4}(\frac{m\pi}{a_r}+\frac{n\pi}{b_r})]}{\frac{m\pi}{a_r}+\frac{n\pi}{b_r}}dz'_{s2}\quad(D.21b)$$

In order to simplify the calculations in (D.21b), integral $\int_{-L}^{L}\sin[\frac{q\pi}{2L}(z'_{s2}+L)]\sin(kz'_{s2}+\frac{d\pi}{2})dz'_{s2}$ is examined. In the above integral, k and d are arbitrary coefficients.

$$I_{i_q} = \int_{-L}^{L} \sin[\tfrac{q\pi}{2L}(z'_{s2}+L)]\sin(kz'_{s2}+\tfrac{d\pi}{2})dz'_{s2} \Rightarrow$$

$$I_{i_q} = \tfrac{1}{2}\int_{-L}^{L}\{\cos[\tfrac{q\pi}{2L}(z'_{s2}+L)-kz'_{s2}-\tfrac{d\pi}{2}]-\cos[\tfrac{q\pi}{2L}(z'_{s2}+L)+kz'_{s2}+\tfrac{d\pi}{2}]\}dz'_{s2} \Rightarrow$$

$$I_{i_q} = \tfrac{1}{2}\left[\frac{\sin[\frac{q\pi}{2L}(z'_{s2}+L)-kz'_{s2}-\frac{d\pi}{2}]}{\frac{q\pi}{2L}-k}\right]_{-L}^{L} - \tfrac{1}{2}\left[\frac{\sin[\frac{q\pi}{2L}(z'_{s2}+L)+kz'_{s2}+\frac{d\pi}{2}]}{\frac{q\pi}{2L}+k}\right]_{-L}^{L} \Rightarrow$$

$$I_{i_q} = \tfrac{1}{2}\frac{\sin(q\pi-kL-\frac{d\pi}{2})-\sin(kL-\frac{d\pi}{2})}{\frac{q\pi}{2L}-k} - \tfrac{1}{2}\frac{\sin(q\pi+kL+\frac{d\pi}{2})-\sin(-kL+\frac{d\pi}{2})}{\frac{q\pi}{2L}+k} \Rightarrow$$

$$I_{i_q} = -\tfrac{1}{2}\frac{\sin(kL-\frac{d\pi}{2})+\cos(q\pi)\sin(kL+\frac{d\pi}{2})}{\frac{q\pi}{2L}-k} - \tfrac{1}{2}\frac{\sin(kL-\frac{d\pi}{2})+\cos(q\pi)\sin(kL+\frac{d\pi}{2})}{\frac{q\pi}{2L}+k} \Rightarrow$$

$$I_{i_q} = -\frac{q\pi}{L}\frac{\sin(kL-\frac{d\pi}{2})+\cos(q\pi)\sin(kL+\frac{d\pi}{2})}{(\frac{q\pi}{2L})^2-k^2}$$

Insertion of I_{i_q} with the apropriate values for k and d leads to the following expression for I_{sb_q}:

$$\begin{aligned} I_{s1b_q} = &-\frac{\sqrt{2}q\pi}{L}\Big\{\frac{\sin[\frac{\sqrt{2}w}{4}(\frac{m\pi}{a_r}-\frac{n\pi}{b_r})]}{\frac{m\pi}{a_r}-\frac{n\pi}{b_r}}\frac{\sin[(\frac{m\pi}{a_r}+\frac{n\pi}{b_r})\frac{\sqrt{2}L}{2}-\frac{(m+n)\pi}{2}]}{(\frac{q\pi}{2L})^2-k^2}+ \\ &+\frac{\cos(q\pi)\sin[(\frac{m\pi}{a_r}+\frac{n\pi}{b_r})\frac{\sqrt{2}L}{2}+\frac{(m+n)\pi}{2}]}{(\frac{q\pi}{2L})^2-k^2}\Big\}- \\ &-\frac{\sqrt{2}q\pi}{L}\frac{\sin[\frac{\sqrt{2}w}{4}(\frac{m\pi}{a_r}+\frac{n\pi}{b_r})]}{\frac{m\pi}{a_r}+\frac{n\pi}{b_r}}\Big\{\frac{\sin[(\frac{m\pi}{a_r}-\frac{n\pi}{b_r})\frac{\sqrt{2}L}{2}-\frac{(m-n)\pi}{2}]}{(\frac{q\pi}{2L})^2-k^2}+ \\ &+\frac{\cos(q\pi)\sin[(\frac{m\pi}{a_r}-\frac{n\pi}{b_r})\frac{\sqrt{2}L}{2}+\frac{(m-n)\pi}{2}]}{(\frac{q\pi}{2L})^2-k^2}\Big\} \quad (D.21c) \end{aligned}$$

$$\begin{aligned} I_{s1b_q} = &-\frac{\sqrt{2}q\pi}{L}\Big\{\frac{\sin[\frac{\sqrt{2}w}{4}(\frac{m\pi}{a_r}-\frac{n\pi}{b_r})]}{\frac{m\pi}{a_r}-\frac{n\pi}{b_r}}\frac{\sin[(\frac{m\pi}{a_r}+\frac{n\pi}{b_r})\frac{\sqrt{2}L}{2}-\frac{(m+n)\pi}{2}]}{(\frac{q\pi}{2L})^2-\frac{1}{2}(\frac{m\pi}{a_r}+\frac{n\pi}{b_r})^2}+ \\ &+\frac{\cos(q\pi)\sin[(\frac{m\pi}{a_r}+\frac{n\pi}{b_r})\frac{\sqrt{2}L}{2}+\frac{(m+n)\pi}{2}]}{(\frac{q\pi}{2L})^2-\frac{1}{2}(\frac{m\pi}{a_r}+\frac{n\pi}{b_r})^2}\Big\}- \\ &-\frac{\sqrt{2}q\pi}{L}\frac{\sin[\frac{\sqrt{2}w}{4}(\frac{m\pi}{a_r}+\frac{n\pi}{b_r})]}{\frac{m\pi}{a_r}+\frac{n\pi}{b_r}}\Big\{\frac{\sin[(\frac{m\pi}{a_r}-\frac{n\pi}{b_r})\frac{\sqrt{2}L}{2}-\frac{(m-n)\pi}{2}]}{(\frac{q\pi}{2L})^2-\frac{1}{2}(\frac{m\pi}{a_r}-\frac{n\pi}{b_r})^2}+ \\ &+\frac{\cos(q\pi)\sin[(\frac{m\pi}{a_r}-\frac{n\pi}{b_r})\frac{\sqrt{2}L}{2}+\frac{(m-n)\pi}{2}]}{(\frac{q\pi}{2L})^2-\frac{1}{2}(\frac{m\pi}{a_r}-\frac{n\pi}{b_r})^2}\Big\} \quad (D.21c) \end{aligned}$$

Summarizing the results from (D.21a) and (D.21b), integral I_{9_q} is otained by:

$$I_{s1_q} = \begin{cases} I_{s1a_q}, \frac{m\pi}{a_r} = \frac{n\pi}{b_r} \\ I_{s1b_q}, \frac{m\pi}{a_r} \neq \frac{n\pi}{b_r} \end{cases} \quad (D.22a)$$

– Evaluation of the integral over the observation points:

$$\begin{aligned} I_{o1_p} &= \iint_{Slot2} f2_{m,n}(z_{s2},x_{s2})v_p(z_{s2},x_{s2})dx_{s2}dz_{s2} \Rightarrow \\ I_{o1_p} &= I_{s1_p} \quad (D.22b) \end{aligned}$$

As aready mentioned before the product $I_{o_p}I_{s_q}$ yields the final expression for $R1_{q,p}$:

$$R1_{q,p} = \frac{\sqrt{2}}{2}I_{o1_p}I_{s1_q} \qquad (D.23)$$

• $R2$

$$R2_{p,q} = \frac{\sqrt{2}}{2}\iint_{Slot2} v_p(\zeta_{s2},\xi_{s2})\iint_{Slot2} G^m_{Hsrw_{\zeta\xi}}(\overrightarrow{r_{s2}}|\overrightarrow{r_{s2}}')u_q(\zeta'_{s2},\xi'_{s2})d\xi'_{s2}d\zeta'_{s2}d\xi_{s2}d\zeta_{s2}$$

where:

$$G^m_{Hsrw_{\zeta\xi}}(\overrightarrow{r_{s2}}|\overrightarrow{r_{s2}}') = \frac{4j}{a_r b_r}\sum_{m=1}^{\infty}\sum_{n=0}^{\infty}\frac{\frac{m\pi}{a_r}\frac{n\pi}{b_r}}{\gamma_{m,n}\varepsilon_m\varepsilon_n k_o^2} f2_{m,n}(\zeta_{s2},\xi_{s2}) f3_{t,s}(\zeta'_{s2},\xi'_{s2}) t3_{n,m}(\eta_{s2},\eta'_{s2}),$$

$$f3_{m,n}(\zeta_{s2},\xi) = \cos[\frac{m\pi}{a_r}(\zeta_{s2}+\frac{a_r}{2})]\sin[\frac{n\pi}{b_r}(\xi_{s2}+\frac{b_r}{2})] \Rightarrow$$

$$f3_{m,n}(z_{s2},x_{s2}) \overset{(C.12)}{=} \cos[A_1(z_{s2},x_{s2})]\sin[A_2(z_{s2},x_{s2})]$$

The elements of matrix $R2$ may be expressed as the product of two integrals:

$$R2_{p,q} = \frac{\sqrt{2}}{2} I_{o1_p} I_{s2_q}, \qquad (D.24)$$

$$I_{s2_q} = \int\int_{Slot2} f3_{m,n}(z'_{s2},x'_{s2}) u_q(z'_{s2},x'_{s2}) dx'_{s2} dz'_{s2}$$

and I_{o1_p} is given by (D.22b)

– Evaluation of integral I_{s2_q}:

$$I_{s2_q} = \int_{-L}^{L}\int_{\frac{a}{2}-\frac{w}{2}}^{\frac{a}{2}+\frac{w}{2}} \cos[A_1(z'_{s2},x'_{s2})]\sin[A_2(z'_{s2},x'_{s2})]\sin[\tfrac{q\pi}{2L}(z'_{s2}+L)]dx'_{s2}dz'_{s2} \Rightarrow$$

$$\begin{aligned} I_{s2_q} = \tfrac{1}{2}\int_{-L}^{L}\int_{\frac{a}{2}-\frac{w}{2}}^{\frac{a}{2}+\frac{w}{2}} \{&\sin[A_1(z'_{s2},x'_{s2})+A_2(z'_{s2},x'_{s2})]- \\ &-\sin[A_1(z'_{s2},x'_{s2})-A_2(z'_{s2},x'_{s2})]\}\sin[\tfrac{q\pi}{2L}(z'_{s2}+L)]dx'_{s2}dz'_{s2} \Rightarrow \end{aligned}$$

I) $\frac{m\pi}{a_r} = \frac{n\pi}{b_r}$:

$$\begin{aligned} I_{s2a_q} = \tfrac{1}{2}\int_{-L}^{L}\int_{\frac{a}{2}-\frac{w}{2}}^{\frac{a}{2}+\frac{w}{2}} \{&\sin[\tfrac{m\pi}{a_r}(\sqrt{2}z'_{s2}+\tfrac{a_r}{2}+\tfrac{b_r}{2})]- \\ &-\sin[\tfrac{m\pi}{a_r}(\tfrac{a_r}{2}-\tfrac{b_r}{2}-\sqrt{2}x'_{s2}+\tfrac{\sqrt{2}}{2}a)]\}\sin[\tfrac{q\pi}{2L}(z'_{s2}+L)]dx'_{s2}dz'_{s2} \Rightarrow \end{aligned}$$

$$\begin{aligned} I_{s2a_q} = &\tfrac{w}{2}\int_{-L}^{L}\sin[\tfrac{m\pi}{a_r}(\sqrt{2}z'_{s2}+\tfrac{a_r}{2}+\tfrac{b_r}{2})]\sin[\tfrac{q\pi}{2L}(z'_{s2}+L)]dz'_{s2}- \\ &-\tfrac{1}{2}\int_{-L}^{L}\sin[\tfrac{q\pi}{2L}(z'_{s2}+L)]\left[\frac{\cos[\frac{m\pi}{a_r}(\frac{a_r}{2}-\frac{b_r}{2}-\sqrt{2}x_{s2}+\frac{\sqrt{2}}{2}a)]}{\sqrt{2}\frac{m\pi}{a_r}}\right]_{\frac{a}{2}-\frac{w}{2}}^{\frac{a}{2}+\frac{w}{2}} dz'_{s2} \Rightarrow \end{aligned}$$

$$\begin{aligned} I_{s2a_q} = \tfrac{w}{4}\int_{-L}^{L} &\{\cos[\tfrac{q\pi}{2L}(z'_{s2}+L)-\tfrac{m\pi}{a_r}(\sqrt{2}z'_{s2}+\tfrac{a_r}{2}+\tfrac{b_r}{2})]- \\ &-\cos[\tfrac{q\pi}{2L}(z'_{s2}+L)+\tfrac{m\pi}{a_r}(\sqrt{2}z'_{s2}+\tfrac{a_r}{2}+\tfrac{b_r}{2})]\}dz'_{s2}- \\ &-\tfrac{1}{2}\int_{-L}^{L}\sin[\tfrac{q\pi}{2L}(z'_{s2}+L)]\frac{\cos[\frac{m\pi}{a_r}(\frac{a_r}{2}-\frac{b_r}{2}-\frac{\sqrt{2}w}{2})]}{\sqrt{2}\frac{m\pi}{a_r}}dz'_{s1}+ \\ &+\tfrac{1}{2}\int_{-L}^{L}\sin[\tfrac{q\pi}{2L}(z'_{s2}+L)]\frac{\cos[\frac{m\pi}{a_r}(\frac{a_r}{2}-\frac{b_r}{2}+\frac{\sqrt{2}w}{2})]}{\sqrt{2}\frac{m\pi}{a_r}}dz'_{s1} \Rightarrow \end{aligned}$$

$$\begin{aligned} I_{s2a_q} = &\tfrac{w}{4}\left[\frac{\sin[\frac{q\pi}{2L}(z'_{s2}+L)-\frac{m\pi}{a_r}(\sqrt{2}z'_{s2}+\frac{a_r}{2}+\frac{b_r}{2})]}{\frac{q\pi}{2L}-\sqrt{2}\frac{m\pi}{a_r}}\right]_{-L}^{L}- \\ &-\tfrac{w}{4}\left[\frac{\sin[\frac{q\pi}{2L}(z'_{s2}+L)+\frac{m\pi}{a_r}(\sqrt{2}z'_{s2}+\frac{a_r}{2}+\frac{b_r}{2})]}{\frac{q\pi}{2L}+\sqrt{2}\frac{m\pi}{a_r}}\right]_{-L}^{L}- \\ &-\sqrt{2}\sin[\tfrac{m\pi}{a_r}(\tfrac{a_r}{2}-\tfrac{b_r}{2})]\sin(\tfrac{m\pi\sqrt{2}w}{2a_r})\frac{a_r}{m\pi}\frac{L}{q\pi}[1-\cos(q\pi)] \Rightarrow \end{aligned}$$

$$I_{s2a_q} = \frac{w}{4}\frac{\sin[q\pi-\frac{m\pi}{a_r}(\sqrt{2}L+\frac{a_r}{2}+\frac{b_r}{2})]+\sin[\frac{m\pi}{a_r}(-\sqrt{2}L+\frac{a_r}{2}+\frac{b_r}{2})]}{\frac{q\pi}{2L}-\sqrt{2}\frac{m\pi}{a_r}} -$$
$$-\frac{w}{4}\frac{\sin[q\pi+\frac{m\pi}{a_r}(\sqrt{2}L+\frac{a_r}{2}+\frac{b_r}{2})]-\sin[\frac{m\pi}{a_r}(-\sqrt{2}L+\frac{a_r}{2}+\frac{b_r}{2})]}{\frac{q\pi}{2L}+\sqrt{2}\frac{m\pi}{a_r}} -$$
$$-\sqrt{2}\sin[\frac{(m-n)\pi}{2}]\sin(\frac{n\pi\sqrt{2}w}{2b_r})\frac{a_r}{m\pi}\frac{L}{q\pi}[1-\cos(q\pi)] \Rightarrow$$

$$I_{s2a_q} = \frac{w}{4}\frac{-\cos(q\pi)\sin[\frac{m\pi\sqrt{2}L}{a_r}+\frac{(m+n)\pi}{2}]+\sin[-\frac{m\pi\sqrt{2}L}{a_r}+\frac{(m+n)\pi}{2}]}{\frac{q\pi}{2L}-\sqrt{2}\frac{m\pi}{a_r}} -$$
$$-\frac{w}{4}\frac{\cos(q\pi)\sin[\frac{m\pi\sqrt{2}L}{a_r}+\frac{(m+n)\pi}{2}]-\sin[-\frac{m\pi\sqrt{2}L}{a_r}+\frac{(m+n)\pi}{2}]}{\frac{q\pi}{2L}+\sqrt{2}\frac{m\pi}{a_r}} -$$
$$-\sqrt{2}\sin[\frac{(m-n)\pi}{2}]\sin(\frac{n\pi\sqrt{2}w}{2b_r})\frac{a_r}{m\pi}\frac{L}{q\pi}[1-\cos(q\pi)] \Rightarrow$$

$$I_{s2a_q} = \frac{w}{4}\frac{q\pi}{L}\frac{\sin[-\frac{m\pi\sqrt{2}L}{a_r}+\frac{(m+n)\pi}{2}]-\cos(q\pi)\sin[\frac{m\pi\sqrt{2}L}{a_r}+\frac{(m+n)\pi}{2}]}{(\frac{q\pi}{2L})^2-2(\frac{m\pi}{a_r})^2} -$$
$$-\sqrt{2}\sin[\frac{(m-n)\pi}{2}]\sin(\frac{n\pi\sqrt{2}w}{2b_r})\frac{a_r}{m\pi}\frac{L}{q\pi}[1-\cos(q\pi)] \quad (D.25a)$$

II) $\frac{m\pi}{a_r} \neq \frac{n\pi}{b_r}$:

$$I_{s2b_q} = \frac{1}{2}\int_{-L}^{L}\sin[\frac{q\pi}{2L}(z'_{s2}+L)]\left[\frac{\cos[A_1(z'_{s2},x'_{s2})+A_2(z'_{s2},x'_{s2})]}{\frac{\sqrt{2}}{2}\frac{m\pi}{a_r}-\frac{\sqrt{2}}{2}\frac{n\pi}{b_r}}\right]_{\frac{a}{2}-\frac{w}{2}}^{\frac{a}{2}+\frac{w}{2}}dz'_{s2} -$$
$$-\frac{1}{2}\int_{-L}^{L}\sin[\frac{q\pi}{2L}(z'_{s2}+L)]\left[\frac{\cos[A_1(z'_{s2},x'_{s2})-A_2(z'_{s2},x'_{s2})]}{\frac{\sqrt{2}}{2}\frac{m\pi}{a_r}+\frac{\sqrt{2}}{2}\frac{n\pi}{b_r}}\right]_{\frac{a}{2}-\frac{w}{2}}^{\frac{a}{2}+\frac{w}{2}}dz'_{s2} \Rightarrow$$

$$I_{s2b_q} = \frac{\sqrt{2}}{2}\int_{-L}^{L}\sin[\frac{q\pi}{2L}(z'_{s2}+L)]\frac{\cos[(\frac{m\pi}{a_r}+\frac{n\pi}{b_r})\frac{\sqrt{2}z'_{s2}}{2}+\frac{\sqrt{2}w}{4}(\frac{n\pi}{b_r}-\frac{m\pi}{a_r})+\frac{(m+n)\pi}{2}]}{\frac{m\pi}{a_r}-\frac{n\pi}{b_r}}dz'_{s2} -$$
$$-\frac{\sqrt{2}}{2}\int_{-L}^{L}\sin[\frac{q\pi}{2L}(z'_{s2}+L)]\frac{\cos[(\frac{m\pi}{a_r}+\frac{n\pi}{b_r})\frac{\sqrt{2}z'_{s2}}{2}+\frac{\sqrt{2}w}{4}(\frac{-n\pi}{b_r}+\frac{m\pi}{a_r})+\frac{(m+n)\pi}{2}]}{\frac{m\pi}{a_r}-\frac{n\pi}{b_r}}dz'_{s2} -$$
$$-\frac{\sqrt{2}}{2}\int_{-L}^{L}\sin[\frac{q\pi}{2L}(z'_{s2}+L)]\frac{\cos[(\frac{m\pi}{a_r}-\frac{n\pi}{b_r})\frac{\sqrt{2}z'_{s2}}{2}-\frac{\sqrt{2}w}{4}(\frac{n\pi}{b_r}+\frac{m\pi}{a_r})+\frac{(m-n)\pi}{2}]}{\frac{m\pi}{a_r}+\frac{n\pi}{b_r}}dz'_{s2} +$$
$$+\frac{\sqrt{2}}{2}\int_{-L}^{L}\sin[\frac{q\pi}{2L}(z'_{s2}+L)]\frac{\cos[(\frac{m\pi}{a_r}-\frac{n\pi}{b_r})\frac{\sqrt{2}z'_{s2}}{2}+\frac{\sqrt{2}w}{4}(\frac{n\pi}{b_r}+\frac{m\pi}{a_r})+\frac{(m-n)\pi}{2}]}{\frac{m\pi}{a_r}+\frac{n\pi}{b_r}}dz'_{s2} \Rightarrow$$

$$I_{s2b_q} = \frac{\sqrt{2}}{2}\int_{-L}^{L}\sin[\frac{q\pi}{2L}(z'_{s2}+L)]\frac{2\sin[(\frac{m\pi}{a_r}+\frac{n\pi}{b_r})\frac{\sqrt{2}z'_{s2}}{2}+\frac{(m+n)\pi}{2}]\sin[\frac{\sqrt{2}w}{4}(\frac{m\pi}{a_r}-\frac{n\pi}{b_r})]}{\frac{m\pi}{a_r}-\frac{n\pi}{b_r}}dz'_{s2} -$$
$$-\frac{\sqrt{2}}{2}\int_{-L}^{L}\sin[\frac{q\pi}{2L}(z'_{s2}+L)]\frac{2\sin[(\frac{m\pi}{a_r}-\frac{n\pi}{b_r})\frac{\sqrt{2}z'_{s2}}{2}+\frac{(m-n)\pi}{2}]\sin[\frac{\sqrt{2}w}{4}(\frac{m\pi}{a_r}+\frac{n\pi}{b_r})]}{\frac{m\pi}{a_r}+\frac{n\pi}{b_r}}dz'_{s2} \Rightarrow$$

$$I_{s2b_q} = -\frac{\sqrt{2}q\pi}{L}\Big\{\frac{\sin[\frac{\sqrt{2}w}{4}(\frac{m\pi}{a_r}-\frac{n\pi}{b_r})]}{\frac{m\pi}{a_r}-\frac{n\pi}{b_r}}\frac{\sin[(\frac{m\pi}{a_r}+\frac{n\pi}{b_r})\frac{\sqrt{2}L}{2}-\frac{(m+n)\pi}{2}]}{(\frac{q\pi}{2L})^2-\frac{1}{2}(\frac{m\pi}{a_r}+\frac{n\pi}{b_r})^2}+$$
$$+\frac{\cos(q\pi)\sin[(\frac{m\pi}{a_r}+\frac{n\pi}{b_r})\frac{\sqrt{2}L}{2}+\frac{(m+n)\pi}{2}]}{(\frac{q\pi}{2L})^2-\frac{1}{2}(\frac{m\pi}{a_r}+\frac{n\pi}{b_r})^2}\Big\}-$$
$$+\frac{\sqrt{2}q\pi}{L}\frac{\sin[\frac{\sqrt{2}w}{4}(\frac{m\pi}{a_r}+\frac{n\pi}{b_r})]}{\frac{m\pi}{a_r}+\frac{n\pi}{b_r}}\Big\{\frac{\sin[(\frac{m\pi}{a_r}-\frac{n\pi}{b_r})\frac{\sqrt{2}L}{2}-\frac{(m-n)\pi}{2}]}{(\frac{q\pi}{2L})^2-\frac{1}{2}(\frac{m\pi}{a_r}-\frac{n\pi}{b_r})^2}+$$
$$+\frac{\cos(q\pi)\sin[(\frac{m\pi}{a_r}-\frac{n\pi}{b_r})\frac{\sqrt{2}L}{2}+\frac{(m-n)\pi}{2}]}{(\frac{q\pi}{2L})^2-\frac{1}{2}(\frac{m\pi}{a_r}-\frac{n\pi}{b_r})^2}\Big\} \quad (D.25b)$$

Combination of (D.24a) and (D.24b) yields:

$$I_{s2_q} = \begin{cases} I_{s2a_q}, \frac{m\pi}{a_r} = \frac{n\pi}{b_r} \\ I_{s2b_q}, \frac{m\pi}{a_r} \neq \frac{n\pi}{b_r} \end{cases} \quad (D.26)$$

• $R3$

$$R3_{p,q} = \frac{\sqrt{2}}{2} \iint\limits_{Slot2} v_p(\zeta_{s2}, \xi_{s2}) \iint\limits_{Slot2} G^m_{Hsrw_{\xi\zeta}}(\overrightarrow{r_{s2}}|\overrightarrow{r_{s2}}') u_q(\zeta'_{s2}, \xi'_{s2}) d\xi'_{s2} d\zeta'_{s2} d\xi_{s2} d\zeta_{s2}$$

where:

$$G^m_{Hsrw_{\xi\zeta}}(\overrightarrow{r_{s2}}|\overrightarrow{r_{s2}}') = \frac{4j}{a_r b_r} \sum_{m=1}^{\infty} \sum_{n=0}^{\infty} \frac{\frac{m\pi}{a_r}\frac{n\pi}{b_r}}{\gamma_{m,n}\varepsilon_m\varepsilon_n k_o^2} f3_{m,n}(\zeta_{s2}, \xi_{s2}) f2_{t,s}(\zeta'_{s2}, \xi'_{s2}) t3_{n,m}(\eta_{s2}, \eta'_{s2})$$

$$R3_{p,q} = \frac{\sqrt{2}}{2} I_{o2_p} I_{s1_q}, \quad (D.27)$$

where $I_{o2_p} = I_{s2_p}$

• $R4$

$$R4_{p,q} = \frac{\sqrt{2}}{2} \iint\limits_{Slot2} v_p(\zeta_{s2}, \xi_{s2}) \iint\limits_{Slot2} G^m_{Hsrw_{\xi\zeta}}(\overrightarrow{r_{s2}}|\overrightarrow{r_{s2}}') u_q(\zeta'_{s2}, \xi'_{s2}) d\xi'_{s2} d\zeta'_{s2} d\xi_{s2} d\zeta_{s2}$$

where:

$$G^m_{Hsrw_{\xi\xi}}(\overrightarrow{r_{s2}}|\overrightarrow{r_{s2}}') = -\frac{4j}{a_r b_r} \sum_{m=1}^{\infty} \sum_{n=0}^{\infty} \frac{k_o^2 - (\frac{n\pi}{b_r})^2}{\gamma_{m,n}\varepsilon_t\varepsilon_s k_o^2} f2_{m,n}(\zeta_{s2}, \xi_{s2}) f2_{m,n}(\zeta'_{s2}, \xi'_{s2}) t3_{m,n}(\eta_{s2}, \eta'_{s2})$$

$$R4_{p,q} = \frac{\sqrt{2}}{2} I_{o2_p} I_{s2_q}, \quad (D.28)$$

The final expression for $GE12_{p,q}$ is obtained after insertion of (D.23), (D.26), (D.27) and (D.28) into (D.20):

$$GE12_{p,q} = -j\omega\varepsilon\tfrac{1}{2}(I_{o1_p} I_{s1_q} + I_{o1_p} I_{s2_q} + I_{o2_p} I_{s1_q} + I_{o2_p} I_{s2_q}) \quad (D.29)$$

Bibliography

[1] N.Marcuwitz, "Waveguide Handbook", *New York: McGraw-Hill*,1953.

[2] J.R.Whinnery, H.W.Jamieson, "Equivalent Circuits for Discontinuities in Transmission Lines", *Proc I.R.E.*, Feb.1945, pp.98-114.

[3] N.Marcuwitz, J.Schwinger, "On the Representation of the Electric and Magnetic Fields Produced by Currents and Discontinuities in Wave Guides", *J. Appl. Phys.*, vol. 23, Jun.1951, pp.806-819.

[4] A.A.Oliner, "Equivalent Circuits for Small Symmetrical Longitudinal Apertures and Obstacles", *IRE Trans. Microwave Theory Tech.*, Jun.1960, pp.72-80.

[5] J.Van Bladel , "Small-hole coupling of resonant cavities and waveguides", *Proc. Inst. Elec. Eng.*, vol.117, Jun.1970, pp.1098-1104.

[6] F.Alessandri, G.Bartolucci, R.Sorrentino, "Admittance Matrix Formulation of Waveguide Discontinuity Problems: Computer-Aided Design of Branch Guide Directional Couplers", *IEEE Trans. Microwave Theory Tech.*, vol. MTT-36, Feb.1988, pp.394-403.

[7] H.A.Mendez, "On the Theory of Low-Frequency Excitation of Cavity Resonators", *IEEE Trans. Microwave Theory Tech.*, vol. MTT-18, Aug.1970, pp.444-448.

[8] J.Van Bladel , "Small holes in a waveguide wall", *Proc. Inst. Elec. Eng.*, vol.118, Jan.1971, pp.43-50.

[9] R.J.Gutmann, K,E.Mortenson, "An Ordered Array of Terminated Metallic Posts as an Embedding Network for Lumped Microwave Devices" ", *IEEE Trans. Microwave Theory Tech.*, vol. MTT-20, March.1972, pp.215-223.

[10] T.E.Rozzi, W.F.G. Mecklenbraeuker, "Wide-Band Network Modeling of Interacting Inductive Irises and Steps", *IEEE Trans. Microwave Theory Tech.*, vol. MTT-23, No.2, Feb.1975, pp.235-245.

[11] H.Rahman, J.Perini, "Analysis of a Wire in a Rectangular Cavity", *IEEE MTT-S Digest*, 1983, pp.230-232.

[12] A.S.Omar, K.F.Schuenemann, "Analysis of Waveguides with Metal Inserts", *IEEE Trans. Microwave Theory Tech.*, vol. MTT-37, Dec.1989, pp.1924-1931.

[13] A.S.Omar, K.F.Schuenemann, "Application of the Generalized Spectral-Domain Technique to the Analysis of Rectangular Wqaveguides with Rectangular and Circular Metal Inserts", *IEEE Trans. Microwave Theory Tech.*, vol. MTT-39, Jun.1991, pp.944-950.

[14] H.Chang, K.A.Zaki, "Evanescent-Mode Coupling of Dual-Mode Rectangular Waveguide Filters", *IEEE Trans. Microwave Theory Tech.*, vol. MTT-39, Aug.1991, pp.1307-1312.

[15] A.Derneryd, J.Gustincic, "The Interpolation of General Active Array Impedance from Multielement Simulators", *IEEE Trans. Antennas Propag.*, vol. AP-27, Jan.1979, pp.68-71.

[16] J.Gustincic, "The Determination of Active Array Impedance with Multielement Wavaguide Simulators", *IEEE Trans. Antennas Propag.*, vol. AP-20, Sept.1972, pp.589-595.

[17] H.A.Wheeler, "A Systematic Approach to the Design of a Radiator Element for a Phased-Array Antenna", *Proc. IEEE*, vol. 56, Dec.1968, pp.1940-1951.

[18] M.A.Balfour, "Active Impedance of a Phased-Array Antenna Element Simulated by a Single-Element in Waveguide", *IEEE Trans. Antennas Propag. (Commun.)*, vol. AP-15, Mar.1967, pp.313-314.

[19] P.W.Hannan, M.A.Balfour, "Simulation of a Phased-Array Antenna in Waveguide", *IEEE Trans. Antennas Propag.*, vol. AP-13, May.1965, pp.342-353.

[20] P.W.Hannan, P.J.Meier, M.A.Balfour, "Simulation of Phased Array Antenna Impedance in Waveguide", *IEEE Trans. Antennas Propag. (Commun.)*, vol. AP-11, Mar.1963, pp.715-716.

[21] S.A.Schelkunoff, "On diffraction and radiation of electromagnetic waves", *Phys.Rev*, vol. 56, Aug.1939.

[22] R.E.Collin, "Field Theory of Guided Waveguides", 2nd ed *Piscataway, NJ: IEEE Press* ,1991.

[23] Probes A.G.Williamson, "Coaxially fed hollow probe in a rectangular waveguide", *Proc. Inst. Elec. Eng.*, vol.132, Oct.1985, Part H, pp.273-285.

[24] J.J.Jarem, "A Multifilament Method-of-Moments Solution for the Input Impedance of a Probe-Excited Semi-Infinite Waveguide ", *IEEE Trans. Microwave Theory Tech.*, vol. MTT-35, Jan.1987, pp.14-19.

[25] B.Wang, "Mutual Impedance between Probes in a Waveguide", *IEEE Trans. Microwave Theory Tech.*, vol. MTT-36, Jan.1988, pp.53-60.

[26] J.F.Liang, H.C.Chang, K.A.Zaki, "Coaxial Probe Modeling in Waveguides and Cavities", *IEEE Trans. Microwave Theory Tech.*, vol. MTT-40, Dec.1992, pp.2172-2180.

[27] H.Yao, K.A.Zaki, "Modeling Generalized Coaxial Probes in Rectangular Waveguides", *IEEE MTTS-S Digest*,1995, pp.979-982.

[28] J.Hirokawa, K.Sakurai, M.Ando, N.Goto, "An Analysis of a Waveguide T Junction with an Inductive Post", *IEEE Trans. Microwave Theory Tech.*, vol. MTT-39, Dec.1991, pp.563-566.

[29] R.L.Eisenhart, P.J.Khan, "Theoretical and Experimental Analysis of a Waveguide Mounting Structure", *IEEE Trans. Microwave Theory Tech.*, vol. MTT-19, Aug.1971, pp.706-719.

[30] J.A.Bradshaw, "Scattering from a Round Metal Post and Gap", *IEEE Trans. Microwave Theory Tech.*, vol. MTT-21, May.1973, pp.313-322.

[31] O.L.El-Sayed, "Generalized Analysis of Parallel Two-Post Mounting Structures in Waveguide", *IEEE Trans. Microwave Theory Tech.*, vol. MTT-25, Jan.1977, pp.24-33.

[32] J.S.Joshi, J.A.F.Cornick, "Analysis of Waveguide Post Configurations: Part I - Gap Immittance Matrices", *IEEE Trans. Microwave Theory Tech.*, vol. MTT-25, Mar.1977, pp.169-172.

[33] J.S.Joshi, J.A.F.Cornick, "Analysis of Waveguide Post Configurations: Part II - Dual-Gap Cases", *IEEE Trans. Microwave Theory Tech.*, vol. MTT-25, Mar.1977, pp.173-181.

[34] V.M.Pandharipande, B.N.Das, "Equivalent Network of a Variable-Height Post in a Rectangular Waveguide", *Proc. Inst. Elec. Eng.*, Vol.124, No.12. Dec.1977 , pp.1160-1162.

[35] A.G.Williamson, "Analysis and Modelling of a Single-Post Waveguide Mounting Structure", *Proc. Inst. Elec. Eng.*, vol.129, Oct.1982, Part H, pp.271-277

[36] Y.Leviatan, P.G.Li, A.T.Adams, J.Perini, "Single-Post Inductive Obstacles in Rectangular Waveguide", *IEEE Trans. Microwave Theory Tech.*, vol. MTT-31, Oct.1983, pp.806-812.

[37] S.W.Lopuch, T.K. Ishi, "Field Distribution of Two Conducting Posts in a Waveguide", *IEEE Trans. Microwave Theory Tech.*, vol. MTT-32, Jan.1984, pp.29-33.

[38] H.Auda, R,F,Harrington, "Inductive Posts and Diaphragms of Arbitrary Shape and Number in a Rectangular Waveguide", *IEEE Trans. Microwave Theory Tech.*, vol. MTT-32, Jun.1984, pp.606-613.

[39] A.G.Williamson, "Variable-length cylindrical post in a rectangular waveguide", *Proc. Inst. Elec. Eng.*, vol.133, Oct.1986, Part H, pp.1-9.

[40] Y.Huang, N.Yang, S.Lin, R.F.Harrington, "Analysis of a post with arbitrary cross-section and height in a rectangular waveguide", *Proc. Inst. Elec. Eng.*, vol.138, Oct.1991, Part H, pp.475-480.

[41] T.Tokohama, E.Sawado, "Functionals in the Variational Method Applied to Equivalent Impedance Matrix of Metallic Posts Unsymmetrically Positioned in a Rectangular Waveguide", *IEEE Trans. Microwave Theory Tech.*, vol. MTT-40, Aug.1992, pp.1655-1660.

[42] O.Maroja, C.P.Filho, L.C.da Silva, "Scattering Matrix of Cylindrical Posts Centered on the Walls of Rectangular Waveguides", *IEEE Trans. Microwave Theory Tech.*, vol. MTT-42, Jul.1994, pp.1198-1206.

[43] H.W.Yao, K.A.Zaki, A.E.Atia, R.Hershtig , "Full Wave Modelling of Conducting Posts in Rectangular Waveguides and Its Applications to Slot Coupled Combine Filters", *IEEE Trans. Microwave Theory Tech.*, vol. MTT-43, No.12, Dec.1995, pp.2824-2830.

[44] J.H.Richmond, "A Wire-Grid Model for Scattering by Conducting Bodies", *IEEE Trans. Antennas Propag.*, vol. AP-14, Nov.1966, pp.782-78

[45] X.Liang, K.A.Zaki, "Modeling of Cylindrical Dielectric Resonators in Rectangular Waveguides and Cavities", *IEEE Trans. Microwave Theory Tech.*, vol. MTT-41, Dec.1993, pp.2174-2181.

[46] C.T.Tai, "Dyadic Green's Functions in Electromagnetic Theory", Scranton, PA: Intext Educational Publishers, 1972.

[47] J.Van Bladel, "Electromagnetic Fields", McGraw-Hill Book Company, Inc. New York, 1964.

[48] J.G.Fikioris, "Electromagnetic Field Inside a Current-Carrying Region", *Journ. Math. Phys.*, vol. 6, Nov.1965, pp.1617-1620.

[49] A.J.Poggio, E.K.Miller, "Integral Equation Solutions of Three-Dimensional Scattering Problems", in *Computer Techniques for Electromagnetics*, R.Mittra, Ed. New York: Pergamon, 1973, pp.159-264.

[50] Y.Rahmat-Samii, "On the Question of Computation of the Dyadic Green's Function at the Source Region in Waveguides and Cavities ", *IEEE Trans. Microwave Theory Tech.*, vol. MTT-23, Sept.1975, pp.762-765.

[51] C.T.Tai, P.Rozenfeld, "Different Representations of Dyadic Green's Functions for a Rectangular Cavity", *IEEE Trans. Microwave Theory Tech.*, vol. MTT-24, Sept.1976, pp.597-601.

[52] J.A.R.Ball, P.J.Khan, "Source region electric field derivation by a dyadic Green's function approach", *Proc. Inst. Elec. Eng.*, vol.127, Oct.1980, Part H, pp.301-304.

[53] P.H.Pathak, "On the Eigenfunction Expansion of Electromagnetic Dyadic Green's Function", *IEEE Trans. Antennas Propag.*, vol. AP-31, Nov.1983, pp.837-846.

[54] M.Bressan, G.Conciauro, "Singularity Extraction from the Electric Green's Function for a Spherical Resonator", *IEEE Trans. Microwave Theory Tech.*, vol. MTT-33, Feb.1985, pp.407-414.

[55] R.Kastner, "On the Singularity of the Full Spectral Green's Dyad", *IEEE Trans. Antennas Propag.*, vol. AP-35, Nov.1987, pp.1303-1307.

[56] W.C.Chew, "Some Observations on the Spatial and Eigenfunction Representation of Dyadic Green's Functions", *IEEE Trans. Antennas Propag.*, vol. AP-37, Oct.1989, pp.1322-1327.

[57] A.F.Peterson, R.L.Scott, R.Mittra, "Computational Methods for Electromagnetics", *Wiley & Sons*, 1997.

[58] N.Christian Albertsen, J.E.Hansen, N.E.Jensen "Computation of Radiation ftom Wire Antennas on Conducting Bodies", *IEEE Trans. Antennas Propag.*, vol. AP-22, March.1974, pp.200-206.

[59] C.A.Klein, R.Mittra "An Application of the 'Condition Number' Concept to the Solution of Scattering Problems in the Presence of thye Interior Resonant Frequencies", *IEEE Trans. Antennas Propag.*, Mar.1975, pp.431-434.

[60] J.R.Mautz, R.F.Harrington, "H-Field, E-Field and Combined-Field Solutions for Conducting Bodies of Revolution, " *AEU* Band 32 Heft 4, 1978, pp.157-164

[61] A.D.Yaghjian, "Augmented electric- and magnetic-field integral equation", *Radio Sci.*, vol. 16, Nov.-Dec.1981, pp.987-1001.

[62] L.M.Correia "A Comparison of Integral Equations with Unique Solution in the Resonance Region for Scattering by Conducting Bodies", *IEEE Trans. Antennas Propag.*, vol. AP-41, Jan.1993, pp.52-58.

[63] S.C.Wu, Y.L.Chow, "An Application of the Moment Method to Waveguide Scattering Problems", *IEEE Trans. Microwave Theory Tech.*, vol. MTT-20, Nov.1972, pp.744-749.

[64] Y.L.Chow, S.C.Wu, "A Moment Method with Mixed Basis Functions for Scatterings by Waveguide Junctions", *IEEE Trans. Microwave Theory Tech.*, vol. MTT-21, Nov.1973, pp.333-340.

[65] X.Zhu, D.Chen, S.Wang, "Method-of-Moments Solution for the Posts in a Circular Waveguide", *IEEE MTTS-S Digest*,1990, pp.693-696

[66] M.R.Barclay, W.V.T.Rusch, "Moment-Method Analysis of Large, Axially Symmetric Reflector Antennas Using Entire-Domain Functions ", *IEEE Trans. Antennas Propag.*, vol. AP-39, Apr.1991, pp.491-496.

[67] B.E.Spielman, R.F.Harrington, "Waveguides of Arbitrary Cross Section by Solution of a Nonlinear Integral Eigenvalue Equation", *IEEE Trans. Microwave Theory Tech.*, vol. MTT-20, Nov.1972, pp.578-585.

[68] N.N.Wang J.H.Richmond, M.C.Gilreath, "Sinusoidal Reaction Formulation for Radiation and Scattering from Conducting Surfaces", *IEEE Trans. Antennas Propag.*, vol. AP-23, May.1975, pp.376-382.

[69] E.H.Newman, D.M.Pozar, "Electromagnetic Modeling of Composite Wire and Surface Geometries", *IEEE Trans. Antennas Propag.*, vol. AP-26, Nov.1978, pp.784-789.

[70] J.J.H.Wang, "Numerical analysis of three-dimensional arbitrarily-shaped conducting scatterers by trilateral surface cell modelling", *Radio Sci.*, vol. 13, Mar.1978, pp.947-952.

[71] S.M.Rao, A.W.Glisson, D.R.Wilton, "A Simple Numerical Solution Procedure for Statics Problems Involving Arbitrary-Shaped Surfaces", *IEEE Trans. Antennas Propag.*, vol. AP-27, Sep.1979, pp.604-607.

[72] A.W.Glisson, D.R.Wilton, "Simple and Efficient Numerical Methods for Problems of Electromagnetic Radiation and Scattering from Surfaces", *IEEE Trans. Antennas Propag.*, vol. AP-28, Sep.1980, pp.593-603.

[73] S.M.Rao, A.W.Glisson, D.R.Wilton, "Electromagnetic Scattering by Surfaces of Arbitrary Shape", *IEEE Trans. Antennas Propag.*, vol. AP-30, May.1982, pp.409-418.

[74] J.J.H.Wang, C.J.Drane, "Numerical Analysis of Arbitrarily Shaped Bodies Modeled by Surface Patches ", *IEEE Trans. Microwave Theory Tech.*, vol. MTT-30, Aug.1982, pp.1167-1173.

[75] J.M.Bornholdt, L.N.Medgyesi-Mitschang, "Mixed-Domain Galerkin Expansions in Scattering Problems", *IEEE Trans. Antennas Propag.*, vol. AP-36, Feb.1988, pp.216-227

[76] K.A.Michalski, D.Zheng, "Electromagnetic Scattering and Radiation by Surfaces of Arbitrary Shape in Layered Media, Part I: Theory", *IEEE Trans. Antennas Propag.*, vol. AP-38, Mar.1990, pp.335-344.

[77] G.Conciauro, M.Bressan, C.Zuffada, "Waveguide Modes Via an Integral Equation Leading to a Linear Matrix Eigenvalue Problem", *IEEE Trans. Microwave Theory Tech.*, vol. MTT-32, Nov.1984, pp.1495-1504.

[78] S.Hashemi-Yeganeh, C.R.Bircher, "Numerical and Experimental Studies of Current distributions on Thin Metallic Posts Inside Rectangular Waveguides", *IEEE Trans. Microwave Theory Tech.*, vol. MTT-42, Jun.1994, pp.1063-1068.

[79] J.M.Reiter, F.Arndt, "Rigorous Analysis of Arbitrary Shaped H- and E- Plane Discontinuities in Rectangular Waveguides by a Full-Wave Boundary Contour Mode-Matching Method", *IEEE Trans. Microwave Theory Tech.*, vol. MTT-43, Apr.1995, pp.796-801.

[80] D.R.Wilton, S.Govind, "Incorporation of Edge Conditions in Moment Method Solution", *IEEE Trans. Antennas Propagat.*, vol. AP-25, No.6, Feb.1977, pp.845-850.

[81] R.Mittra, T.Itoh, T.Li, "Analytical and Numerical Studies of the Relative Convergence Phenomenon Arising in the Solution of an Integral Equation by the Moment Method", *IEEE Trans. Microwave Theory Tech.*, vol. MTT-20, Aug.1972, pp.96-104.

[82] J.R.Mautz, R.F.Harrington, "An E-Field Solution for a Conducting Surface Small or Comparable to the Wavelength", *IEEE Trans. Antennas Propag.*, vol. AP-32, Jan.1984, pp.330-339.

[83] E.Arvas, R.F.Harrington, J.R.Mautz, "Radiation and Scattering from Electrically Small Conducting Bodies of Arbitrary Shape", *IEEE Trans. Antennas Propag.*, vol. AP-34, Jan.1986, pp.66-77.

[84] M.Hashimoto, K.Fujisawa, "Considerations on Matrix Methods and Estimation of Their Errors", *IEEE Trans. Microwave Theory Tech.*, vol. MTT-18, Jul.1970, pp.352-359

[85] E.E.Altschuler, "A Periodic Structure of Cylindrical Posts in a Rectangular Waveguide", *IRE Trans. Microwave Theory Tech.*, Sep.1961 , pp.398-402

[86] W.H.Watson, "The Physical Principles of Wave Guide Transition", *Oxford University Press*, London, 1947.

[87] A.F.Stevenson, "Theory of Slots in Rectangular Waveguides", *J. Appl. Phys.*, vol.19, Jan.1948, pp.24-38.

[88] S.B.Cohn, "Microwave Coupling by Large Apertures", *Proc I.R.E.*, Jun.1952, pp.696-699.

[89] H.Gruenberg, "Theory of Wave-Guide-Fed Slots Radiating into Parallel Plate Regions", *J. Appl. Phys.*, vol.23, Jul.1952, pp.733-737.

[90] H.Gruenberg, "Second-Order Beams of Slotted Wave Guide Arrays", *Canadian Journal of Physics*, vol.31, 1953, pp.55-69.

[91] G.A.Yevstropov, S.A.Tsarapkin, "Investigation of Slotted Waveguide Antennas with Identical Resonant Radiators", *Radio Eng. Electron. Phys.*, vol.10, Sept.1965, pp.1429-1436.

[92] S.M.Prasad, B.N.Das, "Studies on Waveguide-Fed Slot Antenna", *Proc. Inst. Elec. Eng.*, vol.120, May.1973, pp.539-540

[93] K.Forooraghi, P.-S.Kildal, S.R.Rengarajen "Admittance of an Isolated Waveguide-Fed Slot Radiating Between Baffles Using a Spectrum of Two-Dimensional Solutions", *IEEE Trans. Antennas Propag.*, vol. AP-41, Nov.1993, pp.422-428.

[94] K.Forooraghi, P.-S.Kildal "Transverse Radiation Pattern of a Slotted Waveguide Array Radiating between Finite Height Baffles in Terms of a Spectrum of Two-Dimensional Solutions", *Proc. Inst. Elec. Eng. -H*, vol.140, Feb.1993, pp.52-58.

[95] J.Wettergren, P.Kildal "Admittance of a Longitundinal Waveguide Slot Radiating into an Arbitrary Cylindrical Structure", *IEEE Trans. Antennas Propag.*, vol. AP-43, Nov.1995, pp.667-673.

[96] B.N.Das, P.S.Deshmukh, V.M.Pandharipande "Excitation of Planar Slot Array from Rectangular Waveguide", *Proc. Inst. Elec. Eng. -H*, vol.131, Apr.1984, pp.99-101.

[97] H.Y.Yee, "The Design of Large Waveguide Arrays of Shunt Slots", *IEEE Trans. Antennas Propag.*, vol. AP-40, July.1992, pp.775-781.

[98] O.Nell, K.Solbach, J.Creier, "Rundumstrahlende Hohlleiter-Schlitzantenne fuer Horizontalpolarisation", *UKW-Berichte/VHF Communication*, No1, pp.50-55 and No.2, pp.71-77 (two parts), 199.

[99] S.Edelberg, A.A.Oliner, "Mutual Coupling Effects in Large Antenna Arrays. Part I- Slot Arrays", *IEEE Trans. Antennas Propag.*, May.1960, pp.286-297.

[100] F.Arndt, B.Koch, H.J.Orlok, N.Schroeder, "Field Theory Design of Rectangular Waveguide Broad-Wall Metal-Insert Slot Couplers for Millimeter-Wave Applications", *IEEE Trans. Microwave Theory Tech.*, vol. MTT-33, Feb.1985, pp.95-104.

[101] H.Schmiedel, F.Arndt, "Field Theory Design of Rectangular Waveguide Multiple-Slot Narrow-Wall Couplers", *IEEE Trans. Microwave Theory Tech.*, vol. MTT-34, Feb.1986, pp.791-798.

[102] A.A.Oliner, "The Impedance Properties of Narrow Radiating Slots in the Broad Face of Rectangular Waveguide, Part I-Theory", *IRE Trans. Antennas Propagat.*, vol. AP-5, Jan.1957, pp.4-20.

[103] T. Vu Khac, C.T.Karson, "m=0, n=0 Mode and Rectangular Waveguide slot Discontinuity ", *Electronics Letters*, vol.9, No.18, Sep.1973, pp.431-432.

[104] J. Van Bladel, "Contribution of the ψ =constant mode to the modal expansion in a waveguide", *Proc. Inst. Elec. Eng.*, vol.128, Oct.1981, Part H, pp.247-251.

[105] L.G.Josefsson, "Analysis of Longitundinal Slots in Rectangular Waveguides", *IEEE Trans. Microwave Theory Tech.*, vol. MTT-35, Dec.1987, pp.1351-1357.

[106] S.R.Rengarajan, "Analysis of a Centered-Inclined Waveguide Slot Coupler", *IEEE Trans. Microwave Theory Tech.*, vol. MTT-37, May.1989, pp.884-889.

[107] S.R.Rengarajan, "Characteristics of a Longitundinal/Transverse Coupling Slot in Crossed Rectangular Waveguides", *IEEE Trans. Microwave Theory Tech.*, vol. MTT-37, Aug.1989, pp.1171-1177.

[108] S.R.Rengarajan, "Compound Radiating Slots in a Broad Wall of a Rectangular Waveguide", *IEEE Trans. Microwave Theory Tech.*, vol. MTT-37, Sep.1989, pp.1116-1123.

[109] B.N.Das, P.V.D. Somasekhar Rao, A.Chakrabarty, "Narrow Wall Axial-Slot-Coupled T Junction Between Rectangular and Circular Waveguides", *IEEE Trans. Microwave Theory Tech.*, vol. MTT-37, Oct.1989, pp.1590-1596.

[110] B.N.Das, P.V.D. Somasekhar Rao, "Analysis of Cascaded Sections of T Junctions Between Rectangular and Circular Waveguides", *IEEE Trans. Microwave Theory Tech.*, vol. MTT-39, Jan.1991, pp.92-97.

[111] S.N.Sinha, "A generalized network formulation for a class of waveguide coupling problems", *Proc. Inst. Elec. Eng.*, vol.134, Dec.1987, Part H, pp.502-508.

[112] S.M.Prasad, B.N.Das, "Analytical expression for the reactance due to energy stored inside a waveguide", *Proc. Inst. Elec. Eng.*, vol.120, May.1973, pp.539-540

[113] P.K.Park, G.J.Stern, R.S.Elliott, "An Improved Technique for the Evaluation of Transverse Slot Discontinuities in Rectangular Waveguide", *IEEE Trans. Antennas Propag.*, vol. AP-31, May.1983, pp.148-153.

[114] V.M.Pandharipande, B.N.Das, "Equivalent Circuit of a Narrow-Wall Waveguide Slot Coupler ", *IEEE Trans. Microwave Theory Tech.*, vol. MTT-27, Sept.1979, pp.800-804.

[115] Y.Tsunoda, N.Gotto, "Nonuniformly spaced slot arrayed antenna with low sidelobe pattern", *Proc. Inst. Elec. Eng.*, vol.133, Apr.1986, Part H, pp.155-158

[116] A.Datta, A.M.Rajeek, A.Chakrabarty, B.N.Das, "S Matrix of a Broad Wall Coupler between Dissimilar Rectangular Waveguides", *IEEE Trans. Microwave Theory Tech.*, vol. MTT-43, Jan.1995, pp.56-62.

[117] K.Yashiro, S.Ohkawa, "Boundary Element Method for Electromagnetic Scattering from Cylinders", *IEEE Trans. Antennas Propag.*, vol. AP-33, Apr.1985, pp.383-389.

[118] M.Koshiba, M.Suzuki, "Application of the Boundary-Element Method to Waveguide Discontinuities", *IEEE Trans. Microwave Theory Tech.*, vol. MTT-43, Feb.1986, pp.301-307.

[119] W.E.Boyse, K.D.Paulsen, "Accurate Solutions of Maxwell's Equations Around PEC Corners and Highly Curved Surfaces Using Nodal Finite Elements", *IEEE Trans. Antennas Propag.*, vol. AP-45, Dec.1997, pp.1758-1766.

[120] M.Israel, R.Miniowitz, "An Efficient Finite Element Method for Nonconvex Waveguide Based on Hermitian Polynomials", *IEEE Trans. Microwave Theory Tech.*, vol.MTT-35, Nov.1987.

[121] B.Schiff, "Eigenvalues for Ridged and Other Waveguides Containing Corners of Angle 3 /2 or 2 by the Finite Element Method ", *IEEE Trans. Microwave Theory Tech.*, vol.MTT-35, Jun.1991.

[122] J.Helszajn, M.McKay , "Voltage-current definition of impedance of double ridge waveguide using the finite element method", *IEE Proc.-Microw. Antennas Propag.*, vol.45, Feb.1998.

[123] H.Igarashi, T.Honma , "An Analysis of Electromagnetic Waves by a Complementary Finite Element Method", *(*IEEE Trans. Mag. vol.30, Sep.1994.

[124] D.T.McGrath, V.P.Pyati, "Phased Array Antenna Analysis with the Hybrid Finite Element Method", *IEEE Trans. Antennas Propag.*, vol. AP-42, Dec.1994.

[125] S.B.Cohn, "Properties of Ridge Waveguide", *Proc. IRE*, vol.35, Aug.1947, pp.783-788.

[126] S.Hopfer, "The Design of Ridged Waveguides", *IRE Trans. Microwave Theory Tech.*, vol. MTT-3, Oct.1955, pp.20-29.

[127] W.J.Getsinger, "Ridged Waveguide Field Description and Application to Directional Couplers", *IRE Trans. Microwave Theory Tech.*, vol. MTT-10, Jan.1962, pp.41-50.

[128] J.R.Pyle, "The Cutoff Wavelength of the TE_{10} Mode in Ridged Rectangular Waveguide of any Aspect Ratio", *IEEE Trans. Microwave Theory Tech.*, vol. MTT-14, Apr.1966, pp.175-183.

[129] J.P.Montgomery, "On the Complete Eigenvalue solution of Ridged Wvaguide", *IEEE Trans. Microwave Theory Tech.*, vol. MTT-19, Jun.1971, pp.547-555

[130] Y.Utsumi, "Variational Analysis of Ridged Waveguide Modes", *IEEE Trans. Microwave Theory Tech.*, vol. MTT-33, Feb.1985, pp.111-120.

[131] S.Mizushina, N.Kuwabara, H.Kondoh, "Theoretical Analysis of a Ridged-Waveguide Mounting Structure", *IEEE Trans. Microwave Theory Tech.*, vol. MTT-25, Dec.1977, pp.1131-1134.

[132] R.R.Mansour, R.S.K.Tong, R.H.Macphie, "Simplified Description of the Field Distribution in Finlines and Ridge Waveguides and Its Application to the Analysis of E-Plane Discontinuities", *IEEE Trans. Microwave Theory Tech.*, vol. MTT-36, Dec.1985, pp.1825-1832.

[133] S.Amari, J.Bornemann, R.Vahldieck, "Application of a Coupled-Integral-Equations Technique to Ridged Waveguides", *IEEE Trans. Microwave Theory Tech.*, vol. MTT-44, Dec.1996, pp.2256-2264.

[134] J.-W.Tao, H.Baudrand, "Multimodal Variational Analysis of Uniaxial Waveguide Discontinuities", *IEEE Trans. Microwave Theory Tech.*, vol. MTT-39, Mar.1991, pp.506-516.